

INVESTIGATION OF SHORT AND LONG TERM TRENDS IN THE EASTERN  
MEDITERRANEAN AEROSOL COMPOSITION

A THESIS SUBMITTED TO  
THE GRADUATE SCHOOL OF NATURAL AND APPLIED SCIENCES  
OF  
MIDDLE EAST TECHNICAL UNIVERSITY

BY

FATMA ÖZTÜRK

IN PARTIAL FULFILLMENT OF THE REQUIREMENTS  
FOR  
THE DEGREE OF DOCTOR OF PHILOSOPHY  
IN  
ENVIRONMENTAL ENGINEERING

JANUARY 2009

Approval of the thesis:

**INVESTIGATION of SHORT and LONG TERM TRENDS in EASTERN  
MEDITERRANEAN AEROSOL COMPOSITION**

submitted by **FATMA ÖZTÜRK** in partial fulfillment of the requirements for the degree of  
**Doctor of Philosophy in Environmental Engineering Department, Middle East  
Technical University** by,

Prof. Dr. Canan Özgen  
Dean, Graduate School of **Natural and Applied Sciences** \_\_\_\_\_

Prof.Dr.Göksel N.Demirer  
Head of Department, **Environmental Engineering** \_\_\_\_\_

Prof.Dr.Gürdal Tuncel  
Supervisor, **Environmental Engineering Dept., METU** \_\_\_\_\_

**Examining Committee Members**

Prof. Dr. Kahraman Ünlü  
Environmental Engineering Dept., METU \_\_\_\_\_

Prof. Dr. Gürdal Tuncel  
Environmental Engineering Dept., METU \_\_\_\_\_

Prof Dr. Gülen Güllü  
Environmental Engineering Dept., Hacettepe University \_\_\_\_\_

Assoc.Prof.Dr. Mustafa Odabaşı  
Environmental Engineering Dept., Dokuz Eylül University \_\_\_\_\_

Assoc.Prof.Dr. Ayşegül Aksoy  
Environmental Engineering Dept., METU \_\_\_\_\_

**Date:** \_\_\_\_\_

**I hereby declare that all information in this document has been obtained and presented in accordance with academic rules and ethical conduct. I also declare that, as required by these rules and conduct, I have fully cited and referenced all material and results that are not original to this work.**

Name, Last Name: Fatma Öztürk

Signature :

## ABSTRACT

### INVESTIGATION OF SHORT AND LONG TERM TRENDS IN EASTERN MEDITERRANEAN AEROSOL COMPOSITION

Öztürk, Fatma

Ph.D., Department of Environmental Engineering

Supervisor: Prof. Dr. Gürdal Tuncel

January 2009, 451 pages

Approximately 2000 daily aerosol samples were collected at Antalya (30°34'30.54" E, 36°47'30.54"N) on the Mediterranean coast of Turkey between 1993 and 2001. High volume PM<sub>10</sub> sampler was used for the collection of samples on Whatman-41 filters. Collected samples were analyzed by a combination of analytical techniques. Energy Dispersive X-Ray Fluorescence (EDXRF) and Inductively Coupled Plasma Mass Spectrometry (ICPMS) was used to measure trace element content of the collected samples from Li to U. Major ions, namely, SO<sub>4</sub><sup>2-</sup> and NO<sub>3</sub><sup>-</sup>, were determined by employing Ion Chromatography (IC). Samples were analyzed in terms of their NH<sub>4</sub><sup>+</sup> contents by means of Colorimetry. Evaluation of short term trends of measured parameters have been shown that elements with marine and crustal origin are more episodic as compared to anthropogenic ones. Most of the parameters showed well defined seasonal cycles, for example, concentrations of crustal elements increased in summer season while winter concentrations of marine elements were considerably higher than associated values for summer. Seasonal Kendall statistic depicted that there was a decreasing trend for crustal elements such as Be, Co, Al, Na, Mg, K, Dy, Ho, Tm, Cs and Eu. Lead, As, Se and Ge were the anthropogenic elements that decreasing trend was detected in the course of study period. Cluster and Residence time analysis were performed to find the origin of air masses arriving to Eastern Mediterranean Basin. It has been found that air masses reaching to our station resided more on Balkans and Eastern Europe. Positive Matrix Factorization (PMF) resolved eight factors influencing the chemical composition of Eastern



Mediterranean aerosols as local dust, Saharan dust, oil combustion, coal combustion, crustal-anthropogenic mixed, sea salt, motor vehicle emission, and local Sb factor.

Keywords: Aerosol, Cluster Analysis, Eastern Mediterranean Basin, Long Term And Short Term Trends of Pollutants, Major Ions, Positive Matrix Factorization, Potential Source Contribution Function, Turkey, Trace elements, Trend Analysis

## ÖZ

### AKDENİZ AEOSOLLERİNİN KİMYASAL KOMPOZİSYONUN KISA VE UZUN DÖNEMLİ DEĞİŞİMLERİNİN İNCELENMESİ

Öztürk, Fatma

Doktora, Çevre Mühendisliği Bölümü

Tez Yöneticisi: Prof. Dr. Gürdal Tuncel

Ocak 2009, 451 sayfa

Türkiye'nin Akdeniz kıyısında Antalya'da konuşlandırılan bir istasyonda 1993-2001 yılları arasında yaklaşık olarak 2000 aerosol örneği günlük olarak toplanmıştır. Örnekler PM<sub>10</sub> Yüksek Hacimli örnekleyici kullanılarak Whatman-41 selüloz fiber filtre üzerinde toplandıktan sonra eser element içerikleri açısından Enerji Dağılımlı X-Işınları Spektrometre (EDXRF) ve Endüktif Eşleşmiş Plazma Kütle Spektrometre (ICPMS) cihazları ile ve ana iyonlardan SO<sub>4</sub><sup>2-</sup> ve NO<sub>3</sub><sup>-</sup> İyon Kromatografi (IC) cihazı kullanılarak analiz edilmiştir. Örneklerin NH<sub>4</sub><sup>+</sup> içerikleri Kolorimetre ile tayin edilmiştir. Toprak ve deniz kaynaklı parametrelerin kısa dönemde antropojen elementlere göre daha çok değişim gösterdiği belirlenmiştir. Çalışmada ölçülen parametrelerin mevsimsel analizi ise birçok parametrenin çok belirgin bir değişim gösterdiğini, örneğin deniz kökenli parametrelerin kış derişimlerinin yaz oranla daha yüksek olduğunu, buna karşın toprak kökenli elementlerin yaz aylarında derişimlerinin kışa nazaran daha yüksek olduğu belirlenmiştir. Üretilen veri setine uygulanan Mevsimsel Kendall testi özellikle toprak kökenli elementlerde, örneğin, Al, Fe, Na, Mg, K, Cs, Be, Dy, Ho, Er, Eu, Tm gibi, belirgin bir azalan eğilimin olduğunu göstermiştir. Antropojen kökenli elementlerden As, Se, Ge, ve Pb da çalışma süresince % 95 güven aralığında bir azalmanın olduğu da yine Mevsimsel Kendall testi tarafından bulunan bir diğer olgudur. Geri yörünge istatistiğine dayanan Kluster and Rezidans zaman analizleri, Doğu Akdeniz'e ulaşan hava kütlelerinin en çok Balkanlar ve Batı Avrupa üzerinden geldiğini göstermiştir. Doğu Akdeniz aerosolünün kimyasal kompozisyonunu etkileyen kaynakların belirlenmesi amacıyla Pozitif Matriks Faktörizasyonu (PMF) kullanılmış ve bu model yardımıyla sekiz faktör bulunmuştur.

Bunlar, yerel toprak, Sahra tozu, motorlu aralar, deniz tuzu, petrol kullanımı, kmr kullanımı, antropojen-toprak karışımı ve yerel Sb olarak bulunmuştur.

Anahtar Kelimeler: Aerosol, Ana iyonlar, Doęu Akdeniz Havzası, Eser elementler, Eęilim Analizi, Trkiye, Kirleticilerin Uzun ve Kısa Dnem Eęilimleri, Kluster Analizi, Potansiyel Kaynak Katkı Fonksiyonu, Pozitif Matriks Faktrizasyonu

*To My Mother, Arzu Öztürk*

## **ACKNOWLEDGEMENTS**

I like to express my sincere appreciation to my supervisor Prof. Dr. Gürdal Tuncel for his guidance, advice, criticism and encouragement throughout the research.

I want to thank my committee members, Prof. Dr. Gülen Güllü, Prof.Dr. Kahraman Ünlü, Assoc. Prof. Ayşegül Aksoy and Assoc.Prof. Mustafa Odabaşı for their efforts and time spent in evaluating my dissertation.

I wish to express my appreciation to Prof. John Ondov, from Chemistry and Biochemistry Department of University of Maryland (MD, USA), for his comments, suggestions and helps.

I would like to thank Dr. Abdullah Zararsız and Rıdvan Kırmaz from Sarayköy Nuclear Research and Training Center of the Turkish Atomic Authority for the analysis of samples with EDXRF.

I would like to express my appreciation to Serap Tekin and Fehime Şahin from Central Laboratory of METU for the analysis of samples with ICPMS.

Thanks are also due to TÜBİTAK for supporting me in one year research in USA.

I extend my sincere thanks to D.Deniz Genç Tokgöz for her help in digestion my samples and Mihriban Yılmaz Civan in getting meteorology data.

I would like to thank you Murat Varol. He made my life easy by writing scripts and macros.

Special thanks to Süleyman Can, Güray Doğan, Nur Banu Öztaş, Elif Bayındır, Devrim Kaya, Umay Gökçe Özkan Yücel, Kadir Gedik, Firdes Yenilmez for their friendship and helps.

Finally, I would like to express my deepest appreciation to my family for their endless support, understanding and patience not only during this study but also throughout my life.

## TABLE OF CONTENTS

ABSTRACT .....	iv
ÖZ .....	vi
ACKNOWLEDGEMENTS .....	ix
TABLE OF CONTENTS .....	x
LIST OF TABLES.....	xiv
LIST OF FIGURES.....	xvii
LIST OF ABBREVIATIONS.....	xxiii
CHAPTERS	
1. INTRODUCTION .....	1
1.1. Background .....	1
1.2. Motivation .....	3
1.3. Scope of Thesis .....	5
1.4. Novelty of Thesis .....	5
1.5. Organization of Thesis.....	6
2. LITERATURE REVIEW .....	8
2.1. Aerosols .....	8
2.1.1. Definition of Aerosol .....	8
2.1.2. Aerosol Size.....	9
2.1.3. Aerosol Composition.....	12
2.1.4. Classification of aerosols with respect to their origins .....	13
2.1.5. The Role of Aerosols on the Global Atmospheric Chemistry .....	22
2.1.6. The Impact of Aerosols on Health.....	25
2.2. Legal Framework Established for PM.....	31
2.3. Long Range Transport.....	32
2.4. Eastern Mediterranean Aerosol Composition .....	34
2.4.1. Trace Element Composition.....	37
2.4.2. Major Ion Composition.....	40
2.4.3. General Climatology of Eastern Mediterranean Atmosphere.....	43
2.5. Background of Receptor Modelling.....	46
2.5.1. Positive Matrix Factorization (PMF).....	49
2.5.1.1. PMF Mathematics .....	49

2.5.1.1.1. Residual Matrix, E .....	50
2.5.1.1.2. Estimation of Number of Factors .....	51
2.5.1.1.3. Factor Rotations .....	51
2.5.1.1.4. Robust Mode .....	52
2.5.1.1.5. Uncertainty Estimation, $\sigma_{ij}$ , and Treatment of BDL and Missing Data Values .....	52
2.5.1.2. Output Files of PMF Analysis.....	54
2.5.1.3. Mass Apportionment-Scaling Factor.....	55
2.5.1.4. Explained Variation, $EV_{kj}$ .....	56
2.5.1.5. Uniqueness of the Solution .....	56
2.5.2. Potential Source Contribution Function (PSCF) Analysis.....	58
2.5.2.1. Trajectory Analysis .....	58
2.5.2.2. Potential Source Contribution Function (PSCF) .....	58
2.6. Distribution Characteristics of the Atmospheric Variables .....	61
3. EXPERIMENTAL METHODS .....	65
3.1. Sampling Site Description .....	65
3.2. PM-10 High Volume Air Sampler .....	67
3.2.1. High Volume Sampler Calibration.....	69
3.2.2. Aerosol Filter Selection .....	70
3.3. Sample Handling.....	70
3.4. Analytical Techniques .....	72
3.4.1. Ion Measurements .....	73
3.4.1.1. Determination of Major Anions by Ion Chromatography .....	73
3.4.1.1.1. Sample Preparation for IC Analysis.....	74
3.4.1.2. Determination of $NH_4^+$ by Colorimetry .....	74
3.4.1.2.1. Sample Preparation.....	74
3.4.2. Trace Element Measurement.....	75
3.4.2.1. Energy Dispersive X-ray Fluorescence (EDXRF) .....	75
3.4.2.1.1. XRF Analysis.....	79
3.4.2.1.2. Sample Preparation.....	81
3.4.2.1.3. Calibration of the EDXRF Spectrometry .....	83
3.4.2.1.4. Detection Limit of EDXRF.....	86
3.4.2.1.5. Development of Quality Assurance /Quality Control (QA/QC) Protocol for EDXRF Analysis.....	89
3.4.2.1.6. Penetration Depth and Mass Absorption Coefficient of Aerosols.....	98

3.4.2.2. Trace Element Determination by Inductively Coupled Plasma Mass Spectrometry (ICP-MS) .....	102
3.4.2.2.1. Reagents and Gases.....	102
3.4.2.2.2. Sample Preparation.....	103
3.4.2.2.3. ICP-MS Analysis.....	107
3.4.2.2.4. Quality Assurance and Quality Control (QA/QC).....	111
3.4.2.3. Comparison of Analytical Techniques.....	124
4. RESULTS & DISCUSSION.....	127
4.1. General Characteristics of Atmospheric Data.....	127
4.1.1 Distribution Characteristics of the Eastern Mediterranean Aerosols.....	129
4.1.2. Comparison with Literature .....	136
4.2. Flow Climatology of Eastern Mediterranean .....	144
4.2.1. Comparison of Climatologies of Eastern and Western Mediterranean Basin	151
4.2.2. Local Meteorology .....	154
4.3. Regional Background Concentration of Eastern Mediterranean Atmosphere.....	156
4.4. TEMPORAL VARIATIONS OF POLLUTANTS .....	170
4.4.1. Short-Term (Episodic) Variations of elements and ions in the Eastern Mediterranean Atmosphere.....	172
4.4.2. Long-Term (Seasonal) Variations of Elements and Ions in the Eastern Mediterranean Atmosphere.....	193
4.4.3. Year to year Variation in Concentrations of Aerosol Variables in the Eastern Mediterranean Atmosphere – Long-term trends in concentrations of elements and ions.....	211
4.5. INVESTIGATION of TYPES and LOCATIONS of POLLUTANT SOURCES AFFECTING EASTERN MEDITERRANEAN ATMOSPHERE USING DIFFERENT METHODOLOGIES ..	246
4.5.1. Average Concentration of Elements in Different Wind Sectors .....	247
4.5.1.1. Residence Time Analysis .....	248
4.5.1.2. Cluster Analysis .....	259
4.5.1.2.1. Variation of Chemical Composition with Clusters .....	268
4.5.1.2.2. Comparison of Cluster Analysis and Residence Time Analysis.....	280
4.5.2. Correlations between Parameters .....	281
4.5.3. Enrichment Factors.....	288
4.5.3.1. Crustal Enrichment Factor .....	289
4.5.3.2. Marine Enrichment Factor.....	297
4.5.4. Elevated Sulfate over Eastern Mediterranean Atmosphere.....	299



4.5.5. Saharan Dust Transport to the Eastern Mediterranean Region .....	317
4.5.5.1. Identification of Dust Episode Days .....	319
4.5.5.2. Chemical Tracers of Saharan and Middle East Dust.....	330
4.5.5.3. Temporal Variation of Saharan Dust Frequencies.....	333
4.5.6. Source Apportionment with Factor Analysis (FA) and Positive Matrix Factorization (PMF).....	335
4.5.6.1. Factor Analysis .....	337
4.5.6.2. Positive Matrix Factorization (PMF).....	341
4.5.6.2.1. Construction of Input Data Matrix for PMF .....	341
4.5.6.2.2. PMF Analysis .....	345
4.5.6.2.3. PMF Results .....	347
4.5.6.2.4. Particulate Mass (PM) Apportionment .....	373
4.5.7 Potential Source Contribution Function (PSCF) .....	375
4.5.8. Deposition Fluxes of Elements and Ions to the Eastern Mediterranean .....	379
4.5.8.1. Comparison with Literature.....	385
4.5.8.2. Seasonal Variation of Dry Deposition Fluxes.....	387
5. CONCLUSION .....	392
6. FUTURE WORKS AND RECOMMENDATIONS.....	399
7. REFERENCES.....	401
APPENDIX A. SAMPLE BACKTRAJECTORY FILE AND MAP .....	450
VITA .....	451

## LIST OF TABLES

### TABLES

Table 2.1 Estimates (in Tg per year) for the year 2000 of (a) direct particle emissions into the atmosphere and (b) in situ production .....	15
Table 2.2 Chemicals from particles in different emission sources (Chow, 1995).....	21
Table 2.3 Examples of input data pretreatment for PMF in literature .....	54
Table 3.1 Performance Specifications for PM-10 Sampler.....	67
Table 3.2 Analytical techniques employed in the characterization of samples .....	72
Table 3.3 Oxford ED-2000 XRF instrument specifications.....	76
Table 3.4 Optimal excitation conditions of the OXFORD ED-2000 X-ray fluorescence analyzer .....	81
Table 3.5 Detection limits of the measured analytes .....	88
Table 3.6. Comparison of detection limits for EDXRF with the values reported in the literature .....	90
Table 3.7 Elemental composition of filter blanks (ng/ 100 cm <sup>2</sup> filter) .....	93
Table 3.8 Frequency of observance and average statistical uncertainty for the elements analyzed by XRF.....	96
Table 3.9 Calculated percent accuracy for some of the selected elements in SRM 2783 ..	98
Table 3.10 Results of reflectance measurement for blank and samples.....	100
Table 3.11 Quality criteria for argon.....	103
Table 3.12 Operating Program 9 of ETHOS 900 MW digestion system .....	106
Table 3.13 ICP-MS Operating Parameters .....	109
Table 3.14. Selected analyte masses and correlation coefficient and slope of the calibration curves .....	110
Table 3.15 Average Field Blank Concentrations and Standard Deviations .....	112
Table 3.16 The MDL values for the measured parameters.....	117
Table 3.17 Calculated Detection Limits (ng /23.75 cm <sup>2</sup> filter) for the elements measured by ICP MS and sample concentrations .....	118
Table 3.18 Shows the percent accuracy values for selected elements of SRM 1648 .....	121
Table 3.19 Calculated statistical uncertainty and frequency of observation for the elements measured by ICP MS .....	124
Table 4.1 Summary statistics of Eastern Mediterranean Aerosol Data (in terms of ng m <sup>-3</sup> ) .....	130

Table 4.3 Distribution fitting parameters for the measured aerosol variables.....	132
(in terms of $\text{ng m}^{-3}$ ) .....	132
Table 4.5 Comparison of selected elements measured in this study with the literature (Concentrations were given in terms of $\text{ng m}^{-3}$ ).....	141
Table 4.6 Calculated regional background concentrations of measured parameters (in terms of $\text{ng m}^{-3}$ ).....	161
Table 4.4 Calculated regional background concentrations of measured parameters (in terms of $\text{ng m}^{-3}$ ).....	162
Table 4.5 Calculated regional concentrations of each element and ion ( $\text{ng/m}^3$ ) .....	166
Table 4.6 Contributions of episodes on average concentrations of elements .....	169
Table 4.7 Average and median concentrations of elements in summer and winter ( $\text{ng/m}^3$ ) .....	208
Table 4.8 Annual median concentrations of measured aerosol variables ( $\text{ng m}^{-3}$ ) .....	212
Table 4.9 Results of the Van Belle and Hughes' Homogeneity Test.....	222
Table 4.10 Results of the conducted Seasonal Kendall test.....	224
Table 4.11 Calculated Sen's Slope Estimator values .....	226
Table 4.12 Van Belle and Hughes' Homogeneity Test results for summer season .....	234
Table 4.13 Seasonal Kendall Test results for summer season.....	236
Table 4.14 Sen's slope estimator values for summer season.....	238
Table 4.15 Van Belle and Hughes' Homogeneity Test results for winter season .....	240
Table 4.16 Seasonal Kendall test results for winter season .....	242
Table 4.17 Sen's slope estimator values for winter season.....	244
Table 4.18 Average concentrations of measured parameters in different wind sectors ( $\text{ngm}^{-3}$ ).....	250
Table 4.19 Average concentrations within resolved clusters.....	271
Table 4.20 Results of Kruskal-Wallis Test applied on the clusters .....	279
Table 4.21 Binary correlation matrix of measured elements ( $p < 0.05$ indicated only)...	283
Table 4.22 Reported concentrations of $\text{SO}_4^{2-}$ , $\text{NO}_3^-$ and $\text{NH}_4^+$ in Aegean, Black Sea and Mediterranean.....	301
Table 4.23 ANOVA result for $\text{SO}_4^{2-}$ concentration in different clusters .....	312
Table 4.24 Results of multiple comparison test using Tukey's HSD approach .....	313
Table 4.25 Homogenous subsets from Tukey's HSD test .....	313
Table 4.26 Number of data in different groups with respect to years.....	323
Table 4.27 Summary statistics of measured parameters used in the source apportionment analysis .....	338

Table 4.28 Varimax rotated factor loadings obtained from factor analysis .....	342
Table 4.29 Calculated SNR of parameters .....	345
Table 4.30 ANOVA results of MLR performed in PM mass apportionment.....	374
Table 4.31 Deposition velocities and corresponding calculated deposition fluxes of elements and ions .....	383
Table 4.32 Average deposition fluxes of measured aerosol variables reported in the literature ( $\mu\text{g m}^{-2}\text{d}^{-1}$ ) .....	388

## LIST OF FIGURES

### FIGURES

Figure 1.1 Conceptual analysis plan for field data .....	6
Figure 2.1 Different size properties of aerosols in terms of their generation mechanisms .....	10
Figure 2.2 Number, surface and volume distributions for a typical urban model aerosol .....	12
Figure 2.3 Typical composition (by mass) of fine continental aerosol.....	13
Figure 2.4 Steps of bubble bursting mechanisms over the sea surface.....	16
Figure 2.5 The hypothesized marine sulphur-cloud albedo-climate linkage.....	17
Figure 2.6 Major sources and sinks of nitrogen containing gases in the atmosphere .....	18
Figure 2.7 Major sources and sinks of nitrogen containing gases in the atmosphere .....	19
Figure 2.8 Deposition of particles in different regions of the lung for polydisperse aerosol and schematic diagram of human respiratory track.....	27
Figure 2.9 Suggested neuronal translocation pathways in humans for solid nanosized particles and for soluble components ( <i>a</i> :olfactory nerves, <i>b</i> :trigeminal nerves, <i>c</i> :afferent vagal nerves) .....	28
Figure 2.10 The paths and scales of transport and transformation of pollutants over Mediterranean.....	36
Figure 2.11 Mean monthly sea level pressure for August 2001.....	44
Figure 2.12 The paths of atmospheric cyclones over Turkey .....	45
Figure 3.1 Place of the Antalya Station .....	65
Figure 3.2 The platform onto which Hi-Vol sampler anchored .....	66
Figure 3.3 Schematic of High Volume Sampler .....	68
Figure 3.4 High Volume sampler calibration plot at Antalya station on 19.08.1993.....	69
Figure 3.5. SEM photos of aerosols collected on Whatman 41 filter .....	71
Figure 3.6 Basic components of the ion chromatography system .....	75
Figure 3.7 Scheme of the experimental setup for EDXRF.....	77
Figure 3.8 The Oxford ED-2000 XRF instrument.....	78
Figure 3.9 The 8-position sample tray .....	78
Figure 3.10 X-ray fluorescence analysis procedures .....	80
Figure 3.11 Sample spectrum obtained in EDXRF analysis .....	82
Figure 3.12 The custom-made Flexy Glass Cutting Device and cutted filters.....	83

Figure 3.13. Mean, standard deviation and percent relative standard deviation of the analytes for sample collected on 13.02.1993.....	91
Figure 3.14. Average field blank composition .....	92
Figure 3.15 Comparison of field blank composition with the samples.....	94
Figure 3.16 Plot of percent blank subtraction and percent of observance of samples analyzed by XRF.....	95
Figure 3.17 Calculated average percent statistical uncertainty and average frequency of observance of the analytes detected by XRF .....	97
Figure 3.18 Imagined volume of sampled air.....	99
Figure 3.19 Schematical representation of EDXRF for reflectance measurement.....	100
Figure 3.20. Microwave digestion oven and digestion vessels .....	106
Figure 3.21 Sample to blank ratio for the elements detected in ICP MS analysis.....	114
Figure 3.22 Plot of percent frequency of observance versus percent blank subtraction.....	115
Figure 3.23. Proportions of different elements in field blanks, acid blanks and DI water .....	115
Figure 3.24. Shows the calculated precision values for the analyzed parameters .....	122
Figure 3.25. Shows the relationship between calculated average statistical uncertainty and frequency of observance.....	123
Figure 3.26. Comparison of ICP MS and XRF for the measured common parameters ...	125
Figure 3.27 Plot of XRF versus IC for $\text{SO}_4^{2-}$ measurement.....	126
Figure 3.28 Plot of XRF versus IC for $\text{Cl}^-$ measurement .....	126
Figure 4.1 Frequency histograms and associated distribution curves for Na and Mg.....	134
Figure 4.3 Location of sampling points used in the comparison.....	140
Figure 4.4 Comparison of the aerosol variables measured in this station with the literature .....	142
Figure 4.5 Definition of sectors used in the classification .....	146
Figure 4.6 9 year average frequencies of air mass transport from different sectors for three different altitudes.....	148
Figure 4.7 Comparison of summer and winter averages for three different altitudes ....	150
Figure 4.8 Comparison of flow climatology determined in different studies.....	154
Figure 4.9 Surface wind patterns at the sampling point.....	157
Figure 4.10 Histogram for calculation of most frequently occurring value.....	158
Figure 4.11 Year to year variation in the baseline concentrations of selected elements	164
Figure 4.12 Seasonal variations in the baseline concentration of elements .....	165
Figure 4.13 Regional background concentrations calculated for each station.....	167

Figure 4.14 Short term variations in the concentrations of crustal elements .....	174
Figure 4.15 Seasonal variation of dust episode numbers .....	175
Figure 4.16 Monthly apportionment of dust days in three different classes .....	176
Figure 4.17 Short term variations in the concentrations of marine elements.....	178
Figure 4.18 Monthly variations in the concentrations of marine elements.....	179
Figure 4.19 Short term variations in the concentrations of anthropogenic elements.....	181
Figure 4.20 Effect of rain on short term variation in the concentrations of selected elements .....	183
Figure 4.21 The ratio of elemental concentrations in non-raining days to average concentrations in raining days .....	185
Figure 4.22 Variation in concentrations of crustal elements as a function of non-raining days.....	186
Figure 4.23 Variations in concentrations anthropogenic elements as a function of non- raining days .....	187
Figure 4.24 Variations in the concentrations of marine elements as a function of non- raining days .....	188
Figure 4.25 Atmospheric reloading times for the selected anthropogenic, marine and crustal elements.....	190
Figure 4.26 Trajectories corresponding to rainy days .....	191
Figure 4.27 Seasonal variations in the concentrations of marine elements .....	194
Figure 4.28 Seasonal variations in the concentrations of selected crustal and anthropogenic elements.....	197
Figure 4.29 Monthly variation in the concentration of crustal elements.....	198
Figure 4.30 Monthly variation in the concentrations of selected anthropogenic elements .....	199
Figure 4.31 Monthly variation in the concentrations of marine elements .....	201
Figure 4.32 Contribution of crustal and marine Na fractions to measured total Na concentration .....	202
Figure 4.33 Seasonal variation of Cl/Na ratio (Dashed line in the figure represent the [Cl] / [Na] ratio of bulk seawater) .....	203
Figure 4.34 Variation of Cl / Na ratio with respect to (a) $\text{SO}_4^{2-}$ (b) $\text{NO}_3^-$ concentration..	205
Figure 4.35 Summer to winter ratio for the parameters measured in the study .....	210
Figure 4.36 Annual variation observed in the concentrations of selected crustal elements .....	214
Figure 4.37 Annual variation observed in the concentrations of marine elements.....	215

Figure 4.38 Annual variation observed in the concentrations of anthropogenic elements .....	216
Figure 4.39 Time series plot of the $\text{SO}_4^{2-}$ concentrations over 9 years.....	218
Figure 4.40 Schematical description of the trend analysis methodology .....	219
Figure 4.41 Variation of Saharan dust episode number and corresponding Al concentration with time .....	228
Figure 4.42 Past, current and projected annual emissions of trace elements in Mediterranean region (By the courtesy of Pirrone et al., 1999) .....	230
Figure 4.43 The outputs of Mann Kendall test for Pb and $\text{NO}_3^-$ .....	232
Figure 4.44 Sectors used in residence time analysis.....	248
Figure 4.45 Distribution of some of the selected anthropogenic pollutants in different sectors .....	256
Figure 4.46 Distribution of some of the selected crustal elements in different sectors ..	257
Figure 4.47 Distribution of some of the selected rare earth elements in different sectors .....	258
Figure 4.48 Distribution of marine originated elements in different sectors .....	259
Figure 4.49 Percent change in TRMSD versus number of clusters .....	261
Figure 4.50 Percentage of trajectories allocated in each cluster .....	262
Figure 4.51 Trajectories allocated to different clusters .....	264
Figure 4.52 Monthly percentage of trajectories analyzed in cluster number 1, 3 and 9 ..	266
Figure 4.53 Altitude profile of trajectories within (a) Cluster 3 & (b) Cluster 9 .....	267
Figure 4.54 Monthly percentage of trajectories analyzed in cluster number 5, 6 and 8 ..	268
Figure 4.55 Monthly percentage of trajectories analyzed in cluster number 2 and 4.....	269
Figure 4.56 Crustal enrichment factors of elements .....	292
Figure 4.57 $\text{EF}_c$ -Al plots o some of the selected elements with mixed sources .....	293
Figure 4.58 $\text{EF}_c$ -Al plots o some of the selected crustal elements .....	294
Figure 4.59 $\text{EF}_c$ -Al plots o some of the selected crustal elements .....	295
Figure 4.60 $\text{EF}_c$ -Al plots o some of the selected anthropogenic elements .....	296
Figure 4.61 Marine enrichment factors of elements.....	298
Figure 4.62 Comparison of mean concentrations of $\text{SO}_4^{2-}$ measured in EMEP and this study between 1993 and 2000.....	300
Figure 4.63 $\text{SO}_4^{2-}$ concentrations in EMEP and Eastern Mediterranean in 1980, 1990 and 2000, respectively .....	303
Figure 4.64 Variation of $\text{SO}_4^{2-}$ concentrations in (a) Western European and (b) Former USSR (Eastern European) countries .....	304



Figure 4.65 Variation of $\text{NO}_3^-$ concentrations in (a) Western Europe and (b) Eastern Europe .....	306
Figure 4.66 $\text{SO}_4^{2-}$ to $\text{NO}_3^-$ ratio in aerosol in the western European countries and at former USSR countries before 1990 .....	308
Figure 4.67 $\text{SO}_4^{2-}$ to $\text{NO}_3^-$ ratio in aerosol in the western European countries and at former USSR countries after 1990 .....	308
Figure 4.68 Variation in $\text{SO}_4^{2-}$ to $\text{NO}_3^-$ ratio at Antalya between 1993 and 2000 .....	309
Figure 4.69 Monthly variation of $\text{SO}_4^{2-}$ to $\text{NO}_3^-$ ratio at Antalya station .....	310
Figure 4.70 Cluster centers and frequency of air masses in each cluster .....	311
Figure 4.71 $\text{SO}_4^{2-}$ concentration corresponding to each cluster.....	311
Figure 4.72 Size distribution of $\text{SO}_4^{2-}$ , $\text{NO}_3^-$ and $\text{NH}_4^+$ at the Eastern Mediterranean .....	317
Figure 4.73 Time series plot of Al, Ca and Fe between 1992 and 2001 .....	321
Figure 4.74 Time Series plot of Al, Ca and Fe for the first six month of 1992 .....	322
Figure 4.75 Backward trajectory calculated for 28/3/1992 Saharan episode day.....	322
Figure 4.76 Time series plot of measured Al, Ca, Fe and calculated Aerosol Index for March 1998.....	326
Figure 4.77 SeaWiFS image for 26 <sup>th</sup> of March 1998 obtained from NASA web page .....	326
Figure 4.78 A sequence of TOMS images for episode observed on 26 <sup>th</sup> of March, 1998	327
Figure 4.79 Time series plot of measured Al, Ca, Fe and calculated Aerosol Index for April 2000 .....	328
Figure 4.80 A sequence of TOMS images for episodes observed on 16 <sup>th</sup> and 21 <sup>st</sup> of April, 2000 .....	329
Figure 4.81 Saharan dust to local dust ratio of each parameter in descending order ....	331
Figure 4.82 Ratios of elements in different groups.....	332
Figure 4.83 Ratios of elements in different groups.....	333
Figure 4.84 Variation of recorded Saharan dust episode with months.....	335
Figure 4.85 Scree plot of applied factor analysis.....	340
Figure 4.86 Enrichment Factor, Explained Variation, and Floading values for Factor 1..	348
Figure 4.87 Seasonal variation of G score values for Factor 1 .....	349
Figure 4.88 Trajectories corresponding highest 25 G scores for Factor 1.....	350
Figure 4.89 Enrichment Factor, Explained Variation, and Floading values for Factor 2..	351
Figure 4.90 Seasonal variation of G score values for Factor 2 .....	352
Figure 4.91 Enrichment Factor, Explained Variation, and F loading values for Factor 3.	353
Figure 4.92 Seasonal variation of G score values for Factor 3 .....	354
Figure 4.93 Enrichment Factor, Explained Variation, and F loading values for Factor 4.	355

Figure 4.94 Seasonal variation of G score values for Factor 4 .....	356
Figure 4.96 Enrichment Factor, Explained Variation, and Flooding values for Factor 5..	357
Figure 4.97 Short term variations in G score values for Factor 5 .....	358
Figure 4.98 Seasonal variation of G score values for Factor 5 .....	359
Figure 4.99 Enrichment Factor, Explained Variation, and Flooding values for Factor 6..	360
Figure 4.100 Short term variation of G score values for Factor 6.....	361
Figure 4.101 Seasonal variation of G score values for Factor 6 .....	361
Figure 4.102 Enrichment Factor, Explained Variation, and Flooding values Factor 7 .....	362
Figure 4.103 Seasonal variation of G score values for Factor 7 .....	363
Figure 4.104 Enrichment Factor and Explained Variation for Factor 8 .....	364
Figure 4.105 Seasonal variation of G score values for Factor 8 .....	365
Figure 4.106 Trajectories corresponding highest 25 G scores for Factor 8.....	366
Figure 4.107 Relation between observed and predicted concentration of some of the selected rare earth elements .....	368
Figure 4.108 Relation between observed and predicted concentration of some of the selected anthropogenic elements .....	369
Figure 4.109 Relation between observed and predicted concentration of some of the selected marine and crustal elements.....	370
Figure 4.110 Observed to predicted concentration ratios of parameters.....	371
Figure 4.111 Percent contribution of each factor to each parameter .....	372
Figure 4.112 Relation between observed and predicted mass concentration .....	375
Figure 4.113 PSCF bootstrapped distribution of Factor 2 corresponding to highest 25 % G score values.....	376
Figure 4.114 PSCF bootstrapped distribution of Factor 3 corresponding to highest 25 % G score values.....	377
Figure 4.115 PSCF bootstrapped distribution of Factor 4 corresponding to highest 25 % G score values.....	378
Figure 4.116 PSCF bootstrapped distribution of Factor 5 corresponding to highest 25 % G score values.....	378
Figure 4.117 Average monthly precipitation and temperature profile of Antalya between 1993 and 2001.....	380
Figure 4.118 Seasonal variation of dry deposition flux of parameters evaluated in the first group .....	389
Figure 4.119 Seasonal variation of dry deposition flux of parameters evaluated in the second group .....	390

Figure 4.120 Seasonal variation of dry deposition flux of parameters evaluated in the third group .....	391
Figure 4.121 Seasonal variation of dry deposition flux of parameters evaluated in the fourth group .....	391

## LIST OF ABBREVIATIONS

<b>AAS</b>	Atomic Absorption Spectrometry
<b>ARL</b>	Air Resources Laboratory
<b>BC</b>	Black Carbon
<b>BDL</b>	Below Detection Limit
<b>CCN</b>	Cloud Condensation Nuclei
<b>CMB</b>	Chemical Mass Balance
<b>CNS</b>	Central nervous system
<b>DMS</b>	Dimethylsulfide
<b>DMSP</b>	Dimethylsulfoniopropionate
<b>ECMWF</b>	European Center for the Medium Range Weather Forecasts
<b>EDXRF</b>	Energy Dispersive X-Ray Fluorescence
<b>EF</b>	Enrichment Factor
<b>EMEP</b>	European Monitoring and Evaluation Programme
<b>EMR</b>	Eastern Mediterranean Region
<b>EU</b>	European Union
<b>EV</b>	Explained Variation
<b>FA</b>	Factor Analysis
<b>Hi-Vol</b>	High Volume Sample
<b>HYSPLIT</b>	HYbrid Single-Particle Lagrangian Integrated Trajectory
<b>IC</b>	Ion Chromatography
<b>ICPMS</b>	Inductively Coupled Plasma Mass Spectrometry
<b>IDL</b>	Instrument Detection Limit
<b>INAA</b>	Instrumental Neutron Activation Analysis
<b>IPCC</b>	Intergovernmental Panel on Climate Change
<b>ITCZ</b>	Intertropical convergence zone
<b>IUPAC</b>	International Union of Applied and Pure Chemistry
<b>K-S DN</b>	Kolmogorov –Smirnov
<b>MBL</b>	Marine Boundary Layer
<b>MDL</b>	Method Detection Limit
<b>MMD</b>	Mass Median Diameter
<b>MR</b>	Mediterranean Region
<b>MSA</b>	Methanesulphonic Acid

<b>NAAQS</b>	National Ambient Air Quality Standard
<b>NIST</b>	National Institute of Standard and Technology
<b>NOAA</b>	National Oceanic and Atmospheric Administration
<b>PCA</b>	Principal Component Analysis
<b>PDFs</b>	Probability Distribution Functions
<b>PM</b>	Particulate Matter
<b>PM<sub>10</sub></b>	Particulate Matter < 10 µm in diameter
<b>PM<sub>2.5</sub></b>	Particulate Matter <2.5 µm in diameter
<b>PMF</b>	Positive Matrix Factorization
<b>PSCF</b>	Potential Source Contribution Function
<b>QA/QC</b>	Quality Assurance Quality Control
<b>REE</b>	Rare Earth Element
<b>RSD</b>	Relative Standard Deviation
<b>SI</b>	Skewness Index
<b>SRM</b>	Standard Reference Material
<b>SST</b>	Sea Surface Temperature
<b>SXRF</b>	Synchrotron Radiation X-ray Fluorescence
<b>TSP</b>	Total Suspended Particulate
<b>UFP</b>	Ultrafine Particles
<b>USEPA</b>	U.S. Environmental Protection Agency
<b>WHO</b>	World Health Organization

# CHAPTER 1

## INTRODUCTION

### 1.1. BACKGROUND

Several major air pollution episodes in the 20<sup>th</sup> Century including those in Donora Valley (PA, USA) in 1948, and London (England) in 1952 led to legislation aimed at improving the air quality. The need for the regulatory compliance and also scientific curiosity give rise to improvements in particulate matter research. With the increased recognition of the adverse impacts on human health and anthropogenic modification of atmospheric processes, efforts to determine the chemical composition and sources of particulate matter have intensified.

Numerous attempts have been made to understand the general features, the potential impacts and sources of particulate matter over the Mediterranean Region atmosphere as well. Mediterranean Region (MR) encompasses lands around and enclosed by the Mediterranean Sea, which is a sea of Atlantic Ocean. The Mediterranean Sea is surrounded by the portions of three different continents, which are Europe on the North, Africa on the South and finally Asia on the East. The presence of highly industrialized European countries on the North, developing countries on the South and East, the close proximity to the Saharan Desert, and unique climate characteristic have all made the region interesting and attractive for the researchers for many years.

Previous studies conducted to date over the MR demonstrate several important aspects governing the air pollution profile of the region. These can be summarized as follows:

- The Eastern Mediterranean Region (EMR) is continuously receiving polluted air masses from Europe

A substantial number of studies confirm this fact. For instance, Lelieveld *et al.* (2002) have revealed that 60–80 % of the boundary layer CO over the Mediterranean have been transported to the EMR from both Eastern and Western Europe. Sciare *et al.* (2003) have

shown that the contribution of anthropogenic emissions from the Central Europe to the EMR is considerably high. Kidnap *et al.* (2006) report that PM<sub>10</sub> levels detected in the Istanbul exceeded on 11 January 2002 the World Health Organization (WHO) limit of 300 µgm<sup>-3</sup>, about 3 times in some of the episode days when westerly wind blowing towards the city.

- Saharan dust intrusions in EMR influence the chemical composition of the aerosols and chemistry of the atmosphere, accordingly

A large amount of Saharan dust is transported over the Mediterranean due to the characteristic climatology of the region. Previous studies have revealed that the radiative forcing over the MR is among the highest reported in the world, hence region takes special concern in this respect (IPCC, 2001; Lelieveld *et al.* 2002). In addition to dust transported from the Sahara, there are various sort of aerosols from different sources present in the region. Anthropogenic aerosols and natural sources such as forest fires, the earth's crust and Mediterranean Sea lead to observe variation in the aerosol composition. Region receives long-range transported aerosols from North Africa and Asia as well (Lelieveld *et al.* 2002). Saharan dust intrusions can further modify the atmospheric processes by taking part in the heterogeneous reactions, altering temperature and dynamics of the EM atmosphere (Mona *et al.* 2006). Moreover, Saharan dust deposition into the Mediterranean Sea supplies soluble and bioavailable micro nutrients, which can alter the aquatic biogeochemistry (Herut *et al.* 2005). Furthermore, Saharan dust is responsible for PM<sub>10</sub> daily exceedances in southern part of Europe. Meloni *et al.* (2008) reported that about 70 % of daily PM<sub>10</sub> exceedances in Rome is due to Saharan dust intrusions. For this reason, researchers are trying to find the natural tracers of Saharan dust that enable them to estimate Saharan dust contribution to observed daily exceedances. Consequently, researchers can assess the impact of anthropogenic emissions on daily exceedances.

- Elevated levels of SO<sub>4</sub><sup>2-</sup> are observed over the EMR

High concentrations of SO<sub>4</sub><sup>2-</sup> (mean SO<sub>4</sub><sup>2-</sup> concentration was measured as 7.93 µg m<sup>-3</sup> in the course of this study) are reported in the studies conducted over the MR. Glavas and Moschonas (2002) have performed back trajectory analysis and found that samples influence by air from North African sector had SO<sub>4</sub><sup>2-</sup> concentration of 52.4 µeq/l while

average concentration was recorded for all data as 46.1  $\mu\text{eq/l}$ . Avila and Allarcon (1999), Herut *et al.* (2000) and Al-Momani *et al.* (2000 and 2008) have reported similar results. Others claim that the MR atmosphere is enriched in  $\text{SO}_2$  by transport of polluted air masses from Central Europe (Luria *et al.* 1996; Ganor *et al.* 2000; Sciare *et al.* 2003 and Tsitouridou *et al.* 2003). Consequently, the exact reason of the anomalous  $\text{SO}_4^{2-}$  levels have not been clarified yet.

- Flow climatology determines the concentrations of the pollutants over MR atmosphere

Kallos *et al.* (2007) have revealed that MR act as "temporal reservoir" where pollutants are "concentrated" and "aged" before they are advected further. Eastern Mediterranean Sea and Black Sea are considered among these temporal reservoirs. In addition, islands and peninsulas present in the MR behave as obstacles and chimneys, which enhance the formation of relatively strong updrafts leading to release of pollutants from Marine Boundary Layer (MBL) to free troposphere. Consequently, they are transported long distances.

## 1.2. MOTIVATION

Considerable efforts have been expended to determine the chemical composition of aerosols (e.g. Querol *et al.*, 2004; Rodriguez *et al.*, 2007; Salvador *et al.*, 2007) and rainwater ( e.g. Avila and Roda, 2002; Rodrigo *et al.*, 2003; Fiol *et al.*, 2005) associated with the Mediterranean atmosphere since 1980. Nevertheless, these studies were conducted on the Western Mediterranean atmosphere. Though literature published on the particles (Sciare *et al.*, 2003; Vasilakos *et al.*, 2007; Gullu *et al.*, 2000; Gullu *et al.*, 2005; Al Momani *et al.*, 2008) and rainwater composition (Glavas and Moschonas, 2002; Al Momani *et al.*, 2008; Nastos *et al.*, 2007) of Eastern Mediterranean atmosphere have increased recently, there are still gaps in knowledge associated with the Eastern Mediterranean atmosphere. For example, long term variations in the concentrations of man made and natural emissions have not been fully determined. Most of the pollutants have been strictly regulated in European countries since 1980s. However, how and at what extent these reductions affect the chemical composition of Eastern Mediterranean atmosphere has not been clearly answered yet. Furthermore, the literature associated with trace element concentrations is limited to several elements, most of which are soil



originated such as Al, Fe and Ca. Identification of more sources with available receptor modelling approaches needs more parameters be used as tracers. For this reason, determination of more parameters is useful in resolution of more sources in source apportionment studies.

Reliable scientific data on anthropogenic emissions are necessary for the construction of applicable policies and regulation of man made emissions. The generation of database will fill the gaps in the current knowledge of pollution profile of EMR. These two factors are interrelated and are the main driving forces behind this study.

The objectives of this research are to utilize analytical techniques like Inductively Coupled Plasma Mass Spectrometry (ICP-MS), Energy Dispersive X-ray Fluorescence (EDXRF) and Ion Chromatography (IC) to generate a large comprehensive database of elemental and ionic air pollutant concentrations in the EMR, determine trends, sources and origins of these pollutants in the EM atmosphere; and to assess the importance of their deposition on the Eastern Mediterranean Sea.

The generation of a comprehensive pollutant database was an enormous effort requiring the collection and analysis of about 1700 samples. Each sample was collected and analyzed for 60 parameters. The incorporation of ICP-MS enabled measurements of 57 elements, thus greatly expanding the number of potentially useful tracer species, which enable us more sources with multivariate statistical receptor so called Positive Matrix Factorization (PMF).

The trends, origins and sources of EM aerosols were explored by employing different tools. The trends in the concentrations of measured parameters were investigated by analyzing the short and long term variations. Moreover, Mann-Kendall statistic was applied to determine the monotonic increase and decrease in the generated data set. In this study, source term for the pollutants refers to specific industrial activity or specific natural phenomena release the pollutant in the atmosphere. For this purpose, enrichment factors were computed and interpreted, and Positive Matrix Factorization (PMF) was applied to the generated data set to infer the sources of measured pollutants. The geographical region(s) of pollutants origin was investigated by applying Potential Source Contribution Function (PSCF) method, wherein wind back trajectories are analyzed with

conditional probability. Analysis of data collected during the sampling campaign is presented in Figure 1.1 as a simplified plan.

### **1.3. SCOPE OF THESIS**

The objectives of this study are as follows:

1. To determine the general flow climatology of the Eastern Mediterranean by analyzing the back trajectories between 1992-2001
2. To estimate the regional background concentration of the analyzed parameters
3. To characterize the seasonal and short-term variations in the concentrations of anthropogenic and natural pollutants and find out the reasons behind these variations
4. To find long term trends observed in the pollutant concentrations
5. To find the association between the meteorological parameters such as precipitation and pollutant concentrations
6. To determine the sources of the pollutants observed over the region and to quantify the relative contribution of sources located both Europe and Eastern Mediterranean
7. To find the transport mechanisms of pollutants to the region
8. To identify tracers of Saharan dust transported to EMR
9. To determine the dry deposition fluxes of pollutants to the Mediterranean Sea
10. To assess the level of air quality in the Eastern Mediterranean atmosphere
11. To observe the effectiveness of the control strategies conducted on the pollutant emissions by the European countries starting from 1980's

### **1.4. NOVELTY OF THESIS**

A Whatman filter is not a good substrate for the Energy Dispersive X-Ray Fluorescence (EDXRF) analysis, which is surface technique, its sensitivity is inversely related with the depth of filter. A novel method was developed and applied to the analysis of aerosol particles collected on Whatman cellulose fiber filters by EDXRF in this study. The methodology developed here can be utilized by other researchers in analyzing this kind of material.

This study is the most extensive research conducted in the EMR in terms of both the number of parameters investigated and time span covered. Results provided in this study can guide to policy makers to evaluate the efficiencies of control mechanisms taken on the pollutants over the last decade and a useful database for researchers.

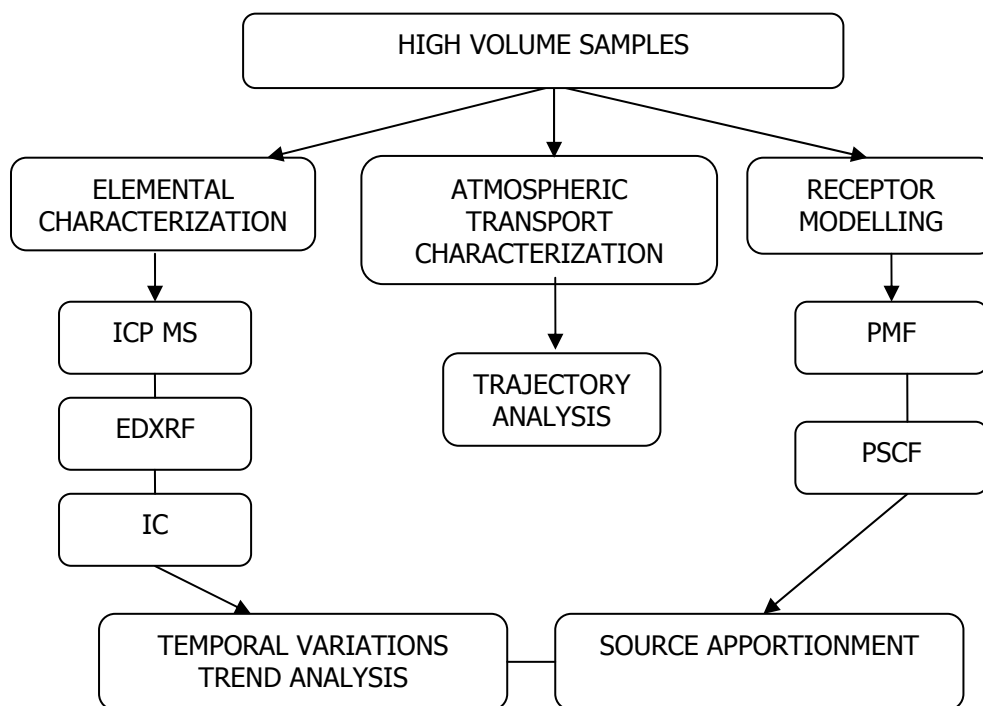


Figure 1.1 Conceptual analysis plan for field data

## 1.5. ORGANIZATION OF THESIS

This study contains five chapters. *As part of this work;*

*Chapter 1-INTRODUCTION* outlines the driving forces behind this study. In addition, the major objectives of the study are listed.

*Chapter 2- LITERATURE REVIEW* provides information on the background of this thesis. The definition of term of aerosol, the chemical composition and origins of aerosols are given. In addition, the role of aerosols on the atmospheric chemistry and the impact on

the health will be provided. Then, a literature review on the general climatology of the Eastern Mediterranean region and previous studies conducted to determine the chemical composition of aerosols will be highlighted in this chapter. Background information of the receptor models employed in this study and brief information on distribution characteristics of atmospheric data are other topics presented in this chapter of study.

*Chapter 3-EXPERIMENTAL METHODS* describes the sampling and analysis techniques. The major operating conditions and specifications of the instruments employed in the study are presented. Some quality assurance quality control issues including the detection limit of the instruments, the ratios of field blanks to samples, uncertainty and precision calculations will be provided in this chapter. In addition to these, comparison of the analytical methods employed for the common parameters will be given in this part of the thesis.

*Chapter 4-RESULTS and DISCUSSIONS* provides the main outcomes of this study. Background concentrations of measured ions and elements and correlations between them will be provided. The short and long term variations of the pollutants will be presented. Sectoral variations in pollutant concentrations will be discussed. Saharan dust transport to Eastern Mediterranean will be evaluated. Reasons behind elevated sulfate concentration in Eastern Mediterranean atmosphere will be evaluated. The results of the source apportionment studies will be highlighted. The deposition fluxes of the pollutants will be given. The reason of the elevated sulfate concentrations over the Eastern Mediterranean atmosphere will be discussed in this chapter.

*Chapter 5- CONCLUSIONS* includes the concluding remarks

*Chapter 6-FUTURE WORKS AND RECOMMENDATIONS* contains recommendations for the future works.

## **CHAPTER 2**

### **LITERATURE REVIEW**

#### **2.1. AEROSOLS**

##### **2.1.1. Definition of Aerosol**

Willeke and Baron defined the aerosol as " an assembly of solid and liquid particles, with the particle diameters in the range of 0.001 to 100  $\mu\text{m}$ , suspended in gaseous medium long enough to be determined and measured (Spurny, 1999). The lower size range is corresponding to molecules and molecular clusters, and upper limit is the size that undergoes rapid sedimentation in the atmosphere (Pöschl, 2005).

The term "aerosol" was first used by F.G.Donnan in about 1918 and Schmauss introduced this term to meteorological literature in 1920 (Spurny, 1999).

Atmospheric particulate matter (PM) is composed of a mixture of solid and aqueous species which are emitted into the atmosphere both by human activity (anthropogenic) and natural sources. Due to the large number of natural and anthropogenic sources, PM may present diverse physical (size, surface, area, density, number) and chemical characteristics in different regions. Both the levels and composition of ambient air PM depend on the strengths of local and regional anthropogenic emissions, on climatology (temperature, humidity, radiation, rain scavenging, re-circulation of air masses versus dispersive conditions) and on the geography including topography, soil cover, proximity to arid zones or to the coast of a given region. Therefore, concentrations, size and composition of atmospheric particles varies considerably in different regions of the world.

In this part of the study, firstly, the information about the general properties of aerosols like size, composition, generation and removal mechanisms will be presented. After that, the studies conducted on the impacts of aerosols on the human health, atmospheric chemistry and climate will be reviewed. The methods and analytical techniques in the

measurement of size and composition of the aerosols will be mentioned, thereafter. The legislations established for the Particulate Matter will be given. The studies showing the long-range transport of the pollutants will be discussed, and previous studies conducted on ionic and trace element content of the Eastern Mediterranean aerosols will also be included in topics discussed in this section. In addition, the general climatology of the Eastern Mediterranean will be described, finally.

### **2.1.2. Aerosol Size**

In the past, total suspended matter (TSP) in the ambient air was the basis for setting national air quality standards. For human health, however, particles with an aerodynamic diameter less than 10  $\mu\text{m}$ , commonly addressed as the  $\text{PM}_{10}$  are of much more concern since these particles are small enough to enter respiratory system. Aerodynamic is defined as the diameter of a sphere of unit density ( $1 \text{ g cm}^{-3}$ ) with the same settling velocity as the subject particle under the same conditions. Still smaller particles with an aerodynamic diameter < 2,5  $\mu\text{m}$  ( $\text{PM}_{2.5}$ ) or even smaller (e.g.  $\text{PM}_1$ ,  $\text{PM}_{0.1}$ ) are thought to be of greatest significance for health and some of the heavy metals associated with these particles become soluble in blood and rapidly enter to the blood circulation.

Aerosols that present ubiquitously in the atmosphere have different sizes. The atmospheric aerosol is composed of mainly (1) a nucleation mode (particles < 0.01  $\mu\text{m}$  radius) from recent gas-to-particle conversion; (2) an accumulation mode (0.01–1  $\mu\text{m}$ ) from condensational growth and coagulation of the nucleation mode; and (3) a coarse mode (> 1  $\mu\text{m}$ ) resulting mostly from direct mechanical generation at the Earth's surface (Jacob, 2000).

The different size properties of aerosols based on their generation mechanisms is presented in the Figure 2.1 (Pitts and Pitts, 2000, originally adapted from Whitby and Sverdrup, 1980).

Most of the aerosol surface area and mass are in the accumulation and coarse modes, which are hence of most interest for heterogeneous chemistry, which covers chemical processes involving aerosol phases (liquid and solid particles) in the atmosphere. The principal component of the fine (accumulation) mode are water, sulfate, nitrate, ammonium, organic compounds, and black carbon soot. Since these smallest particles

are generally formed by gas-to-particle conversions and combustion processes, their composition is complex. The main components of the coarse mode are soil dust (including calcium carbonate, silicates, metal oxides) and sea salt (Jacob, 2000).

The particles in the coarse mode are frequently the most important when considering the optical properties of the atmosphere, due to their size. Coarse particles absorb more light, but scattering tends to be greatest for particles around 0.1  $\mu\text{m}$  in diameter. They have generally shorter lifetimes in the atmosphere compared to other sizes of particle, as they readily lost through gravimetric settling and impaction (processes collectively known as dry deposition).

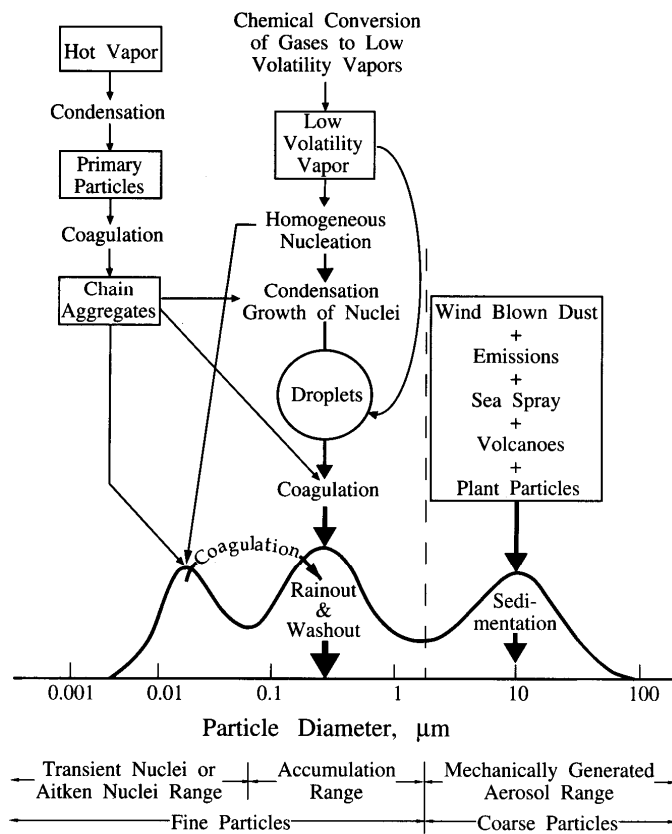


Figure 2.1 Different size properties of aerosols in terms of their generation mechanisms

Accumulation mode particles are generally the most significant when considering gas phase deposition and atmospheric heterogeneous chemistry, as the majority of the chemically active particulate surface area is normally contained within this mode. They also tend to have long atmospheric lifetimes and frequently act as the nuclei for the cloud droplets. The ultimate fate of these particles is often loss in rain and other forms of precipitation (wet deposition).

Atmospheric aerosol nucleation occurs when gases react to form low vapor pressure products. Secondary particles typically form during the late morning and then grow throughout the day reaching growth rates of 1 to 20 nm hour<sup>-1</sup> depends on the chemistry of the condensing species. For example, nitric acid and many organic vapors (vapor), in the continental boundary layer or iodide compounds in coastal environments. However, existing aerosol particles behave as sink for these vapors and for nucleated clusters, and hence inhibit the nucleation of new atmospheric particles. Nucleation seems to be also affected by the magnitude of solar radiation and by atmospheric mixing processes, for example nucleation is different in the continental boundary layer than at the boundary between the stratosphere and troposphere.

There are four types of nucleation processes proposed in the literature: (1) Homogeneous nucleation involving binary mixtures of water and sulfuric acid may present in industrial plumes. (2) Homogeneous ternary (water-sulfuric acid-ammonia) nucleation may take place in the continental boundary layer. (3) Ion-induced nucleation of binary, ternary, or organic vapors may be found in the upper troposphere or lower stratosphere. (4) Finally, homogeneous nucleation involving iodide species may occur in the coastal environment.

The initial steps of growth contain activation of inorganic clusters by soluble organic molecules, heterogeneous nucleation of insoluble organic vapors on inorganic clusters, and chemical reactions of organic molecules at surfaces of inorganic clusters. Finally, cloud condensation nuclei (CCN) form through addition of organic and sulfuric acid molecules (Kulmala, 2003).

Particle distributions can be presented either in terms of number or mass distributions. In terms of number, in an urban environment where motor vehicle emissions are a dominant pollution source, over 80 % or more particulate matter in terms of number is in



the ultrafine range. Their total mass, however, often insignificant in comparison with that of a small number of large particles. Figure 2.2 (Pitts and Pitts, 2000, originally adapted from Whitby and Sverdrup, 1980) shows the mass, number and volume frequency distribution of the aerosols.

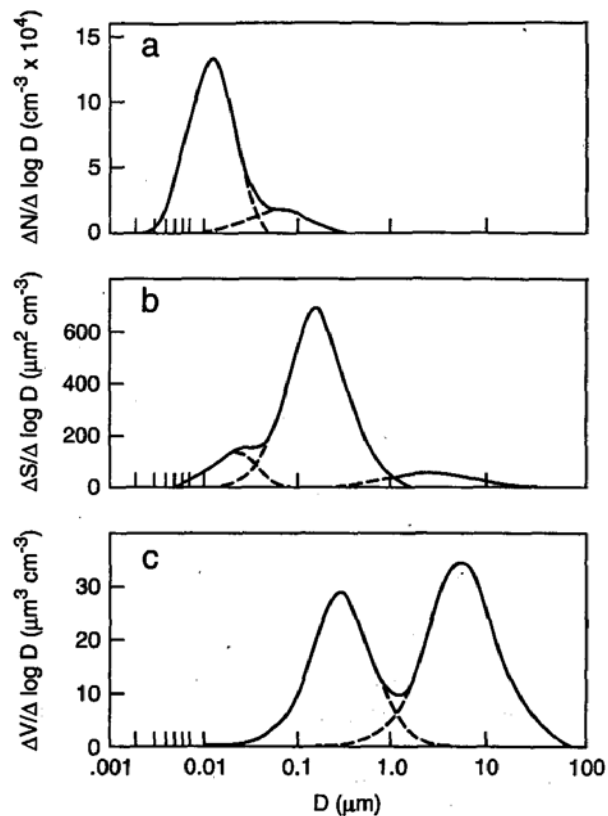


Figure 2.2 Number, surface and volume distributions for a typical urban model aerosol

### 2.1.3. Aerosol Composition

Previous studies have been revealed that there are four major components of PM in the atmosphere. First component contains elemental and organic carbon, which enter into the atmosphere due to the emissions from vehicles, especially from diesel engines. The other major component includes secondary ammonium sulfate and ammonium nitrate. These compounds are formed within the atmosphere as a result of the oxidation of

sulphur dioxide and nitrogen dioxide. Since these components have long atmospheric lifetime, they are transported in the atmosphere and measured as sulfates and nitrates in the measurement sites. Mineral matter, arising from the resuspension of the road dust and soils into the atmosphere by the action of wind and passing traffic, is the other typical component.

The last component is sodium chloride that enters into the atmosphere by a phenomena known as "bubble bursting", which will be discussed in detail in one of the following sections:

The typical composition (by mass) of the fine continental aerosol was described by Jacob (2000) and results of this study was depicted in Figure 2.3:

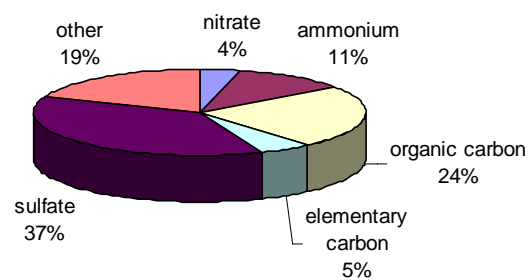


Figure 2.3 Typical composition (by mass) of fine continental aerosol

#### **2.1.4. Classification of aerosols with respect to their origins**

Atmospheric particulate refers to a wide variety of particles from natural sources, e.g. sea spray, airborne natural dust, desert sand, volcanic eruptions, plant pollen and anthropogenic sources, mainly fossil fuel and wood burning, domestic heating, traffic, industrial activities such as bulk handling and wear.

Primary particles often formed by the resuspension of soil, volcanic eruptions, bubble bursting mechanism and such. In contrast to this, atmospheric reactions of sulfur dioxide (SO<sub>2</sub>), nitrogen oxides (NO<sub>x</sub>), volatile organics, and ammonia, originally emitted from fuel burning, traffic, industry, or agriculture results in the formation of secondary particles. The quantity of particle emission and in situ formation shows variation. However, Table 2.1 may be helpful to make a comparison between relative amounts of primary particle emission and in situ formation. Size in Table 2.1 refers to particle diameters (IPCC, 2001; Wallace and Hobbs, 2006).

In this part of the study, information will be provided about the origins of the particles present in the atmosphere.

Natural primary aerosols consist of mainly particles associated with soil dust, sea salt, and biogenic origin. In addition to these, particles generated by the volcanic eruptions and biomass burning can be classified under this category.

The presence of sea salt particles in the atmosphere is due to the ejection of the ocean materials into the atmosphere by a process, which is called as 'bubble bursting'. In bubble bursting process, the material enters into the drops from windblown spray and foam forming air bubbles, and these are burst at the ocean surface. Many small droplets are formed when the air bubble burst, and new formed particles are known as jet droplets. Bubbles greater than 2 mm in diameter each eject 100 to 200 film droplets into the air. The film drops evaporates in the atmosphere and they left the sea salt particles behind with a size of about 0.3 µm. From one to five larger drops break away from each jet that forms when a bubble burst and these are called as jet droplets, which may rise up to 15 cm in the atmosphere. Figure 2.4 demonstrates schematically how the film and jet droplets are formed over the sea surface when the droplets burst.

- Natural primary aerosols:

Sea salt particles are generally associated with the larger particle sizes and their residence time in the atmosphere is short as compared to the anthropogenic ones. Consequently, sea salt particles are observed close to marine environments extensively. M. Koçak *et al.* (2007) have showed that approximately 50 % of the exceedances in PM<sub>10</sub>

concentrations of the samples collected at the Erdemli, Mersin, are due to the sea salt particles. This finding is not surprising for a coastal area.

Table 2.1 Estimates (in Tg per year) for the year 2000 of (a) direct particle emissions into the atmosphere and (b) in situ production

(a) Direct Emissions

	Northern Hemisphere	Southern Hemisphere
Carbonaceous aerosols		
Organic Matter (0-2 $\mu\text{m}$ ) <sup>a</sup>		
Biomass Burning	28	26
Fossil Fuel	28	0.4
Biogenic (>1 $\mu\text{m}$ )	-	-
Black Carbon (0-2 $\mu\text{m}$ )		
Biomass Burning	2.9	2.7
Fossil Fuel	6.5	0.1
Aircraft	0.005	0.0004
Industrial dust, etc. (>1 $\mu\text{m}$ )		
Sea salt		
< 1 $\mu\text{m}$	23	31
1-16 $\mu\text{m}$	1,420	1,870
Total	1,440	1,900
Mineral (soil) dust		
<1 $\mu\text{m}$	90	17
1-2 $\mu\text{m}$	240	50
2-20 $\mu\text{m}$	1,470	282
Total	1,800	349

(b) In situ

	Northern Hemisphere	Southern Hemisphere
Sulfates (as $\text{NH}_4\text{HSO}_4$ )	145	55
Anthropogenic	106	15
Biogenic	25	32
Volcanic	14	7
Nitrate (as $\text{NO}_3^-$ )		
Anthropogenic	12.4	1.8
Natural	2.2	1.7
Organic Compounds		
Anthropogenic	0.15	0.45
Biogenic	8.2	7.4

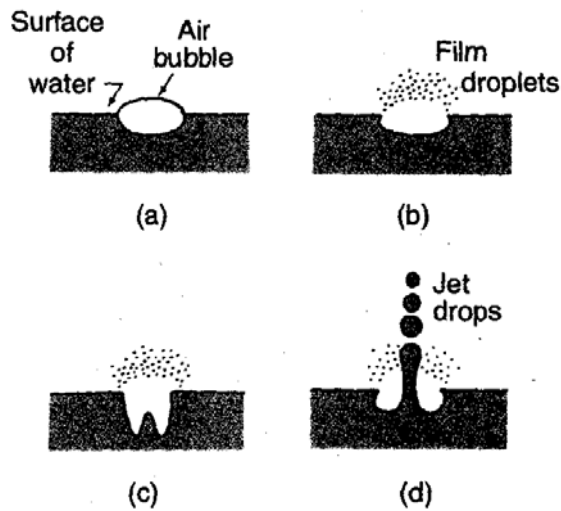


Figure 2.4 Steps of bubble bursting mechanisms over the sea surface

Sea salt particles are mainly associated with Na, Cl, Br and Mg. In addition to these elements, marine bacterioplankton present in the water environment can regulate the sulfur flux to the atmosphere by converting the dimethylsulfoniopropionate (DMSP) either to dimethylsulfide (DMS) or to other sulfur compounds (Howard *et al.*, 2006). DMS is the only naturally reduced sulphur gas responsible for modifying the climate (Nunes *et al.*, 2005). Charlson *et al.* (1987) hypothesized the mechanism by which DMS affect the global climate is demonstrated in Figure 2.5.

According the hypothesized linkage given in Figure 2.5, the marine phytoplankton give rise to the production of volatile DMS, which is further transported to the atmosphere, where it is oxidized to low volatility compounds like methanesulphonic acid (MSA) and sulphuric acid. These end products form the cloud condensation nuclei (CCN) in the atmosphere and hence, increase the albedo of clouds, reflecting more sunlight to the space. This mechanism ultimately results in the cooling of the atmosphere (Cox, 1997; Charlson *et al.*, 1987).

Earth's surface is the source soil dust in the atmosphere. Winds and atmospheric turbulence are the main mechanisms of transport of soil dust particles towards the atmosphere. The wind speed of  $\sim 0.2 \text{ ms}^{-1}$  should be attained to suspend the particles with a diameter range of 20-200  $\mu\text{m}$ . Semiarid regions and deserts, which cover one third

of the Earth's surface, are the main sources of the dust particles in the atmosphere. Aluminium, Fe, Sc, and Si can be considered among the marker elements that strongly related with the soil dust. Similar to sea salt particles, soil dust particles have shorter residence time in the atmosphere owing to their coarser sizes.

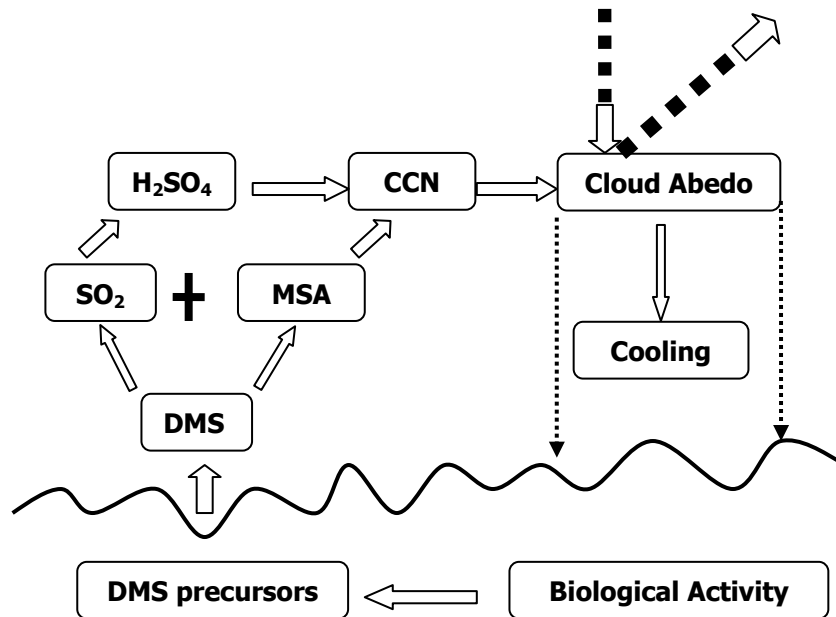


Figure 2.5 The hypothesized marine sulphur-cloud albedo-climate linkage

Volcanoes also eject particles and gases into the atmosphere. Large particles have short residence times whilst smaller ones, which are mainly produced by gas to particle conversion of  $\text{SO}_2$ , can be long range transported. In addition to sulfur, soluble ions like  $\text{Cl}^-$ ,  $\text{F}^-$ ,  $\text{NO}_3^-$ ,  $\text{K}^+$ ,  $\text{Ca}^{2+}$ , and  $\text{Mg}^{2+}$  are ejected from the volcanoes. Such particles are particularly important since they act as cloud condensation nuclei (CCN), and hence modify the energy balance of the earth (Mather *et al.*, 2004).

The other source of primary natural particles is the forest fires. Small smoke particles, particularly, organic compounds and elemental carbon are directly ejected from the forest fires, and they make a peak at  $0.1 \mu\text{m}$  diameter. Due to having this smaller size, particles

arising from the forest fires act as CCN similar to the ones generated by the volcanoes (Wallace and Hobbs, 2006).

Biogenic particles are also present in the atmosphere. These particles can be pollens, fungi, bacteria, and viruses.

- Natural secondary aerosols:
  - Natural sulphur emissions

The majority of secondary natural aerosols results from reaction of sulphur gas emissions. Figure 2.6 has already demonstrated the mechanism of sulfate formation in the atmosphere by the action of phytoplankton activity over the ocean. In addition to this, SO<sub>2</sub> emitted from the volcanoes is considered as a natural source of sulfate present in the atmosphere. The major sources and sinks of sulphur containing gases are depicted in Figure 2.6, which is adopted from Wallace and Hobbs (2006). The numbers near the arrows show the average annual fluxes in Tg(S) per year in Figure 2.6.

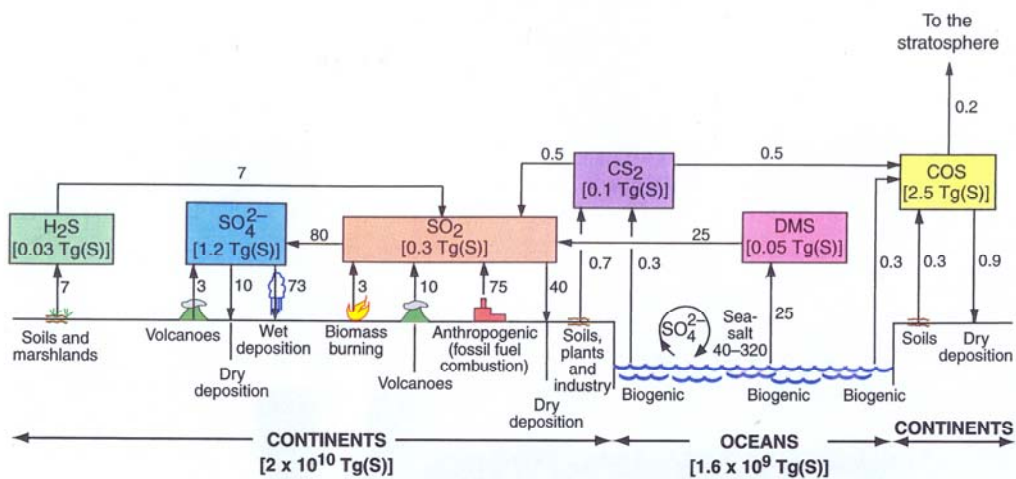


Figure 2.6 Major sources and sinks of nitrogen containing gases in the atmosphere

- Natural nitrogen emissions

Nitrate is formed in the atmosphere from precursor  $\text{NO}_x$  emissions. Natural sources of  $\text{NO}_x$  include biomass burning, and soil emissions from nitrification, denitrification and fertilizers. The nitrogen cycle containing the sources and sinks of nitrogen in the atmosphere is depicted in Figure 2.7, which is adopted from Wallace and Hobbs (2006). The numbers near the arrows show the average annual fluxes in Tg(N) per year in Figure 2.7.

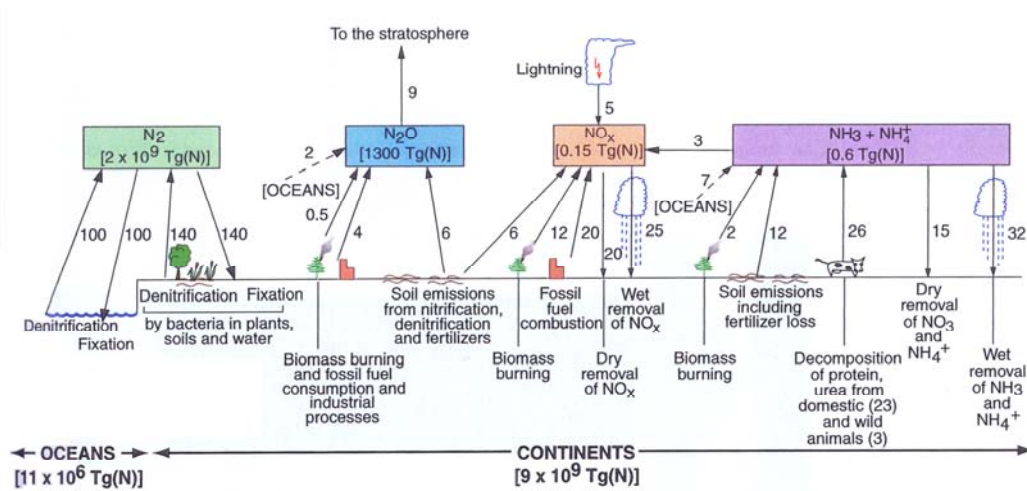


Figure 2.7 Major sources and sinks of nitrogen containing gases in the atmosphere

- Anthropogenic primary aerosols:

Anthropogenic primary particles are directly emitted from the sources and they undergo few changes between sources and receptors. Table 2.2 show the particles emitted from different sources at different size ranges. Average atmospheric concentrations of the primary particles are proportional to quantities that are emitted. Primary particles play an important role in the formation of secondary particles. For example, dust from bare land, roadways, agricultural fields and construction sites is a primary pollutant, however, some components of dust, such as ammonium nitrate fertilizer may volatilize in the atmosphere to form ammonia and nitric acid, thereby contributing to secondary aerosol.



- Anthropogenic secondary aerosols:

Anthropogenic secondary aerosols are formed primarily by means of two mechanisms: homogenous and heterogenous nucleation. Homogenous nucleation describes the processes whereby gas-phase chemical reactions form very tiny particles from specific precursor gases. These tiny particles are captured by the preexisting particles and coagulated to form larger ones. In case of heterogenous nucleation, gas precursors condense on the preexisting ambient particles. The major difference between the homogenous and heterogenous nucleation is that the homogenous process leads to increase in the number and mass of the particles per volume while heterogenous results in the increase of mass of particles per volume. While homogenous reactions occur in the ultrafine size range, heterogenous reactions work both ultrafine and fine size ranges (Derwent and Malcom, 2000).

The sulphur and nitrogen containing secondary aerosols are primarily formed by the photochemical oxidation of anthropogenic  $\text{SO}_2$  and  $\text{NO}_x$  precursors. In contrast, secondary organic compounds have precursors from biogenic emissions. Pandis *et al.* (1991), Zhang *et al.* (1992), and Hoffmann *et al.* (1997) have investigated the aerosol forming potential of the biogenic hydrocarbons in several smog chamber studies. They have found that isoprene ( $\text{C}_5\text{H}_8$ ) photooxidation does not result in the secondary aerosol under ambient conditions. In contrast, the pinenes react with the  $\text{O}_3$ ,  $\text{NO}_3$ , and OH to form secondary aerosol. This is a significant contribution to secondary aerosol budget around the areas with high vegetation. The main chemical constituents of secondary aerosols generally observed in the urban atmosphere are sulphuric acid, ammonium sulfate, ammonium and other nitrates and organic compounds.

Table 2.2 Chemicals from particles in different emission sources (Chow, 1995)

Source Type	Dominant Particle Size	Chemical Abundance in Percent Mass			
		<0.1 %	0.1 to 1 %	1 to 10 %	> 10 %
Paved Road Dust	Coarse (2.5 to 10 $\mu\text{m}$ )	Cr, Sr, Pb, Zr	$\text{SO}_4^-$ , $\text{Na}^+$ , $\text{K}^+$ , P, S, Cl, Mn, Zn, Ba, Ti	Elemental Carbon (EC), Al, K, Ca, Fe	Organic Carbon (OC), Si
Unpaved Road Dust	Coarse	$\text{NO}_3^-$ , $\text{NH}_4^+$ , P, Zn, Sr, Ba	$\text{SO}_4^-$ , $\text{Na}^+$ , $\text{K}^+$ , P, S, Cl, Mn, Ba, Ti	OC, Al, K, Ca, Fe	Si
Construction	Coarse	Cr, Mn, Zn, Sr, Ba	$\text{SO}_4^-$ , $\text{K}^+$ , S, Ti	OC, Al, K, Ca, Fe	Si
Agriculture Soil	Coarse	$\text{NO}_3^-$ , $\text{NH}_4^+$ , Cr, Zn, Sr	$\text{SO}_4^-$ , $\text{Na}^+$ , $\text{K}^+$ , S, Cl, Mn, Ba, Ti	OC, Al, K, Ca, Fe	Si
Natural Soil	Coarse	Cr, Mn, Sr, Zn, Ba	Cl-, $\text{Na}^+$ , Ec, P, S, Cl, Ti	OC, Al, Mg, K, Ca, Fe	Si
Lake Bed	Coarse	Mn, Sr, Ba	$\text{K}^+$ , Ti	$\text{SO}_4^-$ , $\text{Na}^+$ , OC, Al, S, Cl, K, Ca, Fe	Si
Motor Vehicle	Fine (0 to 2.5 $\mu\text{m}$ )	Cr, Ni, Y, Sr, Ba	Si, Cl, Al, P, Ca, Mn, Fe, Zn, Br, Pb	Cl-, $\text{NO}_3^-$ , $\text{SO}_4^-$ , $\text{NH}_4^+$ , S	OC, EC
Vegetative Burning	Fine	Ca, Mn, Fe, Zn, Br, Pb, Rb	$\text{NO}_3^-$ , $\text{SO}_4^-$ , $\text{NH}_4^+$ , S, $\text{Na}^+$	Cl-, $\text{K}^+$ , Cl, K	OC, EC
Residual Oil Combustion	Fine	$\text{K}^+$ , OC, Cl, Ti, Cr, Co, Ga, Se	$\text{NH}_4^+$ , $\text{Na}^+$ , Zn, Fe, Si	V, OC, EC, Ni	S, $\text{SO}_4^-$
Incinerator	Fine	V, Mn, Cu, Ag, Sn	$\text{K}^+$ , Al, Ti, Zn, Hg	$\text{NO}_3^-$ , $\text{Na}^+$ , EC, Si, S, Ca, Fe, Br, La, Pb	$\text{SO}_4^-$ , $\text{NH}_4^+$ , OC
Coal Fired Boiler	Fine	Cl, Cr, Mn, Ga, As, Se, Br, Rb, Zr	$\text{NH}_4^+$ , P, K, Ti, V, Ni, Zn, Sr, Ba, Pb	$\text{SO}_4^-$ , OC, EC, Al, S, Ca, Fe	Si
Oil Fired Power Plant	Fine	V, Ni, Se, As, Br, Ba	Al, Si, P, K, Zn	$\text{NH}_4^+$ , OC, EC, Na, Ca, Pb	S, $\text{SO}_4^-$
Smelter Fine	Fine	V, Mn, Sb, Cr, Ti	Cd, Zn, Mg, Na, Ca, K, Se	Fe, Cu, As, Pb	S
Antimony Roaster	Fine	V, Cl, Ni, Mn	$\text{SO}_4^-$ , Sb, Pb	S	None reported
Marine	Fine and Coarse	Ti, V, Ni, Sr, Zr, Pd, Ag, Sn, Sb, Pb	Al, Si, K, Ca, Fe, Cu, Zn, Ba, La	$\text{NO}_3^-$ , $\text{SO}_4^-$ , OC, EC	Cl-, $\text{Na}^+$ , Na, Cl

### 2.1.5. The Role of Aerosols on the Global Atmospheric Chemistry

The studies conducted up to now have revealed that anthropogenic aerosols exert a radiative influence on climate that is globally comparable to that of greenhouse gases but opposite in sign. Radiative influences of aerosols on climate occur both directly, referring to scattering and absorption of the radiation by the aerosol particles themselves, and indirectly, referring to the influence of aerosols on cloud radiative properties by forming cloud condensation nuclei (CCN). Increase in the droplet number concentration observed with the raising aerosol amount. The increase in the number of drops results in the increase of reflection of solar radiation from clouds to space, which in turn leads to a climate cooling. This is called the first indirect radiative forcing. Unless the condensed moisture inside the cloud is changed by the increase in aerosols, the droplet radius will decrease because of the increase in its number concentration, which result in a decrease in the precipitation efficiency. This direct microphysical effect leads to suppression of precipitation in polluted clouds. In addition, it can also cause to an increase in cloud lifetime and in turn the amount of clouds.

The increase in cloudiness will lead to a further increase in the reflection of solar radiation, giving rise to the so-called second indirect radiative forcing (Ramanathan *et al.*, 2001).

The so-called "Mediterranean Intensive Oxidant Study" has confirmed the aforementioned claim on reduction in the precipitation amount because of the aerosols. In this study the workers employed a climate model with maximum and minimum monthly mean observed Mediterranean sea surface temperature (SST) and they have been found out that large precipitation reductions of 10 to 50 % in the Mediterranean region, the Middle East, and the Eastern Sahel will be possible since aerosol particles reduce solar radiation penetration to the surface leading to suppression of precipitation (Lelieveld *et al.*, 2002).

The overall effect of the atmospheric aerosols on the climate is the cooling of the atmosphere. Charlson *et al.* (1992) have found that the direct aerosol and indirect cloud components each contribute a globally averaged forcing of roughly  $-1 \text{ Wm}^{-2}$  that is confined predominantly to the northern hemisphere. The Intergovernmental Panel on Climate Change (IPCC) has recently estimated the direct effect of sulfate aerosol on the

radiative forcing to range between  $-0.21$  and  $-0.8 \text{ Wm}^{-2}$  with a central value of  $-0.5 \text{ Wm}^{-2}$  (Sharma *et al.*, 1999).

On the other hand, similar to the greenhouse gases aerosols may cause global warming. It has been previously shown that airborne absorbing aerosols play an important role to raise the regional temperature more effectively than  $\text{CO}_2$  by not only transferring the absorbed energy to surface but also reducing the local large scale cloud cover, which is known as "cloud burning" effect. Yu *et al.* (2001) have studied the temperature change patterns and the signals of regional aerosol-inducing forcing in eastern China during the half of the twentieth century. They have found out that high absorbing aerosols, which can be produced by both black carbon (BC) and dust, have a warming effect on the local temperature, especially in winter and when the reduction in local large-scale cloud cover occurs over Eastern China.

Latha and Badarinath (2004) have pointed out that the slope between black carbon aerosols and tropospheric ozone is  $-3.5$  suggesting that every  $1 \mu\text{gm}^{-3}$  increase in black carbon aerosol mass concentration causes a reduction of  $3.5 \mu\text{gm}^{-3}$  surface ozone. This reduction is the result of aerosol particles having large surface area facilitating the heterogeneous reactions to occur especially for the reactive trace gases like ozone. If an ozone molecule hits to the active site on the surface of carbon sample, one of its oxygen atoms gets adsorbed while the resultant oxygen molecule is liberated. The adsorbed oxygen atom can then combine with another adsorbed oxygen atom to form molecular oxygen. This catalytic reaction results in the dramatic ozone depletion in the atmosphere.

The role of non-activated aerosol particles as a medium for chemical processes in the atmosphere was given little attention until recently. It was generally assumed that the small amount of liquid water available in aerosols would prevent reactions in or on aerosols from competing successfully with reactions in cloud droplets.

When the aerosols undergo heterogeneous processes, they also affect gas phase chemistry. In the stratosphere, aerosols take up nitric acid and water at cold temperatures to form polar stratospheric clouds, which play a major role in polar ozone depletion (Murphy *et al.*, 1998).

The first critical step in a series of chemical reactions leading to rapid ozone destruction is:



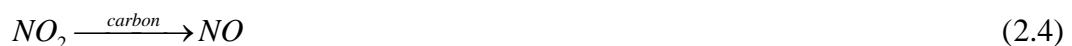
This leads to the formation of catalytically active Cl. This reaction only occurs on the surface or within the particles of polar stratospheric clouds at low temperatures. The liberated active Cl combines with O<sub>3</sub> via following reaction and the net result is the depletion of O<sub>3</sub>:



In addition, it had been shown that the below reaction takes place on stratospheric sulfuric acid particles, leading to conversion of catalytically active NO<sub>x</sub> (NO+NO<sub>2</sub>) to much less reactive HNO<sub>3</sub>:



Furthermore, Tabor *et al.* (1994) have demonstrated that reduction of NO<sub>2</sub> to NO has been observed on fresh black carbon surfaces. Lary *et al.* (1997) point out the resulting catalytic cycle for ozone loss:



Larger particulate aerosols, for example crustal dust with a mass median diameter greater than 1.0 μm, are removed from the air during long range transport and hence composition of the aerosol will change with distance from the land-based sources. As a result, open ocean particulate aerosols remote from the continents represent an integration of material from many sources. Chester *et al.* (1993) supposed that there are

mainly three globally important sources of trace metals to the marine aerosol: a) low temperature weathering of the Earth's surface, that is, crustal source; b) a variety of mainly high temperature anthropogenic processes, that is, anthropogenic source; and c) sea-salt generation, that is, oceanic source.

Mineral dust released from arid and semi-arid regions of the Earth account for the 45 % of the global aerosol emissions. The Saharan Desert is the main source of this soil derived dust, with an annual emissions estimated from 300 to 700 megatons per year (Chiapello *et al.*, 1997). One of the most important characteristics of the desert aerosol is that they can be long-range transported. When they deposited to the sea or ocean or any kind of water body they affect the biogeochemical cycles going on there. This fact was proven with the study conducted by Zhuang *et al.* (1992). They found out that the mineral aerosols originating from the arid regions could enhance biological activity of the open oceans because during long-range transport Fe (III) can be reduced to the Fe (II). In this form iron is bioavailable and hence results in the increased dimethylsulphide (DMS) concentration in the atmosphere.

#### **2.1.6. The Impact of Aerosols on Health**

Although the short-term health effects of particulate pollution have been well established in the literature, the exact mechanism by which these health impacts are produced is still unknown. There is no precise evidence reported upto now indicating that any single major or trace component of the particulate matter is responsible for the recorded adverse health effects.

Harrison and Yin (2000) put forward the factors which may influence the toxicity of particulate matter. The factors comprise the bulk chemical composition; trace element, strong acid, and sulfate contents, and lastly particle size distribution. Although these factors given under different items, they are interrelated, i.e., they can not be separated by the solid lines since one encompasses the other. For example, bulk chemical composition does not only refer to nitrate, ammonium, chloride, elemental and organic carbon, crustal and biological materials but also sulfate. Sulfate, which is derived mainly from the oxidation of sulfur dioxide in the atmosphere, is then converted into the sulfuric acid by the ongoing heterogeneous chemistry and neutralized by atmospheric ammonia.

Lipmann (1998) has argued that the toxicity of airborne particles is owing to their strong acid content. There are many other kinds of toxic substances and materials.

Thurston *et al.* (1994) have ranked the impact of the pollutants associated with the particulate matter as:  $H^+ > \text{sulfate} > PM_{2.5} > PM_{10} > \text{TSP}$

However, Schwartz *et al.* (1996) have found lower correlations between  $H^+$  and health effects than with sulfate and  $PM_{2.5}$  (Schwartz *et al.*, 1996; Anderson, 2000).

The vast number of epidemiological studies have tried to establish a link between total mortality and exposure to the  $PM_{10}$  (e.g., Dockery and Pope, 1994; Lippmann, 1998). Lipmann (1998) claims that total daily mortality increases by approximately 1 % per  $10 \mu\text{g m}^{-3}$  increase in  $PM_{10}$  concentration.

In the literature it is argued that  $PM_{2.5}$  is a better metric for the adverse health effects compared to the  $PM_{10}$  since the penetration efficiency of this smaller size fraction getting into the alveolar region of the respiratory system is higher. However, Lippmann (1998) have revealed that there is little evidence indicating that  $PM_{2.5}$  has more toxic effects than does  $PM_{10}$ . On the other hand, a World Health Organization (WHO) group stated that there is a strong correlation found between fine particles and mortality, and cardiovascular and respiratory endpoints, i.e, they are more hazardous than coarse particles. However, this does not mean that the coarse fraction of  $PM_{10}$  is harmless (Englert, 2004).

Yeh *et al.* (1996) conducted a modelling study to find the deposition of particles in various regions of lung and they summed up their finding in Figure 2.8. (By the courtesy of Yeh *et al.*, 1996 and Hinds, W.C., 1982, respectively). The schematic of human respiratory track is also depicted in Figure 2.8. As it can be seen from this figure, the larger particles are deposited upper portions of the respiratory system, they are trapped in the nose and upper airways. Particles with size smaller than  $0.5 \mu\text{m}$  reach to the pulmonary and tracheobronchial region.

Lingard *et al.* (2005) collected size fractionated roadside samples and they analyzed the collected samples in terms of Cr, Cu, Fe, Mn, Ni and Zn. Aqueous extratcs of these samples were used to measure genotoxic effect of particulate matter on DNA. They have

found out that strand break was induced, the damage was especially higher in the smaller size fractions.

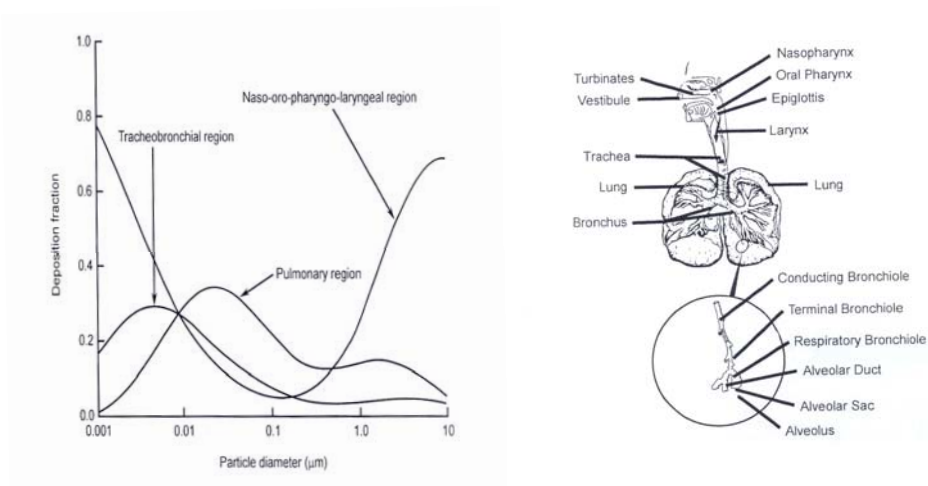


Figure 2.8 Deposition of particles in different regions of the lung for polydisperse aerosol and schematic diagram of human respiratory track

Donaldson and MacNee (1998) have found out that ultrafine particles, which are generally less than 100 nm in size, seem to have significantly greater toxicity per unit mass and their toxicity increases as the particle size decreases. There may be two reasonable explanation of this properties of the particles. First one is that ultrafine particles have larger surface area which increases the available places for the toxic components to reside. Secondly, ultrafine particles are believed to penetrate the pulmonary interstitium.

Oberdörster and his colleagues generated ultrafine elemental  $^{13}\text{C}$  particles with 36 nm in size to determine whether translocation of inhaled ultrafine particles (UFP) to regions of the brain occur. They hypothesize that UFP deposited on the olfactory mucosa of the nasal region will transport along the olfactory nerve into the olfactory bulb. The rat subjects were exposed to generated ultrafine elemental  $^{13}\text{C}$  particles for 6 h. The lungs, cerebrum, cerebellum and olfactory bulbs of the rats were removed after 1, 3, 5, and 7 days. They have found out that there was a significant and persistent increase in added  $^{13}\text{C}$  in the olfactory bulb. The concentration was increased from 0.35  $\mu\text{g/g}$  for 1 day to



0.43  $\mu\text{g/g}$  for 7 day postexposure. They concluded that central nervous system (CNS) can be targeted by ultrafine particles found in the atmosphere. There are the likely mechanisms by which airborne particles transported into the CNS: uptake of these particles into the nerve endings embedded in mucosa of nasal, *route a* and *b*, and tracheobronchial, *route c* in Figure 2.9, region. The biological and toxicological significance of these routes in addition to classical clearance pathways of mucociliary and phagocytic cell transport, dissolution, diffusion, and protein binding remain to be further determined.

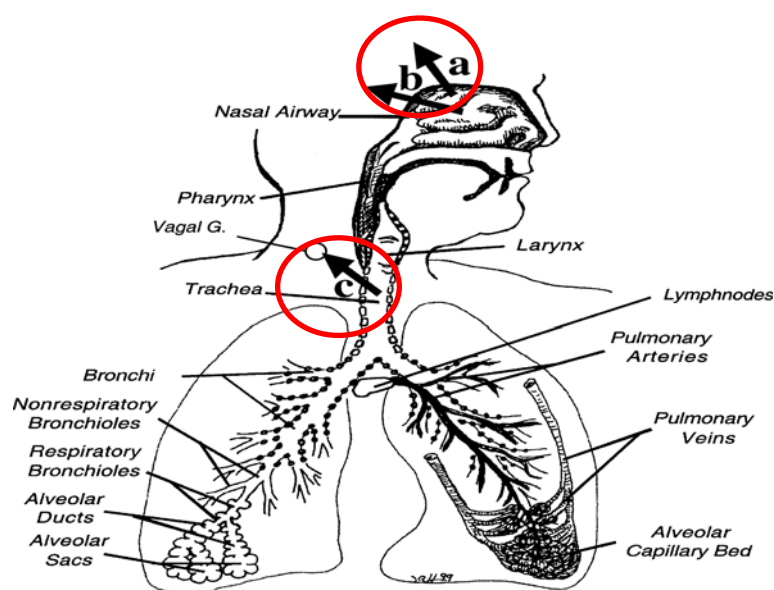


Figure 2.9 Suggested neuronal translocation pathways in humans for solid nanosized particles and for soluble components (*a*:olfactory nerves, *b*:trigeminal nerves, *c*:afferent vagal nerves)

Dorman *et al.* (2004) have also showed the transport of inhaled particles to CNS. They performed a study to determine the nasal toxicity of inhaled  $\text{MnSO}_4$  and manganese phosphate (as hureaulite) in young adult male rats. The rats were exposed to  $\text{MnSO}_4$  at a concentration of 0.01, 0.1 and 0.5  $\text{mg Mn/m}^3$ , and also 0.1  $\text{mg Mn/m}^3$  of hureaulite for 90 days. Nasal pathology, brain glial fibrillary acidic protein (GFAP), and brain manganese concentrations were evaluated at the end of 90 days exposure and 45 days postexposure

time. They came up with the result that the manganese concentration was increased in the olfactory bulb, striatum, and cerebellum after exposure to elevated concentration values. They were also able to demonstrate that high-dose manganese inhalation resulted in nasal toxicity (irritation). However, they could not find any evidence of increased GFAP concentrations in the olfactory bulb, cerebellar or striatum.

Gilmour *et al.* (1996) proposes that transition metals take part in the some non-classical mechanisms through which they adversely affect the health. The fact behind this suggestion is that metals are redox active and hence they are able to induce or catalyze chemical reactions. For example, iron goes into the so-called Fenton reaction to produce hydroxyl radical as given below:



Hydroxyl radical generated by these pathways is known to cause tissue inflammation (Harrison and Yin, 2000).

Theoretically, it has been stated that lung inflammation can result in the release of reductant superoxide and labile hydrogen peroxide ( $H_2O_2$ ) from lung cells, which in the presence of lipids, react in vitro with the transition metals to produce more oxidants. However, there is too much effort should be spent to prove this hypothesis (Chapman *et al.*, 1997).

The reaction sequence given in Equation (6) & (7) is also applicable for other transition metals, which exist in two or more valance states and are thus capable of redox suttling of electrons.

Furthermore, it was previously documented that metals are deposited and remained in the deep lung of living humans, especially in industrialized urban areas. In addition, studies conducted on the laboratory animals have repeatedly demonstrated that metals associated with the particles can be toxic to the lungs, inducing inflammation, changing normal physiological function and impairing host defenses (Chapman *et al.*, 1997; and

references therein). Dye *et al.* (2001) applied the diluted extracts from air filters by instillation to rats and bronchoscopically to human volunteers. They found out that extracts resulted in the local inflammation and hence, they proved that water soluble components, which are rich in terms of metals, are more toxic. Kuschner *et al.* (1997) found out that ZnO particles are more toxic than MgO particles. These all reveal that some components of particulate matter are more toxic than others and the effects depend on the chemical composition and phase of the particles.

Christensen (1995) has conducted very detailed study to highlight the impacts of toxic metal exposure on human health. Arsenic was one of the toxic metals that he investigated. It was stated that the inorganic form of the As is more toxic than other forms since inorganic As is known to be carcinogenic. High dose exposure to inorganic As may lead to lung, skin, liver, bladder and kidney cancer. Besides, inorganic As exposure results in the formation of lipid peroxides and free radicals, and hence, it has a strong association with neurological and cardiovascular diseases. In addition to As, Ni and Ni compounds are also classified as the carcinogens.

Lee and his colleagues (2000) conducted a study covering the seven major cities of Korea to establish the relationship between the air pollution and daily mortality. The results of their study show that SO<sub>2</sub> was a significant indicator for all causes deaths. An increase of 50 ppb in SO<sub>2</sub> concentration corresponds to 1–12 % more deaths. This is consistent with the idea that SO<sub>2</sub> acts well as a surrogate for the fine particles that are thought to be a risk factor of early mortality. Xu *et al.* (1994) have conducted similar study in Beijing, China and found that SO<sub>2</sub> was significantly associated with the increased mortality but Total Suspended Particulate (TSP) were not.

The work conducted by Chapman *et al.* (1997) revealed that both short and long-term exposures to PM<sub>10</sub> and PM<sub>2.5</sub> are associated with increased mortality in adults, especially in people older than 65 years with previous cardiopulmonary illness. In the same study, they also showed that short-term exposures to PM<sub>10</sub> are well correlated with increased hospital visits in elderly adults with respiratory illness. In addition, another study conducted on elderly people suggest that there is a strong association of short-term elevation of ambient PM levels with the reduction of variability in heart rate in elderly subjects (Aburto *et al.*, 1997).

In summary, particle composition and size and duration of the exposure are the key parameters affecting the influence of particulate matter on health. From the discussions presented in this section, possible effects by which aerosol particles and other air pollutants adversely affect the human health can be listed as follows (Pöchl, 2005 and references therein):

- Pulmonary inflammation induced by PM and O<sub>3</sub>
- Free radical and oxidative stress generated by transitional metals or organic compounds, for instance, PAHs
- Covalent modification of key intracellular proteins (e.g. enzymes)
- Inflammation and innate immune effects induced by biological compounds such as endotoxins and glucans
- Stimulating nervous system activity regulating heart rate variability and airway reactivity
- Adjuvant effects in the immune system, for example, transition metals enhancing responses to common environmental allergens
- Procoagulant activity by ultrafine particles accessing the systematic circulation
- Suppression of normal defense mechanisms, for instance, suppression of alveolar macrophage functions

## **2.2. LEGAL FRAMEWORK ESTABLISHED FOR PM**

The first recorded air pollution regulation was identified by Brimblecombe in 1987 as a royal decree in 14<sup>th</sup> century England to decrease the coal consumption. People complained with the black smoke from chimneys, reduced visibility, black deposits on buildings and clothing, and respiratory problems at that time. Although people had no highly sensitive instruments to determine the causes of air pollution, their complaints mainly based on the observation were valid. The reason of their complaints was the sulfur dioxide (Chow, 1995).

With the current high technology instruments, it is possible to detect ultra trace concentrations of pollutants in the atmosphere. Accordingly, regulations, laws and any kind of regulatory tools are concerned with the minimum concentration that can give damage to human health, and associated property. There exists different regulations established for PM<sub>10</sub> and PM<sub>2.5</sub> concentrations in the ambient air in different countries.

The European Union set limit values for the PM<sub>10</sub> and PM<sub>2.5</sub>. In the Air Quality Directive 1999/30/EC it is stated that 24-h average of PM<sub>10</sub> should not be greater than 50 µgm<sup>-3</sup> and not to be exceeded more than 35 times per year by 2005 and 7 by 2010. Under the same directive it is also stated that an annual mean limit value should be 40 and 20 µgm<sup>-3</sup> by 2005 and 2010, respectively. Recently, the EU proposes a shift to the PM<sub>2.5</sub> metrics with the suggestion of an annual PM<sub>2.5</sub> limit value in the range of 12-20 µgm<sup>-3</sup> and a daily limit value of 35 µgm<sup>-3</sup> not to be exceeded more than 35 days per year (Querol *et al.*, 2004).

The National Ambient Air Quality Standard (NAAQS) set by the U.S. Environmental Protection Agency (USEPA) for PM<sub>10</sub> does not permit ambient concentrations to exceed 50 µg/m<sup>3</sup> for annual arithmetic average and 150 µg/m<sup>3</sup> for 24-hour average more than three times a year (EPA/600/P-95/001aF, 1996).

In the UK, running 24-h average for PM<sub>10</sub> is 50 µgm<sup>-3</sup>. Finland has a proposal for a new ambient air quality standard for PM<sub>10</sub> is 70 µgm<sup>-3</sup>. Germany does not only set out standard for PM<sub>10</sub> and PM<sub>2.5</sub>, but also for PM<sub>1</sub>. Japan established air quality standard for PM<sub>10</sub> in 1973, before the emergence of recent evidence of air pollutants on the public health. Their current standard for PM<sub>10</sub> is 200 µg m<sup>-3</sup> as a 1-h average and 100 µgm<sup>-3</sup> as a 24-h average (Sloss and Smith, 2000).

In the Turkish Air Pollution and Quality Control Regulation, short and long term limit values are defined for both general and industrial sources. The short term values of PM<sub>10</sub> are 300 and 400 µgm<sup>-3</sup> for general and industrial regions, respectively. On the other hand, the long term limit values of PM<sub>10</sub> are given as 150 µg m<sup>-3</sup> for general sources and 200 µgm<sup>-3</sup> for industrial counterpart. (Turkish Air Quality Regulation, 2004). Once these values are compared with the standard values sets by the EU, it may be said EU standards are more strict.

### **2.3. LONG RANGE TRANSPORT**

After the recognition of impacts of the long range transported atmospheric pollutants over human health and also the ecosystem, Long Range Transboundary Air Pollution on Persistent Organic Pollutants Convention was adopted in Genoa on 13 November 1979. The convention entered into force in 1983. 47 European countries and Canada and USA

are currently parties of this convention. With this convention parties accepted that emissions of many persistent organic pollutants are transported across international boundaries and are deposited in Europe, North America and Arctic, away from their release point to the atmosphere. Parties were aware that these sorts of pollutants were not degraded in the natural environment and they can biomagnify and may eventually be harmful to the people and other living biota exposed to them.

Significant quantity of work has been done to show the transport of atmospheric pollutants over long distances in the literature. Some examples of these were presented herein.

Kindap *et al.* (2006) has investigated the transport of PM<sub>10</sub> from Eastern European countries to Istanbul, Turkey. The trajectory analysis they have conducted indicated that the PM<sub>10</sub> episodes observed in the Istanbul is corresponding to northwesterly winds suggesting the impacts of sources in Eastern European countries on Istanbul. A sensitivity analysis indicated that aerosol transport from Eastern Europe to Northern and Western Turkey occurred all the time during the simulation period. As a result of their work they suggested that the contribution from the Europe should be considered while assessing the air quality of the Northern or Western Turkey.

Mineral dust is transported over long distances and affects the radiation balance directly and indirectly by scattering and absorbing radiation, and by acting as CCN. Mineral dust also modifies the global biogeochemical cycle by carrying anthropogenic pollutants and some micronutrients like Fe, which can be consumed by the phytoplankton in the ocean and hence, primary productivity of the ocean increased. Long range transported mineral dust particles can act as surfaces for the production of sulfate compounds as well. Han *et al.*, (2007) have showed that sulfate is mainly found in the PM<sub>2.5</sub> but some is formed on the mineral dust particles.

The Mediterranean region's atmosphere is also the receiver of the pollution arriving from central Europe. Ganor *et al.* (2000), Luria *et al.* (1996), Sciare *et al.* (2003), Tsitouridou *et al.* (2003), Zerefos *et al.* (2000) and Saliba *et al.* (2007) have all proven that the air masses originating from Europe enrich the atmosphere of the Mediterranean with sulfur dioxide (SO<sub>2</sub>). Emissions from Europe influence the countries in mainland as well.

Charron *et al.* (2007) and Abdalmogith *et al.* (2006) have showed that secondary inorganic aerosol in the UK is derived from the precursor emissions in Europe.

Erel *et al.* (2006) has showed that Mediterranean region does not only receive air masses from Europe but also from North Africa. They performed sampling campaign in which they have collected aerosol samples on the PTFE filters and analyzed the samples for elemental constituents after sequential extraction. They found that samples were enriched in Pb, Cu, Zn and Ni, significantly while other elements like Na, Ca, Mg, Mn, Sr, U and Th were present at natural concentrations. The increased concentrations in the anthropogenic elements in this study were attributed to air masses carrying pollution from the North Africa.

Tamamura *et al.* (2007) collected aerosol particles for 1 year at a rural area in Japan, and analyzed the collected particles in terms of their Polycyclic Aromatic Hydrocarbon (PAH) contents. They conducted back trajectory analysis to find the sources of high PAH concentrations and they came up with the result that the PAH is transported to this rural site from highly industrialized areas on dust particles. Long range transportation of PAH has also discovered by Sehili and Lammel (2007) in their multicompartamental model study. They illustrated that PAH emitted from Russia and Europe transported to northern latitudes.

Bioaerosols are also transported over long distances. Skjoth *et al.* (2007) showed that Denmark receives significant amount of birch (*Betula*) pollen from Poland and Germany almost every year, and that this increases the complaints of the people having allergies. They suggest that the forecasts that try to quantify the annual pollen production should take long range atmospheric transport into account as well.

#### **2.4. EASTERN MEDITERRANEAN AEROSOL COMPOSITION**

The studies conducted over the Eastern Mediterranean indicated three important sources determining the chemical composition of the aerosols over this region, which are: (i) anthropogenic sources which are located to the north and northwest of the region, i.e., Europe; (ii) crustal source located in North Africa; (iii) Mediterranean Sea itself (Gullu *et al.*, 1998; Tuncer *et al.*, 2001; Kouvarakis *et al.*, 2002; Ganor *et al.*, 2000). Among these sources, the anthropogenic ones, especially located in Europe, is more pronounced as

compared to the others. Kouvarakis *et al.* (2002) have found at least 70 % of the time during the year, the Eastern Mediterranean basin receives, air masses influenced from human activity from Central and Eastern Europe. Luria *et al.* (1996) revealed that the annual average of particulate sulfate is twice as high as predicted for the region by a global model and comparable or sometimes higher than the values reported for the most industrialized parts of the United States.

Lelieveld and his co-workers (2002) claimed that the Eastern Mediterranean is polluted by emissions from Eastern Europe, in particular Poland, the Ukraine, and Russia. They found out that long range CO transport from both Western and Eastern Europe contributes 60 to 80 % of the boundary layer CO that is mostly as a result of fossil fuel use over Mediterranean. Therefore, it can be concluded that the Eastern Mediterranean basin is the major recipient of polluted air masses coming from the Europe.

Herut *et al.* (2001) have confirmed the above findings. They have indicated that air masses arriving to the Eastern Mediterranean originate from three major directions: (i) northwest Europe; (ii) Eastern Europe crossing Turkey; (iii) southwest and southeast air flows from inland North Africa and Arabian continents. The first two air mass back trajectories belong to air masses associated with European and marine sources whilst the third probably to have aerosol populations influenced by mineral components from deserts of North Africa (Sahara), Sinai, and Arabian Peninsula.

All these results indicate that chemical composition of aerosol particles have been affected from these major sources.

Various large scale research projects have been conducted over the Mediterranean region to find the paths and scales of pollution transport and transformation. Some of these research projects employ the modelling tools, and output obtained from these models were validated and improved with the field campaigns (Kallos *et al.*, 2007). The paths and scales of transport and transformation of pollutants over the Mediterranean Region identified so far are depicted in Figure 2.10.



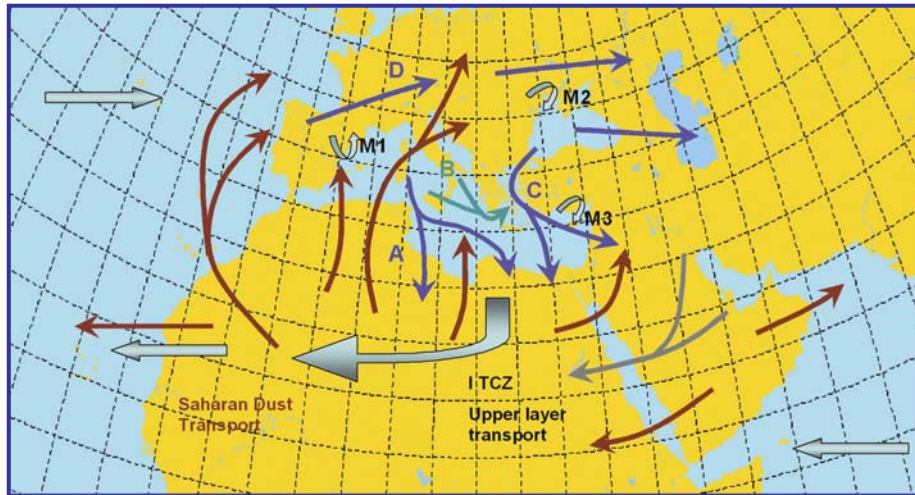


Figure 2.10 The paths and scales of transport and transformation of pollutants over Mediterranean

The blue, gray and greenish arrows in Figure 2.10 show the transport path of the pollutants with anthropogenic origin over the Mediterranean region. The gray arrows depict the upper layer transport, while greenish and blue ones show the transport in the lower-tropospheric layers. The transport of desert dust in the lower troposphere is illustrated with the red-brown arrows. The following conclusions are drawn from Figure 2.10:

- The Mediterranean Sea, North Africa, and the Middle East receive air masses from southern Europe during all seasons, particularly in summer (paths indicated with the letters of *A*, *B*, and *C* in Figure 2.10)
- Even though the long range component is also important, thermal circulations define the air quality at the coastal sides (*M1*, *M2* and *M3* in Figure 2.10)
- Anthropogenic pollutants emitted from the coastal regions are vented toward the free troposphere during the day time and toward the marine boundary layer (MBL) where they are kept and travel long distances before they finally returned to the ground
- Transport over the Mediterranean Sea appears to occur within the MBL, from which anthropogenic pollutants are injected to the free troposphere. The islands behave as the chimneys and take part in the emitting pollutants in the free troposphere

- Some of the places in Black Sea and Eastern Mediterranean act as *temporal reservoirs* in which pollutants are concentrated and aged prior to their further advection. *Path C* in Figure 2.10 stands for this case
- While horizontal transport is dominant in the eastern Mediterranean, vertical transport is significant in the western counterpart and results in the formation of multiple layers in the atmosphere, which is depicted by the *MZ* in Figure 2.10
- Intertropical convergence zone (ITCZ) is placed over Africa, south of the Mediterranean coast line and over southern Libya and Egypt. In order massive upward transport of the aged pollutants to happen, the air masses from the Europe should reach to ITCZ within 4-6 days

#### **2.4.1. Trace Element Composition**

The scavenging efficiency of particles is affected by chemical composition, which is in turn affected by the sources of particles. The globally significant sources of trace metals to aerosol are: (i) low temperature weathering of the Earth's surface (crustal source); (ii) a variety of mainly high temperature anthropogenic processes (anthropogenic source); (iii) sea-salt generation (oceanic source). In addition, volcanic sources can supply trace metals to the atmosphere.

The work conducted by Pirrone *et al.* (1999) have showed that North Africa and Middle East represent the major contributors of Pb, nearly 75 % in 1998, released annually to the atmosphere in the Mediterranean region. On a country-by country basis, Syria is the major Pb emitter (nearly 23.6 %) in the region, followed by France (12.5 %), Italy (11.1 %), Turkey (10.2 %), Egypt (6.8 %), Spain (6.4 %), Israel (5.1 %), Yugoslavia (3.4 %), Greece (2.5), Lebanon (2.3 %) and Albania (0.2 %) according to 1998's estimate.

In the same study the workers have also revealed that emissions from the combustion of fossil fuels as well as from primary and secondary non-ferrous metal smelters represent important sources of Pb, Ni, Cd, and V in the region. More than 50 % of ambient Ni was released from anthropogenic sources from Lebanon, Tunisia, Bulgaria and Cyprus. Lebanon, Tunisia and Bulgaria are the major emitters of Cd in the region while Cu is mainly released by the Libya.

In another study, Tian and Pino (1994) carried out a box model in order to simulate and predict the Pb concentration in the Mediterranean Sea. Researchers suggest that the Mediterranean Sea has acted as a source since 1981 though it was a sink before 1980. In relation to accumulation in the sediments, about half of the total external input of Pb was estimated to have been deposited between 1959 and 1992.

Herut *et al.* (2001) found out that the elements like Cd, Cu, Pb and Zn have originated from the anthropogenic activities while the elements such as Fe, Al, Mn and Cr have natural sources. In the same study it was found that concentrations of crustal derived elements are a factor of 2-3 greater in the Eastern Mediterranean than is observed over the Western Mediterranean. Moreover, the concentrations of elements originating from the anthropogenic activities are reported to be lower than the ones observed over Europe. This fact can be explained by the dilution of air masses coming from the Europe with the ones arriving to the Eastern Mediterranean from the North Africa and Arabian Peninsula.

In relation to the Cd concentration, the finding presented in the previous paragraph has been confirmed by Migon and Caccia (1990). They have demonstrated that the anthropogenic contribution of particulate Cd is about 100 times higher than the natural Cd levels. In contrast to the study of Herut *et al.* (2001), they have failed to illustrate that concentration of anthropogenic particulate Cu is higher. They suggested that the observed Cu concentration over the Mediterranean atmosphere is only due to the long range transport.

With respect to the atmospheric inputs the Mediterranean Sea is of special interest because it is bordered on its northern shore by industrialized regions, which act as a source for the supply of anthropogenic material to the atmosphere, and on its southern and eastern shores by arid and desert regions, which are sources of crustal material. In addition, the meteorological regime over the Mediterranean Sea gives rise to seasonal differences in the inputs of the anthropogenic-rich and crust-rich material.

Kocak *et al.* (2004) have investigated the aerosol composition over the Levantine Basin. They have found out enhanced concentrations of Al, Fe and Mn over the Levantine Basin during Saharan dust events. They have also reported high concentrations of Cr and Cu,

but at lower values compared to Cr. They attributed this high concentration of Cr and Cu to the pollution arising from the local sources.

Kocak *et al.* (2005) have revealed that the atmospheric deposition of some of the anthropogenic elements to the Mediterranean Sea is considerably higher than their corresponding input from the rivers. For instance, riverine input of Pb, Cd and Cu are 0.2, 0.048 and 5.7 tonsyr<sup>-1</sup>, respectively while their minimum atmospheric deposition values are 2120, 3.0 and 450 tonsyr<sup>-1</sup>.

Kubilay and Saydam (1995) also found out that there is no significant difference in the concentrations of atmospheric particulate matter over the entire Mediterranean region. They also presented that concentrations of the crustal elements (Al and Fe) are an order of magnitude higher and of the anthropogenic elements (Cd and Zn) are relatively lower when air masses come from North Africa rather than from north. The Eastern Mediterranean is dominated to a much greater extent by desert particles than its Western counterpart.

As the atmosphere is the source of trace elements in the water bodies, the oceans affect the chemical composition of the atmosphere as well. Comparison of the estimated fluxes from different sources demonstrates that gas phase emission from the ocean could represent up to 60 % of the atmospheric Se with a global input of 5-8 10<sup>9</sup> g Se/yr. This finding is also applicable for the Eastern Mediterranean that maritime emissions are the major source of Se to the atmosphere in the basin (Amouroux and Donard, 1996).

Mateu *et al.* (1996) carried out a study concerning about the particle size distribution and long range transport of metals in atmospheric aerosols over the Majorca, Spain. They come up with the result that the metals originating from the anthropogenic activities associated with the fine particles, whose diameter is less than 0.5 µm. In contrast, natural metals are predominated in coarse particles. They also presented that aerosols from northern Spain, southern and central France, and Sardinia were found to contain high concentrations of metals of anthropogenic origin (Cd, Zn, Ni), whereas those from southern Spain and northern Africa were found to be enriched with metals from natural sources (Ca, Mg, Mn, Fe, K, Cr).

Yatin *et al.* (2000) have investigated the atmospheric trace element composition of the aerosol samples collected in the Ankara, Turkey. They have revealed that the change in the concentrations of anthropogenic elements is consistent with the regulations taken to improve the air quality. Moreover, they have reported a decrease in the concentrations of crustal elements, and they explain this behaviour of crustal elements with the increased urbanization, which led to change in the soil cover.

#### **2.4.2. Major Ion Composition**

Sulfur and nitrogen containing species are emitted from a variety of anthropogenic and natural sources. They are mixed, transported and reacted, and finally removed from the air back to the earth surface.

Sulfur dioxide reacts with hydroxyl radicals in the atmosphere to yield  $\text{SO}_3$ , which in turn reacts rapidly with water vapour to produce sulphuric acid or depending on the meteorological conditions and availability of oxidising substances, the  $\text{SO}_2$  may be transported hundreds of kilometres in the atmosphere without being totally depleted. Similarly,  $\text{NO}$  and  $\text{NO}_2$  can be transported, dry deposited or react to form nitric acid. Gaseous nitric acid combines with the cloud water and converted into nitrate ion ( $\text{NO}_3^-$ ), which then comes back to earth's surface in precipitation. Atmospheric nitric acid ( $\text{HNO}_3$ ) is the major sink for the  $\text{NO}_x$  ( $\text{NO} + \text{NO}_2$ ) and also the main contributor of acid deposition (Johnson *et al.*, 1994).

Nitric acid is also significant because of being precursor of  $\text{NH}_4\text{NO}_3$  particles, which cause visibility degradation and also contribute to the acidity of the suspended particles, rainwater, lakes and vegetation (Appel *et al.*, 1988).

The main source of ammonia to the atmosphere is from the agricultural operations via volatilization. While it is not hazardous at atmospheric levels, it takes part in aerosol formation with  $\text{HNO}_3$  and hence neutralizes the acidity of gaseous and particle phase acids (Finlayson and Pitts, 1986).

Sulfate and nitrate make up the secondary fraction of naturally produced particles. Natural sources of sulfate is the oxidation of  $\text{SO}_2$  emitted from volcanoes and dimethylsulfide (DMS) produced by biogenic activities in the marine environment. In

addition the main natural sources of NO<sub>x</sub> are the soil transpiration (Roelle *et al.*, 2001) and lightning (Priece *et al.*, 1997).

Erduran and Tuncel (2001) carried out a study over the Northeastern Mediterranean to determine the levels of gaseous and particulate pollutants. They illustrated that the concentration of gaseous nitric acid is lowest among compared to the other acid causing agents indicating that it has small contribution to the acidity in the Northeastern Mediterranean atmosphere. NH<sub>3</sub> levels show significantly seasonal pattern, which can be related to the variability of fertilising activities over the region. Sulfate is mostly anthropogenic in origin. They, moreover, carried out backtrajectory analysis and found out that there are four major source regions affecting the observed chemical composition, namely, Western Mediterranean countries, north-eastern Europe, Russia and Anatolia.

Higher concentrations of nitric acid, ammonia and particulate matter was observed in the summer at a Mediterranean coastal site, Patras, Greece. This is due to greater nitric acid production in the summer because of larger hydroxyl radical concentrations and larger ammonia emissions at higher temperatures. The results corresponding to air mass back trajectory analyses are in a good agreement with the ones obtained by Erduran and Tuncel (2001). They demonstrated that the higher concentrations of the long-lived particulate sulfate were long range transported from northern directions. Elevated sulfate concentrations 7-11 µgm<sup>-3</sup> were observed in the summer. Particulate sulfate was 5-15 times larger than particulate nitrate on an equivalent basis indicating that higher sulphur over nitrogen emissions (Danalatos and Glavas, 1999).

In another study conducted over the same region Glavas *et al.* (1995) have revealed that nitric acid showed a clear diurnal variation with maximum concentrations occurring in the afternoon. Gaseous nitric acid is the predominant form of inorganic nitrate. They also indicated that Ca<sup>2+</sup> (as CaCO<sub>3</sub>) is more important neutralizing agent over the region as compared to ammonia.

The study conducted by the Shaka and Saliba (2004) have showed that the inorganic ions such as SO<sub>4</sub><sup>2-</sup>, NO<sub>3</sub><sup>-</sup>, SiO<sub>4</sub><sup>2-</sup>, CO<sub>3</sub><sup>2-</sup>, and NH<sub>4</sub><sup>+</sup> are at higher concentrations in the fine fraction of aerosols as compared to coarse fraction in the Eastern Mediterranean aerosols. Besides, fine fraction is enriched by the organic species for example aliphatic

hydrocarbons, and long chains of alcoholic and carboxylic acids while higher water concentrations were observed in the coarse fraction. Kuloglu and Tuncel (2005) also revealed that  $\text{SO}_4^{2-}$  and  $\text{NH}_4^+$  ions are associated with the smaller size fractions in the Eastern Mediterranean aerosols. They reported that the mass median diameter (MMD) for the  $\text{SO}_4^{2-}$  and  $\text{NH}_4^+$  are 0.63 and 0.45  $\mu\text{m}$ , respectively.

Bardouki *et al.* (2003) identified the  $\text{SO}_4^{2-}$  and  $\text{NH}_4^+$  as the major ionic composition of sub-micrometer particles. On the other hand,  $\text{NO}_3^-$ ,  $\text{Cl}^-$ ,  $\text{Na}^+$  and  $\text{Ca}^{2+}$  are the main components of the super micron particles. Super micron particles also contain the ionic organic compounds such as carboxylic, dicarboxylic and ketoacids.

Kouyoumdjian and Saliba (2005) investigated the seasonal variation of ionic composition of size segregated aerosols in Lebanon. They found out that  $\text{NO}_3^-$  was enriched in the coarse fraction of the aerosols in summer months. They suggest nitric acid is neutralized by the  $\text{CaCO}_3$  present in the coarse fraction and this neutralization reaction occurs at faster rates as compared the reaction between  $\text{NaCl}$  and  $\text{HNO}_3$ . Since  $\text{CaCO}_3$  concentration is higher in summer due to the enhanced resuspension of soil particles, the neutralization process is more probable in summer than in winter.

Danalatos and Glavas (1999) and Peleg *et al.* (2002) observed elevated sulphur concentrations over Israel in summer, which researchers suggested to related to synoptic conditions characteristic of the Eastern Mediterranean. Synoptic analysis indicated that conditions during summer in Israel facilitate the accumulation of pollution species above the Mediterranean basin from the upwind European sources. This season features a shallow mixed layer and weak zonal flow leads to poor ventilation rates, inhibiting an efficient dispersion of these pollutants while being transported eastward.

$\text{SO}_4$  concentrations measured in the Mediterranean coast of Turkey are among the highest measured in the Mediterranean basin. The similarity in the  $\text{SO}_4$  concentrations at Crete, Israel and Antalya indicates that high concentrations is not a unique feature for the Mediterranean coast, but is a common feature in the region. The values reported for the Eastern Mediterranean is higher than the  $\text{SO}_4$  concentrations reported for the Western Mediterranean, which is supposed to have elevated sulfate levels due to the close proximity to the more industrialized Western countries. Although one expect to see elevated  $\text{NO}_3$  concentrations over the Eastern Mediterranean as well, the reverse of this

is true. This situation complicates the problem because polluted air masses not only carry SO<sub>4</sub> but also NO<sub>3</sub> (Uzun, 2000).

### **2.4.3. General Climatology of Eastern Mediterranean Atmosphere**

The characteristic of the local climatology over the region provide information about the transport of the pollutants in changing time scales and locations. For this reason, detailed information about the study region climatology is a prerequisite in understanding the transportation and transformation of pollutants to or from the region.

Kallos *et al.* (2007) have stated that the climatic conditions in the Mediterranean region can be divided into two as cold and warm periods. The cold period of the year is described by the low-index circulation that is related with the intense cyclogenetic activity. The anticyclonic activity during this period is associated with anticyclone generated in central Europe and the Balkan region.

The warm period is mainly due to the high index circulation in which the North Atlantic Ocean low pressure center moves towards Europe and only edges of the fronts contact with the Mediterranean region. This warm period of the year is balanced by the North Atlantic Ocean anticyclonic activity, which extends toward Europe and Mediterranean region and the monsoon activity generated in the Indian Ocean and the Middle East. This balance results in the transport of air masses at various scales. An example of this case is depicted in Figure 2.11, which is generated with the use of mean monthly sea level pressure fields for August 2001 from the European Center for the Medium Range Weather Forecasts (ECMWF) analysis fields.

In Figure 2.11, the monsoon activity over the Indian Ocean and anticyclonic activity over the North Atlantic Ocean are clear. The pressure difference over these two activity is strong enough, about 10-20 hPa from the western to eastern Mediterranean, or between the points *A* and *B*, to results in the trade wind systems like the etesians over the Aegen Sea.

Kostopoulou and Jones (2007) conducted a comprehensive analysis of the climate variability in the Eastern Mediterranean, and their study agree with the findings of Kallos *et al.* (2007). They were able to demonstrate that large scale features situated in Europe



influence the circulation over the study region during winter and spring, whereas the Atlantic (Azores) and the Asian Thermal Low are dominant during summer and autumn.

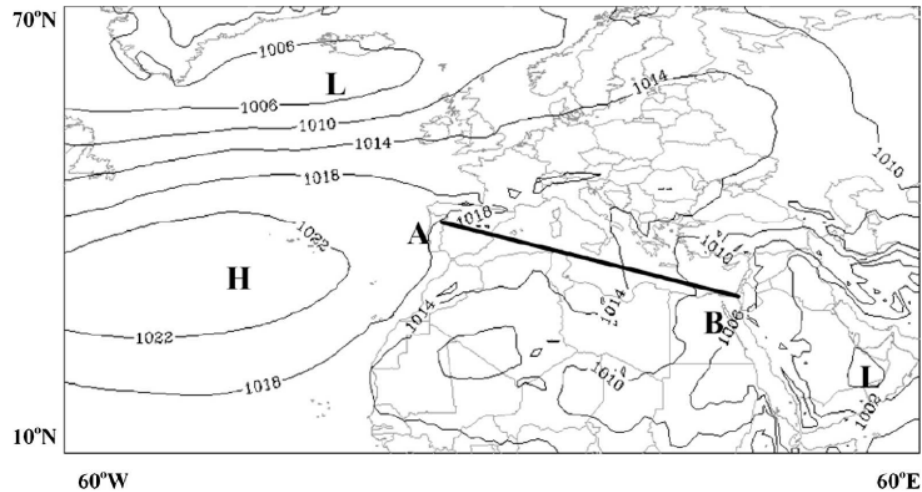


Figure 2.11 Mean monthly sea level pressure for August 2001

The direction of wind is generally from north to south across the Mediterranean region with significant variations in each area during both warm and cold periods. These differences are due to the different heating and cooling pattern of the Mediterranean Sea and southern Europe and North Africa. Variability in landscape and different heating pattern lead to formation of thermal circulation that range from a few hundred meters to a few thousand kilometers (Millan *et al.*1997, 2005).

Kallos *et al.* (2007) have presented information on the height of the mixing layer. In their work, the mixing height was reported as 1-2 km during summer days and 100-1000 m during the winter and transient period for Europe. For the North Africa, the mixing height varies between a few tens of meters during the night and 2-4 km during the day. In contrast to these diurnal variations observed for Europe and North Africa in mixing heights, Mediterranean Sea can be considered as stable in this aspect. The height of mixing layer is approximately 300 m during the diurnal cycle and it slightly changes with the seasonal cycle, around 200-350 m. The presence of islands and peninsulas along the coastal zones of Mediterranean behave as obstacles and chimneys, which lead to sudden

changes in mixing depth. The generated updrafts can inject polluted air masses from the boundary layer to free troposphere.

Karaca *et al.* (2000) have analyzed surface and 500 hPa maps for 15 years and their study has revealed that there are four types of cyclone tracks that influence Turkey. These cyclone tracks were demonstrated in Figure 2.12. The tracks in the Figure 2.12 were assigned with a number of their points of origin from north to south.

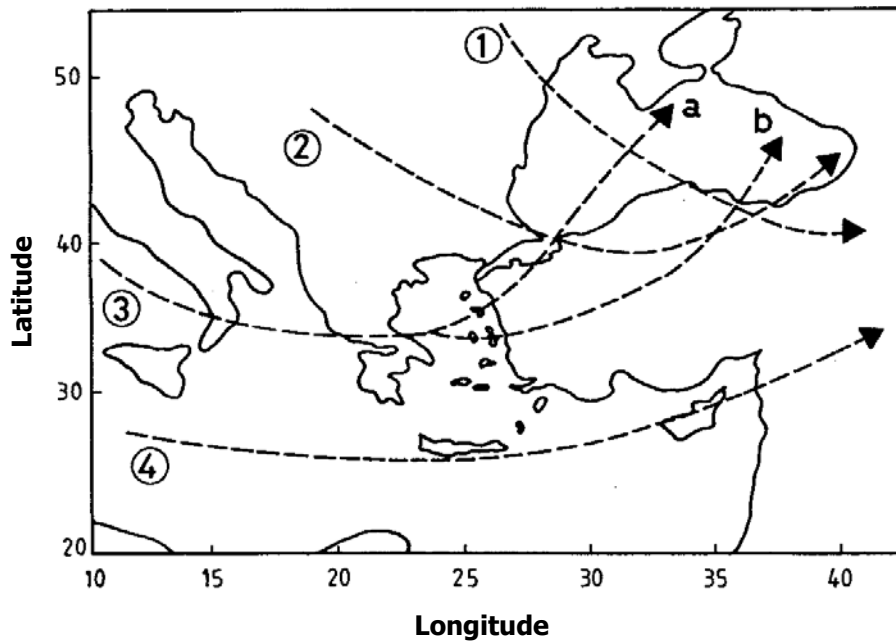


Figure 2.12 The paths of atmospheric cyclones over Turkey

The paths shown in Figure 2.12 can be described as follows:

1. *Path 1* originates from north of Turkey, passes Black Sea and extends towards the southwestern part of Russia
2. *Path 2* starts from Balkans and influence Marmara and Black Sea region, and partly inner parts of Anatolia
3. *Path 3* is produced in Gulf of Genoa and affects Turkey. This path is further split into two at the western part of the Aegean Sea:

- a. *Path a* continues towards the northeast direction and affects northern part of the Aegean sea, whole Marmara region and western and central part of the Black Sea
  - b. *Path b* moves toward the east and influence the western Turkey and middle of Anatolia and then it affects the middle eastern part of Black Sea
4. *Path 4* originates in the middle or western Mediterranean with some cases generated in Gulf of Genoa and with some cases from Sahara and moves towards the Mediterranean. This path influence the counties in Mediterranean like Turkey, Crete, Cyprus and Middle East

## **2.5. BACKGROUND OF RECEPTOR MODELLING**

The development of effective control strategies for particulate matter air pollution needs a broad knowledge of the relative significance of the various sources that contribute to PM concentrations at monitoring sites. In air quality management, there are two types of approaches have been using, namely, source oriented models and receptor oriented models. Source oriented models are generally referred to as dispersion models requires the source information to be run. In some of the sophisticated models, deposition and even chemical transformation mechanisms of pollutants are also taken into account. They are all in computer programs, and user should be aware of the assumptions and constraints used in them. However, these models only give meaningful outputs in case of reliable data available related with the source. Receptor models are developed as alternatives to dispersion models. They are employed to find sources of pollutants and apportion the contributions to the observed concentration at the receptor site.

The receptor modelling is a methodology that based on the conservation of mass principle and used to identify and apportion the sources of airborne particulate matter in the atmosphere (Hopke 1985, 1991). For instance, the total zinc concentration on a specific site can be calculated by taking the contribution of different sources into account. The possible sources of atmospheric zinc are the motor vehicles, incinerators, non-ferrous metal smelters, etc. Therefore, the mass balance equation including the total zinc concentration measured at site can be formulated as follows:

$$Zn_{Total} = Zn_{smelter} + Zn_{auto} + Zn_{incin.} + \dots \quad (2.8)$$

Nevertheless, the smelter not only emits zinc but also other pollutants. For this reason, atmospheric concentration of zinc from the non-ferrous metal smelters in ng/ m<sup>3</sup> ought to be calculated by considering the gravimetric concentration (ng/μg) of zinc in particles emitted from the smelter,  $g_{Zn, smelter}$  and also mass concentration (μg/m<sup>3</sup>) of those particles in the atmosphere,  $f_{smelter}$ . The simple mass balance related with this case is provided below:

$$Zn_{smelter} = g_{Zn, smelter} \cdot f_{smelter} \quad (2.9)$$

The mass balance Equation 2 can be reconstructed in a way that it should consider 'i' chemical species in 'j' samples as contribution from 'p' independent sources. The extended mass balance equation can be written as follows:

$$x_{ij} = \sum_{k=1}^p g_{ik} \cdot f_{kj} + e_{ij} \quad (2.10)$$

Where;

$x_{ij}$  is the elemental concentration of i<sup>th</sup> element in the j<sup>th</sup> sample

$g_{ik}$  is the i<sup>th</sup> element mass fraction from the k<sup>th</sup> source (ng / μg)

$f_{kj}$  is the airborne mass concentration of k<sup>th</sup> source contributing to the j<sup>th</sup> sample (ng /m<sup>3</sup>)

$e_{ij}$  is the residual matrix indicating the error between the measured and predicted concentration of element 'i' from sample 'j'.

Henry (1991) described some major, physical constraints that should be taken in to account while constructing such a model to identify and apportion the sources of airborne particles in a realistic manner:

1. The model must explain the observations; the original data must be reproduced by the model
2. The predicted source compositions must be negative

3. The predicted source contributions can not be negative
4. The sum of the predicted mass fractions should be less than or equal to 1; in other words, it can not be greater than what is determined in the original data

In order to construct such a mass balance equation, large amount of sample should be collected and analyzed for their elemental concentrations. The data, then, can be used to identify and apportion the sources of pollutants in the atmosphere. If number of sources,  $p$ , and composition profile of the source,  $g_{ik}$  are known, then contributions of each source to each sample can be found by using a sort of least square method like Chemical Mass Balance (CMB). However, if only the concentrations of parameters are known then factor analysis methods such as Principal Component Analysis (PCA), and Positive Matrix Factorization (PMF) should be used to identify the number of sources, their mass contribution to sources and their concentration profile.

It may be possible to find the applications of such sort of models in the literature. For example, Schauer *et al.* (1996) has used the organic compounds as tracers in CMB to apportion the sources in California, Plaisance *et al.* (1997) employed PSCF to locate possible sources influencing the chemical composition of precipitation in two rural French sites, Liouy *et al.* (1989) used the trace element data in FA, PCA was used to determine the sources affecting the bulk wet deposition chemistry in Finland (Anttila *et al.*, 1995). Pekney *et al.* (2006) was used UNMIX along with PMF to find the sources of  $PM_{2.5}$  emissions in Pittsburgh. There are many applications of PMF on atmospheric data in the literature (Paateto *et al.*, 2005; Chueinta *et al.*, 2000; Biegalski *et al.*, 2004; Ogulei *et al.*, 2006, etc.).

Enrichment Factors (EF) is also commonly used in the source apportionment studies. In the EF method, the ratio of atmospheric concentrations of elements to a reference element is compared with the same ratios of geological or marine material. Heavy metal enrichments are generally indicating industrial emissions. Potassium enrichment is attributed to cooking or biomass burning. The EF theory was first proposed by the Vinogradov (1959) and then other researchers further evaluated this method such as Turekian and Wedepohl (1961), Taylor (1964), Mason (1966), Gordon *et al.* (1973), Zoller *et al.* (1974), Rahn (1976), Lawson and Winchester (1979a), Reimann and de Caritat (2000) (Watson *et al.*, 2002).

In this study, PSCF and PMF were exploited to identify and apportion the sources that influence the chemical composition of aerosols collected at the sampling site. The detailed information about these methods is provided in the following sub sections.

### **2.5.1. Positive Matrix Factorization (PMF)**

Positive Matrix Factorization (PMF) was first introduced by Paatero and Tapper in 1994 (Paareto and Tapper, 1994). Afterwards, it has been widely applied to apportion the observed concentrations to specific sources in many environmental studies (e.g. Hedberg *et al.*, 2005; Zabalza *et al.*, 2006; Keeler *et al.*, 2006). In this section of the thesis mathematical model of the PMF and associated assumptions are presented.

#### ***2.5.1.1. PMF Mathematics***

Similar to other receptor modelling techniques PMF is based on the mass conservation. Nevertheless, differ from other traditional factor analysis techniques that it does not use correlation matrix in its algorithm. Instead, PMF identifies two matrixes, namely, **G** and **F**. For PMF Equation (2.10) is modified and written in matrix form as:

$$X = G \bullet F + E \tag{2.11}$$

Where;

**X** is a  $i \times j$  concentration matrix of  $i$  species in  $j$  samples

**E** is the residual matrix with the same dimension of  $X$

**G** is the  $i \times k$  source contribution matrix and

**F** is a  $k \times j$  sources composition profile matrix of the  $k$  sources (Johnson *et al.*, 2006; Paatero *et al.*, 2005).

Three years later Paatero (1997) introduced PMF2, a revised version of PMF. PMF2 handles two dimensional arrays. In addition to PMF2, it is possible to find the applications of PMF3, handles with three dimensional arrays, in the literature (e.g., Polissar *et al.*, 1999; Hopke *et al.*, 1998). However, PMF2 is used in this study and described herein.

As a summary, **G** matrix represents information about source contributions (time variation trends), **F** matrix describes source profiles (source chemical compositions) and **E** reveals the portion of data variance unexplained by the p factor model.

The residual matrix, **E**, in Equation 2.11 can be defined as:

$$E_{ij} = X_{ij} - \hat{X} = X_{ij} - \sum_{k=1}^p G_{ik} \cdot F_{kj} \quad (2.12)$$

Where;

i=1,.....,m elements  
 J=1,....., n samples

An objective function, **Q**, can be defined and task of PMF is to minimize **Q** as a function of **G** and **F**;

$$Q = \sum_{i=1}^n \sum_{j=1}^m \left( \frac{E_{ij}}{s_{ij}} \right)^2 \quad (2.13)$$

Where  $s_{ij}$  is an estimate of the “uncertainty” in the  $i^{\text{th}}$  variable measured in the  $j^{\text{th}}$  sample. While doing this job, PMF has subjected to two important constraints, which were previously mentioned in this section, which denote the physically meaningful conditions that sources can not have negative species concentration (i.e.,  $f_{ij} \geq 0$ ) and samples can not have negative contribution (i.e.,  $g_{ik} \geq 0$ ). The Equation 2.13 is solved by trial and error procedure in which **G** and **F** vary simultaneously at each iteration step as described by Paatero (1997).

#### **2.5.1.1.1. Residual Matrix, E**

Matrix **E** (Equation 2.13) stands for the overall error, which includes both measurement and modelling error. Modelling error is corresponding to error at which mathematical model fails to explain what exactly is nature doing. Analytical error forms the largest

portion of the residual matrix E, but other potential causes of this deviation can be listed as follows:

- Variation in the source profile
- Change of the soil composition with the geography, different winds transport different soil to the receptor site
- Pollutants undergo chemical transformation
- Traffic density and associated emissions show variation with time
- Laboratory systematic and random errors

#### ***2.5.1.1.2. Estimation of Number of Factors***

The number of factors should be entered to the model by the user. There is no rule of thumb related with the selection of the number of factors, however, Q value is a good parameter to obtain the optimum number of factors in the PMF.

If uncertainties truly characterize the data, and every point is perfectly modeled, then the calculated **Q** by this method should be equal to number of species multiplied by the number of samples minus number of factors multiplied by number of species. The modeled **Q** value can deviate 50 % from the calculated **Q** in order to obtain a reasonable fit of all observations (Buzcu-Guven et al., 2007).

#### ***2.5.1.1.3. Factor Rotations***

The objective function can be solved in the PMF, successfully, but it does not necessarily imply that it generates unique solution. In addition, the natural physical constraints described by Henry (1991) previously in this section should be satisfied. However, these constraints can be satisfied in ore than one solution, in that case, external constraints, such as rorations, should be applied in order to have unique solution. Linear transformation is also known as rotations and can be described in PMF as follows:

$$X = GTT^{-1}F \tag{2.14}$$

Where T= transformation matrix



A parameter called as  $F_{\text{peak}}$  is used in the PMF to control the rotations. It is used in trial and error by the user. Positive  $F_{\text{peak}}$  values subtract rows from  $\mathbf{F}$  and add column to  $\mathbf{G}$ , while negative values do the opposite, and therefore result in generating more physically realistic solutions.

Experience gained by the application of PMF on the real data set has revealed that non-zero  $F_{\text{peak}}$  values generally yield more realistic results. Although there is no generally accepted rule of choosing  $F_{\text{peak}}$  value, the analyst can make decisions by carefully examining the  $\mathbf{Q}$  value. Typically highest  $F_{\text{peak}}$  value before significant increase in the  $\mathbf{Q}$  value yields more physically interpretable results (Hopke, 1999).

#### **2.5.1.1.4. Robust Mode**

PMF has a robust mode through which it can handle with outliers observed in the data set. Paatero (2000) proposed a robust application of the model to handle extreme values and outliers in the data set and to reduce their influence on the fitted results. In such an application, a measured value  $x_{ij}$  is assumed as an outlier if:

$$(x_{ij} - \sum_{k=1}^p a_{ik} \cdot f_{kj}) / s_{ij} > \alpha \quad (2.15)$$

The  $\alpha$  is called as "outlier distance" and it can take the value of 2, 4, and 8 (Paatero, 2000). PMF has a default value of 4 for the outlier distance and it was generally used in many applications of PMF (Begum *et al.*, 2005; Hedberg *et al.*, 2005; Buzcu *et al.*, 2003; Pekney *et al.*, 2006).

#### **2.5.1.1.5. Uncertainty Estimation, $\sigma_{ij}$ , and Treatment of BDL and Missing Data Values**

One of the most significant advantages of PMF is to allow user to adjust the influence of data point by weighting them individually based on their confidence, which enables using missing or below detection limit (BDL) data with related uncertainty adjusted so that these data points are given less weight in the model results. Different methodology used

in the literature in substituting the BDL and missing values and their associated uncertainties. Table 2.3 shows some example studies reported in recent years.

Polissar *et al.* (1998) suggested following treatment of missing and below detection limit values and associated error estimation:

$$\begin{array}{lll}
 x_{ij} = v_{ij} & \text{For determined values} & \sigma_{ij} = u_{ij} + d_{ij} / 3 \\
 x_{ij} = \bar{d}_{ij} / 2 & \text{For below limit of detection values} & \sigma_{ij} = \bar{d}_{ij} / 2 + d_{ij} / 3 \\
 x_{ij} = \bar{v}_{ij} & \text{For missing values} & \sigma_{ij} = 4\bar{v}_{ij}
 \end{array} \tag{2.16}$$

Where  $v_{ij}$ ,  $u_{ij}$ ,  $d_{ij}$  are measured concentration, analytical uncertainty, and the method detection limit, respectively. In addition,  $\bar{d}_{ij}$  and  $\bar{v}_{ij}$  are the arithmetic mean of the detection limit values and geometric mean of the measured concentrations, respectively.

Alternatively, the error estimates,  $s_{ij}$ , for each data point can be estimated based on the measured concentration and associated uncertainty of the data,  $\sigma_{ij}$ . The  $s_{ij}$  values could be determined according to Equation 2.17 below as recommended by Paatero (2000) for general purpose environmental data.

$$s_{ij} = \sigma_{ij} + C_3 \max_{i,j} \left( x_{ij} \cdot \sum_{k=1}^p g_{ik} \cdot f_{kj} \right) \tag{2.17}$$

In this equation  $C_3$  is a user defined dimensionless parameter between 0.1 and 0.2, and the larger of the measured or fitted values are taken which prevents generating too small standard deviation values. Besides this, producing larger error estimates results in reducing  $Q$  value in accordance with Equation 6.

Reff *et al.* (2007) reported other methods of calculating uncertainties for PMF analysis of particulate matter data available in the literature.

Table 2.3 Examples of input data pretreatment for PMF in literature

Reference	BDL Data	Missing Data	BDL Data $\sigma$	Missing Data $\sigma$
Poirot <i>et al.</i> , 2001; Pollissar <i>et al.</i> , 2001	DLx0.5	Median Concentration	1.5x DL	4xMedian Concentration
Antilla <i>et al.</i> , 1995		Mean Concentration	DL	DL
Song <i>et al.</i> , 2001	DLx0.5	Geometric Mean	DL	4xGeometric Mean
Begum <i>et al.</i> , 2005; Xie and Berkowitz, 2006	DLx0.5	Geometric Mean	5/6x DL	4xGeometric Mean
Brown <i>et al.</i> , 2007	DLx0.5	Median Concentration	1.5x DL	4xMedian Concentration
Chung <i>et al.</i> , 2006	DLx0.5	Geometric Mean	DL	4xGeometric Mean
Chueinta <i>et al.</i> , 2000	DLx0.5	Mean Concentration	DLx0.5	

### 2.5.1.2. Output Files of PMF Analysis

There are three output files that PMF yields, which are, **F factor**, **G factor** and **MISC**. The values in these files are used to interpret the model. In this section these parameters will be explained.

- **F Factor:**

The resolved **F** factor gives information about the source composition. By analyzing the **F** factor values, the identified factors are designated to emission sources.

- **G Factor:**

**G** factor represents the source strength (concentration). The created scatter plots of **G** matrix for different sources are known as **G** space plotting. **G** space plotting helps to identify the edges that show the factors that are independent from each other, thereby reducing the rotational freedom. If there are unrealistic rotations in the solution, then oblique edges will present in the solution, which act as a diagnostic tool indicating that PMF should be modified by adjusting **F<sub>peak</sub>** or other parameters of PMF until the edges aligned with the coordinate axes.

- **MISC:**

There are two important tools present within this file, which are Scaled Residuals and Explained Variation (**EV**) values. Both of these tools are used to interpret the PMF results.

### **2.5.1.3. Mass Apportionment-Scaling Factor**

**F** matrix and **G** matrix are obtained as output files after performing the PMF model calculations. Nevertheless, the numbers are in an arbitrary unit. In order to convert the units the corresponding units of  $x_{ij}$ , a "l" can be introduced into the Equation (2.10) by neglecting the residual matrix  $e_{ij}$ ,

Where,  $l = s_k / s_k$

$$x_{ij} = \sum_{k=1}^p g_{ik} \cdot f_{kj} = \sum_{k=1}^p \left( \frac{g_{ik}}{s_k} \right) \cdot (f_{kj} \cdot s_k) = \sum_{k=1}^p g'_{ik} \cdot f'_{kj} \quad (2.18)$$

The scaling factor **s<sub>k</sub>** is determined by applying multi-linear regression technique on the measured mass (**m<sub>i</sub>**), and regress against the estimated source contribution values as given in Equation (2.19). After the **s<sub>k</sub>** values are obtained, they are applied to **F** and **G** matrices.

$$Mass = m_i = \sum_{k=1}^p g_{ik} \cdot s_k \quad (2.19)$$

#### 2.5.1.4. Explained Variation, $EV_{kj}$

The **EV** is a measure of contribution of each parameter in each source and it is generally used for the qualitative identification of sources. The **EV** value can range from 0 to 1, i.e., from not explaining anything to explaining all of the variance (Hedberg et al., 2005). For example, high **EV** value of vanadium in one factor revealed that this factor corresponding to oil combustion or a factor that explains great proportion (i.e., high **EV** values) of alkenes can be identified as a petrochemical emission source.

The **EV** is defined by Paatero (2000) as:

$$EV_{kj} = \frac{\sum_{i=1}^n |g_{ik} \cdot f_{kj}| / s_{ij}}{\sum_{i=1}^n (\sum_{h=1}^p |g_{ih} \cdot f_{hj}| + |e_{ij}|) / s_{ij}} \quad \text{for } k = 1, \dots, p, \quad (2.20)$$

$$EV_{kj} = \frac{\sum_{i=1}^n |e_{ij}| / s_{ij}}{\sum_{i=1}^n (\sum_{h=1}^p |g_{ih} \cdot f_{hj}| + |e_{ij}|) / s_{ij}} \quad \text{for } k = p + 1 \quad (2.21)$$

Where the (p+1) factor is the unexplained residual.

#### 2.5.1.5. Uniqueness of the Solution

There is no general accepted way to determine the correct number of factors in PMF analysis. The user must select the maximum number of factors that adequately explain in the PM mass, and solutions with duplicate factors or factors with unrealistic composition and contribution must be excluded. For doing this, user should have knowledge about the source types around the sampling station and also about the quality of the data. The

analyst must observe, however, some of the parameters like **Q** value, the distribution of scaled residuals, and also scaling factors from the regression to ensure the good fit of the model results.

The **Q** value is an indicator of goodness of fit and measure of how the modeled values are close to observed ones. If the uncertainties associated with each data point truly represent the uncertainty in the data, then **Q** should be equal to number of data points in the concentration data set.

If uncertainties truly characterize the data, and every point is perfectly modeled, then the calculated **Q** by this method should be equal to number of species multiplied by the number of samples minus number of factors multiplied by number of species. The modeled **Q** value can deviate 50 % from the calculated **Q** in order to obtain a reasonable fit of all observations (Buzcu-Guven et al., 2007).

In addition to **Q** value, the distribution of scaled residuals can be used as a diagnostic tool whether the obtained number of factors truly represents the real case. Ideally, the residuals should be centered around zero and they should have a sharp peak at zero (Anderson *et al.* 2001). It is desirable to have all residuals within  $\pm 3$  standard deviations (Xie *et al.*, 2006; Brown *et al.*, 2007). If distribution of residuals exceeded this criterion, then number of factors identified by the PMF should be reexamined.

The resolved **F** factor by the PMF does not give the absolute source composition and has subjected to a scaling constant,  $s_k$ , that is given in Equation 2.22:

$$x_{ij} = \sum_{k=1}^p g_{ik} \cdot f_{kj} = \sum_{k=1}^p \left( \frac{g_{ik}}{s_k} \right) \cdot (f_{kj} \cdot s_k) = \sum_{k=1}^p g'_{ik} \cdot f'_{kj} \quad (2.22)$$

The measured mass of the constituents analyzed is regressed against the source contribution factors from the PMF subjected to the constraint that scaling constants had to be non-negative (Xie et al., 2006). A regression that produces a negative scaling constant means that the number of factors identified by the PMF was incorrect.

## **2.5.2. Potential Source Contribution Function (PSCF) Analysis**

### ***2.5.2.1. Trajectory Analysis***

A trajectory can be defined as the path of infinitesimally small particles of air as they move through the space and time. The trajectory can either be tracked backward in time from prescribed positions at some initial time (backward trajectories), or can be tracked forward in time from prescribed positions at some initial time (forward trajectories). In other words, backward trajectory indicates the past path of particle while forward trajectory means future path of the particle. Atmospheric trajectory models combine meteorological information with mathematical equations to simulate transport in the atmosphere. Generally, the location of the air masses are computed based on meteorological data like pressure, temperature, humidity, wind speed and direction. In environmental science, trajectories are utilized to establish source-receptor relationship of pollutants.

To determine the possible source regions that influence the chemical composition of the aerosol particles collected at the sampling site air mass backward trajectories were calculated using the HYSPLIT (HYbrid Single-Particle Lagrangian Integrated Trajectory) Version 4.0 model, which is an online service developed by the National Oceanic and Atmospheric Administration (NOAA) Air Resources Laboratory (ARL) (Draxler, R.R. and Rolph, G.D., 2003; Rolph, G.D., 2003). The air parcel movement was described by segment endpoints coordinates in terms of latitude and longitude of each point. The backward trajectories were 5-day long, and they were requested at three different altitudes, namely, 100, 500 and 1500 m above the ground level. Isentropic vertical motion was selected and trajectories were computed for every day at 14 UTC. Rainfall was selected as dump meteorological data along the trajectory. The computations were conducted at the NOAA web site (<http://www.arl.noaa.gov/hysplitarc-bin/traj1arc.pl>) using the archived meteorological data set (REANALYSIS).

### ***2.5.2.2. Potential Source Contribution Function (PSCF)***

Ashbaugh *et al.* (1985) and Malm *et al.* (1986) were originally discovered the Potential Source Contribution Function method in their analysis of particulate composition data

from the measurements conducted near the Grand Canyon. As a result of their study, they accomplished to relate different source types to probable locations in the Western United States.

The structure of the PSCF can be described as follows: If a trajectory endpoint falling in the grid cell  $(i,j)$ , the trajectory is assumed to collect material emitted in the cell. Once aerosol is incorporated into air parcel, it can be transported along the trajectory to the receptor site. There are some assumptions to be kept in mind at this point: (1) The aerosols incorporated into the air parcel do not go into the chemical transformation, (2) The aerosols incorporated into the air parcel are not lost through diffusion, (3) The aerosols, incorporated into the air parcel, are not affected by atmospheric scavenging processes.

The aim is to construct a probability field proposing likely source locations of the material that gives rise to high measured values at the receptor site.

If  $n_{ij}$  is the total number of endpoints that fall in the cell, then the cumulative probability of these endpoints,  $P[A_{ij}]$ , can be given by:

$$P[A_{ij}] = \frac{n_{ij}}{N} \quad (2.23)$$

Where 'N' is the total number of endpoints summarized over all cells in the modeling region. The probability  $P[A_{ij}]$  describes the potential for transport of material from a grid cell to the receptor site. Among the  $n_{ij}$  counts, there will be  $m_{ij}$  points for which the measured aerosol parameter exceeds a threshold value selected for this parameter. The probability that cell  $(i,j)$  is related to the observed high concentrations,  $B_{ij}$ , can be defined as:

$$P[B_{ij}] = \frac{m_{ij}}{N} \quad (2.24)$$

The conditional probability, the PSCF, can then be defined as:



$$PSCF_{ij} = P[B_{ij}/A_{ij}] = \frac{m_{ij}}{n_{ij}} \quad (2.25)$$

(Plaisance *et al.*, 1997)

Therefore, PSCF can be thought as a conditional probability defining the spatial distribution of likely geographical source locations from where pollutant under consideration arriving to the receptor area and causing high concentration over there. In other words, cells related to the high values of PSCF values are the potential areas affecting the pollution load of the receptor site.

However, one should be careful while using PSCF method in this from since small numbers of  $n_{ij}$  can result in the high PSCF value. For instance, it is possible to have a PSCF value of one when only one trajectory segment endpoint fall into that cell, which in turn can misspecify the potential areas that lead to high concentration of pollutants in the receptor site.

In order to minimize the artifact of obtaining high PSCF value completely by chance Vasconcelos *et al.* (1996b) proposed a statistical approach, in which the null hypothesis was tested against that there is no relation between the concentrations and trajectories. Afterwards, Wehrens *et al.* (2000) developed a non-parametric bootstrap method to test the statistical significance of the spatial distribution of the PSCF value. There are two assumptions in the application of this method: (1) the concentration values are independent, (2) they are identically distributed (Lupu and Maenhaut, 2002). In this method, a trajectory is randomly removed from the cluster of trajectories and its relation with a sample whose concentration for the species of concern is above the predefined value. If the correlation of this trajectory with the observed high concentration at the sampling site is strong, then this trajectory is counted in both  $m_{ij}$  and  $n_{ij}$ . Otherwise, the  $n_{ij}$  is incremented but  $m_{ij}$  remains constant (Hopke *et al.*, 1995). Then the PSCF values calculated for each of the grid cells are sorted. Let the number of iterations as B and the significance level as  $\beta$ . If

$$P_{ij} \geq P_{\left( (B+1) \left( 1 - \frac{\beta}{2} \right) \right)_{ij}}^* \quad (2.26)$$

the null hypothesis is rejected at  $(1-\beta)100\%$  confidence level. Then, for the rest of the analysis only PSCF values satisfying the above relation are retained (Lupu and Maenhaut, 2002).

The value of PSCF ranges between 0 and 1. Any grid cell having PSCF of 0 is unlikely to be the source region, while the opposite is true for the PSCF of 1.

The region of interest covers the area between 20°W and 60°E longitude in east-west direction (starts from west of the UK at west and extends to east of the Caspian Sea at east) and between 75°N and 15°N latitudes in north-south direction (starts from the middle of the Siberia at north extends almost to the equator at south). The whole study area was divided into 1°x1° grids resulting in the total of 4800 grids.

## **2.6. DISTRIBUTION CHARACTERISTICS OF THE ATMOSPHERIC VARIABLES**

Due to their dependence on the fluctuations of meteorological and source emission variables, concentrations of air pollutants are inherently random variables. Accordingly, atmospheric concentrations could be described by a probability density function or a frequency distribution. The frequency distributions of the measured air pollutants can be useful for modelling studies that are generally to be used to develop control strategies for the pollutants. They enable the estimation of the frequency of exceedence of a threshold concentration (Cheng *et al.*, 1991, and references therein; Lu and Fang, 2002; Karaca *et al.*, 2005).

There are many types of probability distribution functions (PDFs) that have been used to fit air pollution concentration data. Many PDFs such as logistic, log-normal, Weibul, type V Pearson and gamma distribution are used in several studies (Lu and Fang, 2002; Karaca *et al.*, 2005; Seinfeld and Pandis, 1998; Lu, 2002).

It is largely agreed that there is no reason to expect that atmospheric concentrations should conform to a specific probability distribution though there has been debates on what probability distribution is optimum in representing atmospheric concentrations from a physical point of view. The type of distribution that should best fit the atmospheric data depends on many factors including the type of the pollutant, the time period of interest,

the averaging time of data, the location, and other factors (Georgopoulos and Seinfeld, 1982). For example, Bencala and Seinfeld (1976) claimed that observed data is generally represented as log-normal, although other common statistical distributions are also capable of representing data as well as or better than the log-normal. They put forward also that the log-normal is convenient because mean and variance can be easily determined from the log probability plot of the data. While the basic question of why concentration data approximately log normal can not be answered completely clear, Bencala and Seinfeld (1976) suggested that it is related with the log normal distribution of wind speed.

Ott and Mage (1976) utilized the diffusion equation to show that the concentrations of air pollutants should fit to the three parameter log-normal distribution. Ott (1990) gave the physical explanation to why log-normal distribution fits the atmospheric concentration data as the successive random dilution of pollutants in the atmosphere. Ott also suggested that as the number of dilution that the atmospheric pollutant undergoes increases the associated variance also increases (Rumburg *et al.*, 2001). Furthermore, it was also suggested that deviations from the log-normal distribution is due to the sampling errors (deNevers, 1979). Kao and Friedlander (1994, 1995) claimed that the width of the geometric standard deviation of the fitted distribution increased with the reactivity of the aerosol component.

A two parameter log-normal distribution function has the following form (Cheng *et al.*, 1991):

$$f(x) = \frac{x}{\sqrt{2\pi \ln \sigma_g}} \exp \left[ \frac{-\left(\ln x - \ln \bar{x}_g\right)^2}{2(\ln \sigma_g)^2} \right] \quad (2.27)$$

For concentration,  $x$ , larger than zero, where;

$x$  = concentration of a chemical species in  $\text{ngm}^{-3}$

$\bar{x}_g$  = the geometric mean of the distribution

$\sigma_g$  = the geometric standard deviation of the distribution

The Kolmogorov –Smirnov (K-S DN or DN) is commonly used to test the goodness of fit of data to a log normal distribution. The K-S one sample test includes the whole distribution of the examined variable, not just its central value, and compares the empirical distribution function to that of the hypothesized distribution. The maximum absolute distance between the data and hypothesized distribution is calculated to test the conformance of the two cumulative distribution functions in the case of log-normal distribution.

A value of ALPHA is used to represent the observed significance level for the Kolmogorov-Smirnov DN statistics. The function that was used to calculate the significance of any non-zero values of DN can be written as the following sum (von Mises, 1964):

$$\xi(\lambda) = 2 \sum_{j=1}^{\infty} (-1)^{j-1} \exp(-2j^2 \lambda^2) \quad (2.28)$$

Equation 28 is a monotonic function with limiting values,  $\xi(0) = 1$  and  $\xi(\infty) = 0$ . In terms of Equation (28), the significance level of an observed value of DN, that is, ALPHA, a disproof of the null hypothesis that the distribution is log normal, is given approximately by:

$$ALPHA = \left( \sqrt{N} + 0.12 + \frac{0.11}{\sqrt{N}} \right) \bullet DN \quad (2.29)$$

Equation 2.29 becomes asymptotically accurate as N becomes large. In practice, an N of 20 is large enough for a high significance level of value of 0.01 or smaller (Cheng *et al.*, 1991). The sample size for each measured aerosol variable in this study is greater than 600 enabling enough degrees of freedom to use the DN statistics. For samples greater than 35, the critical value for 95 % confidence limit is given approximately by  $1.36 / \sqrt{N}$ , where N is the sample number (Massey, F.J., 1951). If the computed KS-DN value is less than the critical value calculated for 95 % significance level, one fails to reject the null hypothesis that the distribution of the variable under consideration is not different from the log-normal distribution. Alternatively, one can compare the ALPHA value with the

1.36 for 95 % significance level, the variable accepted to fit log-normal distribution if ALPHA is less than 1.36.

Skewness Index (SI) and Kurtosis are other parameters evaluated herein to investigate the distribution characteristics of atmospheric data. Von Mises (1964) defined the SI as:

$$SI = \frac{n \sum_{i=1}^n (x_i - \bar{x})^3}{(n-1)(n-2)\sigma^3} \quad (2.30)$$

Where  $x_i$  is the concentration of atmospheric species,  $\bar{x}$  is the arithmetic mean of the distribution,  $\sigma$  is the standard deviation of the distribution and  $n$  represent the number of samples for the variable of concern. The positive numbers of SI indicates that tail of the distribution extends out toward the right end, while the reverse is true for the negative SI values.

Kurtosis is a value used to measure the flatness or steepness of a curve with respect to a distribution (Statgraphics Plus User Manual, 1994-1997). Kurtosis allows direct comparison of the tail behaviour and peakedness of a distribution with respect to that of Gaussian or normal distribution. Kurtosis measures the deviation from normality based on the frequency of values either near the mean or far from it relative to the values at an intermediate distance from the mean (Johnson and Kotz, 1985; Cheng *et al.*, 1991). For a normal distribution, Kurtosis coefficient is 0. When the coefficient is less than 0, the curve is flat with short tails. When the coefficient is greater than 0, the curve is either very steep at the center or relatively long tails.

## CHAPTER 3

### EXPERIMENTAL METHODS

#### 3.1. SAMPLING SITE DESCRIPTION

The samples evaluated in this study were collected at Antalya (30°34'30.54" E, 36°47'30.54"N) on the Mediterranean coast of Turkey. The sampling station was located approximately 20 km to the west from the town of Antalya, which is the nearest population center. The location of the sampling site is presented in Figure 3.1.

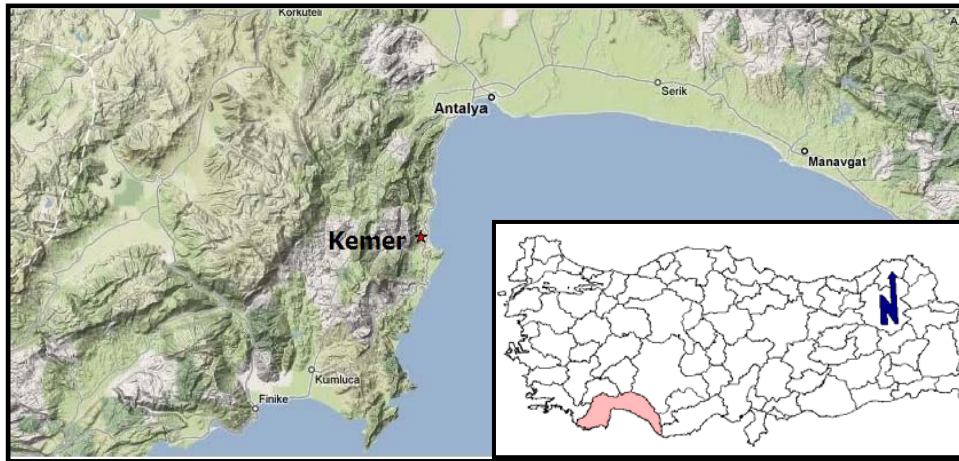


Figure 3.1 Place of the Antalya Station

Having a clean sea environment, 640 km coastal zone, local topography, ancient sites, and a mild climate, Antalya is the capital of tourism activities and has virtually no air polluting industries. After visiting various places, this place was decided as a sampling site because power necessary for the sampling equipment is readily available throughout the sampling campaign, and also, it is protected by the Ministry of Environment and Forestry.

Larsen *et al.* (1999) categorized the sampling sites with respect to the distance between the sites and major emitters close to the site. According to this criterion, *natural background sites* should be placed at least 50 km away from the large pollution sources. In case of *rural background station* this distance should be between 10 and 50 km. *The near city background stations* should be placed 3-10 km away from the large pollution sources. The intensity of the traffic should be less than 2500 vehicle / day in order to classify a site as an *urban background station*. Putuad *et al.* (2004) has added one more category to this classification. They called the stations within the street canyons as *kerbside*. According to these definitions, Antalya station can be classified as a "Rural Background" station because the nearest pollution source, the city of Antalya, is 20 km away. Instruments were housed in a field laboratory mounted on a 4 m x 4 m concrete platform located on a rock structure 20 m above sea level. The platform was surrounded by a 2 m height fence, which was covered by polyethylene wiring in order to prevent the contamination of samples by the corrosion of metals. A wet only precipitation sampler, a wet and dry deposition sampler, a High volume Sampler and High Volume impactor were fixed to the concrete base of the platform. The required power for the equipments was provided from the field laboratory directly as no sockets were placed on the platform to avoid the short circuiting due to sea spray. Pictures of the sampling platform are shown in Figure 3.2.



Figure 3.2 The platform onto which Hi-Vol sampler anchored

The field laboratory consists of a container (3 m x 2 m x 2 m) and contained a storage area, a refrigerator to preserve the samples prior to shipment to Ankara and an area to change the sampling substrates. This area reserved for sample change contained a table covered with polyethylene sheet and 50 cm x 50 cm plexiglass plate which was wiped with a damp tissue paper and then with a dry tissue paper before sample handling. The plate was covered by polyethylene sheet when not in use. All the necessary measures were taken to prevent sample contamination throughout the campaign.

The sampling station was put into operation in January 1992 and continued to operate until April 2001.

### 3.2. PM-10 HIGH VOLUME AIR SAMPLER

Air samples were collected with a SIERRA-ANDERSEN Model SAUV-10H PM<sub>10</sub> High Volume Air Sampler. The specifications of the sampler were summarized in Table 3.1.

Table 3.1 Performance Specifications for PM-10 Sampler

Parameter	Specifications
Flowrate	1.35 m <sup>3</sup> /min
Flowrate stability	Over 24 hours, average flowrate within ± 5 % of initial
Filter media	20 cm x 28 cm Whatman 41 cellulose filter
Inlet collection efficiency	The inlet has a cut-point of 9.7 ± 0.5 µm over a wind speed of 0 to 36 kmh <sup>-1</sup>

The typical high volume system, which is generally called as hi-vol, with shelter to protect the filter from the rain was illustrated in Figure 3.3. In this system air is drawn through the filter at a flowrate of 1.1–1.7 m<sup>3</sup> min<sup>-1</sup>, resulting in the collection of particles larger than 0.3 µm with nearly 100 % efficiency (Finlayson Pitts and Pitts, 1986).



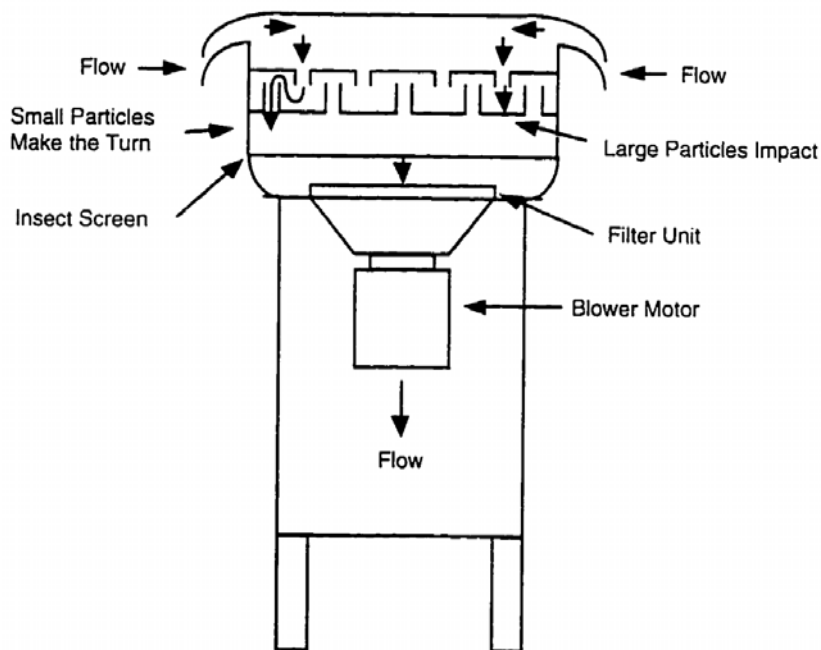


Figure 3.3 Schematic of High Volume Sampler

The sampler was equipped with an inlet impactor to exclude particles with aerodynamic diameter greater than  $10\ \mu\text{m}$ . The impaction surface on the sampler was greased to reduce large particle reentrainment. Only the particles pass through the pre-impactor are collected by the filter.

The ventilation of sample exhaust is necessary if brushless motor is employed in the sampler. Sample contamination, especially with Cu, might be possible if motor exhaust find its way to the sample inlet.

The volumetric flowrate was controlled by a venturi device. The venturi meter is operated in such a way that when the air attains sonic velocity in the throat of the device, a sound pressure barrier which is designed not to allow more air through under the existing temperature and pressure conditions. This system is not affected by the downstream conditions such as motor speed and exit pressure, however, it strongly depends on the upstream conditions, for example, stagnation pressure ratio and temperature. In this system, there is no moving means or electronic parts to control the flowrate. The

engineer designed nozzle, which is the orifice in the flow controller, is functioned as reacting to a specific pressure ratio expressed in absolute term. The total volume of air sampled was calculated by multiplying the air flowrate with the sampling duration. Air concentrations were obtained by dividing the mass deposited on the filter to the total volume of air passed through the filter.

### 3.2.1. High Volume Sampler Calibration

The calibration kit was used to calibrate the sampler each month. A blank filter was taken after each calibration. The calibration involves the correlating the measured flow rate through the high volume sampler with the flow reading on the high volume sampler chart recorder. Figure 3.4 illustrates the result of a sample calibration.

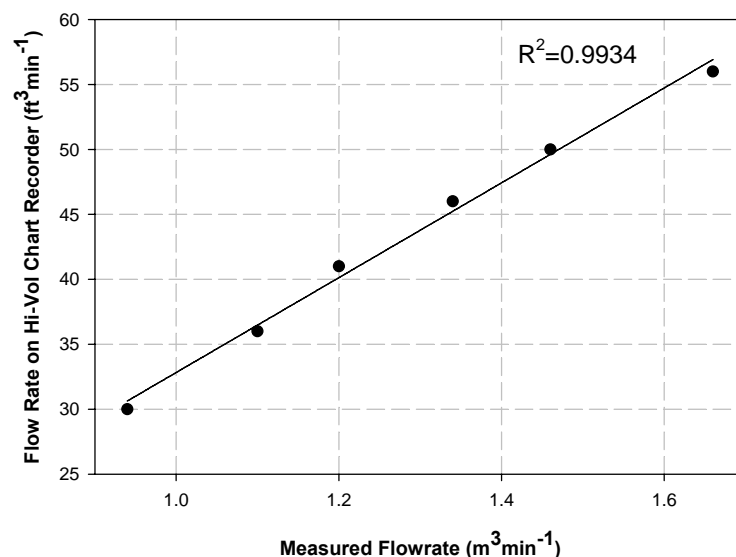


Figure 3.4 High Volume sampler calibration plot at Antalya station on 19.08.1993

The flowrate during the sampling was tried to keep around 1.35 m³min⁻¹. The difference between the flows calculated using the calibrated flow charts and gas meter was always less than 5 %. The high volume chart recorder was checked at the beginning of every sample collection to make sure that its value was the calibrated value. Flowrate should be

controlled regularly to insure proper sample collection. Inappropriate filter installation or the need for sample maintenance could be the reason of irregular flow readings.

### **3.2.2. Aerosol Filter Selection**

Whatman 41 was selected as suitable substrate to collect aerosol samples in this study. Whatman 41 filter is fibrous filter made of cellulose, the corresponding chemical formula is  $(C_6H_{10}O_5)_n$ , has a density of  $8.7 \text{ mg cm}^{-2}$  and its filter efficiency is 58 % at  $0.3 \text{ }\mu\text{m}$  particle size. The small pressure drop and good mechanical strength are the major advantages of this kind of filter. It is possible to find them in suitable size in the market that fits the high volume sampler. The impaction, interception, sedimentation, electrostatic attraction and diffusion are the main mechanisms that make possible the collection of particles onto the filter media. Impaction is the key route at larger particle diameter and high flows while collection by diffusion to the surface is efficient at smaller diameters and flows. The low filtration efficiencies for sub-micrometer particles, their sensitivity to moisture and a large variance in the concentration of certain elements, which is especially important for blank determination, are the typical disadvantages of Whatman-41 filter. In addition to this, they are made of carbon based material, which makes them inappropriate for carbon analysis (Biegalski *et al.*, 1998; Finlayson Pitts and Pitts, 1986; Chow, 1995; EPA/625/R-96/010a, 1999).

Photographs of the several samples were taken by means of Scanning Electron Microscopy (SEM) and they are provided in the Figure 3.5. From Figure 3.5, it can be easily seen that aerosol particles completely penetrated in the filter material, which is a major drawback of the Whatman filter in case it is analyzed by the surface technique such as Energy Dispersive X-Ray Fluorescence (EDXRF) technique.

### **3.3. SAMPLE HANDLING**

Samples were changed at 10:00 am every day by a crew working for the Ministry of Environment and Forestry. Before removing the exposed filter, the power of the sampler was turned off, and the flow appearing on the dry-gasmeter was recorded. The filter cassette was put into the polyethylene bag and transferred to the field laboratory. In field laboratory, the filter was removed from the cassette on the pre-cleaned plexiglass plate

and was transferred to acid washed polyethylene bags and heat sealed. A Sample ID was written on this polyethylene sheet with non-vanishing ink. Then, filter bag and the corresponding sampling information log sheet, including sample ID, date of sampling, recorded flow, temperature and precipitation events, were placed into another clean polyethylene bag and again heat sealed and stored in the 4 °C refrigerator until they were sent to the Laboratory in the Environmental Engineering Department of Middle East Technical University. The unloaded filter cassette was wiped with a damp tissue paper and unused filter was replaced on it, the filter cassette was put into a clean polyethylene bag and carried to the sampling platform. Using flow controller chart recorder, the air flow through the filter was determined and recorded to the sampler information sheet which was prepared for each sample. The indicator reading on flow dry-gas meter was also recorded. Blank filters were treated as samples except that air was drawn them for only one minute. Samples and blanks were sent to Ankara approximately once each month.

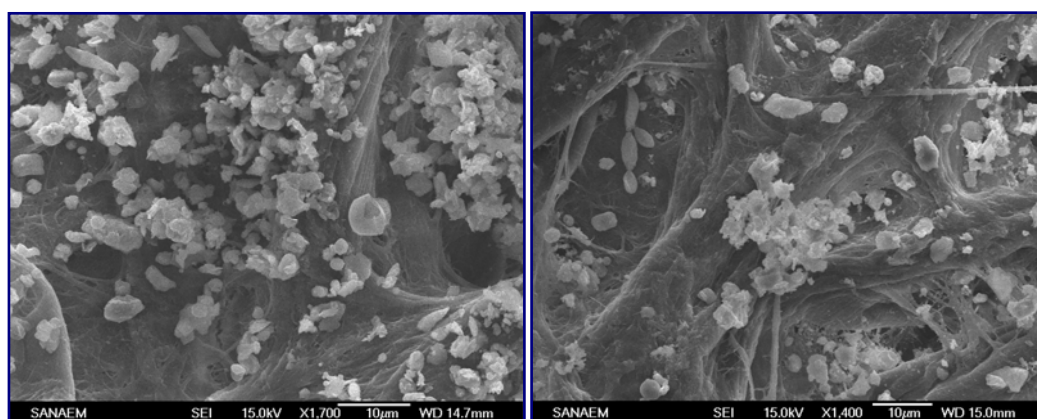


Figure 3.5. SEM photos of aerosols collected on Whatman 41 filter

All the plastic equipment was rinsed with the 10 % reagent grade  $\text{HNO}_3$  and then, washed with deionized water. Plastic tweezers were used to perform throughout the sample loading and uploading procedures. Powder free gloves were used to avoid the contamination of samples with zinc.

Class 100 Clean Room was used for sample handling processes in the Environmental Engineering Department of Middle East Technical University, Ankara, where particle number concentrations are approximately 50 times less than that of outside the room. Samples were stored in the refrigerator in another room, which is separated by a door from the clean room. The cellulose acetate filters were weighed before and after sampling. The filters were kept overnight in the clean room where the room temperature and humidity were almost constant throughout the year to obtain constant weight. The analytical uncertainty associated with mass measurements was estimated to be about 5 %.

### 3.4. ANALYTICAL TECHNIQUES

Table 3.2 summarizes the three different analytical techniques employed in the determination of trace elements and ions.

Table 3.2 Analytical techniques employed in the characterization of samples

<b>Analysis Techniques</b>	<b>Measured Species</b>
Energy Dispersive X Ray Fluorescence Spectrometry (Oxford Instruments, ED 2000)	Cl, Mg, Ca, K, Fe, Cr, Ni, Pb, Mn, Al, Si, P, Ti, Br, Zn
Ion Chromatography (Vaydac Column with Jasco 875 UV-VIS detector)	Cl <sup>-</sup> , SO <sub>4</sub> <sup>2-</sup> , NO <sub>3</sub> <sup>-</sup>
Inductively Coupled Plasma Mass Spectrometer (Perkin Elmer DRC II model ICP-MS)	Be, P, Cr, P, Tl, Lu, Eu, Fe, W, Zn, Ca, Li, In, Sn, Tm, Cd, Gd, Ta, As, Hf, Ba, Dy, Se, Co, V, Tb, Er, Y, Nd, Sm, Mn, Pr, Pb, Ho, Na, Yb, Th, Cs, Sb, Sr, Rb, Ni, Mg, Ti, Al, U, Ce, Bi, La, Pt, Au, Be, Ge
Colorimetric (Nessler's Method)	NH <sub>4</sub> <sup>+</sup>

One fourth of the Whatman 41 filter sample was used for IC. Fifty five mm diameter discs were obtained from second quarter and analyzed by EDXRF. After EDXRF analysis, same samples were digested and analyzed by ICPMS. Third quarter of the samples was analyzed by IC and Colorimetry.

Detailed information about each method is given in the following sections.

### **3.4.1. Ion Measurements**

#### ***3.4.1.1. Determination of Major Anions by Ion Chromatography***

The ion chromatography (IC) technique was first developed by Small et al. (1975) as a physio-chemical separation technique that provides quantitative analysis of inorganic and organic ions from a complex mixture. The technique is simply based on the injection of a filtered aliquot of sample, an analyte, into an eluent stream. Then, pumping system transport the mixture of sample and eluent to the separator column. The eluent ions were kept by the succeeding suppressor column, in which they neutralized, and sample ions are determined quantitatively after being converted to their strong acidic or basic form. The basic components of the IC system are given in Figure 3.6.

In this study,  $\text{SO}_4^{2-}$ ,  $\text{NO}_3^-$  and  $\text{Cl}^-$  were determined by ion chromatography containing a Varian model 2010 HPLC coupled with a VYDAC 302 anion exchange column, which had a diameter of 2.46 cm and its total length was 25 cm, and it connected to the JASCO UV-VIS 875 detector.

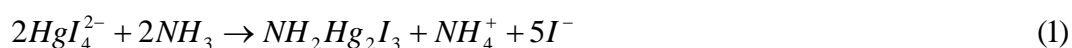
The eluent consisted of 3 mM phthalic acid with a flowrate of 3 mL/min. The pH of the mobile phase was adjusted to 4.95 by using sodium tetraborate solution. The bubbles from the solution were degassed for about 30 min prior to use. The injection volume of samples, blanks, and standards were 100  $\mu\text{L}$ . All solutions were prepared in plastic volumetric flasks to avoid the contamination from the glassware. The standards and mobile phase were newly prepared every day. In order to calibrate the instrument the solution of salts, NaCl,  $\text{K}_2\text{SO}_4$ , and  $\text{NaNO}_3$ , were prepared and they were diluted properly in the dynamic range of the instrument. Peak areas were determined by using Peak 2 software and peak areas were converted to concentrations by using the calibration curve for each analyte.

#### **3.4.1.1.1. Sample Preparation for IC Analysis**

Prior to IC analysis, one quarter of the samples was put into a beaker and 50 ml of distilled deionized water was added. Since the particles penetrated deep into the fiber filter, agitation was performed to extract the water soluble particles into solution for about 40 minutes. In order to prevent system clogging, solutions were filtered through 0.22 µm pore size cellulose acetate filter and 100 µl of the filtrate was directly injected to the IC for analysis. The solutions were preserved in the refrigerator at -4 °C to prevent the loss of sample due to evaporation if they were not analyzed immediately after the extraction. Blank filters were treated as the sample filters, and they were analyzed before the samples in order to prevent the contamination of the blanks with the analytes under consideration.

#### **3.4.1.2. Determination of NH<sub>4</sub><sup>+</sup> by Colorimetry**

Ammonium ion concentration in the collected samples was determined with the Nesslerization Method using Unicam 8625 UV-VIS Spectrometer. This method based on the reaction of Nessler's reagent, an alkaline solution of mercuric iodide, with NH<sub>3</sub>, which results in the formation of yellow-brown colloidal suspension. The reaction between the NH<sub>3</sub> and Nessler's reagent is as follows (3.1):



The absorbance of the formed suspension was measured spectrophotometrically in a glass cell with an optical path length of 1 cm at a wavelength of 425 nm. Ammonium sulfate was used to prepare standard solutions to calibrate the spectrophotometer. For this, ammonium sulfate was first dried at 100 °C and stock solution was prepared by using de ionized water, and intermediate stocks were obtained by diluting this stock solution to appropriate amounts. The absorbance obtained from the sample is directly proportional to the NH<sub>3</sub> concentration in the sample.

#### **3.4.1.2.1. Sample Preparation**

Samples prepared for the IC analysis were also used in the determination of ammonium ion.

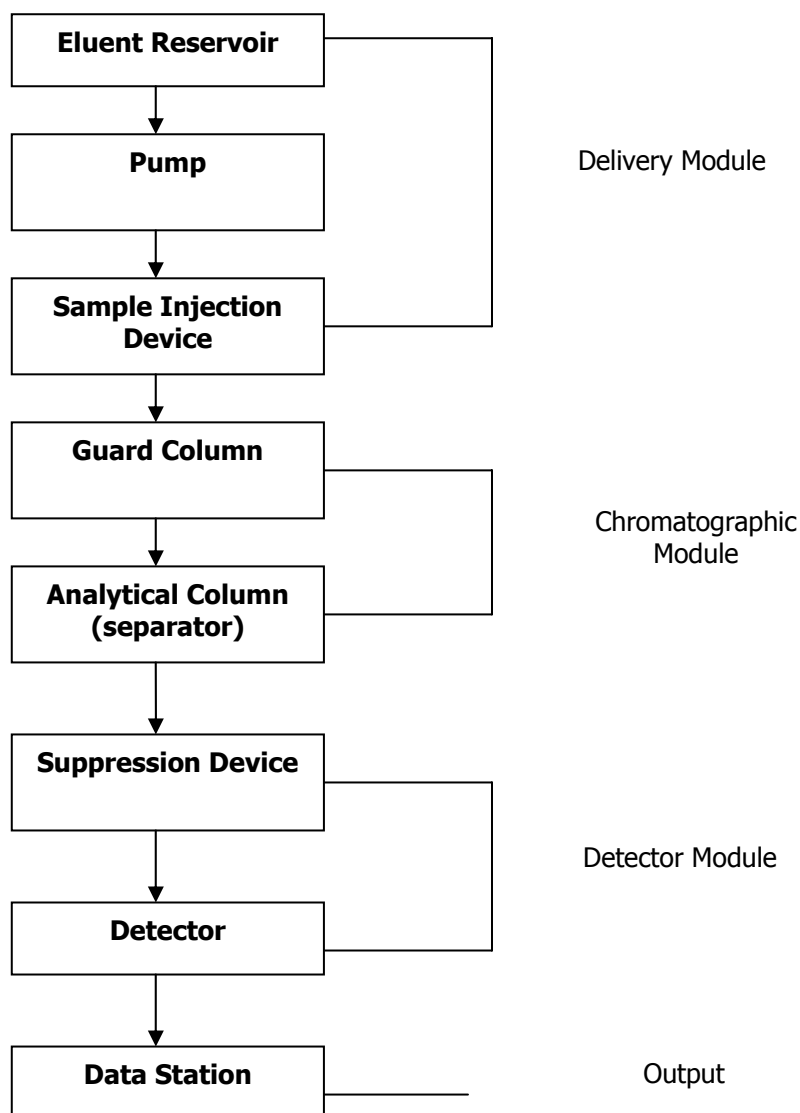


Figure 3.6 Basic components of the ion chromatography system

### 3.4.2. Trace Element Measurement

#### 3.4.2.1. Energy Dispersive X-ray Fluorescence (EDXRF)

Magnesium, Al, Si, S, K, Ca, Ti, Cr, Mn, Fe, Ni, Cu, Zn and Pb were measured by Energy Dispersive X-Ray Fluorescence using an Oxford ED-2000 energy dispersive X-Ray Spectrometer (Figure 3.7). The main components that make up the instrument includes a X-ray chamber with radiation enclosure involving X-ray tube with a Ag anode, filter



changer mechanism and a sample changer mechanism (with a 8 position sample tray), preamplifier, amplifier, ADC, MCA, HV power supply assembly, Lithium Drifted Silicon Si(Li) solid-phase detector cooled with liquid nitrogen and lastly factory configured PC with preloaded XperEase software. Instrument specifications are listed in Table 3.3. The pictures of the instrument and sample tray are given in Figure 3.8 & 3.9, respectively.

Table 3.3 Oxford ED-2000 XRF instrument specifications

Sections of the Instrument	Values
X-Ray tube	
▪ Max. Power	50 W
▪ Max. Voltage	50 kV
▪ Max. Current	1000 mA
Si(Li) Solid-phase Detector	
▪ Resolution Power	160 eV
▪ Cooling Method	Liquid Nitrogen
Sample Tray	
▪ Inner Diameter	47 mm
▪ Outer Diameter	50.5 mm
▪ Thickness	1 mm

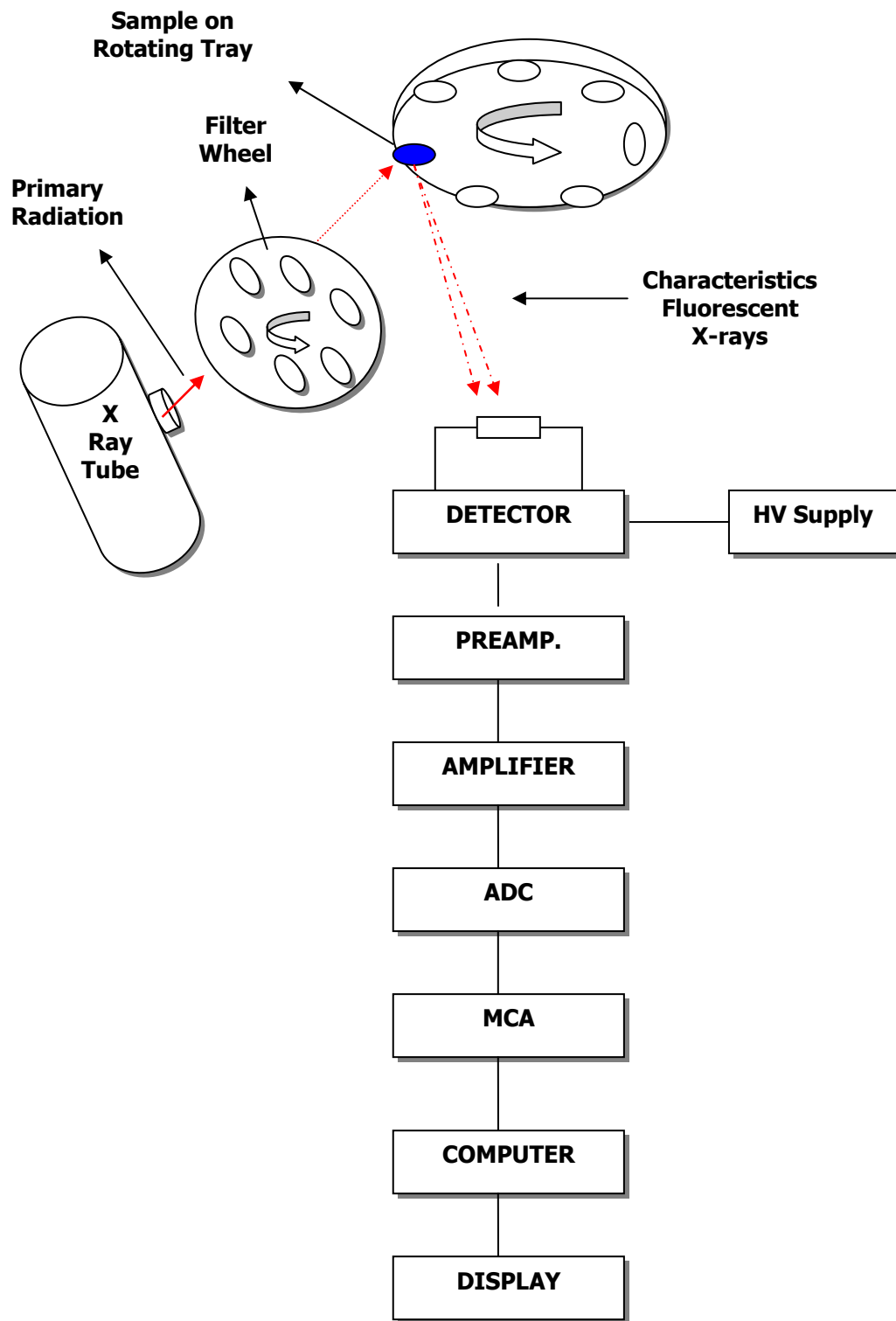


Figure 3.7 Scheme of the experimental setup for EDXRF



Figure 3.8 The Oxford ED-2000 XRF instrument



Figure 3.9 The 8-position sample tray

#### ***3.4.2.1.1. XRF Analysis***

Energy Dispersive XRF spectrometer in Ankara Nuclear Research and Training Center Laboratory was employed in the determination of trace element composition of aerosol samples. The elemental concentrations of Mg, Al, Si, S, K, Ca, Ti, Cr, Mn, Fe, Ni, Cu, Zn, and Pb were measured by this technique.

The processes followed during the XRF analysis run is illustrated in Figure 3.10. Filters are removed from their petri dishes and placed with their deposit sides downward into polycarbonate filter cassettes. A polycarbonate retainer ring keeps the filter flat against the bottom of the cassette. These cassettes are loaded into a carousel in the X-ray chamber containing 8 openings. The filter IDs are recorded on data sheet to correspond to numbered positions in the carousel. The sample chamber is evacuated to  $10^{-3}$  torr and a computer program controls the positioning of the samples and excitation conditions. The samples were presented directly to the unit with the loaded side directed towards X-ray tube. Complete analysis of 8 samples under four excitation conditions requires approximately 140 minutes. After one set of samples were removed from the XRF, sample holders were cleaned and made ready for the new set of samples. Four sets of samples were analyzed throughout a day, which means that the total number of samples analyzed per day was 32.

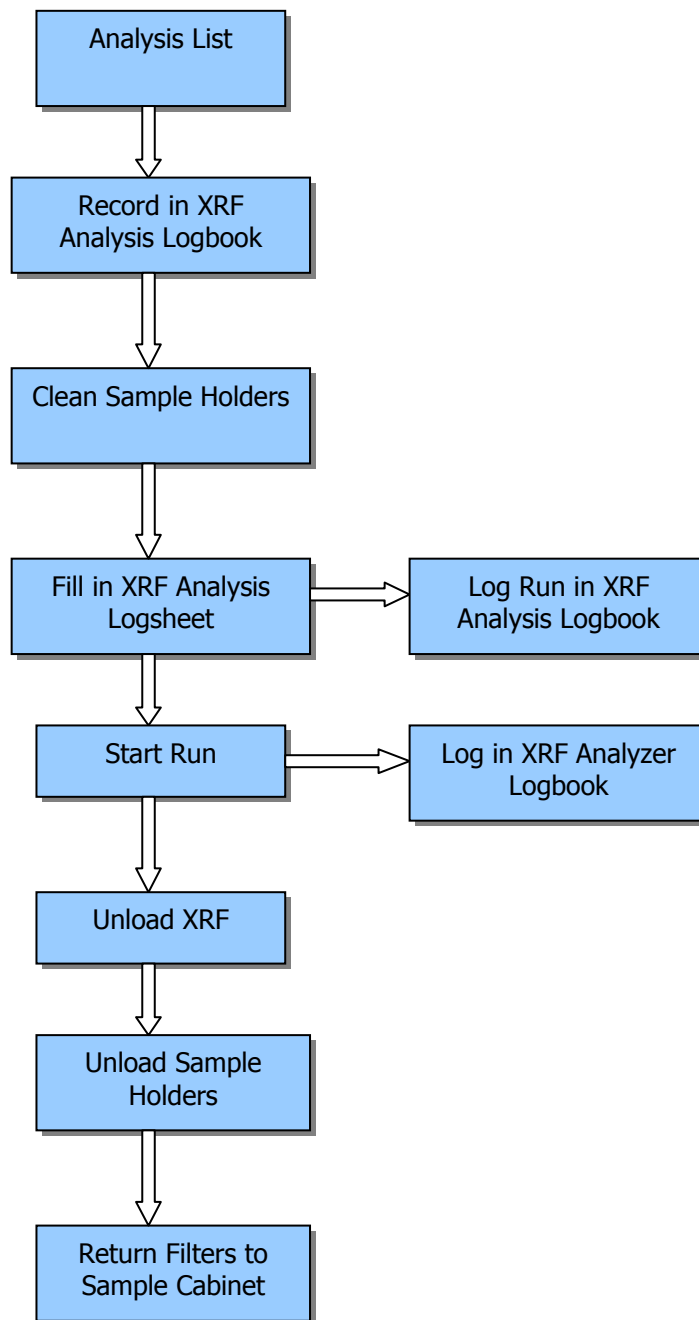


Figure 3.10 X-ray fluorescence analysis procedures

Four different analysis conditions (Very Light Elements: VLE; Solids: S; Steels: St; and Medium Elements: ME) applied during a single analysis run to maximize sensitivity to the full range of elements reported are shown in Table 3.4.

Table 3.4 Optimal excitation conditions of the OXFORD ED-2000 X-ray fluorescence analyzer

Parameter	Condition Number			
	1 (VLE)	2 (S)	3 (St)	4 (ME)
Tube Voltage (keV)	2.5	10	15	22.6
Tube Current (mA)	900	900	1000	494
Direct Excitation (Ag type of anode)				
Filter Thickness	None	Thin Al	Thick Al	Thin Ag
Analysis Time (s)	150	100	100	100
Energy range Analyzed	Na - K	K - Cr	Cr - Fe	Fe - Mo Pb
Elements Analyzed	Mg, Al, Si, P, S, Cl	K, Ca	Ti, Cr, Mn	Fe, Ni, Cu, Zn, Br, Pb

The K lines of Mg, Al, Si, P, S, Cl, K, Ca, Ti, K- $\alpha$  lines of Cr, Fe, Mn Ni, Br, and L- $\beta$  lines of Pb were detected by EDXRF in this study. A sample spectrum obtained by employing XRF is illustrated in Figure 3.11.

#### **3.4.2.1.2. Sample Preparation**

One fourth of the Whatman 41 filter sample was used in the EDXRF analysis. The 55 mm discs were obtained from each sample by using custom made plexiglass device. Figure 3.12 shows the cutting device and also extracted 55 mm filters in petri dishes. This material was selected instead of a metal in order to prevent the contamination of filter material with metal particles.

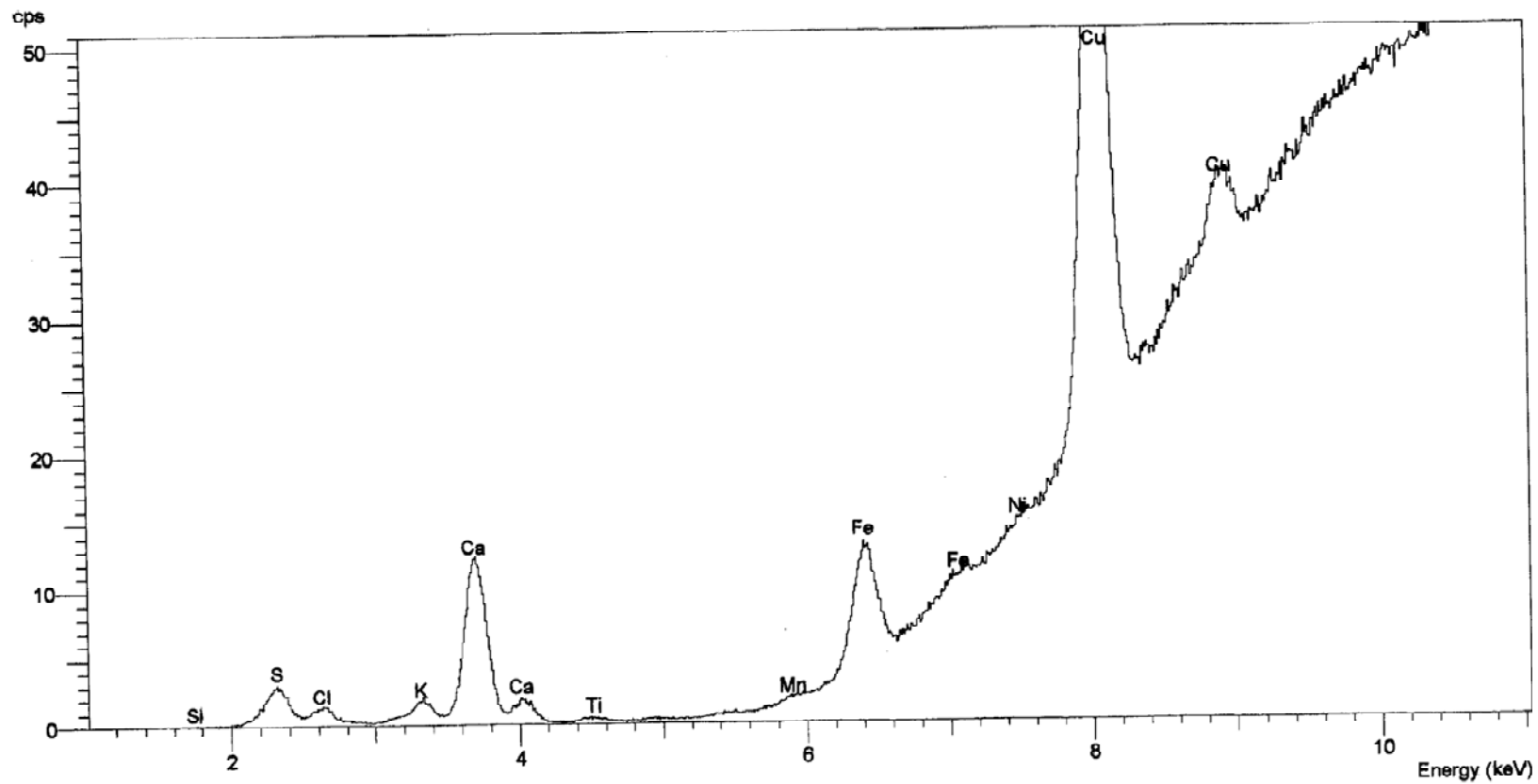


Figure 3.11 Sample spectrum obtained in EDXRF analysis



Figure 3.12 The custom-made Flexy Glass Cutting Device and cutted filters

#### ***3.4.2.1.3. Calibration of the EDXRF Spectrometry***

There are commonly reported three ways of calibration of EDXRF in the literature; vacuum-deposited thin film elements and compounds (Micrometters) (e.g., Marcazzan et al., 2004; Marcazzan, 1998; Bandhu et al., 1996; Lopes et al., 2006), thin glass films provided by the institutions like National Institute of Standard and Technology (NIST) (e.g. Lindgren et al., 2006; Chimidza et al., 2001; Henriksson et al., 2007; Lindgren et al., 1998; Holynska et al., 1997), custom made standards prepared by micropipetting the stock solutions onto the filter media (e.g., Shuvayeva et al., 1998; Braziewicz et al., 2004). Among these, while the vacuum deposits could be used for multielemental analysis since they cover largest number of elements, a separate Micrometters standard should be used to perform the calibration of each analyte. NIST standards are available for a limited number of elements.

The filter substrate used in this studies were generally Polycarbonate and Teflon membrane filter. While the aerosol particles penetrate through the filter material in cellulose esters and fibrous filter (recall that Whatman 41 is a cellulose fiber type of filter and its thickness is 300  $\mu\text{m}$ ), they are collected on the surface of the Polycarbonate and Teflon filters, which are 150 and 10  $\mu\text{m}$  in thickness, respectively. Haupt et al. (1995) and Davis et al. (1977) have previously reported that emitted X-rays with energies less than  $\sim 4$  keV (affecting the elements sodium, magnesium, aluminum, silicon, phosphorus, sulfur, chlorine, and potassium) are absorbed in the filter in case of a thick particle



deposit. Consequently, X-ray attenuation arising from the filter matrix is not a problem in case of polycarbonate and teflon filters, and they could be considered as 'thin films'. Not only the matrix of filter, but also the size distribution and chemical composition of the aerosols are the factors resulting in the X-ray attenuation during the analysis. The corrections related to the particle size and compositions have been estimated and published in the literature (e.g., Lodge, 1989). According to these studies, largest corrections should be applied to the Ca, Na, and Cl since these elements are present in the atmosphere associated with the coarse particle mode, and scattering of the incident (exciting) radiation by the coarser particles are considerably important, causing in the lower signal to noise ratio in the XRF analysis. Nevertheless, corrections for S should be less as the primary source of S is anthropogenic and it presents in the atmosphere in smaller size range. Considering all these discussions, it can be concluded that the standard selected for the calibration of EDXRF should exhibit the fairly similar particle size and composition with the sampled particles. In addition, it should be compatible with the filter material used for the collection of the particles.

The biggest difficulty encountered in this study was to calibrate the EDXRF. Firstly, stock Merck single element solutions were micropipetted onto the clean Whatman 41 filters intermediately, however, solutions were leaked out of the filter, hence, it was decided that these were not proper means of calibration. As a second attempt, SRM 2783, is an air particulate sample reduced in particle size to simulate  $PM_{2.5}$ , was ordered from the NIST. Particulate matter was deposited on a polycarbonate filter membrane in this standard. Since collected particles were  $PM_{10}$  and they were collected on the cellulose fiber substrate in this study, SRM 2783 could not be employed for the calibration as well.

As a third attempt in the calibration of XRF, samples collected in 1993, which were analyzed by using Instrumental Neutron Activation Analysis (INAA) and results were evaluated by Gullu et al (1996), was decided to use. Previously, ten samples corresponding to 1993 were bombarded with the X-rays. Once the results corresponding to both analytical techniques were compared, it was seen that there was a considerable difference between the XRF and INAA results especially for the light elements, whose atomic number is less than those of calcium (Ca). This observed difference in the results is due to the fact that XRF and INNA use different parts of the electromagnetic spectrum to excite the atoms in the samples. INAA technique bombards the filters by  $\gamma$ -rays whose wavelengths range between 0.03 and 0.3  $\text{\AA}$ . However, X-rays are the part of the

electromagnetic spectrum with a wavelength of 0.3 to 30 Å. Hence, INNA method gives higher and hence more accurate results compared to XRF due to the perfect penetration of more energetic  $\gamma$  -rays deep into the Whatman filter.

After noticing this fact, it was decided to use the filters which were previously analyzed by the INAA as standard. As an initial step, 100 samples corresponding to 1993 were counted by the XRF. The obtained 100 intensity values, which were given in terms of count per second (cps), were divided to the concentration values (in nano- grams) obtained from the INNA results. Hence, count per second (cps) per nano-gram (ng) values were calculated for each element. The "cps per ng" values were not changed from one sample to another as it was expected. An average "cps per ng" value was calculated for each element based on the results of analyzed 100 samples. Another set involving 60 samples belonging to 1993 was counted by the XRF and concentrations of elements in the samples in terms of "ng" was computed by using the calculated count per second per nano-gram. The results obtained by the proposed method for this second set were compared by the INNA results and it was seen that the developed methodology yields compatible concentrations with the INNA. After this verification, the proposed method, i.e. the calculated "cps per ng" values, was applied to the rest of the samples that were analyzed by means of EDXRF to convert "cps" values into concentrations.

Calibration curves for Al, Br, Cl, Cr, Fe, K, Mg, Mn, Ti and Zn were plotted by using the regression of XRF to INNA. Same procedure was also applied to  $\text{SO}_4^{2-}$ , recall that it was detected by means of ion chromatography (IC), and related calibration curve was plotted as XRF versus IC. Lead, Ca and Ni plots were formed by using the AAS results, which were generated in our research group before.

Obtained correlation between XRF and INNA for the elements of Mg and K are low, which is due to the lower concentrations of K and Mg reported using the XRF could be the result of absorbance of  $< \sim 4$  keV emitted by these elements by the particulate matter collected on the filter media. The similar conclusion has been made by the previous studies (Wang et al., 1995a; Kulkarni et al., 2003). The correlation coefficients corresponding to Ni and Pb are about 0.46 and 0.31, respectively. Shuvayeva et al. (1998) also found low correlation between the AAS and INNA and synchrotron radiation X-ray fluorescence (SXRF), which was attributed to sample digestion prior to AAS analysis.

#### **3.4.2.1.4. Detection Limit of EDXRF**

As it is known the definition of detection limit is that it is the minimum concentration or weight of the analyte that can be detected at a known confidence level.

International Union of Applied and Pure Chemistry (IUPAC) has defined the detection limit in terms of standard counting error of the background intensity. The standard error for a net count can be expressed as in Equation 3.2:

$$\sigma = \sqrt{\sigma_p^2 + \sigma_b^2} \quad (3.2)$$

Where;

$\sigma_p$  and  $\sigma_b$  are the background and peak counting errors, respectively. In the calculation of detection limit, background and peak counting errors can be assumed to be equal. Hence, Equation 3.2 becomes:

$$\sigma = \sqrt{2\sigma_b^2} \quad (3.3)$$

If Equation 3.3 is rewritten for 95 % confidence level, then counting error will be;

$$2\sigma = 2\sqrt{2\sigma_b^2} \approx 3\sqrt{N_b} \quad (3.4)$$

Where  $N_b$  is the background counts in a given time. Equation 3.4 can be modified further to calculate the detection limit by taking the slope of counts vs. concentration of analytical curve and counting time as follows;

$$C_{DL} = \frac{3}{m} * \sqrt{\frac{N_b}{t}} \quad (3.5)$$

Where;

$C_{DL}$  is the minimum detectable concentration of analyte,  $m$  is the slope of analyte counts-concentration curve and represents the sensitivity of the spectrometer,  $N_b$  background concentration,  $t$  is the measuring time (Tiwari et al., 2005).

Both the spectrometer sensitivity and the measured background vary with the average atomic number of the sample. While X-ray spectrometer has ability to detect low parts per million range, its sensitivity decline dramatically towards the long wavelength limit of the spectrometer mainly due to the low fluorescence yields and the increased absorption. As a consequence of this, poorer detection limits are achieved at the long wavelength extreme of the spectrometer, which corresponds to the lower atomic numbers (Jenkins, 2000). This explains why lower intensities were obtained for Mg in this study.

Equation 4 was employed to calculate the detection limits of elements measured with the EDXRF. Slopes of the calibration curves obtained in the previous section and counting time presented in Table 3.4 were placed in the Equation 3.5. For the background counting, intercept of the calibration curve was used. Detection limits of analytes were calculated and presented in Table 3.5. The average flowrate that passed through the 47 mm diameter filter is about 90.42 m<sup>3</sup> and concentration is based on 17.35 cm<sup>2</sup> irradiated area for a 47 mm filter substrate.

Table 3.5 Detection limits of the measured analytes

<b>Analyte</b>	<b>m (slope) (cps/ng)</b>	<b>I<sub>b</sub> (Intercept) (cps)</b>	<b>R<sup>2</sup> (Correlation Coefficient)</b>	<b>DL (ng)</b>	<b>DL (ng m<sup>-3</sup>)</b>	<b>DL (ng cm<sup>-2</sup>)</b>
<b>Al</b>	0.0012	9.27	0.6562	621.49	6.87	35.82
<b>Fe</b>	0.0107	54.99	0.7515	207.91	2.30	11.98
<b>Pb</b>	0.0065	5.16	0.3072	105.04	1.16	6.05
<b>Ni</b>	0.0036	0.66	0.4637	67.70	0.75	3.90
<b>Br</b>	0.0087	7.37	0.7786	93.61	1.04	5.40
<b>K</b>	0.0028	58.07	0.4202	666.64	7.37	38.42
<b>Mn</b>	0.0025	0.57	0.5709	90.60	1.00	5.22
<b>Cl</b>	0.0104	168.59	0.9075	306.09	3.39	17.64
<b>S</b>	0.0062	643.51	0.8114	1002.22	11.08	57.77
<b>Zn</b>	0.0100	3.96	0.5090	59.70	0.66	3.44
<b>Ti</b>	0.0049	3.70	0.6619	117.77	1.30	6.79
<b>Cr</b>	0.0059	3.02	0.3200	88.36	0.98	5.09
<b>Ca</b>	0.0046	5.15	0.9182	148	1.64	8.53

Detection limit of any kind of analytical technique changes with the type and sensitivity of instrument, operating conditions, and substrate analyzed. Even if the operating conditions are kept constant, it would not be possible to obtain the same detection limit as the previous day for the same instrument and analyte. Hence, different studies reported different detection limits for the EDXRF technique. Comparison of detection limits calculated in this study employing the proposed calibration procedure with the literature can give insight about the accuracy of the used methodology. Therefore, the detection limit values calculated for this study were compared with the ones reported in the literature (Louie et al., 2005; Ladsberger and Creatchman, 1999; Valkovic et al., 1996; Lindgern et al., 2005; Haupt et al., 1997; Bennet et al., 2005) as shown in the Table 3.6.

#### ***3.4.2.1.5. Development of Quality Assurance /Quality Control (QA/QC) Protocol for EDXRF Analysis***

Since the amount of samples to be analyzed is huge, it would be possible to see erroneous experimental results systematically or occasionally. For this reason, it is necessary to establish a detailed QA/QC protocol which will be composed of documentation, and measurement of samples and blanks. Analysis of the samples was initiated after development of this protocol. The proposed QA/QC protocol is mainly composed of three parts. First part encompasses documentation. It was decided to open a file for each sample in the computer and all the information about that sample will be saved in this specific file. The second section of the protocol describes the works associated with the analysis of the samples. In this respect, it was planned to perform the following items in a routine manner: (1) The present standard filter is counted twice a day with the analyzed samples. If results corresponding to subsequent two days is 5 % different from each other, samples are counted again. (2) Five samples over 100 samples will be reserved for the next set and these reserved samples will be distributed in the second set and they will be counted with this second one. If the average count per second values of this 5 samples were different by 10 % from the previous analysis, then second set will be analyzed again. (3) The last section in the QA/QC protocol is related with blank measurements. It was planned to count 2 field and 2 laboratory blanks with each 100 samples. After analyzing first 1000 samples, blank measurement will be reduced by 50 %. By this manner, 20 field blanks will be analyzed with the first 1000 samples and 30 field and 30 laboratory blanks will be counted at the end of the study.

Table 3.6. Comparison of detection limits for EDXRF with the values reported in the literature

<b>Analyte</b>	This Study (ngm <sup>-3</sup> )	Louie et al., 2005 (ngm <sup>-3</sup> )	Ladsberger and Creatchman, 1999	Valkovic et al., 1996 (ngm <sup>-3</sup> )	This study (ngcm <sup>-2</sup> )	Lindgern et al., 2005 (ng cm <sup>-2</sup> )	Haupt et al., 1997 (ng cm <sup>-2</sup> )	Bennet et al., 2005 (ng cm <sup>-2</sup> )
<b>Al</b>	6.87	0.48	5	NA	35.82	NA	108.7	NA
<b>Fe</b>	2.30	0.7	0.7	1	11.98	1.3	41.9	1.8
<b>Pb</b>	1.16	1.4	1	1	6.05	0.92	11.1	1.3
<b>Br</b>	1.04	0.5	0.5	NA	5.40	0.62	1.5	0.88
<b>K</b>	7.37	2.9	3	16	38.42	15	NA	20
<b>Mn</b>	1	0.8	0.8	1	5.22	2.5	11.3	3.5
<b>Cl</b>	3.39	4.8	5	NA	17.64	40	12.8	57
<b>S</b>	11.08	2.4	2	NA	57.77	90	33.2	130
<b>Zn</b>	0.66	0.5	0.5	0.7	3.44	0.89	62.8	1.3
<b>Ti</b>	1.30	1.4	2	3	6.79	5.1	NA	7.2
<b>Cr</b>	0.98	0.9	1	NA	5.09	2.1	18.6	NA
<b>Ni</b>	0.75	0.4	-	1	3.90	1.2	7.6	1.7
<b>Ca</b>	1.64	2.2	2	NA	8.53	8	NA	11

### 3.4.2.1.5.1. Precision Calculation

Precision describes the reproducibility of results, that is, the agreement between numerical values for two or more replicate measurements, or measurements that have been made in exactly the same way. Precision can be formulated as shown in the Equation 3.6 below:

$$\%RSD = \frac{s}{\bar{x}} * 100 \quad (3.6)$$

Where "s" standard deviation of element concentration,  $\bar{x}$  is the mean value of these concentrations. Samples that were used in the calibration of the XRF were counted at every batch and obtained values were compared with the previous one in order to estimate the precision of the measurements. Sample which was collected on 13/02/1993 is one of those samples and corresponding precision of the elements were computed and illustrated in Figure 3.13.

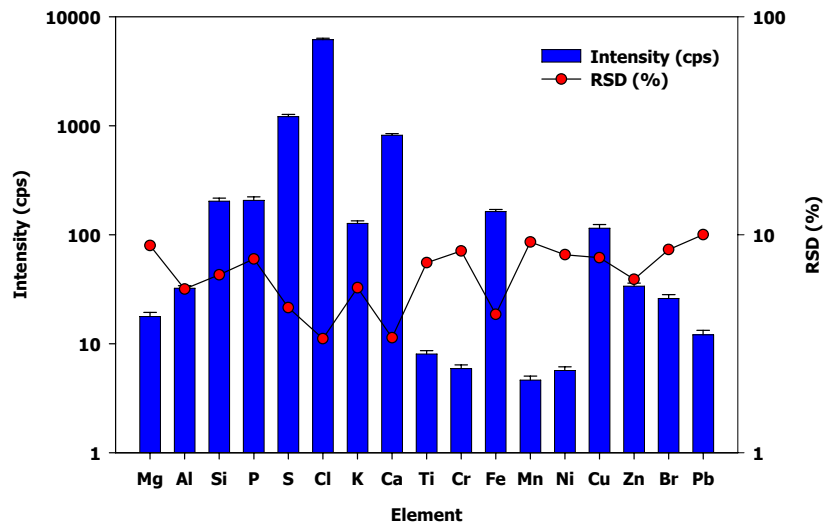


Figure 3.13. Mean, standard deviation and percent relative standard deviation of the analytes for sample collected on 13.02.1993



The relative standard deviations obtained for Mn and Pb were high as compared to other elements, and their corresponding values were 9.26 and 10 %, respectively. For S, Ca, Fe and Cl, the calculated rsd was lower than 5 %. The estimated rsd for the rest of the measured parameters was range from around 6 % to 9 %. With the exception of Pb, all the calculated values for rsd was lower than 10 % implying that precision of the measurements is acceptably good in generating reliable data set.

### 3.4.2.1.5.2. Blank Analysis

Field blanks were collected and treated as the samples except air was allowed to pass through the field blanks only one minute. They were analyzed under the same condition with the samples. XRF analysis results indicated that Whatman filter is free of Cl, Mg, and Br. Si was detected only one blank out of 30, which implies that these filters probably contaminated with this analyte. The average filed blank composition was illustrated in Figure 3.14.

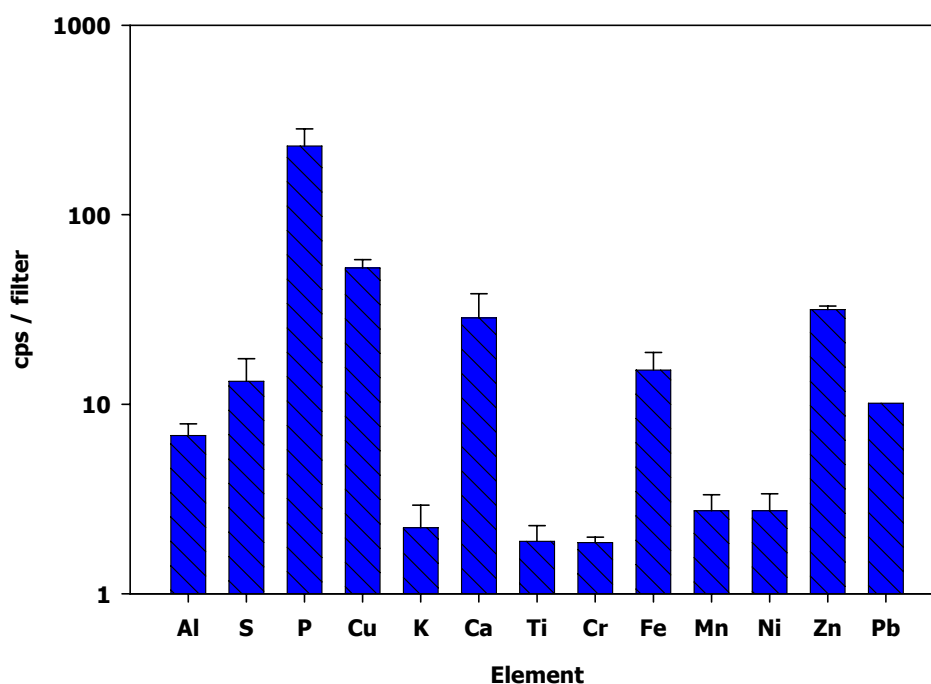


Figure 3.14. Average field blank composition

Figure 3.14 revealed that field blanks contains considerably high concentration of P and Cu. As it was indicated previously, brushless motor was not used in the high volume sampler; consequently, sampler itself contaminated the collected filter with Cu. Another point that can be concluded from Figure 3.14 is that filter has high background concentration of P. Whatman filter matrix itself is the source of P. Therefore, both P and Cu were excluded from the further data analysis and interpretation. Lead was detected in only one blank out of 30; however, it was used in the blank subtraction.

With the exception of Br, average field blank composition was converted from cps per filter to ng per filter by using the slopes of the calibration curves for each analyte and results were tabulated in Table 3.7.

Table 3.7 Elemental composition of filter blanks (ng/ 100 cm<sup>2</sup> filter)

Element	Mean	$\delta$
Al	28.4•10 <sup>3</sup>	4.3•10 <sup>3</sup>
S	10.0•10 <sup>3</sup>	4.6•10 <sup>3</sup>
K	4.7•10 <sup>3</sup>	6.0•10 <sup>3</sup>
Ca	31.2•10 <sup>3</sup>	12.8•10 <sup>3</sup>
Ti	2.8•10 <sup>3</sup>	4.5•10 <sup>3</sup>
Cr	1.0•10 <sup>3</sup>	69.44
Fe	6.7•10 <sup>3</sup>	2.1•10 <sup>3</sup>
Mn	5.3•10 <sup>3</sup>	1.4•10 <sup>3</sup>
Ni	5.8•10 <sup>3</sup>	7.8•10 <sup>3</sup>
Zn	18.0•10 <sup>3</sup>	0.8•10 <sup>3</sup>
Pb	6.1•10 <sup>3</sup>	-

Field blank averages were also compared with those of samples and this comparison was illustrated in Figure 3.15, which clearly showed that sample averages were significantly higher for all of the analytes except Zn. The sample to blank ratio for the Zn was calculated as ~ 1.06, which implies that the contribution of field blanks to contamination of samples is significant especially in obtaining reliable measurement results for Zn.

Another element that we observed low sample to blank ratio was Mn, for which ratio was estimated as 1.86. Nickel and Cr had estimated ratios of around 4. Since Cl, Mg and Br were not detected in the field blanks; the contamination attributed to field blanks in terms of these analytes is not a concern here. For the elements of Al, Ti, Fe, Ca, K and S,

the calculated sample to blank ratio were 10.56, 9.50, 24.14, 29.83, 58.87, and 150.30, respectively indicating that the blank contribution for these elements were negligible to be significant in generating reliable data set. In order to make accurate data analysis, blank contribution needs to be determined. The average concentrations of the field blanks for each analyte were subtracted from those of samples and percent blank subtraction was calculated. The obtained results were provided in Figure 3.16.

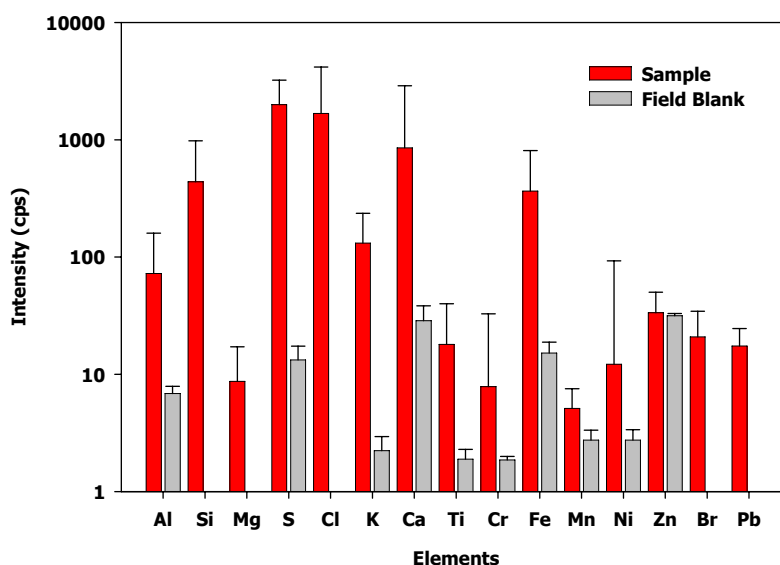


Figure 3.15 Comparison of field blank composition with the samples

Average blank subtraction were about 75 and 80 % for Zn and Ni, respectively. Though having high average blank subtraction, percentage frequency of observance for Ni was about 80 %. Manganese had average blank subtraction about 60 % and it was detected 100 % of the analyzed samples. Higher blank contribution of Ni, Mn and Zn could be due to low ambient concentrations of these elements in the sampling region. Average blank subtraction and frequency of observance for Cr were 41 and 19 %, respectively. There was an inverse relationship between the frequency of observance and average blank subtraction for the analytes of Pb, Mg, Br, S, K, Ca and Fe. Except Mg and Fe, the other elements in this group had been detected about 100 % of the samples. Aluminium and Ti had average blank subtraction around 20 %. There was not any blank subtraction for Si and Cl, these two elements were detected only 40 and 20 % of the samples, respectively. For the elements having blank contribution less than 20 %, it can be concluded that

accurate measurement of the analytes have been achieved by using the proposed analytical and sampling methodology.

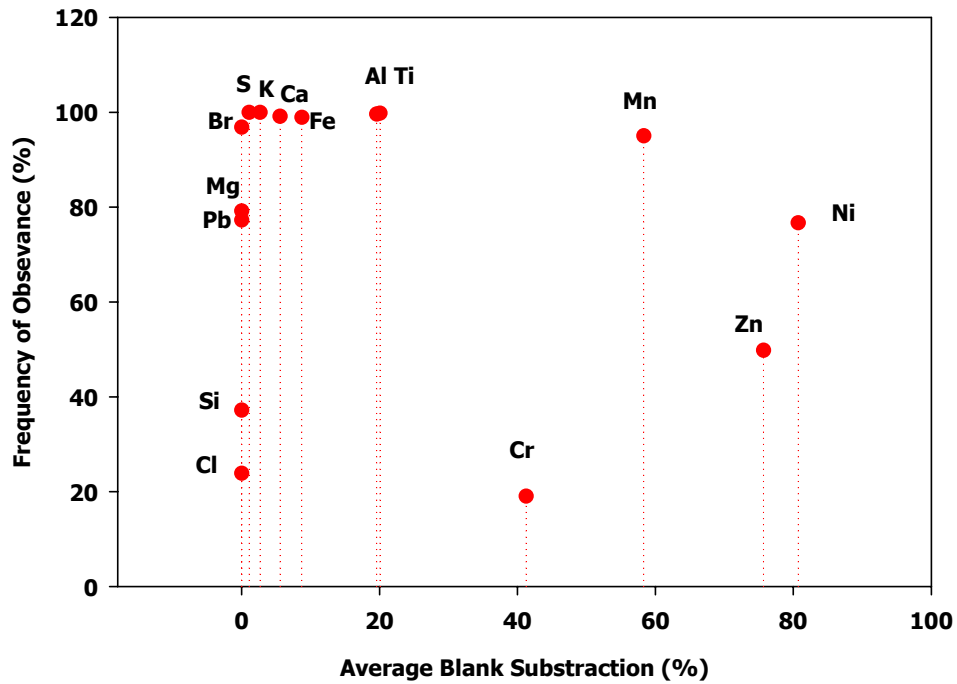


Figure 3.16 Plot of percent blank subtraction and percent of observance of samples analyzed by XRF

### 3.4.2.1.5.3. Uncertainty in EDXRF Measurements

Bevington (1969) defined the total uncertainty,  $\sigma_t$ , as the root sum of square of contributing uncertainties. In order to calculate the total uncertainty in XRF measurements, uncertainties arising from the collection and analyzing steps were taken into account and they were summarized in the following Equation:

$$\sigma_t^2 = \sigma_a^2 + \sigma_c^2 + \sigma_{vol}^2 + \sigma_w^2 \quad (3.7)$$

Where;

$\sigma_a$  = analytical uncertainty,

$\sigma_c$  = calibration uncertainty,  
 $\sigma_{vol}$  = uncertainty in air volume measurements,  
 $\sigma_w$  = uncertainty in weighing of samples

The uncertainty associated with XRF employing Si (Li) detector was previously reported as  $\pm 4\%$  (Braziewicz et al., 2004). However, the uncertainty related to counting of the samples was calculated by dividing the standard deviation of counts to the corresponding mean count rate, and hence an analytical uncertainty value was calculated for each analyte. With exception for Br and Cl, the calibration uncertainty was estimated from the absolute error of the SRM 2783, that is, standard deviation values of the measurements divided with the associated mean for each analyte. SRM 2783 neither include Cl nor Br. For these two analytes, calibration uncertainty was assumed as 5%. The uncertainty corresponding to air volume measurements and weighing of the samples were assumed as 5%. Total uncertainty was calculated by using error propagation law as given in the Equation 6 and results were summarized in Table 3.8. Table 3.8 also shows the percent frequency of observance of each analyte in the samples. The values presented in Table 3.8 were also plotted in Figure 3.17 below.

Table 3.8 Frequency of observance and average statistical uncertainty for the elements analyzed by XRF

Element	Frequency of Observance %	Average Statistical Uncertainty %
Mg	79.19	8.97
Al	99.62	7.86
Si	37.19	7.54
S	99.96	19.37
Cl	23.88	8.66
K	99.96	13.61
Ca	99.13	13.08
Ti	99.77	17.51
Cr	19.03	20.44
Fe	98.94	9.43
Mn	95.03	9.50
Ni	76.69	52.74
Zn	49.81	10.41
Br	96.85	8.66
Pb	77.26	13.82

As it can be concluded from Figure 3.17, with the exception of Zn, Cl and Cr, the rest of the analytes observed in higher than 70 % of the samples. Except for Ni, all the measured analytes had average statistical uncertainty lower than 20 %. In fact, the estimated average uncertainty for Cr was 20.44 %, but it could be also rounding off to 20 %. Excluding Ni the estimated low uncertainty values implied that the measurement results are reliable in generating this data set.

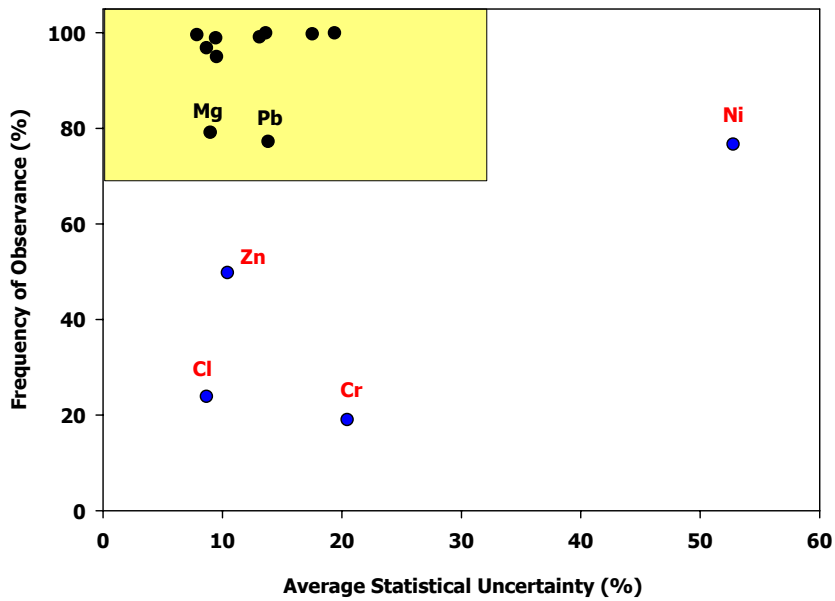


Figure 3.17 Calculated average percent statistical uncertainty and average frequency of observance of the analytes detected by XRF

#### ***3.4.2.1.5.4. Accuracy Determination in EDXRF Measurements***

SRM 2783, air particulate on filter media purchased from the NIST, was counted along with samples to determine the accuracy of the XRF measurements. Percent recovery values were calculated by plugging the measured and certified values into below Equation:

$$A = \frac{(C_m - C_t) * 100}{C_m} \quad (3.8)$$

Where;

$C_m$ : Measured value

$C_t$ : Standart reference material

A: Accuracy (in percent)

From Table 3.9, it can be concluded that the accuracy for all of the analytes was lower than 15 %, except for Al, for which the percent error was estimated as 15.64.

Table 3.9 Calculated percent accuracy for some of the selected elements in SRM 2783

	SRM 2783				Error (%)
	Certified Value (ng)		Measured Value (ng)		
	Mean	$\delta$	Mean	$\delta$	
Si	58600	1600	59500	1550	1.54
S	1050	260	915	165	12.86
K	5280	520	4902	570	7.16
Cr	135	25	146	28	8.15
Mn	320	12	315	20	1.56
Al	23210	530	19580	670	15.64
Zn	1790	130	1609	123	10.11
Fe	26500	1600	30310	1890	14.38
Ca	13200	1700	14990	1650	13.56
Ti	1490	240	1685	270	13.09
Pb	317	54	320	38	0.95

#### ***3.4.2.1.6. Penetration Depth and Mass Absorption Coefficient of Aerosols***

Major difficulty encountered in the calibration of the XRF owing to the high filter thickness. Since particles completely penetrated through the filter media, lower intensities

were detected for the elements. The penetration depth of the particles was calculated in order to get idea of efficiency of X-rays in the measurement.

For this reason, the reflectance (average of 6 readings) was transformed into an "absorption coefficient" according to the Equation 3.9 below:

$$a_p = \frac{A}{2V} \ln \frac{R_0}{R} \quad (3.9)$$

Where;

$a_p$  : absorption coefficient ( $m^{-1}$ )

$A$  : loaded filter area ( $m^2$ )

$V$  : samples volume ( $m^3$ )

$R_0$  : reflectance of the blank filter

$R$  : reflectance of the filter with collected particles

It can be imagined that all sampled volume of air with suspended particles is a roller, which is depicted in Figure 3.18 schematically, with a base surface equal to the filter area. Loaded filter area for 47 mm diameter Whatman cellulose fibrous filter is  $17.35 \text{ cm}^2$  and thickness of the filter,  $X$ , is  $300 \text{ }\mu\text{m}$ , and hence, sample volume could be calculated as  $0.5205 \text{ cm}^3$ . Reflectance of the loaded filters ( $R$ ) and a blank filter ( $R_0$ ) were measured by EDXRF as indicated in Figure 3.19 and values presented in Table 3.10.

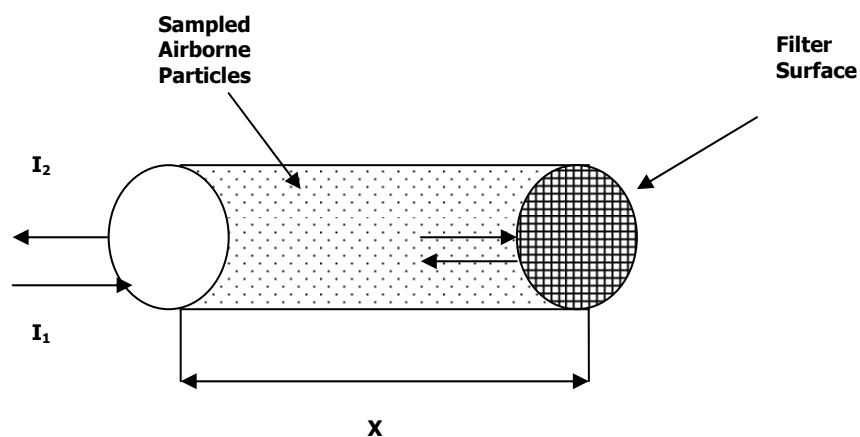


Figure 3.18 Imagined volume of sampled air



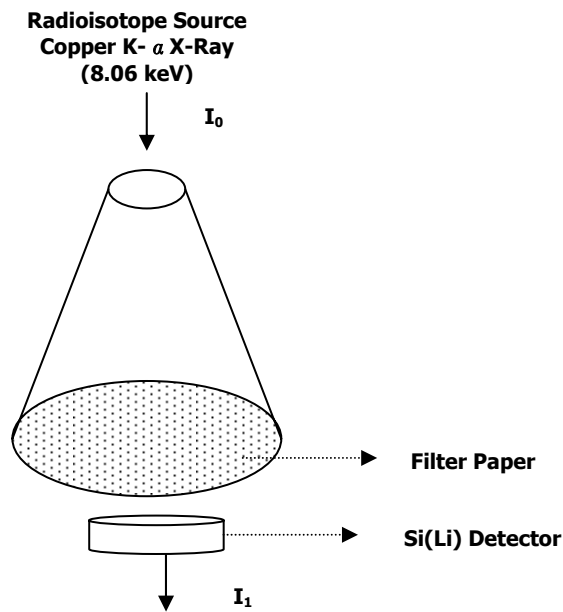


Figure 3.19 Schematical representation of EDXRF for reflectance measurement

Table 3.10 Results of reflectance measurement for blank and samples

	Sample (mean $\pm$ SD), n=6	Blank (mean $\pm$ SD)
$I_1$ (count)	21250 $\pm$ 295	14901 $\pm$ 295
$I_2$ (count)	19448 $\pm$ 230	13968 $\pm$ 240
$R = I_1 / I_2$	1.093 $\pm$ 0.020	
$R_0 = I_1 / I_2$		1.067 $\pm$ 0.028

Known values were plugged into the Equation 7 so as to get absorption coefficient ( $a_p$ );

$$a_p = \frac{17.35 \text{ cm}^2}{2 * 0.5205 \text{ cm}^3} \ln \frac{1.093}{1.067} \cong 0.401 \text{ cm}^{-1} = 401 * 10^{-5} \text{ m}^{-1}$$

Dividing the absorption coefficient  $a_p$  ( $\text{m}^{-1}$ ) by the concentration of aerosol particles, the mass absorption coefficient was calculated as:

$$\sigma_p = \frac{a_p}{C} \tag{3.10}$$

Where;

$\sigma_p$ : mass absorption coefficient ( $m^2 / g$ )

C: concentration of particles ( $\mu g / m^3$ )

The concentration of particles on 47 mm diameter filter is  $2085.3 \mu g / m^3$  and absorption coefficient was calculated previously as  $401 * 10^{-5} m^{-1}$ , and from Equation 3.9, mass absorption coefficient was calculated as;

$$\sigma_p = \frac{401 * 10^{-5} m^{-1}}{2085.3 \mu g / m^3} = 1.9229 m^2 / g$$

The calculated mass absorption coefficient ( $\sigma_p$ ) is less than the values reported in literature which range from  $3 m^2 / g$  (Wolff *et al.*, 1982) to  $17 m^2 / g$  (Truex and Anderson, 1979; Hitzengerger *et al.*, 1999). However, it should be kept in mind that these values were reported for the urban area for which it is not surprising to see high absorption coefficients.

The penetration depth of the X-ray beam ( $x$ ) was calculated as follows;

$$x = \frac{2.69}{\sigma_p * \rho} \tag{3.11}$$

Where;

$\rho$  : density of the sample ( $g / cm^3$ )

$\sigma_p$ : mass absorption coefficient ( $cm^2 / g$ )

Density of the sample,  $\rho$ , is  $0.0097 g / cm^3$  and mass absorption coefficient,  $\sigma_p$ , is  $19229 cm^2 / g$ . Once these two known values were plugged into Equation 3.11, the penetration depth of the X-ray beam was calculated as follows;

$$x = \frac{2.69}{19229 cm^2 / g * 0.0097 g / cm^3} \cong 144 \mu m$$

This last calculation reveals that information is obtained only for a depth of  $144 \mu m$  although the thickness of the filter media is  $300 \mu m$ . The secondary X-rays from elements at a depth of more than  $144 \mu m$  were not detected, because they were

absorbed by the filter material. In a study conducted by Szilagyi and Hartyani (2004), the penetration depth of aerosol particles on the Whatman filter was found as 100 µm or less. The difference in the calculated values might be due to use of different operating conditions. The concluding remark from this section of this study is that correction factor should be applied on the measured intensities to get accurate and reliable results in case of Whatman-41 was used as a substrate in XRF analysis.

### ***3.4.2.2. Trace Element Determination by Inductively Coupled Plasma Mass Spectrometry (ICP-MS)***

Perkin Elmer DRC-II Model Inductively Coupled Plasma Mass Spectrometry (ICP-MS), which is located at the Central Laboratory of METU was used to determine elemental content of the collected aerosol samples.

#### ***3.4.2.2.1. Reagents and Gases***

Merck Suprapur analytical grade more than 65 % HNO<sub>3</sub> and HF acids were used for the digestion of samples and also for the preparation of standards in ICP-MS analysis. Nitric acid contains trace elements ranging from 0.1 ppb for Ga, Ge, and Au to 10 ppb for Na. Tuning solution was ELAN 6100 DRC Setup/Stab/Masscal solution. This solution was a multielement solution and contains Mg, Cu, Rh, Cd, In, Ba, Ce, Pb, and U at 10 ppb concentration each in 2 % HNO<sub>3</sub> acid. Both mixed and single element standards were used to calibrate the instrument. Inorganic Ventures Standards, 1000 ppm each in 5% HNO<sub>3</sub> acid, were used for some of the elements. For rare earths, Inorganic Ventures 100 ppm mixed standard made up in a 5% HNO<sub>3</sub> acid solution used. Multi element standards were Merck brand and could be listed as Merck VI, Merck IX and Merck IV.

In all standard preparation and analyses deionized water was used prepared by Barnstead nanopure ultrapure deionization unit equipped with two ion exchange cartridges to remove ions, a third cartridge to remove the organic and fourth one to remove the particulate matter. The produced water finally has a resistance of 18.3 MΩ.

Argon was used as the ICP torch gas. The quality criteria for argon is listed in Table 3.11 below:

Table 3.11 Quality criteria for argon

Purity	≥ 99.996 %
Oxygen	< 5 ppm
Hydrogen	< 1 ppm
Nitrogen	< 20 ppm
Water	< 4 ppm

#### ***3.4.2.2.2. Sample Preparation***

##### ***Microwave Digestion***

The most important drawback of the ICP-MS technique as compared to XRF is that aerosol samples collected on the Whatman-41 filters should be converted to aqueous solution before aspirating into the ICP-MS. Ideal sample preparation should convert filter samples to aqueous solution, destroy all organic matter, retain all analytes of interest in solution at detectable concentrations, add no interfering ions and adjust sample viscosity to the optimum for analysis.

Generally, two approaches have been applied to airborne particulate matter: leaching (partial dissolution) and total dissolution. Partial dissolution includes a selective dissolution of elements, in which filter on which particulate matter is deposited is not dissolved, but, metals and metalloids in the particulate matter is leached to the solution. In contrast to this, the complete dissolution of sample and filter (total or portion) is of concern in total dissolution. Total dissolution or digestion has advantage over the partial dissolution because of the fact that total dissolution of filter will be more representative of the sample (Arruda, 2006).

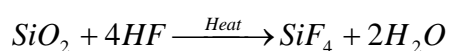
Total digestion can be performed in two ways as open and closed vessel digestion. Closed vessel microwave digestion in the presence of HNO<sub>3</sub> and HF was decided to use as sample preparation procedure in this study. The closed vessel microwave assisted acid digestion has many advantages over the open vessel digestion system such as speeding up the sample preparation process, safe operation of digestion due to fully automated programming, preventing loss of volatile analytes, such as, As, Cd, Sb and Zn, during digestion and eliminating contamination of samples from each other or laboratory

environment. In addition, reaction parameters such as temperature and pressure can be monitored and controlled during digestion bringing the advantage of determining the efficiency of digestion, and higher temperatures obtained in the pressurized closed vessels results in the complete digestion of the samples (Dolgopolova, 2004).

Nitric acid is a common digestion reagent, it is used to destroy organic compounds by breaking down the complex hydrocarbons into CO<sub>2</sub> and H<sub>2</sub>O meanwhile oxidizing metals. Furthermore, nitric acid forms water-soluble salts with most of the elements and hence, precipitation is eliminated during digestion. Most nitrates are less volatile as compared to chlorides and volatilization of the analytes with nitrates is precluded in the digestion system.

Selection of nitric acid as digestion reagent is especially crucial if ICP-MS will be employed for the determination of trace elements in the sample, because, plasma includes H, O and N (Arruda, 2006). 2 % HNO<sub>3</sub> is the maximum preferred amount for ICP-MS since polyatomic ions are not increased and it is readily available in a high purity form in the market. Up to 5 % HNO<sub>3</sub> is preferred, ArN<sup>+</sup> and NOH<sup>+</sup> are the possible interferences over this ratio in the ICP-MS technique (Thermo X Series ICP-MS Operator Manual, 2006).

Although HNO<sub>3</sub> digests the sample as completely as possible, it can not alone completely digest the silica and materials present in the sample bounded to siliceous material. For this reason, HF acid is necessary to extract trace elements associated with relatively insoluble matrices such as siliceous material which is a typical component of atmospheric particulate matter (Wu et al., 1996; Ghose, 1999; Siefert et al., 1999; Swami et al., 2001). Hydrofluoric acid digests the SiO<sub>2</sub> found in the particulate matter according to following reaction:



However, handling free HF is extremely hazardous, and necessitates great care and rigorous laboratory safety protocols. Additionally, because HF is corrosive to standard components (e.g., nebulizer and plasma torch) of commercial instruments, more expensive HF tolerant components need to be purchased unless excess HF is expelled prior to ICP-MS analysis. (Kulkarni et al., 2003; Pekney and Davidson, 2005).

Boric acid could be used to complex the HF at higher concentrations but not used in this study. Other reagents including perchloric and hydrochloric acid could be alternatively used instead of boric acid, neither of which was used in this study since ClO, ClOH, and ArCl can cause interference problems in the measurement of As, Se, V, and Cr by ICP-MS ( USEPA, 1991).

In this study, Whatman filters were put in TFM (Tetrafluormethaxil-regulated trademark of Hoechst) digestion vessels with a capacity of 125 mL. TFM is a PTFE based material, which exhibits many of advantages. It has high density, high working temperature (330°C–350°C). Five of these vessels were used for the sample digestion and one of them is used for acid blanks. Acid mixture of 5 mL HNO<sub>3</sub>+ 1 mL HF was used in order to digest the filters. The digestion vessels were placed in the rotor body and the rotor was placed into microwave cavity. ETHOS 900 Milestone Microwave Digestion Oven was used for sample digestion. Figure 3.20 depicts the microwave digestion oven and digestion vessels. The optimized program on Table 3.12 was used during digestion. It was completed in 24 minutes with 5 minutes ventilation time. High temperature and pressure are reached inside the vessels. It is therefore necessary to cool down the rotor before opening the vessels. After 45 minutes extra cooling under tap water, digestion vessels were opened under the hood with tension wrench. The HF was evaporated without loss of analyte nearly 105 minute over the hot plate operated at a temperature of 80 °C. Then the content of the vessel was transferred into the 50 ml volumetric flask and made up to 50 ml with the ultra-pure water. Volumetric flasks will be emptied into the high density polyethylene (HDPE) bottles. All digestion vessels and flasks were kept in 30 % (v/v) HNO<sub>3</sub> overnight before use.

In all sample preparation and analyses deionized water was used prepared by Barnstead ultrapure deionization unit equipped with two ion exchange cartridges to remove ions, a third cartridge to remove the organic and fourth one to remove the particulate matter. The produced water finally has a resistance of 18.3 MΩ.



Figure 3.20. Microwave digestion oven and digestion vessels

Table 3.12 Operating Program 9 of ETHOS 900 MW digestion system

Step	Time (min)	Power (W)
1	6	250
2	6	400
3	6	650
4	6	250
5	5	Ventilation

### ***Filtration of Samples***

Large quantities of dissolved solids in the sample can deposit on the sampler and skimmer cones of ICP-MS and hence, can affect the results by reducing the orifice size and the instrument performance. For this reason, it is recommended that total solids in samples should be kept below 0.2 % (w/v) or equivalently, 2000 mg/L to minimize solid deposition (USEPA, 1998). Makrolon<sup>®</sup> polycarbonate filter holder with polypropylene filter support obtained from Sartorius AG was used to filter the samples, in which suspended matter was observed after digestion. Sample was poured through the 0.45 µm pore size Millipore brand mixed esters of cellulose filter. HDPE sample bottle was washed with ultra-pure 10 % HNO<sub>3</sub> to ensure that no particle remains in it. Thereafter, filtered sample was transferred back from the filter holder to the sample bottle. One filter was used at a time for one sample. After one sample filtered, filter holder and

associated parts were firstly cleaned three times with 10 % HNO<sub>3</sub> and then all accessories were washed with ultra-pure DI water in order not to contaminate the next sample. Towels were not used to dry the filter apparatus since they may leave lint particles on the filter holder and hence, they may find their way into the next sample.

#### ***3.4.2.2.3. ICP-MS Analysis***

Perkin Elmer DRC-II Model Inductively Coupled Plasma Mass Spectrometry (ICP-MS), with a Pt cone and Pt skimmer and Meinhard Concentric Type A nebulizer, has been employed in this study to carry out the trace element analysis as mentioned in the previous section.

The environment in which the instrument is operated should meet some conditions. For this, room temperature was tried to be kept between 15 and 30 °C. The maximum rate of change of temperature per hour was 2.8 °C, and this was closely observed. For optimum performance relative humidity of the room should be between 20 and 80 %. In order to minimize contamination, this is especially necessary to quantitate ubiquitous elements like Fe, Ca, K, Na etc. below 1 ppb, room was kept free of smoke and other potential contaminant causing materials.

A regulated filtered water was used as a coolant. The pH of the water should be between 6.5 and 8.5. It should be hardness free with less than 1 ppm of heavy minerals. The recirculator operating pressure should be of 344 ± 13 kPa.

In order to start up the instrument, firstly, vacuum pumping was operated and plasma was ignited. Then, analytical conditions including: selection of masses (isotopes), number of times that exposures are counted per analysis, scanning mode and mass regions to be skipped, were all established at this time or previously stored in the system software. Then, it was waited for 30 minutes to warm up the instrument. Afterwards, tuning of the instrument was started.

The instrument was tuned daily using 10 ppb ELAN 6100 DRC Setup/Stab/Masscal solution made up to 2 % HNO<sub>3</sub> acid solution. This multi element tuning solution contains Mg, Cu, Rh, Cd, In, Ba, Ce, Pb and U. Aspiration of the tuning solution was performed to make initial optimization. The purpose of instrument optimization is to achieve maximum signal from atomic, singly charged ions and to reduce formation of interfering polyatomic



ions. Procedures include the following: adjusting the torch position; setting the power and gas flow; setting the MS X-Y position; performing mass calibration, which should be adjusted if any peaks have shifted more than 0.1 amu from the center; optimizing the ion optics; checking and adjusting the channel electron multiplier (CEM) voltage. Low nebulizer argon gas flowrates and adjustment of ion optics voltages generally provide the lowest yields of polyatomic oxides and doubly charged ionic species. Another purpose of using tuning solution was to check the resolution. EPA protocols define good resolution as a peak width of 0.75 amu at 5 % peak height for the Mg isotopes (24, 25, 26) at the low end of the spectrum and Pb isotopes (206, 207 and 208) at the high mass end of the spectrum (Landsberger and Creatchman, 1999). While tuning of the instrument, this principle was followed. Optimized ICP-MS operating parameters followed during the analysis were listed in Table 3.13.

Calibration standards, blanks and samples were then spiked with internal standard. As an internal standard,  $^{103}\text{Rh}$ , was used in order to overcome the physical suppression of the analyte signal owing to the sample matrix components. Rhodium was selected as an internal standard because of following reasons: (1) Qualitative analysis has showed that it is not present in the samples. (2) Sample matrix and analyte elements do not spectrally interfere with it. (3) It has a similar ionization potential with to the groups of analyte elements so they behave similarly in the plasma. A hundred microliter of this standard was spiked into the samples, calibration standards, and blanks at the part per billion (ppb) level to correct for any variations in the response of elements caused by the matrix. As the intensity of internal standard change the element responses were updated every time a sample was analyzed. In addition to the internal standard use for the correction of the interferences, the ELAN Software has its own mathematical correction equations to compensate for spectral interferences.

The final step before the analysis of samples was analytical calibration, which was performed using at least one blank and three calibration standards. The selected analytical masses, and correlation coefficients and slope of the calibration curves of the measured parameters were presented in Table 3.14. Samples were placed into the Perkin Elmer AS 93-plus type of autosampler. There are 157 available places for the samples and standards in the tray of the autosampler. Each result was based on the three integrations. Internal standard element recovery was monitored closely. Recoveries

tried to be kept between 70 % and 120 %. When the recoveries were unacceptably low, samples were diluted and reanalyzed.

Table 3.13 ICP-MS Operating Parameters

a) Instrumental Parameters	
RF power (kW)	1100 Watts
Argon gas flow (L/min)	
• Plasma	15
• Auxiliary	1.2
• Nebulizer	0.97
Peristaltic pump flow (rpm)	18
Sample uptake rate (L/min)	~1
Skimmer Cone	Pt (1.1 aperture diameter in mm)
Sampling Cone	Pt (0.9 aperture diameter in mm)
b) Data acquisition parameters	
Measurement mode	Scanning (Standard)
Number of measurement per peak	50 ms
Mass range (m/z)	5-270 amu
Integration time	1000 ms
Number of repetitions	3
Time per sample measurement	4 min 22 s (including 40 s sample flush)
Rinse time (min)	1 ( plus ~ 30 s read delay )

Table 3.14. Selected analyte masses and correlation coefficient and slope of the calibration curves

<b>Analyte</b>	<b>Mass</b>	<b>Correlation Coefficient (R<sup>2</sup>)</b>	<b>Slope</b>
Li	7	0.999796	0.007
Be	9	0.999979	0.002
B	10	0.999978	0.001
Na	23	0.999748	0.026
Mg	24	0.999912	0.017
Al	27	0.999948	0.026
P	31	0.999968	0.002
K	39	0.999782	0.037
Ca	44	0.999588	0.001
Sc	45	0.999939	0.055
Ti	48	0.999604	0.038
V	51	0.999979	0.054
Cr	52	0.999983	0.047
Fe	54	0.999361	0.004
Mn	55	0.999765	0.069
Ni	58	0.999957	0.035
Co	59	0.999992	0.065
Cu	63	0.999925	0.026
Zn	64	0.999703	0.016
Ge	74	0.999920	0.015
As	75	0.999969	0.006
Se	82	0.999845	0.001
Rb	85	0.999985	0.059
Sr	88	0.999996	0.078
Y	89	0.999989	0.093
Mo	98	0.999992	0.022
Cd	114	0.999822	0.029
In	115	0.999971	0.129
Sn	120	0.999953	0.040
Sb	121	0.999954	0.033
Cs	133	0.999924	0.132
Ba	138	0.999990	0.090
La	139	0.999977	0.122
Ce	140	0.999875	0.113
Pr	141	0.999904	0.142
Nd	144	0.999996	0.033
Eu	151	0.999948	0.061
Sm	152	0.999940	0.034
Gd	158	0.999952	0.029
Tb	159	0.999949	0.121
Dy	162	0.999884	0.031
Ho	165	0.999952	0.115
Er	166	0.999977	0.038
Lu	175	0.999931	0.107
Yb	174	0.999874	0.037
Hf	180	0.986870	0.032

Table 3.14. Selected analyte masses and correlation coefficient and slope of the calibration curves (Continued)

<b>Analyte</b>	<b>Mass</b>	<b>Correlation Coefficient (R<sup>2</sup>)</b>	<b>Slope</b>
Tm	169	0.999953	0.113
Ta	181	0.984751	0.006
W	184	0.999401	0.021
Pt	195	0.999848	0.018
Au	197	0.992332	0.001
Tl	203	0.999871	0.028
Pb	206	0.999876	0.026
Bi	209	0.995542	0.069
Th	232	0.998994	0.091
U	238	0.999921	0.124

#### ***3.4.2.2.4. Quality Assurance and Quality Control (QA/QC)***

##### ***3.4.2.2.4.1. Blank Analysis***

Field, laboratory and reagent blanks were measured in a similar manner with the samples. The measurement of blanks is important to make accurate blank subtraction, especially for low levels of analyte concentrations, and also to calculate the detection limit of the instrument.

Field blanks were collected regularly in a similar manner with the samples except air pull down the filter only for five minutes. Laboratory blanks were un-used Whatman-41 filters. Laboratory and field blanks were treated as the samples and they underwent digestion procedure. Reagent blanks, which are namely HF and HNO<sub>3</sub> acids used in the digestion of the samples, were digested in the Teflon vessels under the same conditions with the samples. After digestion they were diluted to 50 ml with DI water. All these blanks were analyzed by the ICP-MS, for which operating parameters were previously presented in Table 3.13. Average field blank concentration and corresponding standard deviations of the measured parameters was listed in Table 3.15.

Table 3.15 Average Field Blank Concentrations and Standard Deviations  
(ng/100 cm<sup>2</sup> filter)

<b>Element</b>	<b>Mean</b>	<b><math>\delta</math></b>	<b>Element</b>	<b>Mean</b>	<b><math>\delta</math></b>
<b>Li</b>	12.90	4.35	<b>In</b>	0.51	0.34
<b>Be</b>	0.89	0.29	<b>Sn</b>	46	12
<b>B</b>	3350	1850	<b>Sb</b>	11.32	3.29
<b>Na</b>	30500	12500	<b>Cs</b>	0.81	0.35
<b>Mg</b>	7500	2500	<b>Ba</b>	400	245
<b>Al</b>	9800	1940	<b>La</b>	7.95	2.67
<b>P</b>	8100	2900	<b>Hf</b>	1.84	1.20
<b>K</b>	14500	2900	<b>Ta</b>	1.08	0.61
<b>Ca</b>	103500	32120	<b>W</b>	6.26	3.58
<b>Sc</b>	430	190	<b>Pt</b>	0.96	0.18
<b>Ti</b>	662	171	<b>Au</b>	23.52	16.58
<b>V</b>	32.21	7.81	<b>Tl</b>	0.85	0.48
<b>Cr</b>	380	100	<b>Pb</b>	298	97
<b>Mn</b>	130	30	<b>Bi</b>	10.03	5.44
<b>Fe</b>	27820	5200	<b>Ce</b>	12.61	4.86
<b>Co</b>	7.23	3.88	<b>Pr</b>	1.30	0.48
<b>Ni</b>	224	113	<b>Nd</b>	4.31	1.77
<b>Cu</b>	1710	1000	<b>Sm</b>	0.94	0.39
<b>Zn</b>	1060	270	<b>Eu</b>	3.61	3.43
<b>Ge</b>	0.80	0.23	<b>Gd</b>	0.91	0.25
<b>As</b>	5.48	0.88	<b>Tb</b>	0.12	0.05
<b>Se</b>	5.52	3.63	<b>Dy</b>	4.80	4.50
<b>Rb</b>	12.05	2.59	<b>Ho</b>	0.15	0.07
<b>Sr</b>	348	248	<b>Er</b>	0.34	0.06
<b>Y</b>	2.73	1.04	<b>Tm</b>	0.07	0.03
<b>Mo</b>	54.40	35.35	<b>Yb</b>	0.37	0.10
<b>Cd</b>	5.97	1.70	<b>Lu</b>	0.07	0.02
<b>Th</b>	7.21	4.87	<b>U</b>	4.97	3.75

Sample to blank ratios were also calculated based on the average concentrations of samples (N=1458) and those of field blanks (N=24) and results were provided in Figure 3.21. The calculated values range from 2-10 for B, Eu, P, Pt, Ni, Sr, Au, Dy, Ca, Fe, U, Zn, Sn, Cr, and Bi, from 12-30 for Th, Ba, Hf, Co, K, Cd, Li, Ti, La, B, Ce and Al, from 31-52 for Y, Mn, Rb, Mg, Na, Ge, Pr, Tm, Se, Lu, Ho, Sm, Nd, Yb, V, Gd, Tb, and Er, from 58-130 for Sb, Tl, Cs, As, Pb, and Ta. Except for B, Eu, and P, sample to blank ratios for measured elements were larger than 3, indicating that blank subtraction does not have a significant contribution on the observed concentrations. The sample to blank ratios for B, Eu and P were 2.05, 2.50, and 2.79, respectively. It is noteworthy to point out that most of the marker elements for instance, Na, Se, V, Sb, As and Pb, have sample to blank ratio

greater than 20, which in turn means that these elements can easily be detected in the samples.

The percent frequency of observance values were calculated and they were plotted against percent blank subtraction and results were provided in Figure 3.22. Figure 3.22 revealed that most of the elements have less than 30 % blank subtraction while their frequency of observance is around 100 %. As it was discussed in the EDXRF section, Whatman -41 has high P content, which is the reason of around 65 % blank subtraction for P in the ICP-MS analysis. Not only P but also B has high blank subtraction, which is approximately 65 %. In contrast to P, which was detected in 75 % of the samples, B was observed only in 53 % of the analyzed samples. Gold, Eu and Pt have percent blank subtraction between 40 and 60 %, whilst their frequency of observance range from 45 to 63 %.

Average field blank concentrations were also compared with those of DI water and reagent (acid) blanks and results of selected analytes were presented in Figure 3.23. Figure 3.23 revealed that acid blank and DI water compositions were nearly identical, which in turn means that these reagents contributed to contamination at the same proportion. Except for Ge and Pt, field blank concentrations were 50 % higher than those of acid blank and DI water and hence, it can be concluded that most of the contribution is arising from the sample handling and filter itself.

#### ***3.4.2.2.4.2. Detection Limit (DL)***

The United States Environmental Pollution Agency (USEPA) defines the Method Detection Limit (MDL) as 'the minimum concentration that can be determined with 99 % confidence, that the true concentration is greater than zero'. The MDL depends on many factors including equipment, chemicals, methodology, materials, sample composition and even the analysis (USEPA, 1999).

The method detection limit is different from the instrument detection limit (IDL), which is reported by the instrument manufacturers and can only be obtained in case of optimum instrument operating conditions. However, optimum operating conditions can not be achieved all the times.

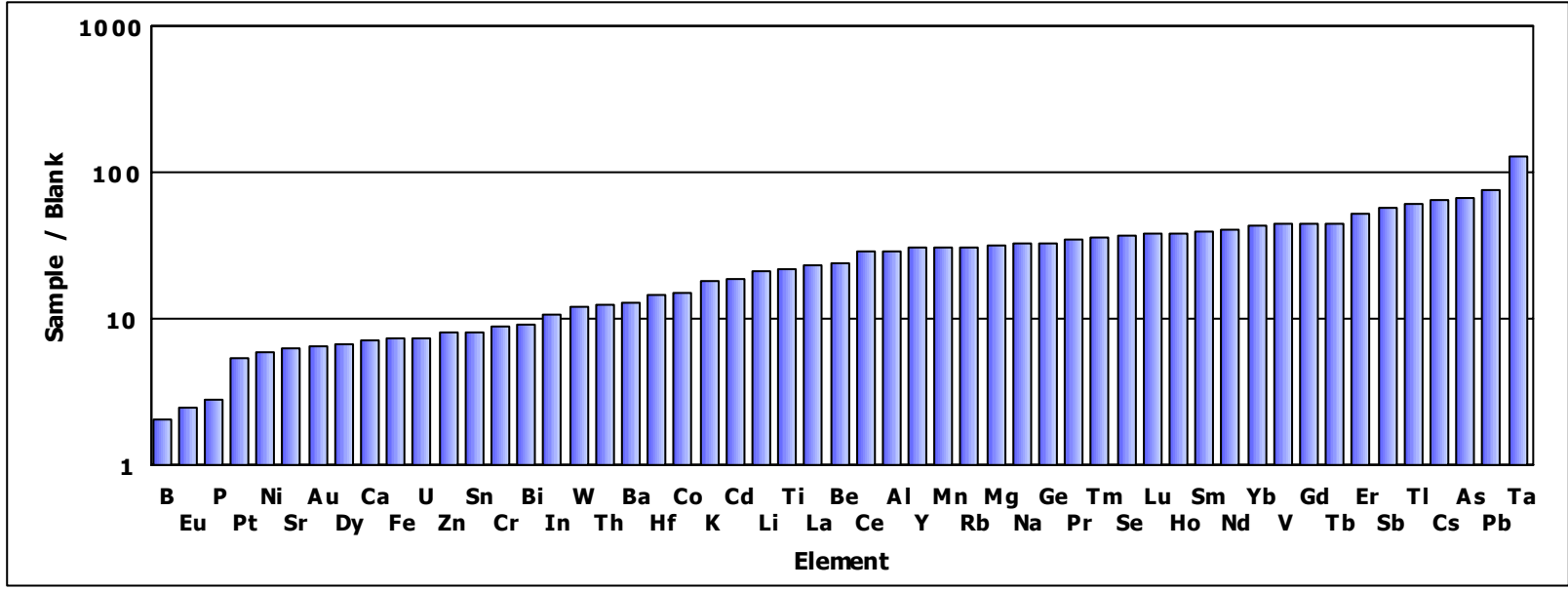


Figure 3.21 Sample to blank ratio for the elements detected in ICP MS analysis

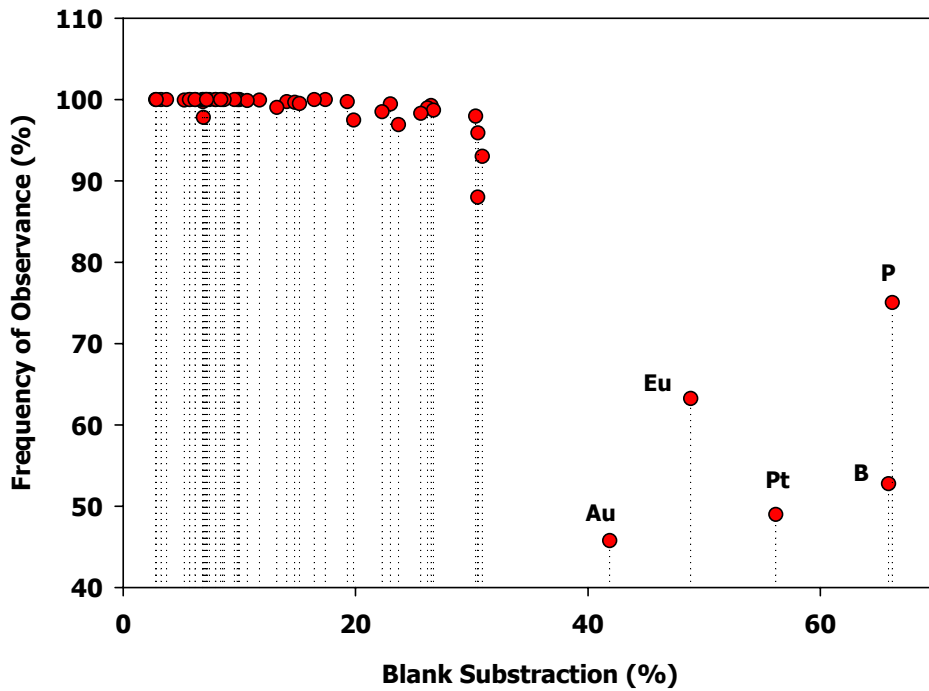


Figure 3.22 Plot of percent frequency of observance versus percent blank subtraction

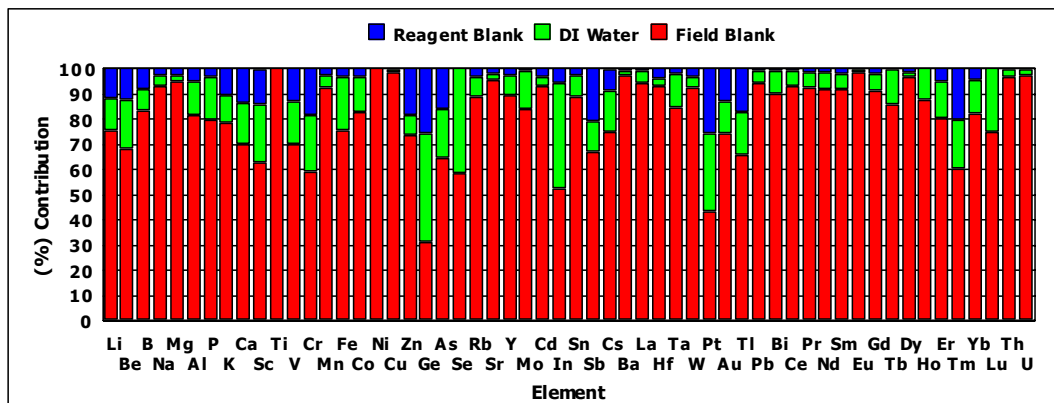


Figure 3.23. Proportions of different elements in field blanks, acid blanks and DI water

For instance, in case of ICP MS, there may be matrix interferences, the sample introduction system may be contaminated by earlier injections, ICP MS cones may not be in perfect condition, or the torch and the injector tube may have deposits. The IDL is a



useful tool in comparing different analytical techniques or different versions of same instrument.

In this study, MDL for each analyte was used to characterize the instrument performance. Standard solutions were prepared in the concentration range from 0.005 ppm to 100 ppm by considering the two to five times of the instrument detection limits. Solutions were aspirated to the ICP MS by ten times. The standard deviation of the results of these multiple runs was then calculated and the associated MDL was computed by following the below equation and results were tabulated in Table 3.16:

$$MDL = t * SD \quad 3.12$$

Where;

MDL=Method Detection Limit

t = Student t value for a 99 % confidence level and a standard deviation estimate with n-1 degrees of freedom (t=2.851 for 10 replicates)

SD= Standard Deviation of 10 replicate analysis

The calculated MDL values range from 0.97 ng/L to 5096 ng/L.

Detection limits based on the standard deviation of the field blanks were also calculated in this study. Galasyn et al. (1987) and Dzubay and Stevens (1984) defined the detection limit in the analysis of atmospheric aerosol as "twice the standard deviation of a number of replicates analysis of field blanks". Table 3.17 shows the calculated detection limits of elements measured in this study. The average concentrations of the elements in samples were also presented in Table 3.17 in terms of ng /23.75 cm<sup>2</sup> filter.

Table 3.16 The MDL values for the measured parameters

<b>Analyte</b>	<b>MDL (ng/L)</b>	<b>Analyte</b>	<b>MDL (ng/L)</b>
<b>Na</b>	2709	<b>Cs</b>	4.79
<b>Mg</b>	3269	<b>Ge</b>	15.17
<b>Al</b>	2416	<b>Hf</b>	14.60
<b>Ca</b>	5096	<b>Co</b>	2.17
<b>Cu</b>	2132	<b>Pt</b>	13.74
<b>K</b>	3120	<b>Tl</b>	16.62
<b>Fe</b>	2758	<b>Bi</b>	25.29
<b>B</b>	864	<b>Cd</b>	12.83
<b>P</b>	1280	<b>In</b>	4.96
<b>Pb</b>	183.83	<b>Ta</b>	12.97
<b>Ti</b>	79.57	<b>Au</b>	76.01
<b>Mo</b>	132.83	<b>Be</b>	28.85
<b>Zn</b>	112.84	<b>Gd</b>	3.28
<b>Mn</b>	114.52	<b>Tb</b>	1.57
<b>Ni</b>	152.04	<b>Pr</b>	0.97
<b>Sr</b>	115.29	<b>Sm</b>	3.96
<b>Ba</b>	86.56	<b>Eu</b>	1.31
<b>V</b>	119.06	<b>Dy</b>	3.68
<b>Cr</b>	130.60	<b>Ho</b>	1.85
<b>As</b>	24.89	<b>Er</b>	3.14
<b>Rb</b>	5.62	<b>Tm</b>	1.54
<b>Sn</b>	6.19	<b>Yb</b>	4.11
<b>Sb</b>	10.78	<b>Lu</b>	1.63
<b>W</b>	15.85	<b>Th</b>	3.51
<b>Se</b>	170.77	<b>U</b>	1.74
<b>Sc</b>	14.97	<b>Nd</b>	3.51
<b>Li</b>	14.31	<b>Y</b>	1.23
<b>Ce</b>	5.45	<b>La</b>	2.14

Table 3.17 Calculated Detection Limits (ng /23.75 cm<sup>2</sup> filter) for the elements measured by ICP MS and sample concentrations

<b>Element</b>	<b>DL</b>	<b>Sample Concentration</b>	
<b>Al</b>	922	6.7•10 <sup>4</sup>	± 16.3•10 <sup>4</sup>
<b>As</b>	0.42	87	± 318
<b>Au</b>	7.88	42.91	± 438.91
<b>B</b>	874	1.7•10 <sup>3</sup>	± 20.5•10 <sup>3</sup>
<b>Ba</b>	116	1.2•10 <sup>3</sup>	± 4.7•10 <sup>3</sup>
<b>Be</b>	0.14	4.94	± 92.69
<b>Bi</b>	2.59	20	± 67
<b>Ca</b>	15255	15.3•10 <sup>4</sup>	± 116.8•10 <sup>4</sup>
<b>Cd</b>	0.81	25.36	± 101.56
<b>Ce</b>	2.31	85	± 211
<b>Co</b>	1.84	24.1	± 78.79
<b>Cr</b>	46.76	780	± 13•10 <sup>3</sup>
<b>Cs</b>	0.16	12.41	± 29.35
<b>Dy</b>	2.14	7.51	± 21.88
<b>Er</b>	0.03	4.18	± 11.65
<b>Eu</b>	1.63	2.25	± 7.7
<b>Fe</b>	2470	42.7•10 <sup>3</sup>	± 311•10 <sup>3</sup>
<b>Gd</b>	0.12	9.68	± 23.69
<b>Ge</b>	0.11	6.2	± 66.21
<b>Hf</b>	0.57	6	± 15.09
<b>Ho</b>	0.03	1.37	± 3.22
<b>In</b>	0.16	1.23	± 13.35
<b>K</b>	1374	5.98•10 <sup>4</sup>	± 89.3•10 <sup>4</sup>
<b>La</b>	1.27	42.84	± 108.71
<b>Li</b>	2.07	63	± 160
<b>Lu</b>	0.01	0.58	± 1.64
<b>Mg</b>	1167	5.5•10 <sup>4</sup>	± 1.3•10 <sup>4</sup>
<b>Mn</b>	13.96	0.93•10 <sup>3</sup>	± 3.2•10 <sup>3</sup>
<b>Na</b>	5900	2.33•10 <sup>5</sup>	± 42.2•10 <sup>4</sup>
<b>Nd</b>	0.84	41	± 98
<b>Ni</b>	53.53	267	± 872
<b>P</b>	1374	4.75•10 <sup>3</sup>	± 97•10 <sup>3</sup>
<b>Pb</b>	45.84	5.3•10 <sup>3</sup>	± 14.4•10 <sup>3</sup>
<b>Pr</b>	0.23	11	± 26
<b>Pt</b>	0.09	1.18	± 18.7
<b>Rb</b>	1.23	87.49	± 259
<b>Sb</b>	1.56	154	± 2.9•10 <sup>3</sup>
<b>Se</b>	1.72	48	± 170
<b>Sm</b>	0.19	8.79	± 21.79
<b>Sn</b>	5.78	79	± 391
<b>Sr</b>	118	445	± 1.4•10 <sup>3</sup>
<b>Ta</b>	0.29	33.58	± 335.6

Table 3.17 Calculated Detection Limits (ng /23.75 cm<sup>2</sup> filter) for the elements measured by ICP MS and sample concentrations (Continued)

<b>Element</b>	<b>DL</b>	<b>Sample Concentration</b>		
Tb	0.02	1.28	±	3.4
Th	2.32	20.17	±	50.56
Ti	81.17	3.27•10 <sup>3</sup>	±	9.96•10 <sup>3</sup>
Tl	0.23	12.11	±	67.36
Tm	0.01	0.57	±	1.39
U	1.78	7.8	±	14.93
V	3.71	335	±	896
W	1.7	17.21	±	224.18
Y	0.5	19.48	±	56.08
Yb	0.05	3.81	±	10.57
Zn	128	1.8•10 <sup>3</sup>	±	11.7•10 <sup>3</sup>

As it can be seen in Table 3.17, the calculated detection limit values are significantly smaller than the observed average concentrations for all of the elements.

#### **3.4.2.2.4.3. Accuracy of Trace Metal Determination by ICP MS**

In the analytical chemistry, accuracy of the measurement is defined as “closeness of the agreement between the results of a measurement and a true value” (Dean, 1997). The true value is the value certified in a standard reference material (SRM) or it is the one that can be obtained by two or more independent procedures employed to get the same value. Accuracy depends on the several factors like purity of the reagents used, the sample matrix, and the chemical form of the analyte. The accuracy of the measurement was determined by employing below equation:

$$A = \frac{(C_m - C_t) * 100}{C_m} \quad 3.13$$

Where;

C<sub>m</sub>: Measured value

C<sub>t</sub>: Standart reference material value

A: Accuracy (in percent)

Since a large data set produced in this study, the determination of accuracy is a crucial step to obtain the reliable results. The Standard Reference Material (SRM) 1648 obtained by the National Institute of Standard and Technology (NIST) was used in the determination of accuracy. SRM 1648 is an urban particulate matter used in the evaluation of methods employed in the analysis of atmospheric particulate matter and materials with a similar matrix.

SRM 1648 was digested in a similar manner with the samples and then aspirated to the ICP MS. Table 3.18 shows the calculated percent error values for some of the selected elements.

Negative accuracy values in Table 3.18 indicate that the corresponding elements could not be completely decomposed during digestion. Except for Co, for which associated accuracy values was found as around 11 %, the accuracy was lower than 10 % for selected elements.

#### ***3.4.2.2.4.4. Precision of Trace Metal Determination by ICP MS***

The definition of the precision was given in the previous section. For the ICP MS analysis, precision values were also computed and results for three samples are provided in Figure 3.24 below. The calculated percent RSD values were based on the 26 samples and 3 sequential runs for each sample. Figure 3.24 revealed that all the calculated precision values are lower than 10 % for all of the analytes determined. The percent RSD values calculated for Dy, Ho, Er are 4.95, 5.66 and 5.18 %, respectively. These analytes have the highest percent RSD values in the generated data set. Since obtained precision values are acceptable, it can be concluded that repeatability of ICP MS results is good.

Table 3.18 Shows the percent accuracy values for selected elements of SRM 1648

Element	Unit	Certified		Measured		Error %
		Mean ± SD		Mean ± SD		
<b>Al</b>	%	3.22 ± 0.16		3.486 ± 0.05		8.26
<b>Ca</b>	%	5.83 ± 0.33		6.38 ± 0.03		9.43
<b>Cd</b>	ppb	72 ± 2		74.29 ± 1.87		3.18
<b>Ce</b>	ppb	55 ± 4		57.71 ± 0.37		4.93
<b>Co</b>	ppb	17.4 ± 1.8		15.42 ± 0.37		-11.38
<b>Cs</b>	ppb	3.5 ± 0.2		3.59 ± 0.04		2.57
<b>Fe</b>	%	3.92 ± 0.24		3.63 ± 0.05		-7.4
<b>K</b>	ppb	1.03 ± 0.5		1.06 ± 0.03		2.91
<b>La</b>	ppb	39 ± 3		39.4 ± 0.04		1.03
<b>Mn</b>	ppb	822 ± 45		769 ± 19.5		-6.45
<b>Na</b>	ppb	4230 ± 230		4564.8 ± 63.25		7.91
<b>Sb</b>	ppb	44 ± 2		41.8 ± 0.4		-5
<b>Se</b>	ppb	24 ± 2		22.3 ± 2.2		-7.08
<b>Sr</b>	ppb	207 ± 15		214.03 ± 4.12		3.4

#### 3.4.2.2.4.5. Uncertainty of Trace Metal Determination by ICP MS

Definition of the uncertainty was provided in the previous section. In ICP MS analysis, uncertainty arising from the digestion of samples was also taken into account in addition to total uncertainty calculated for EDXRF.

$$\sigma_t^2 = \sigma_a^2 + \sigma_c^2 + \sigma_d^2 + \sigma_{vol}^2 + \sigma_w^2 \quad 3.14$$

Where;

$\sigma_t$  = total uncertainty,

$\sigma_a$  = analytical uncertainty,

$\sigma_c$  = calibration uncertainty, and

$\sigma_d$  = digestion uncertainty,

$\sigma_{vol}$  = uncertainty in air volume measurements,

$\sigma_w$  = uncertainty in weighing of samples

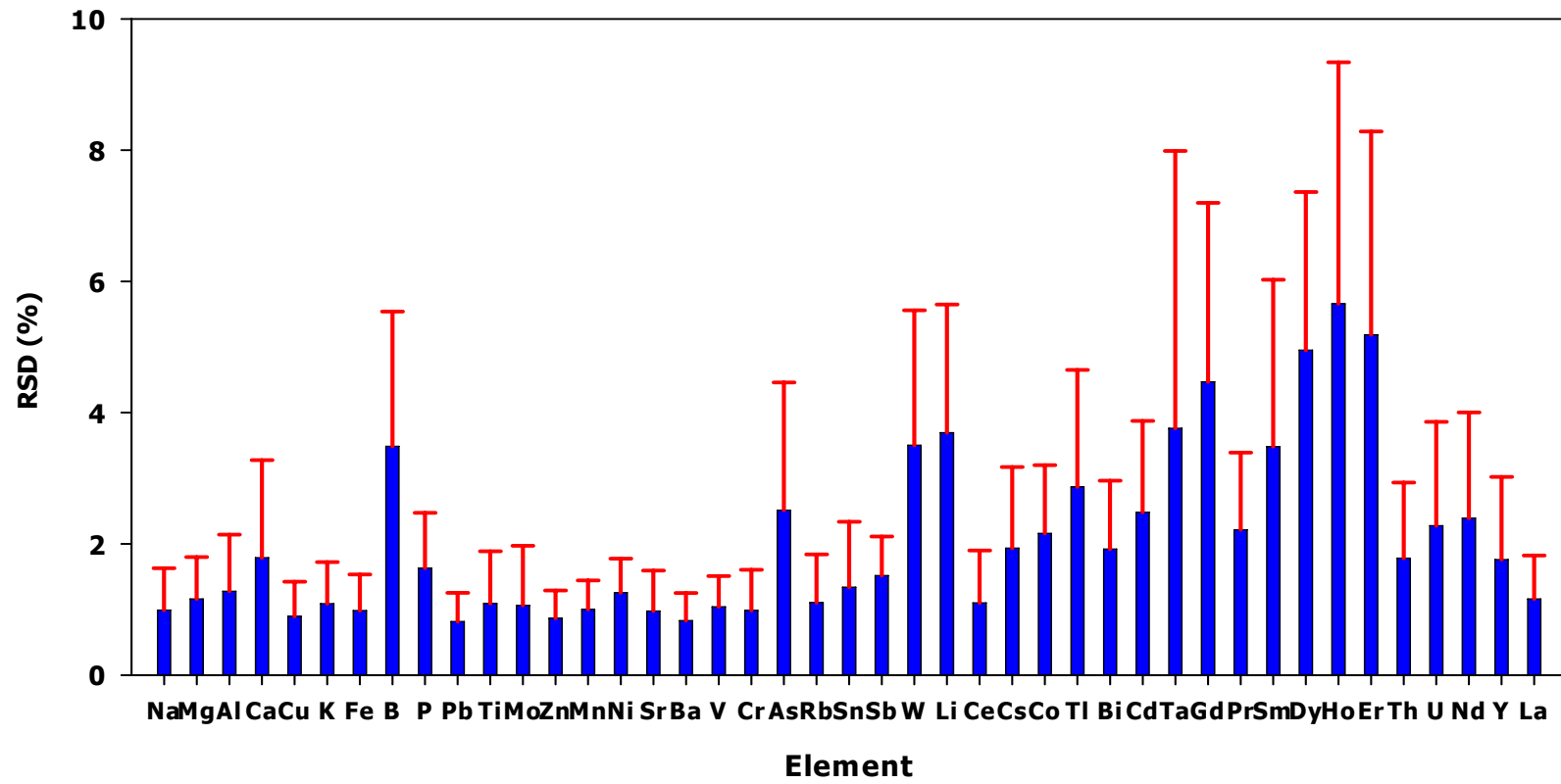


Figure 3.24. Shows the calculated precision values for the analyzed parameters

The uncertainty corresponding to calibration, air volume measurements and weighing of the samples were assumed as 5 % for each. Uncertainty associated with sample digestion was taken as 4 %. For the analytical uncertainty, mean absolute relative standard deviation of the samples was used. The total uncertainty was calculated and results were provided in Figure 3.25 below:

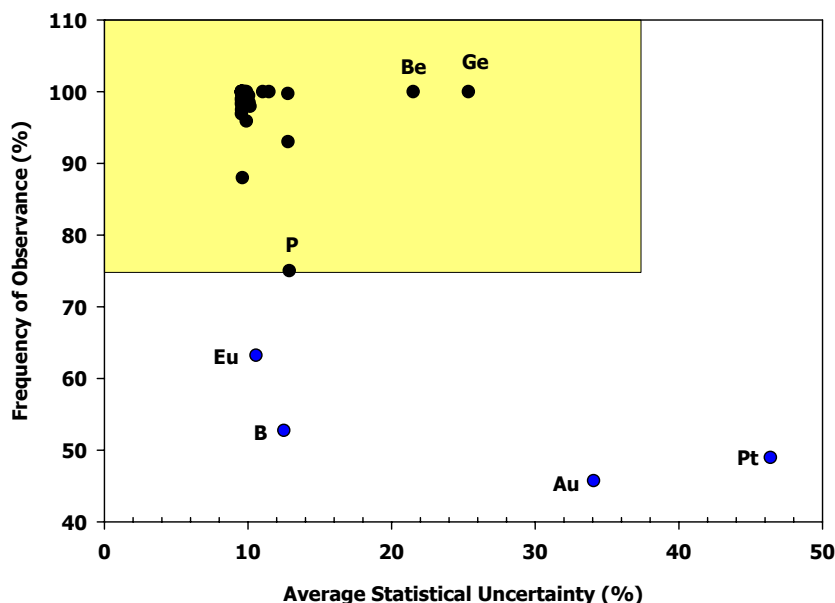


Figure 3.25. Shows the relationship between calculated average statistical uncertainty and frequency of observance

Figure 3.25 points out that most of the calculated uncertainty values were smaller than ~ 15 % except for Be, Ge, Au and Pt, for which calculated uncertainty values were found as 21.5, 25.35, 34.06 and 46.38 %, respectively. Only Eu, B, Au and Pt had frequency of observance lower than 70 %. The contribution of the aforementioned steps on total uncertainty calculation was small to be considered as significant error in measured concentrations based on these calculations. For the elements having frequency of observance value less than 70 %, which are B, Ge, Au and Pt, were not considered as reliable elements and were not included in the further discussions in this study. Percent frequency and average statistical uncertainties were presented in Table 3.19 below.



Table 3.19 Calculated statistical uncertainty and frequency of observation for the elements measured by ICP MS

Element	Statistical Uncertainty	Frequency of Observation	Element	Statistical Uncertainty	Frequency of Observation
	%	%		%	%
<b>Be</b>	22	100	<b>Tb</b>	10	100
<b>P</b>	13	75	<b>Er</b>	10	100
<b>Cr</b>	13	93	<b>Y</b>	10	100
<b>K</b>	13	100	<b>Nd</b>	10	100
<b>Tl</b>	11	100	<b>Sm</b>	10	100
<b>Lu</b>	11	100	<b>Mn</b>	10	100
<b>Eu</b>	11	63	<b>Pr</b>	10	100
<b>Fe</b>	10	98	<b>Pb</b>	10	100
<b>W</b>	10	98	<b>Ho</b>	10	100
<b>Zn</b>	10	99	<b>Na</b>	10	100
<b>Ca</b>	10	99	<b>Yb</b>	10	100
<b>Li</b>	10	100	<b>Th</b>	10	97
<b>In</b>	10	96	<b>Cs</b>	10	100
<b>Sn</b>	10	100	<b>Sb</b>	10	100
<b>Tm</b>	10	100	<b>Sr</b>	10	99
<b>Cd</b>	10	100	<b>Rb</b>	10	100
<b>Gd</b>	10	100	<b>Ni</b>	10	99
<b>Ta</b>	10	99	<b>Mg</b>	10	100
<b>As</b>	10	100	<b>Ti</b>	10	100
<b>Hf</b>	10	100	<b>Al</b>	10	100
<b>Ba</b>	10	100	<b>U</b>	10	97
<b>Dy</b>	10	88	<b>Ce</b>	10	100
<b>Se</b>	10	98	<b>Bi</b>	10	98
<b>Co</b>	10	100	<b>La</b>	10	100
<b>V</b>	10	100			

#### ***3.4.2.3. Comparison of Analytical Techniques***

As it is stated previously ICP MS, EDXRF and IC were the main analytical techniques employed to find the chemical composition of the aerosols in this study. Sulfate and Cl were the common analytes measured both by IC and EDXRF. Magnesium, Ca, Al, Ti, Cr, Fe, Mn, Pb, Ni, Zn and K were analyzed both ICP MS and EDXRF. All samples were analyzed by utilizing these three different techniques. In this section of this study, agreement between these techniques was investigated.

In order to find the degree of correlation between ICP MS and XRF, the ratio of results corresponding to two techniques were calculated and also correlation coefficients were estimated for each common parameter only in 100 samples and results were summarized in Figure 3.26.

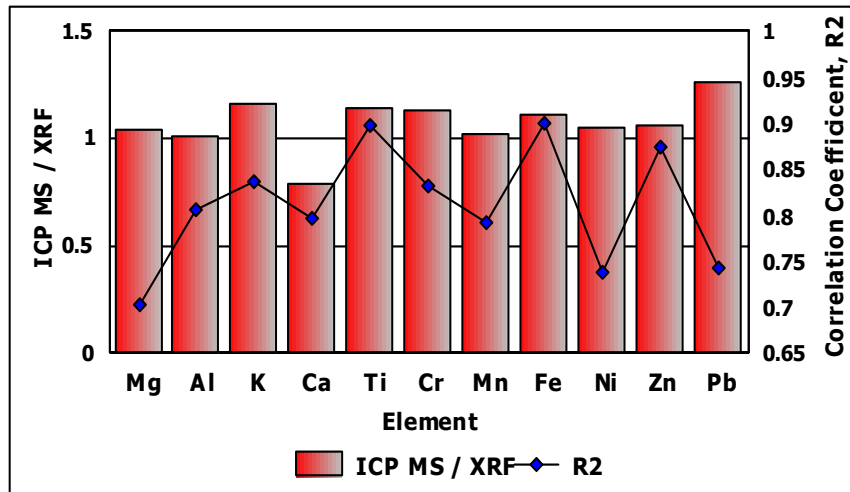


Figure 3.26. Comparison of ICP MS and XRF for the measured common parameters

Figure 3.26 revealed that the agreement between two analytical methods is within 70 % and higher for all of the measured parameters. With the exception of Ca and Pb, the estimated ICP MS to XRF ratio was close to 1 for the rest of the elements. The ICP MS to XRF ratio was calculated as 0.79 and 1.26 for Ca and Pb, respectively.

The agreement between the XRF and IC was also searched in this section; however, comparison was conducted based on the samples collected in 1993. The common analytes, namely,  $\text{SO}_4^{2-}$  and  $\text{Cl}^-$  were regressed to find the correlation between the analytical techniques. Figure 3.27 and 3.28 show the scatter plots of the parameters of concern. Figure 3.27 and 3.28 showed that there is a strong correlation between the measured parameters by XRF and ICP MS. The plots associated to other years in the sampling campaign were also drawn. After the analysis of the plots, it was decided that XRF gave more consistent results as compared to IC and, hence, the IC results of  $\text{SO}_4^{2-}$  were not included in the thesis data. Regarding to  $\text{Cl}^-$ , more reliable results were obtained

in IC analysis associated with the years of 1997, 1998, 1999 and 2000. For the rest of the years in the study period, XRF results were considered for  $\text{Cl}^-$  in the generated data set.

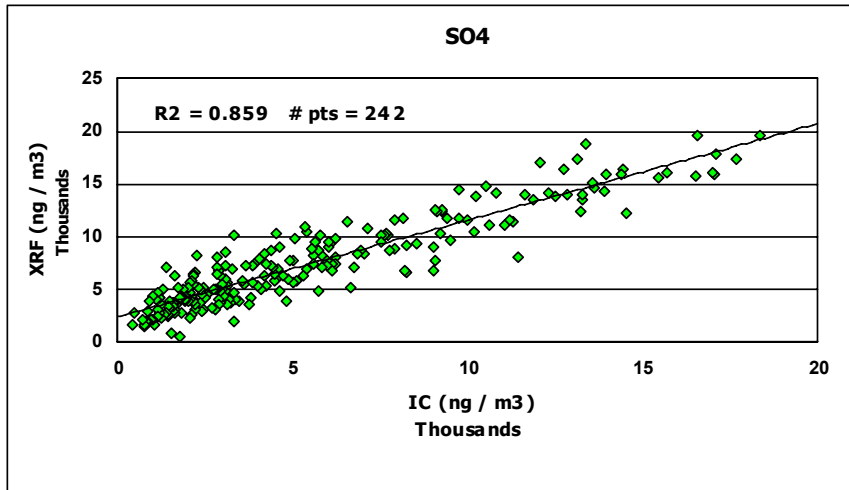


Figure 3.27 Plot of XRF versus IC for  $\text{SO}_4^{2-}$  measurement

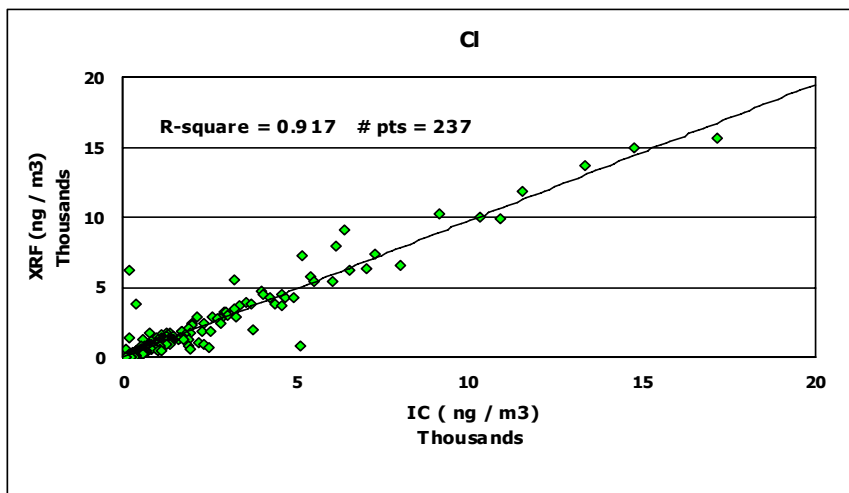


Figure 3.28 Plot of XRF versus IC for  $\text{Cl}^-$  measurement

## CHAPTER 4

### RESULTS & DISCUSSION

#### 4.1. GENERAL CHARACTERISTICS OF ATMOSPHERIC DATA

Three different analytical techniques, namely ICP MS, IC and EDXRF, were employed in this study to find the elemental and ionic compositions of aerosols collected at the Turkish Mediterranean coast, Antalya.

The concentration of aerosol variables and key statistics for each of these variables measured between 1993 and 2001, at Antalya is summarized in Table 1. Table 1 includes the number of samples analyzed in this study for each aerosol variable, their corresponding arithmetic mean, arithmetic standard deviation, mode, median, geometric mean and geometric standard deviation.

The values of the arithmetic mean, median, and mode are identical for a symmetric Gaussian distribution. If the mode < median < arithmetic mean, then the upper tail of the distribution extends toward the larger values (i.e. positively skewed). If the order is reversed, it is negatively skewed. Since these three numbers can be used to describe the location of the center of probability distribution, they are called the location parameters (Cheng et al., 1991). In this study, the order of mode < median < arithmetic mean is hold for most of the variable, and hence variables of concern are positively skewed. For some of the parameters, mode > median and even arithmetic mean, however, it is shown in Section 4.1.1 that all of the measured parameters are positively skewed in this study.

As stated earlier in this section, geometric means and associated geometric standard deviations of the measured variables are also calculated in this study and they are also provided in Table 1. The geometric mean and its standard deviation are defined as follows (Cheng *et al.*, 1991):

$$\bar{x}_g = \exp \left[ \frac{\sum_{i=1}^N \ln x_i}{N} \right] \quad (4.1)$$

While the geometric standard deviation is given in Kao and Friedlander (1995) as:

$$\sigma_g = \exp \left[ \frac{\sum_{i=1}^N (\ln x_i - \ln \bar{x}_g)^2}{(N-1)} \right]^{1/2} \quad (4.2)$$

Where;

$x_i$  : Concentration of element in the  $i^{\text{th}}$  sample,

$N$  : Number of samples,

$\bar{x}_g$  : Geometric mean and

$\sigma_g$  : Geometric standard deviation.

The dimensionless geometric standard deviation for each measured variable stands for the spread in the data around the geometric mean. The geometric standard deviation indicates the various stochastic processes that affect the chemical components. Some physical processes are common to all gas and particle phase pollutants in the atmosphere like meteorological processes, while other physical (e.g., dry and wet deposition) and chemical (e.g., equilibrium relationships) processes change depending on the pollutant type (Kao and Friedlander, 1995). Kao and Friedlander (1995) found that geometric standard deviations of the non-reactive species like Al and Pb were relatively constant,  $1.85 \pm 0.14$ , despite they are released to the atmosphere from different sources while reactive species like  $\text{SO}_4^{2-}$ ,  $\text{NO}_3^-$  and  $\text{NH}_4^+$  had geometric standard deviations larger than that of non-reactive species. Accordingly, it was concluded that geometric standard deviation does not strongly depend on the source type; the variations in non-reactive species should be attributed to the meteorological parameters and deposition mechanisms.

When one compare the arithmetic and geometric mean values for the measured parameters in Table 4.1, it can be easily seen that all the calculated arithmetic means are smaller than the corresponding geometric means, which confirms the previous finding

pointed in this section that all the measured variables are positively skewed. Furthermore, it can be concluded that variables having geometric standard deviations larger than 3 are highly skewed. The concentrations given in Table 1 ranges from 15.4  $\mu\text{g m}^{-3}$  for Ho to 7.93  $\mu\text{g m}^{-3}$  for  $\text{SO}_4^{2-}$ , respectively.

#### **4.1.1 Distribution Characteristics of the Eastern Mediterranean Aerosols**

In order to assess distribution characteristics of measured elements and ions in generated data set, a bunch of parameters such as Skewness Index, Kurtosis Coefficient, KS-DN and ALPHA values were calculated herein. Detailed information on these parameters was provided previously in Section 2.7 and will not be repeated here again. Skewness Index and Kurtosis Coefficient values were determined by using a statistical software package so called MINITAB (MINITAB INC., 15.I.0.0). The KS-DN values were taken from the goodness of fit test output dialog of STATGRAPHICS Plus 3.1 (Statistical Graphics Cooperation, version 3.1), and ALPHA values for each measured parameter were estimated by applying the Equation 2.29 given in Section 2.7 of this manuscript, accordingly. These calculated parameters for each measured aerosol variable were presented in Table 4.2.

When one examined the Table 4.2 in terms of SI values, it can be easily seen that all the measured parameters have positive SI value implying that corresponding distributions are positively skewed, the distribution curves have extend towards right. In addition, the calculated Kurtosis coefficients are also greater than zero indicating that none of the measured aerosol variables fit to the normal distribution.

With the exception of Al, B, Cd, Cl, K, Lu and Sr, the K-S DN test for goodness of fit was performed using STATGRAPHICS Plus 3.1 indicated the elements given in Table 4.2 as log-normally distributed. The calculated ALPHA values for Al, B, Cd, Cl, K, Lu and Sr were less than 1.36 suggesting that these elements also conform to log-normal distribution. None of the rest of the elements shown in Table 4.2 fit any kind of distribution.

Lognormal distribution is common in atmospheric data sets and attributed to dependence of measured concentrations on meteorological parameters. For example, consider a receptor close to a source. When the wind blows from the source, very high pollutant concentrations are measured at the receptor. But if the receptor is not downwind from the source high concentrations will be measured for only one or two hours of the day and

low concentrations will be measured in the rest of the day, when wind carries pollutants to other directions. When frequency distributions are prepared for the receptor, high concentration that were measured for few hours appear as outliers. However, that data are real and not artifacts.

Table 4.1 Summary statistics of Eastern Mediterranean Aerosol Data (in terms of ng m<sup>-3</sup>)

<b>Element</b>	<b>n</b>	<b>Mean</b>	<b>±</b>	<b>δ</b>	<b>Median</b>	<b>Mode</b>	<b>Geometric Mean<sup>1</sup> (δ)</b>
<b>Al</b>	1452	661	±	1424	354	533	332 (3.2)
<b>As</b>	1452	0.82	±	2.42	0.60	0.64	0.58 (2.1)
<b>Au</b>	665	0.40	±	3.65	0.088	0.018	0.081 (3.8)
<b>B</b>	768	15	±	162	3.28	1.67	3.04 (4.9)
<b>Ba</b>	1446	11	±	42	6.86	10	6.58 (2.6)
<b>Be</b>	1445	0.044	±	0.73	0.014	0.011	0.014 (2.9)
<b>Bi</b>	1428	0.21	±	0.77	0.082	0.083	0.082 (3.1)
<b>Ca</b>	1442	1422	±	9171	775	355	741 (2.5)
<b>Cd</b>	1451	0.24	±	0.75	0.17	0.16	0.17 (2.2)
<b>Ce</b>	1450	0.85	±	1.97	0.45	0.53	0.44 (3.0)
<b>Cl</b>	1346	1885	±	2526	1115	297	1069 (3.0)
<b>Co</b>	1448	0.23	±	0.62	0.13	0.04	0.13 (2.8)
<b>Cr</b>	1351	6.77	±	103	2.60	4.63	2.22 (3.2)
<b>Cs</b>	1451	0.12	±	0.23	0.082	0.061	0.081 (2.4)
<b>Dy</b>	1281	0.088	±	0.35	0.035	0.047	0.032 (3.9)
<b>Er</b>	1452	0.045	±	0.18	0.020	0.058	0.02 (3.2)
<b>Eu</b>	921	0.074	±	0.56	0.001	0.005	0.009 (4.3)
<b>Fe</b>	1423	400	±	2450	193	70	174 (3.2)
<b>Gd</b>	1452	0.097	±	0.22	0.047	0.052	0.048 (3.2)
<b>Ge</b>	1451	0.057	±	0.52	0.031	0.052	0.031 (2.2)
<b>Hf</b>	1445	0.060	±	0.13	0.031	0.06	0.030 (3.1)
<b>Ho</b>	1451	0.015	±	0.072	0.007	0.005	0.007 (3.2)
<b>In</b>	1393	0.024	±	0.29	0.003	0.004	0.003 (3.3)
<b>K</b>	1449	536	±	7049	245	490	245 (2.3)
<b>La</b>	1450	0.43	±	1.02	0.24	0.57	0.23 (3.0)
<b>Li</b>	1450	0.61	±	1.32	0.38	0.52	0.37 (2.5)

<sup>1</sup> δ denotes the geometric standard deviation and it is given in the paranthesis for each aerosol variable

Table 4.2 Summary statistics of Eastern Mediterranean Aerosol Data (in terms of ng m<sup>-3</sup>)  
(Continued)

<b>Element</b>	<b>n</b>	<b>Mean</b>	<b>±</b>	<b>δ</b>	<b>Median</b>	<b>Mode</b>	<b>Geometric Mean<sup>2</sup> (δ)</b>
<b>Lu</b>	1449	0.033	±	0.45	0.003	0.006	0.003 (3.2)
<b>Mg</b>	1451	538	±	1104	363	580	366 (2.2)
<b>Mn</b>	1452	8.93	±	24	6	5.4	5.63 (2.5)
<b>Na</b>	1448	2241	±	3551	1296	667	1352 (2.6)
<b>Nd</b>	1451	0.41	±	0.92	0.21	0.56	0.21 (3.1)
<b>NH<sub>4</sub><sup>+</sup></b>	849	1136	±	1142	667	30	589 (3.8)
<b>Ni</b>	1438	2.52	±	6.50	1.75	0.41	1.65 (2.4)
<b>NO<sub>3</sub><sup>-</sup></b>	945	1285	±	1261	924	367	858 (2.6)
<b>Pb</b>	1452	52	±	110	38	57	35 (2.4)
<b>Pr</b>	1451	0.11	±	0.24	0.056	0.089	0.055 (3.0)
<b>Pt</b>	713	0.14	±	0.95	0.002	0.004	0.002 (3.6)
<b>Rb</b>	1452	0.84	±	1.98	0.56	0.76	0.56 (2.3)
<b>Sb</b>	1451	1.77	±	39	0.56	0.53	0.55 (2.0)
<b>Se</b>	1421	0.45	±	1.29	0.23	0.30	0.25 (2.7)
<b>Sm</b>	1452	0.093	±	0.30	0.044	0.065	0.045 (3.1)
<b>Sn</b>	1448	0.75	±	2.91	0.52	0.54	0.50 (2.1)
<b>SO<sub>4</sub><sup>2-</sup></b>	1421	7927	±	5136	6431	2365	6463 (1.9)
<b>Sr</b>	1435	4.28	±	12	2.63	6.05	2.53 (2.6)
<b>Tb</b>	1452	0.024	±	0.27	0.006	0.005	0.006 (3.2)
<b>Th</b>	1417	0.12	±	0.45	0.11	0.061	0.095 (3.6)
<b>Ti</b>	1451	32	±	83	17	6.31	17 (2.9)
<b>Tm</b>	1450	0.034	±	0.44	0.003	0.005	0.003 (3.2)
<b>U</b>	1408	0.083	±	0.22	0.05	0.058	0.045 (3.1)
<b>V</b>	1450	3.17	±	7.0	2.14	5.38	2.1 (2.4)
<b>W</b>	1432	0.20	±	2.5	0.064	0.079	0.059 (2.7)
<b>Y</b>	1452	0.20	±	0.46	0.11	0.055	0.103 (2.9)
<b>Yb</b>	1452	0.038	±	0.094	0.018	0.059	0.018 (3.2)
<b>Zn</b>	1444	17	±	92	9.40	4.67	9.53 (2.4)

<sup>2</sup> δ denotes the geometric standard deviation and it is given in the paranthesis for each aerosol variable



Table 4.3 Distribution fitting parameters for the measured aerosol variables  
(in terms of ng m<sup>-3</sup>)

<b>Element</b>	<b>SI</b>	<b>Kurtosis</b>	<b>KS-DN</b>	<b>Alpha</b>	<b>Distribution Type</b>
<b>Al</b>	13	253	0.033	1.25	Log-normal
<b>As</b>	24	623	0.044	1.68	
<b>Au</b>	20	440	0.056	1.45	
<b>B</b>	26	718	0.049	1.35	Log-normal
<b>Ba</b>	21	464	0.055	2.12	
<b>Be</b>	38	1430	0.045	1.70	
<b>Bi</b>	10	117	0.061	2.32	
<b>Ca</b>	29	919	0.042	1.61	
<b>Cd</b>	30	1010	0.048	1.83	
<b>Ce</b>	13	231	0.022	0.85	Log-normal
<b>Cl</b>	4	28	0.035	1.29	Log-normal
<b>Co</b>	21	554	0.029	1.10	Log-normal
<b>Cr</b>	36	1309	0.085	3.13	
<b>Cs</b>	24	744	0.022	0.84	Log-normal
<b>Dy</b>	16	308	0.039	1.39	
<b>Er</b>	23	659	0.017	0.63	Log-normal
<b>Eu</b>	13	177	0.051	1.55	
<b>Fe</b>	30	994	0.048	1.83	
<b>Gd</b>	12	183	0.014	0.53	Log-normal
<b>Ge</b>	37	1390	0.044	1.70	
<b>Hf</b>	12	186	0.036	1.37	
<b>Ho</b>	29	983	0.018	0.69	Log-normal
<b>In</b>	22	549	0.086	3.24	
<b>K</b>	37	1398	0.035	1.35	Log-normal
<b>La</b>	14	249	0.023	0.87	Log-normal
<b>Li</b>	16	316	0.030	1.15	Log-normal
<b>Lu</b>	18	329	0.034	1.28	Log-normal
<b>Mg</b>	20	484	0.002	0.08	Log-normal
<b>Mn</b>	26	797	0.034	1.30	Log-normal
<b>Na</b>	12	255	0.023895	0.91	Log-normal
<b>Nd</b>	12	201	0.015669	0.60	Log-normal
<b>NH<sub>4</sub><sup>+</sup></b>	1	1	0.086705	2.54	
<b>Ni</b>	30	1025	0.046222	1.76	
<b>NO<sub>3</sub><sup>-</sup></b>	3	15	0.050988	1.57	
<b>P</b>	32	1047	0.086992	2.88	
<b>Pb</b>	28	942	0.04043	1.55	
<b>Pr</b>	12	207	0.016298	0.62	Log-normal
<b>Pt</b>	7	58	0.150976	4.05	
<b>Rb</b>	27	881	0.0224	0.86	Log-normal
<b>Sb</b>	38	1443	0.069485	2.66	
<b>Se</b>	26	836	0.058407	2.21	
<b>Sm</b>	20	517	0.016514	0.63	Log-normal
<b>Sn</b>	28	834	0.037538	1.43	

Table 4.4 Distribution fitting parameters for the measured aerosol variables  
(in terms of  $\text{ng m}^{-3}$ ) (Continued)

<b>Element</b>	<b>SI</b>	<b>Kurtosis</b>	<b>KS-DN</b>	<b>Alpha</b>	<b>Distribution Type</b>
<b>SO<sub>4</sub><sup>2-</sup></b>	1	3	0.037439	1.42	
<b>Sr</b>	19	435	0.033703	1.28	Log-normal
<b>Ta</b>	29	950	0.063257	2.41	
<b>Tb</b>	22	471	0.021439	0.82	Log-normal
<b>Th</b>	14	254	0.04737	1.79	
<b>Ti</b>	17	414	0.023422	0.90	Log-normal
<b>Tm</b>	17	322	0.038979	1.49	
<b>U</b>	21	543	0.058303	2.19	
<b>V</b>	21	511	0.02165	0.83	Log-normal
<b>W</b>	36	1321	0.059387	2.25	
<b>Y</b>	18	468	0.030665	1.17	Log-normal
<b>Yb</b>	13	214	0.019747	0.75	Log-normal
<b>Zn</b>	30	981	0.038221	1.46	

The frequency histograms and associated distribution curves for Na, Mg, SO<sub>4</sub><sup>2-</sup> and NO<sub>3</sub><sup>-</sup>, are given in Figures 4.1 and 4.2, respectively. Among these Na and Mg are the elements with typical lognormal distribution, whereas goodness of the fit test applied to SO<sub>4</sub><sup>2-</sup> and NO<sub>3</sub><sup>-</sup> showed that their distributions are not lognormal within 5% confidence interval. However, it is clear from figure that these two ions have also skewed distributions, but those distributions are not lognormal.

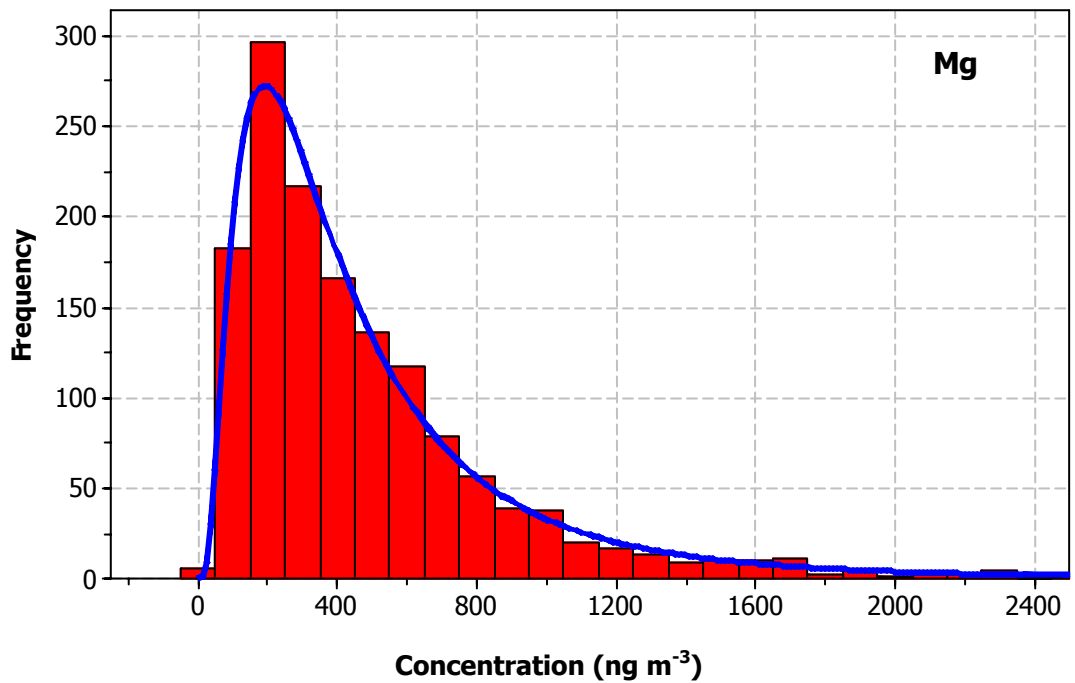
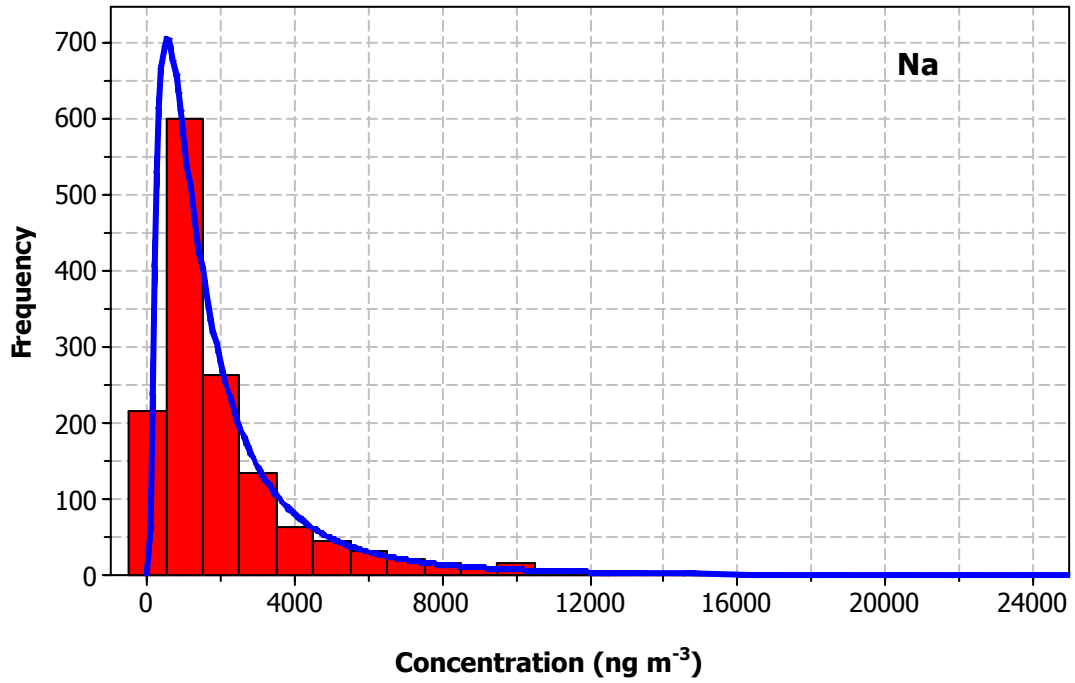


Figure 4.1 Frequency histograms and associated distribution curves for Na and Mg

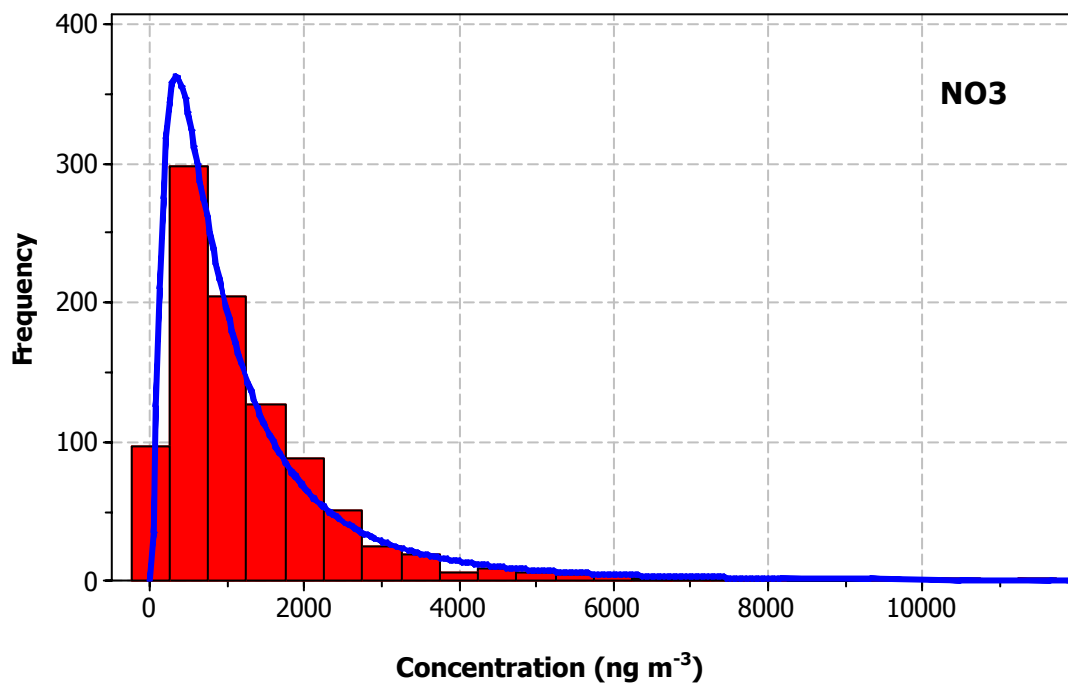
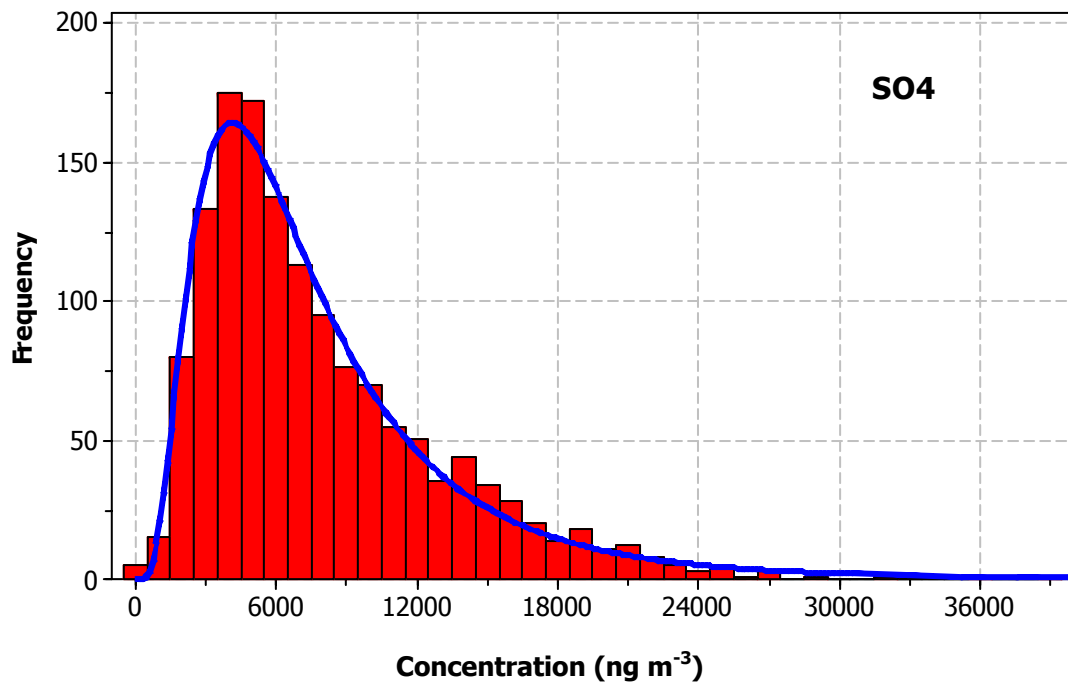


Figure 4.2 Frequency histograms and associated distribution curves for  $\text{SO}_4^{2-}$  and  $\text{NO}_3^-$

#### 4.1.2. Comparison with Literature

In order to give insight about the pollution level at Antalya station, concentration values obtained in this study were compared with those reported for other Mediterranean sites in literature. Two points were considered to make a realistic comparison: (1) Time of data generation and (2) Location of study area. Since concentrations of trace elements and major ions are shown to change (decrease) in time, literature data that were generated more or less at the same period with this study were selected for comparison. Studies performed along or close the coast of Mediterranean Sea was selected as concentration of some of the parameters change if one move from shore to inland.

Although a very extensive comparison with literature were aimed which could very informative, we were limited with the parameters measured in the literature. More than 50 elements were measured in this study using ICP-MS. Since such an extensive data set does not exist in the literature for the Mediterranean region, the comparison was limited with elements commonly measured in the Mediterranean sites.

The detailed information about the sampling sites used for the comparison was provided below:

1. Capo Carbonara Station, Sardinia (Latitude: 39° N, Longitude: 9° E) (Rossini et al., 1999)

This station is a remote coastal one located in southest Sardinia. Samples were collected at this station by employing high volume Sierra Andersen sampler in the period October 1990- October 1992. Sampling time ranged from 48 to 72-h. Graphite furnace and flame atomic absorbtion spectrometry were used together to find out the trace element content of the 55 aerosol samples. Concentrations were given in terms of their arithmetic mean values.

2. Tarragona Stations, Spain (Mareno et al., 2006)

Tarragona station (Longitude: 01° 14' 52" E , Latitude: 41° 07' 29" N) is located on the Mediterranean coast of Spain and it is 98 km southwest of Barcelona. This station is

under the influence of urban environment, port and industrial emissions. The 24-h PM<sub>10</sub> samples were collected at the station during the whole 2001 using Graseby-Andersen high volume sampler. Trace element concentrations were obtained by means of ICP-MS and ICP-OES. Average concentrations were reported in the study.

### 3. Vignola Station, Corsica (Sandroni and Migon, 1997)

Aerosols samples were collected at a coastal site of Vignola, west of Corsica from 26 January 1994 to 16 May 1994 and from 9 September 1994 to 28 November 1994. Sampling station was sheltered from the anthropogenic emissions and is only subjected to medium range influences. A total of 48 samples were collected during these periods. Samples were analyzed by means of GFAAS in order to determine their trace element contents. Results of analyzes were provided in terms of both arithmetic and geometric means.

### 4. Erdemli Station, Turkey (Koçak et al., 2007; Kubilay and Saydam, 1995)

This station (Latitude: 36° 33' 54" N, Longitude: 34° 15' 18" E) was placed at a rural area on the coast of eastern Mediterranean, Erdemli, Turkey. Sampling was started in April 2001 and completed in April 2002. Proton Induced X-Ray Emission (PIXE) was used to determine the trace element contents of the collected samples. Water soluble ions were measured by Ion Chromatography (IC). Mean concentrations of the measured parameters were reported in the study. For some of the parameters, which are Na, Cr, Co and Pb, the previous study conducted on the same sampling station was taken as reference (Kubilay and Saydam, 1995).

### 5. Monagrega Station, Spain (Rodriguez et al., 2004)

This station (Latitude: 40.5° N, Longitude: 0.2° W) is placed at a rural area in the southeastern part of the Ebro basin, 85 km westward of the Mediterranean coast. The PM<sub>10</sub> samples were collected from March, 1999 to July 2000. The collected samples were analyzed by ICP-MS and ICP-OES to determine their trace element contents. Capillary electrophoresis was employed to measure the concentration of ions, SO<sub>4</sub><sup>2-</sup>, NO<sub>3</sub><sup>-</sup>, and Cl<sup>-</sup>, namely. Ammonium ion was determined by means of Colorimetry. Mean concentrations of the measured parameters were provided in the study.

6. Sde Boker Station, Israel (Formenti et al., 2001)

Sde Boker, which is located in the Negev Desert of Israel (Latitude: 30° 51' N, Longitude: 34°47' E), has been operated to investigate the natural and anthropogenic aerosols of Eastern Mediterranean atmosphere. This study was conducted from 20 June to 10 July 1996. Size segregated aerosol samples were collected by means of low pressure impactor samplers and collected samples were analyzed by PIXE. Analysis results were reported in terms of their arithmetic means.

7. South east Italy (Perrone et al., 2006)

Samples were collected at a coastal site of south east Italy (40°34' N, 18°01'E) with a duration of one month only in 2003. Sampling site was located 5 km away from the Adriatic Sea. Collected samples were analyzed by ICP MS and IC to determine the trace element and major ion composition of the samples, respectively. The mean concentration of the measured parameters was provided in the manuscript.

8. Tour du Valat and Blanes Stations (Guieu et al., 1997)

Aerosols, precipitation, total and dry deposition samples were collected on the islands and coastal sites of northwestern Mediterranean. Collected samples were analyzed in terms of Al, Cd, Co, Cr, Cu, Fe, Mn, Ni, Pb and Zn. Average aerosol concentrations were reported in the study.

9. Alfabia Station (Mateu et al., 1996)

Aerosol samples were collected using a cascade impactor at the Alfabia station (1100 m asl in Majorca, Spain) from February to June 1994. Samples were analyzed for Ca, Zn, Mn, Mg, Na, Cu, K, Pb, Cr, Cd, Fe, V, and Ni. Mean concentrations of the measured species were provided in the manuscript.

10. Semaphore Station (Chester et al., 1999)

A series of 10 dry deposition samples were collected at the Semaphore Station 130 m above the sea level on the Cap Ferrat, which is on the Western Mediterranean coast, for

duration of 8 months. Graphite and flame atomic absorption spectrometry were employed to determine the trace elements. Though aerosol concentrations were presented for each individual set in the study, to compare them with the values reported in the literature, the mean of 10 sets were taken herein.

#### 11. Finokalia Station (Simolik et al., 2003)

Finokalia station was located on the island of Crete (35°19' N, 25° 40' E). Aerosol samples were collected on 10-31 July 2000 and 7-14 January 2001. Aerosol samples were collected and segregated into 10 size fractions by two Berner type low pressure cascade impactor. PIXE was used to measure the elemental composition of aerosol particles. The measured elemental concentrations were reported in the study in terms of their geometric mean.

The locations of sampling points used in comparison were shown in Figure 4.3.

In addition, concentrations of the measured parameters used in the comparison were provided in Table 4.3. Though geometric mean of the measured parameters correctly represents the atmospheric data, arithmetic averages were reported for parameters in some of the studies. Arithmetic mean values were used for Antalya station and geometric mean values were written in italics in Table 4.3. Though all the stations are very close to the Mediterranean coast, the concentrations of marine elements like Na and Cl show significant differences at the stations. For example, the concentration of Cl measured in this study has a mean of  $1.9 \mu\text{g m}^{-3}$ , it is reported for the Erdemli station, which is about 100 km away from our station, as  $5.5 \mu\text{g m}^{-3}$ . This is not surprising, because concentrations of marine elements like Na and Cl depends on a number of factors like frequency of storm activity, the strength of storm activity, but most importantly sea salt concentrations depends on the distance of the station to the coast, as sea salt particles are coarse and are quickly removed from atmosphere.





Figure 4.3 Location of sampling points used in the comparison

Concentrations of crustal elements measured in this study and included in the figure (Al, Ca, Ti, Co, Fe, K and Mg) are among the highest measured in the region. Few data in the figure that are higher than those measured in this study are generated at Erdemli, which is located approximately 100 km to the east of our station, Fenolika which is located at only 500 km to the NW of our station and Sde Boker which is on the Negev Desert. These all imply that concentrations of most of the crustal elements are high compared to the sites in the western Mediterranean region. This is not very surprising, because concentrations of soil derived elements are related to the aridity of the region. Mediterranean region in general is arid. That is why concentrations of these elements in Mediterranean countries are higher than the corresponding concentrations measured in the countries located at the central and northern Europe. However, aridity in the Mediterranean basin increases from west to east and north to south. Consequently higher aridity in Turkey compared to western Mediterranean is the main reason for higher concentrations of crustal elements at Antalya station.

Table 4.5 Comparison of selected elements measured in this study with the literature (Concentrations were given in terms of ng m<sup>-3</sup>)

Element	Fin.	Erdemli	Vig.	Tar.	Sem.	T.Val.	Bla.	Alf.	C.Car.	Mon.	S.Bok.	SE. Italy	This Study
<b>Al</b>	496	655	109.4		442.2	380	400		210	400	1880	169	661
<b>As</b>				0.8									0.82
<b>Ca</b>	1093	1888						969	629	930	7080	486	1422
<b>Cd</b>		0.19	0.11	0.3		0.5	0.6	0.14	0.17				0.24
<b>Cl</b>	155	5492								349	1130	509	1885
<b>Co</b>		0.4			0.24	0.26	0.02						0.23
<b>Cr</b>	1	5.7		2.9	2.73		1.8	1.09	0.5	<1		4.4	6.77
<b>Fe</b>	800	351.3	119.5		325.9	275	316	317	84	222	1320	181	400
<b>K</b>	455	360						246	280	203	600		536
<b>Mg</b>								252	615	117	980		538
<b>Mn</b>	16	7.6	1.7	9.2	12.2	13	10	7.96		5	30	3.9	8.93
<b>Na</b>		1900						966	4084	294	1330		2241
<b>NH<sub>4</sub><sup>+</sup></b>		850								1284	1110	1444	1136
<b>Ni</b>	3	3.7	0.97	4.2	3.36	2.3	5.5	6.01		5	5		2.52
<b>NO<sub>3</sub><sup>-</sup></b>		1857								2177	3300	4118	1285
<b>Pb</b>	16	30	8.8	25.5	67.3	55.8	50	5.6	11.7	10	10	8.4	52
<b>SO<sub>4</sub><sup>2-</sup></b>	8739	4953								3803	10470	3884	7927
<b>Ti</b>	79	27.1		22.5						20		9.7	32
<b>V</b>	11	8.7		7.7				4.32		2	8	5.9	3.17
<b>Zn</b>	15	9.7	11.8	35	51.8	60	50	29.9		30	30	14.5	17

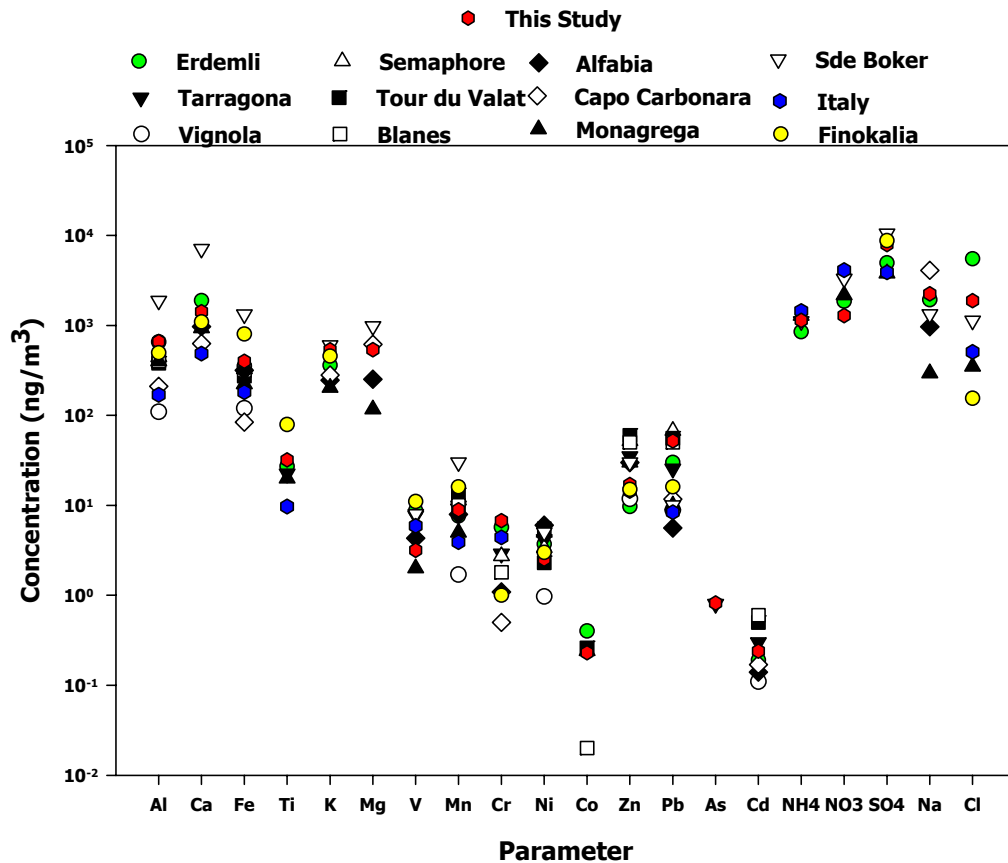


Figure 4.4 Comparison of the aerosol variables measured in this station with the literature

Although a large number of anthropogenic elements were measured in this study, only a limited number is included in Figure 4.4, as multi element data, which can be compared with data generated in this study is very scarce in the Mediterranean region. Concentrations of anthropogenic elements measured in this study, unlike concentrations of crustal and marine elements, comparable with the concentrations measured in other parts of the basin, probably owing to closer proximity of the stations in the western Mediterranean to industrial regions at Western Europe. However, there are two exceptions to this general pattern. Concentrations of SO<sub>4</sub><sup>2-</sup> and Pb measured at Antalya station are significantly higher than ones measured in all stations included in the comparison.

Lead measured at this study is comparable with the values reported for the Tour du Valat and Semaphore, which are more close to the regions with known high industrial

activities, hence, observing at significantly high level of Pb at these stations is not surprising. For Erdemli station, the measured Pb concentration is more or less the same as the value observed at the Antalya station. The major source of Pb in the atmosphere is the motor vehicles (Chow, 1995). The use of leaded gasoline in Turkey was banned in 2002. Since samples at our station and Erdemli were collected before 2002, one can expect to see high concentrations of Pb in the samples not only collected at our station but also at Erdemli.

The most important outcome of this comparison is that anomalously high  $\text{SO}_4^{2-}$  measured at the stations located at the Eastern Mediterranean. The value reported for the Sde Boker is around  $10 \mu\text{g m}^{-3}$ , for Finokalia is  $8.3 \mu\text{g m}^{-3}$  and for Antalya it is around  $8 \mu\text{g m}^{-3}$ . Elevated sulfate concentration for the Eastern Mediterranean was previously reported in the literature by different researchers. For example, Matvev *et al.* (2002) observed elevated sulphur concentrations over the Israel in summer. They related this result with the synoptic conditions characteristic to the Eastern Mediterranean. Synoptic analysis indicated that conditions during summer in Israel facilitate the accumulation of pollution species above the Mediterranean basin from the upwind European sources. This season features a shallow mixed layer and weak zonal flow leads to poor ventilation rates, inhibiting an efficient dispersion of these pollutants while being transported eastward. Furthermore, the backward trajectory analysis conducted by Erduran and Tuncel (2001) have demonstrated that higher concentrations of the long-lived particulate sulfate were long range transported from northern directions to the Eastern Mediterranean. The enrichment of Eastern Mediterranean atmosphere with  $\text{SO}_2$  by the long range transported air masses coming from Central Europe is previously put forward by many scientists (e.g. Luria *et al.* 1996; Ganor *et al.* 2000; Sciare *et al.* 2003 and Tsitouridou *et al.* 2003). Elevated sulfate concentration over Eastern Mediterranean region will be discussed in detail in Section 4.5.4 of this manuscript.

The last group of elements in Figure 4.4 includes Cr, Mn, V and Ni. These are the elements with mixed sources. They all have relatively high concentration in soil, which makes them crustal element. However, their concentrations are also high in industrial emissions

Concentrations of these elements, like the trend observed in anthropogenic elements, are comparable to data generated in other Mediterranean sites. The only exception to this

general trend is Cr. Chromium concentration measured in this study is the highest among all datasets used in this comparison exercise. The reason for high Cr concentration in this area is the mineralogy of the region. The mineralogy of the Turkish Mediterranean coast is characterized by high content of elements like Cr, Ni and Hg. Large number of Hg and Cr mines in the Mediterranean region is an indicator of enrichment by these elements. Because of this, high concentrations of Cr were measured not only in the atmosphere (Güllü et al., 1998; Kubilay and Saydam, 1995), but also in sediments (Sanin et al., 1992).

Similarities and differences between data generated in this study and those reported in the literature for comparable sites in the Mediterranean basin provide some insights about factors affecting chemical composition of aerosols measured at this station, but cannot provide conclusive evidence for sources of measured parameters. Apportionment of sources will be discussed in more detail in the coming sections.

#### **4.2. FLOW CLIMATOLOGY OF EASTERN MEDITERRANEAN**

Assessing the atmospheric pathways of pollutants to a specific geographic region needs a good understanding of the climatology of the region. There are three types of meteorological information, which can help us to understand processes and pathways of the pollutants. First one is the measurement of surface meteorology around the station. Second one includes the investigation of large scale synoptic features. The last one is the data deduced from the numerical weather forecasting models, such as the horizontal and vertical winds and other relevant fields.

Flow climatology provides an improved understanding of typical air-flow patterns and when combined with the ambient monitoring of atmospheric pollutants, it provides information about the variability in measured concentrations of elements and ions. Trajectory models are used extensively to calculate flow climatology for different receptor sites (for example Sancho et al., 1992; Katsoulis et al., 1993).

In this study, 9-year climatology of air flows was calculated for the Eastern Mediterranean basin. Five-day long back trajectories ending at Antalya Station were calculated for the period between of 1993-2001. Approximately 9900 daily trajectories, starting at three altitudes, were used. The Hybrid Single Particle Lagrangian Integrated

Trajectories (HYSPLIT) model was employed for trajectory calculations. The model is developed by the Air Resources Laboratory, U.S. National Oceanic and Atmospheric Administration (ARL, NOAA) and can be applied through their web site (<http://www.arl.noaa.gov/ready-bin/traj>). The model allows user to integrate the trajectories both forward and backward in time. In this study backward option was selected. HYSPLIT\_4 achieved backward trajectories were performed to determine the origin of air parcel arrived at the sampling station.

The isentropic option was selected for the trajectory data since isentropic trajectories are considered to be more realistic as compared to isobaric ones, which does not consider for the vertical motions of adiabatic atmosphere (Stohl, 1998; .Stohl and Seibert, 1998).

After selecting the achieved file and model type (i.e., backward or forward), the next steps include to specify a trajectory starting location and then to set the parameters for starting height, start time and total run time. Five-day long back trajectories were requested. Not only variation of the trajectories with time but also with the altitude was investigated. For this purpose, trajectories were requested at three different altitudes namely, 100, 500 and 1500 meter. The program is run and output files include a text file of end points and a trajectory plot. One can find the vertical motion of the trajectory on the trajectory plot in addition to trajectory which is plotted on the map. An example map and trajectory file was provided in Appendix A.

The requested trajectories were divided into hourly segments and segments in a predefined sector were counted. The calculated segments end points, in fact, reveal the residence time that air mass resides in that sector. Trajectory segments ending at the 100 km radius of the station were excluded from the interpretation since they spin around the sampling point and hence counted in more than one sector, which may led to erroneous results in the computation, that is, sectors could be over presented. In this study, 8 sectors were defined (N, NE, E, SE, S, SW, W, and NW). Definition of sectors used in the classification is shown in Figure 4.5.

Trajectory counting was performed for the whole study period for each of three altitudes and results were depicted in Figure 4.6. This figure reveals that W and NW sectors for altitude of 1500 m accounts for the 52 % of the events for 9 year period. The contributions of N, NE, SW and E sectors to the climatology of region at this altitude are

15, 12, 9 and 7 %, respectively. The frequencies of air masses from the S and SE sectors are negligibly small, 3 % each, as compared to the others. Flow patterns are almost identical at 100 m and 500 m. In these two starting altitudes, the air masses spend relatively equal time in the N and NE sectors as they do in the W and NW sectors. The main difference between flow patterns at three different altitudes is that higher contributions of N, NE and E sectors and lower contribution of W sector to flow pattern observed at 100 and 500 m starting altitudes. In addition to these major differences, residence time of the air masses in the E sector increased from 7 to 12 % at the height of 100 m starting height, while the contributions of SE, SW and S sectors to the overall climatology remained constant at this altitude as compared to the ones observed in the 1500 m.

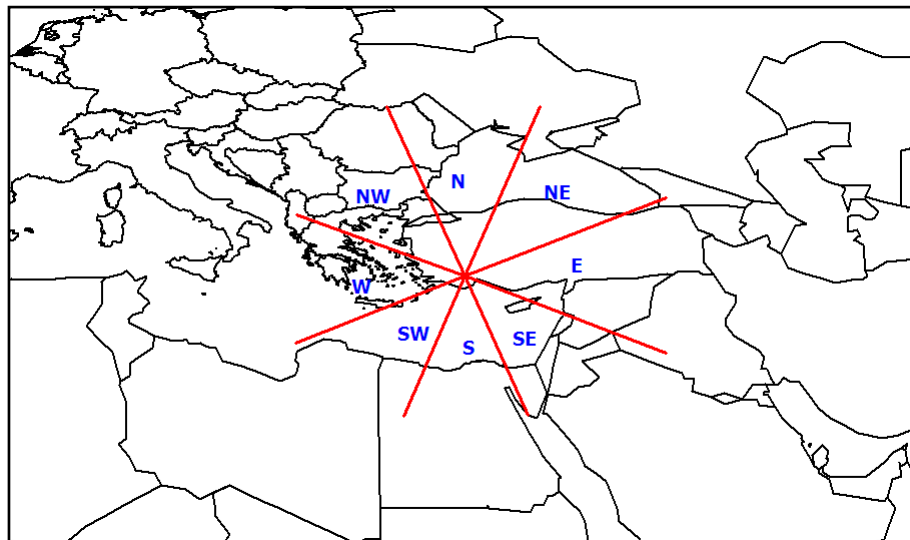


Figure 4.5 Definition of sectors used in the classification

The seasonality of residence time of the air masses in each sector was also investigated. To this end, one sampling period was divided into two as summer, covering the period from May to October, and winter, including the period from November to April. Comparison of frequencies of air masses for three different altitudes both for summer and winter were presented in Figure 4.7. With the exception of 1500 m altitude, air masses spend more time in the W, SW, S, SE and E sectors in the winter time as

compared to summer. On the other hand, air masses in the sectors of N, NE, and NW are more frequent in the summer for all altitudes. The percent residence time of the air masses in the W and NW sectors at 1500 m altitude accounts for 40 in winter time while that is 39 in summer, implying that W/NW are dominant sectors at this altitude over the Eastern Mediterranean regardless of the season. These results are in a good agreement with the previous study conducted by Dayan (1986). It was shown that NNW sector is the prevailing sector in the Mediterranean region both in winter and summer and 30 % of the events are associated with this sector both for summer and winter, that is, there is no seasonal difference in terms of the percent frequency values.



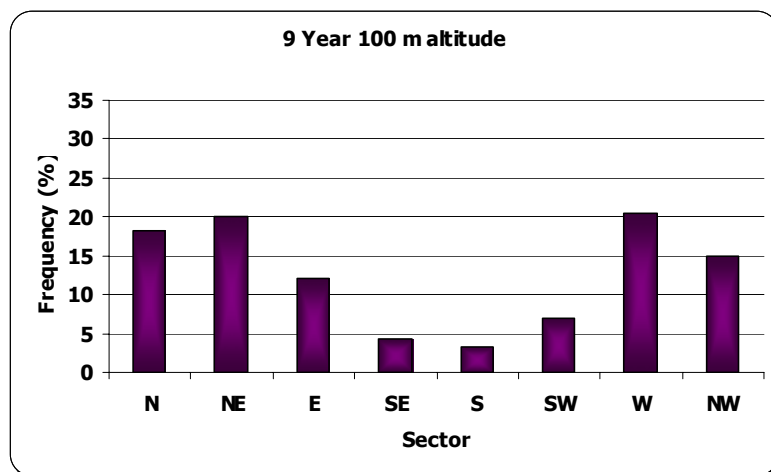
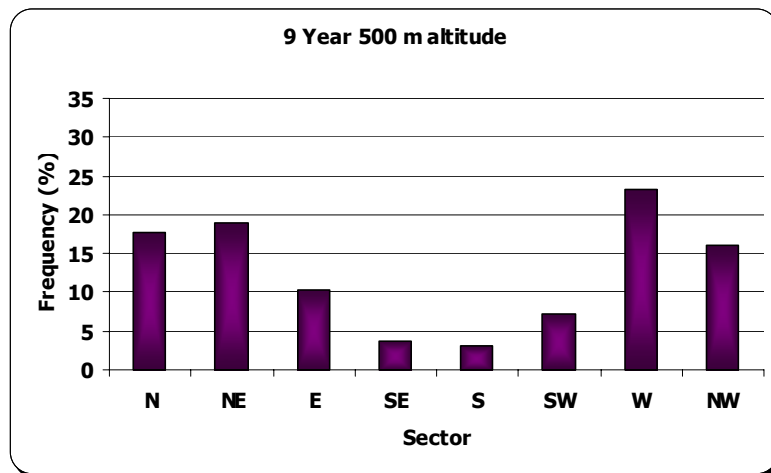
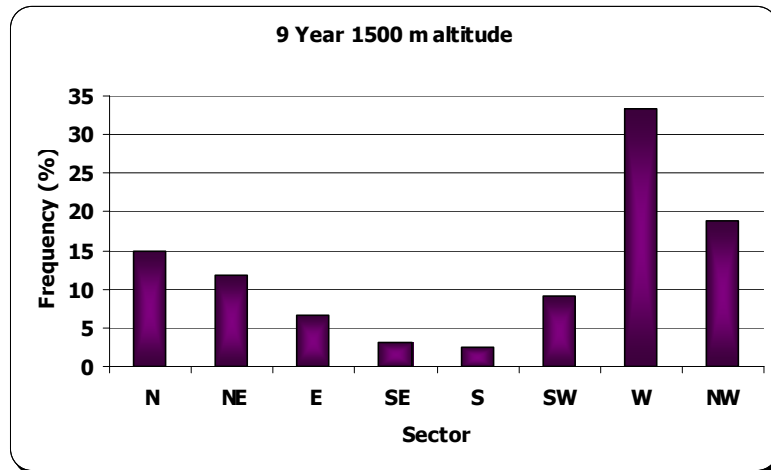


Figure 4.6 9 year average frequencies of air mass transport from different sectors for three different altitudes

Although the W and NW sectors are dominant in both summer and winter flow patterns, the most important difference between summer and winter flows to the Eastern Mediterranean is the significantly higher frequencies observed from N and NE sectors during summer months. This trend is observed at all altitudes. For example winter flow frequencies from N and NE trajectories, for 500 m starting altitudes are 13% and 11% respectively. However, for the summer period frequency of flow is 22% from N sector and 27% from NE sector. Approximately a factor of two increase observed in both sectors. Comparable or even larger differences between summer and winter seasons can be on other sectors. For example larger differences between summer and winter flow frequencies can be seen in SE, S, SW sectors, but the differences in these sectors are not as important as the differences observed in N and NE sectors, because (1) frequencies in these sectors are not high and (2) there are no important sources in these sectors. In other words although the frequencies are substantially different between summer and winter, it does not imply anything on the frequency of pollution transport. However there are strong emission sources in N and NE sectors, including sources in Russia and Ural region. Because of these sources, variations in flow frequencies from these sectors have strong implications in term of pollutant transport.

Summer and winter differences in flow frequencies from W and NW sectors are equally important because they have the contribution to total flow and they carry pollutants from important source regions in Europe to the Eastern Mediterranean. However differences between summer and winter flow frequencies from W and NW sectors are as large as the differences observed in N and NE sectors

The seasonal differences observed for E, SE and S sectors are more pronounced at 100 and 500 m altitudes as compared to ones at 1500 m altitude.

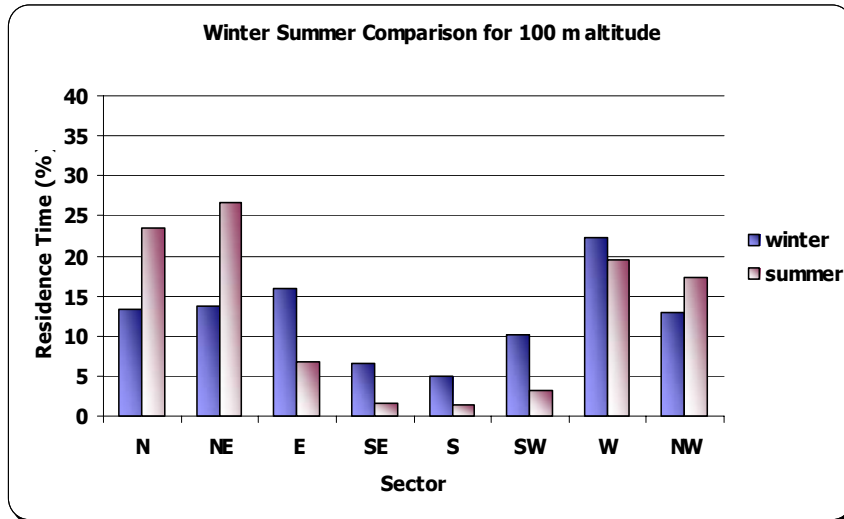
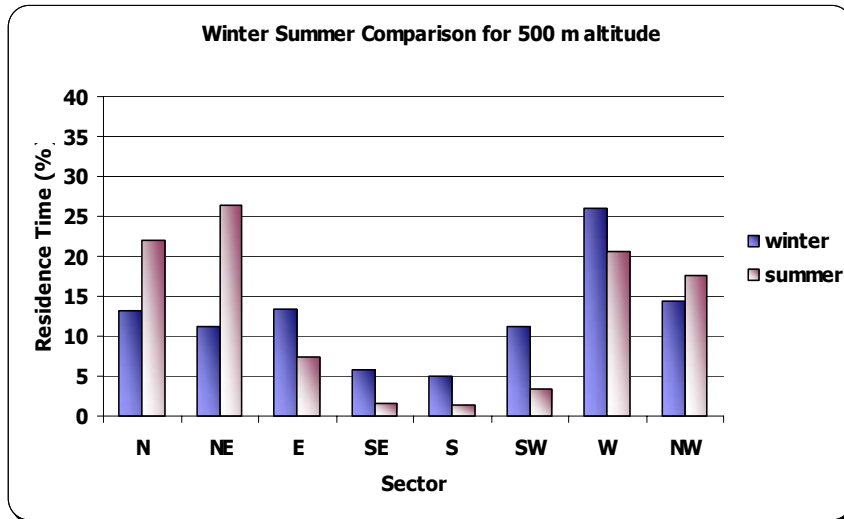
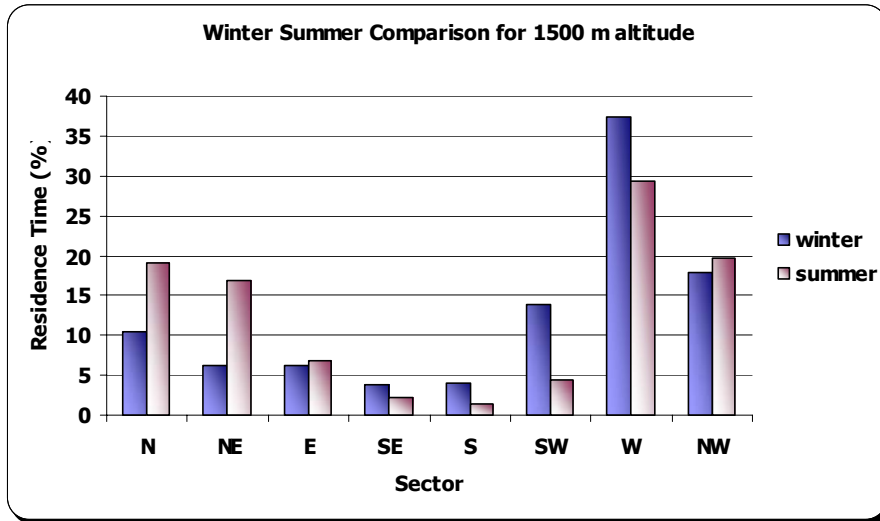


Figure 4.7 Comparison of summer and winter averages for three different altitudes

#### **4.2.1. Comparison of Climatologies of Eastern and Western Mediterranean Basin**

Flow climatology is the least sophisticated and fairly straightforward method to assess source regions that can potentially influence a receptor. In this study, air flow climatology reported in different studies for both Eastern and Western Mediterranean are compared to evaluate the transport of pollutants in different sectors.

Michalopoulos et al. (1997) have evaluated 6 year long trajectory data to find the general climatologic properties of Eastern Mediterranean. Five day long air mass back trajectories obtained from the European Center of Medium Range Weather Forecast (ECMWF) were used in the computation. Eleven sectors have been identified initially, which were reduced to 5 after analysis of results. They identified 3 principal sectors affecting their sampling site at Finokalia, which were N/NW sector accounting for the 61 %, the W for 13 % and S/ SW for 18 % and the rest 8 % of the events on the yearly basis.

Dayan (1986) investigated the climatology of backward trajectories from Israel. Three prevailing sectors were identified in this study as WNW and NNW, representing the air masses originated from the northwest Europe crossing the Mediterranean Sea, N and NE inland flows crossing the Turkey for most of time, and lastly SW and SE sectors including the air masses from inland North Africa and Arabian continents. It was reported that first two sectors are the dominant that influence the chemical character of the atmospheric pollutants measured within the region. The third sector is to have mineral components affecting the aerosol population from the deserts of North Africa (Sahara), Sinai and Arabian Peninsula (Herut et al., 2001).

Study conducted on the same station by Güllü et al. (2000) by taking the averages of backward trajectories corresponding to three years have revealed that Antalya station influenced strongly by the air masses originating from the NW and W sectors. Since these sectors are associated with the high emission areas like Western Europe, former USSR countries, Ukraine, Russia, and western part of the Turkey, they transport most of the pollution to the sampling site. In contrast to results of backward trajectory analysis conducted by Dayan (1986), the frequencies of air mass transport from the SE and E sectors are negligibly small, 2 % and 1 %, respectively. Glavas and Moschonas (2002) performed back trajectory analysis to find the climatology around the sampling site at

Patras, Greece. Air mass back trajectories were calculated for the sampling period using the HYSPLIT 4 model of Air Resources Laboratory of NOAA and FNL database. Trajectories were computed at two different altitudes, 1500 and 3000 m. 48 and 72 hours back trajectories were calculated, and they were sometimes extended to 7 days. Four sectors of origin of air masses were identified based on the backward trajectory analysis, which were North sector, covering the area of NE to NW Europe, N Africa, local and western Mediterranean sector.

Danalatos and Glavas (1999) have also showed that high sulfate emissions observed over the Crete particularly in summer could be attributed the most frequent air masses received from the North sector during summer. Lazaridis et al. (2008) have conducted a study on Akrotiri research station located in Crete. They have reported that 15 % of the air masses arrived from North Africa, Cyprus, and South West Asia on the shore of the Mediterranean Sea. In contrast to this, the frequency of air masses from the north sectors, NE sector accounts for 33.6 % and NW for 51.2 %, is dominant over the sampling site.

Koçak et al. (2004a) classified air trajectories into six airflow sectors according to trajectory direction. These categories are: north-northeast sector (N/NE) include Former Soviet Union, eastern Black Sea and eastern Anatolia, north west sector (NW) covering the area of eastern and western Europe, western part of the Anatolia and Black Sea, southwest sector (SW) encompassing northwest Africa and short trajectories that have flow from the Mediterranean Sea, east southeast sector (E/SE) including the eastern Africa as well as the Arabian Peninsula, western sector includes long fetch of air masses from Mediterranean Sea, and last sector includes trajectories that spend most of their time over the inland of Turkey. However, there is no quantitative information provided about the percent contribution of each sector to the general climatology of the region.

In this section of the study, the flow climatology described for Antalya station was compared with the previously reported studies. For comparison, air flow climatology computed for Tel Shikmona station, located at the coastline of Israel, and Erdemli station, which was placed on the Turkish Mediterranean coast were used. Three day back trajectories requested from ECMWF were calculated at 12 00 UT (Universal Time) at heights of 1000, 850, 700 and 500 hPa. Trajectories were assigned to a particular sector if they reside in that sector more than 50 % of their travel time. Trajectories were

unclassified if they do not obey this criteria (Koçak et al., 2004b). The other study used for the comparison was conducted by Katsoulis and Whelpdale (1993). In this study, isobaric back trajectories at the 850 and 700 hPa were calculated daily at 0 and 12 Z for the years 1983-1987 for the Aliartos, Greece EMEP station, using the Air Resources Laboratory (ARL) trajectory model. Trajectories were classified in terms of both direction and speed, to investigate the monthly, seasonal and annual variability. The other stations used for the comparison were Amasra station located on the Black Sea coast of Turkey and Corsica (Günaydin and Tuncel, 2003). In this last study, the upper layer trajectories were computed for the 4 year period, between 1992 and 1995. For this, 3.5 day-long trajectories at two altitudes, 700 and 850 hPa, ending at the Corsica and Black Sea were calculated for each day of 4 year period. Each trajectory was divided into 84 h segments and each segment was assigned to a wind sector.

One of the difficulties encountered in the comparison of flow climatology provided in different studies was that the definition of wind sector was not standard. The sectoring approach used by Dayan (1986) was assumed as a base, and sectors used in comparison herein were re-defined, accordingly. In this way, North and North East sectors were called as N-NE, East and South East sectors were combined as E-SE, West and North West sectors were coupled as W-NW, and South and South West sectors were taken as they were. Hence, 5 different wind sectors were formed for comparison. In addition, backward trajectories corresponding 850 hPa (1500 m) was used in the comparison since this altitude was chosen in previous studies as the most representative of the transport layer (Dayan, 1986; Güllü, 1996). Comparison of Mediterranean flow climatology reported in these different studies was depicted in Figure 4.8.

From Figure 4.8, it could be concluded that fairly good agreement is observed for Aliartos, Black Sea, and Antalya. Though Erdemli station is located 400 km away from our station, Antalya, N-NE sector is the prevailing at the Erdemli station while W-NW sector is the major sector that air masses reside more before reaching our station. Similar flow pattern is observed for Israel (Dayan, 1986) and Tel Shikmona station whilst E-SE component of flow climatology at the latter one is approximately 70 % higher than the previous one. With the exception of Erdemli station, the major contribution to the calculated flow climatology is from W-NW sector followed by N-NE sector for the rest of the stations located on the Eastern Mediterranean. Frequency of air mass transport in the S sector, in general, is negligible as compared to other sectors for all of the stations.

South sector in general Flow pattern calculated for Western Mediterranean counterpart (Corsica) have approximately 65 % higher contribution of N-NE sector and about 60 % less contribution of W-NW sector compared to flow frequencies calculated in this study.

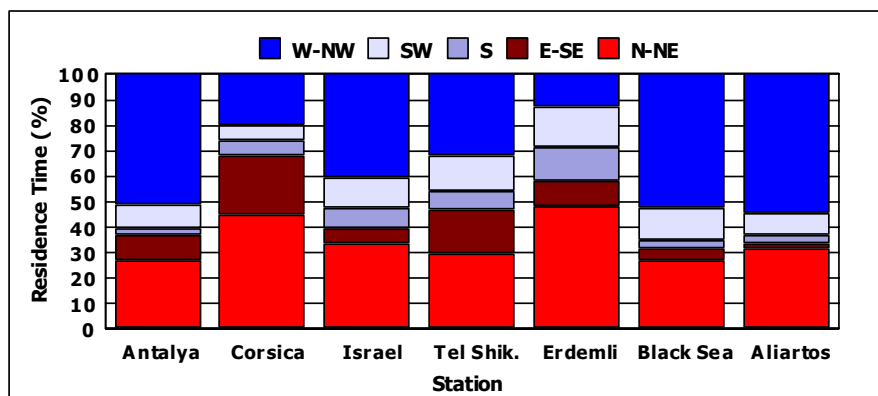


Figure 4.8 Comparison of flow climatology determined in different studies

The differences observed between studies used in this comparison exercise, can be due to several reasons, including the differences in the calculation of trajectories, assignment of segments to wind sectors, location of trajectory start points, and time covered.

More frequent W and NW flow in the Eastern Mediterranean implies that countries located in this region are under the influence of Central and Eastern Europe. In other words, the chemical composition of aerosols and precipitation determined for the Eastern Mediterranean show the fingerprints of the pollutants released from the Western, Central and Eastern Europe. In contrast to this, strong contribution of E and NE sectors on the Western Mediterranean suggest that Western Mediterranean basin is more affected from the former USSR countries.

#### 4.2.2. Local Meteorology

Most of the discussions given in this study are based on upper atmospheric air movements, rather than surface meteorology. However, surface meteorology can provide information on contribution of local sources. The most important local source

that can influence the measurements at our station the city of Antalya, which is approximately 20 km to the northeast of the station. Although the city is not very close, pollution can be transported if the dominant wind direction is from NE. A general discussion of the surface meteorology in the region can reveal information on the effect of the city on measured concentrations of elements.

Mediterranean region has generally warm winter temperatures (from November to February) with frequent rains and a dry summer season (from June to September). The length of the transitional seasons, spring and autumn are very different. The spring season (March through May) is long and autumn usually lasts only 1 month (October) and the change from summer to winter is very abrupt (Brody and Nestor, 1980; Miliman et al., 1992; Koçak et al., 2004).

Local wind direction at the sampling point was also calculated in addition to upper layer atmospheric flow herein. The meteorological hourly data was provided for 16 sectors by State Meteorological Institute. Since wind is a vector, that is, it has both direction and speed, vector computations was performed to process the raw data provided. The description of the computations was given below. The mean east-west,  $V_e$ , and north-south components,  $V_n$ , of the wind from the sequence of  $N$  observations of  $\theta_i$  and  $u_i$  are (<http://www.webmet.com>):

$$V_e = -\frac{1}{N} \sum u_i \sin(\Theta_i) \quad (4.3)$$

$$V_n = -\frac{1}{N} \sum u_i \cos(\Theta_i) \quad (4.4)$$

The resultant wind speed and direction are computed as follows:

$$\bar{U}_{rv} = (V_e^2 + V_n^2)^{1/2} \quad (4.5)$$

$$\bar{\Theta}_{rv} = \text{ArcTan}(V_e / V_n) + \text{Flow} \quad (4.6)$$



Where,

$$Flow = \begin{cases} +180 & \text{for } ArcTan(V_e/V_n) < 180 \\ -180 & \text{for } ArcTan(V_e/V_n) > 180 \end{cases}$$

The average wind speed for the study period was  $1.47 \text{ m s}^{-1}$  and it varies between  $0.5$  to  $3.88 \text{ m s}^{-1}$ . The mean wind direction was also computed and frequency of events that wind blows in each sector were calculated for the whole study period, summer and winter and result of these computations were illustrated in Figure 4.9.

Figure 4.9 reveals that the dominant wind direction around the sampling site is SE, from where wind blows about 40 % of time followed by the S sector with a frequency of 26 %. The contribution of NE winds to total flow is close to 0%, indicating that pollution transport from Antalya is not frequent and can not mask the measurement of long range transported material. The lack of any flow from NW, N and NE sectors is due to high mountains that surrounds the sampling point from north.

One can see quite difference if summer and winter wind profiles presented in Figure 4.9 are compared. It is clear from Figure 4.9 that the predominant wind direction is SE during the winter season, which is also true for the summer period except the contribution of SW direction increased from about 9 % to 17 % in hot season. This difference between summer and winter is probably due to establishment of sea breeze – land breeze system in summer season.

### **4.3. REGIONAL BACKGROUND CONCENTRATION OF EASTERN MEDITERRANEAN ATMOSPHERE**

Average concentration of an element is the combination of its associated background concentration and inputs from local and distant sources. Regional background concentration refers to the concentration not affected by the local and distant emissions and expected to be uniform for the region. It can be very useful to assess episodic nature or contribution of episodes on observed concentrations of elements, which in turn is generally good indication to differentiate between contributions of local and distant sources on elements concentrations.

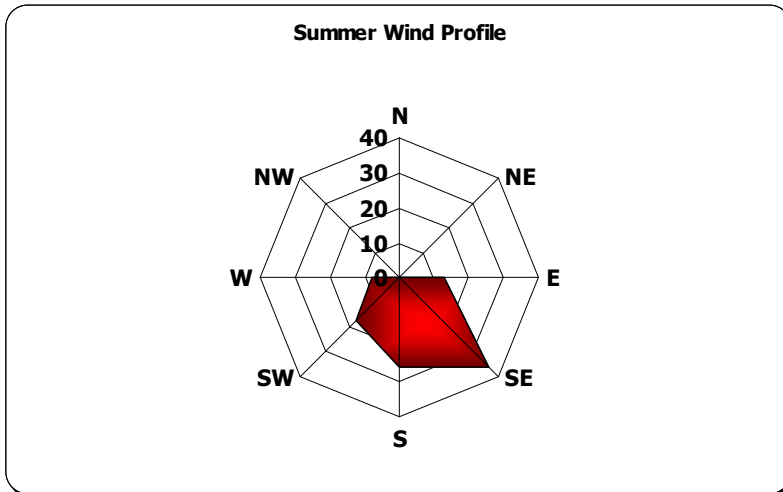
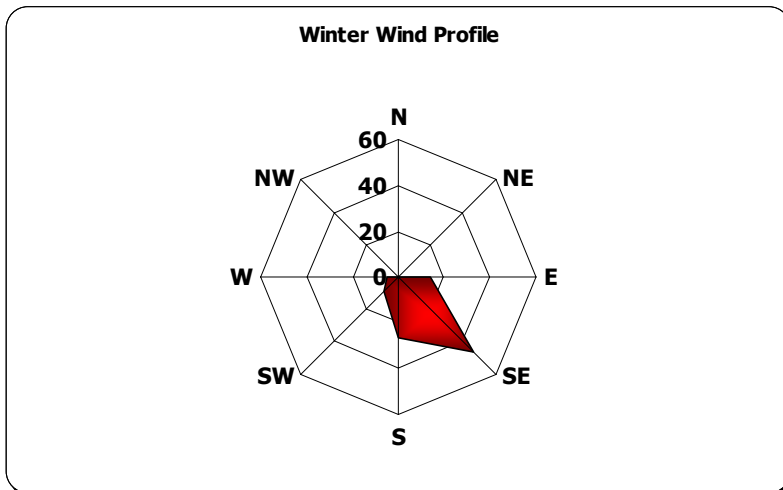
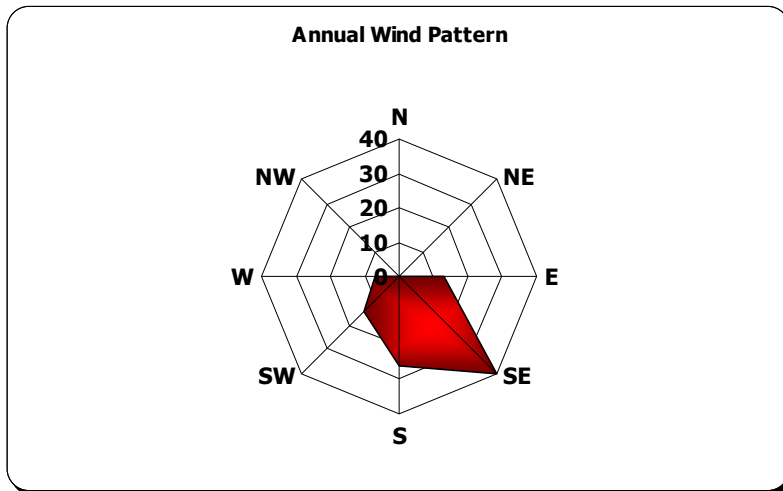


Figure 4.9 Surface wind patterns at the sampling point

Background concentration of the measured aerosol variables were calculated in this study as well. In order to calculate the background concentrations the methodology, which was previously used by Güllü (1996) and Husain et al. (1982), was adopted.

In this methodology, frequency distributions for the aerosol variables were used to calculate the "most frequently occurring value". The peak point of the best fitted distribution is assumed as the most frequently occurring value or in other words, the "background concentration" for the variable of concern. This described methodology is shown in Figure 4.10.

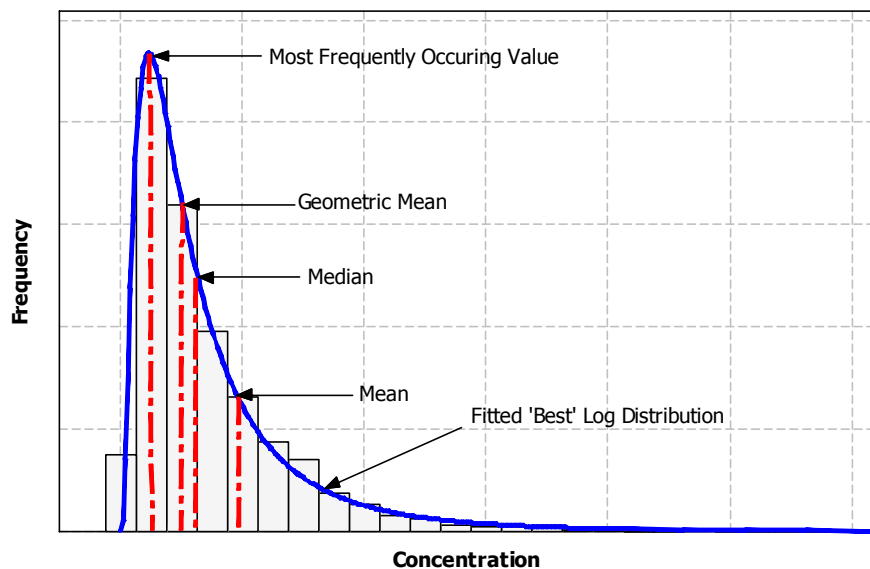


Figure 4.10 Histogram for calculation of most frequently occurring value

The background concentrations of measured aerosol variables were calculated for the 9 year period, and also on a yearly basis. The calculated background concentrations and geometric mean of the measured parameters were provided in Table 4.4.

Table 4.4 reveals that year to year variation in the background concentrations of measured variables does not show significant difference except for 1996 and 1998. In these two years, background concentrations of almost all parameters were higher than

the corresponding concentrations in rest of the years during study period. Year to year variations of some of the selected elements are shown in Figure 4.11. Although Na is a marine element, associated background concentration increased in 1996 and 1998 similar to other crustal elements. This observed trend in Na background concentration can be explained by the crustal contribution to Na levels in atmosphere.

In addition to year to year concentrations, the winter and summer concentrations of the measured parameters were also investigated in this part of the study and results were summarized in Figure 4.12. It can be concluded from Figure 4.12 that the background concentrations of crustal elements like Fe, Al, Ca, Mg, Ti, and K are at least two factors higher in the summer season as compared to the values observed in the winter period. In fact, the summer to winter ratio for the elements of Al, Dy, Er, Fe, Pr, Th, Tm and Y is greater than 4. Higher concentrations of crustal elements were discussed and explained in the previous section. The same trend observed so-called background concentrations indicate that concentrations of crustal elements during non-episode periods also reflect local resuspension process.

Observed year to year and seasonal variation in the background concentrations revealed that pollutants are not only transported to the region with episodes. So called background concentration may also show differences within the region. One can expect to observe similar background concentrations at different stations within same basin. In order to confirm this hypothesis, regional background concentration of aerosol variables that were previously calculated at Uludağ (Tuncel et al., 1994), Çubuk (Yörük, 2004), Antalya (Güllü, 1996) and Amasra (Karakas, 1999) stations were summarized in Table 4.5 and related comparison was demonstrated in Figure 4.13.

Comparison of Uludağ and Çubuk stations with other stations is not easy since very small number of parameters were investigated in these stations. For Amasra and Antalya stations, comparison can be performed easily since most of the parameters were measured at these stations. Though both stations were located close to coast, in fact Amasra at the Black Sea and Antalya at the Mediterranean coast, the calculated background concentrations of Na and Cl were higher at Antalya station. No data reported for Çubuk station, but concentrations of these elements at Uludağ station are lower. This observed pattern is expected; as the station is away from the sea side, the influence of sea salt on the measured concentrations decrease.

When the comparison is conducted in terms of major crustal elements, like Fe, Al and K, there was no significant difference observed between Amasra and Antalya stations, implying that soil input to these stations is not so much different. One biggest observed in the Ca concentrations, which is higher at Antalya station, can be attributed to calcareous soil structure dominating in the region.

For trace crustal elements, for instance, Co, Cs, Dy, Sm, Th, and Sc, regional background concentrations are close for Amasra and Antalya station. However, difference is obvious for other trace crustals including Ce, Hf, Nd, Rb and Tb. This observed difference in regional background concentrations can be explained by variations in the soil profile of two stations. Potassium and Ca are only measured crustal elements in Uludağ and Çubuk stations and their concentrations are relatively lower than ones reported in Amasra and Antalya stations. Background concentrations of Pb, Ni, Zn, As Se and Sb are close in Amasra and Antalya station, but this is not true for Hg,  $\text{NO}_3^-$ ,  $\text{NH}_4^+$  and  $\text{SO}_4^{2-}$ . Concentrations corresponding to these parameters are higher in Amasra station than ones measured in Antalya station. With the exception of  $\text{NH}_4^+$ , calculated regional background concentrations calculated for Uludağ and Çubuk are lower than values associated with Amasra and Antalya station.

Table 4.6 Calculated regional background concentrations of measured parameters (in terms of ng m<sup>-3</sup>)

<b>Element</b>	<b>9 year Geometric Mean</b>	<b>9 year Back.Conc. Mean</b>	<b>1993 Back. Conc.</b>	<b>1994 Back. Conc.</b>	<b>1995 Back. Conc.</b>	<b>1996 Back. Conc.</b>	<b>1997 Back. Conc.</b>	<b>1998 Back. Conc.</b>	<b>1999 Back. Conc.</b>	<b>2000 Back. Conc.</b>	<b>2001 Back. Conc.</b>
<b>Al</b>	332	90	144	35	64	343	88	167	126	49	55
<b>As</b>	0.58	0.35	0.39	0.33	0.41	0.48	0.27	0.45	0.30	0.30	0.21
<b>Au</b>	0.081	0.017	0.016	0.010	0.022	0.042	0.013	0.010	0.023	0.011	0.006
<b>B</b>	3.04	0.54	2.12	0.44	0.43	0.09	0.56	1.27	0.48	0.00	0.85
<b>Ba</b>	6.58	2.80	2.41	1.17	3.58	8.57	3.21	8.30	3.51	2.21	2.07
<b>Be</b>	0.014	0.005	0.006	0.003	0.008	0.011	0.004	0.011	0.005	0.003	0.004
<b>Bi</b>	0.082	0.023	0.009	0.025	0.462	0.090	0.024	0.049	0.022	0.028	0.022
<b>Ca</b>	741	336	376	161	362	766	255	697	362	215	430
<b>Cd</b>	0.17	0.093	0.056	0.055	0.105	0.180	0.075	0.198	0.125	0.119	0.125
<b>Ce</b>	0.44	0.142	0.180	0.049	0.141	0.463	0.127	2.292	0.182	0.085	0.098
<b>Cl</b>	1069	345	320	112	139	288	729	849	1005	427	268
<b>Co</b>	0.13	0.051	0.068	0.033	0.035	0.154	0.036	0.093	0.065	0.025	0.032
<b>Cr</b>	2.22	0.61	0.49	0.28	0.60	1.68	0.72	1.37	0.69	0.43	0.43
<b>Cs</b>	0.081	0.040	0.042	0.028	0.047	0.099	0.034	0.063	0.041	0.027	0.025
<b>Dy</b>	0.032	0.005	0.007	0.008	0.004	0.029	0.002	0.010	0.006	0.006	0.002
<b>Er</b>	0.02	0.006	0.005	0.003	0.007	0.020	0.006	0.014	0.008	0.003	0.004
<b>Eu</b>	0.009	0.001	0.002	0.002	0.001	0.003	0.001	0.002	0.001	0.002	0.001
<b>Fe</b>	174	45	43	17	33	217	44	83	77	33	24
<b>Gd</b>	0.048	0.014	0.016	0.006	0.018	0.046	0.015	0.032	0.018	0.008	0.010
<b>Ge</b>	0.031	0.016	0.025	0.015	0.019	0.027	0.012	0.031	0.013	0.011	0.015
<b>Hf</b>	0.03	0.009	0.007	0.003	0.012	0.029	0.012	0.036	0.010	0.005	0.007
<b>Ho</b>	0.007	0.018	0.002	0.001	0.002	0.006	0.002	0.004	0.003	0.001	0.001
<b>In</b>	0.003	0.001	0.001	0.001	<0.001	0.002	0.001	0.002	0.001	0.001	0.001

Table 4.4 Calculated regional background concentrations of measured parameters (in terms of ng m<sup>-3</sup>)

(Continued)

<b>Element</b>	<b>9 year Geometric Mean</b>	<b>9 year Back.Conc. Mean</b>	<b>1993 Back. Conc.</b>	<b>1994 Back. Conc.</b>	<b>1995 Back. Conc.</b>	<b>1996 Back. Conc.</b>	<b>1997 Back. Conc.</b>	<b>1998 Back. Conc.</b>	<b>1999 Back. Conc.</b>	<b>2000 Back. Conc.</b>	<b>2001 Back. Conc.</b>
<b>K</b>	245	129	178	124	148	270	99	162	130	65	97
<b>La</b>	0.23	0.075	0.112	0.044	0.077	0.229	0.068	0.157	0.093	0.044	0.050
<b>Li</b>	0.37	0.16	0.22	0.06	0.22	0.40	0.13	0.26	0.19	0.13	0.11
<b>Lu</b>	0.003	0.001	0.001	<0.001	0.001	0.003	0.001	0.002	0.001	<0.001	0.001
<b>Mg</b>	366	130	297	169	245	565	145	264	175	135	112
<b>Mn</b>	5.63	3	3	2	3	1	2	4	3	2	2
<b>Na</b>	1352	590	661	457	844	1082	417	784	454	446	206
<b>Nd</b>	0.21	0.065	0.0838	0.0219	0.0668	0.214	0.0603	0.131	0.0812	0.0418	0.0425
<b>NH<sub>4</sub><sup>+</sup></b>	589	109	936	*	36	*	406	*	880	162	*
<b>Ni</b>	1.65	0.79	0.91	0.78	0.49	1.95	0.63	1.37	0.78	0.61	0.60
<b>NO<sub>3</sub><sup>-</sup></b>	858	363	225	*	212	*	682	749	998	462	*
<b>P</b>	8.32	0.0003	2.40	1.22	4.28	4.74	3.39	4.68	0.83	1.06	0.56
<b>Pb</b>	35	16	22	20	44	41	21	31	14	9	6
<b>Pr</b>	0.055	0.017	0.017	0.010	0.018	0.059	0.017	0.036	0.022	0.011	0.012
<b>Pt</b>	0.002	0.0003	0.0004	0.0006	0.0006	0.0004	0.0002	0.0007	0.0002	<0.0001	<0.0001
<b>Rb</b>	0.56	0.27	0.27	0.21	0.29	0.71	0.25	0.38	0.36	0.24	0.19
<b>Sb</b>	0.55	0.31	0.32	0.27	0.49	0.56	0.27	0.33	0.33	0.37	0.28
<b>Se</b>	0.25	0.10	0.05	0.07	0.14	0.28	0.05	0.13	0.15	0.10	0.07
<b>Sm</b>	0.045	0.013	0.013	0.006	0.016	0.046	0.014	0.032	0.018	0.008	0.009
<b>Sn</b>	0.5	0.34	0.2932	0.191	0.472	0.692	0.267	0.438	0.302	0.223	0.2003
<b>SO<sub>4</sub><sup>2-</sup></b>	6463	4167	3972	3556	5599	7864	3619	4169	4752	3580	3354
<b>Sr</b>	2.53	1.00	1.14	0.59	1.26	3.06	0.82	1.64	1.05	0.82	0.41

Table 4.4 Calculated regional background concentrations of measured parameters (in terms of ng m<sup>-3</sup>) (Continued)

<b>Element</b>	<b>9 year Geometric Mean</b>	<b>9 year Back.Conc. Mean</b>	<b>1993 Back. Conc.</b>	<b>1994 Back. Conc.</b>	<b>1995 Back. Conc.</b>	<b>1996 Back. Conc.</b>	<b>1997 Back. Conc.</b>	<b>1998 Back. Conc.</b>	<b>1999 Back. Conc.</b>	<b>2000 Back. Conc.</b>	<b>2001 Back. Conc.</b>
<b>Ta</b>	0.035	0.010	0.004	0.004	0.007	0.017	0.003	0.006	0.024	0.018	0.017
<b>Tb</b>	0.006	0.002	0.002	0.001	0.002	0.006	0.002	0.004	0.025	0.001	0.001
<b>Th</b>	0.095	0.021	0.030	0.017	0.019	0.100	0.014	0.052	0.033	0.009	0.017
<b>Ti</b>	17	5	5	3	5	19	5	9	8	4	3
<b>Tm</b>	0.003	0.0008	0.0011	0.0004	0.0010	0.0027	0.0008	0.0022	0.0011	0.0004	0.0005
<b>U</b>	0.045	0.013	0.029	0.009	0.041	0.036	0.011	0.029	0.010	0.003	0.007
<b>V</b>	2.1	0.728	1.042	0.549	1.086	2.430	0.845	1.360	1.180	0.820	0.747
<b>W</b>	0.059	0.023	0.022	0.012	0.060	0.059	0.012	0.056	0.027	0.015	0.014
<b>Y</b>	0.103	0.300	0.042	0.021	0.029	0.124	0.030	0.065	0.056	0.023	0.022
<b>Yb</b>	0.018	0.005	0.005	0.003	0.007	0.019	0.006	0.012	0.007	0.003	0.004
<b>Zn</b>	9.53	4	3	3	4	10	5	7	6	5	5



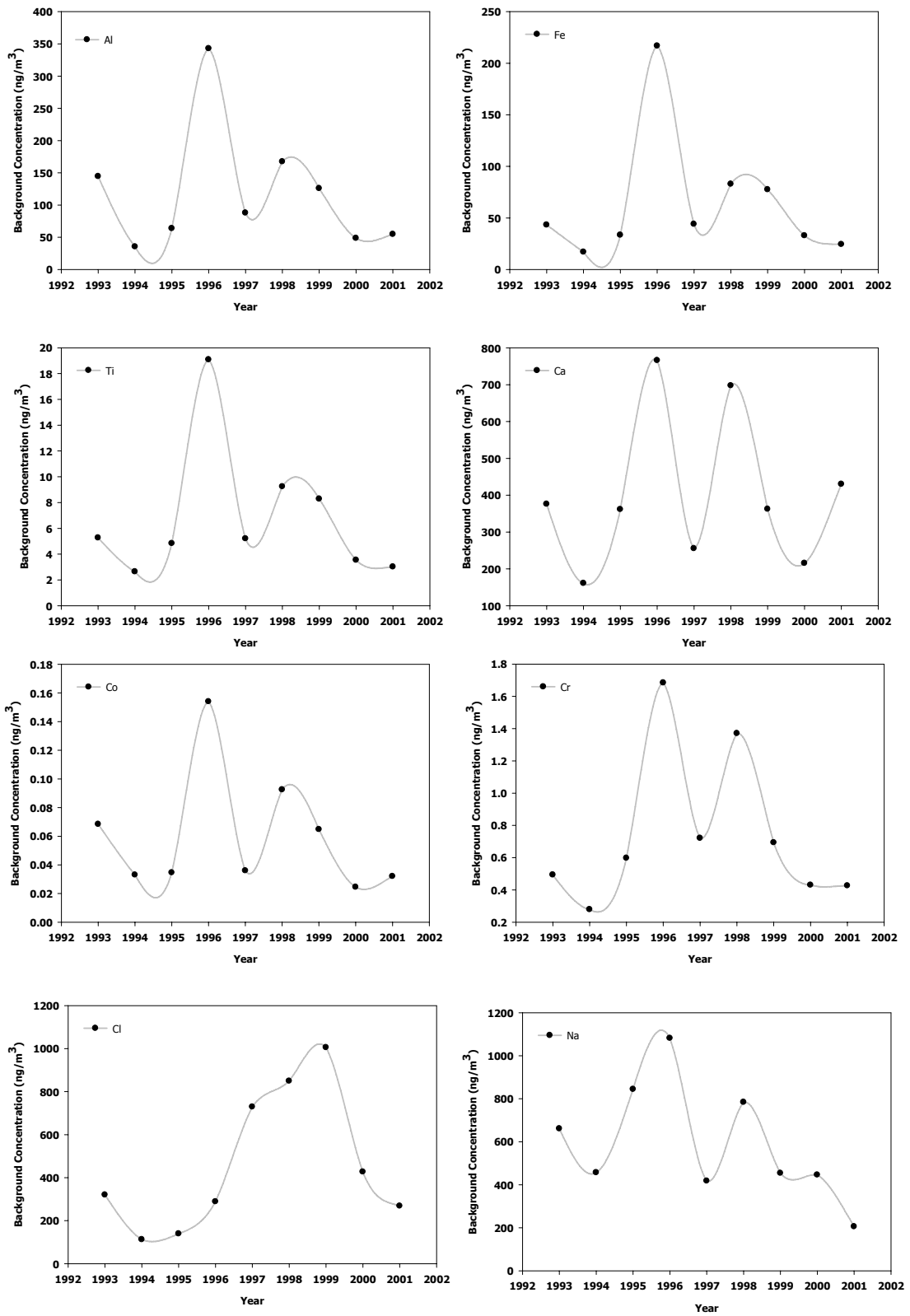


Figure 4.11 Year to year variation in the baseline concentrations of selected elements

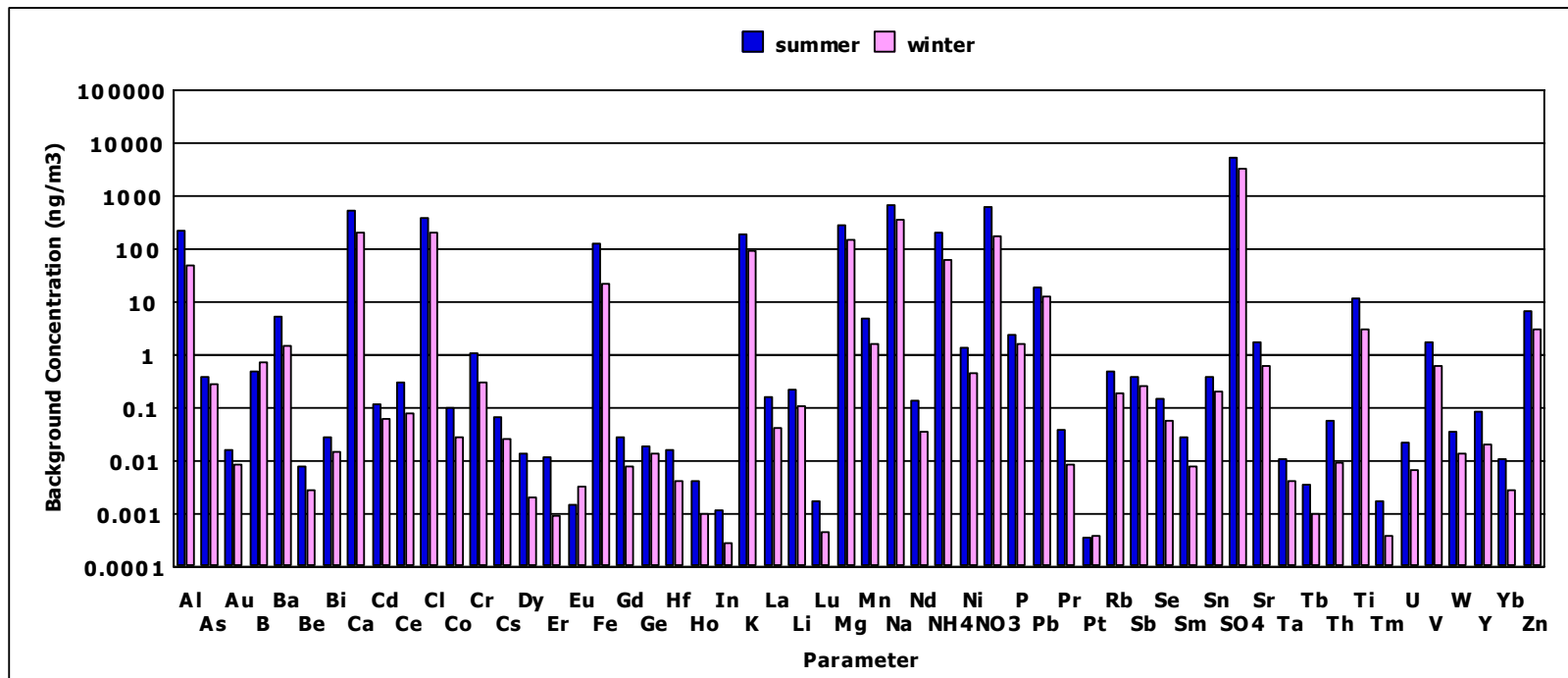


Figure 4.12 Seasonal variations in the baseline concentration of elements

Table 4.5 Calculated regional concentrations of each element and ion (ng/m<sup>3</sup>)

<b>Elements and Ions</b>	<b>Antalya</b>	<b>Amasra</b>	<b>Çubuk</b>	<b>Uludağ</b>
<b>SO<sub>4</sub><sup>2-</sup></b>	2400	3150	300	625
<b>NO<sub>3</sub><sup>-</sup></b>	260	590	73	195
<b>NH<sub>4</sub><sup>+</sup></b>	112.5	875	88	215
<b>Mg</b>	175	60	20	7.5
<b>K</b>	115	80	37	18
<b>Ca</b>	800	93	80	160
<b>Cl</b>	330	105		70
<b>Na</b>	305	185		90
<b>V</b>	0.82	1.4	0.45	
<b>Pb</b>	3.5	5	0.9	
<b>Al</b>	80	85		
<b>Sc</b>	0.015	0.0175		
<b>Ti</b>	11	7.5		
<b>Cr</b>	0.9	0.35		
<b>Mn</b>	2.4	5.2		
<b>Fe</b>	65	95		
<b>Co</b>	0.045	0.035		
<b>Ni</b>	0.575	0.55		
<b>Zn</b>	3.7	3.75		
<b>As</b>	0.65	0.63		
<b>Se</b>	0.15	0.1		
<b>Br</b>	9.5	5		
<b>Rb</b>	0.27	0.08		
<b>Mo</b>	0.011	0.215		
<b>Cd</b>		0.13	17	
<b>Sb</b>	0.2	0.21		
<b>Cs</b>	0.0325	0.025		
<b>La</b>	0.0525	0.075		
<b>Ce</b>	0.125	0.05		
<b>Sm</b>	0.0075	0.009		
<b>Nd</b>	0.08	0.215		
<b>Eu</b>	0.0015	0.003		
<b>Tb</b>	0.0006	0.006		
<b>Dy</b>	0.012	0.015		
<b>Yb</b>	0.0025	0.0035		
<b>Lu</b>	0.0005	0.0003		
<b>Hf</b>	0.0036	0.0015		
<b>Hg</b>	0.0075	0.021		
<b>Th</b>	0.0125	0.01		
<b>NO<sub>2</sub></b>			1150	
<b>TSP</b>		1550		7100
<b>HNO<sub>3</sub></b>			75	
<b>NH<sub>3</sub></b>			65	

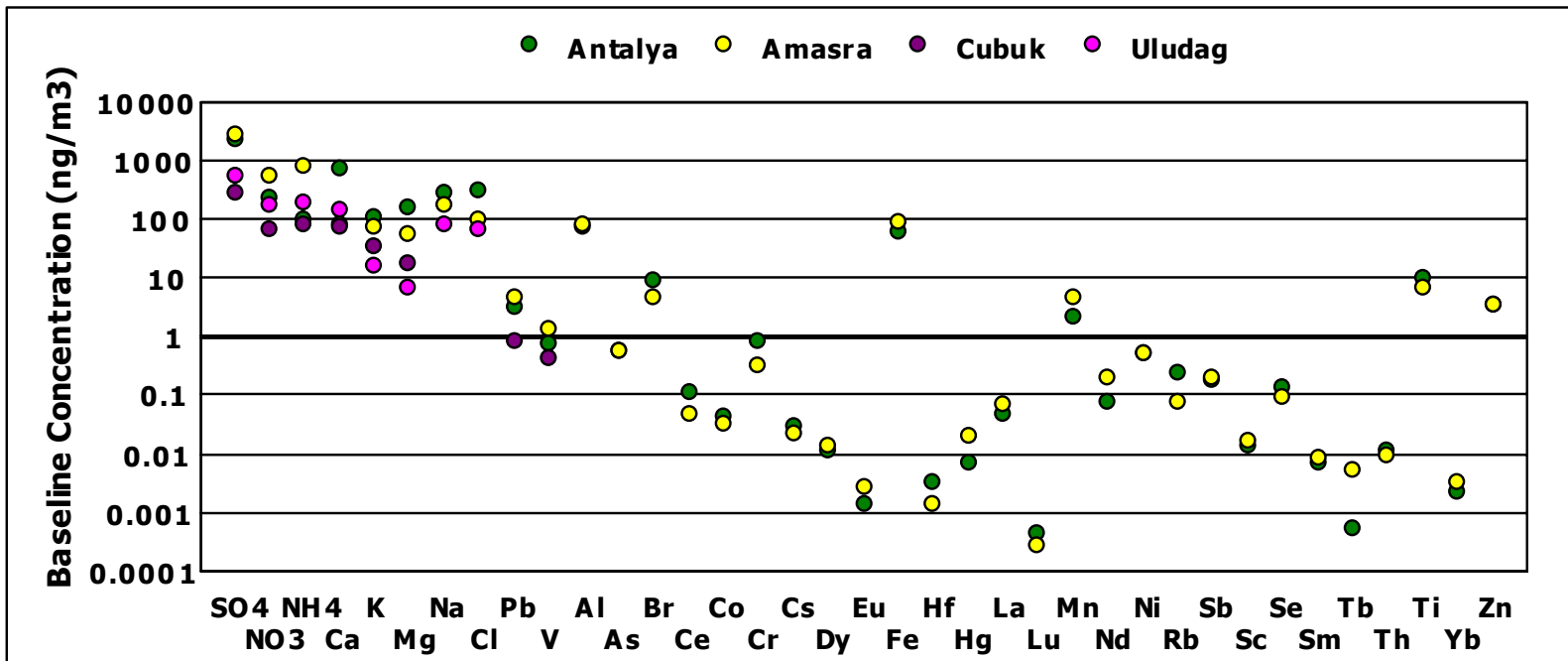


Figure 4.13 Regional background concentrations calculated for each station

In the highlight of information presented so far about the regional background concentrations, it may be concluded that uniformity of regional background concentrations throughout Turkey is not observed though there may be some uniformity in smaller scale. This last finding implies that the employed methodology used in the calculation of regional background concentration should be reviewed.

In order to find influence of episodes on the measured concentrations, percent contribution of episodes was calculated. To end this, baseline (background) concentration of a particular element was divided with its associated arithmetic mean and obtained ratio was subtracted from unity and multiplied with hundred. Contribution of episodes on average concentrations of elements and mean percent contribution for element groups are provided in Table 4.6.

High contribution of episodes indicates that site is under strong influence of local sources. Strong episodic transport from sources to site is expected when the air mass travel from source to station or wind blowing from the source site. However, this is not true for the distant sources, episodes becomes smoother with less maximum concentrations.

As can be seen from Table 4.6, contribution of episodes to observed concentration changes from one element to another. The most episodic behavior was observed for rare earths, for instance, Dy and Eu, having percent episode contribution about 95, while the least was observed for the anthropogenic elements like  $\text{SO}_4^{2-}$  and Sn with value of 47 %. For major crustal markers like Al and Fe, the percent contribution of episodes to observed concentration was 86.

Overall, percent contribution of episodes to elemental concentrations is 76. The percent contribution of anthropogenic (for example,  $\text{SO}_4^{2-}$ ,  $\text{NO}_3^-$ ,  $\text{NH}_4^+$ , Pb, As, Se and Sb) and mixed sources (for example, Cr, Ni, V, K and Mg) to measured mean concentrations is lower than ones calculated for crustal (e.g., Al, Fe and Ca) and marine sources (for example, Na and Cl) as indicated in Table 4.6. This behaviour of mixed and anthropogenic species may be attributed to presence of these sources away from sampling site since only influence of local sources on element concentrations results in strong episodic changes. As concentrations of elements become smoother during transport, concentrations of elements transported from distant sources are not expected as episodic as the ones generated locally.

Table 4.6 Contributions of episodes on average concentrations of elements

<b>Parameter</b>	<b>Avg Concentration (ng/m<sup>3</sup>)</b>	<b>Avg Background Concentration (ng/m<sup>3</sup>)</b>	<b>Contribution of Episodes %</b>
<b>Al</b>	636	90	86
<b>As</b>	0.737	0.353	52
<b>Au</b>	0.170	0.017	90
<b>Ba</b>	9.4	2.8	70
<b>Be</b>	0.024	0.005	80
<b>Ca</b>	1107	336	70
<b>Cd</b>	0.214	0.093	56
<b>Ce</b>	0.776	0.142	82
<b>Cl</b>	1885	345	82
<b>Co</b>	0.213	0.051	76
<b>Cr</b>	3.65	0.61	83
<b>Cs</b>	0.12	0.04	66
<b>Dy</b>	0.07	0.01	92
<b>Er</b>	0.04	0.01	85
<b>Eu</b>	0.02	0.00	95
<b>Fe</b>	316	45	86
<b>Gd</b>	0.093	0.014	85
<b>Ge</b>	0.042	0.016	62
<b>Hf</b>	0.055	0.009	84
<b>In</b>	0.008	0.001	90
<b>K</b>	330	129	61
<b>La</b>	0.404	0.075	81
<b>Li</b>	0.571	0.162	72
<b>Lu</b>	0.005	0.001	84
<b>Mg</b>	517	130	75
<b>Mn</b>	8.19	2.66	68
<b>Na</b>	2179	590	73
<b>Nd</b>	0.385	0.065	83
<b>NH<sub>4</sub><sup>+</sup></b>	1137	109	90
<b>Ni</b>	2.36	0.79	67
<b>NO<sub>3</sub><sup>-</sup></b>	1285	363	72
<b>Pb</b>	48.4	15.6	68
<b>Pr</b>	0.102	0.017	84
<b>Pt</b>	0.0030	0.0003	89
<b>Rb</b>	0.795	0.267	66
<b>Sb</b>	0.667	0.310	54
<b>Se</b>	0.422	0.100	76
<b>Sm</b>	0.084	0.013	85
<b>Sn</b>	0.645	0.340	47
<b>SO<sub>4</sub><sup>2-</sup></b>	7924	4167	47
<b>Sr</b>	4.0	1.0	75
<b>Tb</b>	0.012	0.002	86

Table 4.6 Contributions of episodes on average concentrations of elements  
(Continued)

<b>Parameter</b>	<b>Avg Concentration (ng/m<sup>3</sup>)</b>	<b>Avg Background Concentration (ng/m<sup>3</sup>)</b>	<b>Contribution of Episodes %</b>
<b>Th</b>	0.190	0.021	89
<b>Ti</b>	30.4	5.4	82
<b>Tm</b>	0.0054	0.0008	85
<b>U</b>	0.0757	0.0131	83
<b>V</b>	2.93	0.73	75
<b>W</b>	0.0864	0.0230	73
<b>Yb</b>	0.0355	0.0048	87
<b>Zn</b>	13.17	4.45	66
<b>Anthrop. (%)</b>	69.08	±	16.30
<b>Mixed (%)</b>	72.27	±	6.75
<b>Crustal (%)</b>	80.42	±	9.01
<b>Marine (%)</b>	76.63	±	4.54
<b>All (%)</b>	76.27	±	11.87

As compared to mixed and anthropogenic element groups, contribution of episodes to marine element group is high, in other words, marine elements are more episodic than anthropogenic and mixed elements, which may be explained by presence of sampling station on the coast.

The highest percent contribution, 80.42 %, belongs to crustal element group, which is not surprising since crustal elements associated with aerosols generated in immediate vicinity of the station and their generation strongly depends on wind speed. Since wind speed depicts episodic changes in a daily time scale, it results in similar episodes in atmospheric concentrations of soil related elements. Consequently, one may expect to see higher episodic input of crustal elements.

#### **4.4. TEMPORAL VARIATIONS OF POLLUTANTS**

Temporal variation of aerosol variables including 49 elements from Li to U and 4 major ions, namely,  $\text{SO}_4^{2-}$ ,  $\text{NO}_3^-$ ,  $\text{NH}_4^+$ , and  $\text{Cl}^-$  was investigated to evaluate short- and long-term evolution of the measured parameters, which provided information on the efficiency

of the control actions taken on the anthropogenic emissions and factors affecting levels of natural pollutants.

Dulac et al. (1987) had reported that temporal variation in the concentrations of aerosols over the Western Mediterranean can be explained by flow climatology of the region. However, Miller et al. (1987) have illustrated, in a study based on the 10 years climatology of the region, that there is insignificant seasonality in the flow pattern of the region to impact seasonality of pollutant concentrations. Moreover, the findings of Bergametti et al (1989) conflicted with this study and put forward that the main reason behind the temporal variation of atmospheric concentrations is the local meteorology and source strength of the pollutants. More recently, Rodriguez et al (2002) have reported that variations in the meteorology and orography of the Western Mediterranean region are the important parameters determining the seasonal evolution of airborne particulate pollutants.

The Mediterranean basin is enclosed by the countries having different economical power ranging from the developed ones at north of the basin, such as France and Italy, to semi-industrial ones, like Greece and Turkey, and developing countries which are located on the southern coast. In addition to such uneven distribution of anthropogenic emissions, natural sources are also distributed unevenly around the basin. The strongest natural source is the desert, which generates huge quantities of mineral matter. Desert areas are located on the North Africa and on the Arabic peninsula. Consequently, composition of atmospheric particles in the Mediterranean basin is a function of this assorted distribution of sources. Mediterranean basin receives different types of particles from these contrasting supply areas. As a result, Mediterranean aerosol is a mixture of material transported to the region from the anthropogenic aerosols from North and dust from the Sahara at the south (Kubilay et al., 1997; Güllü et al., 1998).

It is obvious that the distance from the sources and meteorology are the major parameters influencing the variability of atmospheric pollutants. For seasonality of secondary particles, such as, sulfate and  $\text{NO}_3^-$ , photochemistry is also a well documented source of temporal variability (Luria et al., 1996; Mihalopoulos et al., 1997; Kouvarakis and Mihalopoulos, 2002). Both formation and removal of the pollutants depends strongly on the meteorology and physical characteristics of particles. For example, coarser particles are removed from the atmosphere by rain more effectively as compared to the



finer ones. Solubility of particles is another factor determining efficiency of removal through precipitation (Güllü et al, 2000).

Temporal variations in pollutant concentrations are discussed in the following three categories:

1. Short Term (Episodic) Variations
2. Seasonal Variations
3. Year to year Variations- long term trends

#### **4.4.1. Short-Term (Episodic) Variations of elements and ions in the Eastern Mediterranean Atmosphere**

Daily variations in the emission strengths, local meteorology and transport patterns are generally the reasons of observing episodic variations in the concentrations of particle-bound pollutants.

Strong short-term variability in concentrations of atmospheric particles in the Eastern Mediterranean region is well documented (e.g., Güllü et al., 1998; Koçak et al., 2004). Strong short term variations in the concentrations of crustal elements are depicted in Figure 4.14, for Al and Fe. There are two different sources of soil-related material in the Eastern Mediterranean, namely the local soil and dust transported from North Africa, Arabic Peninsula and arid regions of the Middle East. Both of these processes are highly episodic. Saharan dust and dust transported from other regions occur several times in a year in strong episodes. Saharan dust transport to Eastern Mediterranean region will be discussed in detail in Section 4.5.5 later in this manuscript. Local dust concentrations in the atmosphere are observed when strong winds prevail at the sampling point. Since winds are highly episodic, dust generation by resuspension of surface soil is also episodic. Number of episodes occurring per year changes between 64 in 1993 and 8 in 2001. On the average 25 crustal episodes are observed each year.

Number of dust days detected in each month of sampling campaign was depicted in Figure 4.15. It is clear from Figure 4.15 that there is a well defined seasonality in the number of dust episodes with highest values correspond to summer (June, July and August) and early autumn months (September and October). Number of dust episode

days decreases in winter months owing to increase of frequency of precipitation events both around the sampling station and arid regions close to sampling station, from where dust transported to Eastern Mediterranean.

Number of episodes depicted in Figure 4.15 includes total of local, Saharan and Middle East dust episodes. Dust episodes detected in our station was divided into three based on origin of the trajectories. If trajectories arrived to our station from North Africa, corresponding episodes days are called as "Saharan dust days". Episode days are classified as Middle East dust days provided that associated trajectories originated from Middle East.

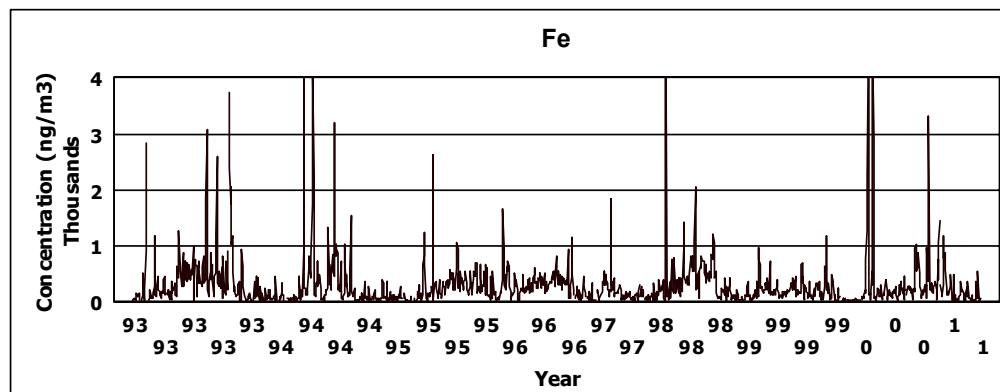
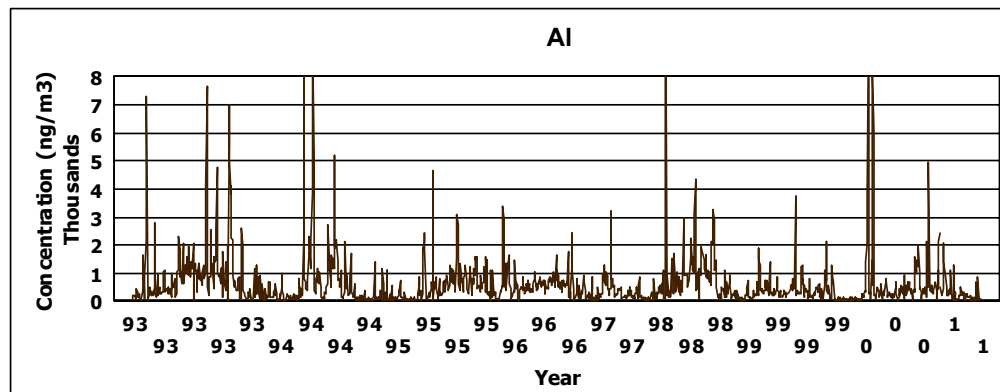


Figure 4.14 Short term variations in the concentrations of crustal elements

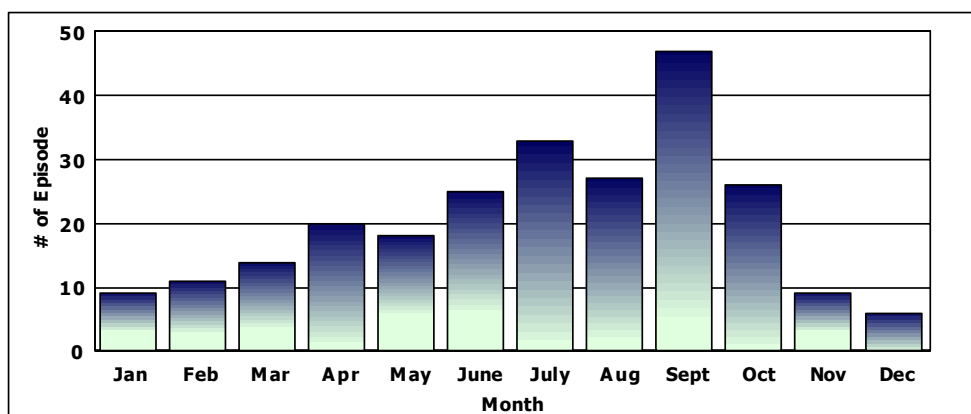


Figure 4.15 Seasonal variation of dust episode numbers

Whether trajectories do not belong to either of these two classes, it is called as "Local dust days". Monthly apportionment of dust days in these three classes was illustrated in Figure 4.16.

It is clear from Figure 4.16 that contribution of Saharan dust episodes to total number of episodes detected at our station increases in spring (March, April and May) and autumn (September, October and November). Same conclusion can be drawn for dust episodes associated with Middle East region. In contrast to this, local dust episodes are more active in summer months (June, July and August) as compared to other seasons. Consequently, one can conclude that the episodes observed at Antalya station in transient seasons are due to dust transport from Middle East and North Africa while occurrence of episodes in summer season, which is particularly true for August, is due to resuspension of local soil. Kubilay et al. (2000) and Goudie et al. (2001) reported that Middle East dust intrusions to Eastern Mediterranean were commonly occurred in early autumn. Middle East dust episodes account for 11 % of total episodes observed in the course of study and there were some days for which samples were neither collected nor analyzed, which may partially explain why the frequency of Middle East dust days recorded in spring and autumn are comparable to each other in this study. Therefore, this observed pattern in Middle East dust does not agree with that of Kubilay et al. (2000) and Goudie et al. (2001).

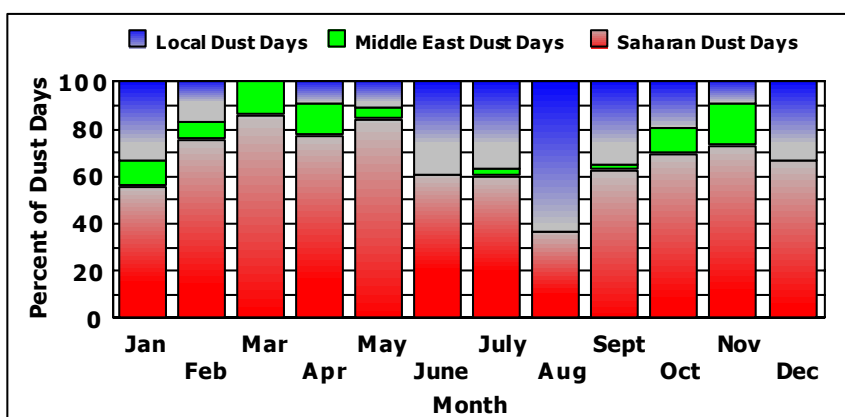


Figure 4.16 Monthly apportionment of dust days in three different classes

The short term changes in the concentrations of Na and Cl are given in Figure 4.17. Concentrations of sea salt elements also show strong episodic behavior. Sea salt particles are produced by bubble bursting process on the surface of the Mediterranean Sea. The magnitude of sea salt production depends on the surface winds on the sea surface. Storm activity which generates large quantities of the sea salt particles is generally associated with passages of frontal systems. Winds increase fairly rapidly immediately before the passage of the front, then gradually decrease. This mechanism generates a sea salt episode. Number of episodes does not change significantly from one month to another. Sea salt episode days were counted based on the concurrent peaks of Na and Cl. Approximately 140 episodes occurred in the course of this study. Seventy three of these episodes were observed in winter months (January, February, March, October, November and December) and 67 occurred during summer season. Although the number of episodes did not change between summer and winter seasons, duration and magnitude of episodes were different in summer and winter seasons. Summer episodes were shorter in duration and smaller in magnitude as compared to winter episodes. Average concentration of summer and winter episodes are  $4.68$  and  $8.41 \mu\text{g m}^{-3}$  as Cl, respectively. Background concentrations of Cl ( $345 \text{ ngm}^{-3}$ ) was reached in the second day proceeding episode day in summer months implying that duration of episode in summer season is two days. However, duration of sea salt episode increased to 4 to 5 days in winter season. These differences in duration and magnitude of sea salt episodes give rise to observed differences in summer and winter season concentrations of sea salt elements. This episodic behaviour of sea salt elements particularly in winter season can

be also clearly observed from Figure 4.18. Both for Cl and Na, episodes are more frequent and also high in magnitude in winter season as compared to summer season. Short term variations in the concentrations of anthropogenic elements are illustrated in Figure 4.19. Variations corresponding to As and Zn was depicted as examples in this figure. Since there is no source of anthropogenic pollutants in the immediate vicinity of the station, transport pattern and removal mechanisms are the driving factors determining the concentrations of these pollutants observed at the sampling station. The episodes in concentrations of pollution-derived elements are generated by changes in transport. High concentrations of anthropogenic elements were observed when air masses come from polluted regions in West, North and Northeast. If the direction of the trajectory changes few days later and air masses come from relatively unpolluted regions on the south and east of the sampling point, concentrations decrease rapidly generating an episode. Rain events can also produce episodes in concentrations of anthropogenic species by washing out particles bearing these elements from atmosphere.

In order to find reasons behind short term variations in the concentrations of selected anthropogenic elements ( $\text{SO}_4^{2-}$ , As and Pb), episodes detected for them were evaluated herein. For  $\text{SO}_4^{2-}$ , fifty four episodes were counted for 9 years of period. Geometric mean concentration for  $\text{SO}_4^{2-}$  is about  $6.5 \mu\text{g m}^{-3}$  while its concentrations increased up to  $\sim 36 \mu\text{g m}^{-3}$  on 26/3/1998. One day later of this high episode, precipitation was recorded and concentration of  $\text{SO}_4^{2-}$  was dropped to  $3.3 \mu\text{g m}^{-3}$  on 28/03/1998. Consequently, duration of this particular episode is just one day. Fifty two episodes were occurred in summer season as expected and two episodes were observed in winter season. Average  $\text{SO}_4^{2-}$  concentration for episodes was 26.4 and  $20.1 \mu\text{g m}^{-3}$  for winter and summer season, respectively.

Fifty two episodes were detected for Pb, seven of them were observed in winter season and forty five was recorded in summer months. Average summer episode concentration was about  $170 \text{ ng m}^{-3}$  while that for winter season was  $228 \text{ ng m}^{-3}$ . Geometric mean Pb concentration was measured as  $35 \text{ ng m}^{-3}$  in the course of study period. The highest Pb episode was recorded on 09/01/1995 as  $382 \text{ ng m}^{-3}$ . Precipitation occurred on this day removed particles bearing elements from the atmosphere and hence, one day after this highest episode day, Pb concentration decreased to  $66 \text{ ng m}^{-3}$ , which is very close to average Pb concentration ( $52 \pm 110 \text{ ng m}^{-3}$ ) measured at Antalya station. For summer season, highest Pb episode was recorded on 17/09/1995 as  $278 \text{ ng m}^{-3}$ .

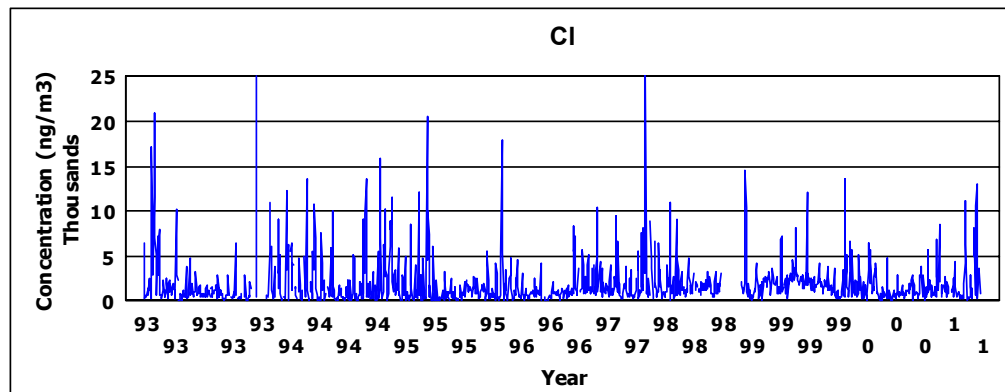
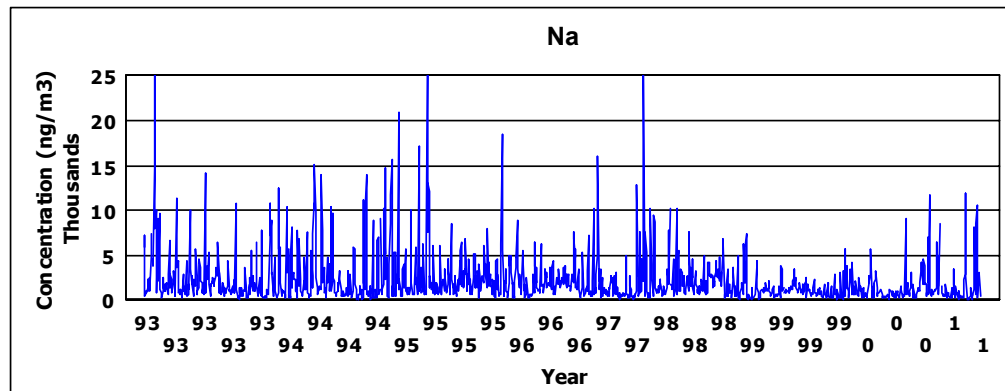


Figure 4.17 Short term variations in the concentrations of marine elements

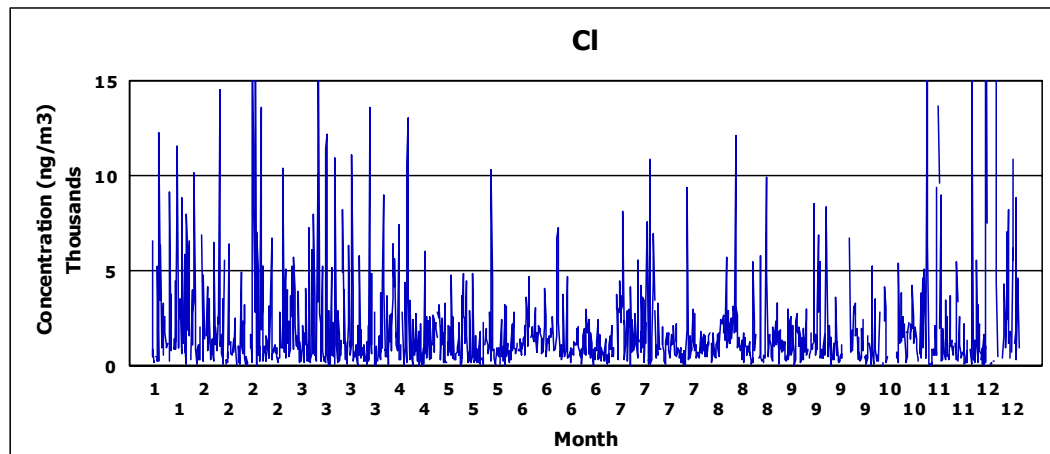
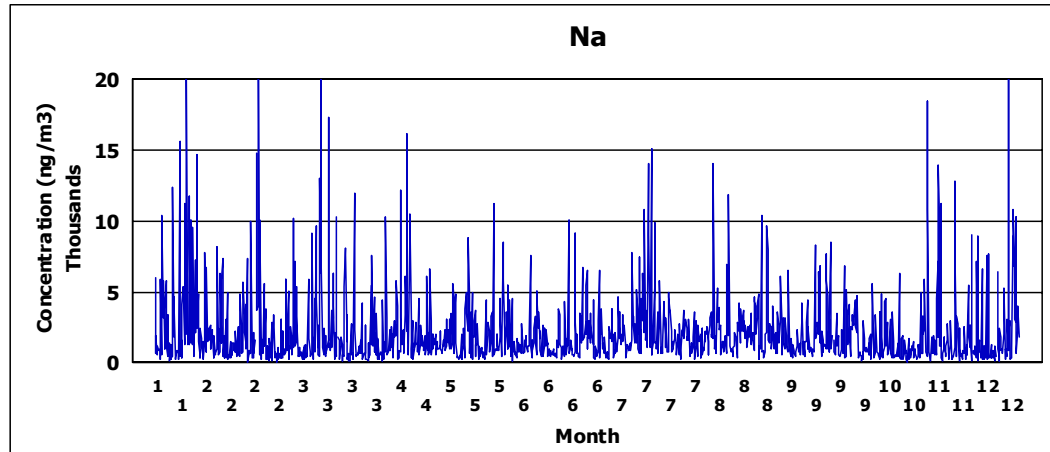


Figure 4.18 Monthly variations in the concentrations of marine elements



There was no rain event was recorded proceeding this episode day, and Pb was measured as 185, 176, 114 and 21 ng m<sup>-3</sup> for 18, 19, 20 and 21 of September, 1995, respectively. As a result, precipitation is the most important factor determining the duration of episodes for anthropogenic pollutants. Frequency of rain events is less in summer season in Antalya region, which leads to longer lifetimes for anthropogenic pollutants.

Unlike SO<sub>4</sub><sup>2-</sup> and Pb, As had more frequent episodes in winter season. A total of 53 episodes were detected for As, thirty three were observed in winter and twenty of them were recorded in summer season. Furthermore, the difference in average summer and winter concentrations is not as high as one observed for SO<sub>4</sub><sup>2-</sup> and Pb. Average summer and winter episode concentrations were 2.66 and 2.86 ng m<sup>-3</sup>, respectively while geometric mean As concentration was measured as 0.58 ng m<sup>-3</sup> during sampling period. Observed difference in summer and winter episode concentrations and more frequent winter episodes implied that As has a local source close to sampling station unlike other long range transported anthropogenic pollutants such as SO<sub>4</sub><sup>2-</sup>. Güllü (1996) performed factor analysis to data generated for Antalya station in 1993. Researcher revealed that there is local As factor influencing the chemical composition of aerosol samples collected at Antalya station. Highest As episode was recorded on 25/04/1995 as 10.03 ng m<sup>-3</sup>. One day later As concentrations dropped to 0.46 ng m<sup>-3</sup> though no rain event was recorded for this day. On 27/04/1995, 1.05 ng m<sup>-3</sup> of As was measured. In the light of this information, it can be concluded that source strength is the major driven factor rather than transport pattern and meteorology in determining short term variations of anthropogenic elements having local sources.

In contrast to marine and crustal pollutants, fewer episodes were recorded for anthropogenic ones. One hundred forty and two hundred fifty five episodes were detected for marine and crustal pollutants, respectively while total number of episodes was around fifty for anthropogenic pollutants. Episodes are more frequent in summer season for anthropogenic and crustal pollutants whilst episode count decreases in summer season for marine elements. Duration of marine episodes is around 4 to 5 days in winter season implying that background concentration reached after 4 to 5 days after the episodes. However, duration for anthropogenic pollutants is around two days in winter season. As expected higher winter episode concentrations were detected for marine elements. This is also true for anthropogenic elements, however, one should keep

in mind that the frequency of winter episodes is significantly smaller than that of summer episodes for anthropogenic pollutants. Short term variations of crustal and marine elements strongly depend on the meteorology including wind speed and precipitation. Nevertheless, source strength and transport pattern are the major factors that should be considered in assessing short term variations of anthropogenic pollutants.

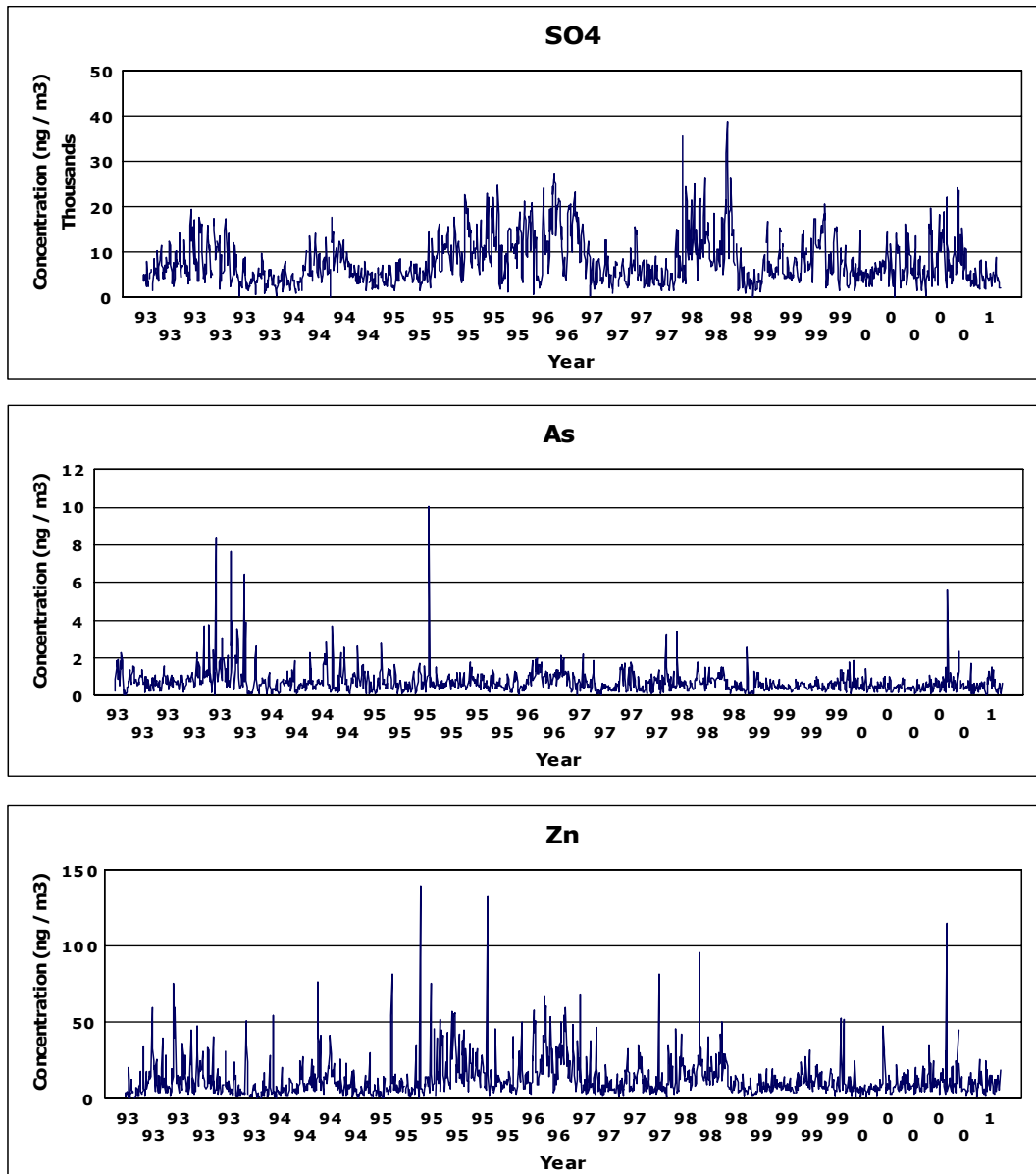


Figure 4.19 Short term variations in the concentrations of anthropogenic elements

Scavenging of particles from atmosphere by rain is an important process affecting temporal behaviors of elements and ions. For most of the parameters measured in this study, rain events correspond to minimum concentrations. Nevertheless, there are few cases in which this observation may not be true, that is, concentrations are high in the day rain event occur. These rare disagreements with general trend are probably due to difficulty of matching rain and concentration data. Aerosol samples were collected daily and rain intensities are also daily averages. However, they do not necessarily start and cease at the same time. For example, if rain starts at 3:00 am at night and stops at 1 pm in the afternoon, this rain event does not affect the sample for that particular day, because samples are collected at 10:30 am every day. For this reason, effect of rain on the concentrations measured can be seen one day after or before the particular day for which it is recorded.

Daily variations in the concentrations of  $\text{SO}_4^{2-}$ , Se, Al and Na are given in Figure 4.20 together with the rainfall in these days. It is clear from Figure 4.20 that the minimum concentrations for crustal (Al) and anthropogenic elements ( $\text{SO}_4^{2-}$  and Se) correspond to high rainfall. Such behaviour of crustal and anthropogenic species is due to removal of the particle bound elements from the atmosphere by washout mechanism. These observations suggest that scavenging by rainfall is an important mechanism determining short term variations in concentrations of elements in the atmosphere, together with transport and changes in the trajectory direction.

Contrary to crustal and anthropogenic elements, Na, which is an indicator element for sea salt particles, follows a different pattern. While for some of the Na minima associated with high rainfall, as observed in crustal and anthropogenic elements. In many cases, maximum Na concentrations correspond to high rainfall events. Observed trend in Na concentrations can be attributed to increase of its concentration immediately after passage of frontal systems. Storms generally move ahead of the fronts, and precipitation starts 1 to 2 hours later after the Na concentration increase in the atmosphere. Since samples evaluated in this study are collected daily, time resolution is not small enough to observe this relationship between precipitation and Na concentration. However, it is clear from the figure that most of the Na episodes are associated with the rain event.

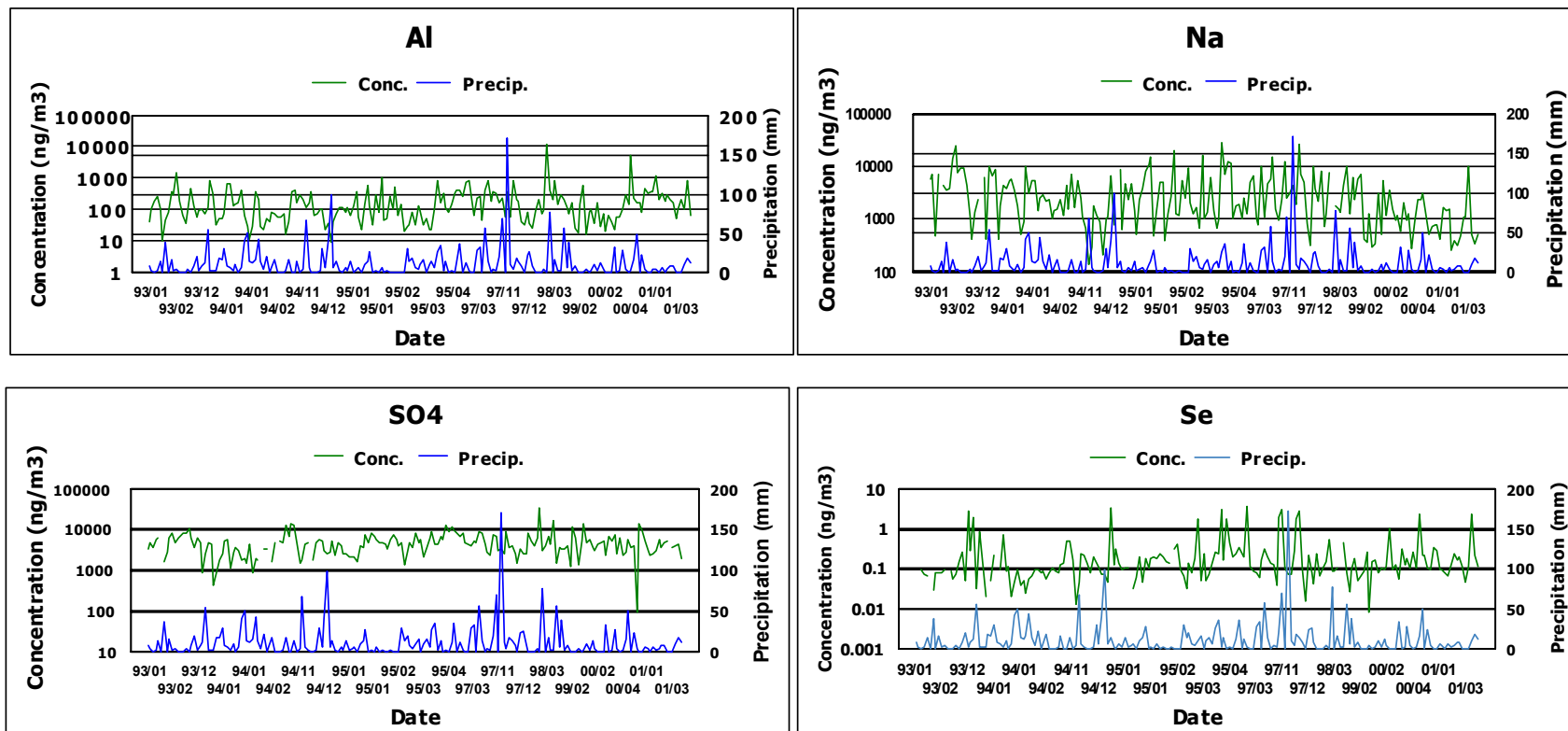


Figure 4.20 Effect of rain on short term variation in the concentrations of selected elements

Non-rainy day to rainy day ratio of the measured parameters, which provides information on the effectiveness of rain in scavenging of elements and ions from atmosphere, were calculated and the results were depicted in Figure 4.21. This ratio for the marine elements such as Na, Cl, Mg and Sr is around 0.5 implying that the rainy day concentrations of these elements are higher than their non-rainy day concentration, which supports the discussion provided in previous paragraph.

Concentrations of crustal elements in non-rainy days are higher by factors changing from 0.5 to 1.5 than the corresponding concentrations in rainy days. This wide range in the non-rain/rain ratio of crustal elements can be explained by partial mixing of rainy and non-rainy days. Since samples were collected on daily basis, it is possible to record a rain event in some portion of the non-rainy day.

Anthropogenic elements such as Cd, Sb,  $\text{NO}_3^-$ , As, Au, and  $\text{NH}_4^+$  have non-rainy day-to-rainy day ratio ranging from 1.5 to 2.0. Once compared with the ratio calculated with the crustal elements, it can be deduced that these elements detected at lower concentrations in the aerosol samples at rainy days. Anthropogenic elements are generally associated with smaller particle sizes in the atmosphere. Consequently, while coarse particles are effectively removed in the atmosphere via precipitation, anthropogenic elements bound to fine particles are not, which explains why we observed high non-rainy day to rainy day ratio for anthropogenic elements as compared crustal ones.

The variation of the concentrations of the elements and ions was also investigated as a function of the duration of non-rainy period. Iron and Cs were selected as indicator parameters for crustal particles. Variation of their concentrations with the duration of non-rainy period is depicted in Figure 4.22. As can be seen from the figure, concentrations of both Cs and Al remained low immediately after rain (day 0). However, their concentrations start to increase gradually 5-7 days after day 0 and continue to increase for about a month. This pattern reflects the drying of the soil. The soil is damp and can not generate crustal aerosol immediately after rain event. It starts to dry and generation of soil aerosol becomes significant only approximately one week after the rain. That is why concentrations of crustal elements Cs and Fe start to with a time gap after the rain. Similar behavior was also observed for other crustal elements such as Al, Ca, K, Ti, Mn, Co, Rb, Ba, La, Sm, Yb, Lu and Th.

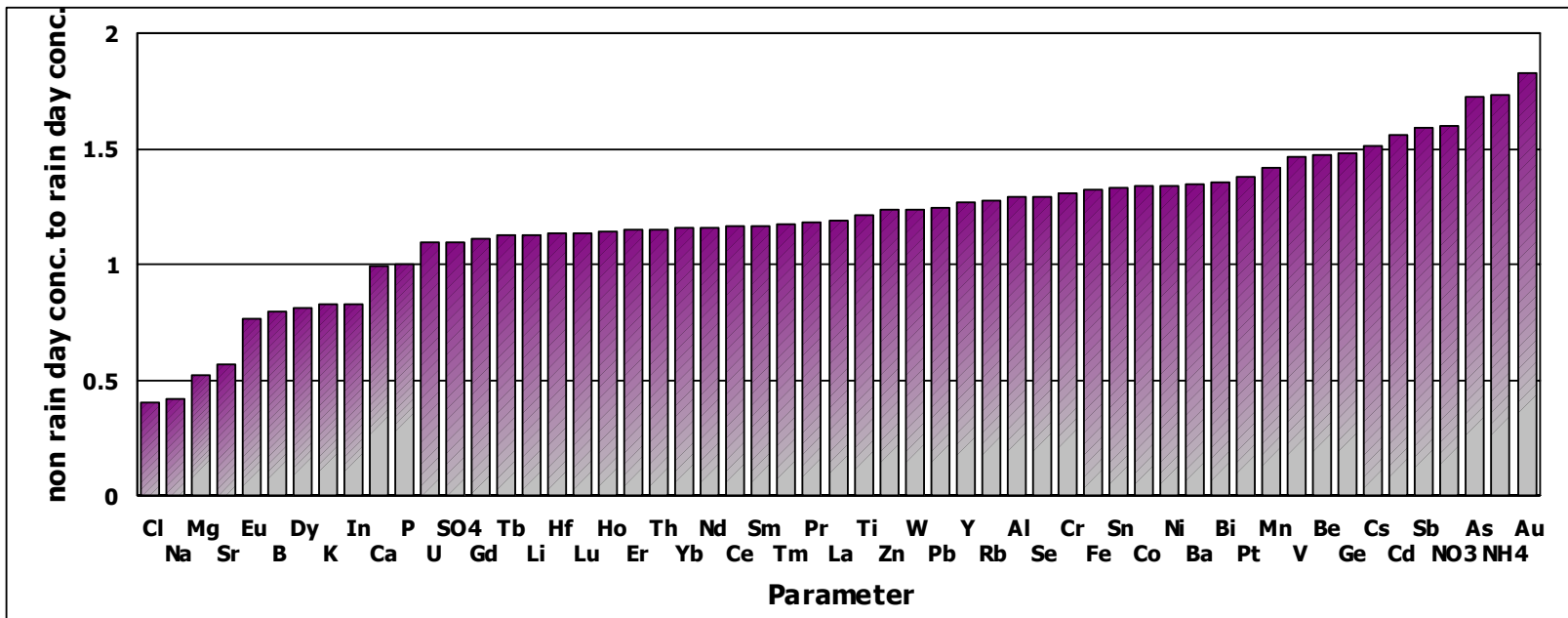


Figure 4.21 The ratio of elemental concentrations in non-raining days to average concentrations in raining days

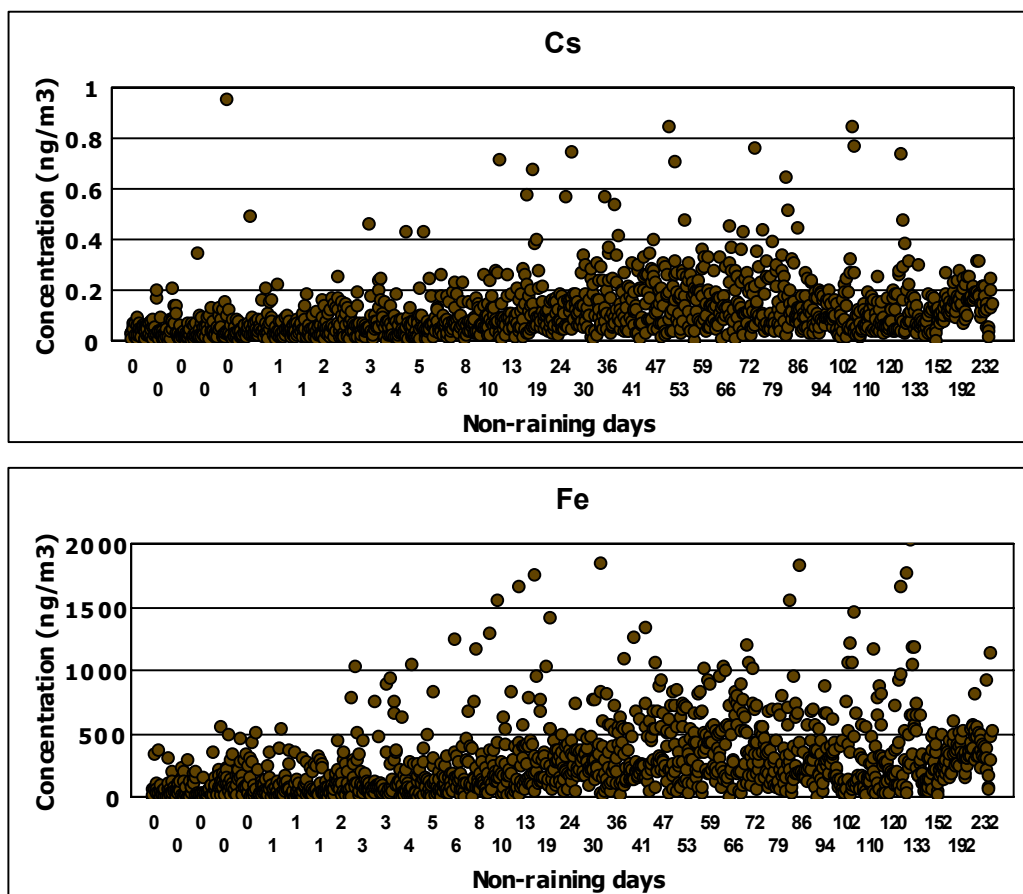


Figure 4.22 Variation in concentrations of crustal elements as a function of non-raining days

Variations in the concentrations of anthropogenic elements,  $\text{SO}_4^{2-}$  and  $\text{NO}_3^-$  as function of non-rainy day are given in Figure 4.23. Unlike crustal elements, concentration of anthropogenic elements started to increase immediately after the rain. This can be observed in the case of  $\text{SO}_4^{2-}$  more clearly. Since these pollutants are long range transported to the region, the transport pattern of the air masses is the main factor determining the concentration of the anthropogenic species rather than the local soil conditions. Therefore, concentrations of anthropogenic pollutants increase in smaller time frame depending on the arrival of pollutant loaded air masses.

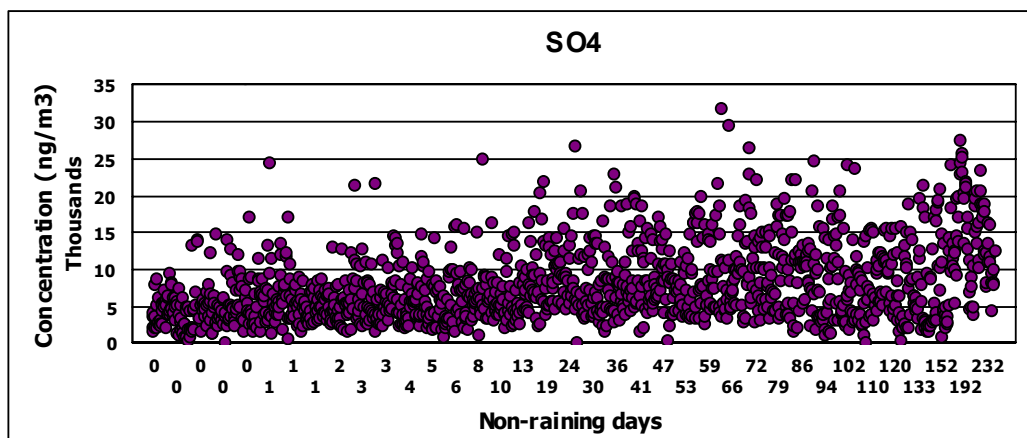
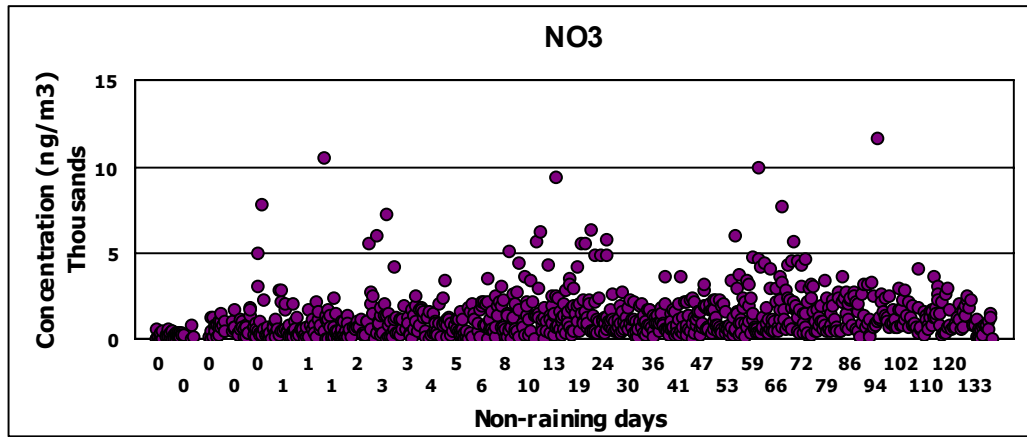


Figure 4.23 Variations in concentrations anthropogenic elements as a function of non-raining days

Variation in concentrations of marine elements (Na and Cl) as a function of non-rainy days is depicted in Figure 4.24. In contrast to anthropogenic and crustal elements, Na and Cl concentrations were high when the rain event occurred, which was named as "day 0" in Figure 4.24. Since marine elements are ejected to the atmosphere through bubble bursting process at the sea surface, their concentrations expected to increase with increasing wind speed. Since strong winds in the region are associated with passage of frontal systems, and since rain almost always follows the front, high sea salt concentrations and high concentrations of Na and Cl, which are associated with sea salt particles are high in the same day with rain. Concentrations of sea salt elements gradually decrease after the passage of the frontal system, as can be seen in Figure 4.24.



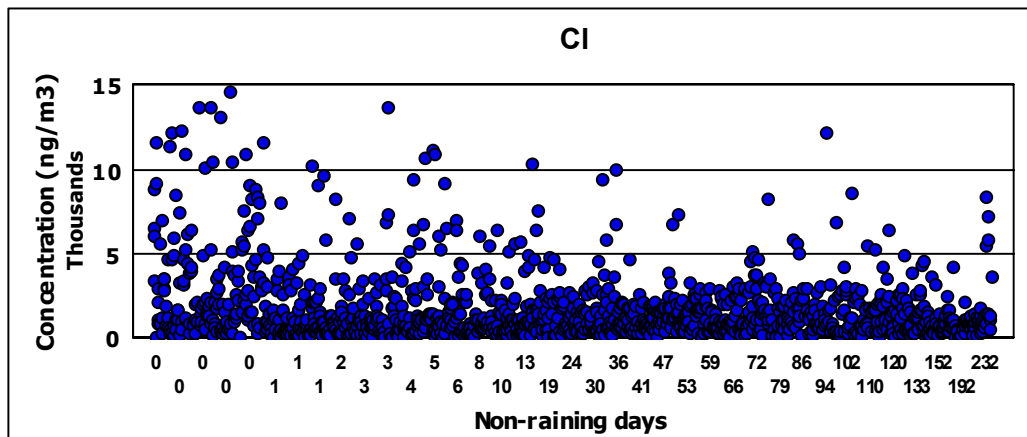
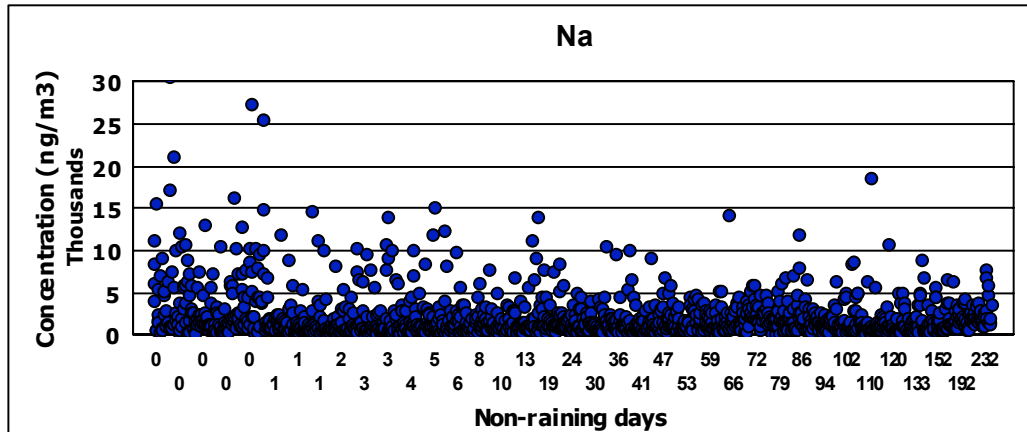


Figure 4.24 Variations in the concentrations of marine elements as a function of non-raining days

Atmospheric reloading time, which is the time necessary for the pollutant to reach its pre-rain concentration, was calculated for each element, to anticipate the influence of precipitation on concentrations of parameters. Atmospheric reloading times for some of the elements and ions measured in this study are depicted in Figure 4.25. In the figure, concentrations of elements corresponding to rainy day were assigned "day 0". Elemental concentrations at 1, 2 and 3 days before rain events were averaged for 9 year-long study period and the average values are depicted as -1, -2 and -3. Thereafter, the value shown as day -1 for Cd is the average Cd concentration for the days that correspond to 1 day before all rain events occurring over the 9 year-long sampling period. The same averaging was also conducted for 1 to 10 days following the rain events and average

values are depicted as days 1-10 in Figure 4.25. Consequently, this figure provides information on the long term average concentrations of pollutants as a function of time from the rain event.

It is obvious from Figure 4.25 that atmospheric reloading times for crustal, anthropogenic and marine pollutants are different. Though trend in anthropogenic and crustal elements are similar, there are two main differences. First, decrease in the concentration of Al at day -1 and day 0 is much larger than decrease observed for  $\text{SO}_4^{2-}$  and Cd. Second difference is that the increase in the Al concentration after the rain event is more gradual as compared to  $\text{SO}_4^{2-}$  and Cd.

Differences in the reloading pattern of anthropogenic and crustal elements can be attributed to the different sources that generate particles associated with these pollutants. Anthropogenic pollutants are transported to the region from different sources and they are scavenged out from the atmosphere with the fine particles bearing them. Nevertheless, the concentrations on the next day depend on the presence of same air mass over the region or arrival of a new pollutant loaded air mass. Low concentration of pollutants will remain same unless new air masses come to the region.

It is well documented, both in this study and other work in literature, that rain has strong influence on atmospheric particles. However, aerosols also affect precipitation. Backtrajectories corresponding to days at which rain occurred (day 0) are depicted in Figure 4.26. Although there is not one-to-one correspondence, most of the trajectories originate from North Africa (Al-Momani et al., 1998). This is because Saharan Dust acts as cloud condensation nuclei and enhances cloud formation and precipitation. Such transport of air masses during rainy days also means that these air masses do not carry pollutants to the region. Clean air masses remain few days in the region.

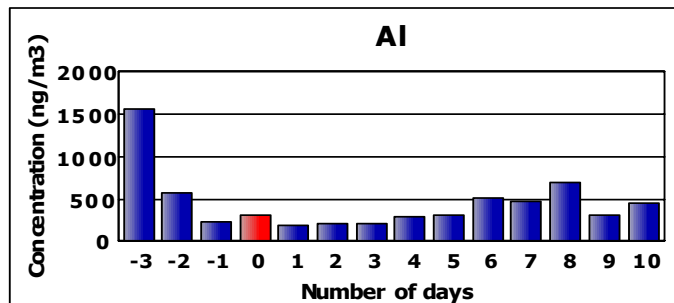
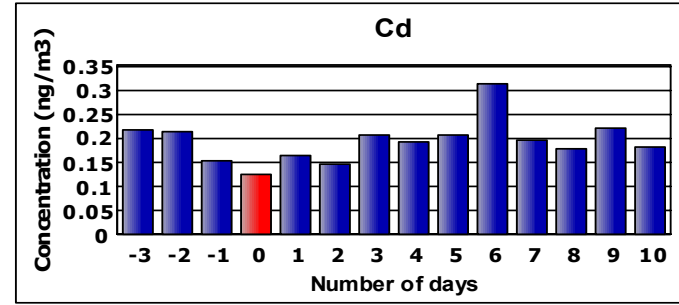
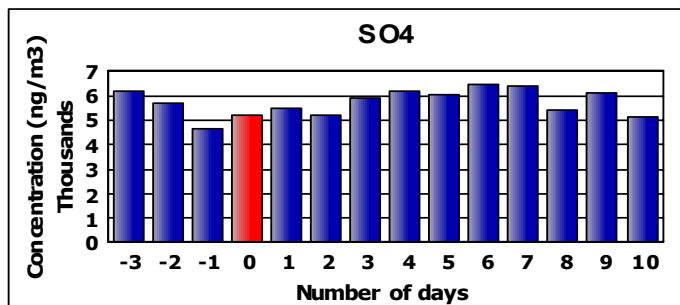
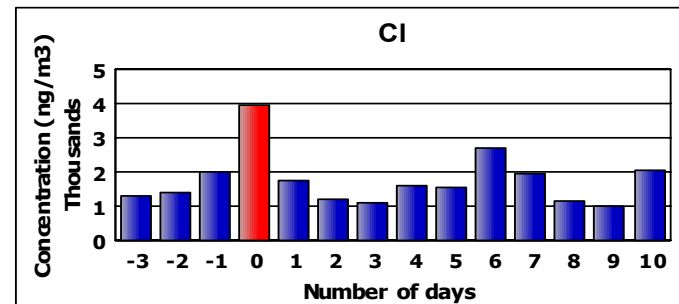
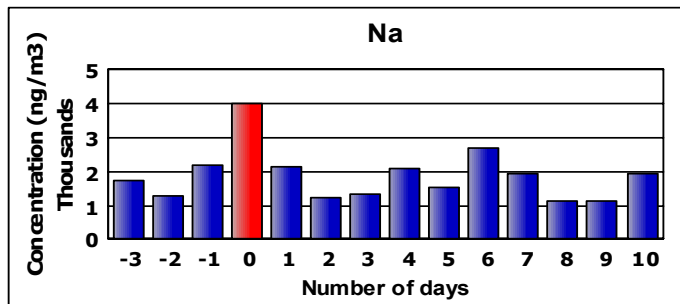


Figure 4.25 Atmospheric reloading times for the selected anthropogenic, marine and crustal elements

During these days concentrations of anthropogenic elements remain low, and then it is replaced by a new air mass. Concentrations of anthropogenic elements depend on the origin of this new air mass. Therefore, unlike crustal elements, the atmospheric reloading time for the anthropogenic elements is much faster (1-3 days after rain).

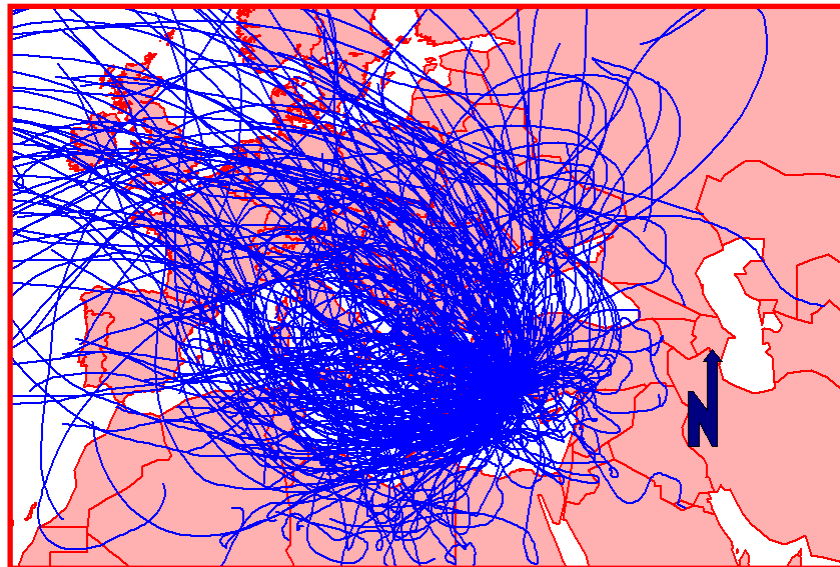


Figure 4.26 Trajectories corresponding to rainy days

In contrast to anthropogenic elements, crustal elements are generated in situ, and their concentration in the atmosphere change with the dryness of soil and wind velocity. When it rains, soil particles in the atmosphere are scavenged out and resulting in the low concentration on the day `0`. The concentration in the following day of rain is low since the resuspension of the soil particles is difficult due to the wet soil surface regardless of the wind speed. Since the concentration of these elements increase as the soil becomes dry, atmospheric reloading of these elements is a relatively slow process and hence reloading time is relatively long. Concentrations of crustal elements levels off 7 – 10 days after rain.

Marine elements, Na and Cl in Figure 4.25, follow different pattern with rainfall. Though Mg and K are also associated with the sea salt particles, there is a significant crustal contribution to these elements. Therefore, the variation of Na and Cl in the course of rain

is depicted in the figure. Their concentration starts to increase before the rain event and become maximum on the '0' day. Marine elements are associated with the sea salt particles which are generated by the bubble bursting process over the sea surface resulting from incorporation of air induced by wind stress. Bubble bursting process had been studied extensively and discussed in the literature (Eg. O'Dowd et al., 1997; Russell and Singh, 2006; Leifer et al., 2006; Pierce and Adams, 2006; O'Dowd and Hoffmann, 2005). These studies had shown that bubbles, which are trapped in the sea, generate film and jet drops on bursting. Waves start to break at the wind speed of 3-4 m s<sup>-1</sup> producing white caps in which bubbles are concentrated (O'Dowd et al., 1997). Each bubble can produce 10 jet drops with sizes ranging from 1-2 µm or that can extend to size greater than 10 µm (Pierce and Adams, 2006). Sea salt particles are injected into marine boundary layer following tearing of wave crests at wind speeds in excess of 7-11 ms<sup>-1</sup> (Leifer et al., 2006).

Güllü et al. (1998) has evaluated the samples collected at the Antalya station between 1992 and 1993. They have investigated the correlation between Na episodes and wind speed and found that the average of the daily wind speed which corresponds to daily episodes, which was assumed as Na concentrations at least 2 standard deviation higher than average, is  $7.4 \pm 2.9 \text{ ms}^{-1}$  while the average wind speed for the non-episode days is  $4.5 \pm 1.6 \text{ ms}^{-1}$ , which confirmed that sea salt episode at the Antalya site are associated with storm activity.

As the generation of sea salt particles depends on the wind speed, strong winds associated with the frontal passages generate considerable quantities of sea salt particles before the rain event which explains why the concentrations of Na and Cl increase just before the rain event, i.e., day '-1' and on the rain day of '0'. Following the rain event, these particles start to scavenge out from the atmosphere owing to their larger sizes and their concentrations decrease from the atmosphere gradually. Consequently, Figure 4.25 reflects the removal time for the marine particles from atmosphere, rather than their reloading time.

#### **4.4.2. Long-Term (Seasonal) Variations of Elements and Ions in the Eastern Mediterranean Atmosphere**

Concentrations of the sea salt elements correlate well with the precipitation rate. The high concentrations of Na and Cl are corresponding to the wet season of the Mediterranean which is due to the rapid reloading of the atmosphere with sea salt particles immediately after rain. During the wet season this is to be expected because precipitation events are associated with the fronts which are the results of synoptic scale meteorological conditions. These fronts carry sea salt particles to the atmosphere, and they are removed very quickly from the atmosphere due to their large size.

Yaalon and Ganor (1979) have previously showed that approximately 25 million tones of dust settle to the eastern Mediterranean annually. The results of the trajectory analysis that they conducted have revealed that the origins of the dust transported to the region are Libyan, Egyptian, Sinai and Negev deserts (Yaalon and Ganor, 1979, Kubilay, 1997). Kubilay et al. (2000) have investigated the seasonality of the dust transport and deposition. They were able to show that highest dust concentrations and depositions rates occur particularly in the transitional months while the region is under influence of the Sharav depressions transporting dust from North Africa and Middle East (Kubilay 1996; Kubilay et al., 2000). Later, Koçak et al. (2004) explained the seasonal variations of crustal elements, particularly, Fe, Al and Mn by the increase frequency and intensity of dust events in transitional period, which is the time covering spring and autumn, and greater washout effect during the winter. They have pointed out that 74 % of the dust events occur in the transitional period, while winter and summer accounted for 22 and 4 %, respectively.

The seasonal variation in the concentrations of marine elements, Na and Cl are selected as representatives, are depicted in Figure 4.27. It is clear from this figure that high concentrations of marine elements corresponds to wet season of the Eastern Mediterranean, which is due to frequent frontal passages during winter months. Since sea surface was calm during summer, bubble bursting mechanism was not effective as in the case of winter. Hence, concentration of sea salt elements was considerably low during summer. A similar trend was also observed in the aerosol samples collected at the Erdemli station, which is another station located on the Turkish Mediterranean coast (Kubilay et al., 1997).

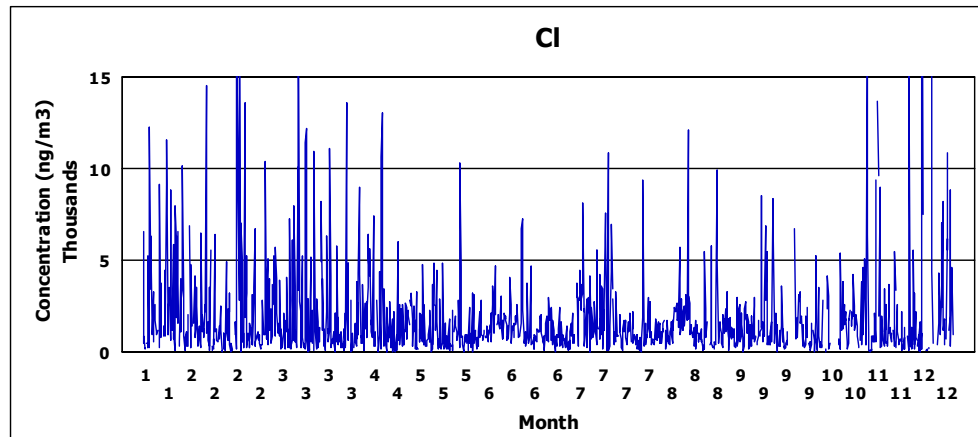
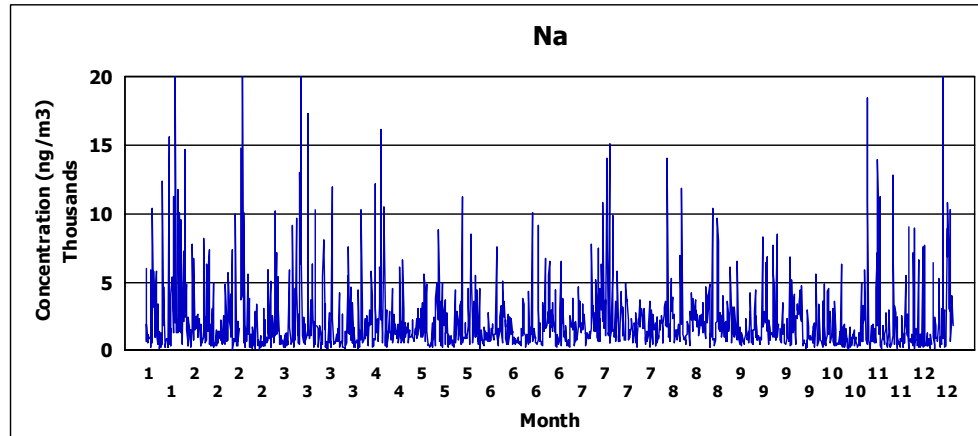


Figure 4.27 Seasonal variations in the concentrations of marine elements

The variation of  $\text{SO}_4^{2-}$  and Al with respect to time was provided in Figure 4.28. Though the concentrations of crustal elements are also determined with the local wind speed, crustal and marine elements show higher concentration and variability in different seasons of the year. There are two different sources of crustal material observed in the Eastern Mediterranean, namely the local soil and dust transported from the Arabian Peninsula and Saharan Desert. The chemical composition of the transported dust also shows seasonal variation. Saharan dust storms generally occur in spring and it is coupled with the low pressure system moving toward east. On the other hand, Arabian dust storms are generally observed in autumn, particularly in October (Kubilay et al., 1997; Kouyoumdjian and Saliba, 2005). As it is shown in Figure 4.28, summer concentration of Al is significantly higher than the corresponding concentrations in winter. This pattern is due to soil conditions around the sampling station and in the Mediterranean region, as discussed previously. Soil was damp in winter period and hence resuspension of the crustal material was more difficult resulting in lower concentrations in winter season.

Seasonal variation of  $\text{SO}_4^{2-}$  is also presented in Figure 4.28. Seasonal trend observed in  $\text{SO}_4^{2-}$  concentration is similar to that of crustal elements, with higher concentrations in summer. This observed seasonality of the  $\text{SO}_4^{2-}$  is well documented in various studies (for instance, Kouyoumdjian and Saliba, 2005; Mazzei et al., 2006; Paatero et al., 2000). Mediterranean region has characteristics of high solar intensity particularly in summer months, giving rise to high photochemical activity. This trend in the  $\text{SO}_4^{2-}$  concentration can be explained by the increase in the photochemical oxidation of  $\text{SO}_2$  which becomes active under summer conditions owing to the high solar radiation and temperatures to produce  $\text{SO}_4^{2-}$ .

Furthermore, Koçak et al. (2004) have found significant correlation between the Saharan dust intrusions and high concentration of  $\text{SO}_4^{2-}$  in summer season. High summer  $\text{SO}_4^{2-}$  concentration in the Mediterranean region was attributed to the dust transport from the Saharan desert by the several other studies in the literature such as Al-Momani et al. (2000; 2008), Avila and Alarcon (2000) and Herut et al. (2000). Mori et al. (1998) have suggested that calcite in the Saharan dust particles absorb ammonium sulfate to form kokaite and finally gypsum. Further, Koçak et al. (2004) recorded two highest  $\text{NO}_3^-$  concentrations during intense Saharan dust event suggesting significant correlation between acidic gaseous components of atmosphere with mineral dust. Concentrations



dropped in the rainy season since the  $\text{SO}_4^{2-}$  bearing particles are removed from the atmosphere by wet deposition.

Monthly variations in the concentrations of Al and other selected crustal elements were also investigated and results were provided in Figure 4.29. In Figure 4.29, concentration of crustal elements started to increase in April and they made maximum in June or August. Nevertheless, concentrations measured in the winter months considerably lower than the ones measured in the summer. This seasonal variation associated with the crustal elements strongly depends on the dryness of the soil condition around the region.

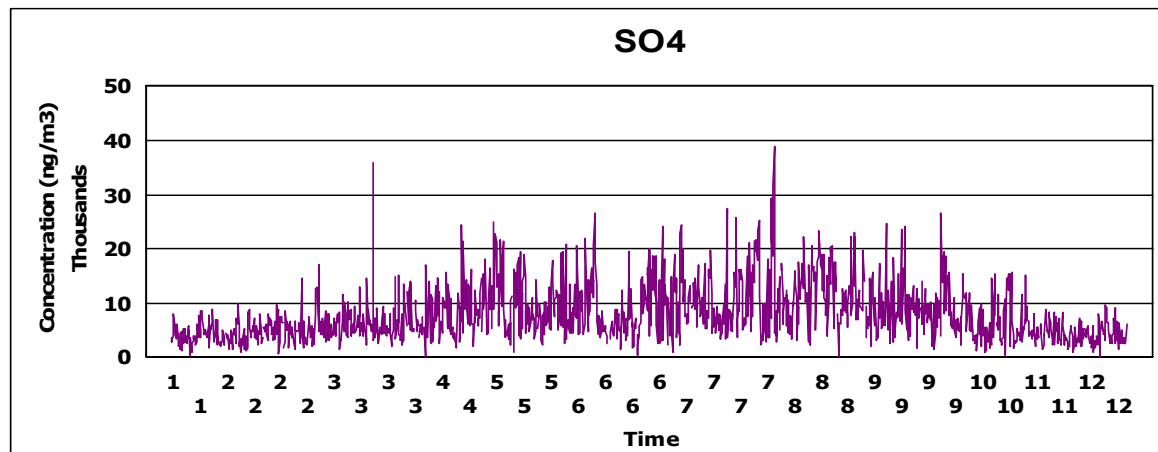
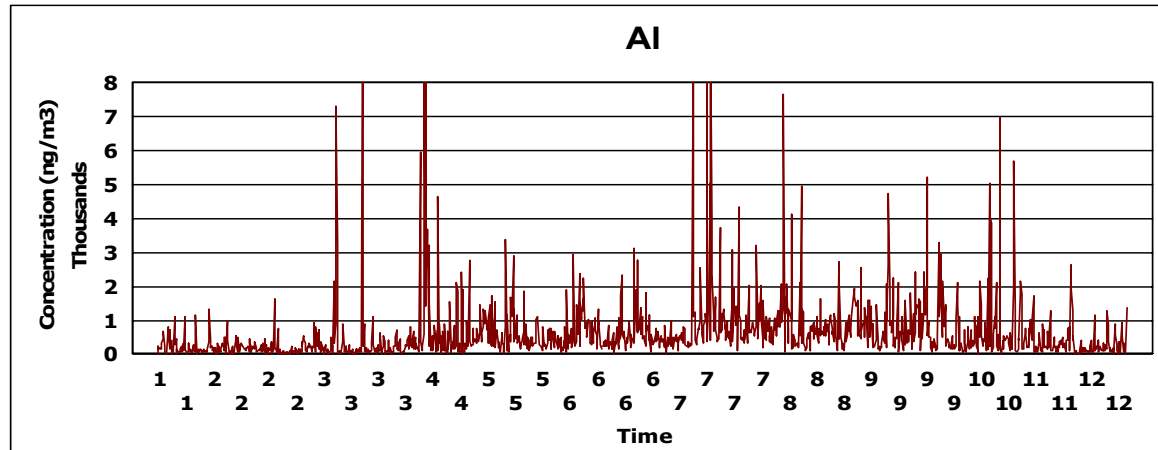


Figure 4.28 Seasonal variations in the concentrations of selected crustal and anthropogenic elements

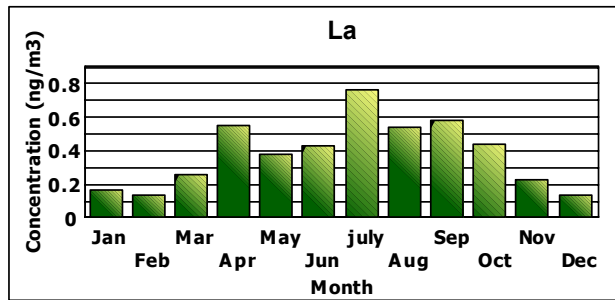
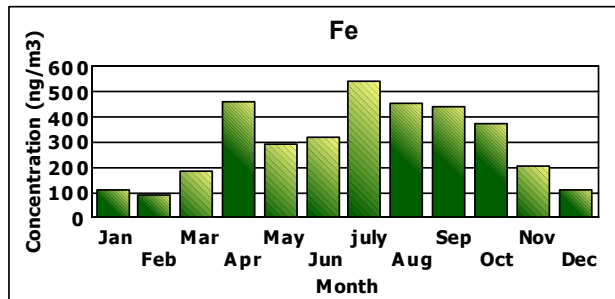
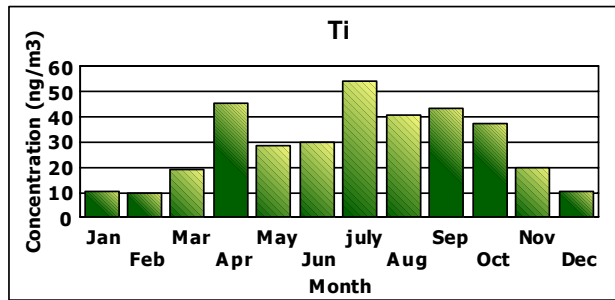
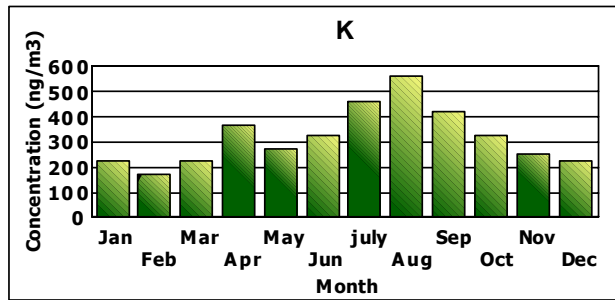
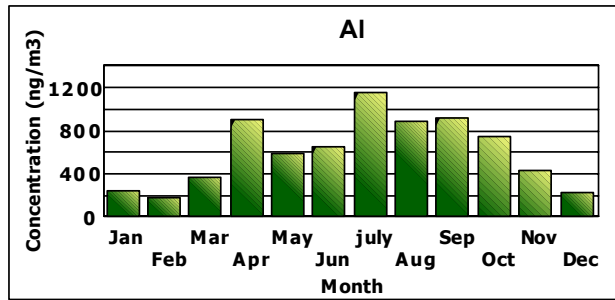


Figure 4.29 Monthly variation in the concentration of crustal elements

Monthly variations in the concentration of selected anthropogenic elements were depicted in Figure 4.30. The trend observed in the anthropogenic elements resemble to the variations in the crustal elements. Anthropogenic elements also have high summer and low winter concentrations. For  $\text{SO}_4^{2-}$ ,  $\text{NO}_3^-$ , and  $\text{NH}_4^+$  high concentrations in summer can be attributed to enhanced photochemical oxidation. In addition to photochemistry, fertilizer application can also modify temporal variations in  $\text{NH}_4^+$  concentrations. Ammonium containing fertilizers are shown to be the main source of  $\text{NH}_3$  in the Mediterranean region (Al Momani et al., 1998; Güllü et al., 1998; 2000). Fertilizers are generally applied to the soil as conditioner in the spring and temperature increase during summer season facilitate both volatilization of  $\text{NH}_3$  from fertilizer containing soil and its conversion to  $\text{NH}_4^+$  ion.

Concentration values measured for the Pb and Cd are also high in summer and low in winter. Since there is no source in close proximity of the sampling station that emits these elements to the atmosphere, observed monthly averages of Pb and Cd may be due to the long range transport of the pollutants to the region. Scavenging of these pollutants from the atmosphere via precipitation along their way to the station is more probable in winter than in summer, explaining their higher concentrations during summer season.

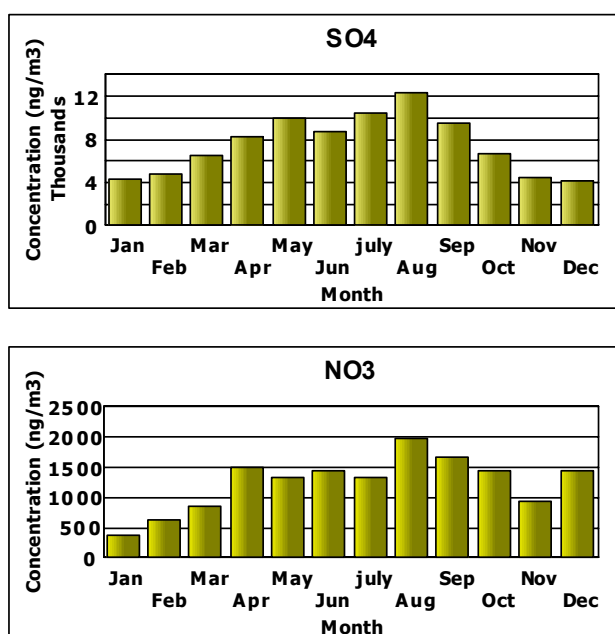


Figure 4.30 Monthly variation in the concentrations of selected anthropogenic elements

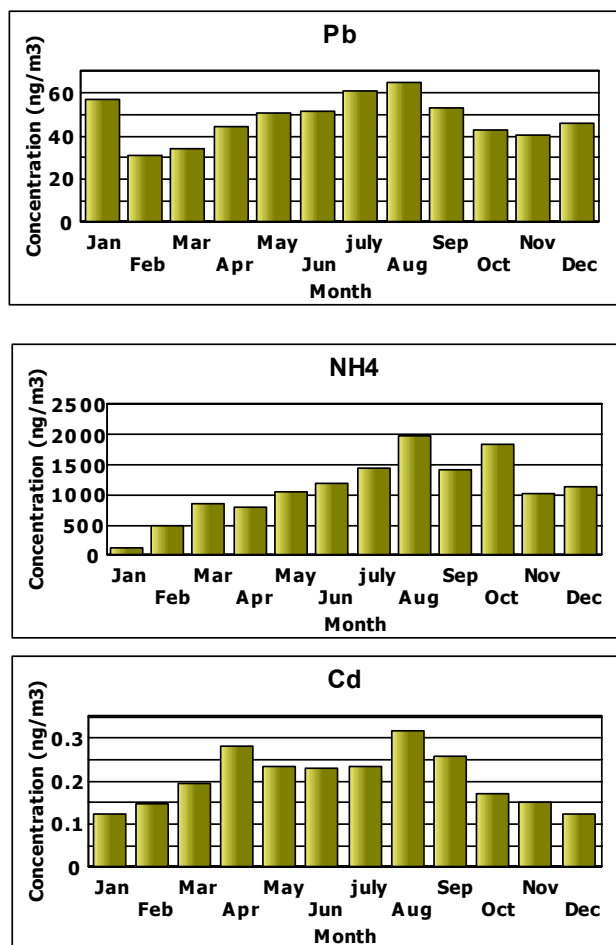


Figure 4.30 Monthly variations in the concentrations of selected anthropogenic elements  
(Continued)

High summer and low winter concentrations of Pb were also reported by Cercasov and Wulfmeyer (2008) in a study performed at Stuttgart, Germany between 1972 and 2005. High summer and low winter concentrations were explained by different vertical exchanges in the boundary layer during winter and summer season and by advection of air masses. In addition to seasonal cycles, a decreasing trend for Pb was also reported by authors and attributed to the shift from leaded to unleaded gasoline in Germany.

The monthly variation in the concentration of Na and Cl are presented in Figure 4.31. Chloride showed a clear seasonal cycle with high concentrations during winter months and relatively low concentrations in summer season. However, Na did not show a similar

seasonal variation. Sodium concentrations in summer months such as July and August were higher than the concentrations observed during the winter months like February, March and November. Lack of seasonality in Na concentrations was attributed to contribution of crustal Na, which is higher during summer season. Calculated sea salt and crustal contributions to measured total Na are depicted in Figure 4.32. In the construction of this figure, contribution of crustal material to measured total Na concentration was calculated using Mason's (1966) soil composition. Then, crustal Na was subtracted from total Na concentration to obtain Na concentration that is accounted for by sea salt. Crustal contribution on measured Na concentrations was generally less than 10%; however, it increases to approximately 20% in summer season. Higher contribution of crustal aerosol on Na concentrations during summer season, can explain lack of seasonal variation in Na concentration.

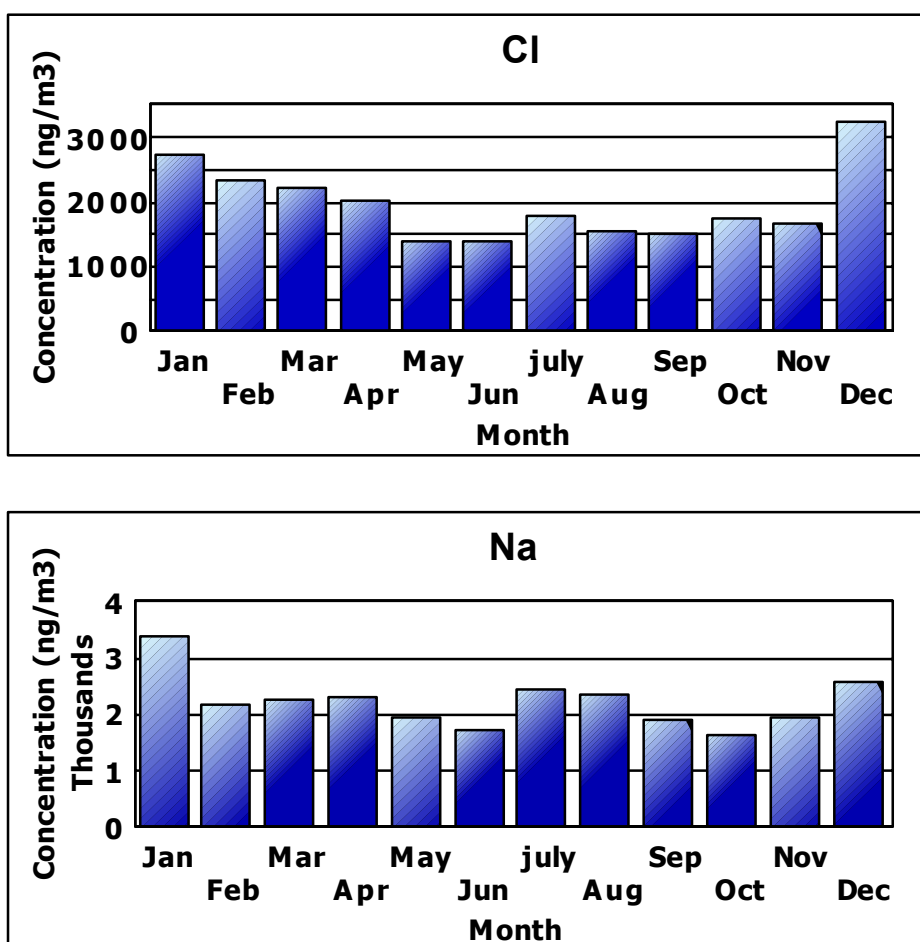


Figure 4.31 Monthly variation in the concentrations of marine elements

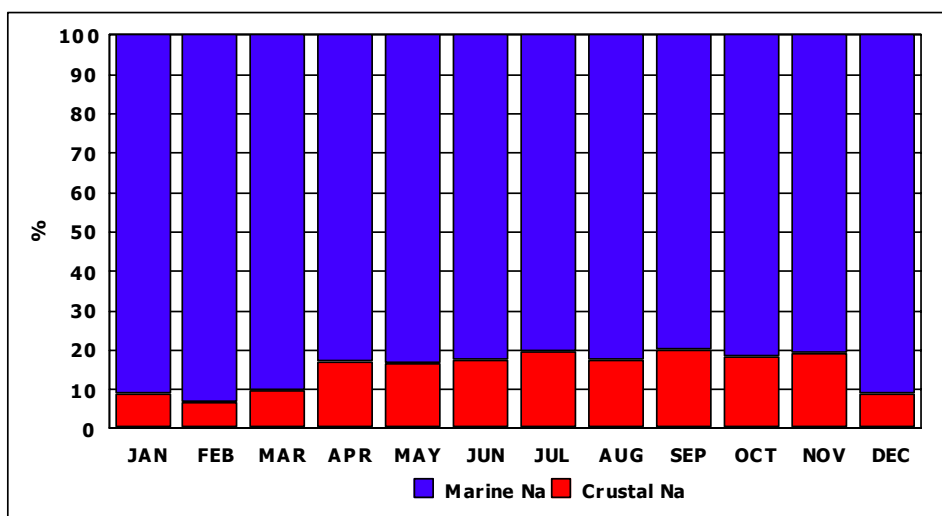


Figure 4.32 Contribution of crustal and marine Na fractions to measured total Na concentration

Though Se is also produced by the biological activity over the sea surface, which is enhanced by the increasing solar intensity (Amourox and Donard, 1996), there is no clear seasonal pattern observed for this element.

### ***Chlorine Deficit***

As it was noted previously, Na and Cl are the major sea salt markers though sea salt is not the only source from which these elements released to the atmosphere. For example, Na has a crustal source and Cl can be emitted from biomass burning (Andrae et al., 1998). Chlorine is not a conservative constituent and it can react with the organic and inorganic acidic species on aerosols, resulting in the depletion of Cl, through evaporations as HCl. Zhuang et al. (1999) had pointed out that chlorine depletion increases with decreasing particle size. In this study binary correlation coefficient between Na and Cl was 0.72, indicating that these two elements were related with 95% statistical confidence. However,  $[Cl^-] / [Na^+]$  ratio showed significant temporal variations as depicted in Figure 4.33.

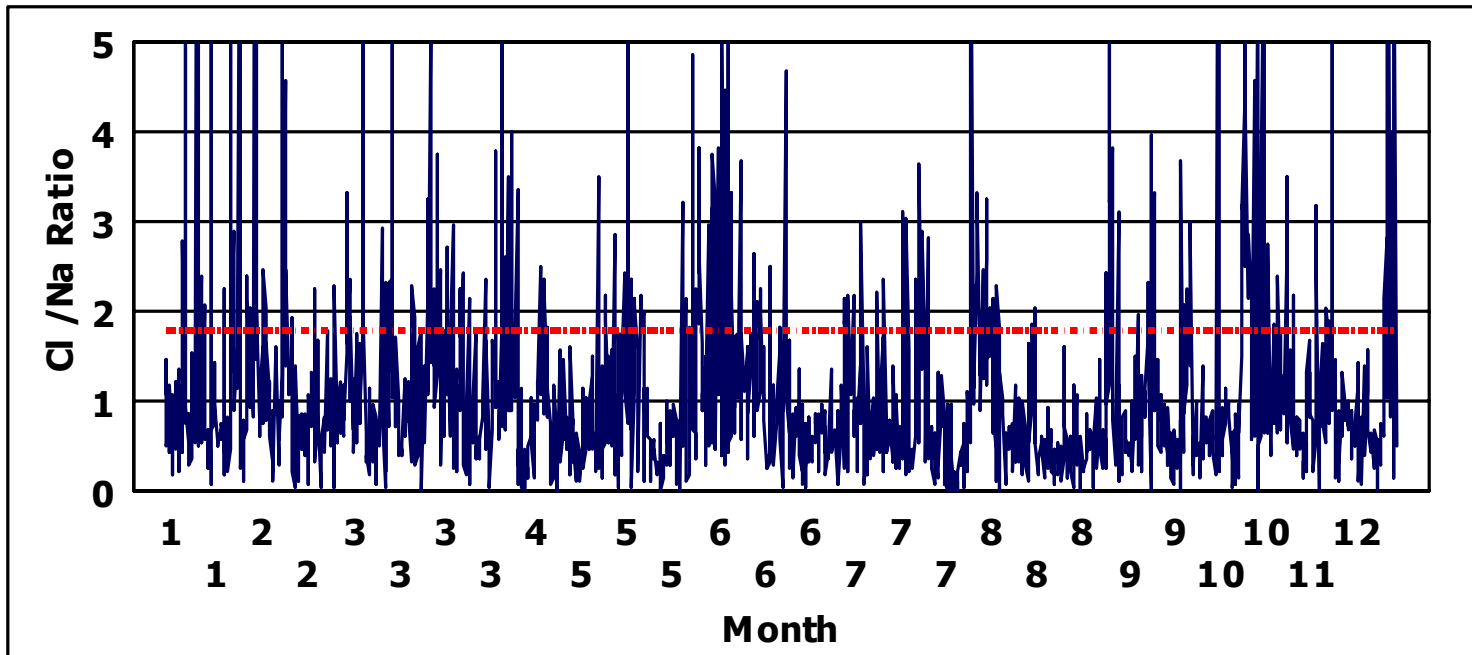
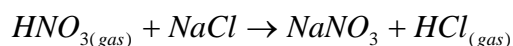


Figure 4.33 Seasonal variation of Cl/Na ratio (Dashed line in the figure represent the  $[Cl] / [Na]$  ratio of bulk seawater)



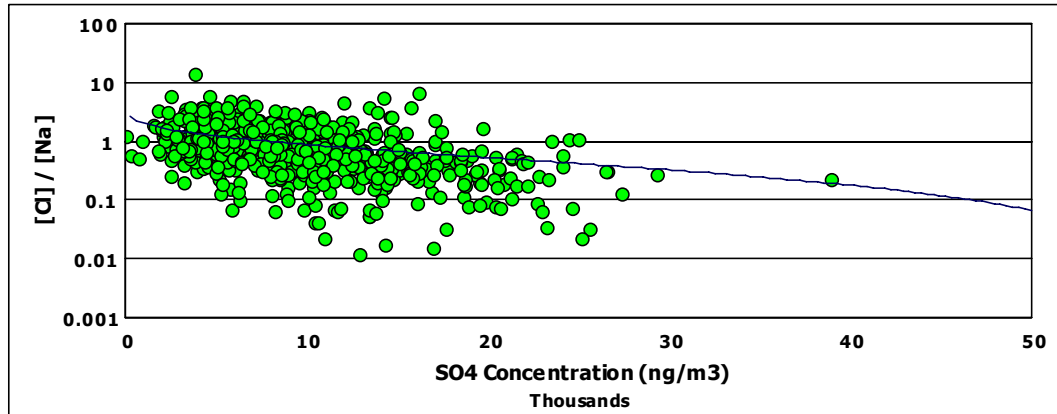
The dashed line in the Figure 4.33 represents  $[\text{Cl}^-] / [\text{Na}^+]$  concentration ratio in bulk sea water, which is 1.8 (Koçak et al., 2004; Hacısalıhoğlu et al., 1991; Kennish 2001; Strayer et al., 2007). The average ratio for the whole data, in this study, was 1.15 while summer and winter ratios were 1.07 and 1.25, respectively. Koçak et al. (2004) have previously estimated this ratio as 1.20 for the summer season for samples collected at Erdemli station, Mersin. Previously, Mihalapoulos et al. (1997) reached a similar conclusion for the samples collected at the Finokalia station, located on the Crete. Hacısalıhoğlu et al. (1991) had collected aerosol samples on a cruise in the Black Sea and they calculated  $[\text{Cl}^-]/[\text{Na}^+]$  ratio as 0.9. Authors claimed that the calculated ratio was low due to the evaporation of Cl as HCl from sea salt particles upon reaction with the  $\text{H}_2\text{SO}_4$ . Bardouki et al. (2003) attributed the Cl deficit to adsorption of  $\text{NO}_3^-$  on the sea salt particles and proposed the following reaction via which HCl is formed:



Later, Koçak et al. (2004) suggested that 20 % of the  $\text{SO}_4^{2-}$  was not neutralized by alkaline species in the atmosphere and the deficiency observed in the summer chlorine concentration could be attributed to the reaction of the sea salt particles with  $\text{SO}_4^{2-}$ . In order to find whether  $\text{HNO}_3$  or  $\text{H}_2\text{SO}_4$  is responsible for summer time  $\text{Cl}^-$  evaporation from filters, variation of  $[\text{Cl}^-] / [\text{Na}^+]$  ratio with respect to  $\text{SO}_4^{2-}$  and  $\text{NO}_3^-$  was investigated as depicted in Figure 4.34. Concentration values measured in summer season was used while constructing this figure.

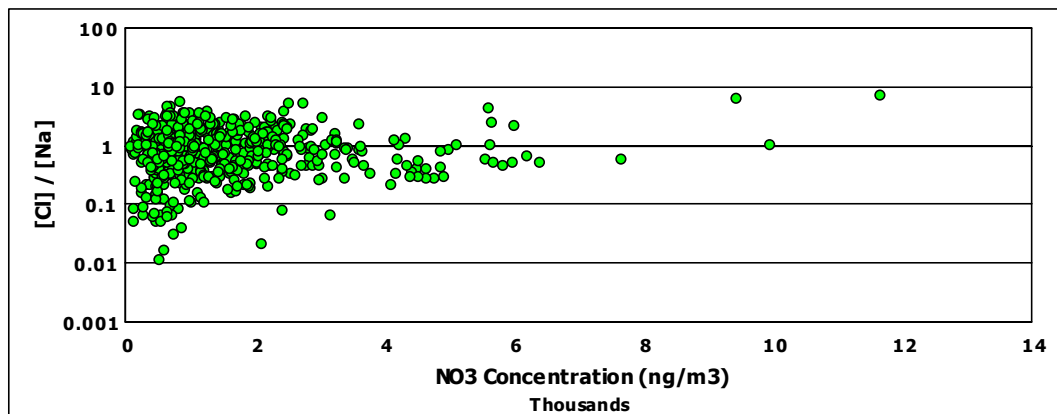
It is obvious from Figure 4.34 that  $[\text{Cl}^-] / [\text{Na}^+]$  ratio decreases with increasing  $\text{SO}_4^{2-}$  concentration while no trend is detected with changing  $\text{NO}_3^-$  concentration. Consequently, it can be concluded that the deficiency observed in the concentration of chlorine can be attributed to the evaporation of chlorine from the aerosol surface due to reaction of sea salt particles with  $\text{H}_2\text{SO}_4$  while reaction with  $\text{HNO}_3$  is not as important as one suggested by Bardouki et al (2003). Similar conclusion was also made for the Black Sea region in Hacısalıhoğlu et al. (1991). Querol et al. (2008) investigated the chemical composition of the aerosol samples collected across the Spain. In this study, authors have also indicated that Cl levels decrease during summer months as a consequence of volatilization as HCl showing a typical Cl/Na summer depletion, particularly true for the inland sites. In another recent study, Favez et al. (2008) evaluated the data generated by analyzing the bulk aerosol samples collected at two different Egyptian sites. The annual cycle of Cl/Na

mass ratio below 1.8 primarily in the summer months was explained by the sea salt chloride depletions.



(a)

Figure 4.34 Variation of Cl / Na ratio with respect to (a) SO<sub>4</sub><sup>2-</sup> (b) NO<sub>3</sub><sup>-</sup> concentration



(b)

Figure 4.34 Variation of Cl / Na ratio with respect to (a) SO<sub>4</sub><sup>2-</sup> (b) NO<sub>3</sub><sup>-</sup> concentration  
(Continued)

Average and median concentrations of measured parameters for winter and summer season were also calculated and results were tabulated in Table 4.7. Winter period extends from November to April and summer period is from May to October. Frequency of rain events is considered while dividing whole year into two seasons. Precipitation at Antalya region is recorded between November and April, while rain event is very rare in the rest of year.

Table 4.7 reveals that the summer concentrations of crustal elements such as Al, Ca, K, Ti, Mn, Fe, Co, Cs, Ba, La, Sm, Yb, Lu and Th were 2 to 4 times higher than the concentration values recorded during winter.

Anthropogenic elements like Sn, Sb, As, Zn, Cd, Cr, Se, Pt, W, and In have also higher summer time concentrations but the difference in summer and winter concentrations is not as pronounced as one observed in crustal elements.

As expected, marine originated elements have higher concentrations in winter season as compared to values recorded in summer months, which is due enhanced sea salt production over sea surface in winter season. Summer to winter ratio for Na and Cl were 1.20 and 1.00, respectively. Calculated ratio for Na is slightly higher than Cl, which can be attributed to contribution of crustal sources of Na concentration in the atmosphere.

The last group of parameters that need to be mentioned in Table 4.7 includes the ions, namely,  $\text{SO}_4^{2-}$ ,  $\text{NO}_3^-$  and  $\text{NH}_4^+$ . These ions are produced by the photochemical activity in the atmosphere and hence, increased solar radiation enhanced the generation of these parameters from their precursors in summer season. Average winter concentration of  $\text{SO}_4^{2-}$  is about  $5.6 \mu\text{g m}^{-3}$  while it rises to  $9.7 \mu\text{g m}^{-3}$  in summer. For  $\text{NO}_3^-$ , summer concentration is 1.8 times higher than the corresponding winter concentration. The difference between summer and winter is more pronounced in  $\text{NH}_4^+$  concentrations and has a ratio of  $\sim 2.6$ . Observed higher summer concentrations of  $\text{NH}_4^+$  as compared to other photochemically produced ions (i.e.,  $\text{SO}_4^{2-}$  and  $\text{NO}_3^-$ ) can be explained both by increased solar radiation as in other two and intensive fertilizer use around the region in spring.

The summer to winter ratio of the measured parameters were sorted in descending order and plotted in Figure 4.35. It has been previously discussed that both anthropogenic and

crustal elements have higher summer concentrations. However, Figure 4.35 revealed that the seasonality of these two different groups of elements is not same though their concentrations are high in dry season.

The elements till Li in the Figure 4.35 are mostly crustal in origin and their summer to winter ratio changes between 2.0 and 4.0. The average summer to winter ratio for the crustal elements is estimated as  $\sim 2.9$ .

Unlike crustal elements, difference in the summer and winter concentrations of anthropogenic elements like Sn, Sb, Zn, In, W, Cd, Cr, Au, Pb and Se is less than 2.0. Summer to winter ratio of these elements is ranging from 1.25 to 1.87. Higher summer time concentration as compared to winter concentration for these elements indicates impact of precipitation and transport pattern on measured values. Particles bearing these elements are removed from the atmosphere by rainout and washout processes in winter season, which explains the difference between winter and summer concentrations for these elements.

Calculated summer to winter ratio was between 1.0 and 1.14 for As, Ge, and Pt. This observed minor difference in summer and winter median concentrations corresponding to this last group of elements implied predominance of local sources in determining atmospheric concentrations of these elements in Antalya region.

Sulfate and  $\text{NO}_3^-$  have summer to winter ratio 1.74 and 1.80, respectively. As it was discussed previously, enhanced photochemical activity in summer season leads to observe increased concentrations for these ions. Although both anthropogenic and crustal elements have high summer concentrations as compared to their winter concentrations, the difference in the summer and winter concentrations of anthropogenic elements are not as high as the difference observed in the crustal elements. This is attributed to different generation and transport pattern for crustal and anthropogenic species. Similar conclusions were drawn by the previous studies conducted over the region and increased summer concentration of anthropogenic elements as compared to their winter concentration was explained by the removal of the anthropogenic particles by rainfall during their transportation to the region (Koçak et al., 2004; Güllü et al., 2004). High summer concentrations of anthropogenic elements can be related to the increased efficiency of the wet precipitation mechanisms during the wet season (winter) over the Mediterranean region.

Table 4.7 Average and median concentrations of elements in summer and winter (ng/m<sup>3</sup>)

	<u>Winter</u>		<u>Summer</u>	
	avg	median	avg	median
<b>Al</b>	379	160	828	538
<b>As</b>	0.75	0.60	0.72	0.61
<b>Au</b>	0.17	0.07	0.17	0.10
<b>Ba</b>	6.90	4.64	11.35	8.97
<b>Be</b>	0.018	0.009	0.029	0.019
<b>Bi</b>	0.098	0.066	0.125	0.091
<b>Ca</b>	864	556	1286	968
<b>Cd</b>	0.17	0.13	0.24	0.20
<b>Ce</b>	0.47	0.22	1.00	0.68
<b>Cl</b>	2336	1110	1551	1117
<b>Co</b>	0.15	0.07	0.26	0.19
<b>Cr</b>	3.04	1.80	4.04	3.13
<b>Cs</b>	0.073	0.052	0.148	0.119
<b>Dy</b>	0.043	0.017	0.085	0.049
<b>Er</b>	0.023	0.010	0.051	0.032
<b>Eu</b>	0.017	0.005	0.021	0.011
<b>Fe</b>	191	91	405	285
<b>Gd</b>	0.055	0.025	0.121	0.074
<b>Ge</b>	0.041	0.029	0.043	0.033
<b>Hf</b>	0.036	0.017	0.068	0.042
<b>Ho</b>	0.008	0.003	0.017	0.011
<b>In</b>	0.008	0.003	0.008	0.004
<b>K</b>	238	176	399	328
<b>La</b>	0.24	0.12	0.53	0.35
<b>Li</b>	0.38	0.24	0.71	0.50
<b>Lu</b>	0.003	0.001	0.007	0.004
<b>Mg</b>	492	273	535	433
<b>Mn</b>	5.12	3.32	10.49	8.65
<b>Na</b>	2400	1163	2013	1399
<b>Nd</b>	0.23	0.10	0.50	0.32
<b>NH<sub>4</sub></b>	761	450	1426	1162
<b>Ni</b>	1.66	1.06	2.87	2.32
<b>NO<sub>3</sub></b>	947	646	1533	1159
<b>Pb</b>	40	31	54	43
<b>Pr</b>	0.059	0.028	0.134	0.085
<b>Pt</b>	0.003	0.002	0.003	0.002
<b>Rb</b>	0.49	0.33	1.02	0.82
<b>Sb</b>	0.59	0.48	0.73	0.60
<b>Se</b>	0.40	0.16	0.44	0.30
<b>Sm</b>	0.050	0.023	0.109	0.069
<b>Sn</b>	0.48	0.37	0.77	0.63
<b>SO<sub>4</sub></b>	5583	4927	9675	8581
<b>Sr</b>	3.31	1.65	4.59	3.43
<b>Tb</b>	0.007	0.003	0.016	0.010
<b>Th</b>	0.11	0.05	0.25	0.17
<b>Ti</b>	19	9	39	26

Table 4.7 Average and median concentrations of elements in summer and winter (ng/m<sup>3</sup>)

	<u>Winter</u>		<u>Summer</u>	
	avg	median	avg	median
<b>Tm</b>	0.003	0.001	0.007	0.004
<b>U</b>	0.054	0.037	0.091	0.065
<b>V</b>	1.79	1.25	3.78	3.02
<b>W</b>	0.067	0.049	0.101	0.075
<b>Y</b>	0.108	0.052	0.232	0.170
<b>Yb</b>	0.021	0.010	0.046	0.029
<b>Zn</b>	9.66	6.68	15.75	11.68

Higher summer and lower winter concentrations of crustal elements, on the other hand, implied enhanced generation of soil aerosol in the summer. Since the soil is damp during the wet season due to the increased frequency and strength of the precipitation, the resuspension of these particles to the atmosphere is difficult. Consequently, concentration the aerosols originated from soil and associated elements have low concentrations in the atmosphere. In contrast to winter, since the region is arid and soil is dry during summer months, resuspension of soil particles are easier and one can observe higher concentrations in the atmosphere.

It is interesting to note that K, Ca, Mg, Bi, Na and Cl are also have lower summer to winter ratio though they are not considered as anthropogenic. In other words, the summer to winter ratio corresponding to these elements are not as high as the other crustal pollutants. It would be worthwhile to note that these elements are also generated over the sea surface and released to the atmosphere by the bubble bursting process as sea salt particles (Chow, 1995). Among them, Na and Cl are well known sea salt markers. As the strength and frequency of the wind increases in the winter time enhancing the release of sea salt particles toward the atmosphere, it is expected to see lower summer to winter ratio for these pollutants.

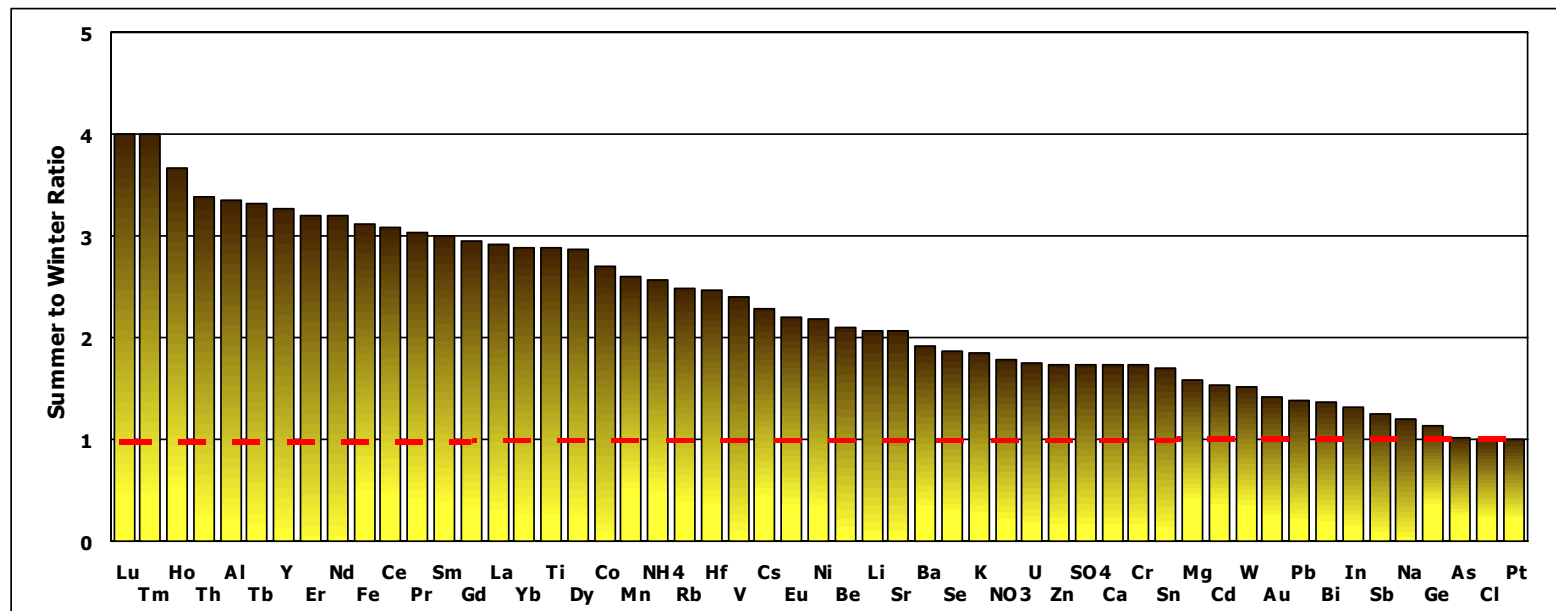


Figure 4.35 Summer to winter ratio for the parameters measured in the study

#### **4.4.3. Year to year Variation in Concentrations of Aerosol Variables in the Eastern Mediterranean Atmosphere – Long-term trends in concentrations of elements and ions**

Nine year-long data enabled us to evaluate the year to year variation of the measured parameters and changes in concentrations of elements that occur in that period. In this section, year to year variation of the measured parameters was discussed. For most of the elements different yearly variations were observed. Annual median concentrations of the measured parameters were presented in Table 4.8.

Highest median concentration values were recorded for  $\text{SO}_4^{2-}$  and lowest ones for Pt. The median concentration of  $\text{SO}_4^{2-}$  varied between  $4.05 \mu\text{g m}^{-3}$  in 2001 and  $13.12 \mu\text{g m}^{-3}$  in 1996. The median Pt concentrations varied between 0.001 and  $0.002 \text{ ngm}^{-3}$ .

Yearly variation in the concentrations of crustal, marine and anthropogenic elements was given in Figures 4.36, 4.37 and 4.38, respectively.

It is clear from Figure 4.36 that crustal elements show decreasing pattern in the course of study period. As it will be discussed later in this section, statistically significant decreasing trend was recorded for crustal elements (e.g., Al, Ca, Fe, Ti, Ce, Pr, Nd, Sm, Eu, Gd, Tb and Dy), some of which is locally generated and rest is transported to the Eastern Mediterranean from North Africa and Middle East.

For marine elements, Na and Cl are selected here as examples, yearly median concentration values do not follow a common increasing or decreasing trend as presented in Figure 4.37 while minor decrease was recorded for Na owing to its crustal contribution.

Unlike marine elements concentrations of all anthropogenic pollutants given in Figure 4.38 decreased after 1996, except for Pb. Lead concentrations increased till 1995 and decreased later on, particularly after 1998.



Table 4.8 Annual median concentrations of measured aerosol variables (ng m<sup>-3</sup>)

<b>Parameter</b>	<b>1993</b>	<b>1994</b>	<b>1995</b>	<b>1996</b>	<b>1997</b>	<b>1998</b>	<b>1999</b>	<b>2000</b>	<b>2001</b>
<b>Al</b>	576	241	327	563	236	514	302	287	139
<b>As</b>	0.81	0.64	0.64	0.87	0.48	0.69	0.49	0.46	0.44
<b>Au</b>	0.083	0.090	0.135	0.106	0.054	0.071	0.084	0.071	0.043
<b>Ba</b>	5.95	5.00	8.20	9.79	7.22	14.18	5.11	5.45	5.41
<b>Be</b>	0.020	0.013	0.019	0.019	0.010	0.023	0.010	0.010	0.008
<b>Bi</b>	0.057	0.083	0.100	0.132	0.072	0.177	0.050	0.056	0.057
<b>Ca</b>	906	680	793	1020	567	1332	587	628	707
<b>Cd</b>	0.11	0.13	0.18	0.26	0.14	0.29	0.17	0.17	0.17
<b>Ce</b>	0.67	0.38	0.44	0.72	0.29	0.78	0.36	0.34	0.24
<b>Cl</b>	845	818	862	843	1414	1451	1905	980	899
<b>Co</b>	0.18	0.12	0.12	0.22	0.09	0.20	0.12	0.11	0.08
<b>Cr</b>	2.31	3.05	2.38	3.93	2.15	3.36	2.53	2.11	2.55
<b>Cs</b>	0.088	0.075	0.092	0.147	0.066	0.135	0.073	0.062	0.049
<b>Dy</b>	0.046	0.039	0.037	0.055	0.018	0.067	0.021	0.024	0.017
<b>Er</b>	0.025	0.018	0.022	0.034	0.012	0.043	0.016	0.016	0.011
<b>Eu</b>	0.013	0.012	0.012	0.011	0.006	0.015	0.005	0.005	0.003
<b>Fe</b>	264	127	172	343	133	274	192	172	87
<b>Gd</b>	0.064	0.043	0.054	0.081	0.028	0.099	0.035	0.032	0.022
<b>Ge</b>	0.039	0.036	0.030	0.041	0.024	0.046	0.021	0.021	0.024
<b>Hf</b>	0.030	0.030	0.036	0.043	0.026	0.078	0.020	0.021	0.020
<b>Ho</b>	0.009	0.006	0.008	0.012	0.005	0.015	0.005	0.005	0.003
<b>In</b>	0.003	0.003	0.003	0.004	0.002	0.004	0.002	0.004	0.003
<b>K</b>	322	228	258	378	189	323	220	172	156
<b>La</b>	0.33	0.19	0.23	0.38	0.14	0.41	0.19	0.18	0.12
<b>Li</b>	0.49	0.29	0.43	0.58	0.24	0.56	0.30	0.32	0.24
<b>Lu</b>	0.003	0.003	0.003	0.005	0.002	0.006	0.002	0.002	0.001

Table 4.8 Annual median concentrations of measured aerosol variables (ng m<sup>-3</sup>) (Continued)

<b>Parameter</b>	<b>1993</b>	<b>1994</b>	<b>1995</b>	<b>1996</b>	<b>1997</b>	<b>1998</b>	<b>1999</b>	<b>2000</b>	<b>2001</b>
<b>Mg</b>	518	396	435	486	253	534	280	225	191
<b>Mn</b>	7.68	4.38	5.53	11.02	4.03	8.15	5.79	5.26	3.27
<b>Na</b>	1518	1203	1873	1904	993	1596	964	848	592
<b>Nd</b>	0.30	0.18	0.20	0.35	0.13	0.38	0.16	0.17	0.10
<b>NH<sub>4</sub><sup>+</sup></b>	1692				915		2021	267	
<b>Ni</b>	2.01	1.35	1.53	2.90	1.25	2.42	1.75	1.54	1.42
<b>NO<sub>3</sub><sup>-</sup></b>	942				1187	2198	1516	821	
<b>Pb</b>	40.1	47.4	73.5	58.5	34.8	56.5	20.7	15.6	13.6
<b>Pr</b>	0.076	0.047	0.057	0.093	0.035	0.102	0.046	0.043	0.025
<b>Pt</b>	0.002	0.002	0.002	0.002	0.001	0.003	0.001	0.001	0.001
<b>Rb</b>	0.67	0.43	0.55	1.06	0.38	0.76	0.61	0.53	0.32
<b>Sb</b>	0.50	0.50	0.73	0.73	0.45	0.77	0.48	0.53	0.50
<b>Se</b>	0.22	0.18	0.27	0.48	0.16	0.29	0.25	0.20	0.13
<b>Sm</b>	0.062	0.039	0.049	0.076	0.027	0.087	0.034	0.034	0.021
<b>Sn</b>	0.49	0.43	0.74	0.87	0.41	0.83	0.46	0.41	0.34
<b>SO<sub>4</sub><sup>2-</sup></b>	5906	5117	8056	13119	4793	8532	6562	6082	4048
<b>Sr</b>	2.95	2.34	2.99	3.80	1.55	3.75	2.23	2.31	1.63
<b>Tb</b>	0.008	0.006	0.006	0.011	0.004	0.013	0.005	0.005	0.003
<b>Th</b>	0.15	0.09	0.09	0.18	0.06	0.20	0.09	0.09	0.05
<b>Ti</b>	23.4	12.2	14.6	30.0	10.6	23.3	16.0	16.3	8.7
<b>Tm</b>	0.004	0.002	0.003	0.005	0.002	0.006	0.002	0.002	0.002
<b>U</b>	0.06	0.05	0.07	0.07	0.03	0.08	0.03	0.03	0.03
<b>V</b>	2.0	1.5	2.1	4.3	1.6	2.9	2.4	2.1	1.1
<b>W</b>	0.05	0.06	0.10	0.08	0.06	0.12	0.04	0.04	0.05
<b>Y</b>	0.14	0.07	0.09	0.19	0.07	0.16	0.10	0.10	0.06
<b>Yb</b>	0.02	0.02	0.02	0.03	0.01	0.04	0.01	0.01	0.01
<b>Zn</b>	8.1	7.1	11.0	17.8	8.5	12.4	9.0	7.9	9.2

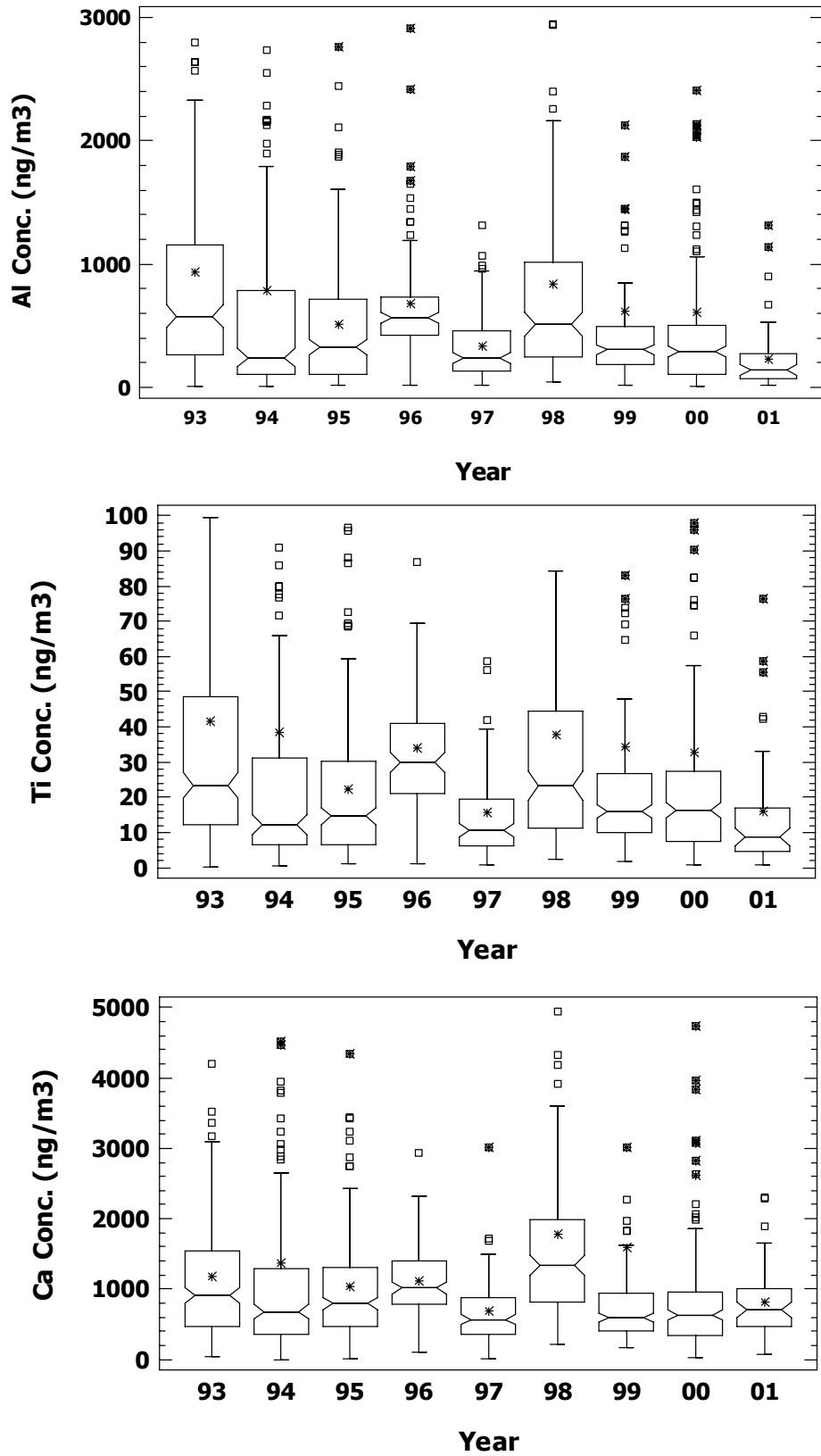


Figure 4.36 Annual variation observed in the concentrations of selected crustal elements

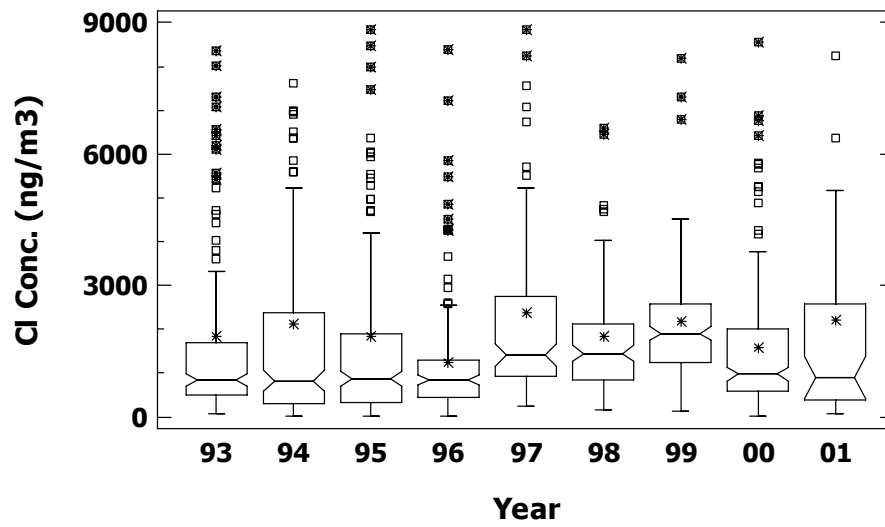
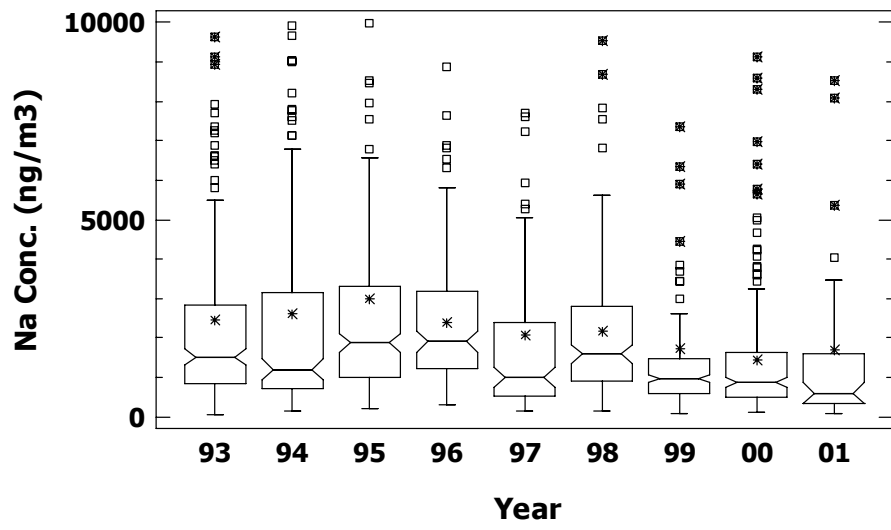


Figure 4.37 Annual variation observed in the concentrations of marine elements

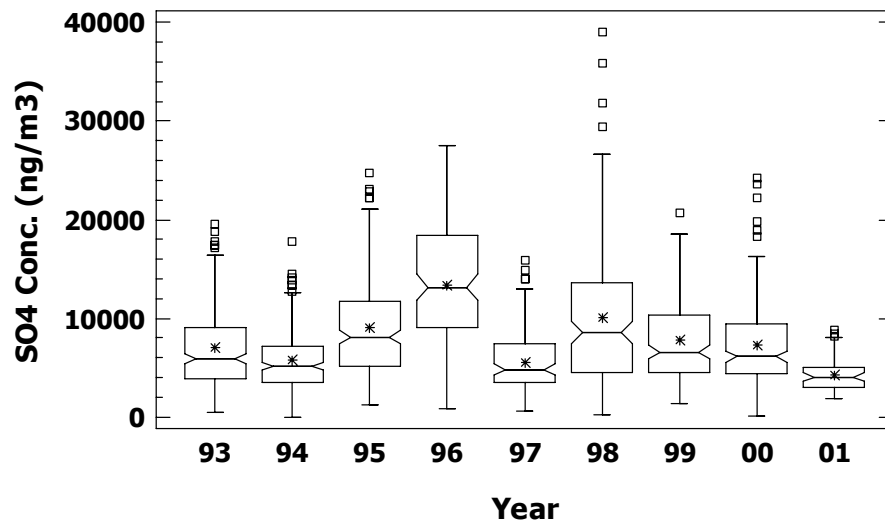
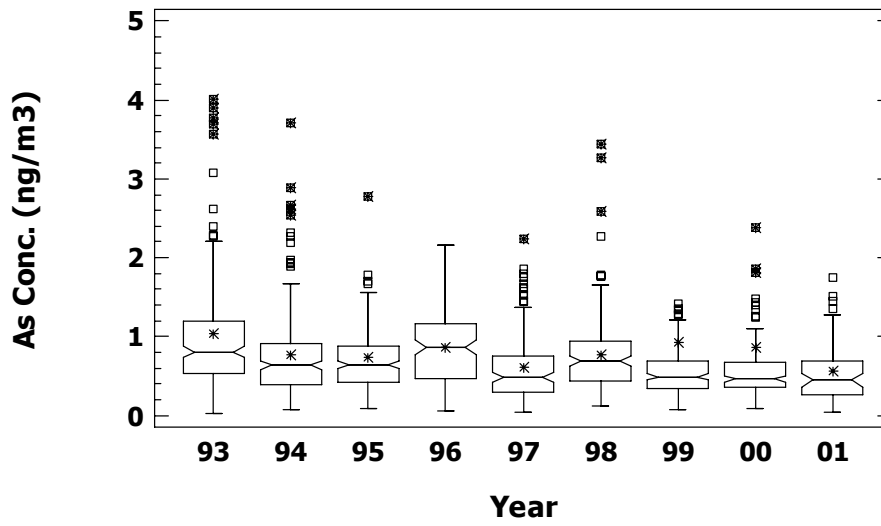
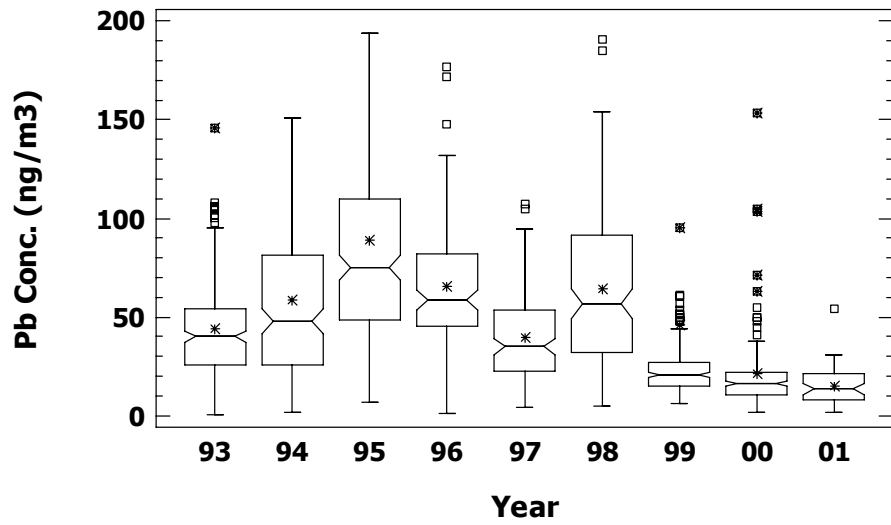


Figure 4.38 Annual variation observed in the concentrations of anthropogenic elements

Time series plot of the  $\text{SO}_4^{2-}$  over 9 years period was given in Figure 4.39. In Figure 4.39,  $\text{SO}_4^{2-}$  concentration made cycles in different years, however, it is hard to interpret whether this pollutant holds increasing or decreasing trend. In order to understand whether the pollutants measured in this study show increasing or decreasing trend, a non-parametric test was applied to generated data set. Time series has three main parts in structural models (Salcedo et al., 1999; Cercasov and Wulfmeyer, 2008):

- Trend that refers to long term variation in the mean
- Cyclical component that include seasonality and other cyclical or quasi cyclical terms
- Random residual that is independent and normally distributed

Although some attempts were made based on short-term measurements, investigation of trends is possible if the long-term time series in the measured parameters are present (Matschullat et al., 2000; Lammel et al., 2002). In order to find the long term changes in measured aerosol variables, the seasonal Kendall test and Sen's slope estimator were applied as non-parametric methods, which are the statistical procedures that require very few assumptions about the underlying population. They are often used when the data do not follow normal (Gaussian) distribution. The normality of the measured parameters was tested earlier in this study, and it was found that some of the parameters conform to log-normal distribution and the rest fit neither Gaussian nor lognormal distributions, but obviously none of them were normally distributed. Since validity of these nonparametric tests do not depend on the distribution of data, they can safely apply to our generated data set.

Hirsch, Slack and Smith (1982) proposed the seasonal Kendall test (Gilbert, 1987). Detection of long term trends can become difficult if there exists seasonal and other cycles in the variations of the measured parameters. This problem can be solved in trend analysis either by removing cycle before applying test or by using statistical tests that are unaffected by the presence of cycles (Gilbert, 1987). The seasonal Kendall test uses the second mentioned approach. The major advantage of Seasonal Kendall test is that it is insensitive to the existence of seasonality. In addition to that, Seasonal Kendall test can be applied to data with missing values and ties, which is referred to as equal-valued data. The methodology used in the trend analysis is schematically outlined in Figure 4.40.

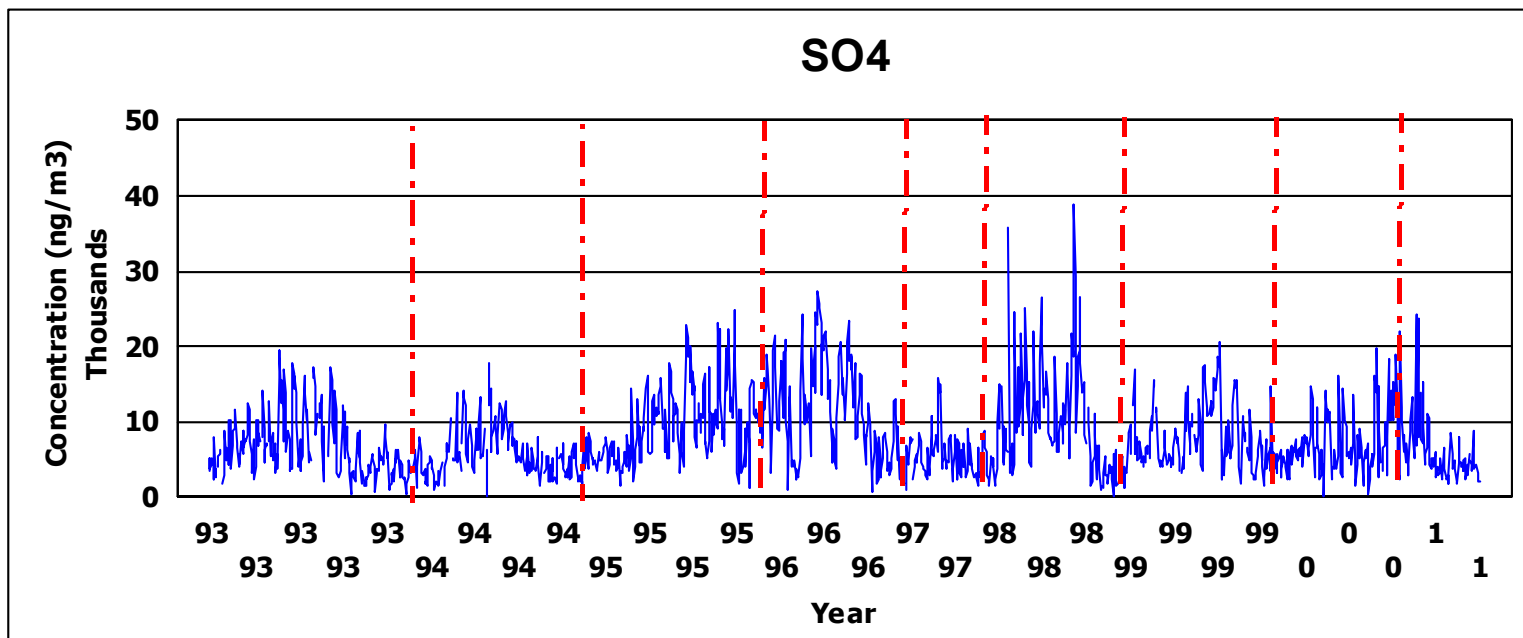


Figure 4.39 Time series plot of the  $\text{SO}_4^{2-}$  concentrations over 9 years

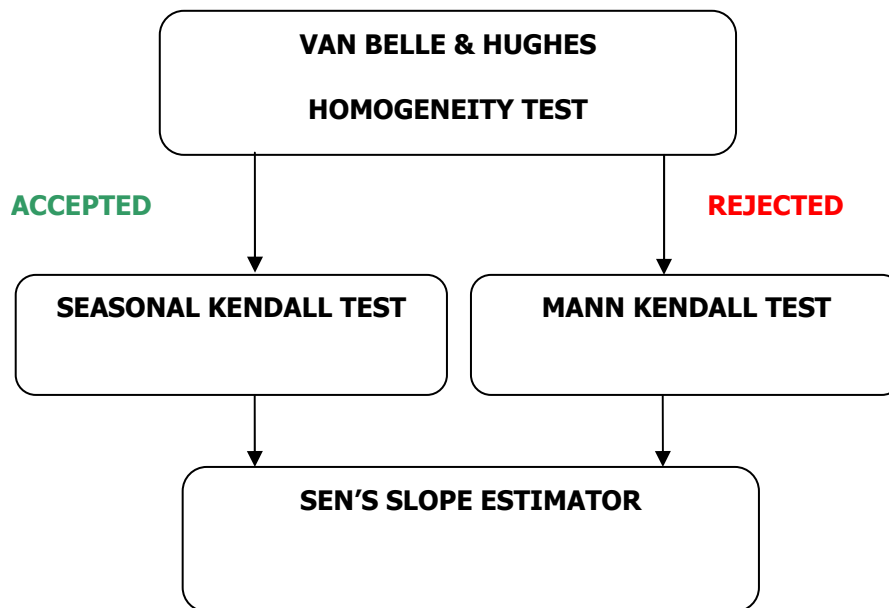


Figure 4.40 Schematical description of the trend analysis methodology

A global trend is meaningful if the trends at all season are in the same direction- that is all upward or all downward. For this reason, homogeneity of the seasons was tested before deciding to use either the Seasonal Kendall test or Mann Kendall test. If homogeneity of the seasons was verified, then Seasonal Kendall test can be used, otherwise Mann Kendal test has to be applied. The Mann-Kendall statistic  $S$  for the data set  $x_i$  of length 'n' is defined in Equation 4.7:

$$S = \sum_{k=1}^{n-1} \sum_{j=k+1}^n \text{sgn}(x_j - x_k) \quad (4.7)$$

Where;

$$\text{sgn}(x_j - x_k) = \begin{cases} +1 & \text{if } (x_j - x_k) > 0 \\ 0 & \text{if } (x_j - x_k) = 0 \\ -1 & \text{if } (x_j - x_k) < 0 \end{cases}$$



The normal test statistics Z can be calculated, thereafter, first estimating the var(S) as it was given in Equation 4.8:

$$z = \begin{cases} \frac{S-1}{\sqrt{\text{Var}(s)}} & \text{if } S > 0 \\ 0 & \text{if } S = 0 \\ \frac{S+1}{\sqrt{\text{Var}(s)}} & \text{if } S < 0 \end{cases} \quad (4.8)$$

A positive value of Z indicates an increasing trend while negative value reveals a decreasing trend. Either an increasing or decreasing trend (two tailed test) can be tested at the  $\alpha$  level of significance against the null hypothesis of,  $H_0$ , no trend.  $H_0$  is rejected if the absolute value of Z is greater than the  $Z_{1-\alpha/2}$ , where  $Z_{1-\alpha/2}$  is obtained from the standard tables.

To determine the global trend, the seasonal trends should have the same direction and magnitude, in other words, they should be homogenous. To test the homogeneity between the seasons Homogeneity Test originally proposed by Van Belle and Hughes (1984) was used. The corresponding test statistic  $\chi^2_{\text{homog}}$  can be computed by using the Equation 4.9 given below:

$$\chi^2_{\text{homog}} = \chi^2_{\text{total}} - \chi^2_{\text{trend}} = \sum_{i=1}^m (Z_i)^2 - m(\bar{Z})^2 \quad (4.9)$$

Where;

$$Z_i = \frac{S_i}{\sqrt{\text{Var}(S_i)}}, \bar{Z} = \frac{1}{m} \sum_{i=1}^m Z_i$$

The computed  $\chi^2_{\text{homog}}$  value was compared with the standard value at the  $\alpha$  level significance and 11 degrees of freedom (df) to test the null hypothesis of,  $H_0$ , homogenous seasonal trend over time (trends in the same direction and of the same magnitude). If the calculated value is greater than the standard one, then the null

hypothesis is rejected. Then, seasonal Kendall test and slope estimate are not meaningful, and one should use the Mann-Kendall test and Sen's slope estimator for each individual season (Gilbert, 1987; Coen et al., 2007). If  $\chi^2_{\text{homog}}$  does not exceed the critical value,  $\chi^2_{\text{trend}}$  is compared with the chi square distribution with 1 degrees of freedom to test presence of a common trend in all seasons.

The outcomes of the conducted Van Belle and Hughes' Homogeneity of Trend test were summarized in Table 4.9. As it can be seen from Table 4.9, all the calculated  $\chi^2_{\text{homog}}$  values are less than the critical  $\chi^2$  (equal to 19.68) with  $df=12-1$  at the  $\alpha = 0.05$  significance level. Therefore, the null hypothesis of homogenous seasonal trends over time can not be rejected. Since the calculated  $\chi^2_{\text{homogenous}}$  values are not significant,  $\chi^2_{\text{trend}}$  values can be compared to the critical  $\chi^2$  value with 1 df at the same significance level ( $\chi^2_{\text{critical}} = 3.84$ ). If the calculated  $\chi^2_{\text{trend}} > \chi^2_{\text{critical}}$  for a parameter, then a common trend is present for that parameter in all seasons. The parameters shaded and written in bold in the Table 4.9 which are Be, Na, Mg, Al, K, Ge, As, Se, Cd, Cs, La, Au, Pb, Eu, Gd, U and  $\text{NO}_3^-$  were passed from the second test, implying that these parameters have common trend in all seasons. As can be concluded from the discussions provided up to now, Van Belle and Hughes' Homogeneity Test is a combined test for the homogeneity and trend. However, it does not give information about the direction of trend in case of it is detected.

As depicted in the Figure 4.40 seasonal Kendall test was applied to the concentrations of parameters that passed from the homogeneity test.

Table 4.9 Results of the Van Belle and Hughes' Homogeneity Test

<b>Van Belle and Hughes Homogeneity Test</b>					
	<b>X<sup>2</sup> homogen</b>	<b>X<sup>2</sup> critical α=0.05 df=11</b>	<b>X<sup>2</sup> trend</b>	<b>X<sup>2</sup> critical α=0.05 df=1</b>	<b>X<sup>2</sup> total</b>
Li	5.438	19.68	3.159	3.84	8.597
<b>Be</b>	<b>2.571</b>	<b>19.68</b>	<b>13.735</b>	<b>3.84</b>	<b>16.306</b>
<b>Na</b>	<b>7</b>	<b>19.68</b>	<b>17.733</b>	<b>3.84</b>	<b>24.733</b>
<b>Mg</b>	<b>7.233</b>	<b>19.68</b>	<b>16.272</b>	<b>3.84</b>	<b>23.505</b>
<b>Al</b>	<b>14.14</b>	<b>19.68</b>	<b>6.007</b>	<b>3.84</b>	<b>20.147</b>
<b>K</b>	<b>8.059</b>	<b>19.68</b>	<b>11.526</b>	<b>3.84</b>	<b>19.585</b>
Ca	13.388	19.68	0.157	3.84	13.544
Ti	9.454	19.68	1.655	3.84	11.109
V	15.974	19.68	0.414	3.84	16.388
Cr	13.48	19.68	2.451	3.84	15.931
Mn	15.329	19.68	1.656	3.84	16.985
Fe	8.794	19.68	1.101	3.84	9.895
Co	11.957	19.68	2.775	3.84	14.732
Ni	14.711	19.68	0.003	3.84	14.714
Zn	15.277	19.68	0.185	3.84	15.462
<b>Ge</b>	<b>5.946</b>	<b>19.68</b>	<b>5.29</b>	<b>3.84</b>	<b>11.236</b>
<b>As</b>	<b>9.28</b>	<b>19.68</b>	<b>8.381</b>	<b>3.84</b>	<b>17.661</b>
<b>Se</b>	<b>9.539</b>	<b>19.68</b>	<b>4.624</b>	<b>3.84</b>	<b>14.164</b>
Rb	15.266	19.68	1.899	3.84	17.165
Sr	10.089	19.68	2.968	3.84	13.058
Y	8.871	19.68	1.297	3.84	10.168
<b>Cd</b>	<b>9.296</b>	<b>19.68</b>	<b>5.942</b>	<b>3.84</b>	<b>15.238</b>
In	8.067	19.68	0.041	3.84	8.108
Sn	4.309	19.68	1.426	3.84	5.735
Sb	6.83	19.68	0.066	3.84	6.896
<b>Cs</b>	<b>13.276</b>	<b>19.68</b>	<b>7.277</b>	<b>3.84</b>	<b>20.552</b>
Ba	11.914	19.68	0.077	3.84	11.991
<b>La</b>	<b>14.207</b>	<b>19.68</b>	<b>4.098</b>	<b>3.84</b>	<b>18.305</b>
Hf	13.037	19.68	0.336	3.84	13.374
W	4.418	19.68	1.785	3.84	6.203
Pt	4.781	19.68	1.14	3.84	5.921
<b>Au</b>	<b>11.18</b>	<b>19.68</b>	<b>8.384</b>	<b>3.84</b>	<b>19.564</b>
<b>Pb</b>	<b>7.085</b>	<b>19.68</b>	<b>22.715</b>	<b>3.84</b>	<b>29.8</b>
Bi	6.463	19.68	0.798	3.84	7.261
Ce	13.924	19.68	3.221	3.84	17.145
Pr	13.995	19.68	2.231	3.84	16.227
Nd	13.437	19.68	2.97	3.84	16.407
Sm	12.993	19.68	2.067	3.84	15.06
<b>Eu</b>	<b>7.072</b>	<b>19.68</b>	<b>4.539</b>	<b>3.84</b>	<b>11.612</b>

Table 4.9 Results of the Van Belle and Hughes' Homogeneity Test (Continued)

<b>Van Belle and Hughes Homogeneity Test</b>					
	<b>X<sup>2</sup> homogen</b>	<b>X<sup>2</sup> critical α=0.05 df=11</b>	<b>X<sup>2</sup> trend</b>	<b>X<sup>2</sup> critical α=0.05 df=1</b>	<b>X<sup>2</sup> total</b>
<b>Gd</b>	<b>13.082</b>	<b>19.68</b>	<b>4.286</b>	<b>3.84</b>	<b>17.367</b>
Tb	12.533	19.68	3.13	3.84	15.663
Dy	15.676	19.68	3.033	3.84	18.709
Ho	12.864	19.68	3.656	3.84	16.52
Er	13.231	19.68	3.656	3.84	16.887
Tm	11.917	19.68	2.596	3.84	14.512
Yb	12.948	19.68	3.388	3.84	16.336
Lu	13.231	19.68	3.656	3.84	16.887
Th	14.766	19.68	2.866	3.84	17.632
<b>U</b>	<b>8.054</b>	<b>19.68</b>	<b>12.083</b>	<b>3.84</b>	<b>20.137</b>
Cl	12.974	19.68	0.876	3.84	13.851
SO <sub>4</sub> <sup>2-</sup>	8.452	19.68	1.469	3.84	9.92
<b>NO<sub>3</sub><sup>-</sup></b>	<b>2.258</b>	<b>19.68</b>	<b>4.535</b>	<b>3.84</b>	<b>6.794</b>
NH <sub>4</sub> <sup>+</sup>	5.938	19.68	2.46	3.84	8.398

In the seasonal Kendall test monthly averages were used and 12 seasons, actually 12 months of the year, were taken as the time periods. The null hypothesis,  $H_0$ , of no trend versus the alternative hypothesis,  $H_A$ , of either an upward or downward trend (a two tailed test) was tested at the  $\alpha = 0.05$  significance level. The critical value at this significance level is equal to 1.96. The computed absolute value of Z is compared with this critical Z value. The two sided null hypothesis of increasing or decreasing trend was accepted if computed Z value greater than the  $Z_{critical}$ . The results of the Seasonal Kendall test were provided in Table 4.10.

Approximately 55 % of the parameters (29 out of 53) have decreasing trend between 1993 and 2001, but to different extent. For the rest of the parameters neither decreasing nor increasing trend was detected. The parameters that have decreasing trend include Be, Na, Mg, Al, K, Co, Ge, As, Se, Sr, Cs, La, Au, Pb, Ce, Pr, Nd, Sm, Eu, Gd, Tb, Dy, Ho, Er, Tm, Yb, Lu, Th and U. The elements in this list are crustal in origin, except for As, Se, Au and Pb, which anthropogenic in nature.

Though Van Belle and Hughes' Homogeneity test detected a common trend for Cd and NO<sub>3</sub><sup>-</sup>, neither increasing or decreasing trend was detected for these two parameters by seasonal Kendall test. For Co, Sr, Ce, Pr, Nd, Tb, Dy, Ho, Er, Tm, Yb, Lu, and Th, downward trend was detected by seasonal Kendall test while no common trend was found by Van Belle and Hughes' Homogeneity test.

Table 4.10 Results of the conducted Seasonal Kendall test

	<b>Mann Kendall Statistic S</b>	<b>Z</b>	<b>Zcritical α=0.05</b>	<b>Trend</b>	<b>Trend Direction</b>
Li	-41	-1.876	1.96	Absent	
<b>Be</b>	<b>-83</b>	<b>-3.753</b>	<b>1.96</b>	<b>Present</b>	↓
<b>Na</b>	<b>-95</b>	<b>-4.289</b>	<b>1.96</b>	<b>Present</b>	↓
<b>Mg</b>	<b>-89</b>	<b>-4.021</b>	<b>1.96</b>	<b>Present</b>	↓
<b>Al</b>	<b>-65</b>	<b>-2.949</b>	<b>1.96</b>	<b>Present</b>	↓
<b>K</b>	<b>-79</b>	<b>-3.574</b>	<b>1.96</b>	<b>Present</b>	↓
Ca	-21	-0.983	1.96	Absent	
Ti	-33	-1.519	1.96	Absent	
V	5	0.179	1.96	Absent	
Cr	25	1.072	1.96	Absent	
Mn	-37	-1.698	1.96	Absent	
Fe	-29	-1.34	1.96	Absent	
<b>Co</b>	<b>-47</b>	<b>-2.144</b>	<b>1.96</b>	<b>Present</b>	↓
Ni	3	0.089	1.96	Absent	
Zn	-21	-0.983	1.96	Absent	
<b>Ge</b>	<b>-53</b>	<b>-2.413</b>	<b>1.96</b>	<b>Present</b>	↓
<b>As</b>	<b>-65</b>	<b>-2.949</b>	<b>1.96</b>	<b>Present</b>	↓
<b>Se</b>	<b>-51</b>	<b>-2.323</b>	<b>1.96</b>	<b>Present</b>	↓
Rb	-33	-1.519	1.96	Absent	
<b>Sr</b>	<b>-47</b>	<b>-2.144</b>	<b>1.96</b>	<b>Present</b>	↓
Y	-35	-1.608	1.96	Absent	
Cd	43	1.876	1.96	Absent	
In	-5	-0.268	1.96	Absent	
Sn	-29	-1.34	1.96	Absent	
Sb	3	0.089	1.96	Absent	
<b>Cs</b>	<b>-71</b>	<b>-3.217</b>	<b>1.96</b>	<b>Present</b>	↓
Ba	-11	-0.536	1.96	Absent	
<b>La</b>	<b>-59</b>	<b>-2.681</b>	<b>1.96</b>	<b>Present</b>	↓
Hf	-27	-1.251	1.96	Absent	
W	-35	-1.608	1.96	Absent	
Pt	-21	-0.983	1.96	Absent	

Table 4.10 Results of the conducted Seasonal Kendall test (Continued)

	<b>Mann Kendall Statistic S</b>	<b>Z</b>	<b>Zcritical α=0.05</b>	<b>Trend</b>	<b>Trend Direction</b>
<b>Au</b>	<b>-69</b>	<b>-3.127</b>	<b>1.96</b>	<b>Present</b>	↓
<b>Pb</b>	<b>-107</b>	<b>-4.825</b>	<b>1.96</b>	<b>Present</b>	↓
Bi	-27	-1.251	1.96	Absent	
<b>Ce</b>	<b>-53</b>	<b>-2.413</b>	<b>1.96</b>	<b>Present</b>	↓
<b>Pr</b>	<b>-45</b>	<b>-2.055</b>	<b>1.96</b>	<b>Present</b>	↓
<b>Nd</b>	<b>-51</b>	<b>-2.323</b>	<b>1.96</b>	<b>Present</b>	↓
<b>Sm</b>	<b>-43</b>	<b>-1.966</b>	<b>1.96</b>	<b>Present</b>	↓
<b>Eu</b>	<b>-57</b>	<b>-2.591</b>	<b>1.96</b>	<b>Present</b>	↓
<b>Gd</b>	<b>-59</b>	<b>-2.681</b>	<b>1.96</b>	<b>Present</b>	↓
<b>Tb</b>	<b>-51</b>	<b>-2.323</b>	<b>1.96</b>	<b>Present</b>	↓
<b>Dy</b>	<b>-55</b>	<b>-2.502</b>	<b>1.96</b>	<b>Present</b>	↓
<b>Ho</b>	<b>-55</b>	<b>-2.502</b>	<b>1.96</b>	<b>Present</b>	↓
<b>Er</b>	<b>-55</b>	<b>-2.502</b>	<b>1.96</b>	<b>Present</b>	↓
<b>Tm</b>	<b>-47</b>	<b>-2.144</b>	<b>1.96</b>	<b>Present</b>	↓
<b>Yb</b>	<b>-53</b>	<b>-2.413</b>	<b>1.96</b>	<b>Present</b>	↓
<b>Lu</b>	<b>-55</b>	<b>-2.502</b>	<b>1.96</b>	<b>Present</b>	↓
<b>Th</b>	<b>-51</b>	<b>-2.323</b>	<b>1.96</b>	<b>Present</b>	↓
<b>U</b>	<b>-83</b>	<b>-3.753</b>	<b>1.96</b>	<b>Present</b>	↓
Cl	27	1.162	1.96	Absent	
SO <sub>4</sub> <sup>2-</sup>	-29	-1.34	1.96	Absent	
NO <sub>3</sub> <sup>-</sup>	41	1.787	1.96	Absent	
NH <sub>4</sub> <sup>+</sup>	-35	-1.608	1.96	Absent	

Finally, the rate of change in the concentration of elements per time was determined with another non-parametric tool, namely, Sen's slope estimator, developed by Sen (1968b). This technique also allows missing values in the data set and it is insensitive to outliers. In this method, slope estimates of n pairs of data are first computed by Equation 4.10:

$$Q_i = \frac{x_j - x_k}{j - k} \quad \text{for } i = 1, \dots, n \quad (4.10)$$

Where  $x_j$  and  $x_k$  are the data values at times  $j$  and  $k$  ( $j > k$ ) respectively. Then median of these  $n$  values of  $Q_i$  is taken as Sen's slope estimator. Afterwards, median value of  $Q_i$  is tested by a two sided test at the  $100(1-\alpha)$  % confidence interval and true slope is obtained (Partal and Kahya, 2006). The calculated Sen's slope values were provided in Table 4.11.

Table 4.11 Calculated Sen's Slope Estimator values

	Mean % Change (per annum)	Slope Estimate (ng/m <sup>3</sup> /yr)	95 % Confidence Interval	
			Lower (ng/m <sup>3</sup> /yr)	Upper (ng/m <sup>3</sup> /yr)
Li	-5.0	-0.024	-0.049	0.004
<b><i>Be</i></b> <sup>‡</sup>	<b><i>-10.6</i></b>	<b><i>-0.002</i></b>	<b><i>-0.003</i></b>	<b><i>-0.001</i></b>
<b><i>Na</i></b>	<b><i>-10.7</i></b>	<b><i>-209</i></b>	<b><i>-289</i></b>	<b><i>-121</i></b>
<b><i>Mg</i></b>	<b><i>-9.4</i></b>	<b><i>-42.5</i></b>	<b><i>-65.6</i></b>	<b><i>-21.7</i></b>
<b><i>Al</i></b>	<b><i>-8.3</i></b>	<b><i>-40.5</i></b>	<b><i>-74.7</i></b>	<b><i>-13.0</i></b>
<b><i>K</i></b>	<b><i>-5.3</i></b>	<b><i>-15.4</i></b>	<b><i>-27.3</i></b>	<b><i>-8.2</i></b>
Ca	-2.6	-26	-96	30
Ti	-3.7	-0.936	-2.599	0.638
V	1.1	0.027	-0.081	0.119
Cr	2.3	0.084	-0.095	0.282
Mn	-5.3	-0.37	-0.704	0.05
Fe	-3.2	-8.4	-23.5	4.2
<b><i>Co</i></b>	<b><i>-4.1</i></b>	<b><i>-0.008</i></b>	<b><i>-0.021</i></b>	<b><i>0</i></b>
Ni	0.61	0.014	-0.1	0.167
Zn	-2.2	-0.273	-0.933	0.358
<b><i>Ge</i></b>	<b><i>-8.1</i></b>	<b><i>-0.003</i></b>	<b><i>-0.005</i></b>	<b><i>-0.001</i></b>
<b><i>As</i></b>	<b><i>-6.2</i></b>	<b><i>-0.042</i></b>	<b><i>-0.067</i></b>	<b><i>-0.012</i></b>
<b><i>Se</i></b>	<b><i>-5.6</i></b>	<b><i>-0.022</i></b>	<b><i>-0.044</i></b>	<b><i>-0.003</i></b>
Rb	-2.8	-0.019	-0.046	0.008
<b><i>Sr</i></b>	<b><i>-5.2</i></b>	<b><i>-0.182</i></b>	<b><i>-0.362</i></b>	<b><i>-0.015</i></b>
Y	-4.8	-0.007	-0.014	0.002
Cd	4.4	0.009	-0.001	0.019
Sn	-3.1	-0.018	-0.041	0.009
Sb	0.32	0.002	-0.029	0.027
<b><i>Cs</i></b>	<b><i>-8.2</i></b>	<b><i>-0.008</i></b>	<b><i>-0.012</i></b>	<b><i>-0.003</i></b>
Ba	-2.1	-0.176	-0.552	0.562
<b><i>La</i></b>	<b><i>-7.8</i></b>	<b><i>-0.025</i></b>	<b><i>-0.048</i></b>	<b><i>-0.005</i></b>
Hf	-4.4	-0.002	-0.004	0.002
W	-3.8	-0.003	-0.008	0.001
<b><i>Au</i></b>	<b><i>-10.8</i></b>	<b><i>-0.014</i></b>	<b><i>-0.026</i></b>	<b><i>-0.006</i></b>
<b><i>Pb</i></b>	<b><i>-16.5</i></b>	<b><i>-5.5</i></b>	<b><i>-8.5</i></b>	<b><i>-3.6</i></b>
Bi	-4.1	-0.004	-0.011	0.004
<b><i>Ce</i></b>	<b><i>-6.8</i></b>	<b><i>-0.043</i></b>	<b><i>-0.086</i></b>	<b><i>-0.007</i></b>
<b><i>Pr</i></b>	<b><i>-6.2</i></b>	<b><i>-0.005</i></b>	<b><i>-0.01</i></b>	<b><i>0</i></b>
<b><i>Nd</i></b>	<b><i>-6.7</i></b>	<b><i>-0.02</i></b>	<b><i>-0.041</i></b>	<b><i>-0.004</i></b>
<b><i>Sm</i></b>	<b><i>-6.1</i></b>	<b><i>-0.004</i></b>	<b><i>-0.01</i></b>	<b><i>0</i></b>

<sup>‡</sup> Statistically significant slope values at 5 % significance level were written in bold and italics

Table 4.11 Calculated Sen's Slope Estimator values (Continued)

	Mean % Change (per annum)	Slope Estimate (ng/m <sup>3</sup> /yr)	95 % Confidence Interval	
			Lower (ng/m <sup>3</sup> /yr)	Upper (ng/m <sup>3</sup> /yr)
<i>Eu</i>	<b>-7.4</b>	<b>-0.001</b>	<b>-0.003</b>	<b>0</b>
<i>Gd</i>	<b>-7.1</b>	<b>-0.005</b>	<b>-0.011</b>	<b>-0.001</b>
<i>Tb</i>	<b>-10.7</b>	<b>-0.001</b>	<b>-0.001</b>	<b>0</b>
<i>Dy</i>	<b>-6.0</b>	<b>-0.003</b>	<b>-0.006</b>	<b>-0.001</b>
<i>Ho</i>	<b>-9.9</b>	<b>-0.001</b>	<b>-0.001</b>	<b>0</b>
<i>Er</i>	<b>-6.7</b>	<b>-0.002</b>	<b>-0.004</b>	<b>0</b>
<i>Yb</i>	<b>-7.3</b>	<b>-0.002</b>	<b>-0.003</b>	<b>0</b>
<i>Th</i>	<b>-8.2</b>	<b>-0.012</b>	<b>-0.018</b>	<b>-0.001</b>
<i>U</i>	<b>-12.0</b>	<b>-0.007</b>	<b>-0.011</b>	<b>-0.003</b>
Cl	4.0	74	-31	159
SO <sub>4</sub> <sup>2-</sup>	-1.9	-130	-355	106
NO <sub>3</sub> <sup>-</sup>	4.4	62	-6.14	133
NH <sub>4</sub> <sup>+</sup>	-9.2	-75	-213	23

For In, Pt, Tm and Lu, the calculated Sen's slope estimator was less than 0.001 ng m<sup>-3</sup> per year and values corresponding to these parameters were not included in Table 4.11. It is worthwhile to note that all the elements having decreasing trend are released to the atmosphere from the earth crust with the exception of As, Se and Pb. The rate of change for the rare earth elements such as Ce, Pr, Nd, Sm, Eu, Gd, Dy, Tb, Ho, Er, Yb and Th are very low, ranging from -0.001 ng m<sup>-3</sup> per year to -0.043 ng m<sup>-3</sup> per year. The reason of this observation is not clear, but may indicate the decrease frequency of Saharan dust transport or changes occur in the climatology of the region due to global warming. However, these speculations are very serious and needs further detailed investigations.

Chemical tracers of Saharan dust and seasonal variation of Saharan dust transport frequencies will be discussed in "Saharan Dust Transport to Eastern Mediterranean Atmosphere" section of this manuscript. However, variation of number of Saharan dust episodes with time was discussed herein briefly. Figure 4.41 shows the number of Saharan dust episodes detected at our station between 1993 and 2001 in addition to median Al concentration, which is the most abundant element in earth crust and can be used as indicator for dust, corresponding to these episode days. With the exception of 1998, Al concentration detected in these episodes days declined. Number of Saharan



dust episodes recorded at our station had decreasing trend during sampling campaign except for 2000, when 24 Saharan dust episodes were detected.

Furthermore, Mann Kendall statistic “S” was calculated both for Saharan dust episode numbers and Al concentration associated with these episodes. Calculated “S” values were -1 and -16 for Saharan dust episode numbers and Al concentration, respectively. Negative “S” values calculated herein implied that measurements taken earlier tend to be greater than one measured later in the study period. Based on this information, one can conclude that both the intensity and number of Saharan dust episodes decreased during the study period. Recently, Foltz and McPhaden (2008) were able to show that precipitation in Sahel region of North Africa increased between 1980 and 2006. Researchers found very pronounced dustiness across western Africa and North Atlantic Oscillation within same period associated with this increased precipitation. Consequently, our finding related with Saharan dust episodes agree with one proposed by Foltz and McPhaden (2008).

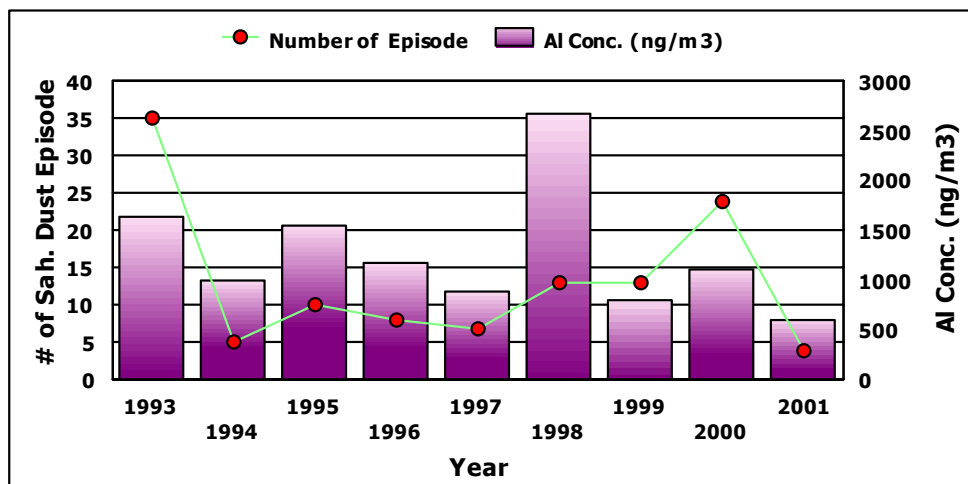


Figure 4.41 Variation of Saharan dust episode number and corresponding Al concentration with time

Gong and Barrie (2005) investigated the trends of heavy metal components in the Arctic aerosols between 1980 and 2000 and their relationship to the emissions in the Northern Hemisphere. They observed a slight decrease for soil components, especially, for Al, Fe

and Ti. They explained this pattern of the decreasing pattern of crustal elements by the declining trend of Asian dust emissions recorded in the same period by Zhang et al., 2003. Husain et al. (2004) evaluated the long term trends in atmospheric concentrations of sulfate, nitrate and trace elements at two different sites in the northeastern United States for about 20 years. The concentrations at both sites indicated remarkable decrease over time. Lead was one of the elements for which 14 and 10 % decrease per year observed. The interesting finding in this study was that crustal elements like Sc, Fe, Mn and K also showed decreases of 3-5 % per year.

There is no statistically significant long-term change was observed in the concentrations of  $\text{SO}_4^{2-}$  and  $\text{NO}_3^-$ , which are known to be the acidifying compounds though 66% increase in the concentrations of acidifying substances between 1990 and 2002 was reported for Turkey by European Environment Agency (EEA, 2005). The EU countries and accession countries have achieved 39 and 53 % emission reduction in acidifying compounds respectively between 1990 and 2000 (EEA, 2003b). In a recent study, significant negative trend of  $-6.6\%$  / yr was detected for  $\text{SO}_2$  from 1995 to 2005 at high alpine site Jungfrauoch (Coen et al., 2007). Işıkdemir (2006) performed least square linear model to find the time trend of ions and elements measured in the precipitation samples collected from the Eastern Mediterranean atmosphere between 1992 and 1999. Among the parameters investigated,  $\text{H}^+$ ,  $\text{NO}_3^-$ , Mg and Al show a decreasing trend in time, whereas,  $\text{NH}_4^+$ , Ca, K, Cd, Cr, Zn and Fe indicate an increasing trend. The decrease in  $\text{H}^+$  trend may be attributed to  $\text{SO}_2$  reductions observed following the Helsinki protocol on the reduction of Sulphur emissions was entered into force in 1987 in Europe.

Calculated Sen's slope estimator for Pb is  $-5.5\text{ ng m}^{-3}$  per year. It is very interesting to see decreasing trend for Pb in this study, because aerosol samples evaluated herein were collected till 2001. The use of leaded gasoline was banned in Turkey in 2002 after installation of catalytic converters while unleaded gasoline was introduced before 2002. The decreasing pattern observed in Pb concentrations is due to phasing out of Pb from gasoline in Europe, which occurred earlier. In the content of this law, the lead content in the gasoline was first reduced to 0.4 g Pb/L and then further decreased to 0.15 g Pb/L in 1976. It takes 10 years to introduce the unleaded gasoline in Europe (Bundesminister den Inneren, 1971 cited in Cercasov and Wulfmeyer, 2008). The current EU Directive 1999/30/CE for 2005 that fixed the Pb concentration as  $500\text{ ng m}^{-3}$  (Querol et al., 2008).

It was previously shown that Turkey is receiving pollutant loaded air masses originating from Europe. Consequently, the decrease in the Pb concentration in Europe is affecting the Pb content of the aerosol samples collected at our station. Cercasov and Wulfmeyer (2008) also showed strong decreasing trend in the Pb concentration with a mean trend of – 10.8 % per year in their study conducted in the city of Stuttgart, Germany. Gong and Barrie (2005) revealed that emissions reductions for Pb for EMEP (The Cooperative Programme for Monitoring and Evaluation of the Long-range Transmission of Air Pollutants in Europe) and Russian Federation were 70 and 35 %, respectively, between 1990 and 2001.

Pirrone et al. (1999) presented the past and current annual emissions of Pb, Ni, Cu, Cd and V to the atmosphere from major anthropogenic sources in the Mediterranean Sea region and provided the projected emissions till 2015. Emissions in this inventory were calculated on the basis of trace element emission factors (the amount of an element released per the quantity of raw material consumed and / or produced) and the amount of ore, coal consumed and production of industrial goods. Emissions of various elements between 1983 and 2015, provided by Pirrone et al. (1999), are shown in Figure 4.42. As it can be seen from Figure 4.42 that most significant drop was observed in the Pb emissions while Cr emissions remained almost same. Whilst both Ni and V emissions showed increasing trends, increase observed in V emission was significant; it was almost doubled from 1983 to 2015.

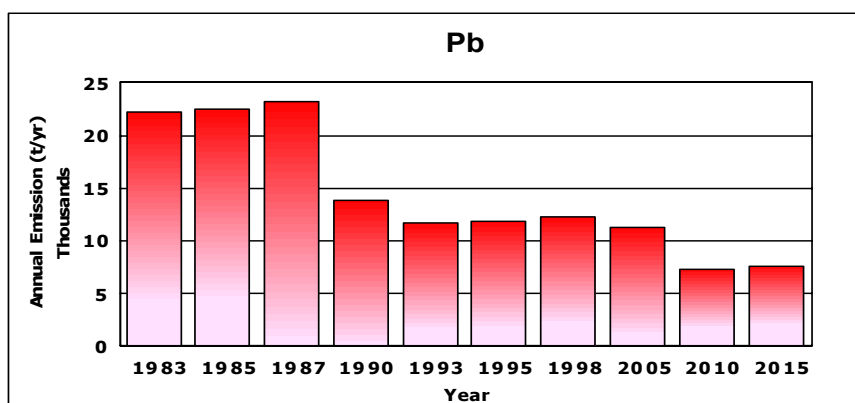


Figure 4.42 Past, current and projected annual emissions of trace elements in Mediterranean region (By the courtesy of Pirrone et al., 1999)

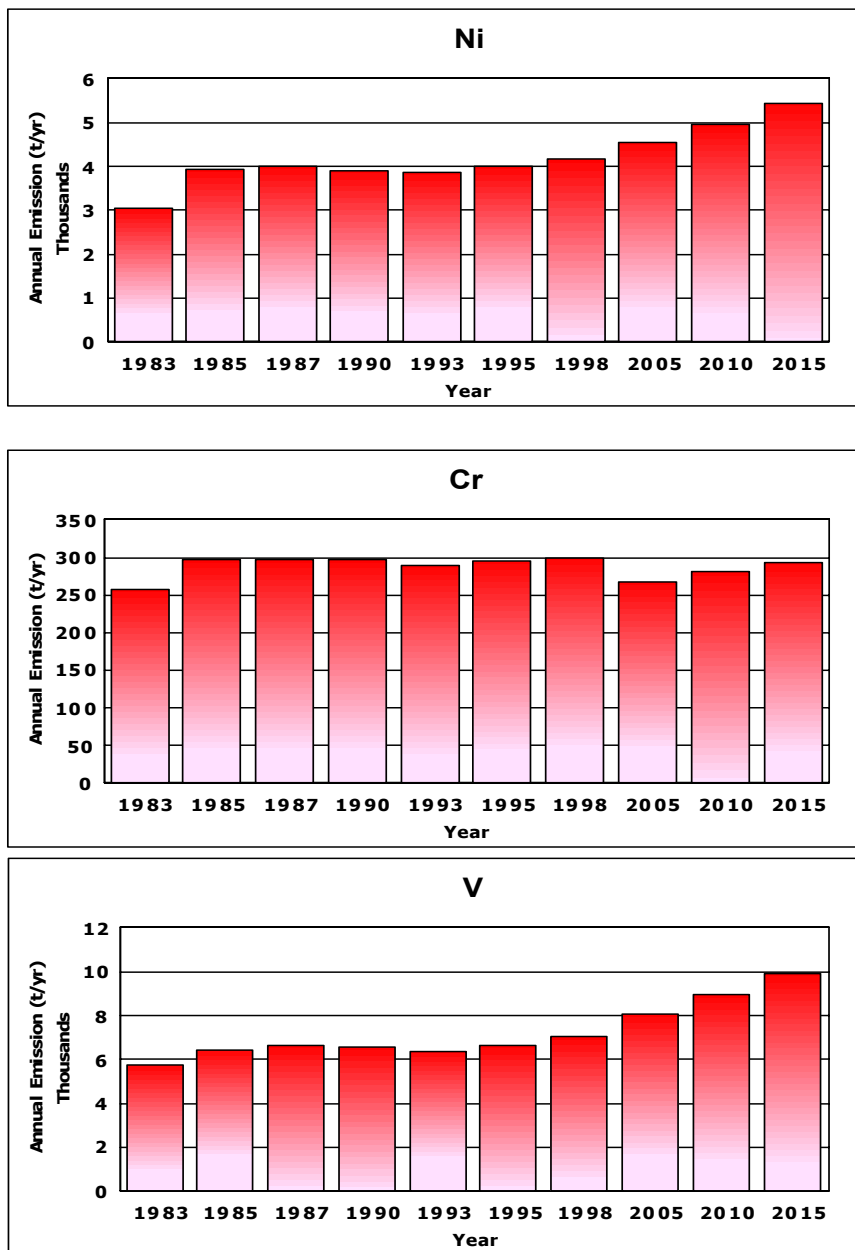


Figure 4.42 Past, current and projected annual emissions of trace elements in Mediterranean region (Continued)

Nonparametric Mann Kendall test was applied to the yearly data to find the statistical significance of trends in the concentrations of Pb and  $\text{SO}_4^{2-}$  and results are depicted in Figure 4.43. The dashed red line in the figure stands for the critical value of Z at 95 %

confidence interval. As it can be seen from Figure 4.43, there is an increasing trend in the concentration of  $\text{SO}_4^{2-}$  for 1995, 1999 and 2000 while a downward trend was detected for 1993. For the rest of the years in the study period,  $\text{SO}_4^{2-}$  concentration stayed stable, in other words, neither upward nor downward trend was found at 5 % significance level.

Lead concentrations increase within 1993 and 1995 while Mann Kendal test identified no statistically significant trend for the remaining years in the course of study period.

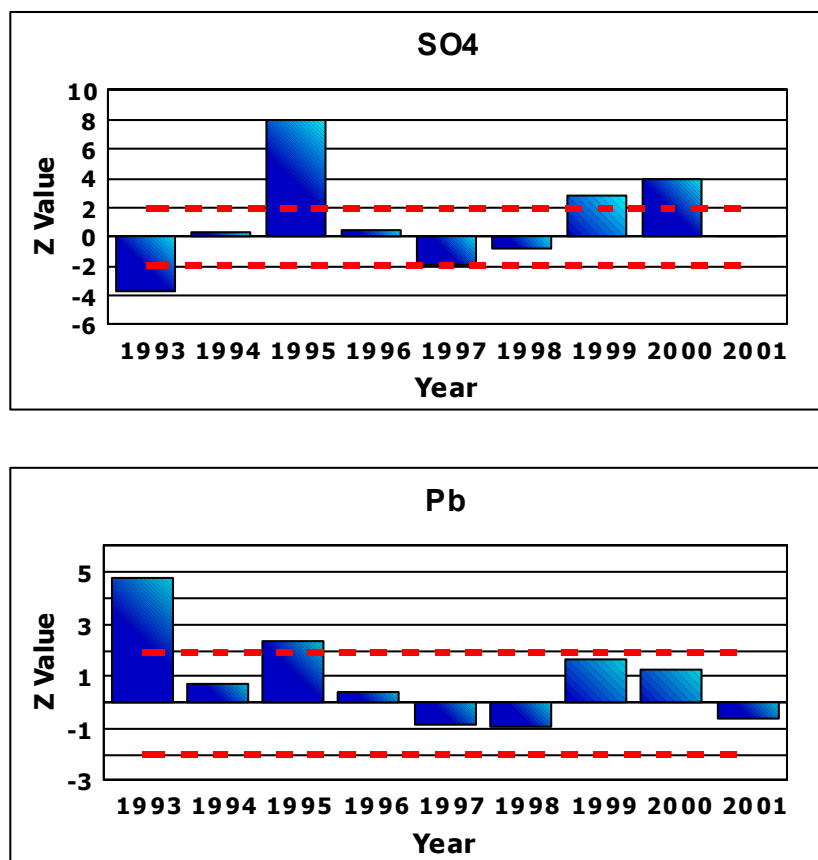


Figure 4.43 The outputs of Mann Kendall test for Pb and  $\text{NO}_3^-$

The input data were divided into two seasons as summer (from May to October) and winter (from November to April) to understand which season contribute to observed long term trends. The methodology described earlier in Figure 4.40 was again applied

separately to two data sets. The outputs corresponding to Van Belle and Hughes' Homogeneity test, seasonal Kendall test, and Sen's slope estimator values were provided for summer and winter seasons in Table 4.12-4.17.

All the parameters passed the homogeneity test, and a common trend was found for Be, Na, Mg, Al, K, Ca, Mn, Co, Cs, La, Pb, Ce, Pr, Nd, Sm, Gd, Tb, Dy, Eu, Ho, Er, Tm, Yb, Lu, U, Th, Cl and  $\text{NO}_3^-$  for summer season as depicted in Table 4.12. With the exception of Cl and  $\text{NO}_3^-$ , decreasing trend was found for all of the parameters for which common trend was found by the homogeneity test. No trend was detected for  $\text{SO}_4^{2-}$  and  $\text{NH}_4^+$ . For the sea salt markers, the decreasing trend was found for Na with a slope of  $64 \text{ ng} / \text{m}^3/\text{yr}$  while increasing trend was observed in case of Cl with a slope of  $126 \text{ ng} / \text{m}^3/\text{yr}$ .

It is worthwhile to divide the crustal elements into two with respect to their rate of decrease, which was presented in Table 4.14. For rare earth elements such as Sm, Gd, Tb, Dy, Eu, Ho, Er, Tm, Yb, Lu and Th the rate of decrease, which is in fact Sen' slope estimator value, is ranging from 0.01 to  $0.001 \text{ ng} / \text{m}^3/\text{yr}$ . For the second group of elements the rate of decrease is considerably higher than that of the rare elements. Magnesium, Al, K and Ca are considered in the second group. The rate of decrease for these elements is ranging from 25 to  $105 \text{ ng} / \text{m}^3/\text{yr}$  and Ca is the one showing the strongest decrease between 1993 and 2001. The difference in the rate of decrease in two groups can be attributed to the presence of two different sources of crustal material over the Eastern Mediterranean region. Presence of two crustal components in Eastern Mediterranean aerosol will be discussed in more detail in the source apportionment section of the manuscript. For Li and Pt, the calculated Sen's slope values were smaller than  $0.001 \text{ ng} \text{ m}^{-3}$  per year and these values were not included in Table 4.14.

Table 4.12 Van Belle and Hughes' Homogeneity Test results for summer season

<b>Van Belle and Hughes Homogeneity Test</b>					
	$\chi^2_{\text{homogen}}$	$\chi^2_{\text{critical}}$	$\chi^2_{\text{trend}}$	$\chi^2_{\text{critical}}$	$\chi^2_{\text{total}}$
		<b><math>\alpha=0.05</math></b>		<b><math>\alpha=0.05</math></b>	
		<b>df=5</b>		<b>df=1</b>	
<b>Li</b>					
<b>Be</b>	0.535	11.07	9.221	3.84	9.756
<b>Na</b>	3.251	11.07	11.887	3.84	15.138
<b>Mg</b>	0.62	11.07	13.614	3.84	14.234
<b>Al</b>	2.441	11.07	6.845	3.84	9.286
<b>K</b>	3.483	11.07	5.622	3.84	9.106
<b>Ca</b>	3.365	11.07	4.226	3.84	7.591
<b>Ti</b>	1.856	11.07	1.952	3.84	3.808
<b>V</b>	6.456	11.07	0.01	3.84	6.466
<b>Cr</b>	4.024	11.07	0.919	3.84	4.943
<b>Mn</b>	5.21	11.07	4.137	3.84	9.347
<b>Fe</b>	1.833	11.07	2.698	3.84	4.53
<b>Co</b>	0.904	11.07	8.492	3.84	9.395
<b>Zn</b>	7.262	11.07	1.637	3.84	8.9
<b>Ge</b>	3.552	11.07	3.47	3.84	7.022
<b>As</b>	5.896	11.07	3.323	3.84	9.219
<b>Se</b>	3.701	11.07	2.608	3.84	6.309
<b>Ni</b>	2.395	11.07	2.282	3.84	4.677
<b>Sr</b>	2.372	11.07	2.657	3.84	5.029
<b>Y</b>	2.108	11.07	3.402	3.84	5.51
<b>Cd</b>	2.375	11.07	1.343	3.84	3.718
<b>In</b>	1.823	11.07	0.454	3.84	2.277
<b>Sn</b>	2.22	11.07	1.647	3.84	3.867
<b>Cs</b>	2.436	11.07	12.266	3.84	14.701
<b>Sb</b>	3.234	11.07	0.113	3.84	3.347
<b>Rb</b>	5.413	11.07	2.996	3.84	8.409
<b>Ba</b>	1.944	11.07	1.516	3.84	3.46
<b>La</b>	1.406	11.07	8.366	3.84	9.772
<b>W</b>	1.274	11.07	3.256	3.84	4.53
<b>Pt</b>	2.811	11.07	0.265	3.84	3.076
<b>Au</b>	5.753	11.07	0.852	3.84	6.605
<b>Pb</b>	2.171	11.07	16.538	3.84	18.709
<b>Bi</b>	3.415	11.07	0.081	3.84	3.496
<b>Ce</b>	1.919	11.07	7.122	3.84	9.041
<b>Pr</b>	2.526	11.07	5.597	3.84	8.123
<b>Nd</b>	1.065	11.07	7.238	3.84	8.303
<b>Sm</b>	0.802	11.07	6.705	3.84	7.507
<b>Hf</b>	2.717	11.07	3.356	3.84	6.073
<b>Gd</b>	0.694	11.07	7.355	3.84	8.048
<b>Tb</b>	0.802	11.07	6.705	3.84	7.507

Table 4.12 Van Belle and Hughes' Homogeneity Test results for summer season  
(Continued)

<b>Van Belle and Hughes Homogeneity Test</b>					
	$\chi^2_{\text{homogen}}$	$\chi^2_{\text{critical}}$	$\chi^2_{\text{trend}}$	$\chi^2_{\text{critical}}$	$\chi^2_{\text{total}}$
		<b><math>\alpha=0.05</math></b>		<b><math>\alpha=0.05</math></b>	
		<b>df=5</b>		<b>df=1</b>	
<b>Dy</b>	0.622	11.07	6.705	3.84	7.327
<b>Eu</b>	1.14	11.07	6.346	3.84	7.486
<b>Ho</b>	0.802	11.07	6.705	3.84	7.507
<b>Er</b>	0.82	11.07	7.238	3.84	8.058
<b>Tm</b>	0.743	11.07	6.593	3.84	7.336
<b>Yb</b>	0.802	11.07	6.705	3.84	7.507
<b>Lu</b>	0.82	11.07	7.238	3.84	8.058
<b>Th</b>	2.981	11.07	5.873	3.84	8.854
<b>U</b>	1.119	11.07	11.179	3.84	12.297
<b>Cl</b>	1.196	11.07	6.192	3.84	7.388
<b>SO<sub>4</sub><sup>2-</sup></b>	1.43	11.07	0.161	3.84	1.59
<b>NO<sub>3</sub><sup>-</sup></b>	0.992	11.07	4.682	3.84	5.674
<b>NH<sub>4</sub><sup>+</sup></b>	1.541	11.07	0.014	3.84	1.556



Table 4.13 Seasonal Kendall Test results for summer season

	<b>Mann Kendall Statistic S</b>	<b>Z</b>	<b>Zcritical <math>\alpha=0.05</math></b>	<b>Trend</b>	<b>Trend Direction</b>
Li	0	0	1.96	Absent	
<b>Be</b>	<b>-52</b>	<b>-3.102</b>	<b>1.96</b>	<b>Present</b>	↓
<b>Na</b>	<b>-58</b>	<b>-3.453</b>	<b>1.96</b>	<b>Present</b>	↓
<b>Mg</b>	<b>-62</b>	<b>-3.687</b>	<b>1.96</b>	<b>Present</b>	↓
<b>Al</b>	<b>-46</b>	<b>-2.75</b>	<b>1.96</b>	<b>Present</b>	↓
<b>K</b>	<b>-42</b>	<b>-2.516</b>	<b>1.96</b>	<b>Present</b>	↓
<b>Ca</b>	<b>-36</b>	<b>-2.165</b>	<b>1.96</b>	<b>Present</b>	↓
Ti	-24	-1.463	1.96	Absent	
V	2	0.059	1.96	Absent	
Cr	-18	-1.112	1.96	Absent	
<b>Mn</b>	<b>-36</b>	<b>-2.165</b>	<b>1.96</b>	<b>Present</b>	↓
Fe	-28	-1.697	1.96	Absent	
<b>Co</b>	<b>-50</b>	<b>-2.985</b>	<b>1.96</b>	<b>Present</b>	↓
Zn	-26	-1.58	1.96	Absent	
Ge	-32	-1.931	1.96	Absent	
As	-32	-1.931	1.96	Absent	
Se	-28	-1.697	1.96	Absent	
Ni	-26	-1.58	1.96	Absent	
Sr	-28	-1.697	1.96	Absent	
Y	-32	-1.931	1.96	Absent	
Cd	18	0.995	1.96	Absent	
In	-12	-0.761	1.96	Absent	
Sn	-24	-1.463	1.96	Absent	
Cs	-60	-3.57	1.96	Absent	
Sb	-8	-0.527	1.96	Absent	
Rb	-30	-1.814	1.96	Absent	
Ba	-22	-1.346	1.96	Absent	
<b>La</b>	<b>-50</b>	<b>-2.985</b>	<b>1.96</b>	<b>Present</b>	↓
W	-32	-1.931	1.96	Absent	
Pt	-8	-0.527	1.96	Absent	
Au	-14	-0.878	1.96	Absent	
<b>Pb</b>	<b>-68</b>	<b>-4.038</b>	<b>1.96</b>	<b>Present</b>	↓
Bi	-8	-0.527	1.96	Absent	
<b>Ce</b>	<b>-46</b>	<b>-2.75</b>	<b>1.96</b>	<b>Present</b>	↓
<b>Pr</b>	<b>-40</b>	<b>-2.399</b>	<b>1.96</b>	<b>Present</b>	↓
<b>Nd</b>	<b>-46</b>	<b>-2.75</b>	<b>1.96</b>	<b>Present</b>	↓
<b>Sm</b>	<b>-44</b>	<b>-2.633</b>	<b>1.96</b>	<b>Present</b>	↓

Table 4.13 Seasonal Kendall Test results for summer season (Continued)

	<b>Mann Kendall Statistic S</b>	<b>Z</b>	<b>Zcritical <math>\alpha=0.05</math></b>	<b>Trend</b>	<b>Trend Direction</b>
Hf	-32	-1.931	1.96	Absent	
<b>Gd</b>	<b>-46</b>	<b>-2.75</b>	<b>1.96</b>	<b>Present</b>	↓
<b>Tb</b>	<b>-44</b>	<b>-2.633</b>	<b>1.96</b>	<b>Present</b>	↓
<b>Dy</b>	<b>-44</b>	<b>-2.633</b>	<b>1.96</b>	<b>Present</b>	↓
<b>Eu</b>	<b>-42</b>	<b>-2.516</b>	<b>1.96</b>	<b>Present</b>	↓
<b>Ho</b>	<b>-44</b>	<b>-2.633</b>	<b>1.96</b>	<b>Present</b>	↓
<b>Er</b>	<b>-46</b>	<b>-2.75</b>	<b>1.96</b>	<b>Present</b>	↓
<b>Tm</b>	<b>-44</b>	<b>-2.633</b>	<b>1.96</b>	<b>Present</b>	↓
<b>Yb</b>	<b>-44</b>	<b>-2.633</b>	<b>1.96</b>	<b>Present</b>	↓
<b>Lu</b>	<b>-46</b>	<b>-2.75</b>	<b>1.96</b>	<b>Present</b>	↓
<b>Th</b>	<b>-42</b>	<b>-2.516</b>	<b>1.96</b>	<b>Present</b>	↓
<b>U</b>	<b>-56</b>	<b>-3.336</b>	<b>1.96</b>	<b>Present</b>	↓
<b>Cl</b>	<b>42</b>	<b>2.399</b>	<b>1.96</b>	<b>Present</b>	↑
SO <sub>4</sub> <sup>2-</sup>	-8	-0.527	1.96	Absent	
<b>NO<sub>3</sub><sup>-</sup></b>	<b>36</b>	<b>2.048</b>	<b>1.96</b>	<b>Present</b>	↑
NH <sub>4</sub> <sup>+</sup>	0	0	1.96	Absent	

Table 4.14 Sen's slope estimator values for summer season

	Mean % Change (per annum)	Slope Estimate (ng/m <sup>3</sup> /yr)	95 % Confidence Interval	
			Lower (ng/m <sup>3</sup> /yr)	Upper (ng/m <sup>3</sup> /yr)
Li	0	0	0	0
<b><i>Be</i></b> <sup>§</sup>	<b><i>-12.5</i></b>	<b><i>-0.003</i></b>	<b><i>-0.005</i></b>	<b><i>-0.001</i></b>
<b><i>Na</i></b>	<b><i>-9.3</i></b>	<b><i>-164</i></b>	<b><i>-274</i></b>	<b><i>-95</i></b>
<b><i>Mg</i></b>	<b><i>-12.0</i></b>	<b><i>-56</i></b>	<b><i>-78</i></b>	<b><i>-20</i></b>
<b><i>Al</i></b>	<b><i>-11.5</i></b>	<b><i>-81</i></b>	<b><i>-147</i></b>	<b><i>-20</i></b>
<b><i>K</i></b>	<b><i>-6.8</i></b>	<b><i>-25</i></b>	<b><i>-47</i></b>	<b><i>-7</i></b>
<b><i>Ca</i></b>	<b><i>-9.2</i></b>	<b><i>-105</i></b>	<b><i>-187</i></b>	<b><i>-7.6</i></b>
Ti	-7.8	-2.65	-5.74	1.01
V	0.80	0.028	-0.225	0.27
Cr	-3.9	-0.152	-0.383	0.081
<b><i>Mn</i></b>	<b><i>-6.2</i></b>	<b><i>-0.601</i></b>	<b><i>-1.289</i></b>	<b><i>-0.056</i></b>
Fe	-6.1	-22	-57	7.63
<b><i>Co</i></b>	<b><i>-9.4</i></b>	<b><i>-0.023</i></b>	<b><i>-0.042</i></b>	<b><i>-0.006</i></b>
Zn	-5.4	-0.768	-1.865	0.271
Ge	-7.4	-0.003	-0.006	0
As	-4.3	-0.03	-0.071	0.001
Se	-5.4	-0.022	-0.05	0.005
Ni	-3.6	-0.097	-0.228	0.049
Sr	-6.8	-0.272	-0.609	0.028
Y	-6.7	-0.014	-0.031	0.002
Cd	2.2	0.005	-0.013	0.02
In	0	0	-0.001	0
Sn	-4.6	-0.032	-0.073	0.013
Cs	-8.1	-0.011	-0.019	-0.006
Sb	-1.0	-0.007	-0.042	0.039
Rb	-4.1	-0.039	-0.105	0.007
Ba	-4.5	-0.478	-1.243	0.517
<b><i>La</i></b>	<b><i>-11.3</i></b>	<b><i>-0.05</i></b>	<b><i>-0.091</i></b>	<b><i>-0.015</i></b>
W	-7.5	-0.007	-0.014	0.001
Pt	0	0	0	0
Au	-4.0	-0.006	-0.021	0.004
<b><i>Pb</i></b>	<b><i>-17.0</i></b>	<b><i>-7.01</i></b>	<b><i>-11.58</i></b>	<b><i>-3.84</i></b>

<sup>§</sup> Statistically significant slope values at 5 % significance level were written in bold and italics

Table 4.14 Sen's slope estimator values for summer season (Continued)

	Mean % Change (per annum)	Slope Estimate (ng/m <sup>3</sup> /yr)	95 % Confidence Interval	
			Lower (ng/m <sup>3</sup> /yr)	Upper (ng/m <sup>3</sup> /yr)
Bi	-3.6	-0.004	-0.014	0.009
<b>Ce</b>	<b>-11.3</b>	<b>-0.098</b>	<b>-0.163</b>	<b>-0.021</b>
<b>Pr</b>	<b>-8.7</b>	<b>-0.01</b>	<b>-0.022</b>	<b>-0.001</b>
<b>Nd</b>	<b>-10.3</b>	<b>-0.043</b>	<b>-0.091</b>	<b>-0.013</b>
<b>Sm</b>	<b>-11.2</b>	<b>-0.01</b>	<b>-0.019</b>	<b>-0.001</b>
Hf	-9.0	-0.005	-0.009	0
<b>Gd</b>	<b>-12.5</b>	<b>-0.012</b>	<b>-0.022</b>	<b>-0.004</b>
<b>Tb</b>	<b>-7.9</b>	<b>-0.001</b>	<b>-0.003</b>	<b>0</b>
<b>Dy</b>	<b>-12.4</b>	<b>-0.008</b>	<b>-0.017</b>	<b>-0.002</b>
<b>Eu</b>	<b>-13.3</b>	<b>-0.002</b>	<b>-0.004</b>	<b>0</b>
<b>Ho</b>	<b>-14.6</b>	<b>-0.002</b>	<b>-0.003</b>	<b>0</b>
<b>Er</b>	<b>-12.3</b>	<b>-0.005</b>	<b>-0.009</b>	<b>-0.001</b>
<b>Tm</b>	<b>-17.8</b>	<b>-0.001</b>	<b>-0.001</b>	<b>0</b>
<b>Yb</b>	<b>-10.8</b>	<b>-0.004</b>	<b>-0.008</b>	<b>-0.001</b>
<b>Lu</b>	<b>-17.9</b>	<b>-0.001</b>	<b>-0.001</b>	<b>0</b>
<b>Th</b>	<b>-7.7</b>	<b>-0.016</b>	<b>-0.043</b>	<b>-0.005</b>
<b>U</b>	<b>-16.3</b>	<b>-0.012</b>	<b>-0.017</b>	<b>-0.003</b>
<b>Cl</b>	<b>8.4</b>	<b>126</b>	<b>5</b>	<b>210</b>
SO <sub>4</sub> <sup>2-</sup>	-1.1	-98	-491	457
<b>NO<sub>3</sub><sup>-</sup></b>	<b>8.0</b>	<b>98</b>	<b>7.5</b>	<b>260</b>
NH <sub>4</sub> <sup>+</sup>	-0.32	-2.01	-182	301

With the exception of Dy, all of the measured parameters passed from the homogeneity test for winter season. The common trend was detected for Be, Na, Mg, K, K, Cr, As, Cd, Au, Pb, NO<sub>3</sub><sup>-</sup> and NH<sub>4</sub><sup>+</sup>. Seasonal Kendall test identified decreasing trend for Be, Na, K, As, Au, Pb and NH<sub>4</sub><sup>+</sup> while NO<sub>3</sub><sup>-</sup> and Cr had upward trend. Though common trend was found for Mg and Cd, neither increasing nor decreasing trend was identified for Mg and Cd. The highest rate of increase was observed for NO<sub>3</sub><sup>-</sup> with a slope of 263 ng m<sup>-3</sup>/ yr whilst the strongest drop was recorded for Na with a value of 244 ng m<sup>-3</sup>/yr as provided in Table 4.15. For Li, Pt, Tm and Lu, the calculated Sen's slope values were smaller than 0.001 ng m<sup>-3</sup> per year and these values were not depicted in Table 4.15.

Table 4.15 Van Belle and Hughes' Homogeneity Test results for winter season

<b>Van Belle and Hughes Homogeneity Test</b>					
	$\chi^2_{\text{homogen}}$	$\chi^2_{\text{critical}}$ <b><math>\alpha=0.05</math></b> <b>df=5</b>	$\chi^2_{\text{trend}}$	$\chi^2_{\text{critical}}$ <b><math>\alpha=0.05</math></b> <b>df=1</b>	$\chi^2_{\text{total}}$
Li		11.07		3.84	
<b>Be</b>	<b>1.69</b>	<b>11.07</b>	<b>4.86</b>	<b>3.84</b>	<b>6.55</b>
<b>Na</b>	<b>3.307</b>	<b>11.07</b>	<b>6.288</b>	<b>3.84</b>	<b>9.595</b>
<b>Mg</b>	<b>5.211</b>	<b>11.07</b>	<b>4.06</b>	<b>3.84</b>	<b>9.271</b>
Al	10.139	11.07	0.722	3.84	10.861
<b>K</b>	<b>4.573</b>	<b>11.07</b>	<b>5.906</b>	<b>3.84</b>	<b>10.479</b>
Ca	3.717	11.07	2.236	3.84	5.954
Ti	7.122	11.07	0.178	3.84	7.301
V	9.263	11.07	0.659	3.84	9.922
<b>Cr</b>	<b>0.923</b>	<b>11.07</b>	<b>10.064</b>	<b>3.84</b>	<b>10.988</b>
Mn	7.592	11.07	0.046	3.84	7.638
Fe	5.34	11.07	0.025	3.84	5.365
Co	5.025	11.07	0.312	3.84	5.337
Zn	6.111	11.07	0.451	3.84	6.562
Ge	2.282	11.07	1.932	3.84	4.214
<b>As</b>	<b>3.284</b>	<b>11.07</b>	<b>5.159</b>	<b>3.84</b>	<b>8.443</b>
Ni	7.528	11.07	2.508	3.84	10.036
Se	5.82	11.07	2.034	3.84	7.854
Rb	8.708	11.07	0.048	3.84	8.756
Sr	7.378	11.07	0.651	3.84	8.029
Y	4.604	11.07	0.055	3.84	4.658
<b>Cd</b>	<b>6.283</b>	<b>11.07</b>	<b>5.236</b>	<b>3.84</b>	<b>11.52</b>
In	5.682	11.07	0.149	3.84	5.831
Sn	1.704	11.07	0.164	3.84	1.868
Sb	3.06	11.07	0.489	3.84	3.549
Cs	5.753	11.07	0.098	3.84	5.851
Ba	5.892	11.07	2.639	3.84	8.531
La	8.532	11.07	0.001	3.84	8.533
Hf	6.276	11.07	1.024	3.84	7.301
W	1.665	11.07	0.007	3.84	1.672
Pt	1.017	11.07	1.431	3.84	2.448
<b>Au</b>	<b>0.953</b>	<b>11.07</b>	<b>8.847</b>	<b>3.84</b>	<b>9.8</b>
<b>Pb</b>	<b>3.944</b>	<b>11.07</b>	<b>7.147</b>	<b>3.84</b>	<b>11.091</b>
Bi	2.806	11.07	0.959	3.84	3.765
Ce	8.087	11.07	0.017	3.84	8.104
Pr	8.04	11.07	0.064	3.84	8.104
Nd	8.04	11.07	0.064	3.84	8.104
Sm	7.244	11.07	0.309	3.84	7.553
Eu	3.244	11.07	0.665	3.84	3.909

Table 4.15 Van Belle and Hughes' Homogeneity Test results for winter season  
(Continued)

<b>Van Belle and Hughes Homogeneity Test</b>					
	$\chi^2_{\text{homogen}}$	$\chi^2_{\text{critical}}$ <b><math>\alpha=0.05</math></b> <b><math>df=5</math></b>	$\chi^2_{\text{trend}}$	$\chi^2_{\text{critical}}$ <b><math>\alpha=0.05</math></b> <b><math>df=1</math></b>	$\chi^2_{\text{total}}$
Tb	8.148	11.07	0.008	3.84	8.156
Dy**	11.366	11.07	0.016	3.84	11.382
Ho	9	11.07	0.013	3.84	9.013
Er	8.829	11.07	0	3.84	8.829
Tm	7.092	11.07	0.084	3.84	7.176
Yb	8.829	11.07	0	3.84	8.829
Lu	8.829	11.07	0	3.84	8.829
Th	8.777	11.07	0.001	3.84	8.778
U	5.367	11.07	2.473	3.84	7.839
Gd	9.272	11.07	0.047	3.84	9.319
Cl	6.288	11.07	1.022	3.84	7.31
SO <sub>4</sub> <sup>2-</sup>	6.607	11.07	1.723	3.84	8.33
<b>NO<sub>3</sub><sup>-</sup></b>	<b>1.287</b>	<b>11.07</b>	<b>16.98</b>	<b>3.84</b>	<b>18.267</b>
<b>NH<sub>4</sub><sup>+</sup></b>	<b>1.51</b>	<b>11.07</b>	<b>5.981</b>	<b>3.84</b>	<b>7.491</b>

\*\* The null hypothesis of homogenous trend direction and magnitude was rejected for this element

Table 4.16 Seasonal Kendall test results for winter season

	<b>Mann Kendall Statistic S</b>	<b>Z</b>	<b>Z<sub>critical</sub> α=0.05</b>	<b>Trend</b>	<b>Trend Direction</b>
Li					
<b>Be</b>	<b>-31</b>	<b>-2.213</b>	<b>1.96</b>	<b>Present</b>	↓
<b>Na</b>	<b>-37</b>	<b>-2.629</b>	<b>1.96</b>	<b>Present</b>	↓
Mg	-27	-1.937	1.96	Absent	
Al	-19	-1.383	1.96	Absent	
<b>K</b>	<b>-37</b>	<b>-2.629</b>	<b>1.96</b>	<b>Present</b>	↓
Ca	15	0.968	1.96	Absent	
Ti	-9	-0.692	1.96	Absent	
V	3	0.138	1.96	Absent	
<b>Cr</b>	<b>43</b>	<b>2.905</b>	<b>1.96</b>	<b>Present</b>	↑
Mn	-1	-0.138	1.96	Absent	
Fe	-1	-0.138	1.96	Absent	
Co	3	0.138	1.96	Absent	
Zn	5	0.277	1.96	Absent	
Ge	-21	-1.522	1.96	Absent	
<b>As</b>	<b>-33</b>	<b>-2.352</b>	<b>1.96</b>	<b>Present</b>	↓
Ni	29	1.937	1.96	Absent	
Se	-23	-1.66	1.96	Absent	
Rb	-3	-0.277	1.96	Absent	
Sr	-19	-1.383	1.96	Absent	
Y	-3	-0.277	1.96	Absent	
Cd	25	1.66	1.96	Absent	
In	7	0.415	1.96	Absent	
Sn	-5	-0.415	1.96	Absent	
Sb	11	0.692	1.96	Absent	
Cs	-11	-0.83	1.96	Absent	
Ba	11	0.692	1.96	Absent	
La	-9	-0.692	1.96	Absent	
Hf	5	0.277	1.96	Absent	
W	-3	-0.277	1.96	Absent	
Pt	-13	-0.987	1.96	Absent	
<b>Au</b>	<b>-43</b>	<b>-3.104</b>	<b>1.96</b>	<b>Present</b>	↓
<b>Pb</b>	<b>-39</b>	<b>-2.767</b>	<b>1.96</b>	<b>Present</b>	↓
Bi	-19	-1.383	1.96	Absent	
Ce	-7	-0.553	1.96	Absent	
Pr	-5	-0.415	1.96	Absent	
Nd	-5	-0.415	1.96	Absent	
Sm	1	0	1.96	Absent	

Table 4.16 Seasonal Kendall test results for winter season (Continued)

	<b>Mann Kendall Statistic S</b>	<b>Z</b>	<b>Z<sub>critical</sub> α=0.05</b>	<b>Trend</b>	<b>Trend Direction</b>
Eu	-19	-1.411	1.96	Absent	
Tb	-7	-0.553	1.96	Absent	
Dy	-11	-0.83	1.96	Absent	
Ho	-11	-0.83	1.96	Absent	
Er	-9	-0.692	1.96	Absent	
Tm	-3	-0.277	1.96	Absent	
Yb	-9	-0.692	1.96	Absent	
Lu	-9	-0.692	1.96	Absent	
Th	-9	-0.692	1.96	Absent	
U	-27	-1.937	1.96	Absent	
Gd	-13	-0.968	1.96	Absent	
Cl	-13	-0.968	1.96	Absent	
SO <sub>4</sub> <sup>2-</sup>	-21	-1.522	1.96	Absent	
<b>NO<sub>3</sub><sup>-</sup></b>	<b>57</b>	<b>3.874</b>	<b>1.96</b>	<b>Present</b>	↑
<b>NH<sub>4</sub><sup>+</sup></b>	<b>-31</b>	<b>-2.213</b>	<b>1.96</b>	<b>Present</b>	↓



Table 4.17 Sen's slope estimator values for winter season

	Mean % Change (per annum)	Slope Estimate (ng/m <sup>3</sup> /yr)	95 % Confidence Interval	
			Lower (ng/m <sup>3</sup> /yr)	Upper (ng/m <sup>3</sup> /yr)
<i>Be<sup>++</sup></i>	<i>-6.7</i>	<i>-0.001</i>	<i>-0.003</i>	
<i>Na</i>	<i>-12.1</i>	<i>-244</i>	<i>-5925</i>	<i>-51</i>
Mg	-7.7	-34	-75	1.18
Al	-5.6	-18	-51	15
<i>K</i>	<i>-5.8</i>	<i>-13</i>	<i>-22</i>	<i>-2.21</i>
Ca	3.4	28	-26	78
Ti	-2.7	-0.453	-1.255	1.62
V	1.6	0.027	-0.046	0.114
<i>Cr</i>	<i>15.6</i>	<i>0.427</i>	<i>0.167</i>	<i>0.776</i>
Mn	-0.6	-0.028	-0.505	0.397
Fe	-1.2	-2.017	-10.808	12.186
Co	3.0	0.004	-0.011	0.022
Zn	0.5	0.044	-0.495	1.035
Ge	-8.7	-0.003	-0.006	0.001
<i>As</i>	<i>-7.5</i>	<i>-0.051</i>	<i>-0.089</i>	<i>-0.008</i>
Ni	10.6	0.171	-0.006	0.299
Se	-7.0	-0.023	-0.054	0.008
Rb	-1.1	-0.005	-0.033	0.032
Sr	-4.6	-0.138	-0.301	0.097
Y	-3.1	-0.003	-0.009	0.005
Cd	7.1	0.012	-0.003	0.031
In	0.0	0	-0.001	0.001
Sn	-2.4	-0.011	-0.035	0.03
Sb	1.8	0.01	-0.035	0.051
Cs	-4.4	-0.003	-0.009	0.006
Ba	3.7	0.229	-0.338	1.299
La	-3.7	-0.008	-0.029	0.019
Hf	3.1	0.001	-0.003	0.005
W	0.0	0	-0.005	0.008
<i>Au</i>	<i>-16.8</i>	<i>-0.02</i>	<i>-0.036</i>	<i>-0.008</i>
<i>Pb</i>	<i>-15.2</i>	<i>-4.53</i>	<i>-7.79</i>	<i>-0.68</i>
Bi	-4.4	-0.004	-0.013	0.006
Ce	-3.7	-0.016	-0.046	0.034

†† Statistically significant slope values at 5 % significance level were written in bold and italics

Table 4.17 Sen's slope estimator values for winter season (Continued)

	Mean % Change (per annum)	Slope Estimate (ng/m <sup>3</sup> /yr)	95 % Confidence Interval	
			Lower (ng/m <sup>3</sup> /yr)	Upper (ng/m <sup>3</sup> /yr)
Pr	-3.8	-0.002	-0.005	0.004
Nd	-4.5	-0.009	-0.02	0.015
Sm	0.0	0	-0.005	0.005
Eu	-8.6	-0.001	-0.002	
Tb	0.0	0	-0.001	0.001
Dy	-2.9	-0.001	-0.003	0.003
Ho	0.0	0	-0.001	0.001
Er	-5.0	-0.001	-0.002	0.003
Yb	0.0	0	-0.002	0.003
Th	-4.3	-0.004	-0.011	0.011
U	-8.8	-0.004	-0.009	0.002
Gd	-2.1	-0.001	-0.006	0.006
Cl	-4.8	-106	-322	170
SO <sub>4</sub> <sup>2-</sup>	-3.3	-179	-391	101
<b>NO<sub>3</sub><sup>-</sup></b>	<b>35.2</b>	<b>263</b>	<b>111</b>	<b>364</b>
<b>NH<sub>4</sub><sup>+</sup></b>	<b>-45.2</b>	<b>-158</b>	<b>-233</b>	<b>-9.61</b>

#### **4.5. INVESTIGATION OF TYPES AND LOCATIONS OF POLLUTANT SOURCES AFFECTING EASTERN MEDITERRANEAN ATMOSPHERE USING DIFFERENT METHODOLOGIES**

Influence of Eastern Mediterranean atmosphere by pollutants exported from Europe and North Africa is shown in previous studies. Occasionally unexpected poor air quality in Western and Northwestern part of Turkey was attributed to long range transport of pollutants from European countries (Kindap et al., 2006). Güllü et al. (2005) highlighted the source regions of pollutants determined at Turkish Mediterranean coast. Researchers indicated the various countries including Ukraine, Russia, Georgia, Poland, Bellarus, France, Spain and Italy as potential source regions. In addition, Israel was also encountered in this list. Kallos et al. (2007) showed the main paths of atmospheric transport to and from Mediterranean region. It has also been indicated that air pollutants are accumulated and aged in this region. In addition to anthropogenic sources, marine (Mediterranean Sea) and crustal (North Africa and Middle East) sources are considered as other factors affecting the pollution profile of Eastern Mediterranean region.b

Temporal variations of parameters evaluated in this study are discussed in Section 4.4. However, identification of sources and source regions affecting chemical composition of aerosol are also important to asses the air quality of region of concern. In this part of the study, main pathways of airmass transport to Eastern Mediterranean were determined by using two different approaches and variation of the concentrations of natural and anthropogenic pollutants with sectors is investigated. Enrichement of pollutants with respect to crustal and marine composition are determined. Elevated sulfate concentration over Eastern Mediterranean is highlighted and ppobable sources are speculated. Dust transport from Africa is evaluated and potential tracers of Saharan dust are discussed. Positive Matrix Factorization is used to apportion elemental concentrations into their sources and major source regions affecting chemical composition of aerosols collected at our stations are determined using Potential Source Contribution Function (PSCF) approach. Lastly, dry deposition fluxes of the parameters were calculated and seasonal evolution of these calculated fluxes was assessed.

#### **4.5.1. Average Concentration of Elements in Different Wind Sectors**

Temporal variation of the pollutants was discussed in detail in previous sections of the study. However, investigation of spatial distribution of the pollutants is also important in order to find the source regions affecting our sampling site. In flow climatology section of this study Section 4.2, it has been shown that air masses arrive to Antalya station from different locations. During their transport, they pick up both natural and anthropogenic emissions from variety of potential source locations that lies on the path of air mass trajectory. Certain fraction of these species is scavenged from the atmosphere during transport, while some transformed to other forms. In order to evaluate the impact of different wind sectors on the measured aerosol chemical composition, two different methodologies were applied herein, namely, (1) residence time analysis and (2) cluster analysis.

Employing these two techniques enable us to link concentration data with sources of pollutants using air mass back trajectories to establish this link. As it was previously stated, HYSPLIT 4 (Hybrid Single Particle Lagrangian Integrated Trajectory) model was used herein. Although trajectories were downloaded for three different starting altitudes (100, 500 and 1500 m), ones arriving at our station at 1500 m altitude were taken into account since this altitude represents free boundary layer in the atmosphere.

Air mass back trajectories are used extensively in atmospheric chemistry to establish source-receptor relationship of pollutants. For example, Koçak et al (2007) used cluster analysis to find the influence of location on the chemical constituents of aerosol samples collected at Erdemli station, Turkey. Cape et al. (2000) used back trajectory clustering to interpret trace gas measurements at Mace Head, Ireland. Kim et al. (2005) classified air masses to find the sources of Asian aerosols. Salvador et al. (2008) combined backward trajectories and aerosol chemistry to characterize long range transport episodes of particulate matter in the Madrid air basin. Aircraft vertical profiles of trace gases and aerosol pollution over the mid-Atlantic United States was evaluated by employing meteorological cluster analysis in Taubman et al. (2006).

Results of two different approaches, i.e., cluster and residence time analysis and comparison of two will be presented in this section of this study.

#### **4.5.1.1. Residence Time Analysis**

In this methodology, trajectory corresponding to particular day was allocated to a specific sector provided that trajectory spend greater than 80 % of its total time in that sector. There is no established criterion for trajectory allocation and it is somewhat subjective. Traub et al. (2003) used 55 % of trajectory lifetime to assign the trajectories to specific sectors.

In order to allocate the trajectories to a particular sector, hourly trajectory segments was counted in sectors, which was depicted in Figure 4.44, by using available tools of MapInfo 7.5 software. Then if >80% of the trajectory segments was counted in a particular wind sector, that trajectory was assigned to that particular wind sector. If >80% of the trajectory segments did not occur in any of the sectors, that trajectory was excluded from the sector averages exercise. Initially, the study region was divided into 8 different sectors (North, North East, East, South East, South, South West, West and North West) and trajectories were assigned to their corresponding sectors. Nevertheless, very few samples were assigned to southern sectors (South, South West and South East) due to dominant Northwesterly flow pattern of the region. Consequently, South, South West and South East sectors were combined and total number of sectors was reduced to 6 as it was shown in Figure 4.44.

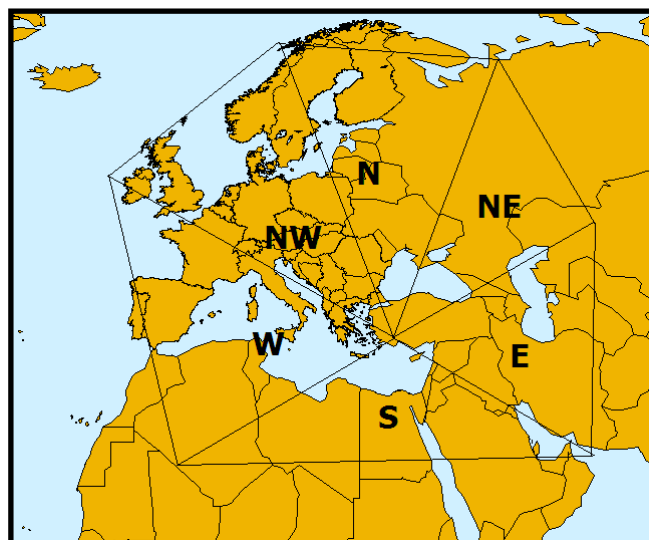


Figure 4.44 Sectors used in residence time analysis

Average concentration of measured parameters in each sector was taken as a result of conducted residence time analysis and results were summarized in Table 4.18. The number of trajectories assigned in each sector was shown in parenthesis. In addition, number of data points used to find average concentrations of elements in each particulate sector was also provided in Table 4.18.

Variations of concentration of some of the selected anthropogenic elements in different sectors were depicted in Figure 4.45. Highest  $\text{SO}_4^{2-}$  concentration was found in North sector followed by West sector. This trend in  $\text{SO}_4^{2-}$  concentration in different wind sectors can be explained by presence of significant sources in the areas covered by these sectors. Like  $\text{SO}_4^{2-}$ , Zn was also high in N, W sectors in addition to NE sector. This is typical behavior of pollution derived elements, including Cd, Ge, Se, Sn, W and Zn, which are not included in the figure. The situation is different in case of Pb. Lead is fairly uniformly distributed between sectors. Elements As, Sb, and Au also show relatively uniform distribution among sectors and closely resemble Pb in that sense. It is worthwhile to note that Güllü et al. (1998) had pointed to local sources of these elements, not because of uniform distribution of their concentrations, but due to similarities on their concentration in summer and winter seasons.

Sectoral variations of some of the selected soil derived elements (Al, Ti and Fe) were illustrated in Figure 4.46. Highest concentrations of cluster elements are associated with the air masses that spend their most of time in the south sector. This behaviour can be explained by the Saharan dust transport from North Africa. In addition to major crustal elements, we have observed highest concentrations of rare earth elements like Nd, Dy and Er in S sector as depicted in Figure 4.47. From this discussion it can be concluded that there is an important contribution of Saharan dust on the crustal contents of the samples collected in addition to local dust.

Variation of selected marine originated elements in different sectors was depicted in Figure 4.48. Air masses resided on south and west sector have high concentrations of Na and Cl. This is an expected outcome because trajectories assigned to these sectors are passing over Mediterranean Sea and some of them originated from Atlantic Ocean. Airflow from these regions swept sea salt particles generated by bubble bursting mechanism over sea surface and brought to our station.

Table 4.18 Average concentrations of measured parameters in different wind sectors (ngm<sup>-3</sup>)

	North (30)			North East (41)			East (21)		
	avg	sd	#	Avg	sd	#	avg	sd	#
<b>Al</b>	473	365	30	669	485	39	1068	1766	21
<b>As</b>	0.72	0.41	30	0.83	0.59	39	1.26	1.65	21
<b>Au</b>	0.079	0.064	19	0.504	1.410	19	0.096	0.057	8
<b>Ba</b>	9.1	7.2	30	10.1	6.6	39	11.4	14.5	21
<b>Be</b>	0.018	0.013	30	0.025	0.018	39	0.030	0.044	21
<b>Bi</b>	0.119	0.086	30	0.146	0.107	39	0.110	0.064	21
<b>Ca</b>	1035	739	30	1105	653	39	1494	2471	21
<b>Cd</b>	0.228	0.118	30	0.284	0.312	39	0.193	0.111	21
<b>Ce</b>	0.660	0.535	30	0.839	0.592	39	1.121	1.685	21
<b>Cl</b>	1595	1026	30	1299	846	34	1710	2560	20
<b>Co</b>	0.166	0.113	30	0.260	0.327	39	0.357	0.581	21
<b>Cr</b>	3.07	2.75	29	3.74	2.73	37	7.52	17.64	21
<b>Cs</b>	0.121	0.086	30	0.167	0.141	39	0.138	0.168	21
<b>Dy</b>	0.053	0.052	29	0.071	0.064	38	0.081	0.126	21
<b>Er</b>	0.034	0.030	30	0.045	0.037	39	0.049	0.069	21
<b>Eu</b>	0.012	0.012	22	0.015	0.015	33	0.025	0.037	15
<b>Fe</b>	240	174	30	319	217	39	540	951	21
<b>Gd</b>	0.079	0.069	30	0.104	0.082	39	0.118	0.166	21
<b>Ge</b>	0.034	0.019	30	0.060	0.091	39	0.055	0.060	21
<b>Hf</b>	0.046	0.038	30	0.063	0.051	39	0.060	0.074	21
<b>Ho</b>	0.011	0.010	30	0.015	0.013	39	0.017	0.024	21
<b>In</b>	0.004	0.004	28	0.005	0.009	39	0.007	0.010	21
<b>K</b>	314	213	30	418	339	39	410	497	21

Table 4.18 Average concentrations of measured parameters in different wind sectors (ng m<sup>-3</sup>) (Continued)

	North (30)			North East (41)			East (21)		
	avg	sd	#	Avg	sd	#	avg	sd	#
<b>La</b>	0.34	0.28	30	0.43	0.29	39	0.57	0.86	21
<b>Li</b>	0.46	0.31	30	0.62	0.43	39	0.79	1.20	21
<b>Lu</b>	0.005	0.004	30	0.006	0.005	39	0.007	0.010	21
<b>Mg</b>	417	228	30	517	281	39	524	510	21
<b>Mn</b>	7.64	4.71	30	10.10	5.81	39	12.02	18.57	21
<b>Na</b>	1768	1298	30	2016	1664	39	1478	914	21
<b>Nd</b>	0.32	0.26	30	0.41	0.31	39	0.52	0.78	21
<b>NH<sub>4</sub><sup>+</sup></b>	1081	1155	17	1687	1453	18	902	853	12
<b>Ni</b>	2.16	1.69	30	2.38	1.33	39	4.28	8.22	21
<b>NO<sub>3</sub><sup>-</sup></b>	1090	729	22	1330	993	23	2000	3107	11
<b>Pb</b>	52.9	45.4	30	57.5	36.0	39	47.2	44.0	21
<b>Pr</b>	0.08	0.07	30	0.11	0.08	39	0.14	0.20	21
<b>Pt</b>	0.00	0.00	17	0.003	0.002	20	0.002	0.001	9
<b>Rb</b>	0.72	0.42	30	0.90	0.53	39	1.11	1.52	21
<b>Sb</b>	0.77	0.49	30	0.64	0.30	39	0.71	0.53	21
<b>Se</b>	0.55	0.75	30	0.40	0.50	38	0.22	0.15	20
<b>Sm</b>	0.07	0.06	30	0.091	0.072	39	0.11	0.15	21
<b>Sn</b>	0.70	0.38	30	0.82	0.49	39	0.79	0.82	21
<b>SO<sub>4</sub><sup>2-</sup></b>	8555	4781	30	8787	5884	36	7123	3586	20



Table 4.18 Average concentrations of measured parameters in different wind sectors (ngm<sup>-3</sup>) (Continued)

	North (30)			North East (41)			East (21)		
	avg	sd	#	Avg	sd	#	avg	sd	#
<b>Sr</b>	2.96	1.54	30	3.60	2.39	39	4.22	5.67	21
<b>Tb</b>	0.010	0.009	30	0.013	0.011	39	0.016	0.022	21
<b>Th</b>	0.177	0.171	30	0.218	0.175	39	0.245	0.372	21
<b>Ti</b>	21.4	14.1	30	27.9	18.9	39	53.0	93.5	21
<b>Tm</b>	0.005	0.004	30	0.006	0.005	39	0.007		21
<b>U</b>	0.072	0.064	30	0.089	0.058	38	0.094		21
<b>V</b>	2.63	2.64	30	2.73	1.93	39	2.87	0.010	21
<b>W</b>	0.092	0.060	30	0.117	0.106	39	0.085	0.119	21
<b>Y</b>	0.142	0.093	30	0.184	0.124	39	0.270	0.445	21
<b>Yb</b>	0.031	0.028	30	0.042	0.036	39	0.046	0.064	21
<b>Zn</b>	12.8	11.0	30	16.1	16.2	39	11.7	8.4	21

Table 4.18 Average concentrations of measured parameters in different wind sectors (ngm<sup>-3</sup>) (Continued)

	SE-S-SW (22)			West (187)			North West (57)		
	avg	sd	#	avg	sd	#	avg	sd	#
<b>Al</b>	1128	1563	22	615	850	187	438	646	57
<b>As</b>	0.51	0.50	22	0.62	0.47	187	0.98	1.31	57
<b>Au</b>	0.080	0.090	11	0.159	0.292	87	0.186	0.253	22
<b>Ba</b>	12.9	12.7	22	8.6	7.2	187	7.2	5.6	55
<b>Be</b>	0.046	0.071	22	0.023	0.024	186	0.025	0.057	57
<b>Bi</b>	0.092	0.084	21	0.090	0.076	175	0.162	0.181	54
<b>Ca</b>	1281	1111	22	1028	1061	185	789	1066	57
<b>Cd</b>	0.140	0.083	22	0.201	0.143	187	0.329	0.497	57
<b>Ce</b>	1.340	1.643	22	0.760	0.931	187	0.554	0.772	57
<b>Cl</b>	3251	6521	21	2379	2897	177	1380	1478	56
<b>Co</b>	0.273	0.284	22	0.209	0.300	186	0.211	0.292	57
<b>Cr</b>	4.25	4.52	20	3.49	3.47	177	4.94	11.10	49
<b>Cs</b>	0.115	0.101	22	0.104	0.091	187	0.138	0.231	57
<b>Dy</b>	0.116	0.142	21	0.063	0.081	162	0.045	0.071	48
<b>Er</b>	0.067	0.078	22	0.035	0.043	187	0.026	0.038	57
<b>Eu</b>	0.034	0.039	16	0.018	0.022	114	0.016	0.033	29
<b>Fe</b>	496	626	22	298	376	184	241	365	55
<b>Gd</b>	0.166	0.193	21	0.084	0.106	187	0.062	0.088	57
<b>Ge</b>	0.034	0.025	22	0.036	0.037	187	0.056	0.071	57
<b>Hf</b>	0.112	0.211	22	0.051	0.056	182	0.035	0.041	56
<b>Ho</b>	0.023	0.027	22	0.012	0.015	187	0.009	0.013	57
<b>In</b>	0.008	0.021	20	0.005	0.008	174	0.009	0.020	53

Table 4.18 Average concentrations of measured parameters in different wind sectors (ngm<sup>-3</sup>) (Continued)

	SE-S-SW (22)			West (187)			North West (57)		
	avg	sd	#	avg	sd	#	avg	sd	#
<b>K</b>	375	283	22	329	237	187	285	415	57
<b>La</b>	0.66	0.81	22	0.38	0.46	187	0.30	0.41	57
<b>Li</b>	0.82	0.84	22	0.56	0.53	187	0.44	0.61	57
<b>Lu</b>	0.009	0.011	22	0.005	0.006	187	0.004	0.005	57
<b>Mg</b>	672	421	22	564	476	187	372	425	57
<b>Mn</b>	10.36	11.24	22	7.45	7.10	187	7.60	12.03	57
<b>Na</b>	2480	2744	22	2738	2639	186	1636	2000	57
<b>Nd</b>	0.66	0.81	22	0.3614	0.450561	187	0.26	0.38	57
<b>NH<sub>4</sub><sup>+</sup></b>	835	1077	10	1167	1180	113	944	1016	41
<b>Ni</b>	2.61	2.38	22	2.35	2.25	185	2.26	3.04	56
<b>NO<sub>3</sub><sup>-</sup></b>	1690	2339	12	1356	1201	124	1097	1488	39
<b>Pb</b>	59.0	34.4	22	46.3	35.9	187	47.4	45.3	56
<b>Pr</b>	0.17	0.21	22	0.095	0.115	187	0.069	0.099	57
<b>Pt</b>	0.003	0.003	11	0.003	0.005	96	0.005	0.009	24
<b>Rb</b>	0.97	1.02	22	0.767	0.680	187	0.719	1.041	57
<b>Sb</b>	0.69	0.48	22	0.611	0.427	187	0.776	1.007	57
<b>Se</b>	0.29	0.35	21	0.430	0.568	182	0.392	0.630	56
<b>Sm</b>	0.14	0.17	22	0.077	0.095	187	0.060	0.101	56
<b>Sn</b>	0.54	0.28	22	0.600	0.439	187	0.738	1.123	57
<b>SO<sub>4</sub><sup>2-</sup></b>	5707	2871	22	8435	5113	182	8671	5408	56

Table 4.18 Average concentrations of measured parameters in different wind sectors (ngm<sup>-3</sup>) (Continued)

	<b>S-SW-SE (22)</b>			<b>West (187)</b>			<b>North West (57)</b>		
	<b>avg</b>	<b>sd</b>	<b>#</b>	<b>avg</b>	<b>sd</b>	<b>#</b>	<b>avg</b>	<b>sd</b>	<b>#</b>
<b>Sr</b>	5.10	3.68	22	4.22	4.26	184	2.85	5.56	56
<b>Tb</b>	0.021	0.024	22	0.011	0.014	187	0.008	0.011	57
<b>Th</b>	0.286	0.358	22	0.172	0.209	178	0.139	0.212	55
<b>Ti</b>	54.8	72.8	22	29.5	41.2	187	20.2	27.5	57
<b>Tm</b>	0.009	0.011	22	0.005	0.006	187	0.004	0.005	57
<b>U</b>	0.096	0.096	22	0.070	0.074	178	0.074	0.134	55
<b>V</b>	2.95	1.96	22	3.26	2.70	187	3.29	5.46	57
<b>W</b>	0.070	0.050	22	0.080	0.064	180	0.095	0.134	54
<b>Y</b>	0.289	0.365	22	0.172	0.205	187	0.130	0.171	57
<b>Yb</b>	0.060	0.071	22	0.032	0.039	187	0.024	0.033	57
<b>Zn</b>	10.4	8.5	22	12.4	10.5	184	15.0	14.0	56

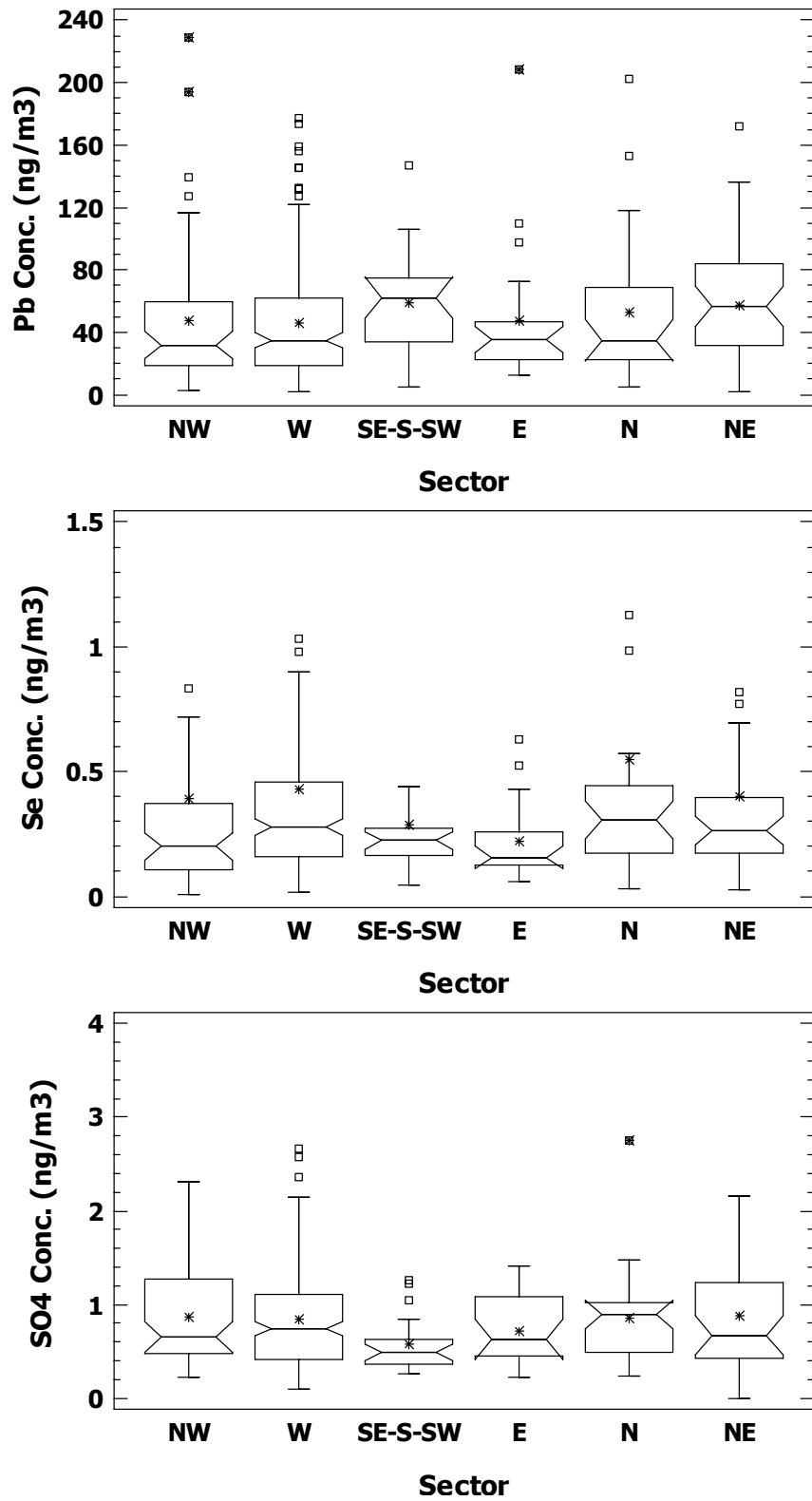


Figure 4.45 Distribution of some of the selected anthropogenic pollutants in different sectors

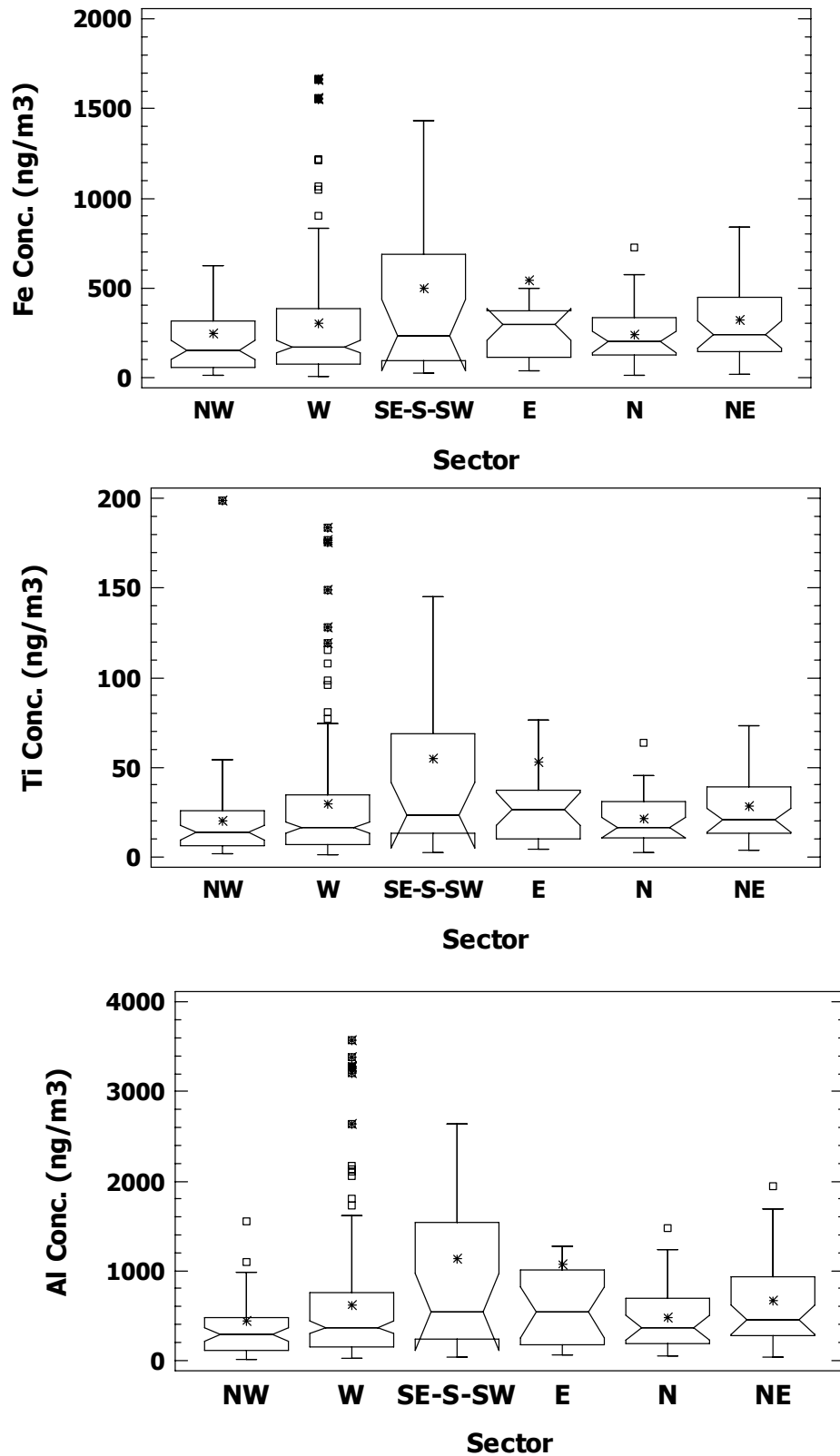


Figure 4.46 Distribution of some of the selected crustal elements in different sectors

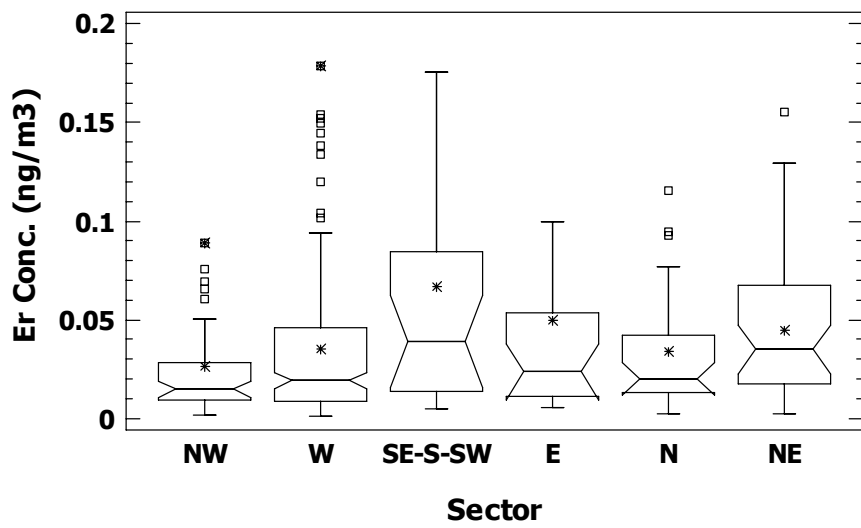
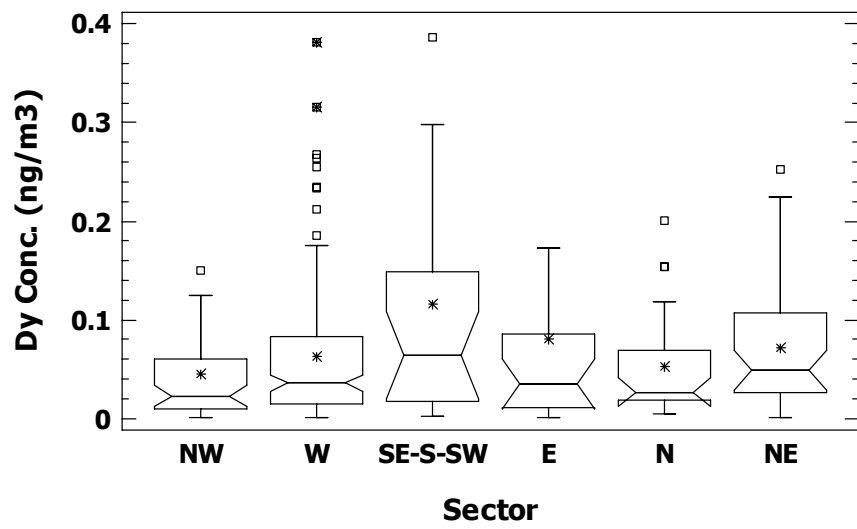
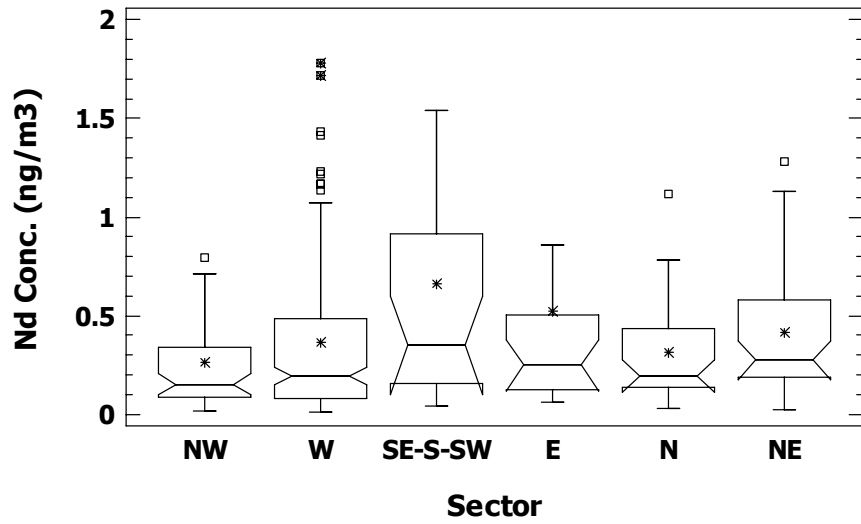


Figure 4.47 Distribution of some of the selected rare earth elements in different sectors

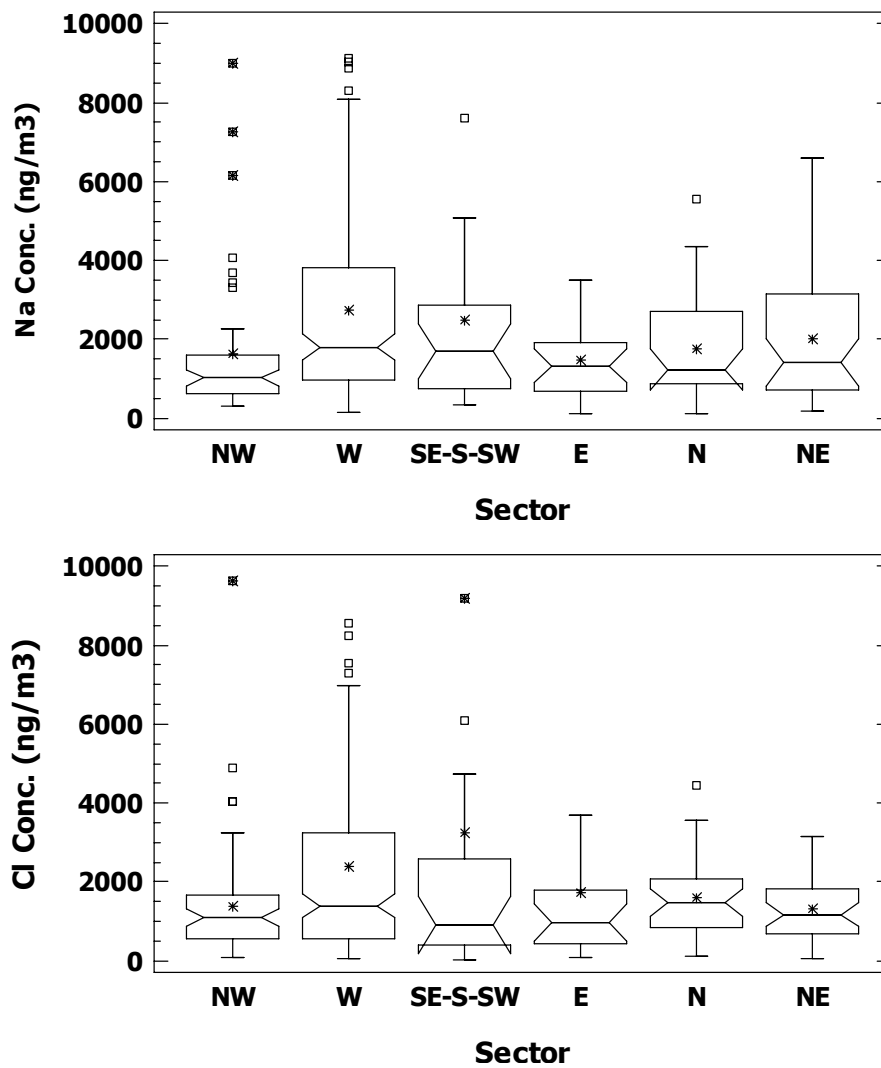


Figure 4.48 Distribution of marine originated elements in different sectors

#### 4.5.1.2. Cluster Analysis

Cluster analysis of trajectories has been generally employed to classify the large amounts of trajectories into similar sub-groups, which are called as 'clusters'. The objective of cluster analysis is to minimize the variance within a particular cluster and maximize the variance between the clusters based on the horizontal speed and direction of air masses.

The Euclidean distance,  $D$ , between the trajectory points is calculated by following equation (Taubman et al., 2006):



$$D_{ij} = \sqrt{\sum_{k=1}^n (x_{ik} - x_{jk})^2 + (y_{ik} - y_{jk})^2 + (z_{ik} - z_{jk})^2} \quad (4.11)$$

In this equation, D is the three dimensional distance between the two trajectories for which comparison is made and denoted by subscript 'i' and 'j'. Longitude, latitude and pressure, or in other words altitude of air masses, are presented as 'x', 'y' and 'z', respectively in this equation, and 'k' stands for the hourly time steps, which is 121 in our case. In this study, the altitude of the air masses was not taken into account and hence, last term in the square root was dropped. Consequently, two-dimensional equation was used instead of three.

For 9 year period, 3159 (365 daily trajectories times 9 years minus trajectories that were unavailable in the web site) 5 day-long backward trajectories at 1500 m starting altitude were requested. Trajectory length was chosen as 5 days since it is compatible with the lifetime of most secondary air pollutants formed in the atmosphere from their precursors (Wojcik and Chang, 1997; Abdalmogith and Harrison, 2005). However, the total length of 165 trajectories was shorter than 3 days (or 72 hours). These short in length trajectories were not considered in cluster analysis in order not to affect the final data interpretation. For the total of 2994 trajectories, 121 longitudinal and 121 latitudinal coordinates in hourly time resolution was used as input to cluster analysis run. Rectangular data matrix including the variables of latitude and longitude in columns and rows correspond to each days was formed (He et al., 2003; Kim et al., 2005).

K-means clustering, which was previously proposed by Dorling et al. (1992), was used to classify the trajectories. This algorithm is a routine available in SPSS 15 (SPSS Inc., 2006). In K means clustering approach, the initial cluster centers should be entered as 'seed' and seed file should represent the all trajectories. Minimum number of seeds used in clustering was suggested as 30 in Brankov et al. (1998). Seed file used in this study was composed of 99 trajectories and 121 longitudinal and 121 latitudinal coordinates, and it was constructed randomly from the cluster analysis input file. Distance between each of the real trajectory in input file and seed was estimated and trajectory was assigned to a seed with the smallest distance. Afterwards, average trajectory of each cluster was re-calculated. Distances between the clusters were estimated and if the

distance was small, clusters were linked with dendrograms to form larger clusters. Consequently, trajectories which are similar directionality and velocity were put into same cluster. However, there are some trajectories which were not classified in any of the cluster. In this study, 253 trajectories that made up of 8.4 % of total trajectories were not allocated to any cluster.

After calculating the average trajectory or trajectory center for each cluster, the appropriate number of clusters can be decided. The root mean square deviation (RMSD) of each trajectory from average trajectory was calculated for each cluster. The calculated RMSDs were then summed up to obtain Total Root Mean Square Deviations (TRMSD). To decide the appropriate number of clusters from cluster analysis, TRMSD was plotted against number of clusters as it was shown in Figure 4.49. The methodology used in finding cluster numbers was previously proposed and used in many studies (e.g., Cape et al., 2000; Brankov et al., 1998; Taubman et al., 2006; Owega et al., 2006).

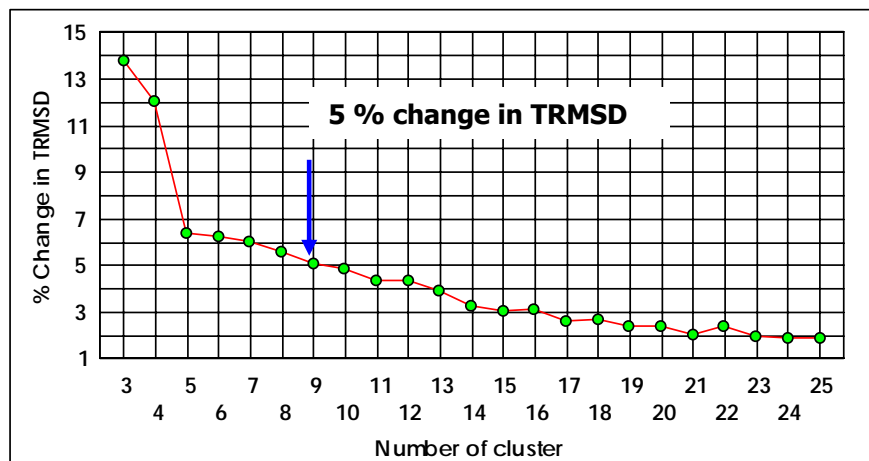


Figure 4.49 Percent change in TRMSD versus number of clusters

As it was demonstrated in Figure 4.49, 25 clusters were tried and corresponding percentage change in TRMSD was estimated. As cluster number decreases, percentage changes in TRMSD increases implying that clusters with significantly different velocity and direction are merged in a cluster. Consequently, the correct number of clusters can be found preceding the large percent change in TRMSD. A threshold of 5 % was proposed

by Dorling et al. (1992), Brankov et al. (1998) and Jorba et al., (1994). The 5 % change in TRMSD threshold in this analysis corresponding to 9 clusters as it was depicted in Figure 4.49. Accordingly, 9 clusters were retained to further interpret the origin of air masses influencing the chemical composition of aerosols collected at our station. The percentage of trajectories assigned to each cluster was illustrated in Figure 4.50.

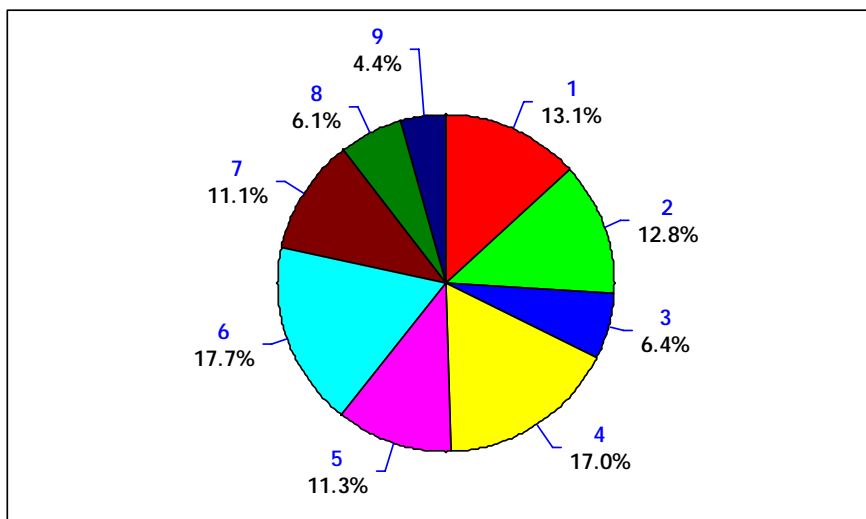


Figure 4.50 Percentage of trajectories allocated in each cluster

Trajectories those were assigned to each sector are depicted in Figure 4.51. The red line in each trajectory cluster shows the final cluster center obtained from the last iteration of cluster analysis. Characteristics of each cluster can be defined as follows:

1. *Cluster 1:* Cover Mediterranean Sea and part of North Africa. This cluster includes 13.1 % of the trajectories.
2. *Cluster 2:* Cover Western Mediterranean Sea and countries surrounding it, include long fetch of air masses and hence, fast moving air masses. This cluster accounts for 12.8 % of of the trajectories

3. *Cluster 3:* Cover European countries and include long fetch of air masses. Some of the backtrajectories in this group extends all the way to North America. Cluster 3 include 6.5 % of the trajectories
4. *Cluster 4:* Cover Western part of Turkey, Balkan countries and Central European countries, such as Hungary, Czech Republic etc. These are trajectories with moderate length. Trajectories in this group accounts for 17 % of total trajectories.
5. *Cluster 5:* Cover Black Sea, Ukraine and some part of Russia, include long fetch of air masses. Trajectories in this cluster are fast moving ones. This cluster represents 11.3 % of total trajectories.
6. *Cluster 6:* Cover western part of Turkey, Greece, and some part of Eastern European countries, and include short fetch of air masses. This cluster accounted for 17.7 % of trajectories.
7. *Cluster 7:* Cover eastern part of Turkey, and some part of Middle East including Syria, Iran and Iraq. These are short trajectories indicating very slow movement of air masses. The cluster includes 11.1 % of total air masses.
8. *Cluster 8:* Cover former USSR countries like Ukraine and Moldova, and include long range transport with fast moving air masses. 6.1 % of trajectory data set belongs to this cluster.
9. *Cluster 9:* This cluster includes the fastest moving air masses. Backtrajectories in this cluster cover most of the Europe, and also crosses Atlantic Ocean and extends to North America. This interesting cluster accounts for only 4.4 % of trajectories.

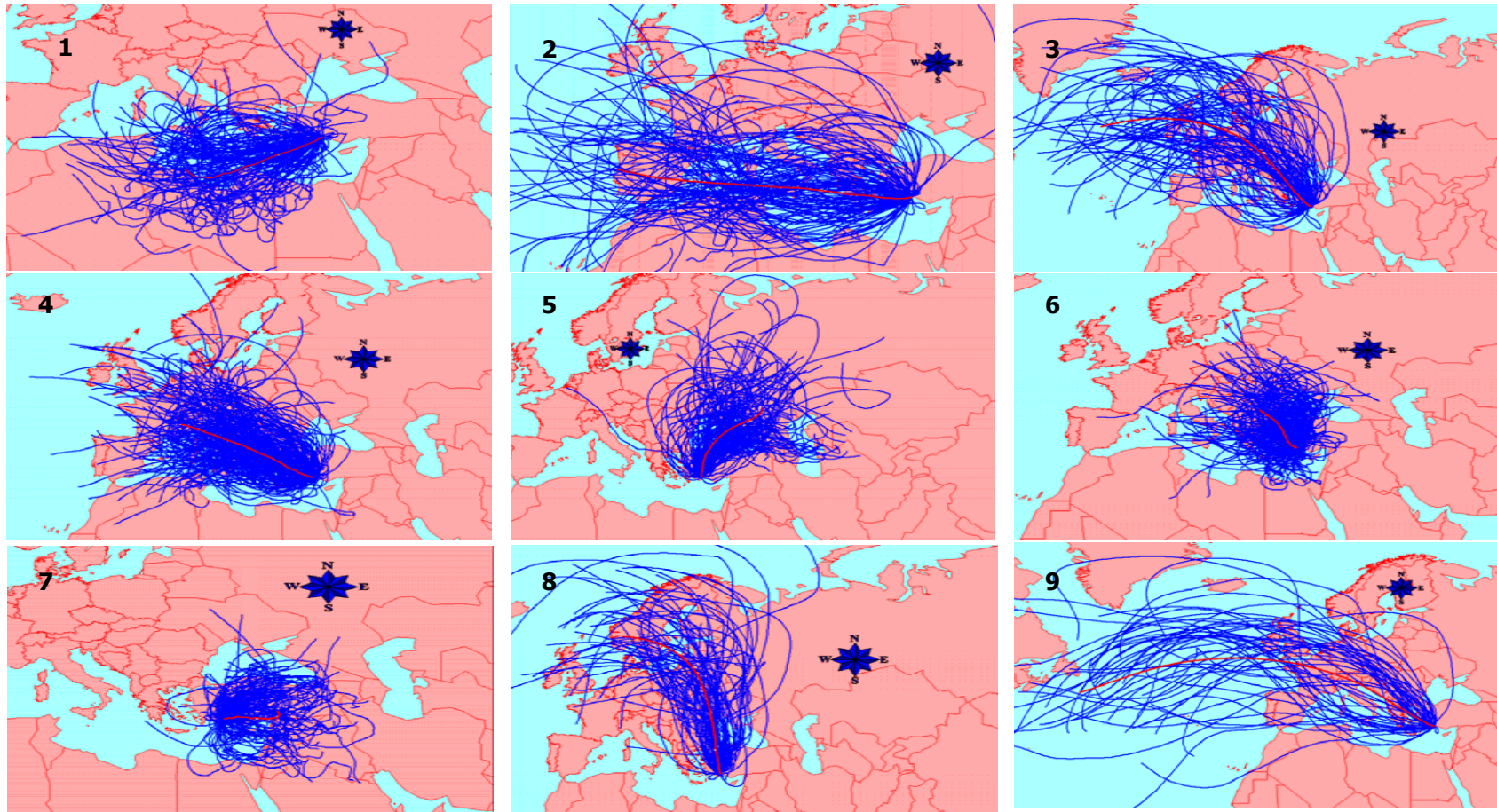


Figure 4.51 Trajectories allocated to different clusters

Salvador et al. (2008) conducted cluster analysis for a background station in central Spain between 1999 and 2005. Researchers identified 8 clusters in this analysis. Clustering pattern found in this study was very similar to one that we obtained with the exception Cluster number 8 from northern direction, which was not identified in Salvador et al. (2008). Riccio et al. (2007) performed trajectory cluster analysis for Southern Italy and come up with 8 cluster solution for 10 years long data. Cluster number 7 found in this study was missing in researchers' solution. Katragkou et al. (2009) used trajectory clustering technique in Thessaloniki, Greece between 2001 and 2004. Performed analysis revealed 8 cluster of trajectories. Koçak et al. (2007) used average three day air mass trajectories for 850 hPa pressure level to classify the trajectories arriving at Erdemli station, Mersin. Seven clusters were determined in conducted cluster analysis. Cluster number 8 and 9 found in this study were not identified for Erdemli station. It should be noted that Koçak et al. (2007) used trajectories for one year interval (April 2001 and 2002). However, it has been widely accepted that analysis of results for a long time period yield more robust results in trajectory clustering (Riccio et al., 2007).

Seasonal variations of trajectories assigned to each cluster were also investigated. To this end monthly percentage of trajectories in each defined cluster were calculated. Clusters were separated into three groups depending on their seasonal trends. The first group included clusters 1, 3, 7 and 9. Monthly percentage of trajectories accounted for by these three groups is depicted in Figure 4.52. These clusters are important and responsible for transport to the Eastern Mediterranean in the winter season. Cluster 7 involves shortest (slowest moving) trajectories and is related with the easterly flow to the region. It should also be noted that trajectories associated with clusters 3 and 9 are fast moving and reaches to North America in 5 days. When they are compared, trajectories in Cluster 9 are longer than trajectories associated with Cluster 3.

The difference in these two clusters was further investigated by plotting altitude of trajectories as a function of backward time and results were demonstrated in Figure 4.53. Since trajectories in Cluster 9 are longer, one may expect to observe higher altitudes for these trajectories than in Cluster 3. However, such a difference can not be concluded from Figure 4.53.

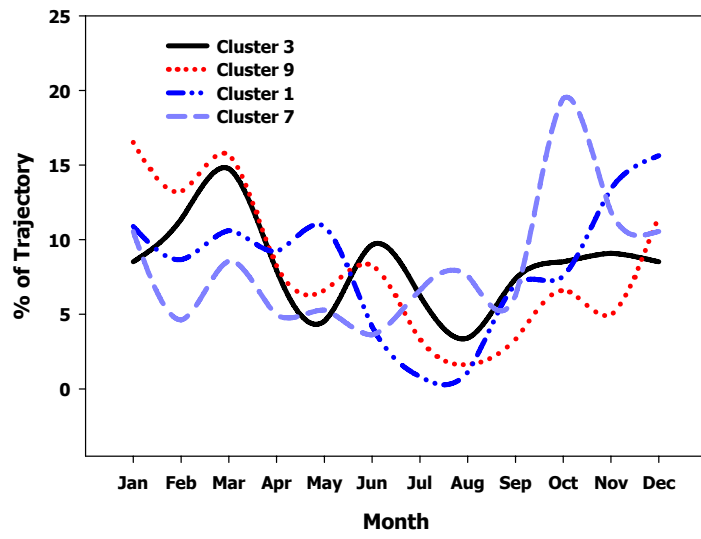
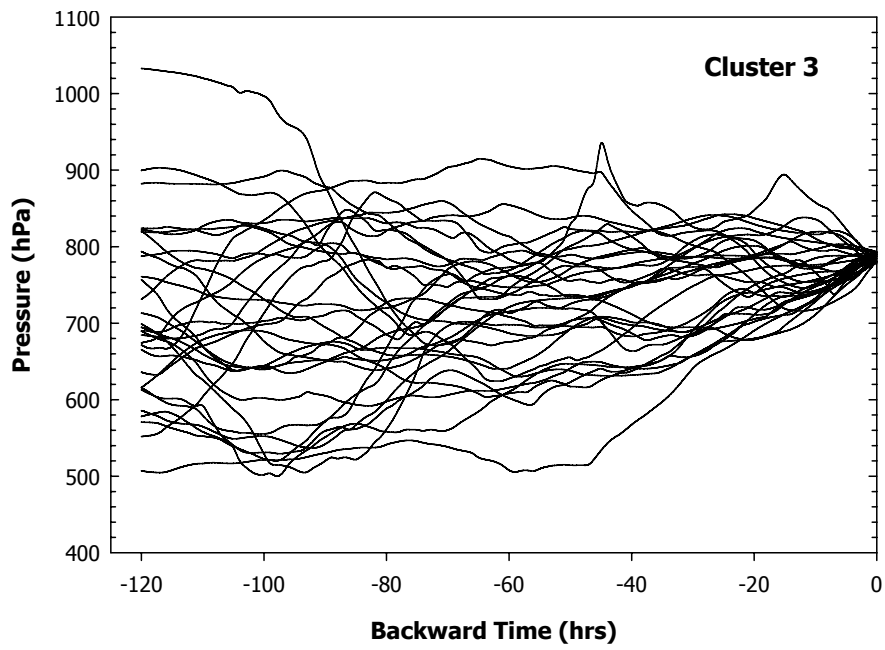
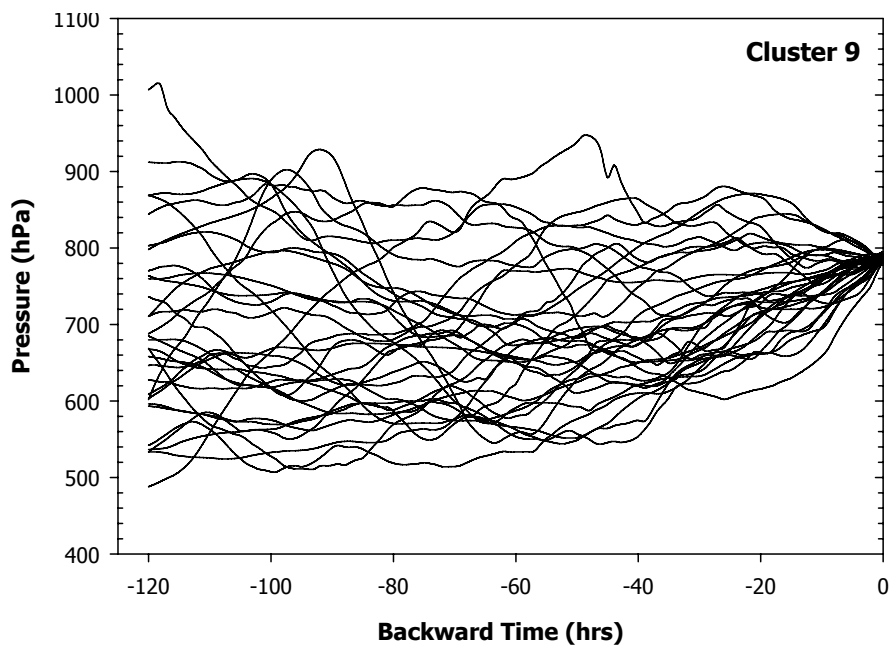


Figure 4.52 Monthly percentage of trajectories analyzed in cluster number 1, 3 and 9



(a) Cluster 3



(b) Cluster 9

Figure 4.53 Altitude profile of trajectories within (a) Cluster 3 & (b) Cluster 9



The second group includes Clusters 5, 6 and 8. Seasonal frequencies of these clusters are illustrated in Figure 4.54. Trajectories included in these clusters are more frequent in summer season. Cluster 5 and 8 include longer trajectories as compared to ones in Cluster 6, which is associated with westerly air mass systems. Clusters 5 and 8, on the other hand, are associated with air mass systems from north and northeast direction, respectively.

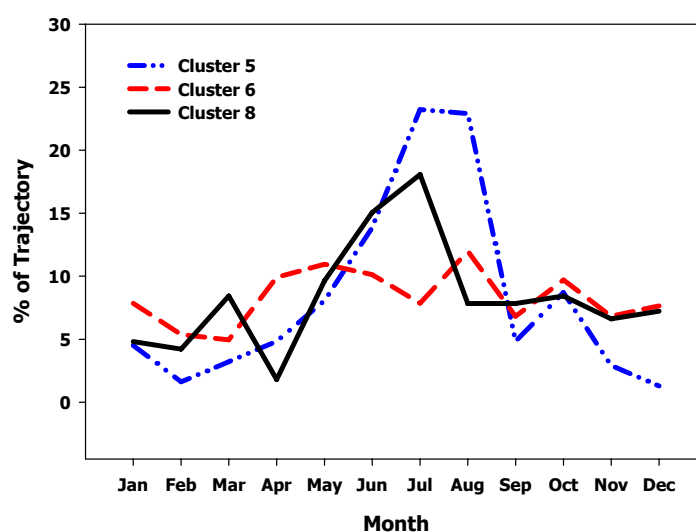


Figure 4.54 Monthly percentage of trajectories analyzed in cluster number 5, 6 and 8

Seasonal variation of trajectories associated with the third cluster group, which includes Clusters 2 and 4 are given in Figure 4.55. Frequencies of these clusters do not change significantly from one season to another and trajectories in clusters 2 and 4 are associated with westerly flow of air masses. Cluster 2 includes longest (fastest moving) trajectories in this group of cluster.

#### ***4.5.1.2.1. Variation of Chemical Composition with Clusters***

Average concentrations of elements in samples corresponding to trajectories included in each cluster are given in Table 4.19. Discussion on the relative abundance of measured concentrations for some of the selected parameters in different sectors was provided in

residence time analysis before, hence, will not be repeated here again. However, it should be noted that concentrations of soil derived species such as Al, Ca, Ti, Ce, Co, Dy, Er, Fe, Ge, Hf, Ho, In, La, Li, Lu, Pr and Yb are found to be higher in trajectories assigned to Cluster number 1 and Cluster number 7.

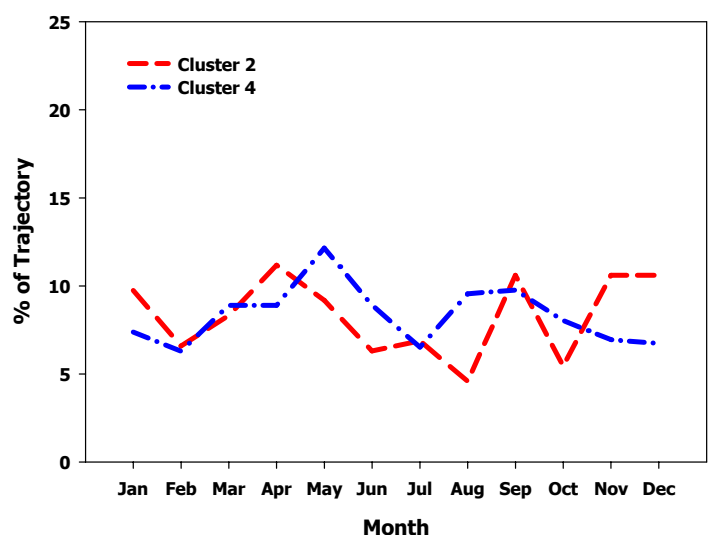


Figure 4.55 Monthly percentage of trajectories analyzed in cluster number 2 and 4

Trajectories in Cluster number 1 have south-westerly direction, some of them originated from North Africa, while trajectories allocated to Cluster number 7 have south easterly flow, some of them originated from Middle East and eastern part of Turkey. These regions covered by clusters 1 and 7 include arid regions in general and desert areas at the Middle East and North Africa. Consequently, it is not surprising to see high concentrations of crustal elements within these clusters. Moreover, marine originated elements, Sr, Mg Na and Cl, observed at their highest concentrations in Cluster number 1 owing to passage of trajectories in this cluster over Mediterranean Sea. These clusters and chemical composition of samples associated with them closely resemble the combined S sector discussed previously in residence time analysis.

Highest concentrations of anthropogenic elements are associated with trajectories assigned with Clusters 5 and 6. For example, Sb, Sn, Se, As and  $SO_4^{2-}$  present at elevated concentrations in clusters 5 and 6. These two clusters cover western Turkey, which is

the most heavily industrialized part of Turkey, Balkan countries, Ukraine and Russia. This difference between concentrations of pollution-derived elements in different cluster groups indicates that concentrations of elements measured in Eastern Mediterranean is probably contributed by sources that are close to the basin, rather than sources at distant western European countries. Locations of potential source areas will be further discussed later in the manuscript.

There are several interesting points that worth noting when individual elements are discussed. While highest average concentration of  $\text{NH}_4^+$  ( $1.4 \mu\text{gm}^{-3}$ ) is associated with trajectories assigned to Cluster number 7,  $\text{NO}_3^-$  concentration was observed in Cluster number 6 ( $\sim 1.7 \mu\text{gm}^{-3}$ ) is higher than one observed in this cluster ( $1.5 \mu\text{gm}^{-3}$ ). These observed concentrations of  $\text{NO}_3^-$  and  $\text{NH}_4^+$  can be attributed the presence of considerable amounts of greenhouses in this part of Turkey.

Furthermore, distribution of  $\text{NO}_3^-$  concentrations among cluster groups resemble to those of crustal and marine elements, with relatively high concentrations associated with cluster 1 and 7. This is probably due to well-documented formation of  $\text{NaNO}_3$  and  $\text{Ca}(\text{NO}_3)_2$  on sea salt and crustal particles by reactions between  $\text{HNO}_3$  and  $\text{NaCl}$  on sea salt particles and between  $\text{HNO}_3$  and  $\text{CaCO}_3$  on crustal particles. (Kuloğlu and Tuncel, 2005)

Table 4.19 Average concentrations within resolved clusters

	Cluster 1			Cluster 2			Cluster 3			
	avg	sd	#	avg	sd	#	avg	sd	#	
<b>Al</b>	693	1240	140	579	645	131	424	627	89	<b>Al</b>
<b>As</b>	0.64	0.50	140	0.61	0.42	131	0.70	0.38	89	<b>As</b>
<b>Au</b>	0.16	0.46	61	0.18	0.32	63	0.18	0.33	43	<b>Au</b>
<b>Ba</b>	9.19	10.68	140	9.38	8.31	131	7.91	7.19	88	<b>Ba</b>
<b>Be</b>	0.024	0.031	140	0.022	0.022	130	0.016	0.021	88	<b>Be</b>
<b>Bi</b>	0.100	0.102	136	0.102	0.085	124	0.112	0.108	82	<b>Bi</b>
<b>Ca</b>	1127	1521	139	949	808	131	865	733	88	<b>Ca</b>
<b>Cd</b>	0.17	0.11	140	0.19	0.12	131	0.19	0.14	89	<b>Cd</b>
<b>Ce</b>	0.86	1.35	139	0.79	0.93	131	0.56	0.82	89	<b>Ce</b>
<b>Cl</b>	2683	4100	127	2235	2799	123	1524	1694	82	<b>Cl</b>
<b>Co</b>	0.22	0.36	139	0.18	0.14	131	0.17	0.19	89	<b>Co</b>
<b>Cr</b>	3.99	4.94	129	3.46	3.44	121	3.00	2.94	80	<b>Cr</b>
<b>Cs</b>	0.099	0.100	140	0.104	0.079	131	0.093	0.077	89	<b>Cs</b>
<b>Dy</b>	0.078	0.148	119	0.071	0.092	111	0.048	0.081	74	<b>Dy</b>
<b>Er</b>	0.042	0.079	140	0.038	0.048	131	0.027	0.041	89	<b>Er</b>
<b>Eu</b>	0.021	0.039	91	0.021	0.024	77	0.015	0.024	45	<b>Eu</b>
<b>Fe</b>	330	585	139	279	293	129	218	316	86	<b>Fe</b>
<b>Gd</b>	0.098	0.174	139	0.091	0.118	131	0.064	0.099	89	<b>Gd</b>
<b>Ge</b>	0.044	0.069	140	0.035	0.030	131	0.041	0.037	89	<b>Ge</b>
<b>Hf</b>	0.061	0.120	138	0.053	0.059	125	0.043	0.059	86	<b>Hf</b>
<b>Ho</b>	0.0140	0.0263	140	0.0130	0.0163	131	0.0093	0.0140	89	<b>Ho</b>
<b>In</b>	0.0084	0.0403	129	0.0056	0.0111	124	0.0087	0.0207	88	<b>In</b>
<b>K</b>	317	271	140	316	211	131	244	199	89	<b>K</b>
<b>La</b>	0.42	0.66	139	0.39	0.44	131	0.28	0.37	89	<b>La</b>
<b>Li</b>	0.60	0.81	140	0.56	0.55	131	0.43	0.57	88	<b>Li</b>
<b>Lu</b>	0.0058	0.0113	139	0.0052	0.0066	131	0.0038	0.0056	87	<b>Lu</b>

Table 4.19 Average concentrations within resolved clusters (Continued)

	Cluster 1			Cluster 2			Cluster 3			
	avg	sd	#	avg	sd	#	avg	sd	#	
<b>Mg</b>	576	656	140	524	427	131	387	364	89	<b>Mg</b>
<b>Mn</b>	7.82	10.56	140	7.12	5.64	131	5.99	5.89	89	<b>Mn</b>
<b>Na</b>	2684	4077	140	2482	2196	130	1853	2595	89	<b>Na</b>
<b>Nd</b>	0.41	0.69	140	0.38	0.46	131	0.27	0.40	89	<b>Nd</b>
<b>NH<sub>4</sub><sup>+</sup></b>	1060	898	75	1269	1329	69	898	949	55	<b>NH<sub>4</sub><sup>+</sup></b>
<b>Ni</b>	2.28	2.66	138	2.16	1.75	129	1.73	1.40	87	<b>Ni</b>
<b>NO<sub>3</sub><sup>-</sup></b>	1430	1592	82	1153	977	80	1055	835	58	<b>NO<sub>3</sub><sup>-</sup></b>
<b>Pb</b>	50	48	140	51	43	131	41	34	89	<b>Pb</b>
<b>Pr</b>	0.106	0.172	140	0.099	0.117	131	0.070	0.100	89	<b>Pr</b>
<b>Pt</b>	0.0034	0.0052	69	0.0024	0.0023	64	0.0025	0.0034	45	<b>Pt</b>
<b>Rb</b>	0.76	0.83	140	0.75	0.63	131	0.58	0.57	89	<b>Rb</b>
<b>Sb</b>	0.61	0.43	140	0.64	0.43	130	0.54	0.28	89	<b>Sb</b>
<b>Se</b>	0.44	0.63	138	0.38	0.52	129	0.33	0.52	86	<b>Se</b>
<b>Sm</b>	0.089	0.153	140	0.083	0.102	131	0.059	0.089	89	<b>Sm</b>
<b>Sn</b>	0.56	0.43	139	0.64	0.45	131	0.51	0.33	88	<b>Sn</b>
<b>SO<sub>4</sub><sup>2-</sup></b>	6615	4031	137	8074	5464	128	6277	4149	87	<b>SO<sub>4</sub><sup>2-</sup></b>
<b>Sr</b>	4.28	4.34	138	3.91	3.45	130	2.91	3.04	87	<b>Sr</b>
<b>Tb</b>	0.013	0.023	140	0.012	0.015	131	0.008	0.013	89	<b>Tb</b>
<b>Th</b>	0.195	0.335	136	0.183	0.209	125	0.140	0.203	81	<b>Th</b>
<b>Ti</b>	34	60	140	27	31	131	21	33	89	<b>Ti</b>
<b>Tm</b>	0.006	0.011	140	0.005	0.007	131	0.004	0.006	89	<b>Tm</b>
<b>U</b>	0.072	0.095	135	0.077	0.068	123	0.059	0.068	85	<b>U</b>
<b>V</b>	2.71	2.38	140	3.16	2.85	131	1.95	1.78	89	<b>V</b>
<b>W</b>	0.075	0.067	138	0.090	0.075	127	0.077	0.068	86	<b>W</b>
<b>Y</b>	0.19	0.30	140	0.17	0.18	131	0.12	0.15	89	<b>Y</b>
<b>Yb</b>	0.038	0.072	140	0.035	0.044	131	0.025	0.038	89	<b>Yb</b>
<b>Zn</b>	11	8	138	13	10	130	11	16	89	<b>Zn</b>

Table 4.19 Average concentrations within resolved clusters (Continued)

	Cluster 4			Cluster 5			Cluster 6			
	avg	sd	#	avg	sd	#	avg	sd	#	
<b>Al</b>	641	1152	210	725	1252	154	635	861	198	<b>Al</b>
<b>As</b>	0.77	0.54	210	0.77	0.80	154	0.84	0.85	198	<b>As</b>
<b>Au</b>	0.16	0.28	91	0.14	0.19	80	0.17	0.22	100	<b>Au</b>
<b>Ba</b>	10.29	12.29	209	10.89	11.41	154	9.95	8.63	196	<b>Ba</b>
<b>Be</b>	0.028	0.070	208	0.024	0.034	154	0.024	0.029	197	<b>Be</b>
<b>Bi</b>	0.127	0.126	205	0.114	0.092	153	0.121	0.105	191	<b>Bi</b>
<b>Ca</b>	1160	2863	206	1107	1315	154	1052	1291	196	<b>Ca</b>
<b>Cd</b>	0.23	0.17	210	0.27	0.25	154	0.27	0.34	198	<b>Cd</b>
<b>Ce</b>	0.83	1.61	209	0.92	1.73	154	0.80	1.01	197	<b>Ce</b>
<b>Cl</b>	1642	2148	196	1560	1934	146	1590	1937	180	<b>Cl</b>
<b>Co</b>	0.21	0.33	209	0.22	0.27	154	0.21	0.26	198	<b>Co</b>
<b>Cr</b>	3.44	3.54	197	3.68	3.50	150	3.67	5.95	190	<b>Cr</b>
<b>Cs</b>	0.124	0.125	210	0.146	0.148	154	0.129	0.147	198	<b>Cs</b>
<b>Dy</b>	0.074	0.181	187	0.080	0.184	148	0.069	0.095	181	<b>Dy</b>
<b>Er</b>	0.041	0.093	210	0.048	0.099	154	0.040	0.052	198	<b>Er</b>
<b>Eu</b>	0.021	0.048	136	0.021	0.050	112	0.019	0.028	133	<b>Eu</b>
<b>Fe</b>	310	551	205	363	571	152	321	441	195	<b>Fe</b>
<b>Gd</b>	0.100	0.228	209	0.115	0.249	154	0.094	0.122	197	<b>Gd</b>
<b>Ge</b>	0.040	0.036	210	0.051	0.079	154	0.044	0.052	198	<b>Ge</b>
<b>Hf</b>	0.055	0.111	208	0.064	0.110	154	0.055	0.063	193	<b>Hf</b>
<b>Ho</b>	0.0140	0.0317	209	0.0162	0.0329	154	0.0135	0.0175	198	<b>Ho</b>
<b>In</b>	0.0065	0.0107	202	0.0053	0.0093	152	0.0072	0.0199	193	<b>In</b>
<b>K</b>	335	471	210	392	477	154	345	311	198	<b>K</b>
<b>La</b>	0.42	0.79	209	0.46	0.82	154	0.40	0.49	197	<b>La</b>
<b>Li</b>	0.61	0.88	210	0.64	0.99	154	0.57	0.61	198	<b>Li</b>
<b>Lu</b>	0.0057	0.0132	210	0.0068	0.0136	154	0.0056	0.0072	198	<b>Lu</b>

Table 4.19 Average concentrations within resolved clusters (Continued)

	Cluster 4			Cluster 5			Cluster 6			
	avg	sd	#	avg	sd	#	avg	sd	#	
<b>Mg</b>	562	1462	210	505	561	154	467	438	198	<b>Mg</b>
<b>Mn</b>	8.24	10.63	210	9.90	10.62	154	8.86	9.90	198	<b>Mn</b>
<b>Na</b>	1993	2107	208	2031	2541	154	1913	2015	198	<b>Na</b>
<b>Nd</b>	0.40	0.84	210	0.45	0.90	154	0.39	0.50	197	<b>Nd</b>
<b>NH<sub>4</sub><sup>+</sup></b>	1100	1038	130	1173	1045	82	1346	1351	109	<b>NH<sub>4</sub><sup>+</sup></b>
<b>Ni</b>	2.52	2.54	208	2.54	2.37	154	2.49	2.33	198	<b>Ni</b>
<b>NO<sub>3</sub><sup>-</sup></b>	1240	1216	142	1276	897	98	1662	1713	126	<b>NO<sub>3</sub><sup>-</sup></b>
<b>Pb</b>	54	39	210	52	42	154	52	41	197	<b>Pb</b>
<b>Pr</b>	0.105	0.206	210	0.117	0.224	154	0.113	0.208	198	<b>Pr</b>
<b>Pt</b>	0.0026	0.0026	93	0.0029	0.0064	89	0.0027	0.0042	107	<b>Pt</b>
<b>Rb</b>	0.82	0.96	210	0.96	1.16	154	0.84	0.85	198	<b>Rb</b>
<b>Sb</b>	0.66	0.41	210	0.75	0.81	153	0.81	0.83	198	<b>Sb</b>
<b>Se</b>	0.37	0.46	206	0.43	0.61	151	0.56	0.77	196	<b>Se</b>
<b>Sm</b>	0.089	0.188	210	0.101	0.206	154	0.086	0.113	198	<b>Sm</b>
<b>Sn</b>	0.67	0.45	209	0.75	0.56	154	0.76	0.78	198	<b>Sn</b>
<b>SO<sub>4</sub><sup>2-</sup></b>	9239	5360	205	8635	5361	152	9997	6570	197	<b>SO<sub>4</sub><sup>2-</sup></b>
<b>Sr</b>	4.50	15.75	207	4.05	5.86	154	3.92	5.18	194	<b>Sr</b>
<b>Tb</b>	0.013	0.030	210	0.015	0.031	154	0.012	0.016	198	<b>Tb</b>
<b>Th</b>	0.202	0.367	204	0.227	0.411	153	0.196	0.249	193	<b>Th</b>
<b>Ti</b>	30	59	210	33	59	154	30	43	198	<b>Ti</b>
<b>Tm</b>	0.006	0.013	209	0.007	0.013	154	0.006	0.007	198	<b>Tm</b>
<b>U</b>	0.084	0.132	206	0.084	0.119	152	0.079	0.097	193	<b>U</b>
<b>V</b>	3.08	2.55	209	3.26	3.53	154	3.87	3.97	198	<b>V</b>
<b>W</b>	0.093	0.105	209	0.113	0.152	154	0.089	0.095	196	<b>W</b>
<b>Y</b>	0.18	0.31	210	0.20	0.31	154	0.18	0.24	198	<b>Y</b>
<b>Yb</b>	0.038	0.085	210	0.044	0.089	154	0.036	0.047	198	<b>Yb</b>
<b>Zn</b>	15	16	208	17	16	153	16	13	197	<b>Zn</b>

Table 4.19 Average concentrations within resolved clusters (Continued)

	Cluster 7			Cluster 8			Cluster 9			
	avg	sd	#	avg	sd	#	avg	sd	#	
<b>Al</b>	787	1203	110	824	2642	74	327	346	52	<b>Al</b>
<b>As</b>	0.81	0.91	110	0.77	0.53	74	0.82	0.95	52	<b>As</b>
<b>Au</b>	0.17	0.44	48	0.21	0.55	30	0.11	0.13	21	<b>Au</b>
<b>Ba</b>	9.45	8.77	109	10.39	19.69	74	6.31	4.96	52	<b>Ba</b>
<b>Be</b>	0.030	0.048	110	0.028	0.076	74	0.013	0.011	52	<b>Be</b>
<b>Bi</b>	0.106	0.091	108	0.130	0.118	73	0.105	0.146	49	<b>Bi</b>
<b>Ca</b>	1307	1799	109	1714	5747	73	720	460	52	<b>Ca</b>
<b>Cd</b>	0.18	0.10	109	0.22	0.15	74	0.21	0.17	52	<b>Cd</b>
<b>Ce</b>	0.88	1.22	109	0.65	0.63	73	0.41	0.39	52	<b>Ce</b>
<b>Cl</b>	1723	2442	104	1553	1724	71	2006	2452	48	<b>Cl</b>
<b>Co</b>	0.25	0.39	109	0.24	0.49	74	0.121	0.097	51	<b>Co</b>
<b>Cr</b>	4.49	8.93	106	3.48	3.49	67	3.34	3.92	46	<b>Cr</b>
<b>Cs</b>	0.112	0.104	109	0.134	0.192	74	0.077	0.053	52	<b>Cs</b>
<b>Dy</b>	0.070	0.101	105	0.102	0.402	67	0.034	0.041	41	<b>Dy</b>
<b>Er</b>	0.042	0.055	110	0.055	0.200	74	0.020	0.023	52	<b>Er</b>
<b>Eu</b>	0.019	0.028	79	0.029	0.116	50	0.010	0.011	23	<b>Eu</b>
<b>Fe</b>	406	638	108	392	1252	73	155	135	51	<b>Fe</b>
<b>Gd</b>	0.098	0.130	110	0.134	0.517	74	0.048	0.053	52	<b>Gd</b>
<b>Ge</b>	0.042	0.038	110	0.044	0.047	74	0.039	0.038	52	<b>Ge</b>
<b>Hf</b>	0.059	0.071	109	0.075	0.237	74	0.028	0.030	52	<b>Hf</b>
<b>Ho</b>	0.0142	0.0187	110	0.0187	0.0698	74	0.0067	0.0075	52	<b>Ho</b>
<b>In</b>	0.0052	0.0107	108	0.0054	0.0102	72	0.0046	0.0050	49	<b>In</b>
<b>K</b>	342	324	109	353	584	73	241	150	52	<b>K</b>
<b>La</b>	0.45	0.61	109	0.58	2.11	74	0.22	0.20	52	<b>La</b>
<b>Li</b>	0.63	0.83	109	0.64	1.62	74	0.37	0.25	52	<b>Li</b>



Table 4.19 Average concentrations within resolved clusters (Continued)

	Cluster 7			Cluster 8			Cluster 9			
	avg	sd	#	avg	sd	#	avg	sd	#	
<b>Lu</b>	0.0059	0.0078	110	0.0075	0.0269	74	0.0028	0.0031	52	<b>Lu</b>
<b>Mg</b>	536	524	109	552	1224	74	440	325	52	<b>Mg</b>
<b>Mn</b>	9.45	12.00	110	10.10	21.92	74	5.08	3.24	52	<b>Mn</b>
<b>Na</b>	1612	1911	109	1879	2364	74	2314	2814	52	<b>Na</b>
<b>Nd</b>	0.42	0.57	109	0.55	2.12	74	0.19	0.19	52	<b>Nd</b>
<b>NH<sub>4</sub><sup>+</sup></b>	1400	1369	60	652	691	38	989	1220	30	<b>NH<sub>4</sub><sup>+</sup></b>
<b>Ni</b>	2.97	4.44	110	2.08	1.42	73	1.58	1.02	50	<b>Ni</b>
<b>NO<sub>3</sub><sup>-</sup></b>	1501	1578	63	927	733	44	937	772	36	<b>NO<sub>3</sub><sup>-</sup></b>
<b>Pb</b>	47	37	110	47	44	74	46	40	50	<b>Pb</b>
<b>Pr</b>	0.110	0.147	109	0.143	0.535	74	0.052	0.050	52	<b>Pr</b>
<b>Pt</b>	0.0021	0.0022	47	0.0061	0.0109	34	0.0034	0.0053	22	<b>Pt</b>
<b>Rb</b>	0.86	1.02	110	0.90	1.91	74	0.51	0.30	52	<b>Rb</b>
<b>Sb</b>	0.70	0.45	109	0.66	0.45	74	0.69	0.61	52	<b>Sb</b>
<b>Se</b>	0.36	0.57	106	0.50	0.85	74	0.37	0.57	50	<b>Se</b>
<b>Sm</b>	0.089	0.117	110	0.119	0.449	74	0.042	0.044	52	<b>Sm</b>
<b>Sn</b>	0.64	0.53	110	0.70	0.67	74	0.61	0.48	52	<b>Sn</b>
<b>SO<sub>4</sub><sup>2-</sup></b>	7306	4461	108	6761	3748	73	7045	4323	51	<b>SO<sub>4</sub><sup>2-</sup></b>
<b>Sr</b>	4.02	4.75	109	6.18	24.64	73	2.49	1.88	52	<b>Sr</b>
<b>Tb</b>	0.013	0.017	110	0.017	0.067	74	0.006	0.007	52	<b>Tb</b>
<b>Th</b>	0.192	0.261	108	0.278	1.001	72	0.095	0.100	51	<b>Th</b>
<b>Ti</b>	39	64	110	40	153	74	14	11	52	<b>Ti</b>
<b>Tm</b>	0.006	0.008	109	0.008	0.028	74	0.003	0.003	52	<b>Tm</b>
<b>U</b>	0.073	0.078	108	0.100	0.292	74	0.047	0.040	50	<b>U</b>
<b>V</b>	3.10	2.55	109	2.63	3.10	74	2.26	1.95	52	<b>V</b>
<b>W</b>	0.067	0.047	109	0.089	0.104	73	0.078	0.093	50	<b>W</b>
<b>Y</b>	0.22	0.33	110	0.23	0.75	74	0.092	0.080	52	<b>Y</b>
<b>Yb</b>	0.038	0.051	110	0.050	0.178	74	0.019	0.021	52	<b>Yb</b>
<b>Zn</b>	12	9	109	13	11	74	11	10	52	<b>Zn</b>

Kruskal Wallis test was employed to test the whether the concentrations corresponding in one of the clusters is statistically different from rest of the clusters. This test is a non-parametric one implying that it does not depend on the distribution of the measured parameters and has been applied by many researchers after interpreting data allocated to sectors by cluster analysis (e.g., Brankov et al., 1998; Abdalmogith and Harrison, 2005). In this test, non-detect and tie (repeated) values can be handled. The null hypothesis  $H_0$  of the populations from which the '9' data set have been drawn have the same mean is tested against the alternative hypothesis  $H_A$  of at least one population has a mean larger or smaller than at least one other population. The null hypothesis is rejected if the calculated  $\chi^2$  value is larger than standard value obtained from related chi square distribution tables at a certain degrees of freedom and significance level.

Results of applied Kruskal-Wallis test were tabulated in Table 4.20. The null hypothesis was tested against the alternative hypothesis at 5 % significance level. As it can be deduced from Table 4.20 that all of the parameters are statistically different at least in one of the sectors with the exception of Pb,  $\text{NO}_3^-$ ,  $\text{NH}_4^+$ , Cl, W, Pt, Au, Ca and Cr. These elements seem not to vary from one to another at 95 % confidence interval.

As a major merker of sea salt, Cl is expected to be associated with Cluster 1 and other clusters moving over the Mediterranean Sea, Black Sea and Atlantic Ocean. Consequently, one may expect to see sharp differences between clusters including air masses passing over water bodies and lands. However, as stated before, no statistically difference was found between the clusters after the application of Kruskall Wallis test. Observed homogeneity of sea salt elements among the clusters is not clear, however, this situation can be attributed to location of the sampling point. The station in Antalya is located on the shore and air masses has to go over a sea at certain duration of their transport before reaching the Eastern Mediterranean no matter which cluster they are associated with. For instance, if they come from south and south west, they have to travel over the Mediterranean Sea. If they originate from West and Northwest, they have to cross the Eagen Sea. Air masses travel over the Black Sea if they come from North and Northeast. This can generate the homogeneity observed in concentrations of sea salt elements. It should also be noted that Cl is an important marker of biomass combustion (Lobert et al., 1999; Prodi et al., 2008) and it is released to atmosphere from traffic as well (Salvador et al., 2008). If these sources were significant, they would contribute to observed homogeneity of Cl concentrations over the clusters. Contribution of forest fires

and traffic on observed Cl concentrations is not quantified, but they are expected to be small compared to marine source.

Similar to Cl,  $\text{NO}_3^-$  and  $\text{NH}_4^+$  did not show any spatial variation. This scheme corresponding to  $\text{NO}_3^-$  and  $\text{NH}_4^+$  could be attributed to use of extensive fertilizer in greenhouses in the Mediterranean region of Turkey. Whatever the direction of air flow intercepted at the sampling station, it is likely to be contaminated with resuspended fertilizer.

Lead is a well known marker of gasoline. It was previously noted that we observe a decreasing trend in lead concentration recorded at our sampling site. The invariable Pb concentrations with changing sectors can be linked to local source of Pb very close to sampling site. Whether the air masses from Europe or Mediterranean or Black Sea intercepted at the sampling site they are polluted with the motor vehicle emissions from traffic activities close to station. Consequently, the influence of air mass origin on observed Pb concentrations is negligible.

Calcium and Cr are crustal elements while Cr is also released to the atmosphere from certain anthropogenic activities, such as smelters and steel production (Chow, 1995). It is well documented that the soil in most of the Mediterranean region is enriched with Cr and Ni (Kubilay and Saydam 1995; Güllü et al., 1998; Güvenç et al., 2003). The lack of variation in the concentrations of these elements can also be due to local sources around the station. Air masses intercepted at sampling point picks up local soil wherever they come from, which leads to statistically insignificant variations in their concentrations with respect to sectors.

There are many non-detect values for Au, Pt, U and W in our data set. Although Kruskal-Wallis test can accommodate non-detect values, there is no published information on the percent of non-detects which can be handled in this test. Accordingly, considerable amount of non-detect may lead to invariable spatial concentrations of this aforementioned elements.

Table 4.20 Results of Kruskal-Wallis Test applied on the clusters

	$\chi^2$ calculated	df	p	$\chi^2$ critical at 95 % conf interval
Al	33.348971	8	$5.33 \cdot 10^{-5}$	15.51
As	23.609818	8	0.002663	15.51
<b>Au</b>	<b>12.26627</b>	<b>8</b>	<b>0.13971</b>	15.51
Ba	16.72237	8	0.033133	15.51
Be	24.392259	8	0.001969	15.51
Bi	19.11804	8	0.01424	15.51
<b>Ca</b>	<b>7.60761</b>	<b>8</b>	<b>0.47271</b>	<b>15.51</b>
Cd	36.302243	8	$1.55 \cdot 10^{-5}$	15.51
Ce	26.538365	8	0.000849	15.51
<b>Cl</b>	<b>13.09774</b>	<b>8</b>	<b>0.10853</b>	15.51
Co	17.356515	8	0.026604	15.51
<b>Cr</b>	<b>10.88257</b>	<b>8</b>	<b>0.20844</b>	<b>15.51</b>
Cs	35.380966	8	$2.28 \cdot 10^{-5}$	15.51
Dy	25.509649	8	0.001274	15.51
Er	24.790343	8	0.001687	15.51
Eu	21.304275	8	0.006382	15.51
Fe	41.322503	8	$1.81 \cdot 10^{-6}$	15.51
Gd	22.534931	8	0.004016	15.51
Ge	8.1181608	8	0.422014	15.51
Hf	20.276173	8	0.00934	15.51
Ho	24.487742	8	0.001897	15.51
In	16.162069	8	0.040118	15.51
K	23.323008	8	0.002973	15.51
La	24.549804	8	0.001852	15.51
Li	17.414928	8	0.026067	15.51
Lu	25.049603	8	0.001525	15.51
Mg	20.309426	8	0.009227	15.51
Mn	44.870488	8	$3.89 \cdot 10^{-7}$	15.51
Na	24.710206	8	0.00174	15.51
Nd	26.154867	8	0.000988	15.51
<b>NH<sub>4</sub><sup>+</sup></b>	<b>6.246269</b>	<b>8</b>	<b>0.61967</b>	15.51
Ni	30.802337	8	0.000152	15.51
<b>NO<sub>3</sub><sup>-</sup></b>	<b>6.539823</b>	<b>8</b>	<b>0.58699</b>	15.51
<b>Pb</b>	<b>12.69942</b>	<b>8</b>	<b>0.12262</b>	15.51
Pr	26.378202	8	0.000905	15.51
<b>Pt</b>	<b>7.393902</b>	<b>8</b>	<b>0.49479</b>	15.51
Rb	37.095209	8	$1.11 \cdot 10^{-5}$	15.51
Sb	21.754772	8	0.005391	15.51
Se	44.133431	8	$5.37 \cdot 10^{-7}$	15.51

Table 4.20 Results of Kruskal-Wallis Test applied on the clusters (Continued)

	$\chi^2_{\text{calculated}}$	df	p	$\chi^2_{\text{critical}}$ at 95 % conf interval
Sm	25.016452	8	0.001545	15.51
Sn	31.839634	8	$9.95 \cdot 10^{-5}$	15.51
SO <sub>4</sub> <sup>2-</sup>	61.041903	8	$2.91 \cdot 10^{-10}$	15.51
Sr	19.470408	8	0.012537	15.51
Tb	25.11604	8	0.001486	15.51
Th	26.104392	8	0.001008	15.51
Ti	34.366698	8	$3.49 \cdot 10^{-5}$	15.51
Tm	22.159073	8	0.00463	15.51
<b>U</b>	<b>14.67224</b>	<b>8</b>	<b>0.06584</b>	15.51
V	45.945566	8	$2.43 \cdot 10^{-7}$	15.51
W	24.833902	8	0.001659	15.51
Y	32.80042	8	$6.69 \cdot 10^{-5}$	15.51
Yb	22.52313	8	0.004034	15.51
Zn	36.421965	8	$1.47 \cdot 10^{-5}$	15.51

#### 4.5.1.2.2. Comparison of Cluster Analysis and Residence Time Analysis

Two different methodologies applied here to find the relation between observed levels of pollutants with varying direction in the air masses intercepted at our sampling location, namely, cluster analysis and residence time analysis.

In residence time analysis, we divided the study region into six main sectors and we assigned trajectories to a particular sector provided that trajectory spend more than 80 % of time in that particular sector. The constraint set here is somewhat subjective since different limits was used in different studies. In addition to this, dividing the study region into six sectors by considering the possible areas affecting Antalya region was also a subjective decision. However, cluster analysis is a statistical technique which does not involve the decisions of the user as compared to residence time analysis and based on the classification of trajectories according to their speed and direction.

In residence time analysis, 15 % of the trajectories were associated with South direction (which is actually combination of S, SE and SW sectors). However, 13.1 % of trajectories

were allocated to cluster 1, covering great portion of the Mediterranean Sea, alone. With the exception of Cluster 5 and 8, all clusters have trajectories passing over Mediterranean Sea. Trajectories assigned to Cluster number 7 are 11 % of total trajectories, while percentage of trajectories allocated to Eastern sector accounts for 7 % of trajectories in residence time analysis. Consequently, one can conclude that airflow frequencies obtained from these two methods are slightly different since high frequencies were found for Eastern and Southern sectors in cluster analysis. Similar finding was also put forward by Koçak (2001) and attributed this difference to classification methodology of trajectories applied in two methods.

#### **4.5.2. Correlations between Parameters**

A detailed discussion on probable sources of pollutants affecting Eastern Mediterranean atmosphere will be presented later in this manuscript. Calculation of binary correlations between elements and ions is a preliminary step for such an apportionment, and a useful tool to investigate characteristics of data set. Correlations between the elements measured in the atmosphere indicate either they are generated by the same source before emitted to the atmosphere or they have similar transport pattern in the atmosphere prior to sampling. In urban atmosphere, high correlation between parameters indicate that they are produced by the same mechanism, because the distance between source and receptor is small and transport over such a short distance do not affect apportionment. Nevertheless, this is not true in rural atmosphere. Pollutants were transported over long distances before sampling. During their transport, they are scavenged out from the atmosphere at certain extent or air parcel is reloaded by a secondary emitter on the way to the sampling station. Consequently, strong correlation observed for the species of samples collected at rural station does not necessarily mean that they are generated by the same mechanisms before released to the atmosphere and can be an artifact of similar transport mechanisms.

Binary correlations of the measured aerosol variables were calculated and results were given in Table 4.21. Only statistically significant non-zero correlations, for which significance level ( $p$ ) is smaller than 0.05, at 95 % confidence level was shown in Table 4.21.

As expected, crustal elements (Al, Mn, Ti, Fe and rare earths, for example, Ce, Pr, Nd, Sm, Eu, Gd, Tb, Dy, Ho, Er, Tm, Yb and Lu) are strongly correlated ( $r > 0.9$ ) between one another, implying that they are primarily originate from soil either local or remote. In addition to this, Mg, K and Ca is significantly correlated among themselves, having  $r > 0.7$ . Correlations of Co, V, Zn, Ni and Cr with purely crustal elements like Al, Ti and Fe are relatively low, with correlation coefficients ( $r$ ) around 0.4, which is due to fact that these elements have also anthropogenic sources.

Correlations between Na, Cl and Mg is considerably high ( $r > 0.7$ ). These elements are expected to be correlated with each other, because they are produced by bubble bursting at the sea surface. Strontium and K are also sea salt markers, while Sr are emitted from various other sources including natural soil, paved road dust, and motor vehicle emissions (Chow, 1995), whereas soil and biomass burning are other sources of K (Watson and Chow, 2001). However, very low correlations were observed for these elements and Na, Cl and Mg.

Poor correlation was obtained between Pb and other anthropogenic elements like V, Mn, Zn and Cd. Although correlation between these elements are statistically significant at 95% confidence level, calculated correlation coefficients varies between 0.32 and 0.40, which is fairly low, for this group of elements. However, correlation of Pb with Sn and Sb is relatively high,  $r > 0.55$ . In addition, Cs, Ba, Li and K have correlation coefficients around 0.3 with Pb implying that Pb transported to atmosphere on the soil particles.

Sulfate has moderate correlation ( $r > 0.5$ ) with V, Zn and Cd. Vanadium and Zn are mainly released to the atmosphere from oil combustion and smelters. Consequently, moderate correlation of  $\text{SO}_4^{2-}$  with this elements indicated that they are generated from combustion activities. Sulfate showed poor correlation ( $r \sim 0.3$ ) with other anthropogenic elements like Sb and Pb.

Secondary pollutants, that is,  $\text{SO}_4^{2-}$ ,  $\text{NO}_3^-$  and  $\text{NH}_4^+$  ions are moderately correlated with each other ( $r < 0.4$ ). They also showed weak correlations with other anthropogenic elements. Correlation among these secondary pollutants can be explained with the similar chemical reactions that they undergo in the atmosphere.

Table 4.21 Binary correlation matrix of measured elements (p< 0.05 indicated only)

	<b>Li</b>										
<b>Be</b>	0.67	<b>Be</b>									
<b>Na</b>	0.19	0.13	<b>Na</b>								
<b>Mg</b>	0.73	0.51	0.70	<b>Mg</b>							
<b>Al</b>	0.93	0.69	0.14	0.72	<b>Al</b>						
<b>K</b>	0.84	0.63	0.37	0.82	0.84	<b>K</b>					
<b>Ca</b>	0.85	0.62	0.17	0.83	0.86	0.81	<b>Ca</b>				
<b>Ti</b>	0.91	0.68	0.12	0.72	0.98	0.82	0.89	<b>Ti</b>			
<b>V</b>	0.59	0.43	0.15	0.42	0.58	0.69	0.48	0.56	<b>V</b>		
<b>Cr</b>	0.40	0.31		0.32	0.36	0.48	0.41	0.38	0.44	<b>Cr</b>	
<b>Mn</b>	0.90	0.67	0.11	0.69	0.93	0.90	0.87	0.93	0.71	0.51	
<b>Fe</b>	0.93	0.69	0.13	0.72	0.98	0.86	0.89	0.98	0.62	0.42	
<b>Co</b>	0.67	0.57		0.58	0.73	0.71	0.72	0.77	0.53	0.53	
<b>Ni</b>	0.33	0.26		0.26	0.32	0.45	0.33	0.34	0.52	0.70	
<b>Zn</b>	0.21	0.16	0.08	0.17	0.21	0.35	0.19	0.19	0.54	0.24	
<b>Ge</b>	0.29	0.33		0.21	0.32	0.39	0.33	0.33	0.36	0.37	
<b>As</b>	0.23	0.31	-0.07	0.11	0.23	0.35	0.23	0.22	0.39	0.40	
<b>Se</b>			0.07	0.07		0.17			0.27	0.11	
<b>Rb</b>	0.91	0.69	0.14	0.67	0.93	0.92	0.83	0.92	0.73	0.48	
<b>Sr</b>	0.81	0.58	0.34	0.90	0.81	0.81	0.94	0.84	0.46	0.34	
<b>Y</b>	0.94	0.69	0.13	0.72	0.98	0.85	0.89	0.98	0.60	0.38	
<b>Cd</b>	0.20	0.20		0.12	0.17	0.38	0.18	0.16	0.58	0.39	
<b>In</b>								0.08		0.10	
<b>Sn</b>	0.36	0.27	0.10	0.22	0.30	0.47	0.28	0.27	0.60	0.42	
<b>Sb</b>	0.30	0.23	0.06	0.16	0.23	0.40	0.22	0.20	0.48	0.37	
<b>Cs</b>	0.71	0.64	0.07	0.50	0.72	0.79	0.66	0.70	0.68	0.53	
<b>Ba</b>	0.86	0.63	0.09	0.62	0.84	0.78	0.77	0.81	0.56	0.38	
<b>La</b>	0.93	0.72	0.15	0.73	0.97	0.82	0.89	0.96	0.54	0.34	
<b>Hf</b>	0.87	0.64	0.14	0.71	0.88	0.77	0.85	0.88	0.50	0.34	
<b>W</b>	0.49	0.37	0.13	0.43	0.45	0.52	0.46	0.42	0.38	0.33	
<b>Pt</b>	0.26	0.20	0.15	0.23	0.25	0.31	0.25	0.24	0.22	0.15	
<b>Au</b>	0.13	0.14		0.09	0.16	0.16	0.13	0.15	0.14	0.15	
<b>Pb</b>	0.33	0.23	0.11	0.20	0.26	0.34	0.21	0.19	0.33	0.20	
<b>Bi</b>	0.12	0.12		0.06	0.10	0.18	0.09	0.10	0.24	0.14	
<b>Ce</b>	0.94	0.65	0.13	0.70	0.96	0.82	0.82	0.94	0.54	0.36	
<b>Pr</b>	0.89	0.66	0.14	0.70	0.91	0.77	0.84	0.91	0.52	0.31	
<b>Nd</b>	0.94	0.69	0.15	0.74	0.96	0.81	0.89	0.96	0.53	0.32	
<b>Sm</b>	0.94	0.68	0.16	0.74	0.95	0.81	0.89	0.94	0.53	0.33	
<b>Eu</b>	0.94	0.70	0.20	0.78	0.95	0.81	0.89	0.94	0.49	0.32	
<b>Gd</b>	0.93	0.67	0.16	0.75	0.94	0.80	0.88	0.93	0.50	0.31	
<b>Tb</b>	0.94	0.66	0.15	0.75	0.94	0.80	0.89	0.93	0.51	0.32	
<b>Dy</b>	0.94	0.67	0.17	0.78	0.94	0.80	0.88	0.93	0.49	0.31	
<b>Ho</b>	0.94	0.66	0.15	0.76	0.94	0.81	0.89	0.93	0.51	0.32	
<b>Er</b>	0.94	0.66	0.15	0.75	0.94	0.80	0.88	0.93	0.52	0.32	
<b>Tm</b>	0.94	0.67	0.15	0.75	0.94	0.81	0.88	0.93	0.51	0.32	



Table 4.21 Binary correlation matrix of measured elements (p< 0.05 indicated only)  
(Continued)

	<b>Li</b>	<b>Be</b>	<b>Na</b>	<b>Mg</b>	<b>Al</b>	<b>K</b>	<b>Ca</b>	<b>Ti</b>	<b>V</b>	<b>Cr</b>
<b>Yb</b>	0.94	0.66	0.15	0.76	0.94	0.81	0.88	0.93	0.51	0.32
<b>Lu</b>	0.94	0.66	0.15	0.76	0.94	0.81	0.88	0.92	0.51	0.32
<b>Th</b>	0.93	0.72	0.16	0.72	0.95	0.81	0.87	0.94	0.54	0.33
<b>U</b>	0.89	0.70	0.20	0.73	0.88	0.80	0.87	0.86	0.51	0.36
<b>Cl</b>	0.08		0.72	0.41		0.20	0.09	0.05		
<b>SO<sub>4</sub></b>	0.24	0.13	0.14	0.22	0.18	0.33	0.15	0.16	0.63	0.14
<b>NO<sub>3</sub></b>	0.25	0.10		0.09	0.22	0.24	0.16	0.21	0.40	0.15
<b>NH<sub>4</sub></b>			-0.08		0.10	0.09		0.08	0.22	

Table 4.21 Binary correlation matrix of measured elements (p< 0.05 indicated only)  
(Continued)

	<b>Mn</b>										
<b>Fe</b>	0.96	<b>Fe</b>									
<b>Co</b>	0.79	0.78	<b>Co</b>								
<b>Ni</b>	0.48	0.39	0.50	<b>Ni</b>							
<b>Zn</b>	0.37	0.24	0.27	0.36	<b>Zn</b>						
<b>Ge</b>	0.43	0.37	0.61	0.29	0.25	<b>Ge</b>					
<b>As</b>	0.39	0.28	0.33	0.37	0.34	0.53	<b>As</b>				
<b>Se</b>	0.13	0.06	0.06	0.19	0.23	0.10	0.30	<b>Se</b>			
<b>Rb</b>	0.98	0.95	0.76	0.46	0.36	0.42	0.37	0.11	<b>Rb</b>		
<b>Sr</b>	0.79	0.82	0.65	0.26	0.16	0.26	0.15		0.77	<b>Sr</b>	
<b>Y</b>	0.95	0.99	0.75	0.35	0.22	0.34	0.23		0.95	0.85	<b>Y</b>
<b>Cd</b>	0.38	0.22	0.42	0.38	0.59	0.55	0.50	0.17	0.38	0.15	0.20
<b>In</b>			0.19	0.06							
<b>Sn</b>	0.47	0.33	0.31	0.41	0.57	0.25	0.44	0.13	0.47	0.22	0.31
<b>Sb</b>	0.38	0.27	0.24	0.34	0.40	0.26	0.44	0.16	0.38	0.15	0.24
<b>Cs</b>	0.84	0.75	0.81	0.47	0.43	0.64	0.49	0.08	0.85	0.58	0.73
<b>Ba</b>	0.83	0.83	0.63	0.32	0.27	0.29	0.23		0.84	0.71	0.84
<b>La</b>	0.90	0.95	0.70	0.28	0.19	0.30	0.20		0.91	0.86	0.97
<b>Hf</b>	0.83	0.87	0.71	0.27	0.19	0.32	0.15		0.83	0.82	0.90
<b>W</b>	0.50	0.44	0.35	0.25	0.24	0.20	0.25		0.50	0.44	0.45
<b>Pt</b>	0.30	0.26	0.23	0.12	0.21	0.21	0.17		0.31	0.23	0.26
<b>Au</b>	0.18	0.17	0.15	0.12		0.12	0.18		0.20	0.11	0.17
<b>Pb</b>	0.32	0.23	0.18	0.21	0.40	0.13	0.26		0.32	0.14	0.23
<b>Bi</b>	0.18	0.11	0.24	0.16	0.32	0.26	0.26		0.18	0.05	0.11
<b>Ce</b>	0.87	0.94	0.67	0.35	0.22	0.27	0.20		0.89	0.78	0.96
<b>Pr</b>	0.84	0.90	0.65	0.25	0.18	0.27	0.17		0.85	0.82	0.92
<b>Nd</b>	0.88	0.94	0.68	0.26	0.18	0.28	0.17		0.89	0.87	0.97
<b>Sm</b>	0.87	0.93	0.67	0.25	0.18	0.28	0.17		0.88	0.87	0.96
<b>Eu</b>	0.87	0.92	0.68	0.21	0.10	0.32	0.18		0.88	0.88	0.95
<b>Gd</b>	0.85	0.91	0.66	0.24	0.17	0.27	0.15		0.86	0.87	0.94
<b>Tb</b>	0.86	0.92	0.67	0.24	0.18	0.27	0.15		0.87	0.87	0.95
<b>Dy</b>	0.85	0.91	0.66	0.23	0.15	0.29	0.14		0.86	0.87	0.94
<b>Ho</b>	0.86	0.92	0.67	0.25	0.18	0.27	0.15		0.87	0.86	0.94
<b>Er</b>	0.86	0.92	0.67	0.25	0.18	0.27	0.15		0.87	0.86	0.94
<b>Tm</b>	0.86	0.92	0.67	0.25	0.18	0.27	0.15		0.87	0.86	0.94
<b>Yb</b>	0.86	0.92	0.67	0.25	0.18	0.27	0.15		0.87	0.86	0.94
<b>Lu</b>	0.86	0.92	0.67	0.25	0.18	0.27	0.15		0.86	0.86	0.94
<b>Th</b>	0.88	0.93	0.67	0.26	0.19	0.29	0.19		0.89	0.84	0.95
<b>U</b>	0.84	0.86	0.62	0.26	0.22	0.29	0.24		0.84	0.84	0.87
<b>Cl</b>					-0.11	-0.09	-0.17				0.21
<b>SO<sub>4</sub></b>	0.30	0.19	0.21	0.31	0.55	0.16	0.21	0.19	0.31	0.17	0.20
<b>NO<sub>3</sub></b>	0.25	0.23	0.21	0.22	0.20	0.10		0.08	0.26	0.08	0.24
<b>NH<sub>4</sub></b>	0.11	0.08	0.08	0.14	0.14		0.10	0.11	0.10		0.08

Table 4.21 Binary correlation matrix of measured elements (p< 0.05 indicated only)  
(Continued)

	<b>Cd</b>										
<b>In</b>	0.10	<b>In</b>									
<b>Sn</b>	0.64	0.04	<b>Sn</b>								
<b>Sb</b>	0.50		0.62	<b>Sb</b>							
<b>Cs</b>	0.64		0.56	0.46	<b>Cs</b>						
<b>Ba</b>	0.28		0.44	0.37	0.74	<b>Ba</b>					
<b>La</b>	0.17		0.31	0.23	0.71	0.85	<b>La</b>				
<b>Hf</b>	0.21		0.34	0.25	0.69	0.82	0.92	<b>Hf</b>			
<b>W</b>	0.36		0.46	0.45	0.51	0.54	0.48	0.49	<b>W</b>		
<b>Pt</b>	0.24		0.30	0.24	0.29	0.29	0.25	0.27	0.20	<b>Pt</b>	
<b>Au</b>	0.11		0.15	0.11	0.18	0.13	0.14	0.13	0.25	0.19	<b>Au</b>
<b>Pb</b>	0.35		0.61	0.55	0.44	0.44	0.26	0.29	0.41	0.18	0.08
<b>Bi</b>	0.51	0.29	0.39	0.27	0.35	0.24	0.12	0.17	0.25	0.14	
<b>Ce</b>	0.21		0.36	0.30	0.69	0.84	1.00	0.89	0.47	0.21	0.13
<b>Pr</b>	0.16		0.29	0.21	0.67	0.81	1.00	0.88	0.45	0.22	0.13
<b>Nd</b>	0.15		0.29	0.22	0.70	0.86	1.00	0.93	0.48	0.24	0.12
<b>Sm</b>	0.17		0.31	0.24	0.70	0.86	0.99	0.93	0.50	0.24	0.12
<b>Eu</b>	0.13	0.08	0.24	0.22	0.69	0.86	0.99	0.92	0.48	0.29	0.10
<b>Gd</b>	0.14		0.29	0.22	0.68	0.85	0.98	0.93	0.49	0.23	0.11
<b>Tb</b>	0.15		0.29	0.22	0.68	0.85	0.98	0.93	0.49	0.23	0.11
<b>Dy</b>	0.13		0.26	0.20	0.68	0.85	0.98	0.93	0.48	0.24	0.10
<b>Ho</b>	0.15		0.30	0.23	0.69	0.86	0.98	0.93	0.50	0.24	0.10
<b>Er</b>	0.16		0.30	0.24	0.69	0.86	0.98	0.93	0.50	0.24	0.11
<b>Tm</b>	0.16		0.31	0.24	0.69	0.86	0.98	0.93	0.50	0.24	0.11
<b>Yb</b>	0.16		0.31	0.24	0.69	0.87	0.98	0.93	0.50	0.24	0.11
<b>Lu</b>	0.16		0.31	0.24	0.69	0.86	0.98	0.93	0.50	0.23	0.11
<b>Th</b>	0.17		0.33	0.25	0.72	0.87	0.99	0.92	0.51	0.25	0.14
<b>U</b>	0.24		0.40	0.30	0.73	0.86	0.93	0.87	0.59	0.24	0.14
<b>Cl</b>	-0.11		-0.08	-0.08	-0.08		0.06	0.07			
<b>SO<sub>4</sub></b>	0.50		0.47	0.31	0.37	0.27	0.18	0.20	0.24		
<b>NO<sub>3</sub></b>	0.22		0.21	0.23	0.23	0.28	0.24	0.28	0.13		
<b>NH<sub>4</sub></b>					0.09				-0.07		

Table 4.21 Binary correlation matrix of measured elements (p< 0.05 indicated only)  
(Continued)

	<b>Pb</b>										
<b>Bi</b>	0.35	<b>Bi</b>									
<b>Ce</b>	0.35	0.14	<b>Ce</b>								
<b>Pr</b>	0.25	0.11	1.00	<b>Pr</b>							
<b>Nd</b>	0.27	0.11	1.00	1.00	<b>Nd</b>						
<b>Sm</b>	0.29	0.12	0.99	0.95	1.00	<b>Sm</b>					
<b>Eu</b>	0.23	0.08	0.98	0.99	0.99	1.00	<b>Eu</b>				
<b>Gd</b>	0.29	0.12	0.98	0.99	0.99	1.00	1.00	<b>Gd</b>			
<b>Tb</b>	0.30	0.12	0.98	0.95	0.99	1.00	1.00	1.00	<b>Tb</b>		
<b>Dy</b>	0.27	0.11	0.98	0.94	0.99	1.00	1.00	1.00	1.00	<b>Dy</b>	
<b>Ho</b>	0.31	0.13	0.98	0.94	0.99	1.00	1.00	1.00	1.00	1.00	<b>Ho</b>
<b>Er</b>	0.31	0.13	0.98	0.94	0.99	1.00	0.99	1.00	1.00	1.00	1.00
<b>Tm</b>	0.31	0.13	0.98	0.94	0.99	1.00	0.99	1.00	1.00	1.00	1.00
<b>Yb</b>	0.32	0.14	0.98	0.94	0.99	1.00	0.99	1.00	1.00	1.00	1.00
<b>Lu</b>	0.32	0.13	0.98	0.94	0.99	0.99	0.99	1.00	1.00	1.00	1.00
<b>Th</b>	0.30	0.14	0.98	0.94	0.99	0.99	0.99	0.98	0.98	0.98	0.98
<b>U</b>	0.40	0.18	0.89	0.93	0.93	0.94	0.95	0.93	0.93	0.93	0.94
<b>Cl</b>	-0.11	-0.11	0.06		0.06	0.06	0.14	0.06	0.06	0.09	0.06
<b>SO<sub>4</sub></b>	0.39	0.34	0.24	0.18	0.19	0.19	0.10	0.19	0.20	0.17	0.20
<b>NO<sub>3</sub></b>	0.07	0.15	0.24	0.32	0.24	0.24	0.18	0.24	0.24	0.21	0.24
<b>NH<sub>4</sub></b>	-0.07			0.09							

Table 4.21 Binary correlation matrix of measured elements (p< 0.05 indicated only)  
(Continued)

	<b>Er</b>									
<b>Tm</b>	1.00	<b>Tm</b>								
<b>Yb</b>	1.00	1.00	<b>Yb</b>							
<b>Lu</b>	1.00	1.00	1.00	<b>Lu</b>						
<b>Th</b>	0.98	0.98	0.98	0.98	<b>Th</b>					
<b>U</b>	0.94	0.94	0.94	0.94	0.95	<b>U</b>				
<b>Cl</b>	0.06	0.06	0.06	0.06	0.06		<b>Cl</b>			
<b>SO<sub>4</sub></b>	0.20	0.20	0.21	0.20	0.20	0.22		<b>SO<sub>4</sub></b>		
<b>NO<sub>3</sub></b>	0.24	0.24	0.24	0.24	0.25	0.15	0.14	0.43	<b>NO<sub>3</sub></b>	
<b>NH<sub>4</sub></b>								0.34	0.42	

### 4.5.3. Enrichment Factors

Like correlation analysis, calculation of Enrichment Factor (EF) is a preliminary step in assignment of sources using aerosol chemical composition. Crustal enrichment factor calculations provide information whether measured concentration of an element can be accounted for by crustal particles in the atmosphere. This is an important question to answer, because crustal material is a ubiquitous component of aerosol and contributes to the concentrations of many lithophilic elements. Enrichment factor calculation is not limited to crustal component. Similar calculations can also provide information on contribution of sea salt on measured concentrations of elements, with a proper selection of marker element. Enrichment Factor (EF) can be defined as the ratio of atmospheric concentration of element to a reference element is compared to same ratio in geological or marine sample (Watson et al., 2008). This definition can be formulated in the following equation:

$$EF = \frac{(C_x / C_{Al})_{sample}}{(C_x / C_{Al})_{reference}} \quad (4.12)$$

In geological samples, Al, Sc, and Fe commonly are taken as reference element since these elements are most abundant ones in earth's crust. In addition, Al can be reliably measured by various analytical techniques. Sodium is generally used as reference element for marine samples. Though, Cl is also marker element of sea salt, it is not preferred in calculating enrichment factors due to its high volatility. Denominator in above equation is the ratio of element under consideration to reference element in the crustal or sea water composition. Generally global compilations of crustal composition, such as those given in Mason (1966), Taylor (1964), Turekian and Wedepohl (1971), and measured concentrations of elements in sea water (e.g., Goldberg, 1963). Elements for which crustal material is the only source have  $EF_c = 1.0$ . Deviation from unity indicates non-crustal sources of that element.

In this section of this study, both crustal and marine EF of the measured aerosol parameters was discussed.

#### **4.5.3.1. Crustal Enrichment Factor**

Crustal enrichment factors of elements and ions measured in this study were calculated and results are given in Figure 4.56.

As pointed before, if crustal enrichment factor ( $EF_c$ ) for a particular element is close to 1, then crustal particles are assumed to be its main source in the atmosphere. Deviations from  $EF_c = 1.0$  indicate contribution(s) of non-crustal source(s) on measured concentrations of that element. Nevertheless, elements with  $EF_c$ 's between 1 and 10 are not considered enriched, because such slight enrichments may arise from differences in chemical compositions of global reference soil compilations used in calculating  $EF_s$  and that of local soil actually affecting samples. Elements are classified as moderately enriched when their  $EF_c$ 's are between 10 and 100, and they are considered highly enriched when  $EF_c$  is greater than 100 (Al-Momani, 2003).

Based on the criteria discussed in the previous paragraph, elements between Y and Ge in Figure 4.56 are not enriched. Elements Ca, Mg, U, Cs, Ni and Cr are in transition. Their  $EF_c$ s are  $<10$ , but close to be classified as moderately enriched. Slightly  $<10$   $EF_c$  values of these may both indicate different soil composition or contribution of non crustal sources. Relatively high  $EF_c$  of U is probably due to differences in soil compositions, because there is no well documented non- crustal source for U. For Ca, Ni and Cr, probably both differences in soil composition and non-crustal sources contribute to their close-to-10  $EF_c$ 's. It is well documented that Saharan Dust affecting region and local dust in the Mediterranean region have unusually high Ca concentration (Özsoy and Saydam, 2000; Kubilay and Saydam, 1995; Koçak et al., 2007). On the other hand, sea salt also affects Ca concentrations when it is measured at stations close to sea. The same argument is also valid for Cr and Ni. Concentrations of these two elements in soil on the Mediterranean coast of Turkey is high (Koçak et al., 2004; Güllü et al., 1998; [www.mta.gov.tr/madenler/turmaden/ic.asp](http://www.mta.gov.tr/madenler/turmaden/ic.asp); Kubilay and Saydam, 1995) and also there are anthropogenic sources with high Cr and Ni emissions (smelters, steel production, metallurgical industry for Cr and oil combustion for Ni). (Gordan, 1980; Chow, 1995) Relatively high  $EF_c$  of Mg and Cs is probably due to contribution of sea salt (Koçak et al., 2007; Tuncel, 1989).

Among remaining elements, Ge, Na, In, Ta, Sn and Zn are moderately and Sn, W, As, Cd, Pb, Sb, Se, S, Cl and Au are highly enriched. Among this group of elements enrichments of Na and Cl are due to contribution of sea salt on their concentrations. Large difference between  $EF_c$ 's of Na and Cl is due to higher concentration of Na in soil. The calculated EF values for Au, S, Se, Sb and Pb are between 1000 and 10000. However, EF for As, W, and Cd lie between 100 and 1000. Chlorine has also EF value above 1000, high enrichment of this element with respect to soil is due to release of it to atmosphere mainly from marine environment.

As pointed earlier in this section, elements with  $EF_c$ 's  $<10$  are not considered enriched because slight enrichments can be an artifact due to different compositions of average soil used in  $EF_c$  calculations and local soil that actually affect samples. However, Slight enrichments of elements may also be due to contribution of non-crustal sources.  $EF_c - Al$  diagrams can be a useful tool to differentiate between these two groups of elements.

In  $EF_c - Al$  diagrams, as its name implies,  $EF_c$  of an element is plotted against Al concentration. If an element has only crustal source, then its  $EF_c$  will be independent of Al concentration. In this case the plot of  $EF_c$  vs Al concentration will be a horizontal line. If the concentration of that crustal element in average soil used in  $EF_c$  calculation is similar to its concentration in actual soil affecting samples, the line will pass through  $EF_c = 1.0$ . However, if the concentration of the crustal element in average soil is different from that in actual soil, the line will pass through a different  $EF_c$  value, but it will still be a horizontal line.

Enrichment factor – Al diagrams are prepared for all elements with  $EF_c < 10$ .  $EF_c - Al$  plots for selected elements in this group are given in Figures 4.57 – 4.60. Based on these diagrams, elements with  $EF_c < 10$  can be divided into following three groups:

1. The first group consisted of Li, Mg, Cr, U, V, K, Be, U, Mn, Ni, and Sr. These elements have high  $EF_c$  values at low Al concentrations, but  $EF_c$  values decrease to 1 with increasing Al concentrations indicating that these elements have sources other than soil. For instance, Mg and Sr are also associated with sea salt, V is emitted various man made activities like oil and coal burning plants (Chow, 1996). However, these sources are masked by soil at typical soil loadings in the atmosphere.  $EF_c$ -Al diagram for selected elements in this group are depicted in Figure 4.57.

2. The second group consists of Fe, Co, Dy, Be, Hf, Co, and Eu. Elements in this group have  $EF_c$  values close to unity at all Al concentrations. The only source of these elements in Eastern Mediterranean atmosphere is the crustal material.  $EF_c$ -Al diagram for selected elements in this group are depicted in Figure 4.58.
  
3. The third group consisted of, Ce, Sm, Tb, Lu, Nd, Gd, La, and Y. These elements have  $EF_c$  values higher than unity at very low Al concentrations indicating there are non-crustal sources for these elements. However, these sources are so weak that they show typical crustal behavior at Al concentrations  $>100 \mu\text{g m}^{-3}$ . In other words, these weak sources are masked by crustal source at Al  $>100 \mu\text{g m}^{-3}$ . For the practical objectives of this study, these group 3 elements can be combined with group two elements and considered as purely crustal elements.  $EF_c$ -Al diagram for selected elements were depicted in Figure 4.59. Another point that should be noted in this figure is that horizontal portions (after Al  $>100 \mu\text{g m}^{-3}$ ) do not pass through  $EF_c = 1.0$  for La and Ce, but passes through  $EF_c = 1.0$  for Ti. This behavior observed in La and Ce is typical for all rare earth elements and shows that rare earth composition of soil affecting collected samples at our station is different from the rare earth composition in Masons (1966) global average soil composition. This characteristics of rare earth elements is used to differentiate between local soil and Saharan dust as will be discussed in detail later in the manuscript.

In addition to slightly enriched elements, the  $EF_c$ -Al diagram was also constructed for highly enriched elements and is depicted for some of the selected elements in Figure 4.60. High enrichment of these parameters as compared to crustal contribution revealed that they have anthropogenic in origin. Other pollutants such as Se, Sb and Sn have similar trends with these pollutants. As indicated in  $EF_c$ -Al diagram, high  $EF_c$  values observed even if at high concentrations of Al. They all show a clear decrease in their  $EF_c$ 's with increasing Al concentration. Some of these pollutants are locally produced but some of them are long range transported to our sampling station from different regions.



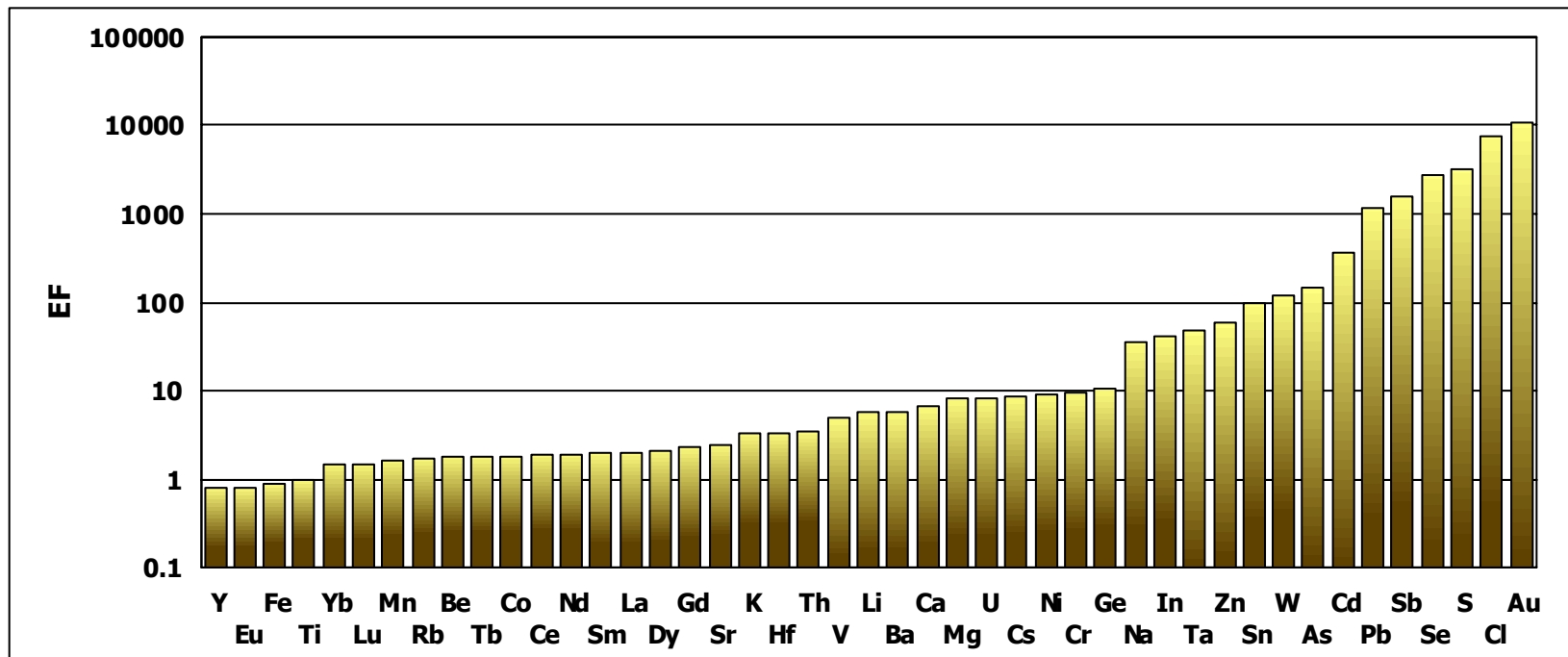


Figure 4.56 Crustal enrichment factors of elements

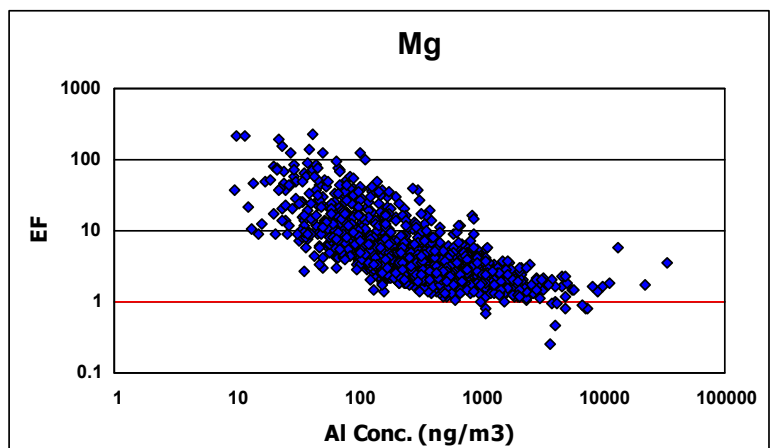
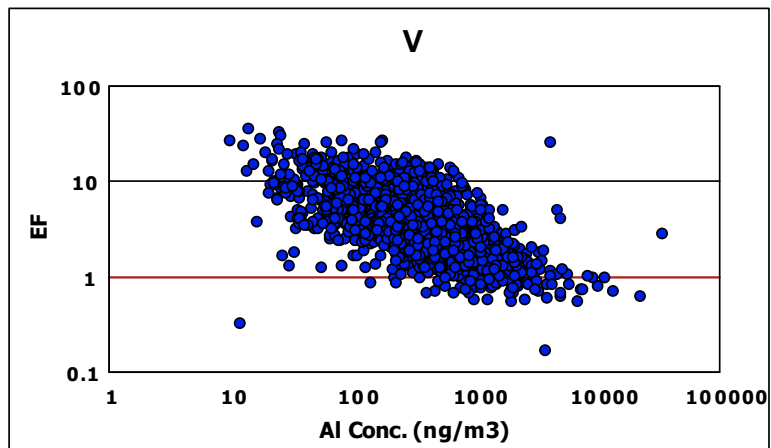
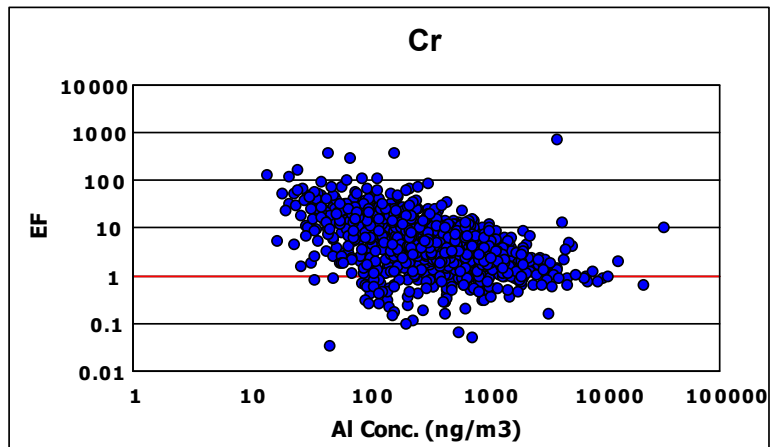


Figure 5.57 EF<sub>c</sub>-Al plots of some of the selected elements with mixed sources

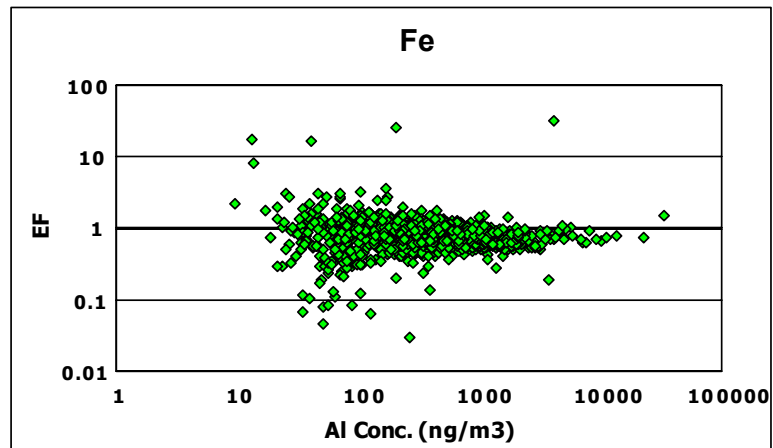
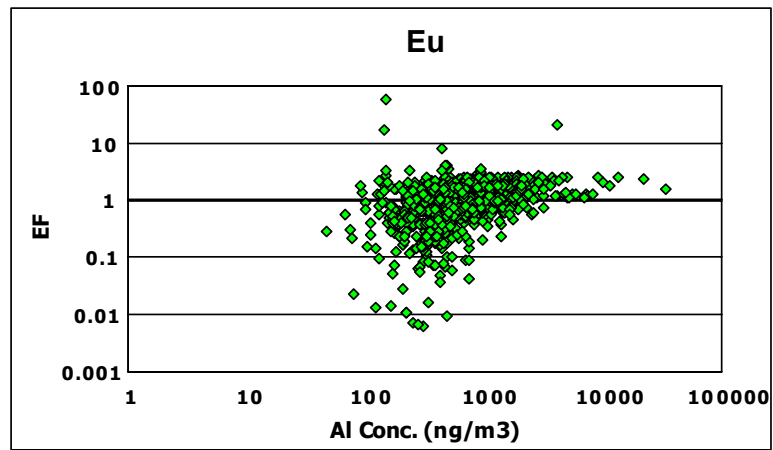
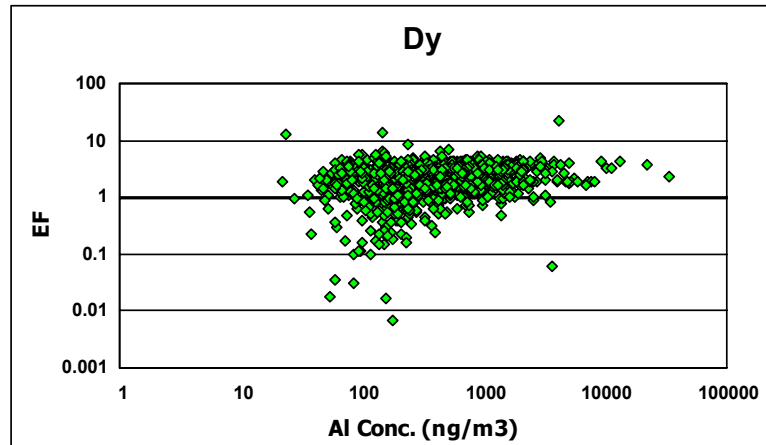


Figure 4.58  $EF_c$ -Al plots of some of the selected crustal elements

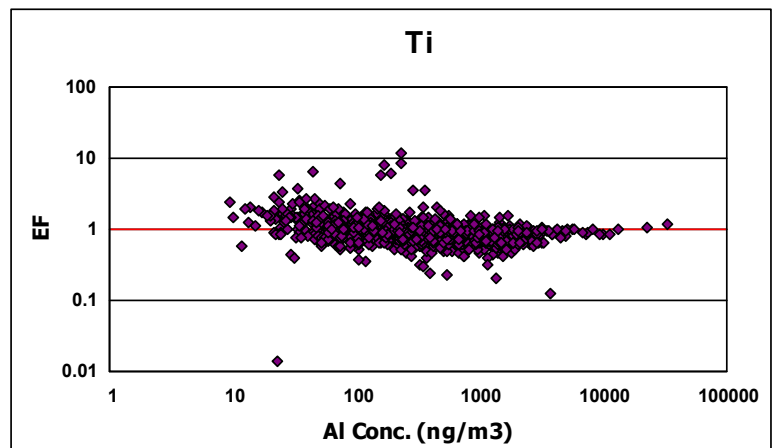
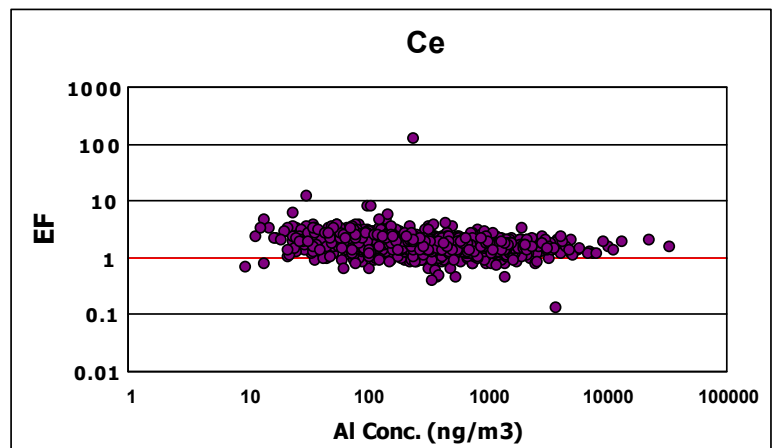
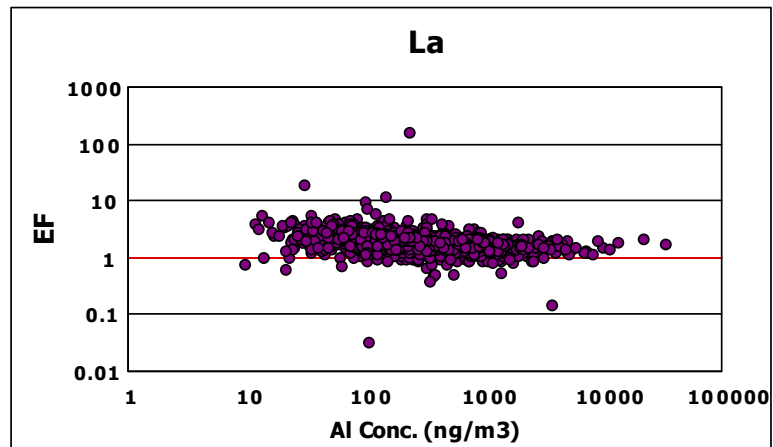


Figure 4.59  $EF_c$ -Al plots of some of the selected crustal elements

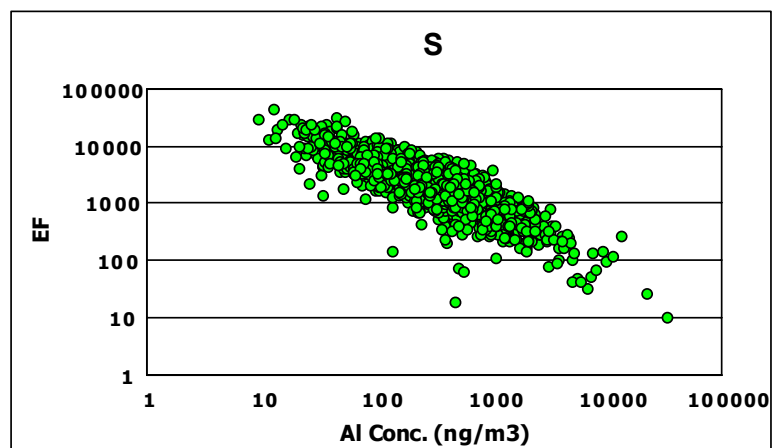
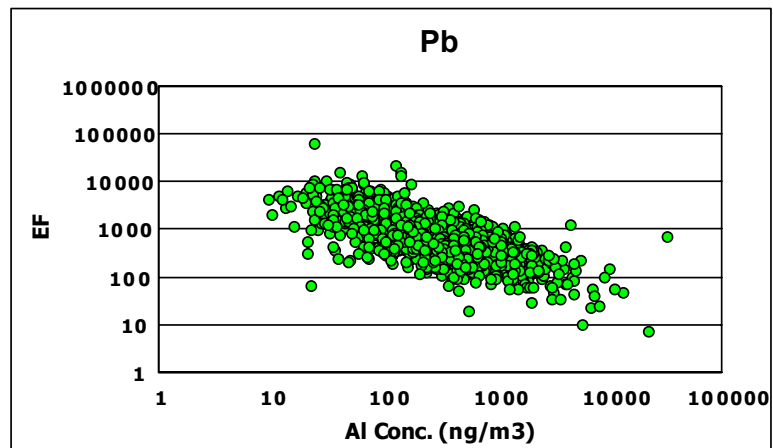
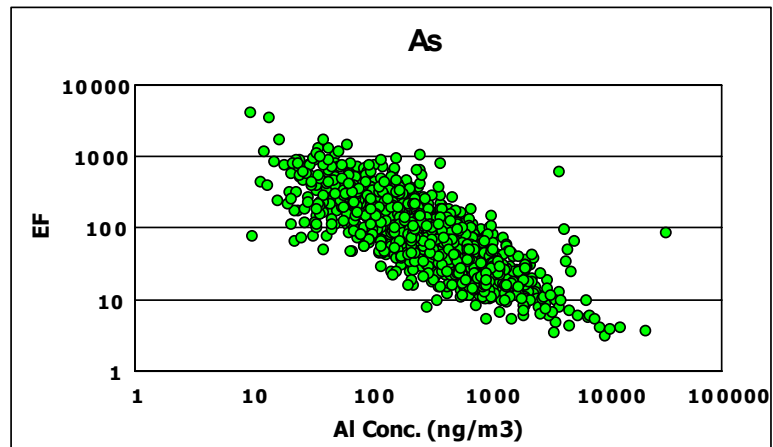


Figure 4.60  $EF_c$ -Al plots of some of the selected anthropogenic elements

#### 4.5.3.2. Marine Enrichment Factor

Goldberg's sea water composition was used to find the marine contributions to observed aerosol concentrations. Calculation of marine enrichment factor ( $EF_m$ ) was very similar to the calculation of  $EF_{Cr}$ , the only difference was to use Na instead of Al as a reference element and to use a sea water composition instead of composition of soil. The following equation was used in estimation:

$$EF_{marine} = \frac{(C_x / C_{Na})_{sample}}{(C_x / C_{Na})_{reference}} \quad (4.13)$$

Calculated  $EF_m$  values for measured parameters were depicted in Figure 4.61. By using the criteria followed in  $EF_{Cr}$ , measured parameters can be classified in three groups in terms of their calculated  $EF_m$  values.

Calculated  $EF_m$  for Cl is smaller than one which can be attributed to volatilization of Cl from samples. Magnesium, Sr and K have  $EF_m$  values between 1 and 10 indicating that these elements have other sources than sea salt. Calcium, Li, Rb and S have  $EF_m$  values between 10 and 100 implying that these elements are moderately enriched. Sulfur has  $EF_m$  greater than 100. High  $EF_m$  for S can be attributed to release of this parameter from other anthropogenic sources in addition to its arrival to sampling location with long range transport. Selenium has  $EF_m$  around 1000. Like Sulfur, this element has biogenic sources in sea. Gas phase emission of Se from ocean to atmosphere can represent for about 60 % of atmospheric Se with a flux of 5-8 10<sup>9</sup> g Se per year (Amouroux and Donard, 1996; Mosher and Duce, 1987). Considerably high  $EF_m$  values for S and Se can be interpreted as predominance of other sources on the measured concentrations of these two elements over sea salt.

Rest of the elements, for which  $EF_m$  calculated as greater than 1000, are highly enriched indicating that the impact of other sources releasing these parameters to the atmosphere is much more pronounced as compared to their marine source, or, in other words, marine contribution to these parameters is negligible.

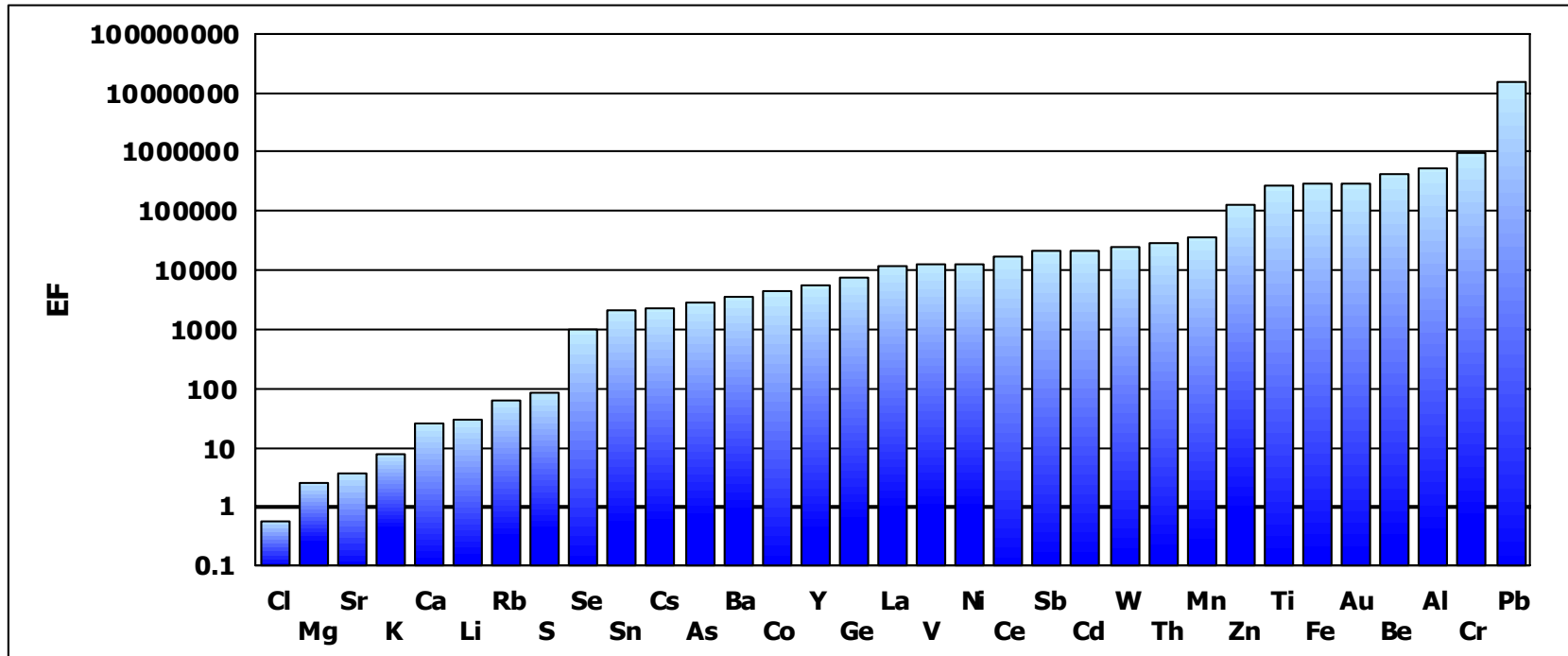


Figure 4.61 Marine enrichment factors of elements

#### 4.5.4. Elevated Sulfate over Eastern Mediterranean Atmosphere

Unusually high sulfate concentrations in the Eastern Mediterranean are frequently reported in the literature. Such elevated  $\text{SO}_4^{2-}$  concentration associated with Eastern Mediterranean was first noticed in a study conducted in Black Sea in 1989 (Hacisalıhođlu et al., 1992), later several researchers reported similar concentrations for the Eastern Mediterranean (Benkovitz et al., 1994; Luria et al., 1996; Güllü et al., 1998; Mihalopoulos et al., 1997). Recently, Rudich et al. (2008) have estimated by remote sensing that 0.025-0.062 Tg  $\text{SO}_4^{2-}$  as S was transported to the region on annual basis. Sulfate,  $\text{NO}_3^-$  and  $\text{NH}_4^+$  concentration values reported in the literature for Eastern Mediterranean are given in Table 4.22.

There are some points in Table 4.22 that need to be highlighted:

- $\text{SO}_4^{2-}$  concentrations measured in Eastern Mediterranean region is significantly higher than average values reported for EMEP stations and this difference seems to increase especially after 1990. Figure 4.62 illustrates the mean concentration of  $\text{SO}_4^{2-}$  measured in EMEP stations located in Western Europe and one measured in this study between 1993 and 2000. Black circles in the middle of boxes indicate mean  $\text{SO}_4^{2-}$  values. In order to show that two data sets are statistically significant from each other their means were compared by using two sample t-test. The null hypothesis ( $H_0$ ), the difference in the means of two groups is zero, was tested at 95 % confidence level against the alternative hypothesis ( $H_a$ ) of true difference in means is not equal to zero. The confidence interval for the difference between the means at 5 % significance level was ranging from -7.85 to -3.87, and calculated *t value* is -6.31 and corresponding significant level (*p value*) is zero. . Since *p value* smaller than 0.05 indicates significant differences between two means and confidence interval does not contain the value 0.0, it can be concluded that there is a significant difference in means of Western EMEP and one corresponding to this study in terms of  $\text{SO}_4^{2-}$  concentrations.
- When such a comparison was performed in terms of  $\text{NO}_3^-$ , the difference in concentrations between Eastern Mediterranean and EMEP stations is not as pronounced as one observed in  $\text{SO}_4^{2-}$  concentrations. Though both  $\text{NO}_3^-$  and  $\text{NH}_4^+$



levels measured in Eastern Mediterranean is higher than average values reported in EMEP stations, difference is not statistically significant at 95% confidence interval, as in the case of  $\text{SO}_4^{2-}$  concentrations.

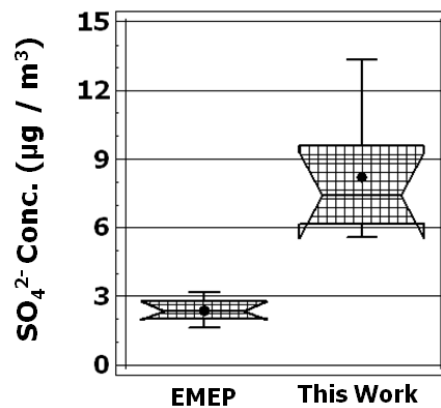


Figure 4.62 Comparison of mean concentrations of  $\text{SO}_4^{2-}$  measured in EMEP and this study between 1993 and 2000

- Elevated  $\text{SO}_4^{2-}$  concentrations are not only observed in Eastern Mediterranean but also in Aegean and Black Sea regions. Consequently, the term "Eastern Mediterranean" refers the region encompasses areas of eastern part of Greece in Mediterranean, Aegean and Black Sea.

The questions of why  $\text{SO}_4^{2-}$  concentrations in Eastern Mediterranean region including Turkey is considerably higher than ones measured in EMEP stations and why similar difference is not observed in  $\text{NH}_4^+$  and  $\text{NO}_3^-$  concentrations are tried to be answered in this section of the study.

Table 4.22 Reported concentrations of  $\text{SO}_4^{2-}$ ,  $\text{NO}_3^-$  and  $\text{NH}_4^+$  in Aegean, Black Sea and Mediterranean

Place	$\text{SO}_4^{2-}$ ( $\mu\text{gm}^{-3}$ )	$\text{NO}_3^-$ ( $\mu\text{gm}^{-3}$ )	$\text{NH}_4^+$ ( $\mu\text{gm}^{-3}$ )	Reference
Athens, Spring (1987)	10.4	2.0	-	Danalatos and Glavas (1999)
Black Sea (1988)	8.1	2.96	-	Güllü et al. (1998)
Athens (1989–1990)	13.4	5.4	7.9	Kirkitsos and Sikiotis (1991)
Etzion (Israel), (1989)	6.72	-	-	Luria et al., (1996)
Jerusalem (Israel), (1990)	12.3	-	-	Luria et al., (1996)
Ashdod (Israel), (1990)	10.7	-	-	Luria et al., (1996)
Caeserea (Israel), (1993)	10.2	-	-	Luria et al., (1996)
Finokalia (Crete) (1994–1995)	9.0	1.5	1.0	Mihalopoulos et al. (1997)
Haifa, Summer (1995)	5.5	1.6	-	Ganor et al. (1998)
Tel Aviv, Summer (1996)	7.1	1.8	-	Ganor et al. (1998)
Sde Boker (1996)	10.5	3.3	1.11	Formenti et al., (1996)
Amasra (1995–1997)	4.13	0.81	1.26	Karakaş et al., (2004)
Erdemli (Mersin), (1996–1999)	7.5	3.34	2.22	Koçak et al. (2004)
Finokalia (Crete), (1996–1999)	3.9	-	-	Kouvarakis and Mihalopoulos (2002)
Finokalia (Crete), Summer (2000)	6.9	2.8	2.4	Bardouki et al. (2003)
Antalya (1993–2001)	7.93	1.29	1.14	This work
Athens (Greece, urban) (2004)	6.7	0.34	1.52	Karageorgos et al., (2006)
Patras (Greece) (2004–2005)	3.2	1.6	0.4	Glavas et al. (2008)

Since European countries suffered a lot from the acid rain problem,  $\text{SO}_4^{2-}$  concentration and concentration of other acidifying substances were monitored in rural parts of Europe through the EMEP measurement network since 1975. European Monitoring and Evaluation Program (EMEP) is a web of international stations to monitor the rural pollution in whole Europe. While the number of stations within this network was not high in 1970's, it increased very rapidly and there are about 100 stations working for this network. There is one EMEP station in Turkey located in Kızılcahamam, Ankara and it is operated by Refik Saydam Hıfzıssıha Center of Ministry of Health. The data generated in the network is sent to a center located in Norway where they are processed further. These data is particularly used in the calibration of models developed by EMEP. However, these produced data is also interpreted to highlight the pollution profile of Europe at the beginning of monitoring studies. EMEP does not evaluate the generated data in detail to prevent conflicts between the countries. Very rough and regional assessments were conducted. As time proceeds, not only number of stations but also the parameters investigated in the collected samples are increased in this network. While  $\text{SO}_4^{2-}$  and  $\text{NO}_3^-$  were only two parameters analyzed in the middle of 1970's, gaseous pollutants, particulate matter and its chemical composition and volatile organic compounds (VOCs) are measured in at least some of the EMEP stations today.

Even though the detailed statistical data evaluation is not performed at EMEP secretariat, generated vast data set enabled researchers to see how  $\text{SO}_4^{2-}$  and  $\text{NO}_3^-$  concentrations change with time in Europe. Moreover, EMEP data formed basis for all the protocols associated with the reductions of emissions over Europe. Variation of  $\text{SO}_4^{2-}$  concentrations between 1980 and 2000 in Europe was depicted in Figure 4.63. Measured  $\text{SO}_4^{2-}$  concentrations between 1990 and 2000 were also depicted in Figure 4.63 to highlight the difference between Europe and Eastern Mediterranean in terms of  $\text{SO}_4^{2-}$  levels.

It is very clear from Figure 4.63 that  $\text{SO}_4^{2-}$  concentrations declined very sharply in Europe between 1980 and 2000. The mean  $\text{SO}_4^{2-}$  concentration was reported as  $6 \mu\text{g m}^{-3}$  in 1980, and then it was dropped to  $4 \mu\text{g m}^{-3}$  in 1990. Average  $\text{SO}_4^{2-}$  concentrations was measured as  $2.4 \mu\text{g m}^{-3}$  in 2000 while the 9-year average  $\text{SO}_4^{2-}$  concentration measured in our station is  $7 \mu\text{g m}^{-3}$ .

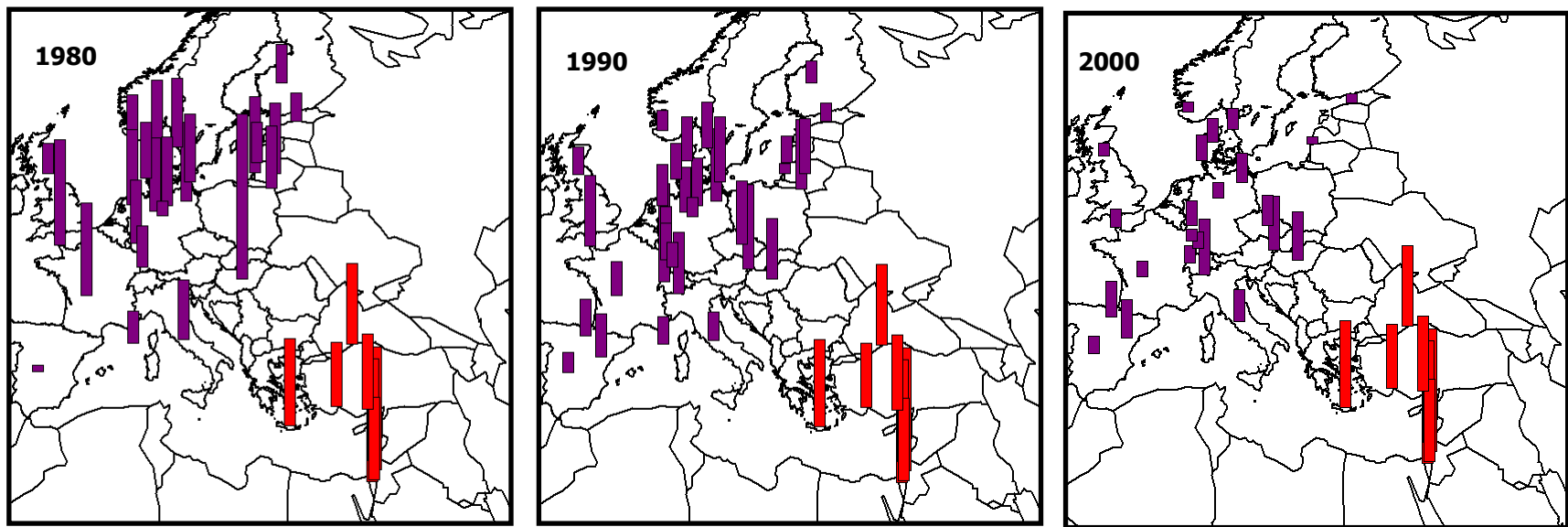


Figure 4.63  $\text{SO}_4^{2-}$  concentrations in EMEP and Eastern Mediterranean in 1980, 1990 and 2000, respectively

It would be better to divide Europe into two regions, as Western and Eastern (or former USSR countries) Europe, to investigate temporal trends in  $\text{SO}_4^{2-}$  concentration. There are significant differences between these two parts of Europe in terms of emissions. Considerable reductions were achieved in  $\text{SO}_2$  emissions in Western Europe as results of regulations, which strictly control emission sources starting from beginning of 1970's. On the other hand, emission control strategies were not implemented in Eastern Europe until 10 years ago and  $\text{SO}_2$  emissions did not decrease significantly.

However, accession of some of the former USSR countries to European Union and allocation of substantial budgets for the implementation of air pollution control technologies results in significant reduction of emissions and  $\text{SO}_4^{2-}$  concentrations associated with these emissions within these countries, but such reductions are observed only recently. For these reasons, variation of  $\text{SO}_4^{2-}$  concentrations for these two parts of Europe was illustrated in two separate plots in Figure 4.64. It is obvious from Figure 4.64 that a rapid reduction were achieved in Western European countries starting from early 80's. This decrease in  $\text{SO}_4^{2-}$  concentrations are as high as 70% in the central parts of Europe (EMEP). However, similar trend was not observed in Eastern Europe due to reasons described previously.

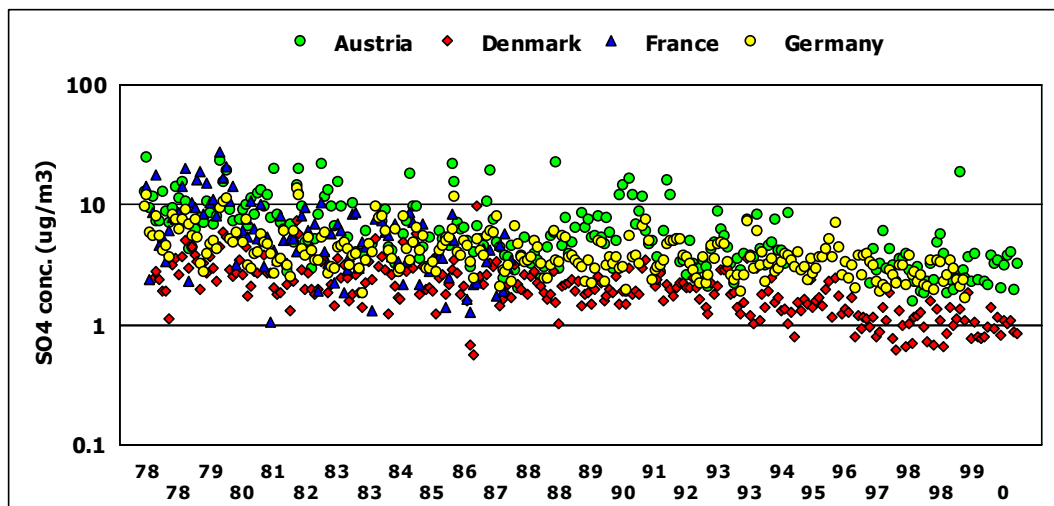


Figure 4.64 Variation of  $\text{SO}_4^{2-}$  concentrations in (a) Western European and (b) Former USSR (Eastern European) countries

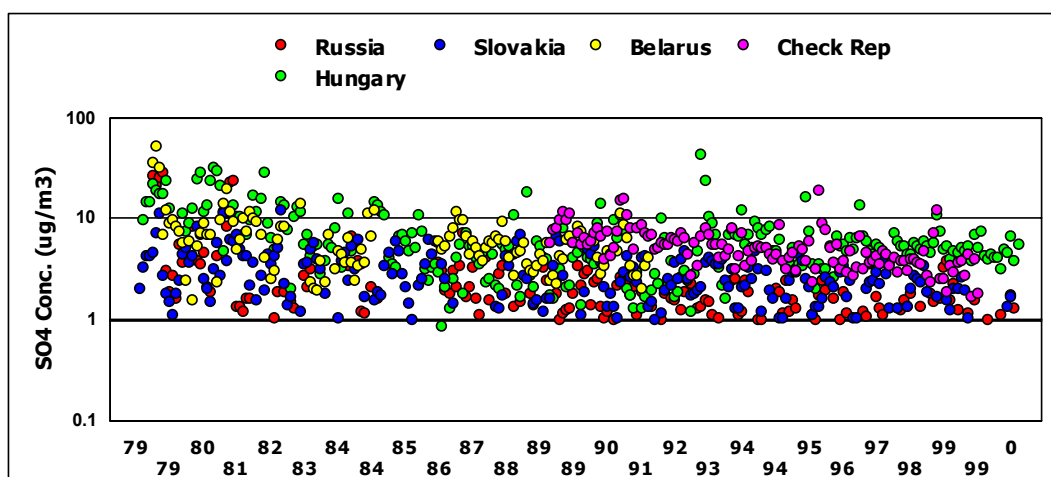


Figure 4.64 Variation of  $\text{SO}_4^{2-}$  concentrations in (a) Western European and (b) Former USSR (Eastern European) countries (Continued)

Variation of  $\text{NO}_3^-$  in Europe with respect to time is different from the trends observed in  $\text{SO}_4^{2-}$  concentrations. Trend in  $\text{NO}_3^-$  ion concentrations measured in Western and Eastern Europe between 1986 and 2000 was depicted in Figure 4.65.

It is obvious from Figure 4.65 that one could not see very clear decrease in terms of  $\text{NO}_3^-$  as compared to  $\text{SO}_4^{2-}$  concentrations. While very small decreasing trend was recorded in Western Europe, it is not as pronounced as decline recorded for  $\text{SO}_4^{2-}$ . This difference in measured  $\text{SO}_4^{2-}$  and  $\text{NO}_3^-$  concentrations in EMEP network is related with the effectiveness of control strategies taken on the emission sources throughout the Europe.

Precautions taken against the reduction of both  $\text{SO}_2$  and  $\text{NO}_x$  emissions gained a legal dimension with the sulphur and nitrogen protocols under the annexes of Convention on Long-Range Transboundary Air Pollution. The Convention on Long Range Transboundary Air Pollution, which is generally referred as Air Pollution or abbreviated as CLRTAP, was opened for signature on 13/11/1979 and entered into force on 16/03/1983. The major objectives of the CLRTAP are to protect human environment against air pollution, to reduce air pollution slowly and to prevent air pollution including rural pollution originating from long-range transboundary transport of pollutants. In fact, history of this convention goes back to 1960s, when scientist discovered that emissions released from the continental Europe resulted in the acidification of lakes within boundary of Scandinavian countries (CIA World Factbook, 2003 Edition; <http://www.unece.org/env/lrtap>). Later,

the CLRTAP has been extended by eight protocols including "The 1985 Protocol on the Reduction of Sulphur Emissions or their transboundary fluxes by at least per cent" and "The 1988 Protocol concerning the Control of Nitrogen Oxides or their Transboundary Fluxes".

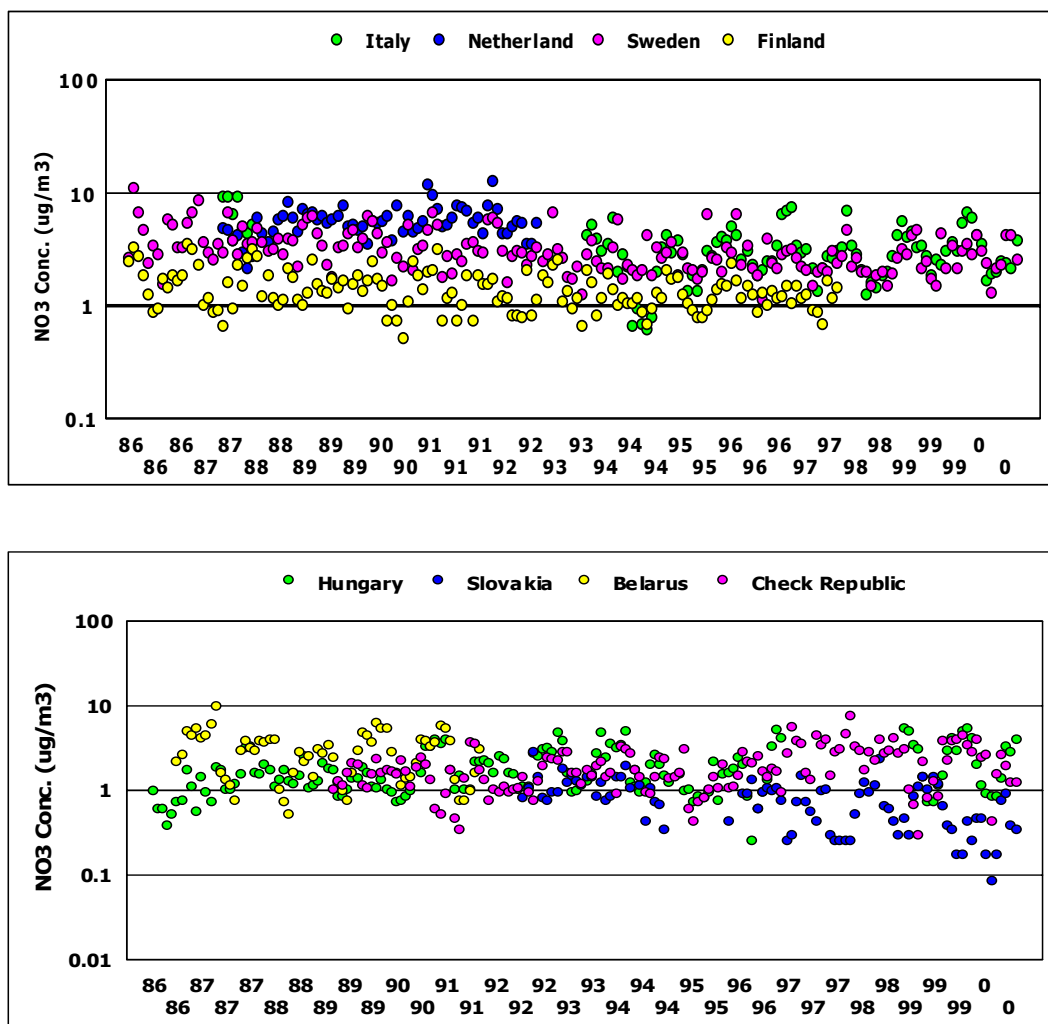


Figure 4.65 Variation of NO<sub>3</sub><sup>-</sup> concentrations in (a) Western Europe and (b) Eastern Europe

Thereafter, some modifications were performed on first Sulphur Protocol and reopened to signature as Second Sulphur Protocol in 1994. However, reductions in SO<sub>2</sub> emissions started immediately after 1985. Results of these emissions could be easily observed in

recorded  $\text{SO}_4^{2-}$  concentrations in rural parts of Europe. On the other hand, Nitrogen protocol for the reduction of nitrogen emissions was opened to signature in the late 1980's due to deficiencies in the technological infrastructure, which explains why decline in  $\text{NO}_x$  emissions initiated after the mid of 1990's.

The difference in the control of  $\text{SO}_2$  and  $\text{NO}_x$  emissions is expected to yield significantly different  $\text{SO}_4^{2-}$  to  $\text{NO}_3^-$  ratios at two different part of Europe. In eastern part of the continent, both of these pollutants are not regulated as strictly as western part of Europe. Therefore,  $\text{SO}_4^{2-}$  to  $\text{NO}_3^-$  ratio calculated for Eastern Europe remained more or less same to the values observed in 1970's all over the world. Nevertheless, sulphur emissions declined in Western Europe significantly but  $\text{NO}_x$  emissions did not until recently. Consequently, it will not be surprising to see decreasing  $\text{SO}_4^{2-}$  to  $\text{NO}_3^-$  ratios with time for this part of the continent. In order to see the impact of regulatory actions on emissions,  $\text{SO}_4^{2-}$  to  $\text{NO}_3^-$  ratios before 1990 and after 1990 were calculated both for Eastern and Western Europe and results are depicted in Figure 4.66 & 4.67.

As it can be seen from Figure 4.66, estimated  $\text{SO}_4^{2-}$  to  $\text{NO}_3^-$  ratio for Western Europe before 1990 is ranging from 0.7 to 1.6 and has a mean of ~1.1. On the other hand, as it was suggested, this ratio has a mean value of 2.5 for Eastern Europe and it is more than a factor-of-two higher than value calculated for western counterpart. Figure 4.67 demonstrates the calculated ratios after 1990. Mean  $\text{SO}_4^{2-}$  to  $\text{NO}_3^-$  ratio in EMEP stations located at the Western European countries decreased to 0.8. It can also be seen in Figure 61, that  $\text{SO}_4^{2-}$  to  $\text{NO}_3^-$  ratios in most of the stations at the Western Europe has values <1.0.

On the other hand, there only a minor change is observed in  $\text{SO}_4^{2-}$  to  $\text{NO}_3^-$  ratio observed at EMEP stations located at the Eastern Europe, between before 1990 and after 1990. The ratio covers a range between 1.3 and 4.5 with a mean value of 2.4. For Eastern Europe, mean ratio was calculated as 2.41 while it is ranging from 1.3 to 4.5. This implies that the relative contributions of  $\text{H}_2\text{SO}_4^{2-}$  and  $\text{HNO}_3^-$  on the acidity of precipitation in Eastern and Western Europe are now different. Until 1985 2/3 of the acidity in rain water was accounted for by  $\text{H}_2\text{SO}_4$  and 1/4 is accounted for by  $\text{HNO}_3$ . This corresponds to  $\text{SO}_4^{2-}$  to  $\text{NO}_3^-$  ratio of approximately 2.5. However, mean value of the  $\text{SO}_4^{2-}$  to  $\text{NO}_3^-$  ratio observed in the Western Europe, which is 0.8 after 1990 suggest that the contribution of  $\text{HNO}_3$  to the rain water exceeded to that of  $\text{H}_2\text{SO}_4$ . The ratio is still 2.4 in the Eastern Europe and Balkan Countries, indicating that earlier ratio is preserved.



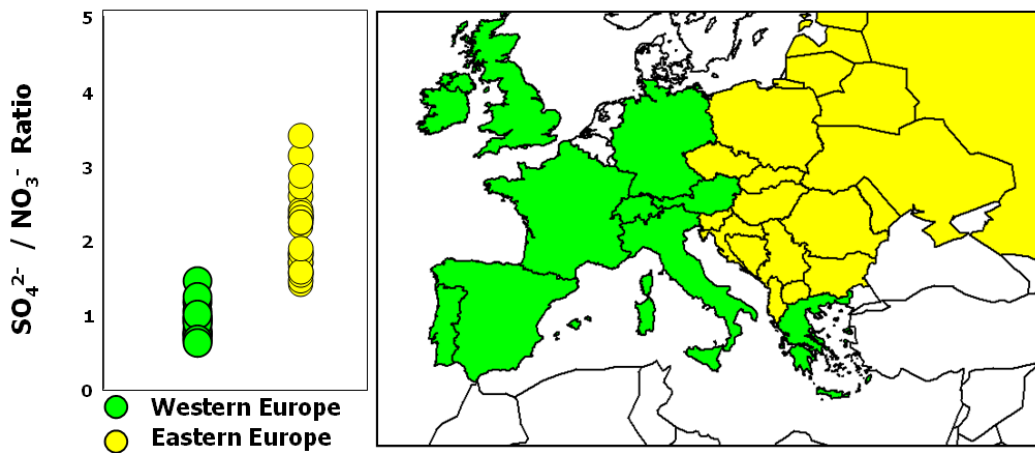


Figure 4.66  $\text{SO}_4^{2-}$  to  $\text{NO}_3^-$  ratio in aerosol in the western European countries and at former USSR countries before 1990

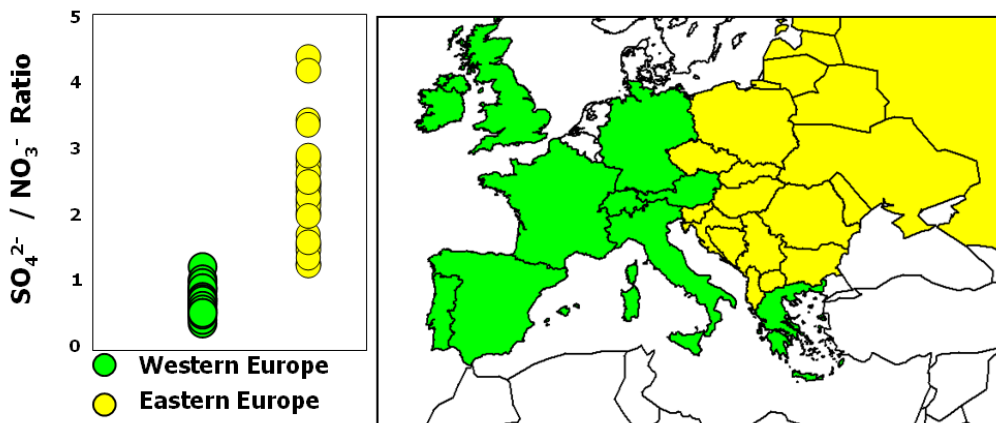


Figure 4.67  $\text{SO}_4^{2-}$  to  $\text{NO}_3^-$  ratio in aerosol in the western European countries and at former USSR countries after 1990

Since different  $\text{SO}_4^{2-}$  to  $\text{NO}_3^-$  ratios were calculated for two different parts of Europe, and then these ratios can be used as tracers to differentiate the influence of Western and Eastern part of Europe on the measured  $\text{SO}_4^{2-}$  concentrations in Mediterranean region.

Variation of  $\text{SO}_4^{2-}$  to  $\text{NO}_3^-$  ratio in Antalya station between 1993 and 2000 was illustrated in Figure 4.68.

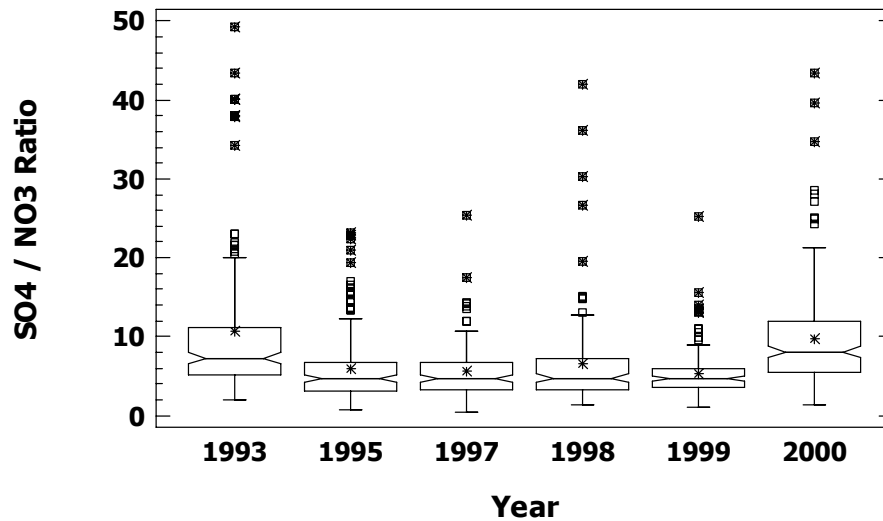


Figure 4.68 Variation in  $\text{SO}_4^{2-}$  to  $\text{NO}_3^-$  ratio at Antalya between 1993 and 2000

Mean  $\text{SO}_4^{2-}$  to  $\text{NO}_3^-$  ratio between 1993 and 2000 is 6.5 (median is 5.5) for Antalya station, which is more in line with the ratios reported for the Eastern Europe, and much higher than the ratios reported for the Western European stations. This indicates that Eastern Mediterranean is under the influence of Eastern Europe, Balkan Countries, including Turkey itself, where this ratio is high. The effect of Western Europe on the chemical composition of particles in the Eastern Mediterranean is not much. Calculated  $\text{SO}_4^{2-}$  to  $\text{NO}_3^-$  ratio for the Eastern Mediterranean does not change significantly between 1993 and 2000. This is also similar to the trend (or lack of trend) observed in Eastern Europe and Balkan Countries. As pointed out before, existing different  $\text{SO}_4^{2-}$  to  $\text{NO}_3^-$  ratios in the Western Europe vs Eastern Europe and Balkan countries provided fairly reliable information on the source regions of anomalously high  $\text{SO}_4^{2-}$  levels in the Eastern Mediterranean region.

Monthly average  $\text{SO}_4^{2-}$  to  $\text{NO}_3^-$  ratio calculated for the Eastern Mediterranean is depicted in Figure 4.69. As can be seen in the figure, there is not an obvious seasonal variation in the  $\text{SO}_4^{2-}$  to  $\text{NO}_3^-$  ratio in the Eastern Mediterranean. This is understandable because, as

discussed in the Section 4.4.2, both  $\text{SO}_4^{2-}$  and  $\text{NO}_3^-$  concentrations are higher during summer months resulting in similar  $\text{SO}_4^{2-}$  to  $\text{NO}_3^-$  ratios throughout the year.

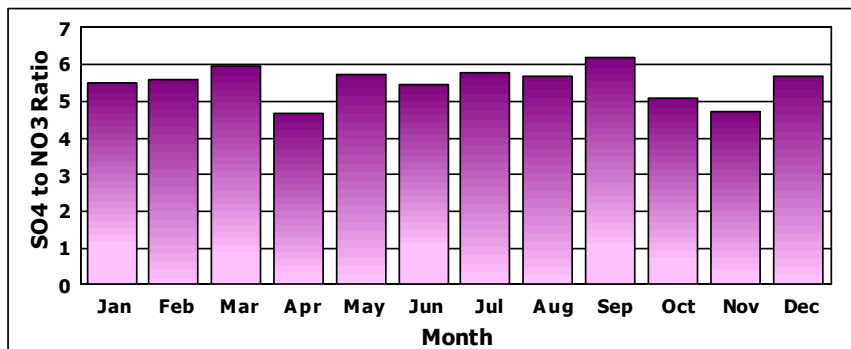


Figure 4.69 Monthly variation of  $\text{SO}_4^{2-}$  to  $\text{NO}_3^-$  ratio at Antalya station

Cluster analysis to determine transport pathways of air masses to Eastern Mediterranean was discussed in Sections 4.5.1.2 – 4.5.1.3. Centers of nine clusters, which were shown earlier in Figure 4.51, are depicted in Figure 4.70.

Sector averages of all measured parameters were discussed previously in Section 4.5.1.4. Only that of  $\text{SO}_4^{2-}$  will be presented here to highlight few points related to anomalously high  $\text{SO}_4^{2-}$  concentrations. Sulfate concentration measured in aerosol samples assigned to each cluster is depicted in Figure 4.71. It is clear from Figure 4.71 that, mean concentration of  $\text{SO}_4^{2-}$  ( $\sim 10 \mu\text{g m}^{-3}$ ) in Cluster 6 is significantly higher than concentrations corresponding to other clusters. This cluster represents for 17.1 % of total air mass transported to our station and consists of trajectories coming from Balkan Countries, particularly from Bulgaria. Cluster 6 is followed by Cluster 4, including 17 % of total air mass, had average  $\text{SO}_4^{2-}$  concentration of  $9.2 \mu\text{g m}^{-3}$ . Cluster 5, which represents 11.3 % of total airflow, had mean  $\text{SO}_4^{2-}$  concentration of  $8.6 \mu\text{g m}^{-3}$ . Trajectories associated with Cluster 4 spend their most of time over Western Europe while those assigned to Cluster 5 resided longer in Russia. Consequently, elevated  $\text{SO}_4^{2-}$  concentration content of aerosol samples collected at our station is influenced more from the airflow transported to Eastern Mediterranean Region from Eastern Europe since Cluster 6 and 5 together represent 28.4 % of total airflow.



Figure 4.70 Cluster centers and frequency of air masses in each cluster

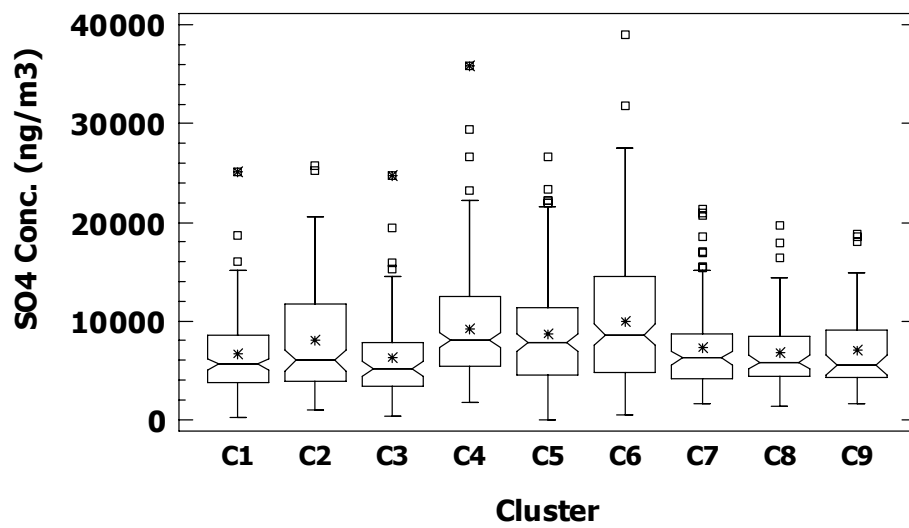


Figure 4.71  $\text{SO}_4^{2-}$  concentration corresponding to each cluster

From Figure 4.71, it is obvious that measured  $\text{SO}_4^{2-}$  concentrations in each cluster are not the same. Statistical significance of mean concentration of  $\text{SO}_4^{2-}$  in each cluster was tested with analysis of variance (ANOVA) and results are tabulated in Table 4.23. Since

the  $p$  value of F test is less than 0.05 as provided in Table 4.23, there is a statistically significant difference between the means of nine clusters at 95 % confidence level.

Table 4.23 ANOVA result for  $\text{SO}_4^{2-}$  concentration in different clusters

	<i>Sum of Squares</i>	<i>df</i>	<i>Mean Square</i>	<i>F Ratio</i>	<i>p value</i>
Between Groups	$1.95 \cdot 10^9$	8	$2.43 \cdot 10^8$	9.12	0.00
Within Groups	$3.08 \cdot 10^{10}$	1156	$2.66 \cdot 10^7$		
Total	$3.28 \cdot 10^{10}$	1164			

After ANOVA, multiple comparison tests using Tukey's post hoc routine available in SPSS 15.0 was performed to determine which means amongst a set of means differ from the rest. Tukey's multiple comparison test is also known as Tukey's honestly significant difference test or Tukey's HSD. Statistically significant mean differences at 0.05 significance level was tabulated in Table 4.24. From this table, it can be deduced that mean  $\text{SO}_4^{2-}$  concentration in Cluster 1 is statistically different from mean  $\text{SO}_4^{2-}$  concentrations determined for Cluster 4, 5 and 6. Similarly, mean  $\text{SO}_4^{2-}$  concentration corresponding to Cluster 6 is different from ones associated with Cluster 1, 2, 3, 7, 8 and 9 at 5 % significance level. Following multiple comparison test, homogenous subsets are formed and results are provided in Table 4.25. This table is a summary of major differences among the means. It organizes the means of the nine clusters into "homogenous subsets". Subsets of means that do not differ from each other at 5 % significance present in the same column, and subsets for which corresponding means do not differ present in separate columns. Clusters that are not in the same column are significantly different from each other at alpha ( $\rho$ ) < 0.05 according to Tukey's multiple comparison test procedure. From Table 4.25, it can be concluded that means corresponding to Cluster 2, 4, 5 and 6 are not statistically significant from each other and consequently, these clusters (or subsets) are included in the same column. Similarly, Cluster 1, 2, 3, 7, 8 and 9; Cluster 1, 2, 7, 8 and 9; and Cluster 2,4,5,7 and 9 are separated in three columns. Therefore, clusters (subsets) evaluated in terms of their  $\text{SO}_4^{2-}$  concentrations are classified in four groups. Mean  $\text{SO}_4^{2-}$  concentration associated with each cluster in each class do not show significant difference while each class includes clusters having means statistically different than do clusters in other three classes.

Table 4.24 Results of multiple comparison test using Tukey's HSD approach

Cluster #	Cluster #	Mean Difference	Std. Error	95% Confidence Interval	
				Upper Bound	Lower Bound
1	4	-2625	570	-4397	-852
	5	-2078	610	-3974	-183
	6	-3383	575	-5170	-1596
2	6	-1923	587	-3747	-100
3	4	-2963	661	-5018	-907
	5	-2416	696	-4578	-254
	6	-3721	665	-5789	-1653
4	1	2625	570	852	4397
	3	2963	661	907	5018
	7	1933	615	23	3843
	8	2478	705	288	4667
5	3	2416	696	254	4578
6	1	3383	575	1596	5170
	2	1923	587	100	3747
	3	3721	665	1653	5789
	7	2692	619	768	4615
	8	3236	708	1035	5437
	9	2952	812	428	5476
7	4	-1933	615	-3843	-23
	6	-2692	619	-4615	-768
8	4	-2478	705	-4667	-288
	6	-3236	708	-5437	-1035
9	6	-2952	812	-5476	-428

Table 4.25 Homogenous subsets from Tukey's HSD test

Cluster #	N	Subset for $\rho = .05$			
		1	2	3	4
3	87	6277			
1	137	6615	6615		
8	73	6761	6761		
9	51	7045	7045	7045	
7	108	7306	7306	7306	
2	128	8074	8074	8074	8074
5	151		8693	8693	8693
4	205			9239	9239
6	197				9997
Sig.		0.22	0.09	0.06	0.15

Discussions in this section provided clues on the source regions responsible for elevated  $\text{SO}_4^{2-}$  concentrations measured by various researchers in the Eastern Mediterranean. Results of the discussions can be summarized as:

- Before 1990,  $\text{SO}_4^{2-}$  concentration was high in most of the Europe, including Eastern Mediterranean. Concentrations of  $\text{SO}_4^{2-}$  started to decrease in western European countries with application of effective  $\text{SO}_2$  emission control measures, through enforcement of S protocol since 1985. In some of the EMEP stations in Western Europe decrease in  $\text{SO}_4^{2-}$  concentrations was as high as 70%, compared to pre-1985 levels. This resulted in substantial reduction in  $\text{SO}_4^{2-}$  to  $\text{NO}_3^-$  ratio in these stations, because  $\text{SO}_4^{2-}$  concentrations decreased but  $\text{NO}_3^-$  concentrations did not.  $\text{SO}_2$  emissions at the Eastern Europe did not decrease in the same period; this resulted in higher  $\text{SO}_4^{2-}$  to  $\text{NO}_3^-$  in the Eastern Europe. The trends in Balkan Countries were very similar to trends observed in Eastern European countries. High  $\text{SO}_4^{2-}$  to  $\text{NO}_3^-$  ratio observed in the Eastern Mediterranean suggests that high  $\text{SO}_4^{2-}$  concentrations in this region are determined by  $\text{SO}_2$  emissions in the Eastern Europe and/or Balkan countries. High  $\text{SO}_4^{2-}$  concentration associated with short trajectories originating from Balkans, lack of change in the  $\text{SO}_4^{2-}$  to  $\text{NO}_3^-$  ratio between 1992 and 2000 supports the Eastern European source for the  $\text{SO}_4^{2-}$  observed at the Eastern Mediterranean. This conclusion also means that future variations in the  $\text{SO}_4^{2-}$  concentrations in the Eastern Mediterranean and the Black Sea will be determined by  $\text{SO}_2$  control in Balkan countries.
- It is interesting to note that, although  $\text{SO}_4^{2-}$  concentrations in the Eastern Mediterranean are very high compared to other parts of Europe, a similar trend is not observed in  $\text{NO}_3^-$  concentrations. This is because  $\text{NO}_3^-$  concentrations did not decrease in Europe as fast as the decrease observed in  $\text{SO}_4^{2-}$  concentrations. In the year 2001, when our sampling was terminated,  $\text{NO}_3^-$  concentrations were high everywhere in Europe including Western Europe.
- Marmer and Langmann (2005) have performed a regional atmospheric chemistry model to determine seasonal variability of secondary trace gases and aerosols, their origin and impact on Mediterranean climate. Researchers investigated partitioning of  $\text{SO}_x$  emissions into land and water sources and their effect on sulfate aerosol concentration, its total burden and direct radiative forcing. Authors have found that 54

% of total sulfate column burden over Mediterranean is due to ship emissions, which contribute over 50 % to the direct radiative forcing.

- There are two additional sources that can also affect  $\text{SO}_4^{2-}$  concentrations in eastern Mediterranean. One of these sources is the sea salt  $\text{SO}_4^{2-}$  and the other one is biogenic  $\text{SO}_4^{2-}$ . Sea salt  $\text{SO}_4^{2-}$  accounts for approximately 20% of the measured  $\text{SO}_4^{2-}$  concentrations. However, it can not be responsible for the elevated  $\text{SO}_4^{2-}$  concentrations at the Eastern Mediterranean, because its contribution to total  $\text{SO}_4^{2-}$  is same at every coastal station. There is no reason to believe in higher contribution of sea salt  $\text{SO}_4^{2-}$  in the Eastern Mediterranean then elsewhere.

- Contribution of biogenic  $\text{SO}_4^{2-}$  on total  $\text{SO}_4^{2-}$  concentrations at the Eastern Mediterranean had been studied by different researchers. Kouvarakis and Mihalopoulos (2002) concluded that the contribution of biogenic sulfur to total S in the Eastern Mediterranean varies between 1 % during winter to 17 % during. Similar low contributions of biogenic  $\text{SO}_4^{2-}$  were also reported by Ganor et al. (2000) and Uzun (1997).

- There is one other interesting point in cluster averages that needs to be highlighted. As pointed previously highest  $\text{SO}_4^{2-}$  concentrations are associated with clusters 4, 5 and 6. Averages of  $\text{SO}_4^{2-}$  concentrations in samples corresponding to trajectories associated with Clusters 1 (from South) and cluster 7 (from east) are low compared to average  $\text{SO}_4^{2-}$  concentrations corresponding to clusters 4, 5 and 6. Average  $\text{SO}_4^{2-}$  concentration in clusters 1, 4, 5 and 6 are  $6600 \text{ ng m}^{-3}$ ,  $9200 \text{ ng m}^{-3}$ ,  $8600 \text{ ng m}^{-3}$  and  $10\,000 \text{ ng m}^{-3}$ , respectively. Although cluster 1 average ( $6600 \text{ ng m}^{-3}$ ) is lower than averages for the clusters 4, 5 and 6, it is significantly higher than  $\text{SO}_4^{2-}$  concentrations measured in whole Europe. This suggests that, a substantial  $\text{SO}_4^{2-}$  transport occurs when air masses are coming from south. However, we know that there is no significant  $\text{SO}_4^{2-}$  source in North Africa. Then the main question that should be answered is: *What is the source of this high  $\text{SO}_4^{2-}$  concentrations coming to our station from south?*

- Koçak et al. (2004) reported an increase in  $\text{SO}_4^{2-}$  and  $\text{NO}_3^-$  concentrations when air masses arrive Erdemli from south. Authors tried to explain this by in the south sector. This increase was attributed to take up of  $\text{HNO}_3$  and  $\text{SO}_2$  by Saharan dust particles from the atmosphere. However, size distribution data generated by our



group does not support this hypothesis. The size distributions of  $\text{SO}_4^{2-}$ ,  $\text{NO}_3^-$  and  $\text{NH}_4^+$  at our Antalya station are depicted in Figure 4.72. Size distributions of  $\text{SO}_4^{2-}$  and  $\text{NH}_4^+$  are fairly similar and most of their mass occurs in submicron size range. This is expected because both  $\text{SO}_4^{2-}$  and  $\text{NH}_4^+$  are secondary particles and secondary particle generation mechanisms do produce small particles in the submicron range. Since  $\text{NO}_3^-$  is also a secondary particle, its size distribution is expected to be similar to that of  $\text{SO}_4^{2-}$  and  $\text{NH}_4^+$ . However, as can be seen in Figure 4.72, approximately 70% of the  $\text{NO}_3^-$  occurs in size range between 4.2 and 2.1  $\mu\text{m}$ . In these stages of the impactor  $\text{NO}_3^-$  correlates strongly with Na, but not with Ca and other soil-related elements. Association of  $\text{NO}_3^-$  with sea salt particles is well documented in the literature. If high  $\text{SO}_4^{2-}$  concentration coming from south is due to picking up of  $\text{SO}_2$  or due to reaction between  $\text{H}_2\text{SO}_4$  and  $\text{CaCO}_3$  on dust particles, then a significant fraction of the  $\text{SO}_4^{2-}$  mass should also occur in large size bins of the impactor. Since >80% of the  $\text{SO}_4^{2-}$  mass occur in submicron size, pick up of  $\text{SO}_2$  by crustal  $\text{CaCO}_3$  particles is not warranted at our sampling station.

- Another possibility is recycling of  $\text{SO}_4^{2-}$  between Eastern Mediterranean and North Africa. The  $\text{SO}_4^{2-}$  sources affecting Eastern Mediterranean lies to the North and Northwest of the region. Each year a significant amount of  $\text{SO}_4^{2-}$  transported from these source regions at the North to the Eastern Mediterranean. What happens then is not known. Probably  $\text{SO}_4^{2-}$  in the air masses coming from N and NW continue their journey to North Africa until they reach Equator. It is well documented that interhemispheric transport of air masses (and pollutants they carry) is very limited. Since  $\text{SO}_4^{2-}$  carried from Balkan Countries to Equator can not penetrate to Southern hemisphere, it builds up at the tropics. Some of this  $\text{SO}_4^{2-}$  scavenged out by both wet and dry deposition processes, but some is transported back to the Eastern Mediterranean, but this time coming from south. A mechanism, very similar to the one proposed here is reported by Kallos et al. (1998). Unfortunately there is no data for  $\text{SO}_4^{2-}$  and other elements on the African continent to test this hypothesis.

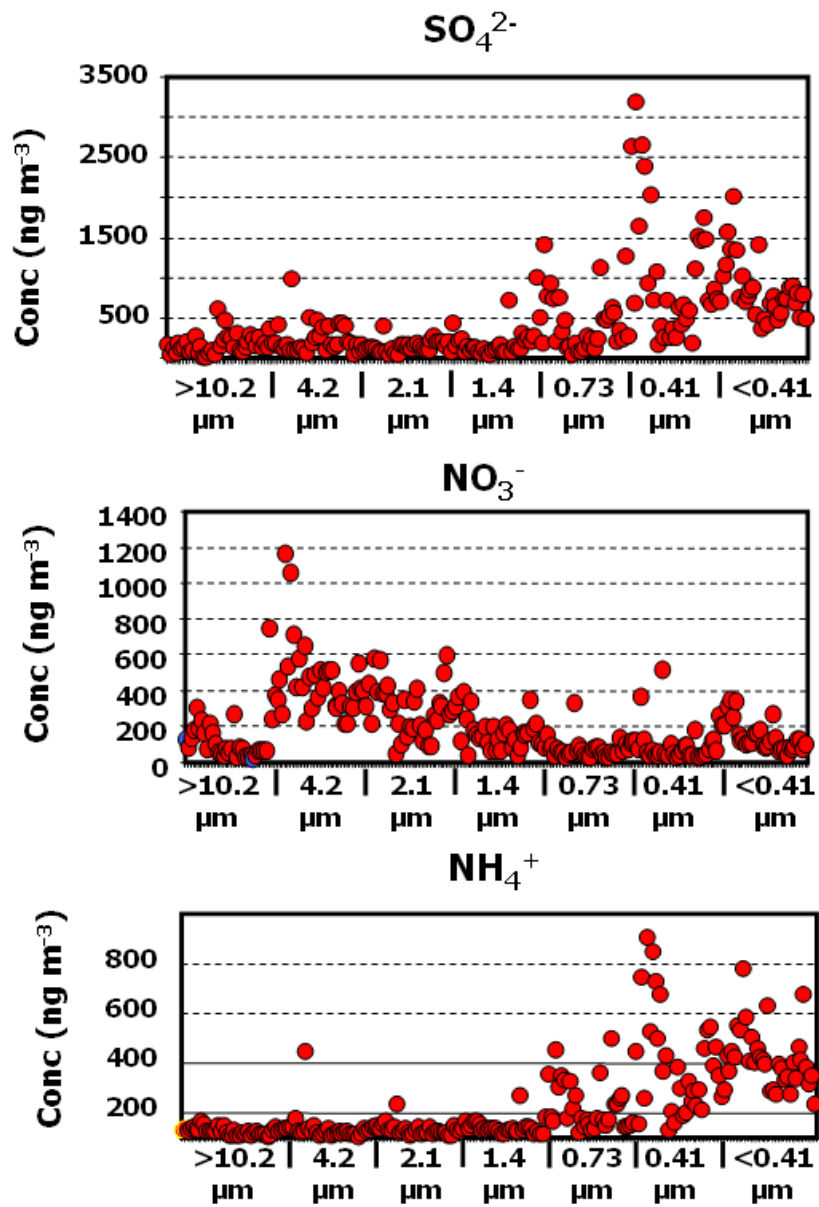


Figure 4.72 Size distribution of  $\text{SO}_4^{2-}$ ,  $\text{NO}_3^-$  and  $\text{NH}_4^+$  at the Eastern Mediterranean

#### 4.5.5. Saharan Dust Transport to the Eastern Mediterranean Region

Arid and semi-arid regions of the world are responsible for the 45 % of the global aerosol emissions by releasing mineral dust to the atmosphere. The most significant producer of this dust is the Saharan Desert with calculated annual emissions of 300 to 700 megatons

(Chiapello et al., 1997; and references therein). Recently, Laurent et al. (2008) modeled Saharan dust emissions from the Saharan desert using new surface properties and soil database. Researchers simulated annual Saharan dust emissions from 1996 to 2001 ranging from 585 to 759 Tg. One of the most important properties of the dust released from Saharan Desert is that it can be transported over long distances. For instance, Saharan dust intrusions were reported in Black Sea (Kubilay et al., 1995); Netherlands (Reiff et al., 1986); north Atlantic (Prospero and Nees, 1987); toward the Amazon basin (Swap et al., 1992) and recently, Barbados and Miami (Muhs et al., 2007; Trapp et al., 2008).

There are many crucial environmental impacts of Saharan dust. Dust particles absorb and scatter solar radiation, which affect air temperatures (Li et al., 1996; Moulin et al., 1997; Alpert et al., 1998). Secondly, they act as cloud condensation nuclei and they have impact on the precipitation pattern. Thirdly, Saharan dust provides considerable amounts of nutrients to the water environment. For instance, Swap et al. (1996) estimated the mean westward mass flux of  $K^+$ ,  $NH_4^+$ ,  $NO_3^-$ , and  $PO_4^{3-}$  as  $4.9 \cdot 10^{11}$ ,  $5.2 \cdot 10^{11}$ ,  $14.7 \cdot 10^{11}$ , and  $1.1 \cdot 10^{11}$  g year<sup>-1</sup>, respectively between 1989 and 1992. In addition, Zhu et al. (1997) reported that aeolian dust contains significant amount of iron, which facilitates the plankton productivity by stimulating  $N_2$  fixation. Prospero et al. (1996), Jickells et al. (2005) and Mahowald et al. (2005) are all agree that Fe is an important micro-nutrient in oceans. Shinn et al. (2000) suggested that disease spreading spores were transported along with dust particles to Caribbean and they found strong correlation with dust episodes and coral reef die off. Lastly, dust deposition influences the characteristic of sediments. Guerzoni et al. (1997) showed that Saharan dust deposition has larger than 80 % contribution to sediments in the offshore waters of whole Mediterranean region.

Saharan dust intrusions, their effects and characteristics have been extensively studied by many researchers in different parts of the world. For example, Kubilay et al. (2000) studied in the Eastern Mediterranean region; continental Europe was investigated by Schiwikowski et al. (1995); Ryall et al. (2002) worked on British Isles and Western Mediterranean was studied by Guerzoni et al. (1997), Avila et al. (1997) and Rodriguez et al. (2001).

This study covers a very long period, which includes numerous Saharan Dust episodes. Good tracers that can mark interception of Saharan Dust at our station, like Al, Si, Ca and a host of lithophilic elements were measured in every sample. This allowed us to isolate a

group of samples that are impacted by the Saharan dust transported to our station from the rest of the data set. This Saharan Dust data subset was used to differentiate composition of the Saharan Dust from that of local soil and to determine their relative contributions to total concentration of crustal material in our samples. The data set was also used to investigate year-to-year variability of Saharan dust incursions to the Eastern Mediterranean in the following sections.

#### ***4.5.5.1. Identification of Dust Episode Days***

Different techniques have been applied to identify the Saharan dust intrusions. The use of models, images and satellite data (Goudie and Middleton, 2001; Washington et al., 2003) and backward trajectory calculations (Koçak et al., 2007) are examples. Moreover, the ratios of Ti/Ca and Ti/Al were used as tracers of Saharan dust in many studies (Bonelli et al., 1996; Marengo et al., 2006; Borbely-Kiss et al., 2004). Avila et al. (1997) linked particulate phosphorus deposition with red rains, which is the rain containing dust. Çetin (2002) also used the phosphorus content of the aerosols collected at Antalya, Turkey, to identify the Saharan dust intrusions to Eastern Mediterranean. Koçak et al. (2007) used Fe concentration of  $500 \text{ ng m}^{-3}$  as a threshold value along with backtrajectories and TOMS images to determine Saharan dust episodes in Eastern Mediterranean atmosphere. Recently, Muhs et al. (2007) used relative abundance of less mobile elements and rare earth elements (REEs) to show the intrusions of North African dust to Florida Keys, Bahamas and Barbados. In a more recent study, Trapp et al. (2008) found statistically significant difference for high dust load samples and low dust load samples for some elements, particularly, Lanthanides. However, they also reported that the absolute difference for these elements in two groups of samples is quite small.

In this study, four different criteria were used to identify dust episodes at our sampling station. As a first criterion, high Al days were selected from the data set since Al is a good marker for all sorts of aluminasilicate based material. Previously, Güllü (1996), Kubilay and Saydam (1995), Guerzoni et al. (1999) used Al, which is the major constituent of aluminasilicate matrix, as a marker of Saharan dust. Since possible sample contamination and measurement artifacts might result in high Al concentration, other criteria was also established to separate dust impacted samples from others. Since Al is a soil derived element, samples with high Al concentrations should contain other soil derived elements like Fe, Ca, Mn and Ti in elevated concentrations. Consequently, Fe and

Ca were chosen as second and third criteria in determining dust episode days. Time series plot of Al, Ca, and Fe between 1992 and 2001 was depicted in Figure 4.73. Days (samples) in which Al, Fe and Ca peaks together were identified as the "dust episode" day.

It was previously mentioned that the regional background concentrations of Al, Ca and Fe at our station, found by using "most frequently occurring value" concept are 90, 336, and 45  $\text{ngm}^{-3}$ , respectively. Koçak et al. (2007) have found that Fe concentrations were ranged from 500 to 7000  $\text{ngm}^{-3}$  during dust events, the upper range is about 21 times higher than Fe background concentration (336  $\text{ngm}^{-3}$ ) calculated in this study.

However, it should be highlighted that identification of a dust episode does not necessarily mean that it is a Saharan Dust, because these elements, that is, Fe, Ca and Al, are also rich in local soil. In order to differentiate the Saharan dust episodes from local dust episodes, backtrajectories with starting altitudes 500, 700 and 900 hPa was calculated for each day of the sampling campaign. Dust episode days were assigned to "Saharan Dust Episode" and "Middle East Dust Episode" provided that one of the calculated trajectories (either 500 hPa, 700 hPa or 900 hPa) originated from North Africa and Middle East, respectively.

Figure 4.74 and 4.75 showed the time series plot of Al, Ca and Fe for the first half of 1992 along with air mass backtrajectories calculated for the episode day of 28/03/1992. Since all three criteria elements make peak on 28/03/1992, this day was assigned to "dust episode day". In order to further confirm that this is a "Saharan Episode Day" backtrajectory was calculated for this particular day. It is clear from Figure 4.75 that trajectories arriving to our station at 700 and 900 hPa level from North Africa. Consequently, this day is identified as a "Saharan Episode Day". Same methodology applied for whole generated data. Table 4.26 summarizes the number of data in different groups with respect to years.

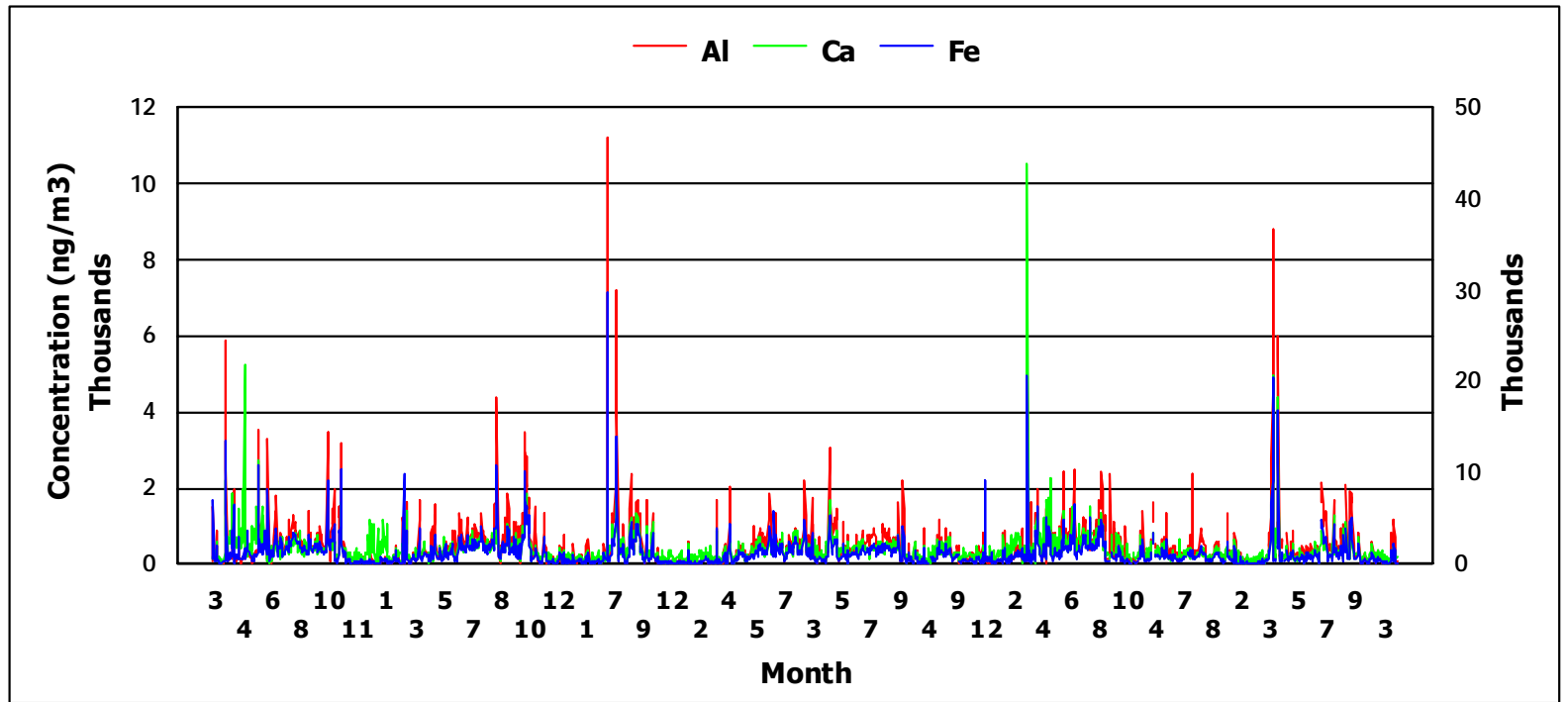


Figure 4.73 Time series plot of Al, Ca and Fe between 1992 and 2001

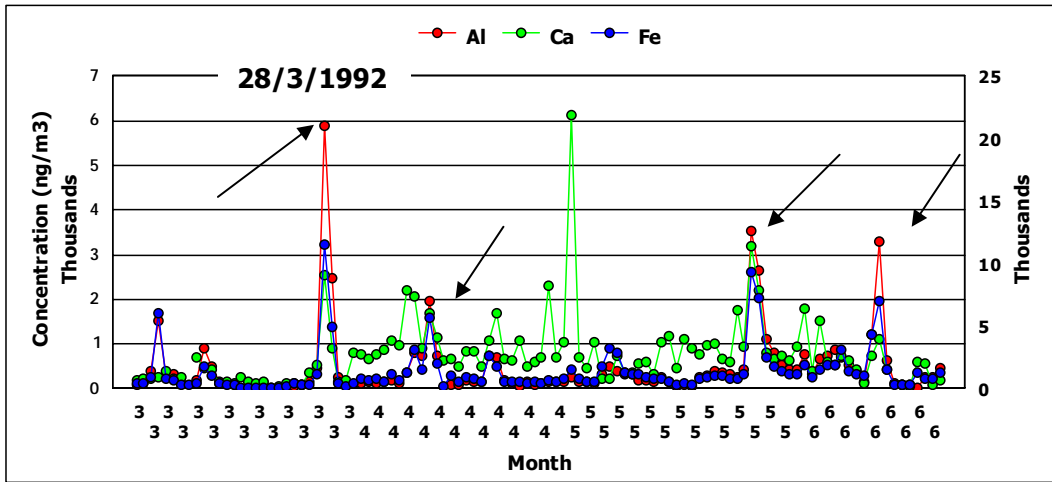


Figure 4.74 Time Series plot of Al, Ca and Fe for the first six month of 1992

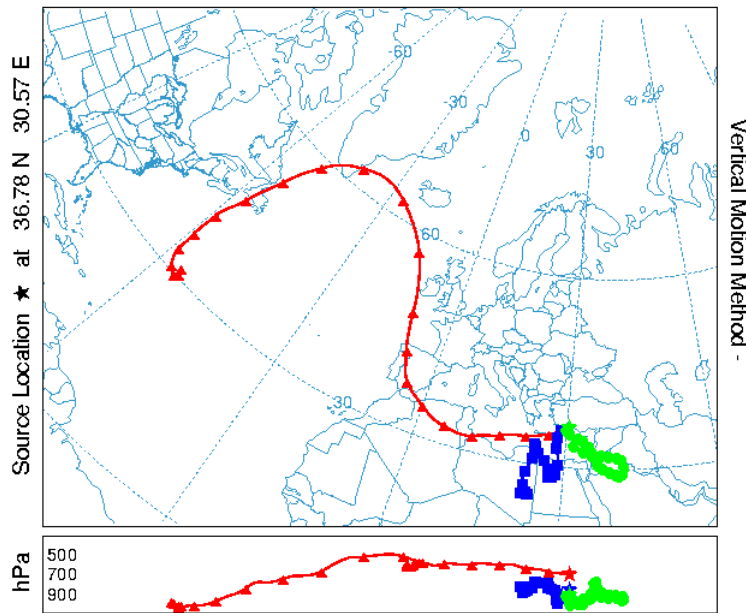


Figure 4.75 Backward trajectory calculated for 28/3/1992 Saharan episode day

Table 4.26 Number of data in different groups with respect to years

Year	Samples Analyzed	Dust Episode	Number of		
			Dust Episode	Saharan Dust Episode	Local Dust Episode
<b>1992</b>	285	18	4	10	4
<b>1993</b>	338	64	8	35	21
<b>1994</b>	197	26	4	5	17
<b>1995</b>	223	16		10	6
<b>1996</b>	172	22		8	14
<b>1997</b>	162	13	3	7	3
<b>1998</b>	231	24	4	13	7
<b>1999</b>	190	19	1	13	5
<b>2000</b>	210	35	3	24	8
<b>2001</b>	71	8		4	4
<b>Total</b>	<b>2079</b>	<b>245</b>	<b>27</b>	<b>129</b>	<b>89</b>

As it can be noticed from Table 4.26, there are some local dust episodes days. These days correspond to resuspension of local soil in the close vicinity of sampling location. Previously mentioned that local soil is also enriched in terms of Al, Ca and Fe thus concurrent high concentrations for these elements represent local dust episodes and should be differentiated from the Saharan and Middle East dust episodes in order to identify the signatures of Saharan dust.

Total Ozone Mass Spectrometer (TOMS) images have been used by many researchers to confirm the finding of measurements and backtrajectories indicating dust intrusions to the study areas (e.g., Koçak et al., 2007; Kaskaoutis et al., 2008). Moreover, TOMS images are also used to find the source regions of dust in North Africa and Middle East (Goudie and Middleton, 2001). TOMS instruments flew onboard on the satellites controlled by National Aeronautics and Space Administration Goddard Space Flight Center. The first TOMS instrument flew onboard the Nimbus 7 spacecraft and has data for the period from November of 1978 through May 6, 1993 when the instrument failed. Data are also available from the TOMS that flew on the Earth Probe (EP) spacecraft (July 1996 - present). TOMS measured the solar irradiance and radiance backscattered by the

<sup>g</sup> ME stands for Middle East



earth's atmosphere in the selected six wavelength band (379.95 nm, 359.88 nm, 339.66 nm, 331.06 nm, 317.35 nm, and 312.34 nm) in the ultraviolet.

In addition to total ozone, aerosol index is another product of TOMS instrument. TOMS aerosol index is a measure of how much the wavelength dependence of backscattered UV radiation from atmosphere containing aerosols (Mie scattering, Rayleigh scattering and absorption) different from that of a pure molecular atmosphere (pure Rayleigh scattering). Aerosol Index (AI) can be defined as:

$$AI = 100 \log_{10} \frac{(I_{360}^{measured})}{(I_{360}^{calculated})} \quad (4.14)$$

Where;

AI: Aerosol Index and calculated and measured EP (Earth Probe) TOMS radiance at 360 nm. In general, positive AI values indicate that measured radiance is greater than calculated one for Rayleigh atmosphere implying that absorbing aerosols (i.e., mineral dust and smoke) are present in the atmosphere. However, negative AI values showed the presence of non-absorbing aerosols (i.e. sulfate particles and sea salt) in the atmosphere (<http://macuv.gsfc.nasa.gov/TOMSAerosol.md>). AI value from TOMS sensor can be obtained on a daily basis on a 1° (Latitude) and 1.25° (Longitude) resolution from the web page of the instrument.

AI values from TOMS instrument were calculated at the approximate location of our sampling point for March 1998 and April 2000, when the highest Ca concentration was observed at our data set (43850 ngm<sup>-3</sup> for 26<sup>th</sup> of March 1998; 20600 and 18255 ngm<sup>-3</sup> for 5<sup>th</sup> and 19<sup>th</sup> of April 2000, respectively). Calcium background concentration determined at our station (336 ng m<sup>-3</sup>) was exceeded by 61 times on 5<sup>th</sup> of April, 2000 and about 131 times on 26<sup>th</sup> of March, 1998.

Spatially averaged AI values were calculated for these episode days along with time series plot of Ca, Fe and AI were depicted in Figure 4.76 for March 1998.

Besides TOMS, Goddard Space Flight Center of NASA provides satellite pictures of Sea-viewing Wide Field of view Sensor (SeaWiFS), which enables visually inspect Saharan

dust with a high resolution as compared to TOMS. SeaWiFS image corresponds to 26<sup>th</sup> of March, 1998 was requested from NASA's webpage and depicted in Figure 4.77. It is very clear from Figure 4.77 that Saharan dust plume cover the atmosphere over Turkey in this particular day.

Though considerably high AI values were determined by TOMS on 15<sup>th</sup> and 16<sup>th</sup> of March, 1998, we did not observe any concurrent elevated values in Al, Ca and Mg concentrations according to ground measurements performed at our station. This pattern in AI value can be attributed with the passage of dust loaded air masses above the mixing height without depositing any dust related material over the region in which our station is located. This suggestion was consistent with the findings of Martin et al. (1990) and Kubilay et al. (2000). Researchers have shown that African air is generally present at upper layers of air from other source regions in the boundary layer because of the frontal air patterns carrying dust to the north. While we detected dust episode on 18<sup>th</sup> of March, 1998 with Al, Ca and Fe concentrations of 8319, 13313 and 4777 ngm<sup>-3</sup>, respectively, corresponding AI value was calculated as 1.71. Hsu et al. (1999) and Kaskaoutis et al. (2008) reported decrease of sensitivity of TOMS below 1000 m in the atmosphere. Consequently, any aerosol below 1000 m is unlikely detected by TOMS, which might explain why we observed dust episode on 18<sup>th</sup> of March, 1998, but corresponding TOMS AI value was small. On 26<sup>th</sup> of March, 1998, we observed anomalously high soil derived element concentrations (Ca: 43850 ngm<sup>-3</sup>; Al: 7699 ngm<sup>-3</sup>; and Fe: 4942 ngm<sup>-3</sup>), particularly for Ca. Corresponding AI value for this particular day was about 26. A sequence of TOMS images for this episode (one day before the episode, episode day and one day after the episode day) was presented in Figure 4.78. On 25 March, 1998, sky over Turkey was clear as it can be seen in Figure 4.78. One day later, episode day, TOMS recorded a dust plume above our sampling station. On 27 March, 1998, dust plume above our sampling station disappeared.

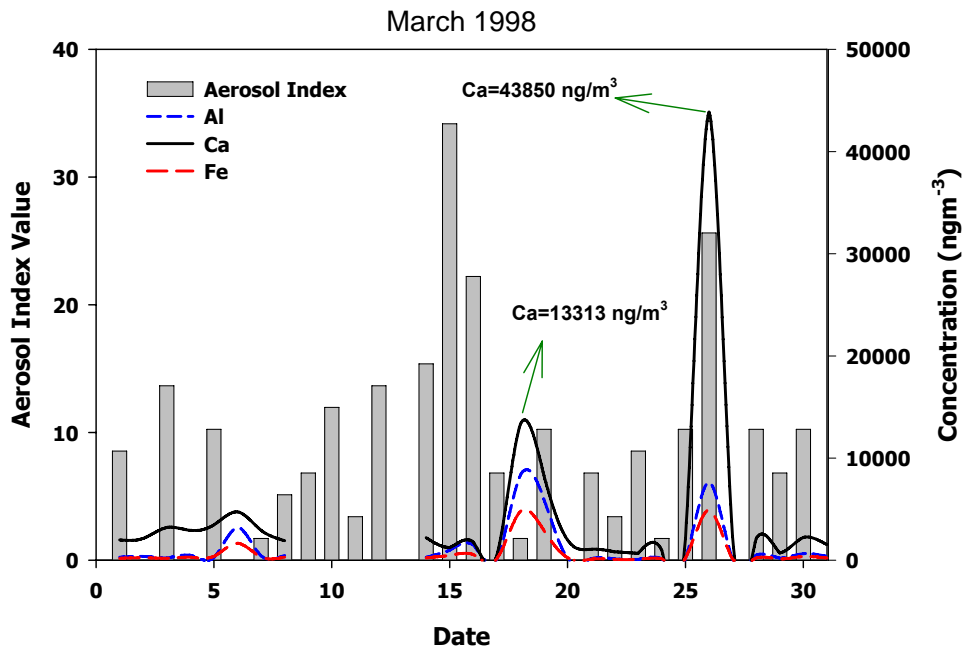


Figure 4.76 Time series plot of measured Al, Ca, Fe and calculated Aerosol Index for March 1998

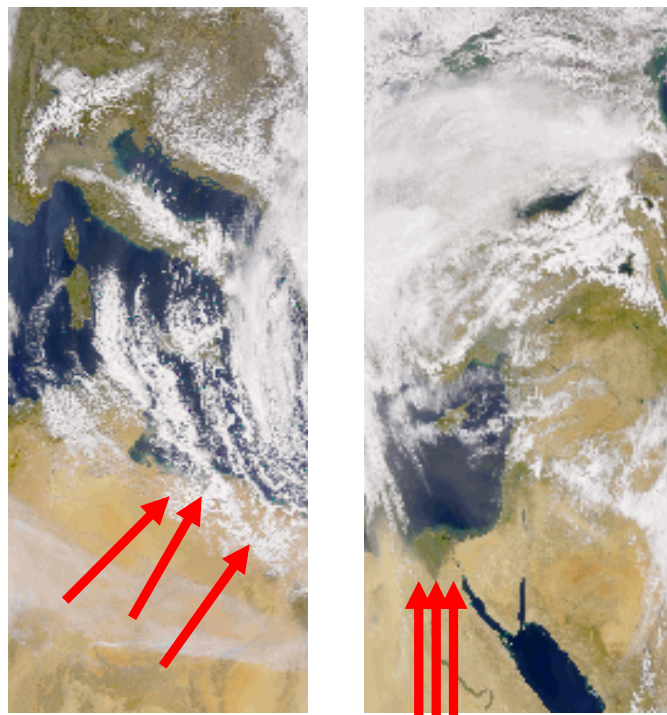


Figure 4.77 SeaWiFS image for 26<sup>th</sup> of March 1998 obtained from NASA web page

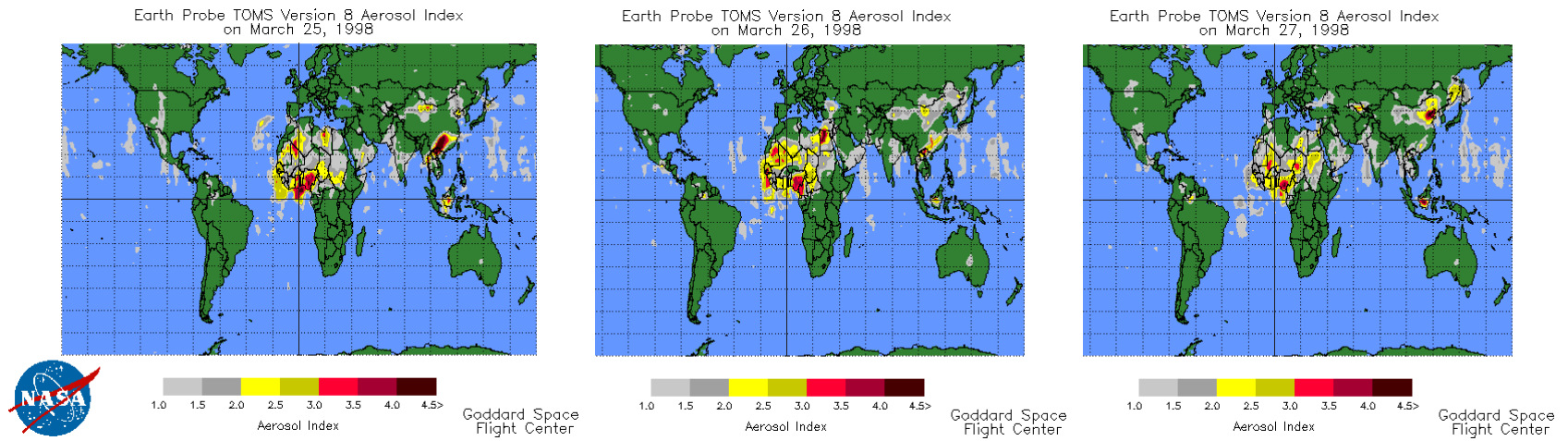


Figure 4.78 A sequence of TOMS images for episode observed on 26<sup>th</sup> of March, 1998

Spatially averaged AI values were calculated for these episode days along with time series plot of Ca, Fe and Al were depicted in Figure 4.79 for March 1998. Regarding to episodes observed in April, 2000, synchronous increase in soil derived elements used to identify Saharan dust episodes with high AI value obtained from TOMS instrument for 5<sup>th</sup>, 18<sup>th</sup> and 19<sup>th</sup> of April, 2000. There were significantly high AI values were calculated at our station in some of the days, for instance, 1<sup>st</sup>, 10<sup>th</sup> and 25<sup>th</sup> of April, 2000. However, we did not record high Al, Ca, and Fe concentrations for the samples collected in these days. The reason was described earlier as passage of air masses over the mixing height without scavenging of particles from loaded air masses. A sequence of TOMS images between 16<sup>th</sup> and 21<sup>st</sup> April was provided in Figure 4.80. There is a good agreement between TOMS images and measured Al, Ca and Fe concentrations with the exception of 17<sup>th</sup> of April. Sample collected in this day was not analyzed. There was a dust plume over the sampling station on 16<sup>th</sup>, 17<sup>th</sup>, 18<sup>th</sup> and 19<sup>th</sup> of April, 2000 as depicted in Figure 4.80. Dust plume disappeared on 20<sup>th</sup> and 21<sup>st</sup> of April, 2000.

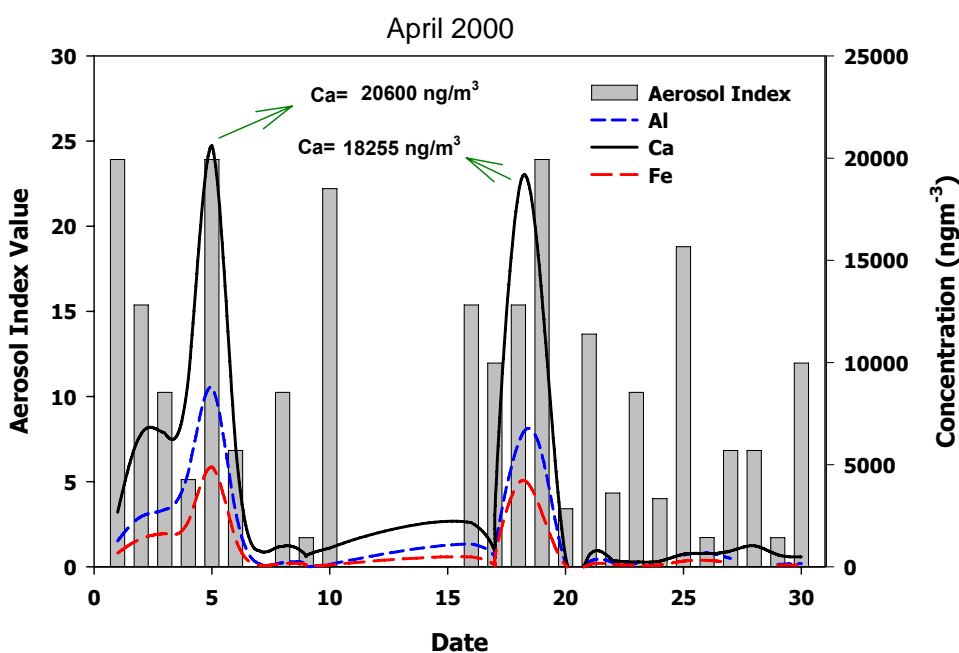


Figure 4.79 Time series plot of measured Al, Ca, Fe and calculated Aerosol Index for April 2000

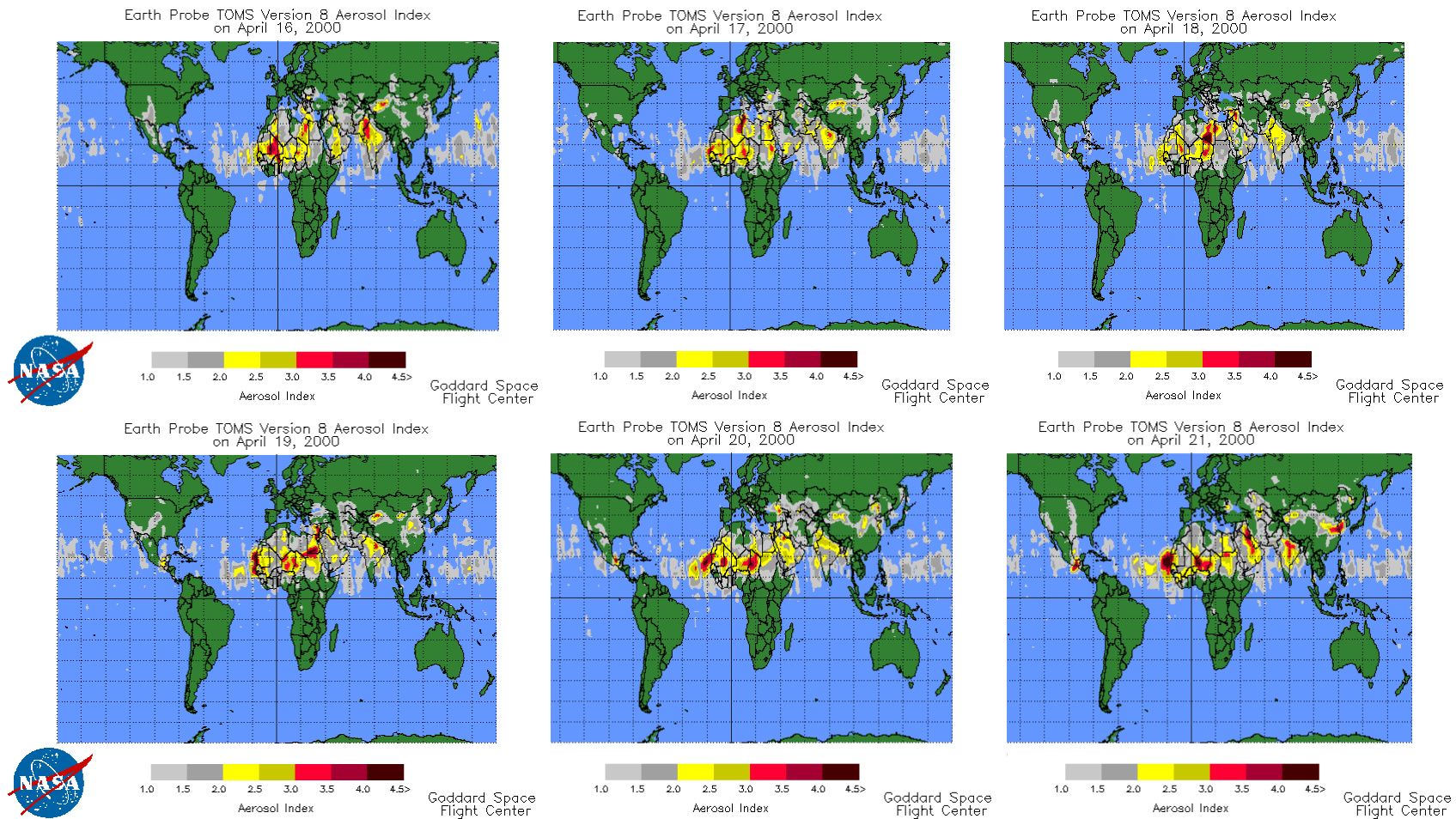


Figure 4.80 A sequence of TOMS images for episodes observed on 16<sup>th</sup> and 21<sup>st</sup> of April, 2000

#### **4.5.5.2. Chemical Tracers of Saharan and Middle East Dust**

As stated previously there are important environmental impacts of Saharan dust. In addition to this, there is a legal concern related with Saharan dust outbreaks in some of the countries, especially ones located Southern part of Europe. Daily limit established for daily PM<sub>10</sub> exceedance in Europe by 1999/30/CE Directive is 50 µg m<sup>-3</sup> (Meloni et al., 2008). Gobbi et al. (2007) have reported that Saharan Dust was responsible for 63-68 % of daily exceedance at a rural station in Rome. Consequently, it is crucial for countries close to North Africa to differentiate Saharan dust from dust emitted to the atmosphere by resuspension of local soil or PM<sub>10</sub> generated from anthropogenic sources. To this end one should find the markers of Saharan dust that should be unique in composition. The dominance of SiO<sub>2</sub> in dust transported from Africa is well known. In addition to this, Fe<sub>2</sub>O<sub>3</sub>, MgO and CaO are in considerable amounts in Saharan dust. Although these compounds are good tracers of soil, they are not useful in differentiating Saharan dust from other dust sources. The high CaCO<sub>3</sub> content of Saharan dust has a very important implication. Özsoy and Saydam (2000) linked increase of precipitation pH recorded in Eastern Mediterranean to close proximity of sampling location to North Africa.

Clay mineralogy of Saharan dust has been investigated extensively. Caquineau et al. (1998) investigated the clay minerals in collected dust samples at Sal Island. Researchers were able to show that highest amount of *illite* present in dust samples originating from North and West Sahara whereas *kaolinite* was associated with air masses from Sahelian origin. Although the amount of *illite* could not be detected in south and central Sahara, *kaolinite* was present in these regions in considerable amounts. Foucault and Melieres (2000) claimed that *kaolinite* is the most important aeolian clay mineral input transported from Africa to the Eastern end of the Mediterranean.

Though clay mineralogy was studied to differentiate dust originating from Africa (e.g., Molinaroli, 1996), there is not a unique tracer of African dust determined in the literature. Recently, Trapp et al. (2008) used analyzed the samples collected at Barbados in terms of their lanthanides (Ce, Dy, Eu, Er, Gd, Ho, Lu, Nd, Pr, Sm and Tm) content and tried to use the lanthanides as marker of dust transported from Africa.

Since considerable amount of trace elements were analyzed in this study, we decided to use these elements to differentiate local dust from dust originated from Africa. Crustal

enrichment factors calculated previously indicated for some of the parameters anthropogenic contribution is significant. Consequently, these parameters such as Pb,  $\text{SO}_4^{2-}$ , As, Sb, Se and Cd were impacted by the man made sources and not taken into account in this apportionment exercise. The rest of the parameters were normalized with Al since upper earth crust is rich in this element, which enable us to detect any significant difference between local soil and other groups given in Table 4.26.

After normalization with Al, median element concentrations were calculated in each group tabulated in Table 4.26. Median values were used since it better represents the log-normally distributed data. Afterwards, median concentration of particular element in one group (one of Saharan, Middle East or local dust) was divided to corresponding median concentration in the second group to calculate "Saharan Dust to Local Dust", "Middle East Dust to Local Dust" and "Saharan Dust to Middle East Dust" ratios. These calculated ratios were depicted in Figure 4.81 – 4.83. Calculated Saharan dust to local dust ratio was illustrated in Figure 4.81 in descending order. For most of the Lanthanides such as Dy, Ho, Tm, Lu, Yb, Er, Sm, Eu, Nd, Hf, Ce and Pr calculated ratio is greater than one implying that these elements can be used as signatures of Saharan dust. Alkali metals (K and Cs) and alkaline earth metals (Mg, Ca and Ba) present in high concentration in local soil than Saharan dust. Trapp et al. (2008) reported that Eu, Ho and Lu are commonly associated with pollutants. Consequently, one should be careful in using these elements as fingerprints of Saharan dust.

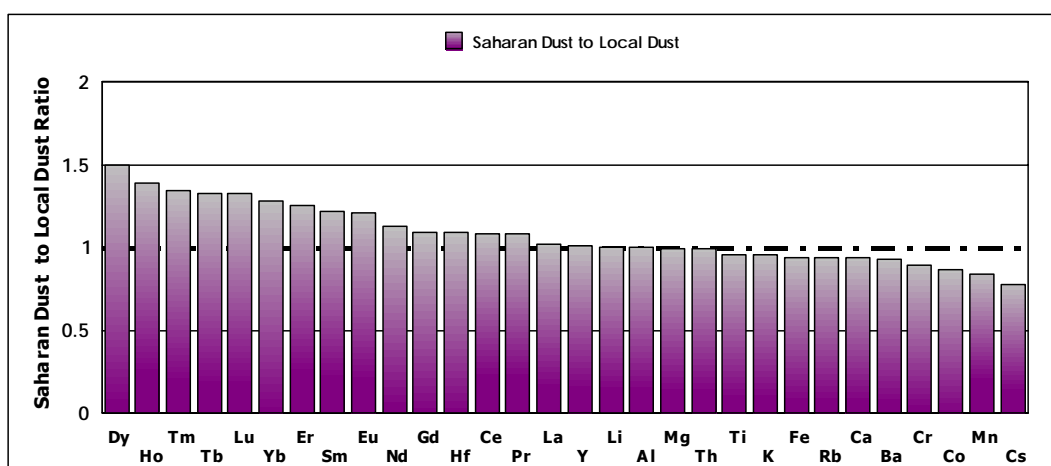


Figure 4.81 Saharan dust to local dust ratio of each parameter in descending order



Difference between Saharan and Middle East dust was calculated and results were presented in Figure 4.82. With the exception of Fe, Al, Co, Mg and Ca, elements in Saharan dust are higher than elements associated with the air masses originating from Middle East (calculated ratio greater than one). Consequently, Saharan dust composition is significantly different from local soil and Middle East. Middle East dust to local dust ratio was also calculated for each element to see at what extent elements in these two groups are different from each other as depicted in Figure 4.83. For all elements, except for Ca and Mg concentrations in local dust is significantly higher than corresponding concentrations in Middle East dust.

The calculated ratios for three different groups indicate that Saharan dust composition significantly differs from Middle East dust composition and local soil in the vicinity of our sampling location, particularly for Lanthanides (Dy, Ho, Tm, Lu, Yb, Er, Sm, Eu, Nd, Hf, Ce and Pr).

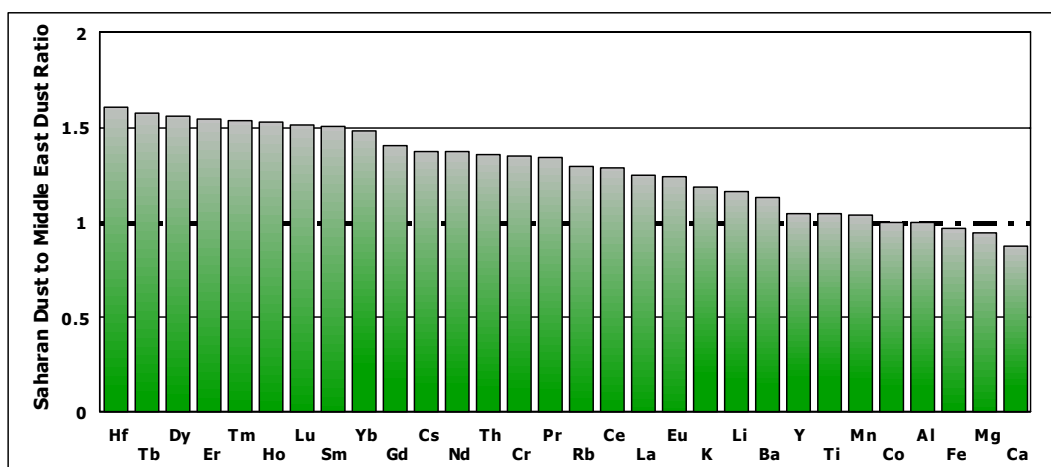


Figure 4.82 Ratios of elements in different groups

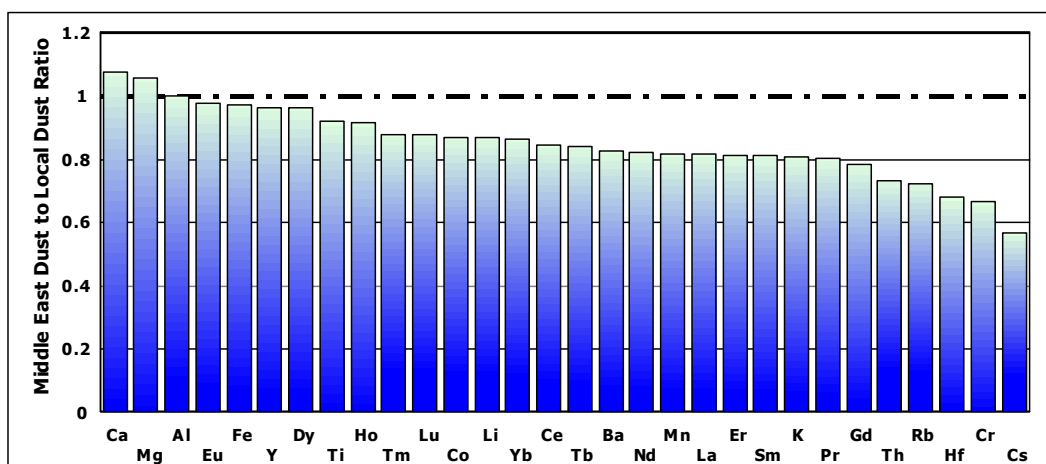


Figure 4.83 Ratios of elements in different groups

#### 4.5.5.3. Temporal Variation of Saharan Dust Frequencies

Variation of dust episodes with time is not well established in the literature. Zhu et al. (1997) suggested that the frequency of Saharan dust episode increase in recent years but researcher did not give an exact time of increase. Goudie and Middleton (1992) and Middleton (1985) claimed that dust storm frequency increased in 1960s, which is concurrent with the droughts observed in the Sahelian zone, which is south of 30 °N latitude in North Africa. Later, N'Tchayi Mbourou et al. (1997) suggested that both the frequency and annual duration o Saharan dust increased since the late 1950's. Zhu et al. (1997) have shown that Saharan dust concentrations increased in the station of Barbados between 1965 and 1992. Prospero (1996) put forward that the concentrations detected in Barbados were inversely related with the precipitation data recorded in Sahelian Africa.

Two sided Mann Kendall test at 5 % significance level was applied to annual Saharan dust episodes numbers given in Table 21. Mann Kendall test statistic was found as  $S=-1$ . The negative sign in calculated "S" value indicates that episodes detected at our station later in time tend to be smaller. However, number of data points used in the calculation was not enough to test the statistical significance of this finding, implying that there is not enough evidence to determine whether there is a decreasing or increasing trend in Saharan dust frequencies. The highest frequencies of Saharan dust episodes were

determined at our stations in 1993 with a number of 35 followed by 24 in 2000. However, it should be noted that there were missing days when samples were not collected or when collected samples were not analyzed. The discussion on the temporal variations of pollutant concentrations presented in Section 4.4.3 indicated that there is a decreasing trend in the concentrations of soil derived elements particularly in the concentrations of rare earth elements. Since rare earth elements are important signatures of dust transported from North Africa, Saharan dust may have a decreasing trend between 1993 and 2001. In a recent paper, Foltz and Mcphaden (2008) confirmed our finding. Researchers illustrated that there is a decreasing trend in Aerosol Optical Depth (AOD) covering all over the North Africa and the tropical North Atlantic Ocean, which further implies that there was a considerable decrease in dust production between 1980 and 2006. Researchers linked this declining trend in dust production with significant increase in Sahel precipitation data within this period.

Dust transport from North Africa to Eastern Mediterranean generally observed during spring months and is generally associated with the eastward passage of frontal low pressure systems. In contrast to this, Middle East dust transport to Eastern Mediterranean occurs in the autumn (Kubilay et al., 2000; Goudie et al., 2001). Koçak et al. (2007) have also pointed out that mineral dust transport from North Africa can be observed at any time of the year while the frequency of events is higher in March, April, May and October while air masses are associated with the cyclonic activity. Monthly variation of Saharan dust intrusions observed at Antalya station between 1992 and 2001 was depicted in Figure 4.84.

The high variability of African dust was previously reported in the literature. Prospero and Lamb (2003) reported means of dust records showed seasonal variations by a factor of ten while annual means varied by a factor of four over the 40 years in Barbados, USA. Researchers have linked this variability to climate changes such as drought cycle in Africa. Later, Ginoux et al. (2004) attributed this variability to El Niño events and the North Atlantic Oscillation.

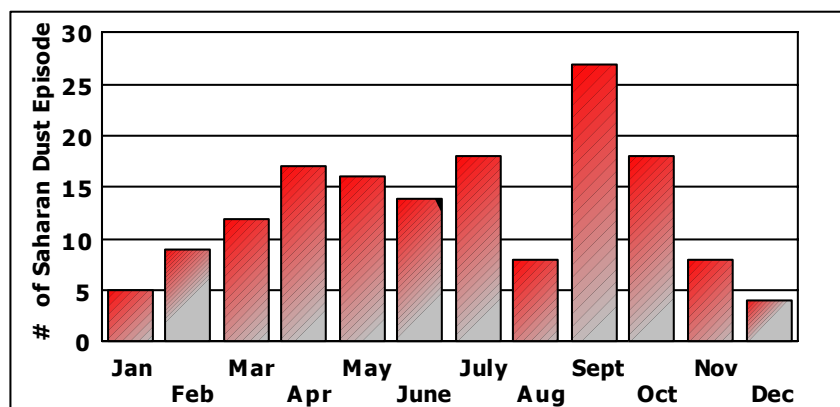


Figure 4.84 Variation of recorded Saharan dust episode with months

#### 4.5.6. Source Apportionment with Factor Analysis (FA) and Positive Matrix Factorization (PMF)

There are three approaches that are commonly used in source apportionment: (1) Techniques based on the assessment of the monitoring data. For example, use of correlation of wind direction with measured concentrations to identify source regions (e.g., Henry et al., 2002) or use of correlations between particulate matter and gaseous pollutants to find associations can be considered in the first approach. Techniques used in this approach can be considered as tools for preliminary data treatment that can be useful in more sophisticated source apportionment techniques. (2) Source oriented techniques that bases on emission inventories and dispersion models (e.g., Visser et al., 2001). A major drawback of this approach is that they require emission inventories, which are not available all the time. (3) Receptor oriented techniques that bases on chemical composition data of particulate matter or gaseous species at the receptor site (receptor models). Two types of statistical tools are commonly used in receptor modeling, namely, multivariate statistical tools, such as multilinear engine (e.g., Hopke et al., 2003), factor analysis (e.g., Ogulei et al., 2005; Plaisance and Guillermo, 1997), principal component analysis (e.g., Anttila et al., 1995) and cluster analysis (e.g., Abdalmogith and Harrison, 2005) and statistical methods that base on least square fitting, such as chemical mass balance (e.g., Schauer et al., 1996) and positive matrix factorization (the PMF can be placed in both categories) (e.g., Poirot et al., 2001).

Viana et al. (2008) reported that Principal Component Analysis, which is a receptor modelling approach, was used 30 % of the studies conducted in Europe till 2005. This is followed by Lenschow approach and back-trajectory analysis with 11 % each. Positive Matrix Factorization (PMF) and Chemical Mass Balance (CMB) were used in 8 and 7 % of studies, respectively.

Güllü et al. (2004) applied varimax rotation factor analysis to data generated at Antalya station. Researchers identified 4 factors influencing the chemical composition of Eastern Mediterranean as crustal, sea salt, long range transport and local As.

In order to find sources of pollutants affecting chemical composition of aerosol collected at our station, we have used two kinds of statistical techniques: (1) Factor Analysis (FA); (2) Positive Matrix Factorization (PMF). Both FA and PMF have advantages and disadvantages. One of the biggest advantages of PMF is the non-negativity constraint, that is, contribution from sources can not be negative. However, negative factor loadings can be obtained in FA, and this is hard to interpret. The other advantage of PMF is that this model can handle with missing values. In case of FA, elements with high missing values should be removed from input data matrix. While source apportionment can be performed quantitatively in PMF, application of Multiple Linear Regression is necessary after FA to quantify the contribution of sources. Though PMF has significant advantages over FA, application of FA before PMF can be useful for researcher.

The most important drawback of PMF is that there is predefined criterion to determine the number of factors. Generally, number of factors resolved by PMF is somehow subjective and researcher should retain the factors that can be physically interpretable. Nevertheless, there are studies in which one element or one ion can be retained such as  $\text{SO}_4^{2-}$  factor or Organic Carbon factor (Hopke et al., 2003) though they are physically meaningless. In contrast to this, number of factors that can be extracted with FA is almost known. Although there are different approaches for this, the most commonly applied one is known as "Kaizer Method", in which factors having eigenvalues greater than 1 is retained in the analysis. Both of these techniques are used in receptor modelling and they do not rely on the source profiles. Factor analysis approach was applied in order to gain information on number and profile of the factors prior to Positive Matrix Factorization (PMF). As will be discussed later about 80 % of the system variance was explained by both of these techniques. Though it is not expected to obtain one to one correspondence in factor number and factor profiles obtained by FA and PMF, high

percentage of system variance explained by both of these techniques implied that corresponding results were not so different from each other.

Number and percentage of below detection limit data in addition to missing values used in input data matrix in both techniques was summarized in Table 4.27.

#### ***4.5.6.1. Factor Analysis***

In order to have an opinion on the number of factors that might be extracted in Positive Matrix Factorization (PMF), factor analysis was initially performed on the generated data set. Factor analysis, identifies minimum number of common factors whose variance often accounts for most of the variance of the parameters of concern.

In this study, varimax rotation was used in factor analysis to improve the orthogonality of the resolved factors. After first run using 1448 sample points, samples having factor score values greater than absolute of 7 were deleted from the data set and factor analysis was run again till no factor scores greater than 7 remained for each factor. Although there is no established criterion in factor analysis to find the minimum number of factors, some general guidelines were presented here: (1) Number of factors identified in the factor analysis should be less than parameters investigated. (2) Communalities of parameters included in the factor analysis should be close to 1. (3) Factors having eigenvalues greater than 1 should be retained in the factor analysis since eigenvalues less than 1 indicated insignificant contribution to system variance. (4) Even if a factor has eigenvalue greater than one, it may be physically meaningless in the factor analysis. Consequently, researcher should assess whether the obtained factor has a physical meaning or not. With the exception of U, Sr, Eu, Dy, Au, In,  $\text{NO}_3^-$  and  $\text{NH}_4^+$ , for which the percentage of the data points smaller than corresponding Method Detection Limit (MDL) was greater than 20 %, the rest of the parameters presented in Table 4.27 were included in factor analysis.

Factor Analysis can not handle with the missing values and hence, missing values in the data matrix should be replaced with appropriate numbers. However, whichever the method used in filling the missing values, there is not always possible to obtain correct values instead of missing ones. For this reason, if missing values account for 70 % of data points for a particular parameter, then this parameter should be excluded from input

data matrix. Güllü (1996) replaced the missing values with the regional background concentration prior to FA. In this study, missing values in data matrix used in factor analysis were replaced with half of the corresponding detection limit value.

Table 4.27 Summary statistics of measured parameters used in the source apportionment analysis

	<b># of Data Points</b>	<b># of Missing Values</b>	<b># of BDL Values</b>	<b>% of Missing Values</b>	<b>% of BDL Values</b>
<b>Al</b>	1450	2	4	0.14	0.28
<b>As</b>	1450	2	0	0.14	0.00
<b>Au</b>	659	793	396	54.61	27.27
<b>Ba</b>	1442	10	97	0.69	6.68
<b>Be</b>	1443	9	48	0.62	3.31
<b>Bi</b>	1396	56	262	3.86	18.04
<b>Ca</b>	1439	13	106	0.90	7.30
<b>Cd</b>	1449	3	7	0.21	0.48
<b>Ce</b>	1445	7	14	0.48	0.96
<b>Cl</b>	1344	108	5	7.44	0.34
<b>Co</b>	1446	6	88	0.41	6.06
<b>Cr</b>	1349	103	178	7.09	12.26
<b>Cs</b>	1449	3	1	0.21	0.07
<b>Dy</b>	1277	175	601	12.05	41.39
<b>Er</b>	1450	2	5	0.14	0.34
<b>Eu</b>	917	535	704	36.85	48.48
<b>Fe</b>	1418	34	132	2.34	9.09
<b>Gd</b>	1447	5	6	0.34	0.41
<b>Ge</b>	1449	3	0	0.21	0.00
<b>Hf</b>	1428	24	166	1.65	11.43
<b>Ho</b>	1449	3	18	0.21	1.24
<b>In</b>	1391	61	492	4.20	33.88
<b>K</b>	1447	5	7	0.34	0.48
<b>La</b>	1446	6	16	0.41	1.10
<b>Li</b>	1448	4	10	0.28	0.69
<b>Lu</b>	1447	5	10	0.34	0.69
<b>Mg</b>	1449	3	0	0.21	0.00
<b>Mn</b>	1450	2	2	0.14	0.14
<b>Na</b>	1446	6	3	0.41	0.21
<b>Nd</b>	1448	4	8	0.28	0.55
<b>NH<sub>4</sub><sup>+</sup></b>	847	605	37	41.67	2.55
<b>Ni</b>	1437	15	227	1.03	15.63
<b>NO<sub>3</sub><sup>-</sup></b>	943	509	25	35.06	1.72

Table 4.27 Summary statistics of measured parameters used in the source apportionment analysis (Continued)

	<b># of Data Points</b>	<b># of Missing Values</b>	<b># of BDL Values</b>	<b>% of Missing Values</b>	<b>% of BDL Values</b>
<b>Pb</b>	1447	5	1	0.34	0.07
<b>Pr</b>	1449	3	7	0.21	0.48
<b>Pt</b>	705	747	268	51.45	18.46
<b>Rb</b>	1450	2	1	0.14	0.07
<b>Sb</b>	1447	5	1	0.34	0.07
<b>Se</b>	1420	32	11	2.20	0.76
<b>Sm</b>	1448	4	11	0.28	0.76
<b>Sn</b>	1446	6	16	0.41	1.10
<b>SO<sub>4</sub><sup>2-</sup></b>	1420	33	0	2.27	0.00
<b>Sr</b>	<i>1433</i>	<i>19</i>	<i>452</i>	<i>1.31</i>	<i>31.13</i>
<b>Tb</b>	1450	2	12	0.14	0.83
<b>Th</b>	1406	46	247	3.17	17.01
<b>Ti</b>	1450	2	11	0.14	0.76
<b>Tm</b>	1448	4	14	0.28	0.96
<b>U</b>	<i>1406</i>	<i>46</i>	<i>367</i>	<i>3.17</i>	<i>25.28</i>
<b>V</b>	1448	4	1	0.28	0.07
<b>W</b>	1426	26	208	1.79	14.33
<b>Y</b>	1450	2	6	0.14	0.41
<b>Yb</b>	1450	2	8	0.14	0.55
<b>Zn</b>	1439	13	32	0.90	2.20

Scree plot obtained from the factor analysis was depicted in Figure 4.85. As it can be seen from Figure 4.85, calculated eigenvalue was greater than 1 for seven factors, while it is very close to 1 (0.958) for eight factor results. Following the guideline provided above, seven factors were retained in this factor analysis and results were tabulated in Table 4.28.

Since an advanced factor analysis technique (PMF) was also applied in this study, detailed information on the conducted factor analysis will not be provided herein. As it can be seen from Table 4.28, all of the parameters included in the factor analysis had communalities greater than 0.60 with the exception of Be, Bi, Pt and W. Seven extracted factors account for ~ 80 % of the total variance. Factor loadings given in Table 4.26 are significant if their corresponding value is greater than 0.25. For this reason, factor loadings larger than this criterion was demonstrated in bold. It is obvious that factor one



is a crustal factor since it includes considerably high loadings of soil derived elements such as Al, Ca, Fe and rare earths (e.g., La, Lu, Gd, Tm and Tb). This factor accounts for ~ 54 % of the system variance alone. It was previously shown that the major tracers of the Saharan dust are rare earth elements. Since high loadings of these elements were not observed in other factors, it can be suitable to call this factor as "Saharan Dust" factor.

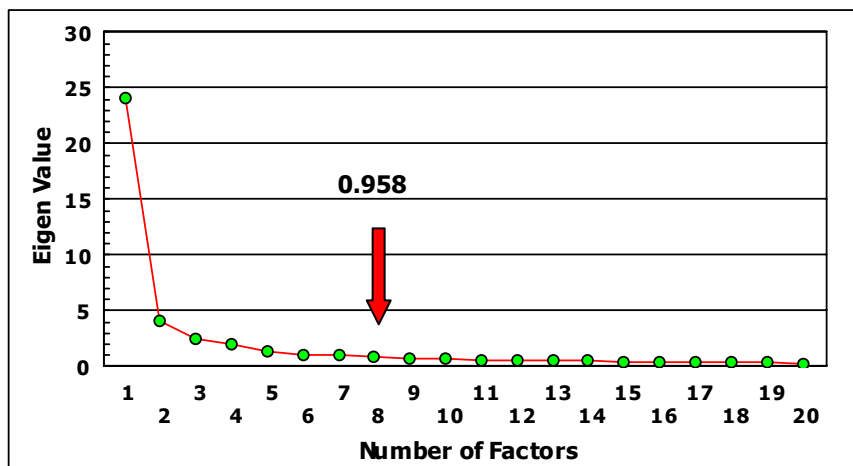


Figure 4.85 Scree plot of applied factor analysis

High loadings of  $\text{SO}_4^{2-}$ , V and Zn implied that this factor is sort of anthropogenic in origin. All of these elements are well known markers of coal ( $\text{SO}_4^{2-}$ , Zn) and oil combustion (V). It was previously shown by Güllü et al. (2004) that long range transported material to Eastern Mediterranean had similar composition with one observed here. This factor is responsible for ~ 9 % of the system variance.

Third factor has high loadings of Na, Cl, and Mg and moderate loading of K. These elements are markers of sea salt and hence, this factor is called as "sea salt" factor, which responsible for ~ 5.4 % of the total variance.

Moderate loadings of Y, V, Ti, Rb, Mn, K, Fe, Cs, Co and Ca in addition to high loadings of Cr and Ni implied that fourth factor is crustal factor. Local soil around the sampling station contains considerable quantities of Cr and Ni (Güllü et al., 2004).

Fifth factor accounts for about 3 % of the total variance and has high loadings of As and Ge along with moderate loadings of Cs, Co, Cd, Bi and Be are observed. Arsenic and Ge are typical tracers of coal combustion. For this reason, is called as coal combustion factor.

Sixth factor is highly loaded in Pb, Pt, Sb, Sn and W. Lead is the major signature of gasoline use from motor vehicle emissions in the atmosphere. Consequently, we called this factor as motor vehicle emission factor. This factor accounts for 2.5 % of system variance.

Last factor contains high loadings of Se and weak loadings of As and Bi. Selenium is mainly emitted from coal combustion. Consequently, this factor is another coal combustion factor.

#### **4.5.6.2. Positive Matrix Factorization (PMF)**

Detailed information on Positive Matrix Factorization was provided previously in Section 2.5.1. However, construction of input data matrix, assumptions made for the PMF analysis and PMF results will be discussed in the following sections.

##### **4.5.6.2.1. Construction of Input Data Matrix for PMF**

For each of the measured value, an uncertainty was calculated as described in Baumann et al., (2008). Below given equation was used in uncertainty calculation:

$$UNC = \sqrt{\left(\frac{MDL}{3}\right)^2 + (P \times CONC)^2} \quad (4.15)$$

Where;

UNC= uncertainty

MDL= method detection limit

P= concentration dependent precision

CONC= concentration of the parameter of concern

Table 4.28 Varimax rotated factor loadings obtained from factor analysis

	<b>Factor 1</b>	<b>Factor 2</b>	<b>Factor 3</b>	<b>Factor 4</b>	<b>Factor 5</b>	<b>Factor 6</b>	<b>Factor 7</b>	<b>Communality</b>
<b>Al</b>	<b>0.91</b>	0.10	0.07	0.20	0.10	0.00	0.10	0.91
<b>As</b>	0.04	0.21	-0.16	0.02	<b>0.67</b>	<b>0.25</b>	<b>0.37</b>	0.73
<b>Ba</b>	<b>0.73</b>	0.20	-0.03	0.08	0.08	<b>0.33</b>	-0.11	0.71
<b>Be</b>	<b>0.57</b>	-0.03	0.09	-0.06	<b>0.32</b>	0.09	0.14	0.47
<b>Bi</b>	0.11	<b>0.45</b>	-0.03	-0.10	<b>0.35</b>	0.19	<b>-0.40</b>	0.55
<b>Ca</b>	<b>0.68</b>	0.02	0.19	<b>0.40</b>	0.19	<b>0.24</b>	0.06	0.75
<b>Cd</b>	0.12	<b>0.70</b>	-0.03	0.15	<b>0.42</b>	<b>0.21</b>	-0.16	0.77
<b>Ce</b>	<b>0.97</b>	0.11	0.04	0.11	0.06	0.09	0.01	0.98
<b>Cl</b>	-0.04	-0.10	<b>0.84</b>	0.01	-0.09	-0.09	-0.02	0.72
<b>Co</b>	<b>0.51</b>	0.19	0.03	<b>0.48</b>	<b>0.49</b>	-0.10	-0.13	0.79
<b>Cr</b>	0.22	0.11	-0.02	<b>0.73</b>	0.17	<b>0.23</b>	-0.02	0.67
<b>Cs</b>	<b>0.63</b>	<b>0.40</b>	-0.01	<b>0.25</b>	<b>0.44</b>	0.16	-0.13	0.85
<b>Er</b>	<b>0.96</b>	0.13	0.04	0.01	0.02	0.17	-0.08	0.98
<b>Fe</b>	<b>0.86</b>	0.16	0.05	<b>0.34</b>	0.13	-0.03	0.13	0.93
<b>Gd</b>	<b>0.96</b>	0.12	0.04	0.01	0.03	0.16	-0.06	0.97
<b>Ge</b>	0.11	0.12	-0.04	0.19	<b>0.87</b>	-0.02	-0.05	0.83
<b>Hf</b>	<b>0.78</b>	0.11	0.05	0.10	0.12	0.18	-0.15	0.69
<b>Ho</b>	<b>0.96</b>	0.13	0.04	0.02	0.03	0.17	-0.08	0.98
<b>K</b>	<b>0.67</b>	<b>0.30</b>	<b>0.40</b>	<b>0.29</b>	0.18	0.13	0.14	0.84
<b>La</b>	<b>0.96</b>	0.12	0.04	0.11	0.08	0.10	0.02	0.97
<b>Li</b>	<b>0.89</b>	0.13	0.12	0.14	0.03	0.11	0.07	0.86
<b>Lu</b>	<b>0.96</b>	0.13	0.04	0.01	0.03	0.18	-0.08	0.98
<b>Mg</b>	<b>0.45</b>	0.08	<b>0.82</b>	0.10	0.04	0.11	0.07	0.92
<b>Mn</b>	<b>0.77</b>	<b>0.34</b>	0.03	<b>0.38</b>	0.19	0.10	0.15	0.92

Table 4.28 Varimax rotated factor loadings obtained from factor analysis (Continued)

	<b>Factor 1</b>	<b>Factor 2</b>	<b>Factor 3</b>	<b>Factor 4</b>	<b>Factor 5</b>	<b>Factor 6</b>	<b>Factor 7</b>	<b>Communality</b>
<b>Na</b>	0.04	0.09	<b>0.91</b>	-0.07	-0.06	0.06	0.02	0.85
<b>Nd</b>	<b>0.98</b>	0.11	0.04	0.07	0.05	0.10	-0.02	0.99
<b>Ni</b>	0.19	<b>0.35</b>	-0.01	<b>0.69</b>	0.04	0.06	0.10	0.64
<b>Pb</b>	<b>0.33</b>	<b>0.40</b>	0.02	-0.11	0.11	<b>0.61</b>	-0.09	0.67
<b>Pr</b>	<b>0.82</b>	0.12	0.02	0.04	0.03	0.05	0.01	0.69
<b>Pt</b>	0.05	-0.09	0.03	0.21	-0.06	<b>0.52</b>	0.09	0.34
<b>Rb</b>	<b>0.83</b>	<b>0.32</b>	0.05	<b>0.32</b>	0.15	0.05	0.11	0.93
<b>Sb</b>	0.19	<b>0.31</b>	-0.03	0.11	0.14	<b>0.65</b>	0.11	0.60
<b>Se</b>	-0.03	0.20	0.06	0.03	0.08	0.02	<b>0.78</b>	0.65
<b>Sm</b>	<b>0.97</b>	0.13	0.04	0.05	0.04	0.14	-0.04	0.98
<b>Sn</b>	0.28	<b>0.57</b>	-0.01	0.15	0.08	<b>0.52</b>	-0.04	0.70
<b>SO<sub>4</sub><sup>2-</sup></b>	0.20	<b>0.85</b>	0.08	0.03	0.01	0.04	0.10	0.79
<b>Tb</b>	<b>0.97</b>	0.13	0.04	0.02	0.03	0.15	-0.06	0.98
<b>Th</b>	<b>0.94</b>	0.14	0.04	0.05	0.06	0.18	-0.04	0.95
<b>Ti</b>	<b>0.87</b>	0.09	0.05	<b>0.33</b>	0.11	-0.07	0.10	0.89
<b>Tm</b>	<b>0.96</b>	0.13	0.04	0.02	0.03	0.18	-0.08	0.97
<b>V</b>	0.38	<b>0.71</b>	0.05	<b>0.29</b>	0.00	-0.03	0.22	0.79
<b>W</b>	0.29	0.18	0.05	-0.06	0.09	<b>0.54</b>	-0.18	0.46
<b>Y</b>	<b>0.92</b>	0.15	0.04	<b>0.26</b>	0.08	-0.02	0.09	0.95
<b>Yb</b>	<b>0.96</b>	0.13	0.03	0.01	0.03	0.18	-0.08	0.98
<b>Zn</b>	0.10	<b>0.72</b>	-0.01	0.16	0.10	0.19	0.16	0.63
<b>Eigenvalue</b>	24.15	4.03	2.42	2.04	1.41	1.13	1.02	
<b>% Variance</b>	53.68	8.96	5.38	4.52	3.12	2.50	2.27	<b>80.44</b>

Signal to Noise ratio (SNR) was calculated for each parameter by using the following equation:

$$S/N = \frac{1}{2} \times \sqrt{\frac{\sum CONC^2}{\sum UNC^2}} \quad (4.16)$$

Calculated SNRs were tabulated in Table 4.29. Buzcu-Guven et al. (2007) categorized the parameters used in PMF analysis in three groups according to their calculated SNR. Parameters having SNR greater than 2 were considered as "*strong*" variables. If calculated SNR was between greater than and equal to 0.2 and less than and equal to 2, then parameters are assigned to "*weak*" variables group. "*Bad*" variables have SNR was less than 0.2. Paatero and Hopke (2003) recommended exclusion of bad variables in PMF analysis. Moreover, uncertainties corresponding to weak variables were increased by a factor of five to reduce their impact on PMF solution (Kim and Hopke, 2008). As it can be concluded from Table 4.29, all of the parameters have SNR greater than 2 indicating that there is no variable considered as weak and bad variable in the input data matrix.

The methodology developed by Kim and Hopke (2008) was used for handling of below detection limit (BDL) and missing data. In this approach, BDL data was replaced by half of the MDL values and their corresponding uncertainty values were set to 5/6 times MDL. Missing concentrations were replaced by the geometric mean of the concentrations and their uncertainties were set 4 times their corresponding concentrations. The percentage of BDL values was also important in the PMF analysis. Kim and Hopke (2008) recommended that uncertainties of parameters having values above 50 % below MDL should be increased by a factor of three. Furthermore, Buzcu-Guven et al. (2007) suggested that parameters having greater than 70 % below detection limit data should be excluded from the PMF analysis. However, weak variables having less than 70 % below detection limit data should be included in PMF analysis but they should be down weighted by increasing their uncertainty by three fold. As it can be seen from Table 4.27, there is no parameter in the data matrix having 50 % BDL data. However, parameters (W, Pt, Bi, Be) having calculated communalities less than 0.6 in factor analysis exercise was excluded from the input data matrix. Moreover, Au, Eu, U and In were not considered in PMF analysis since calculated precision values were small for these parameters, which was thought to influence PMF solution.

Table 4.29 Calculated SNR of parameters

<b>Parameter</b>	<b>SNR</b>	<b>Parameter</b>	<b>SNR</b>
<b>Al</b>	6.9	<b>Mn</b>	5.2
<b>As</b>	3.1	<b>Na</b>	3.9
<b>Au</b>	3.0	<b>Nd</b>	8.6
<b>Ba</b>	5.2	<b>NH<sub>4</sub><sup>+</sup></b>	6.6
<b>Be</b>	3.1	<b>Ni</b>	3.4
<b>Bi</b>	3.4	<b>NO<sub>3</sub><sup>-</sup></b>	6.4
<b>Ca</b>	5.1	<b>Pb</b>	3.2
<b>Cd</b>	3.9	<b>Pr</b>	8.6
<b>Ce</b>	7.9	<b>Pt</b>	1.5
<b>Cl</b>	15.0	<b>Rb</b>	5.1
<b>Co</b>	5.6	<b>S</b>	10.8
<b>Cr</b>	3.6	<b>Sb</b>	3.5
<b>Cs</b>	5.2	<b>Se</b>	2.7
<b>Dy</b>	5.8	<b>Sm</b>	7.8
<b>Er</b>	8.5	<b>Sn</b>	3.1
<b>Eu</b>	2.3	<b>Sr</b>	4.9
<b>Fe</b>	5.6	<b>Tb</b>	8.5
<b>Gd</b>	9.7	<b>Th</b>	6.8
<b>Ge</b>	2.8	<b>Ti</b>	6.8
<b>Hf</b>	5.6	<b>Tm</b>	7.4
<b>Ho</b>	9.2	<b>U</b>	4.4
<b>In</b>	8.2	<b>V</b>	3.8
<b>K</b>	4.2	<b>W</b>	4.2
<b>La</b>	8.0	<b>Y</b>	6.8
<b>Li</b>	6.2	<b>Yb</b>	7.9
<b>Lu</b>	7.9	<b>Zn</b>	4.3
<b>Mg</b>	5.8		

In this study, chlorine and SO<sub>4</sub><sup>2-</sup> were determined by both IC and XRF. As previously indicated, we obtained good correlation between XRF S and IC SO<sub>4</sub><sup>2-</sup>. In addition, correlation between the IC and XRF chlorine was good. For these reasons, both chlorine and SO<sub>4</sub><sup>2-</sup> data were used from XRF analysis to provide homogeneity in the data matrix.

#### ***4.5.6.2.2. PMF Analysis***

PMF version 4.2 software developed by Paatero (2002) was used to apportion the measured parameters. Detailed information on this software was previously provided and hence will not be repeated here again. After concentration and uncertainty data matrix

were constructed, the parameters in the PMF software itself were adjusted to obtain optimum solution.

Outlier data was handled by running PMF in robust mode, in which outlier distance ( $\alpha$ ) was set to default value of 4. This value of outlier distance has been used in many other studies in the literature (Begum et al., 2005; Hedberg et al., 2005; Buzcu et al., 2003; and Pekney et al., 2006). In this way, the influence of extreme values and outliers in the data set were reduced.

Another parameter that analyst can change in PMF analysis is the  $F_{\text{peak}}$  value, which controls the rotations. More realistic solutions can be obtained by changing  $F_{\text{peak}}$  value in trial and error procedure during PMF runs. Though there is no accepted rule of choosing  $F_{\text{peak}}$  value, user should carefully examine variation of Q value with changing  $F_{\text{peak}}$  value.  $F_{\text{peak}}$  value resulted in minimum Q in analysis was selected as the best one.

T

he size of concentrations and uncertainty matrix was 1448 x 46 (number of samples times number of parameters evaluated in analysis). This matrix size also corresponds to theoretical Q value. As a first run,  $F_{\text{peak}}$  value was set to zero. Obtained Q value ( $Q_{\text{calculated}}$ ) was compared with the theoretical one. If convergence of two values were achieved, then used  $F_{\text{peak}}$  value was thought to be optimum but if not  $F_{\text{peak}}$  value was changed with 0.1 increments and software was run again. This trial and error step was continued until  $Q_{\text{calculated}}$  and  $Q_{\text{theoretical}}$  values become converged. In this analysis, minimum Q value was achieved at  $F_{\text{peak}}$  of 0.1.

This trial and error procedure was repeated for each factor ranging from 4 to 10. For each factor, the physical meanings of the results were checked. In addition, scaled residuals should be between  $\pm 2$  for optimum solution, which is the other parameter considered in PMF analysis. Furthermore, autocorrelation between the factors was checked in order to ensure not to resolve factors more than actual. Based on the calculated Q value and obtaining physically interpretable results, eight factors were retained in final PMF solution. Consequently, all the discussion from now on will be performed these eight factors.

#### **4.5.6.2.3. PMF Results**

As discussed before, eight factors were extracted from PMF analysis. In order to assign each factor to a specific source, Explained Variation (EV) and F loading, which are the outputs of PMF solution, plots were constructed for each parameter. Furthermore, seasonal variation of G score, which is another output file of PMF solution, was investigated. Crustal enrichment factors (EF) of parameters were calculated for each factor by using factor loading values.

F loading actually represents the concentration of each measured species in each factor in PMF analysis. Nevertheless, it would be misleading to interpret the results based on F loading alone. For example, S was present at higher loading rates in Factor 2-5; however, this does not mean that all these factors are from coal combustion. Sodium is enriched in Factor 5 and 8 as it can be seen in Figure 4.96 and 4.104. However, Factor 8 was classified as sea salt factor only. For this reason, F loading was coupled with EV, EF and G score in the interpretation of PMF solution. Eight factors in the solution accounts for about 85 % of the system variance, which is fairly good value, particularly for the data generated at a rural station.

EV, EF and F loading values corresponding to Factor 1 was plotted and depicted in Figure 4.86. Crustal EF values for soil derived elements (e.g., Li, Mg, Al, Ca, Ti, Fe, Co, Cr, Mn, Rb, Sr and Y) were close to unity. In addition, large portion of the variance was explained by these soil derived elements. Consequently, this factor is a crustal factor and called as "*local soil*". This factor accounts for 13.5 % of the total variance.

Seasonal variation of G score values for this factor was illustrated in Figure 4.87. It is clear from Figure 4.87 that G score values increase in summer time, when scavenging of pollutants less from the atmosphere with rain in Eastern Mediterranean region, while started to decrease in winter months. This pattern observed in G score further confirmed that this is a soil derived factor since we observed similar trend for crustal elements in Section 4.4.3, where temporal variations of elements were discussed.



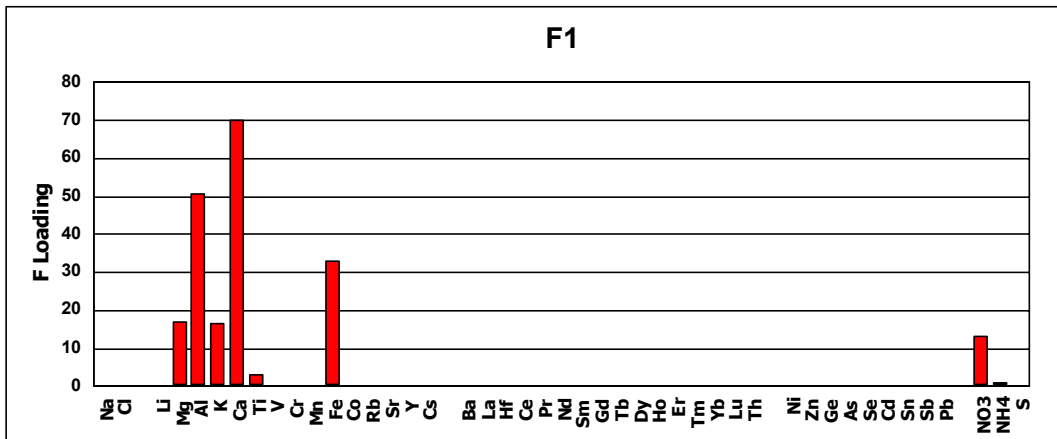
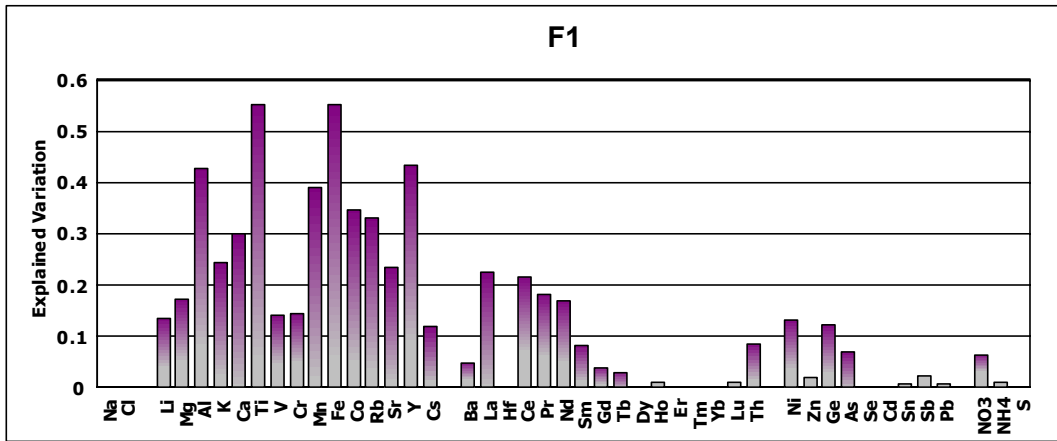
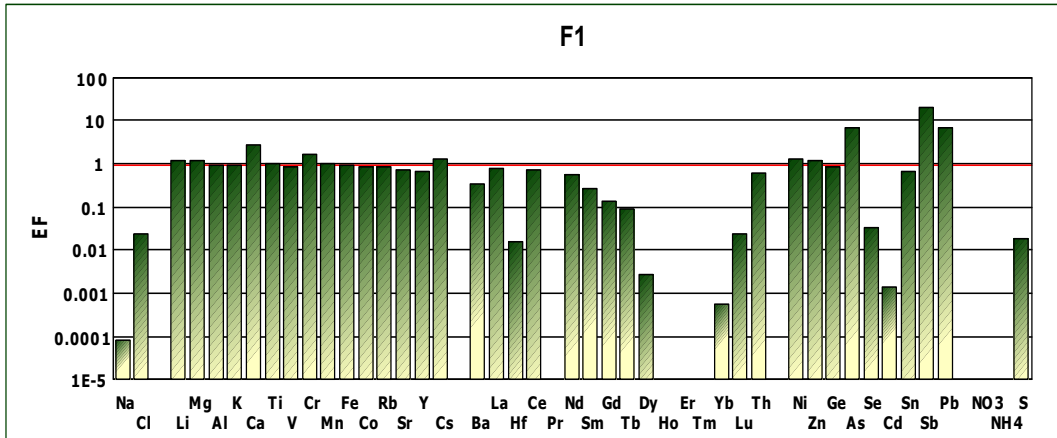


Figure 4.86 Enrichment Factor, Explained Variation, and Flooding values for Factor 1

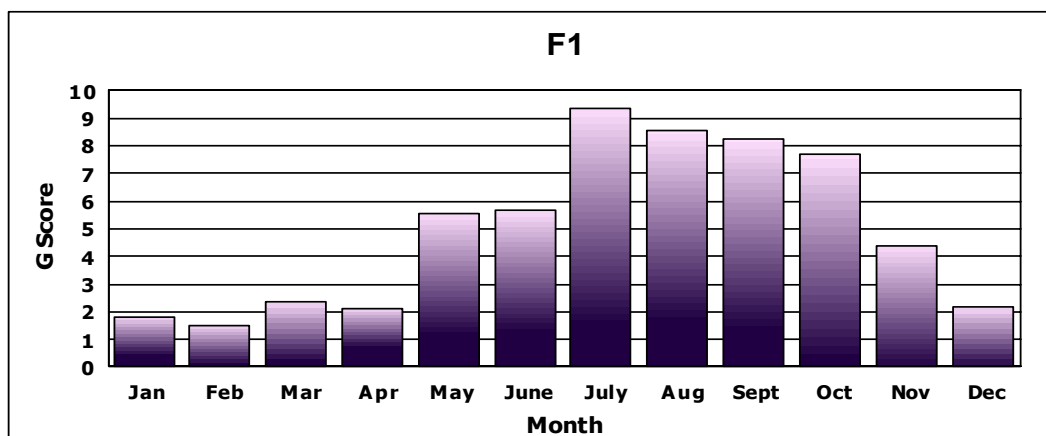


Figure 4.87 Seasonal variation of G score values for Factor 1

Trajectories corresponding to highest 25 G score values for Factor 1 were calculated at 1500 m altitude and depicted in Figure 4.88. It is clear from Figure 4.88 that there is no unique region where trajectories originated before intercepted at our station, which means that all the air masses carry soil related material to Antalya station regardless of their origin.

Figure 4.89 and 4.90 showed the PMF output for Factor 2. This factor is enriched in V, Ni, Zn, Ar, Sn, Cd, Pb, Se and S. Factor explained 10 – 30% of the variances in data for these elements, except for V. The factor explains approximately 60% of the variance of V data. Selenium and S are the most important markers of coal combustion (e.g., Yatin et al., 2000; Al-Momani et al., 2005; Ölmez and Gordon, 1985) while V and Ni are well documented tracers of oil combustion (e.g., Yatin et al., 2000; Al-Momani et al., 2005; Ölmez and Gordon, 1985; Vallius et al., 2003; Artaxo et al., 1999) in the atmosphere. Since anthropogenic elements are enriched and factor 2 explains 20% and 60% of the variances of Ni and V, respectively, this factor is defined as “oil combustion” factor. Seasonal variation of G scores corresponding to this factor was depicted in Figure 4.90. High G score values in summer and low ones in winter suggest that this factor might be long range transported factor. If these pollutants were generated in close proximity of the station, then one should observe high G score values in winter time as well. During their long range transport these pollutants were scavenged from the atmosphere with

precipitation in winter, which explains the well defined seasonality of pollutants in this factor. Oil combustion factor explains about 7 % of system variance.

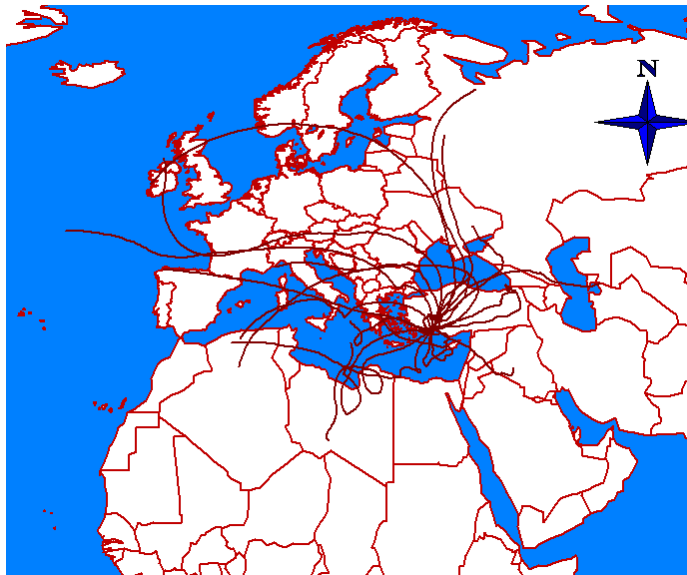


Figure 4.88 Trajectories corresponding highest 25 G scores for Factor 1

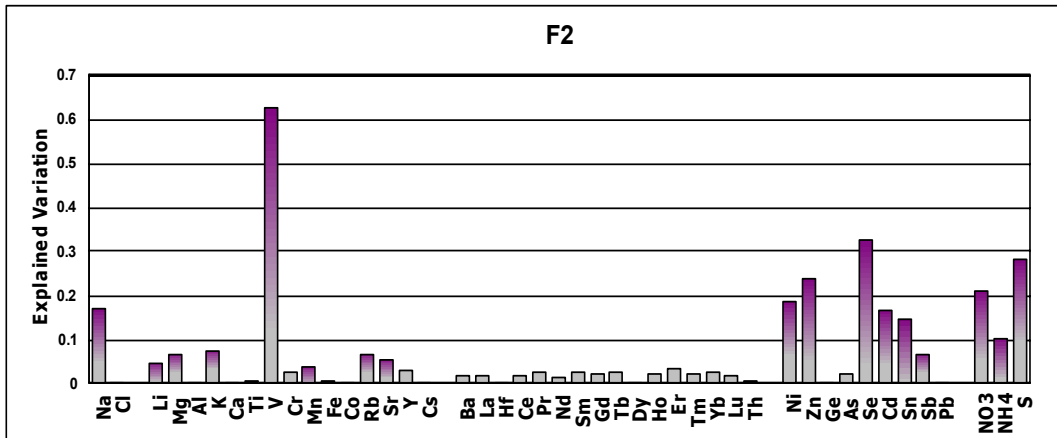
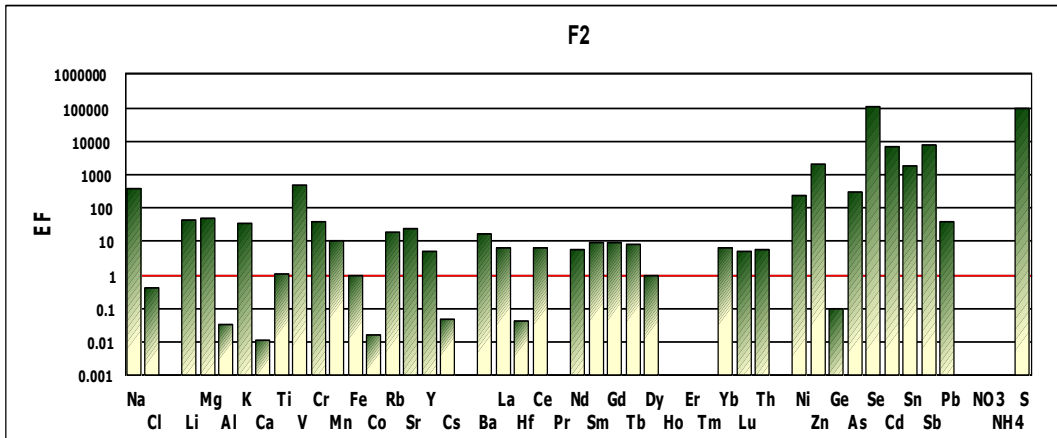


Figure 4.89 Enrichment Factor, Explained Variation, and Flooding values for Factor 2

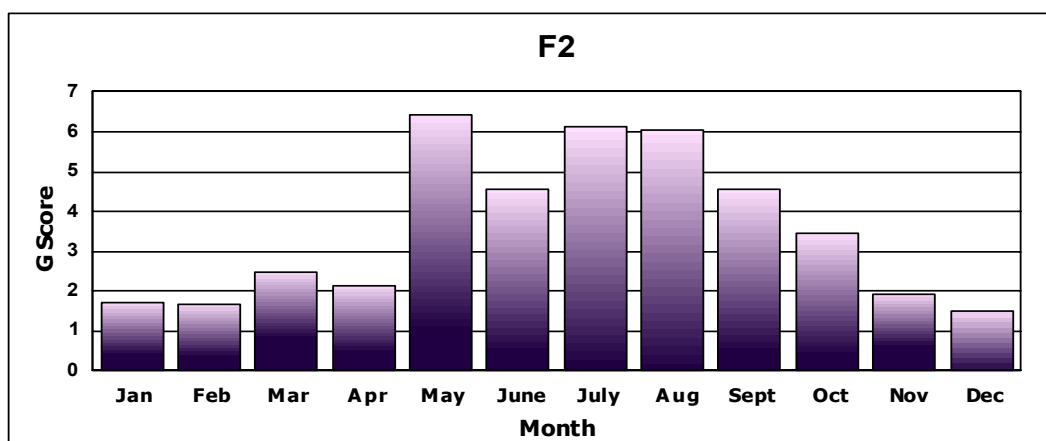


Figure 4.90 Seasonal variation of G score values for Factor 2

EF, EV and F loading values were demonstrated in Figure 4.91 for Factor 3. Calculated EF values for soil derived elements like Ca, Fe, Co and Rb were close to one while Se, Cd, Sn, Pb and S were enriched in this factor. Factor 3 explains most of the variance of K, Cr, Mn, Co, Rb, Cs, Ni, Zn, Cd and Zn. Both soil derived and anthropogenic elements are present in this factor. Consequently, this factor is called as "*anthropogenic-crustal mixed factor*". Seasonality of this factor is depicted in Figure 4.92. Factor 3, like factors 1 and 2, shows high seasonality with higher G scores values in summer and lower ones in winter. One likely source for the anthropogenic component in this factor is biomass burning. The factor explains >20% of the variance in K data, an element which is well documented tracer for biomass burning. At this point, assignment of biomass burning to this factor is a speculation, and further data, particularly on dates of forest fires close to station is needed for positive identification of biomass burning as the source of enrichment of anthropogenic elements in Factor 3. Approximately 10 % of the system variance was explained by this factor.

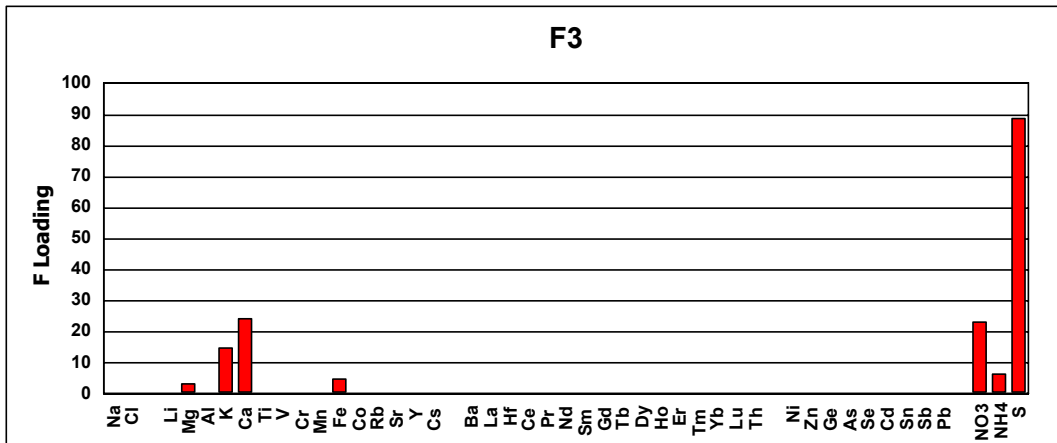
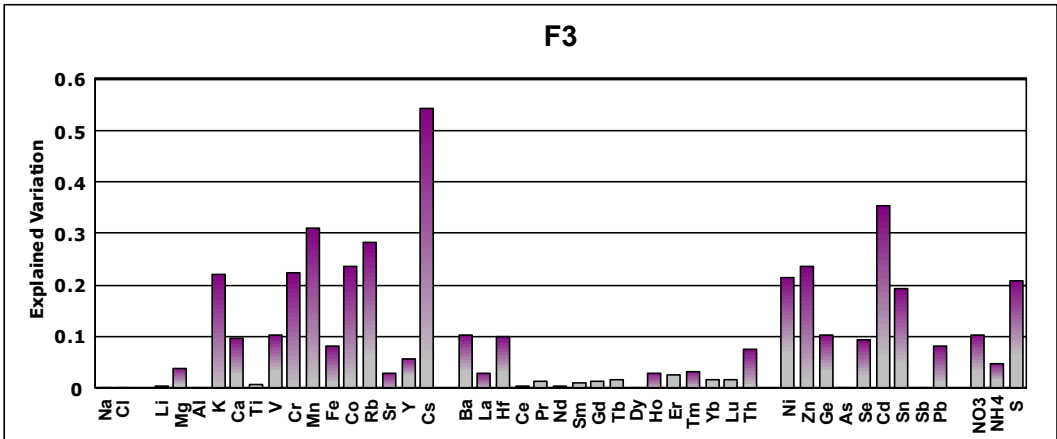
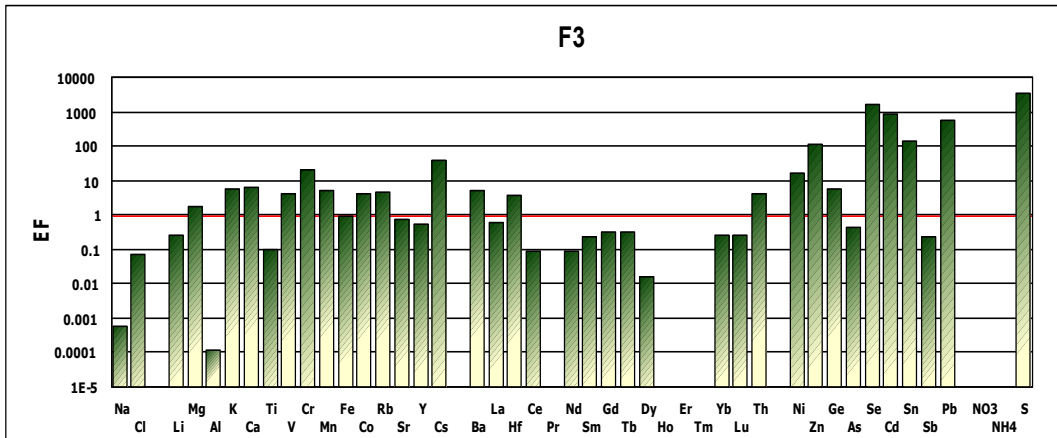


Figure 4.91 Enrichment Factor, Explained Variation, and F loading values for Factor 3

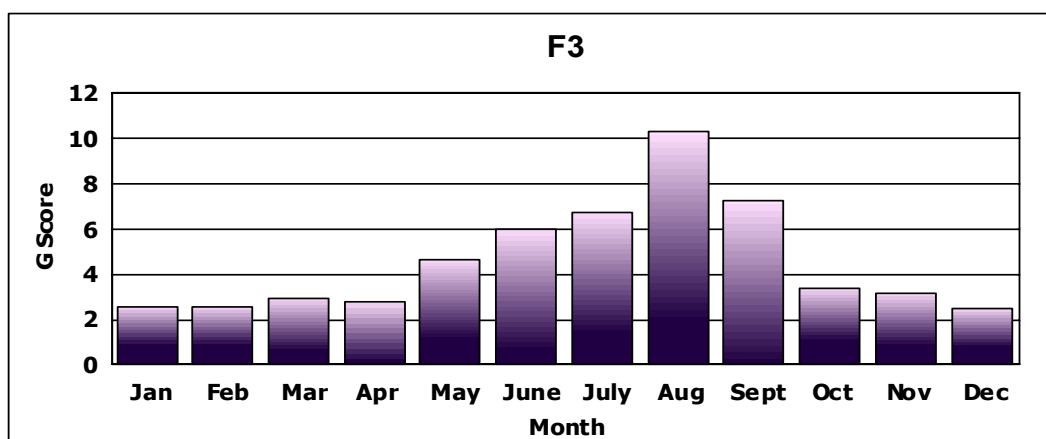


Figure 4.92 Seasonal variation of G score values for Factor 3

Factor 4 is enriched in Cr, Ni, Zn, As, Ge, Se, Cd, Sn, Sb, Pb and S as demonstrated in Figure 4.93. Factor 4 explains approximately 40% and 80% of the variances in Ge and As data, respectively. Concentrations of  $\text{SO}_4^{2-}$ ,  $\text{NH}_4^+$  and  $\text{NO}_3^-$  were high. Therefore, factor 4 describes an anthropogenic source. Germanium and As are well known markers of power plants. The seasonality of G score values associated with Factor 4 was shown in Figure 4.94. While high winter and low summer values for the G score was seen, this observed seasonality is not as pronounced as ones obtained for previously discussed three factors. This observed pattern in seasonality indicated that this factor should be more local. The local does not necessarily refer to immediate vicinity of the stations. It means source regions located on the western part of Turkey and Balkan countries, but not at the Central Europe, Western Europe and Russia. Low G score values in summer months may simply be due to lower mixing height in winter. Based on this argument, Factor 4 is identified as "*local coal combustion*". Factor 4 accounts for ~ 5.5 % of the total variance.

Trajectories corresponding to highest 25 G scores were calculated at 1500 m altitude and presented in Figure 4.95. It is obviously seen from Figure 4.95 that trajectories are mainly originated from Europe and they spend some time over western part of Turkey, where heavy industrial activities and most of our powerplants are located.

Enrichment factor, EV, F-loading and G-score plots for Factor 5 is illustrated in Figure 4.96, 4.97 and 4.98. Crustal associated elements such as Na, Li, Ca, Mn, Cr, Cs and La are slightly enriched in this factor.

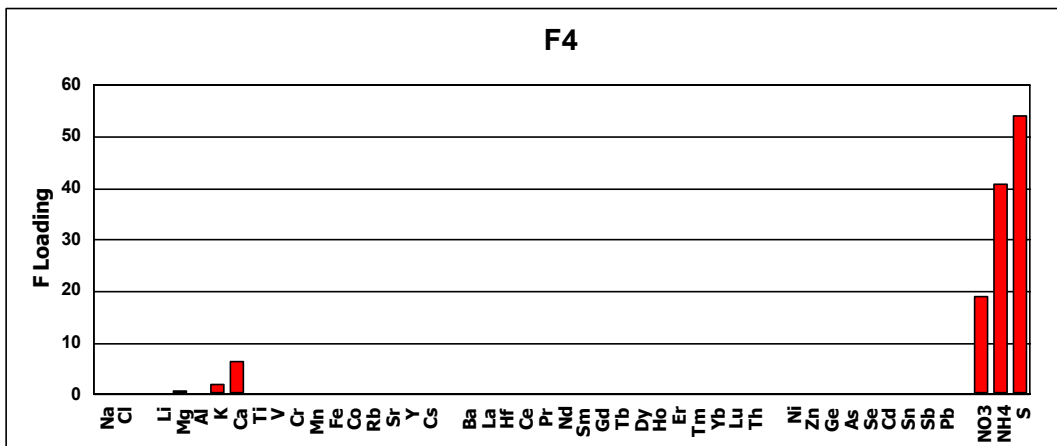
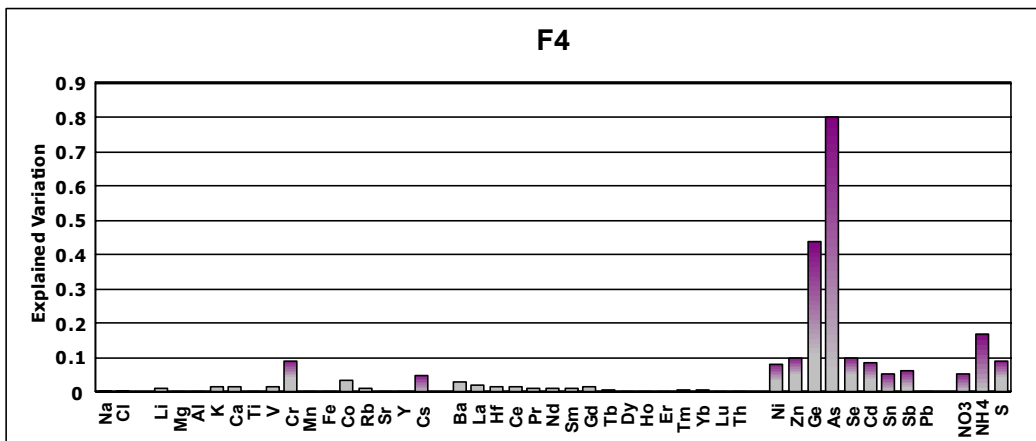
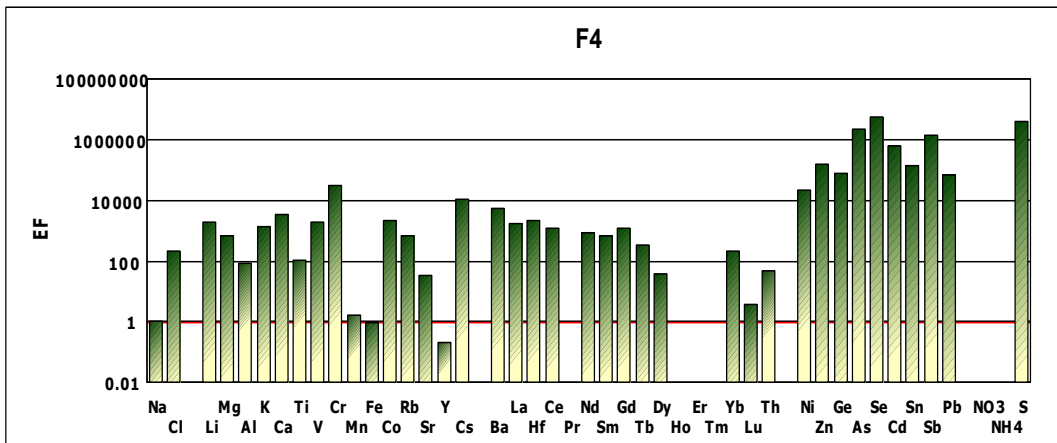


Figure 4.93 Enrichment Factor, Explained Variation, and F loading values for Factor 4



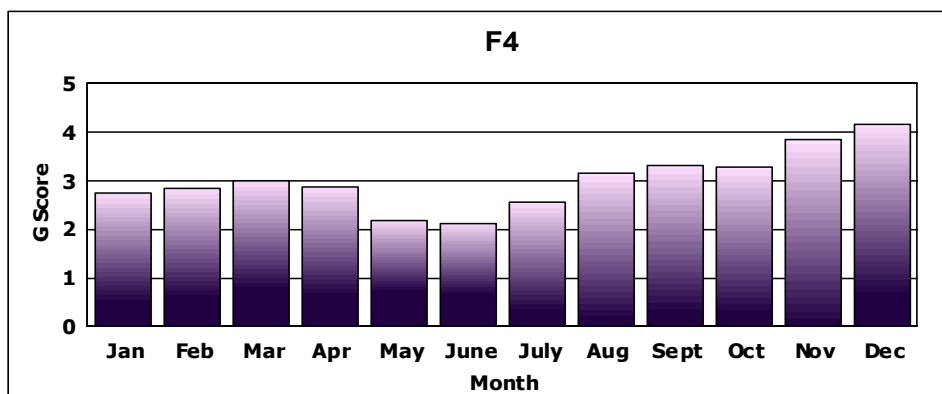


Figure 4.94 Seasonal variation of G score values for Factor 4



Figure 4.95 Trajectories corresponding highest 25 G scores for Factor 4

On the other hand, Zn, As, Se, Cd, Pb, Sn, Sb, Pb and S are highly enriched. The most important feature in the figures is that Factor 5 explains large fraction of the variances of Pb, Sb and Sn data. In the past Pb was used as a tracer for "motor vehicle emissions". It should be noted that Pb was not phased out from gasoline in most of our sampling period. Consequently, this factor was identified as "motor vehicle" factor.

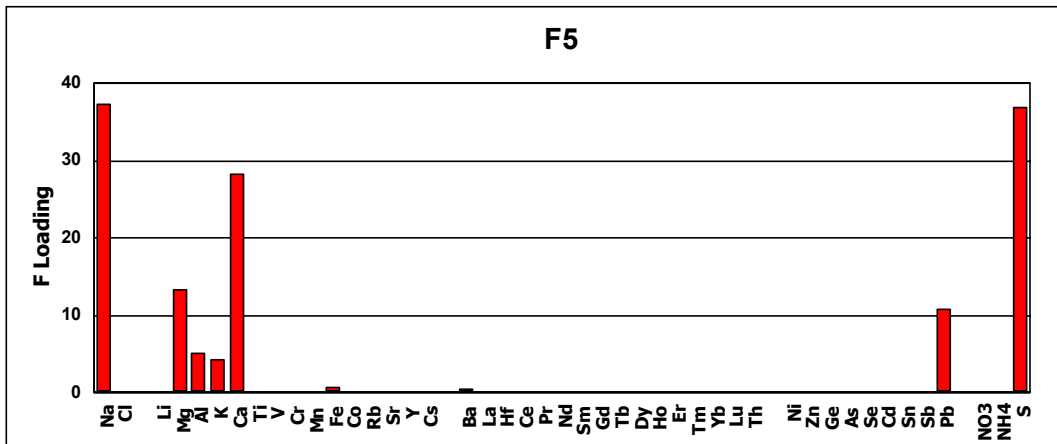
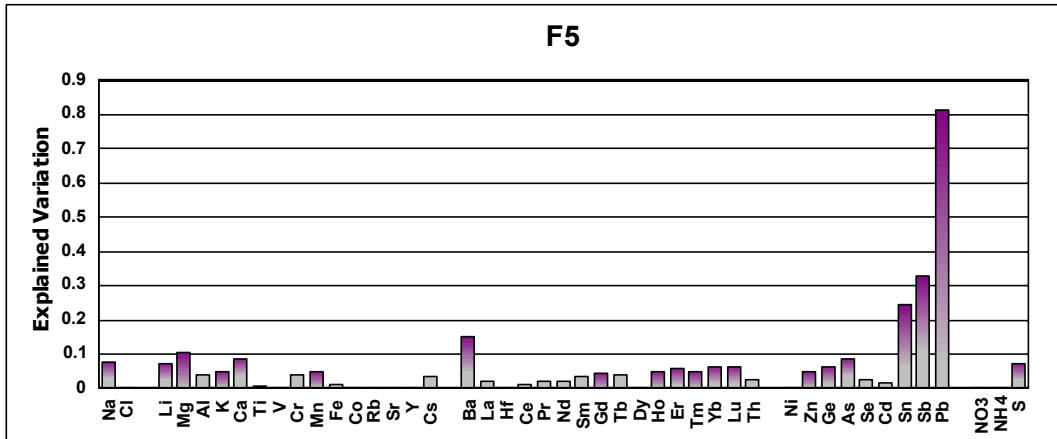
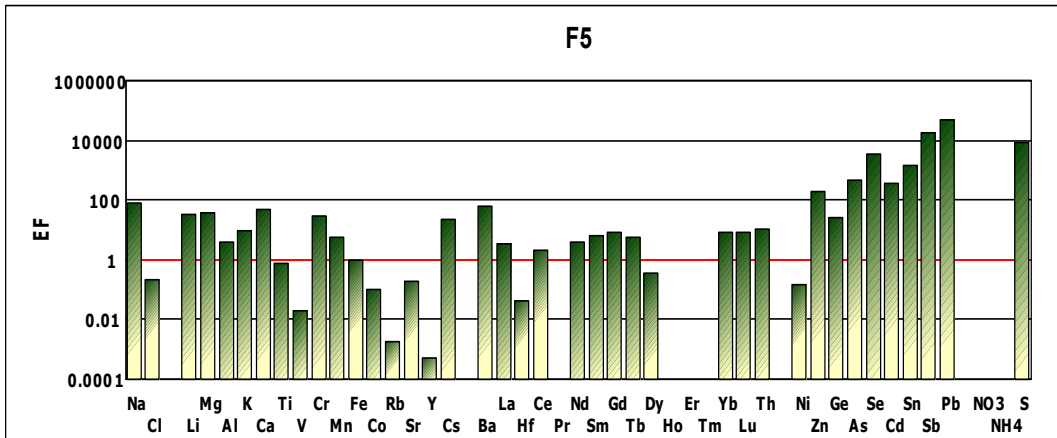


Figure 4.96 Enrichment Factor, Explained Variation, and Floading values for Factor 5

In order to further test this source, short term variations in G score values were also examined and depicted in Figure 4.97. It is interesting to note that Factor 5 scores remained relatively constant from the beginning of sampling period until 1998, then decrease relatively rapidly in the last three years of our sampling period. Phasing out of Pb in Europe started in 80's. The market share of unleaded gasoline in most western European countries was >80% in 1994, which means that phasing out of Pb from Western European gasoline was almost completed in the middle of 90s (World Bank, 1998). However, the situation is different in Balkan Countries. The Market Share of unleaded Gasoline in Greece, Turkey, Bulgaria and Romania were 33%, 18%, 5% and 6%, respectively (World Bank 1998). Considering that leaded gasoline is totally banned in all Balkan Countries now, it would be correct to state that phasing out of Pb from gasoline in Balkan countries took place between 1996 and 2004. The decrease in Factor 5 scores after 1997 is due to increase in the share of unleaded gasoline in Turkey and other Balkan countries.

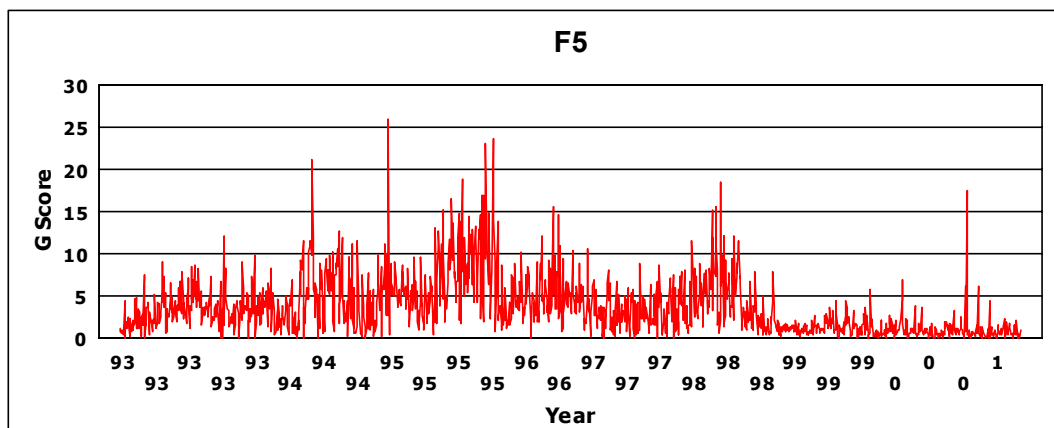


Figure 4.97 Short term variations in G score values for Factor 5

High summer, low winter G score values are indicating good seasonality. About 6.5 % of the total variance was explained by this factor.

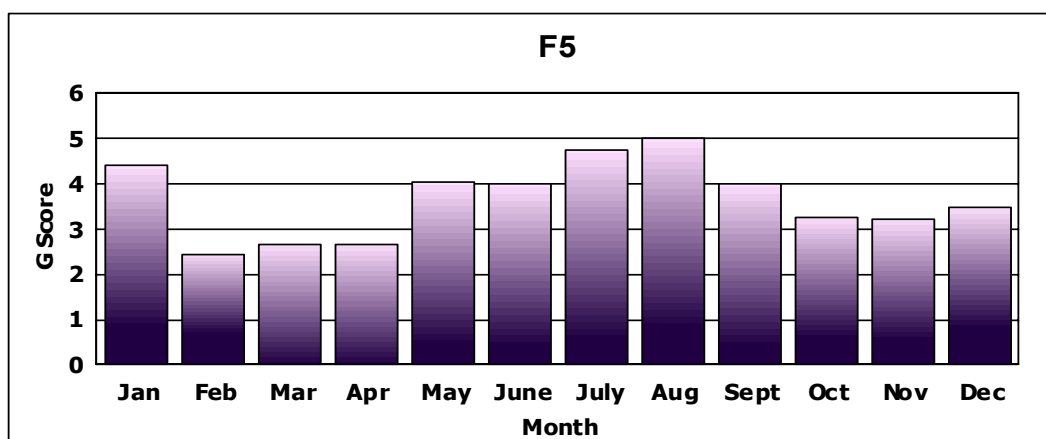


Figure 4.98 Seasonal variation of G score values for Factor 5

Explained Variation, EF and F loading values associated with Factor 6 are provided in Figure 4.99. Chlorine, Se, Sb, Cd and Sn are enriched in this factor. Factor 6 explains approximately 45 % of variance in Sb data. Most of the variance was explained by Sb as depicted by EV variation plot. High loadings of Se, Sb, Cd and Sn indicated that this factor is obviously anthropogenic factor. Antimony is mainly released to the atmosphere from antimony roaster with a chemical abundance ranging from 0.1 to 1 % in mass (Chow, 1995). Episodic variation of this factor was also investigated using G scores and illustrated in Figure 4.100. It is interesting to note that G scores for this factor is increasing gradually in time. Seasonal variations in G score were demonstrated in Figure 4.101. A small difference between values of G scores between summer and winter months seem to suggest that sources responsible for this factor are relatively close to our station. Factor 6 accounts about 5.7 % of total variance. Sources generating Factor 6 are not clear at this point.

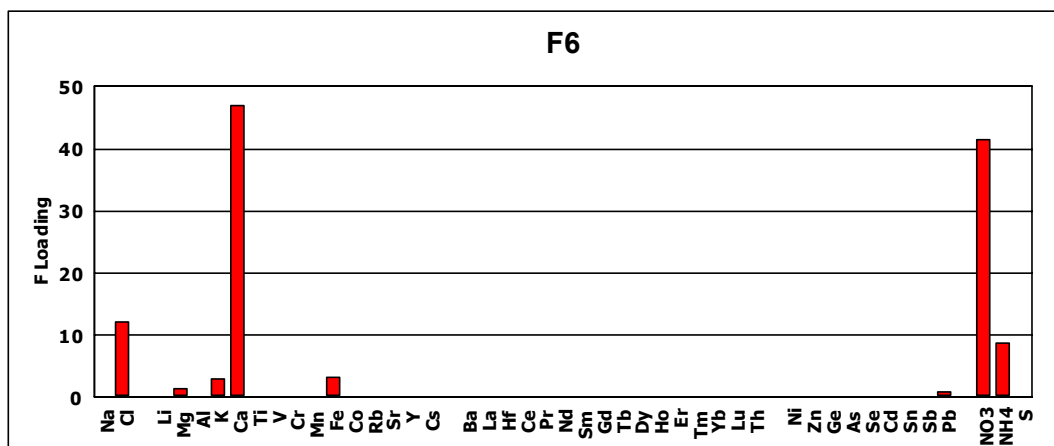
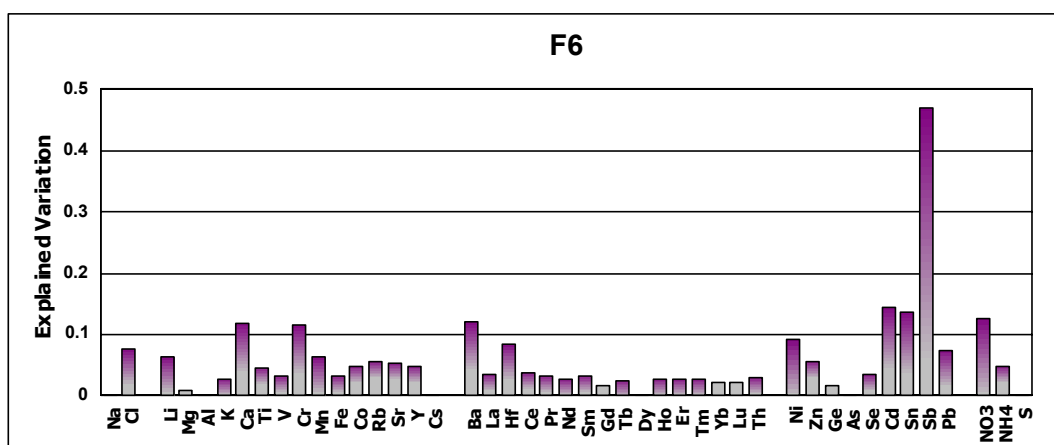
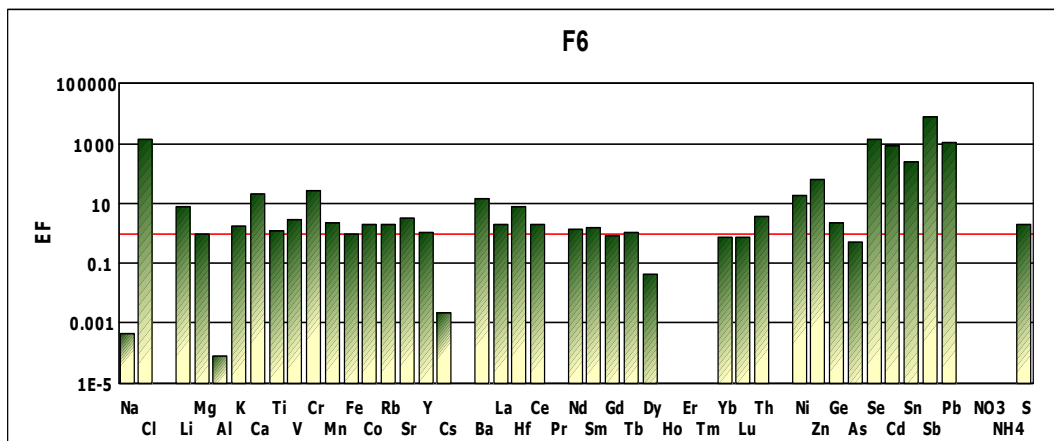


Figure 4.99 Enrichment Factor, Explained Variation, and Floading values for Factor 6

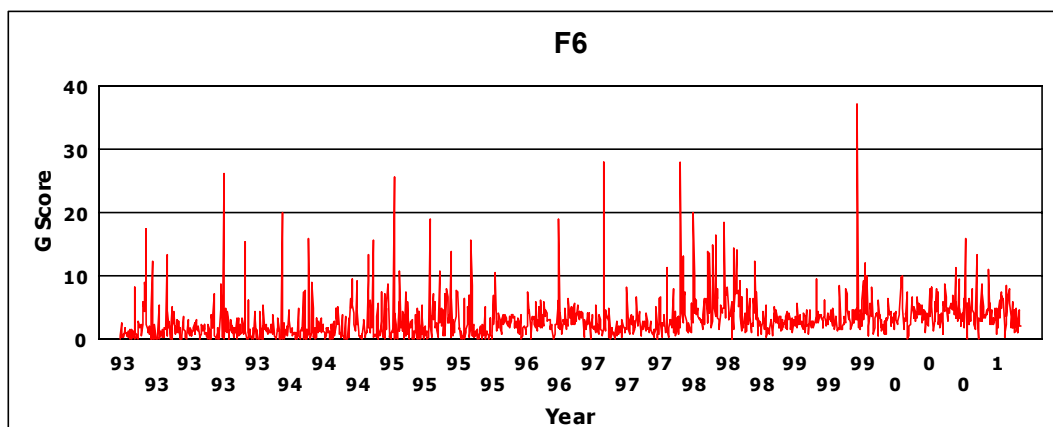


Figure 4.100 Short term variation of G score values for Factor 6

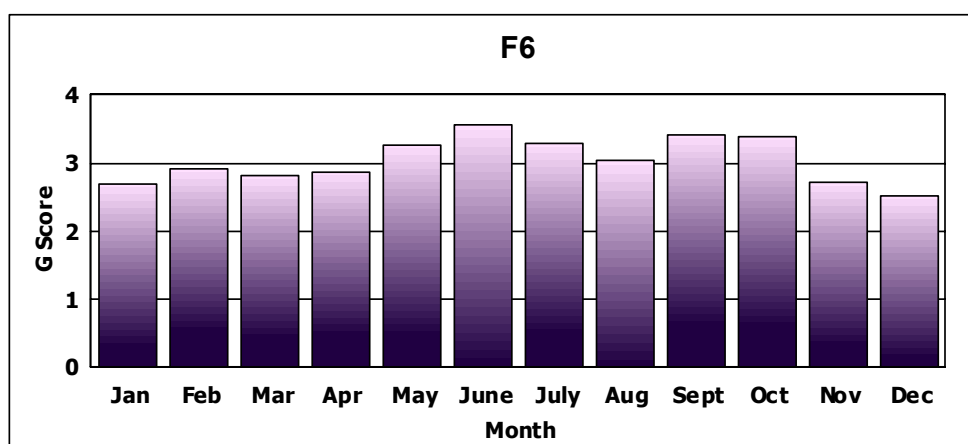


Figure 4.101 Seasonal variation of G score values for Factor 6

Enrichment Factor, EV and F loading plots for Factor 7 were illustrated in Figure 4.102. Calculated crustal EF values were close to unity for Mg, Al, Ti, Fe, Ca and K. In addition, rare earth elements such as La, Hf, Ce, Nd, Sm, Gd, Tb, Dy, Yb and Lu had  $EF_c$  between one and ten. It is obvious that Factor 7 is a crustal factor. Once EV plot was investigated, it can be seen that Factor 7 explains 60 %- 80 % of the variances in rare earth elements. Besides, F loading plot depicts that Ca, Al and Fe present in this factor at high concentrations. This factor accounts for ~ 32 % of total system variance. Applied Mann Kendall test on G score values associated with Factor 7 indicated that there is a decreasing trend at 95 % significance level ( $Z_{\text{calculated}} = |-6.07| > Z_{\text{critical}} = 1.96$ ). It was previously shown in this study that dust transported from North Africa has a different

chemical composition than local soil particularly for some of the rare earth elements such as Dy, Ho, Tm, Lu, Yb, Er, Sm, Eu, Nd, Hf, and Ce. For these elements Saharan dust to local dust ratio of median concentrations was found to be greater than one.

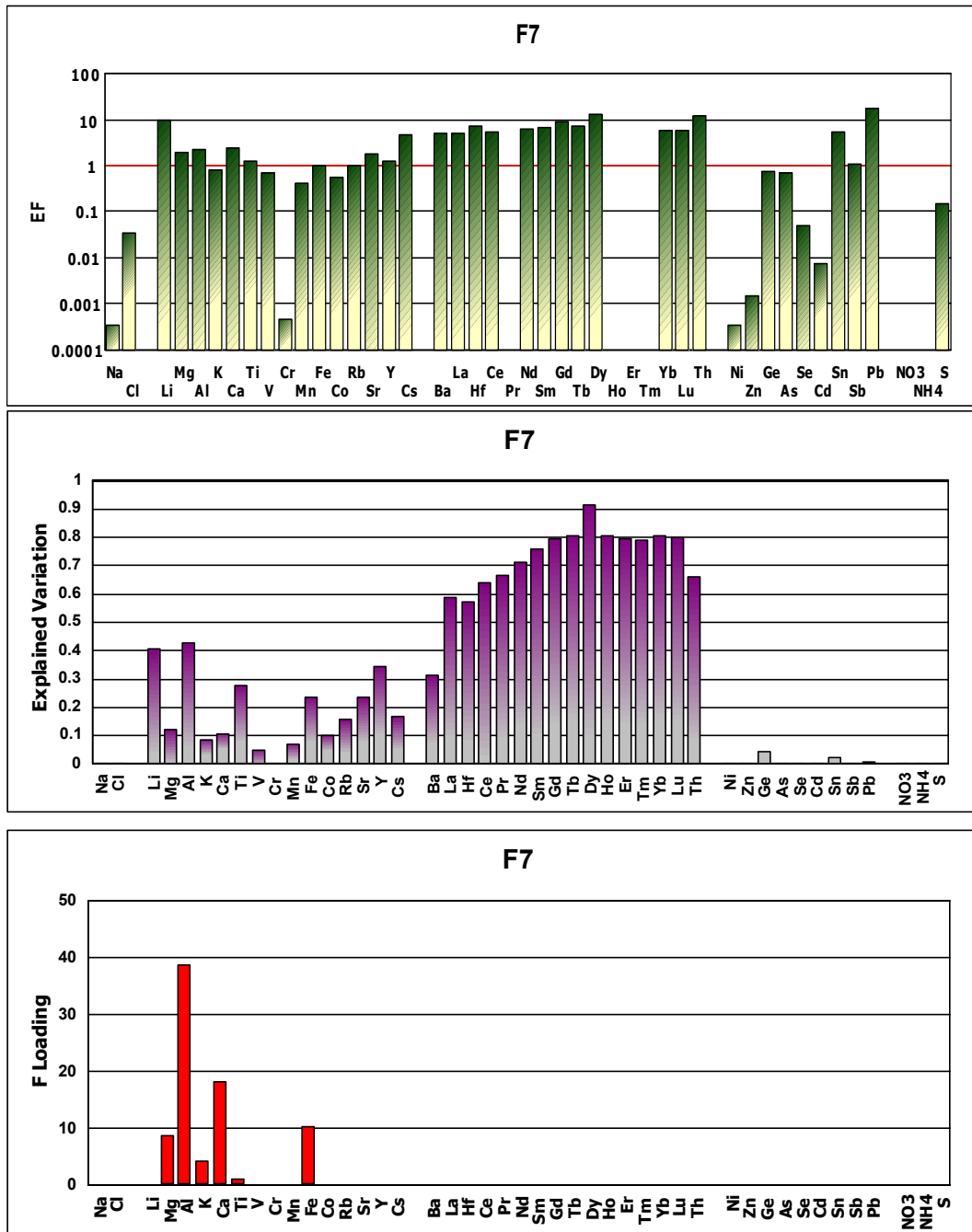


Figure 4.102 Enrichment Factor, Explained Variation, and Flooding values Factor 7

The difference in chemical composition of Saharan dust and local dust implied that this second crustal factor is “*Saharan Dust*” factor. To our knowledge, Saharan dust factor was identified only one study in the literature. Nicolás et al. (2008) found strong correlation between African dust and Ti found in the samples collected in intrusion days. Consequently, researchers used Ti as tracer of African dust transport to urban background station located in Elche, southeastern Spain. Nevertheless, local soil around the vicinity of our sampling station contains comparable amounts of Ti (Al normalized median concentration of Ti in local dust is  $0.0505 \text{ ng m}^{-3}$  while that for Saharan dust is  $0.0486 \text{ ngm}^{-3}$ ). Rare earth elements were used as markers of African dust transport to USA in a recent study (Trapp et al., 2008) as well. Seasonal variation of G scores corresponding to Factor 7 was depicted in Figure 4.103. Well defined seasonality was observed for this factor with increasing G score values in summer and decreasing ones in winter. This pattern in seasonality inversely correlated with precipitation events observed in Eastern Mediterranean.

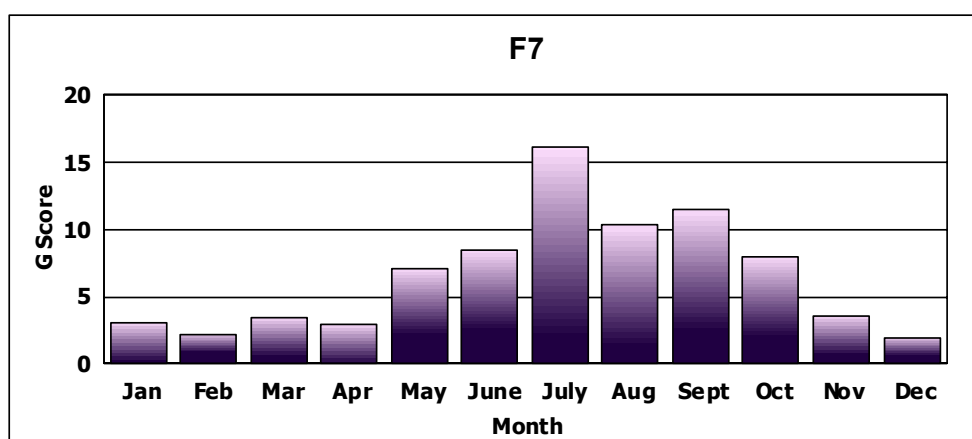


Figure 4.103 Seasonal variation of G score values for Factor 7

Calculated crustal EF, EV and F loading values for Factor 8 was demonstrated in Figure 4.104. Sodium and Cl highly enriched in this factor in addition to Se and S. The factor explains most of the variance in Na, Cl, Mg and Sr data. In addition, loadings of Na and Cl were high. Factor 8 primarily characterized by Na and Cl, which are well known marker of sea salt formed over sea surface and transported to the atmosphere. Since sampling station was also located along Turkish Mediterranean shore it was expected to extract



sea salt factor in PMF. Seasonality of G scores was investigated in Figure 4.105. High winter G score values were observed in winter while lower ones were observed in summer months. This trend also confirm sea salt source of Factor 8 because as pointed out earlier in the manuscript, sea salt concentrations measured at our station is closely related to magnitude of bubble bursting at the sea surface, which is significantly higher in winter.

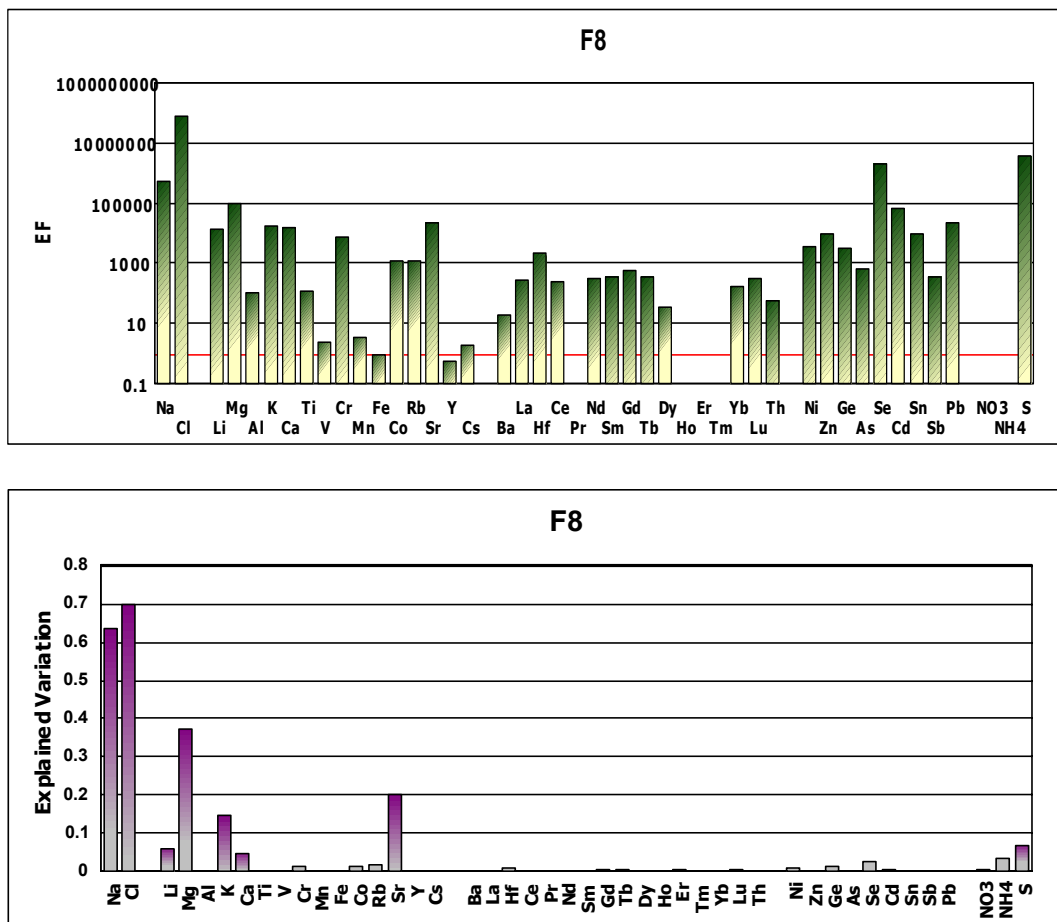


Figure 4.104 Enrichment Factor and Explained Variation for Factor 8

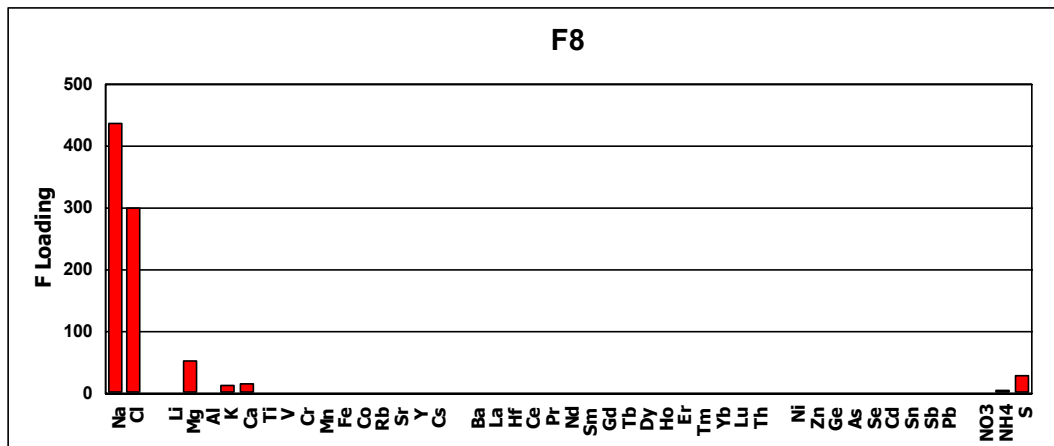


Figure 4.104 Floading values for Factor 8 (Continued)

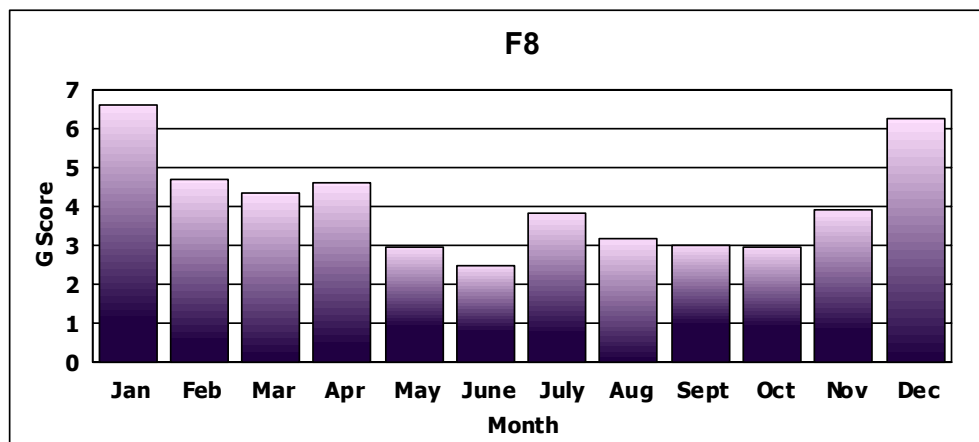


Figure 4.105 Seasonal variation of G score values for Factor 8

Trajectories corresponding to highest 25 G scores values at 1500 m altitude were illustrated in Figure 4.106 for Factor 8. It is obvious from Figure 4.106 that about 90 % of them passed over Mediterranean Sea before reaching to our station in addition to ones originated from Atlantic Ocean.

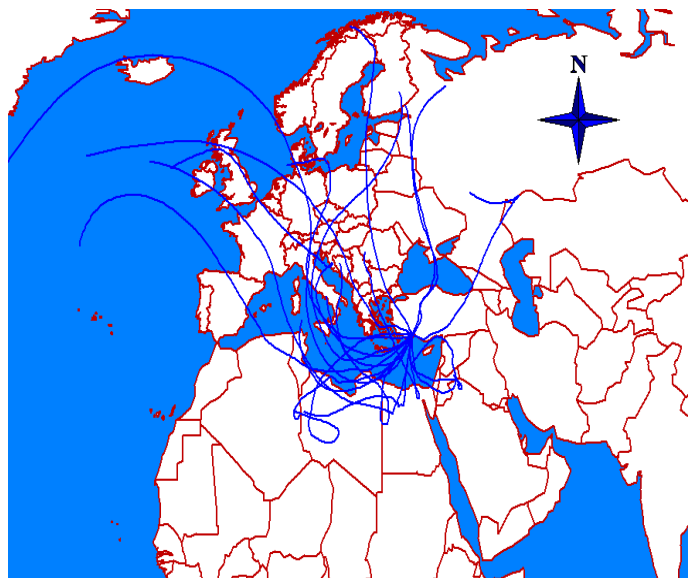


Figure 4.106 Trajectories corresponding highest 25 G scores for Factor 8

Daily predicted concentration for each measured species was obtained by multiplying F loading values for that element with G scores and then summation was performed in row wise manner. Calculated (predicted) concentrations were then regressed against observed concentrations and results were depicted for some of the selected rare earth elements, anthropogenic elements and lastly, crustal and marine elements in Figure 4.107 to 4.109.

Excellent fit were observed particularly for rare earth elements as shown in Figure 4.107. All the correlation coefficients were higher than 0.9, slope close to unity and intercepts are around 0, which all indication of goodness of fit in the applied model. Agreement between the model results and measured concentrations may be attributed to unique sources of rare earth elements. Since contribution of other sources to observed concentrations of these elements are negligible, we observed perfect fit of the predicted concentrations to observed ones.

Another parameter that should be considered in the measurement of PMF model fit to observed concentrations is the calculation of observed to predicted ratio (OPR) for each element. Ratio of observed to predicted concentrations was taken for each sample and then median of all samples were taken to construct Figure 4.110.

Observed to predicted ratios of modeled parameters were close to unity except for  $\text{NO}_3^-$ ,  $\text{SO}_4^{2-}$  and  $\text{NH}_4^+$ . Nitrate (OPR=1.62) and  $\text{NH}_4^+$  (OPR=0.69) have both high volatility. In addition to this, percentage of missing values for these two parameters is considerably high (42 % for  $\text{NH}_4^+$  and 31 % for  $\text{NO}_3^-$ ). For these reasons, the lack of fit for these parameters can be attributed to their high volatility and high percentage of missing values in the input data matrix of PMF. Therefore, excellent results were obtained for the apportionment of particulate matter with PMF in this study.

Contribution of each factor to each modeled parameter was also calculated and depicted in Figure 4.111. To this end daily concentration of each element in each factor was divided to total predicted concentration for that particular day. This process was repeated for all days in input data matrix and then average was taken for each factor.

As it can be concluded from Figure 4.111, soil derived elements like Ti, Ca, Al, Fe, Fe, Y, Co and Ca is due to Factor 1, which is called as "local soil". Factor 2, identified as "coal combustion factor" accounts 39 % of observed  $\text{SO}_4^{2-}$  and 47 % of measured Se concentrations. 31 % of Cr, 35 % of Mn, 29 % of Ni, 26 % of Ca, 43 % of Cd, 29 % of Ni and 32 % of Zn are due to Factor 3, anthropogenic crustal mixed factor. Factor 4 accounts for 79 % of measured concentration of As and 53 % of observed concentration of Ge, which are two marker elements of coal combustion. 77 % measured concentration of Pb was allocated to Factor 5. We could not identify Factor 6, which account for 47 % of the measured Sb concentration. Saharan dust accounts for 97 % of Dy, 77 % of Tb, 76 % of Ho, 77 % of Yb, 77 % of Lu and highest percentage of the rest of the rare earths. 88 % of Cl, 65 % of Na, 9.8 % of Mg, 25 % of Sr, 6 % of Se and 9 % of S are allocated to sea salt factor, Factor 8.

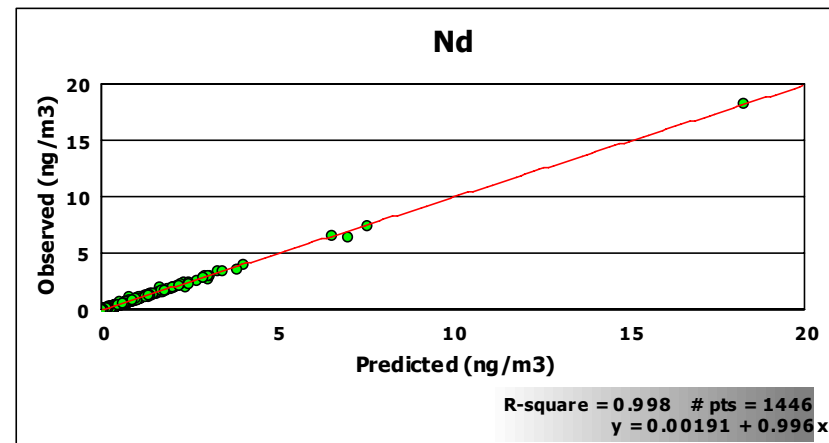
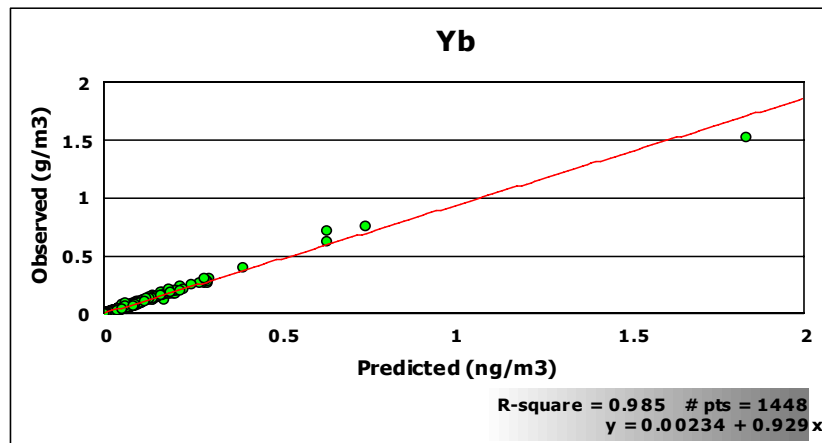
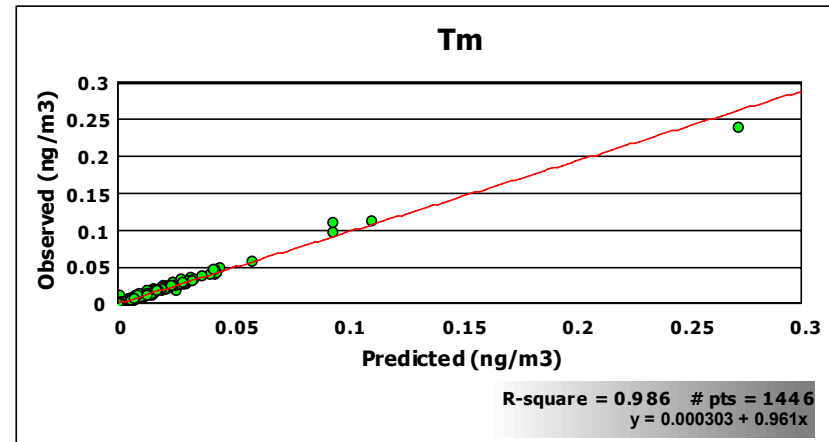
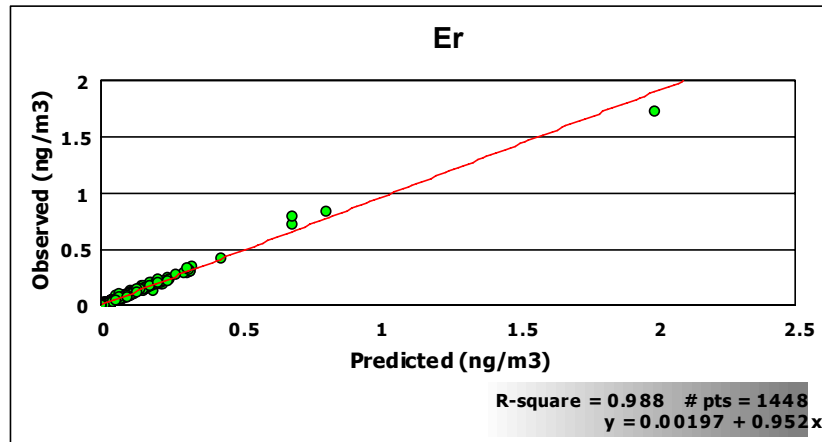


Figure 4.107 Relation between observed and predicted concentration of some of the selected rare earth elements

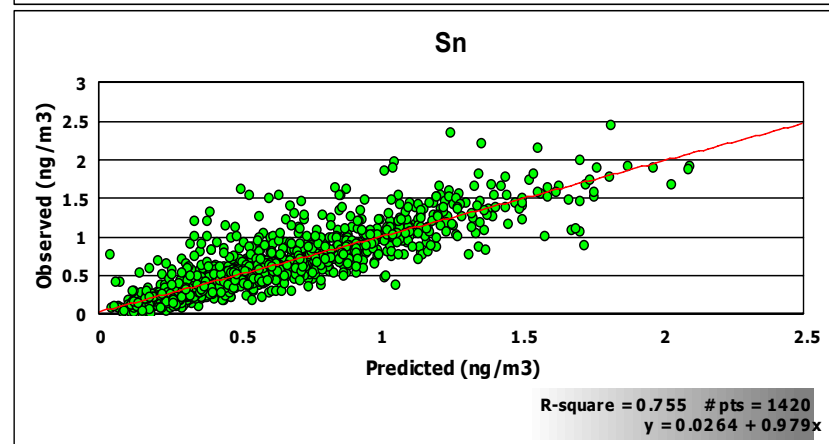
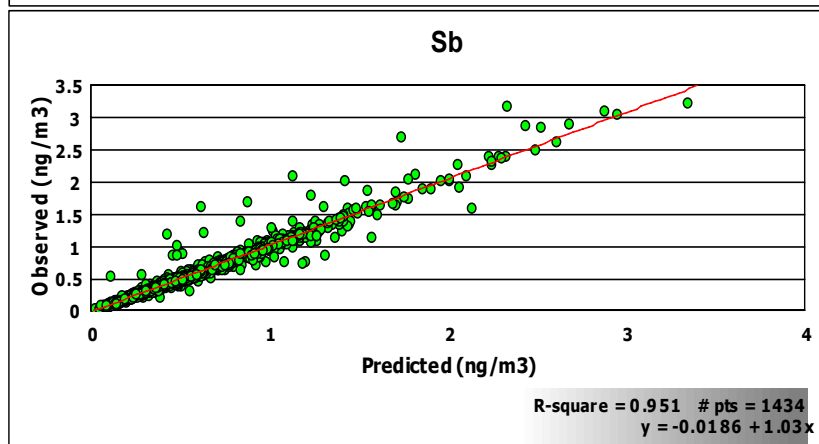
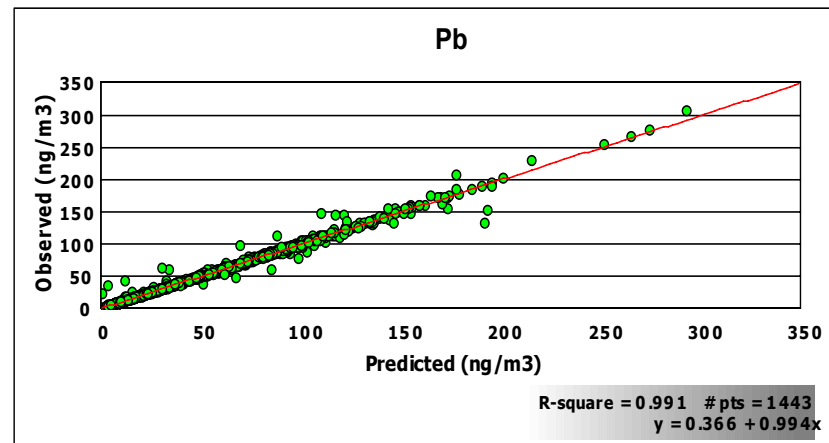
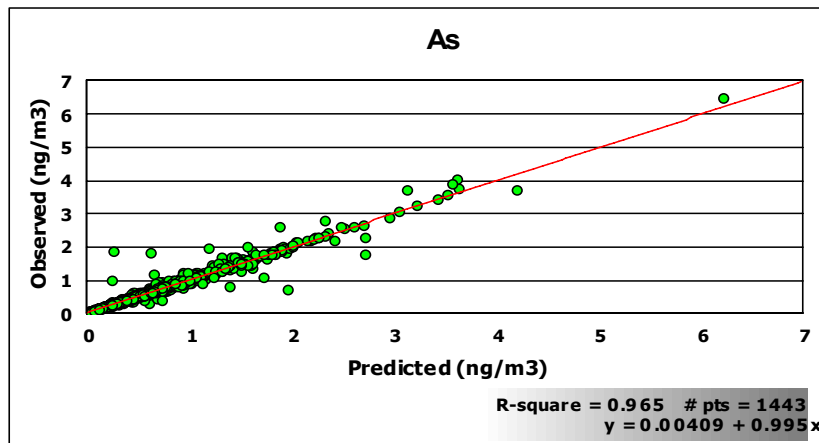


Figure 4.108 Relation between observed and predicted concentration of some of the selected anthropogenic elements

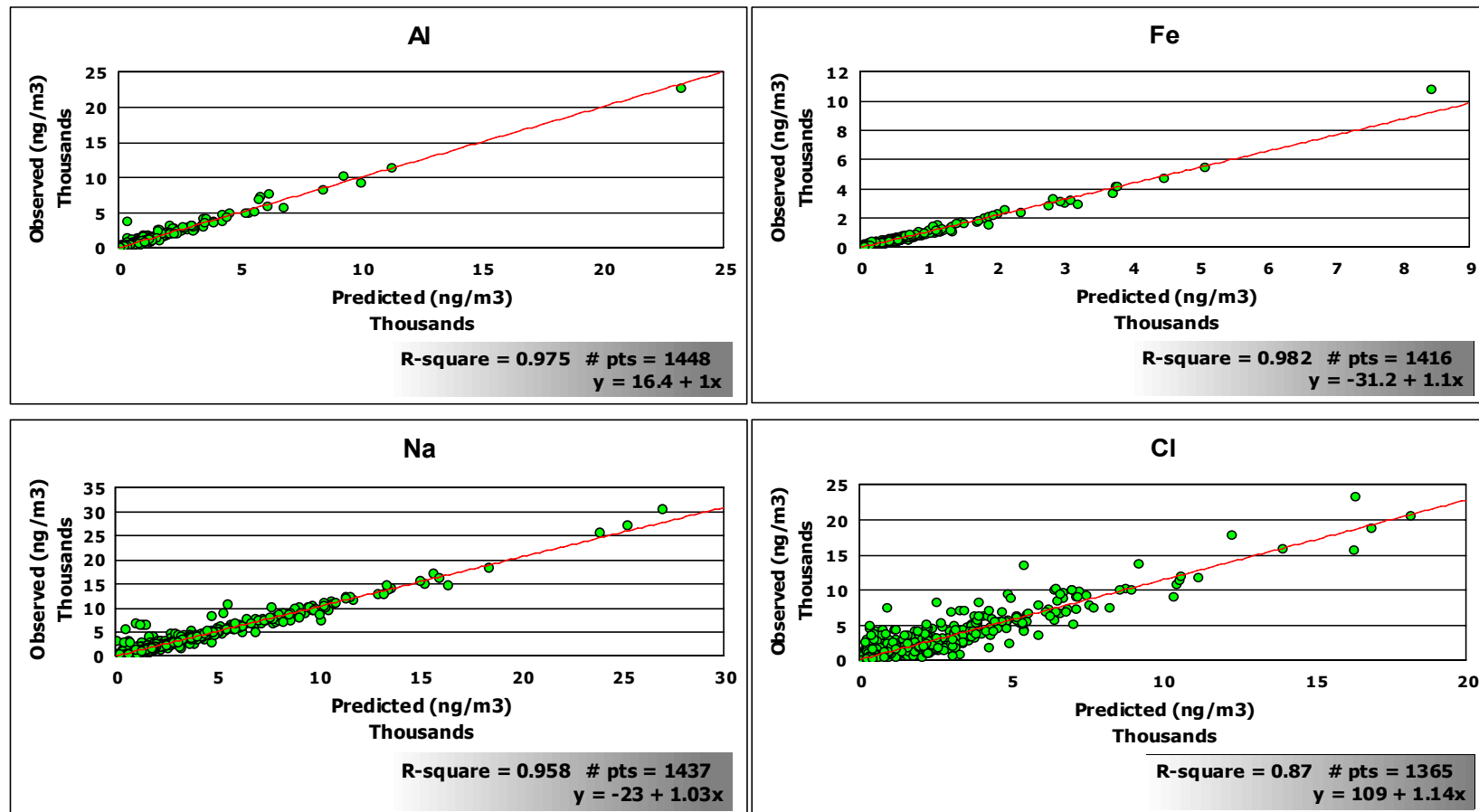


Figure 4.109 Relation between observed and predicted concentration of some of the selected marine and crustal elements

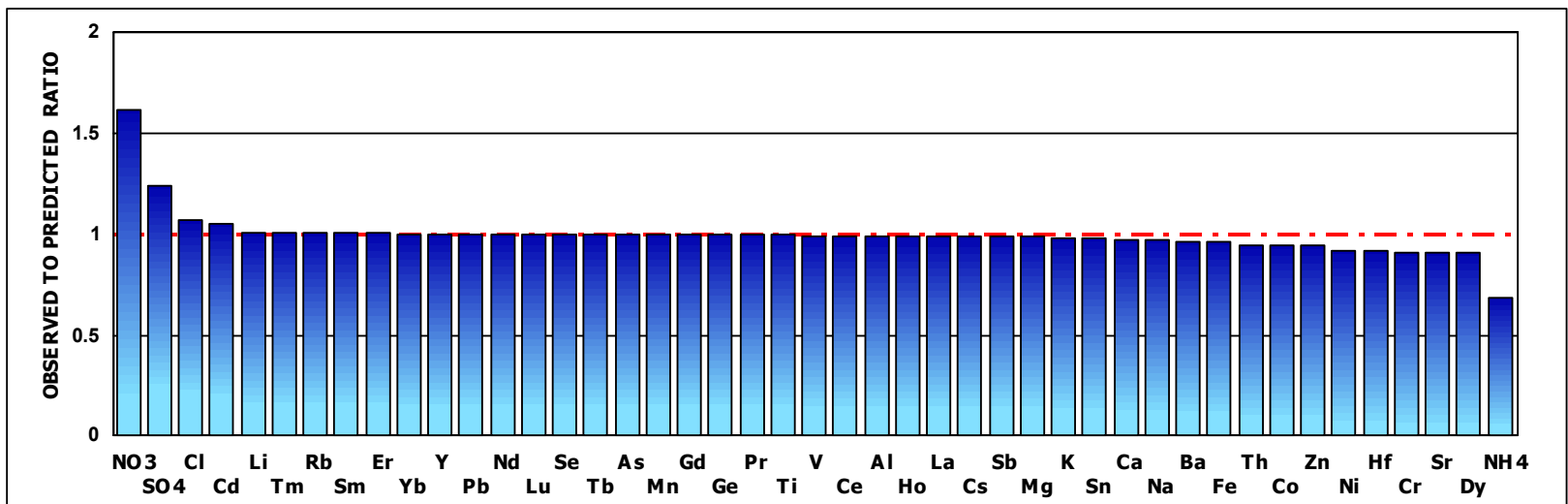


Figure 4.110 Observed to predicted concentration ratios of parameters



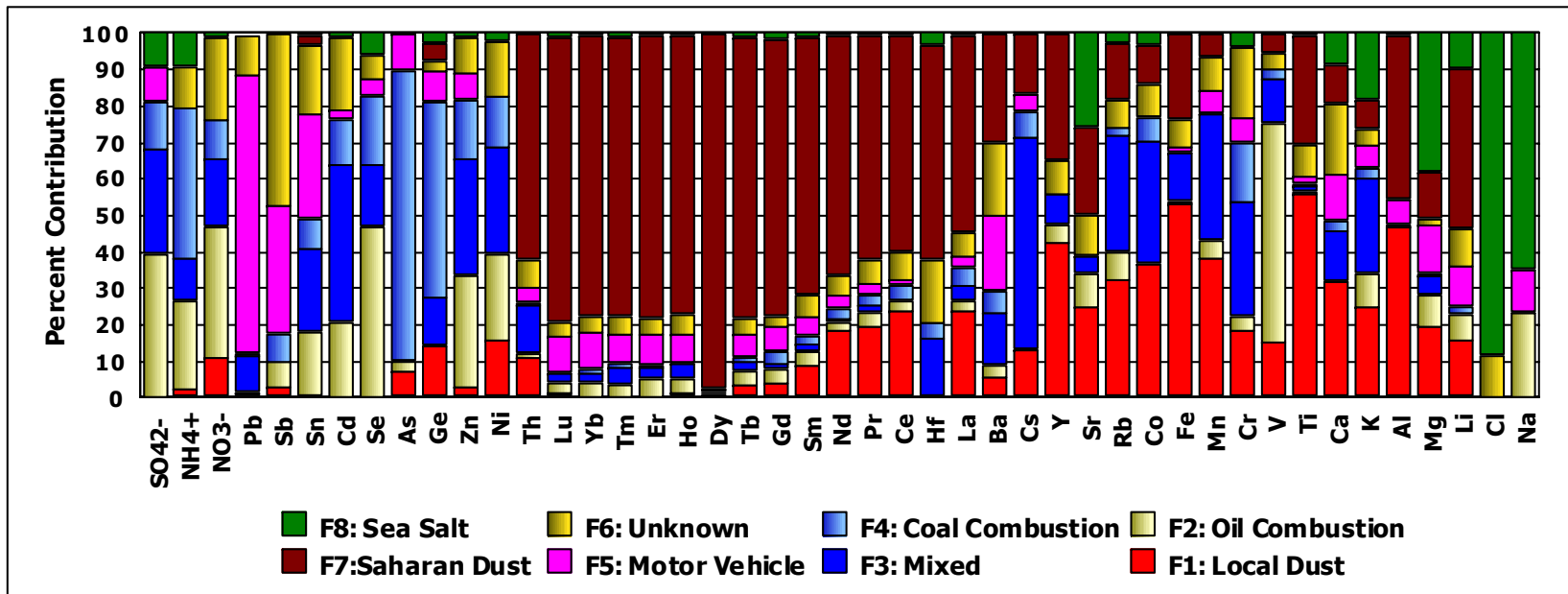


Figure 4.111 Percent contribution of each factor to each parameter

#### **4.5.6.2.4. Particulate Mass (PM) Apportionment**

There are commonly reported two approaches on particulate mass (PM) apportionment in PMF. In this first approach, particulate mass was considered with the other input variables by including in the data matrix of PMF (Kim et al., 2005a; Kim et al., 2005b). Once PM is included in the data matrix, it would be apportioned to factor as other parameters. Recently, some researchers suggested to substantially increasing uncertainty of PM while using in the data matrix so not to impact PMF results (Kim et al., 2005b). Recently, Reff et al. (2007) claimed that inclusion of PM in the PMF data matrix might be considered as double counting of PM in the PMF run because all of the parameters in the data matrix are parts of the particulate matter itself.

For this reason, we decided to use second approach followed in PM apportionment. In this approach, PM was excluded from the data matrix and factor contributions from PMF were regressed against PM measurements as given in the following equation:

$$PM_i = \sum_{k=1}^p g_{ik} \cdot a_{ik} \quad (4.17)$$

Where;

$PM_i$  = is the total PM mass measurement from sample I

$a_k$  = is the regression coefficient for factor "k" from performed regression

$g_{ik}$  = factor contributions

At Antalya station samples were collected on Whatman 41 (cellulose) filters. These fiber filters has very attractive features for sampling atmospheric particles for subsequent trace element measurements, such as low resistance for the passage of air and relatively low metal blanks. However, it's the only disadvantage in this type of studies is that it is hydroscopic, which means its weight changes depending on relative humidity of the air. Because of this, it has to be brought to the constant weight before it is weighted. In our group filter weighting is performed in a constant humidity chamber. Constant humidity chamber was constructed in 1999. For this reason, the PM measurements correspond to 1999-2001 were used in this regression analysis. Multiple Linear Regression (MLR) was

performed in order to find coefficients ( $a_{ik}$ ). The Analysis of Variance (ANOVA) results for this MLR was summarized in Table 4.30. In MLR, F statistics was used to test whether calculated coefficients ( $a_0, \dots, a_n$ ) of independent variables in MLR are zero ( $H_0$ , null hypothesis). Alternative hypothesis ( $H_A$ ) include a statement that calculated coefficients are different than zero. F critical calculated from test is also related to goodness of fit,  $r^2$ . If calculated F value (F ratio in Table 4.30) is greater than F critical, then null hypothesis is rejected, which means that calculated coefficients are greater than zero and goodness of fit is statistically significant.

Table 4.30 ANOVA results of MLR performed in PM mass apportionment

	<i>df</i>	<i>Sum of Squares</i>	<i>Mean of Squares</i>	<i>F Ratio</i>	<i>p</i>
<b>Regression</b>	8	$4.28 \cdot 10^8$	$5.35 \cdot 10^7$	12.80	$3.86 \cdot 10^{-16}$
<b>Residual</b>	343	$1.43 \cdot 10^9$	$4.18 \cdot 10^6$		
<b>Total</b>	351	$1.86 \cdot 10^9$			

Critical F found from statistical charts corresponding to 8 and 343 degrees of freedom and  $\alpha=0.05$  significance level is 0.34. Since  $F_{critical}$  (0.34) is less than  $F_{calculated}$  (12.8) and  $p$  value ( $3.86 \cdot 10^{-16}$ ) is also less than  $\alpha=0.05$ , the null hypothesis was rejected. In other words, calculated MLR coefficients ( $a_0, \dots, a_k$ ) are found to be greater than zero and goodness of fit is statistically significant in 95 % confidence interval.

After coefficients were determined by MLR, matrix multiplication was performed with factor contributions and then mass in each factor was summed up to find the total mass for each sample. Consequently, we obtained predicted mass for each sample. Relation between observed to predicted concentration for PM mass is depicted in Figure 4.112. Though obtained correlation coefficient,  $r^2 \approx 0.62$ , is not as good as ones corresponding to other species modeled by PMF, ANOVA analysis found it statistically significant at 95 % significant level.

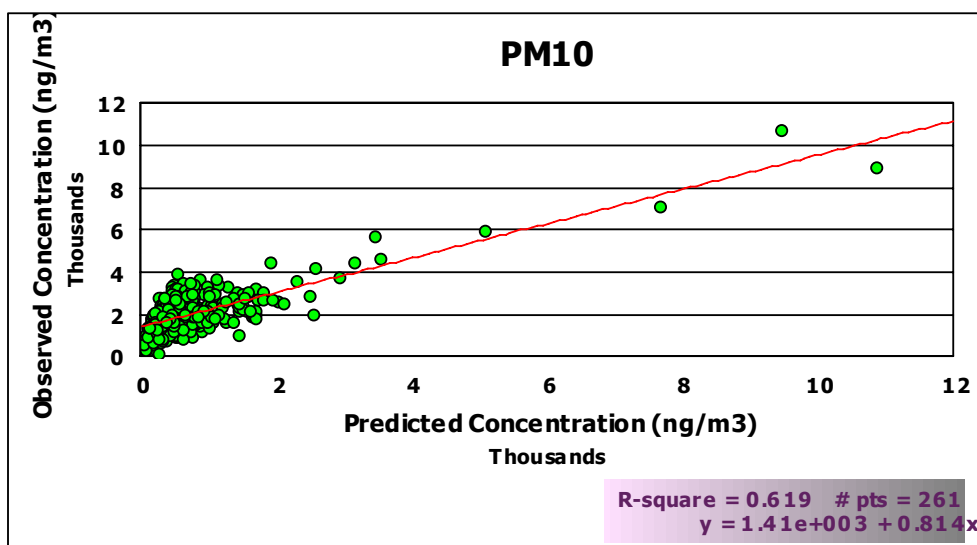


Figure 4.112 Relation between observed and predicted mass concentration

#### 4.5.7 Potential Source Contribution Function (PSCF)

Potential Source Contribution Function (PSCF) was employed extensively in the literature to find the most probable areas affecting the chemical composition of pollutants collected at a specific receptor site (e.g. Raman and Hopke, 2007; Zhao and Hopke, 2006). Güllü et al. (2005) identified anthropogenic source regions of aerosols collected at Antalya station between March 1992 and December 1993 through bootstrapping PSCF calculation. Major source regions for pollutants arriving in Eastern Mediterranean was determined as southern and western part of Turkey, central and eastern parts of Ukraine, east of Belarus, Greece, Georgia, Romania, coastal regions along France, Spain and Black Sea.

To assist in the interpretation of anthropogenic factors identified in Positive Matrix Factorization (PMF), potential source regions of Factor 2, 3, 4 and 5 were determined using PSCF with bootstrapping. Detailed information on bootstrapping in PSCF calculation was provided in Chapter 2. However, simply, source regions were ranked according to their relative contributions to high pollutant concentrations at the receptor site by using trajectory statistics. Trajectories corresponding to highest 25 % of G score days in each factor moving at 900 hPa pressure level were used in PSCF calculation. Trajectory endpoints within the area of 20°W-60°E and 15°N-75°N were included in the analysis.

3000 bootstrapping iteration was performed in calculation. Afterwards, output obtained from bootstrapping was interpolated with a GIS software package programme, Map Info Professional Version 7.5. The artifacts of PSCF associated with trajectory segment counts were previously reported in the literature. If the total number of endpoints is less in a certain cell, it can cause high PSCF value with high uncertainty (Cheng et al., 1993; Lupu and Maenhaut, 2002). Güllü et al. (2005) shown that trajectory segments corresponding to region extending from the South of Scandinavia in the north and to the middle of Algeria, Libya and Egypt in the south are too less that it may result in misleading PSCF values. Consequently, observed high PSCF values for these regions should be interpreted carefully.

Distribution of calculated bootstrapped PSCF values for Factor 2 is depicted in Figure 4.113. High loadings of V detected in this factor further implying that it is a oil combustion factor. It is clear from Figure 4.113 that western part of Turkey, which is highly industrialized, Spain, France, Armania, and Georgia are seem to be the main source regions of pollutants encountered in this factor.

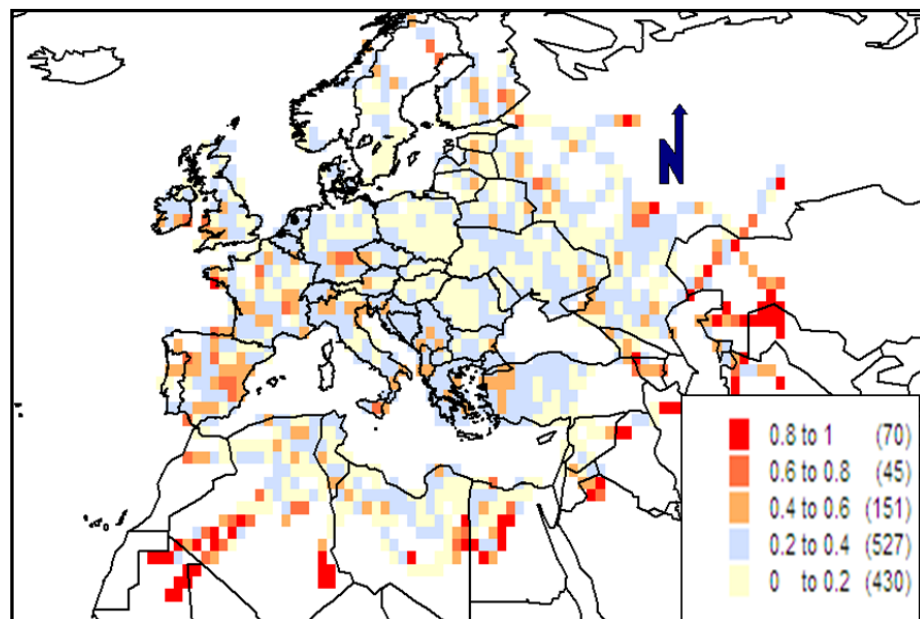


Figure 4.113 PSCF bootstrapped distribution of Factor 2 corresponding to highest 25 % G score values

Factor 3 is the mixed crustal-anthropogenic factor. The potential areas affecting this factor were depicted in Figure 4.114. As it can be seen from Figure 4.114, major source regions for this factor are Georgia and Russia. In addition, northern part of Turkey, Romania, Ukraine, Spain and France are regions contributing to observed concentrations of pollutants including in this factor.

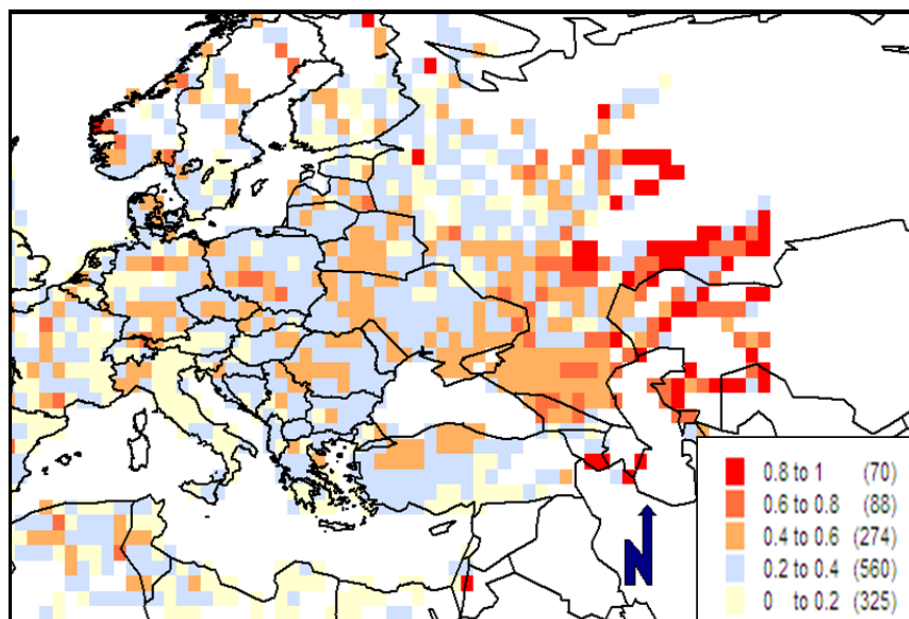


Figure 4.114 PSCF bootstrapped distribution of Factor 3 corresponding to highest 25 % G score values

Distribution of PSCF values for Factor 4 and 5 were depicted in Figure 4.115 and 4.116, respectively. Factor 4 was attributed to coal combustion since most of the variance was explained by As and Ge, which are tracers of coal combustion in the atmosphere. Romania, Bellarus, Hungary and Germany are regions affecting chemical composition of parameters evaluated in this factor as depicted in Figure 4.115.

Figure 4.116 implies that Check Republic, Ukraine, Romania, Germany, Spain are the distant sources influencing parameters encountered in Factor 5.

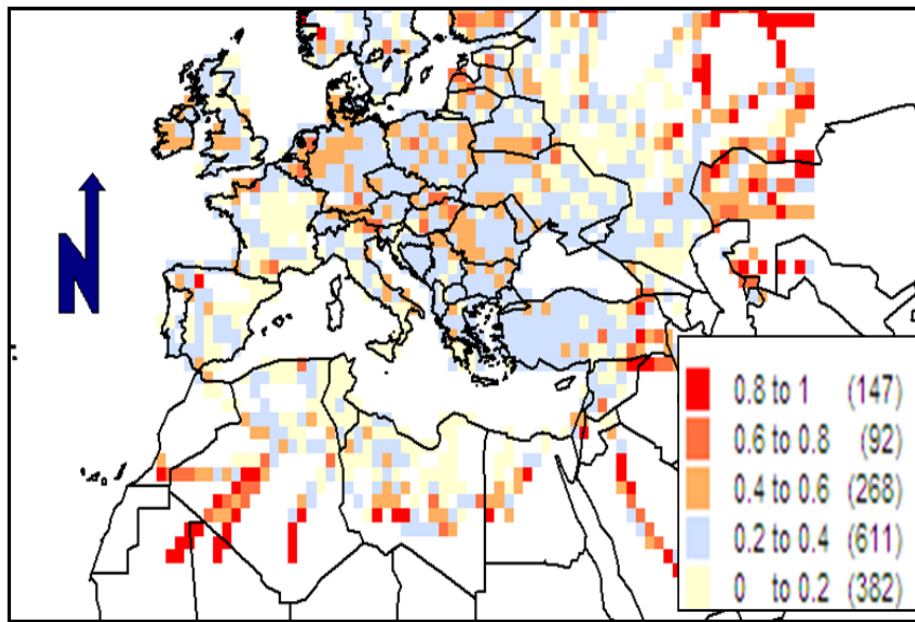


Figure 4.115 PSCF bootstrapped distribution of Factor 4 corresponding to highest 25 % G score values

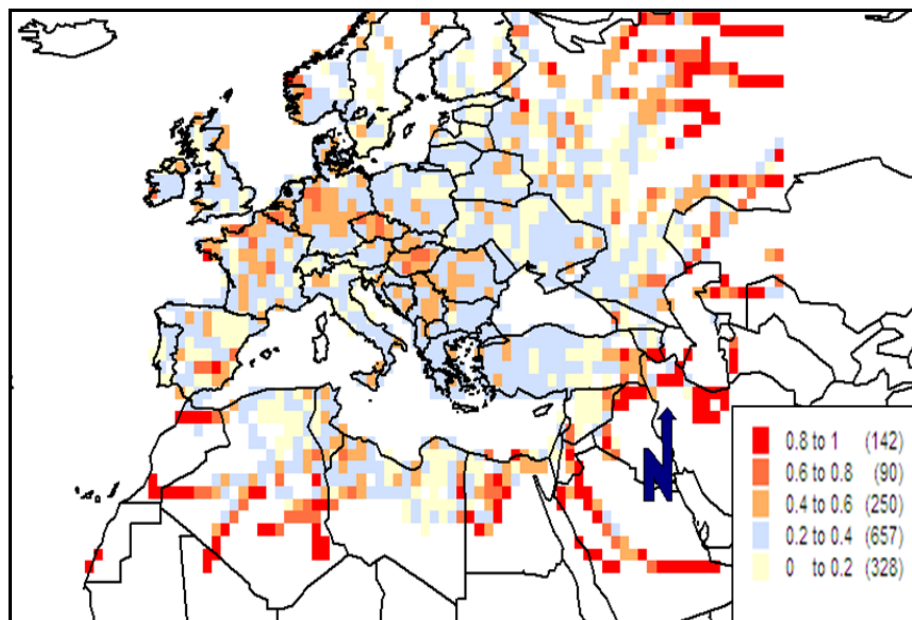


Figure 4.116 PSCF bootstrapped distribution of Factor 5 corresponding to highest 25 % G score values

#### 4.5.8. Deposition Fluxes of Elements and Ions to the Eastern Mediterranean

Dry deposition can be defined as the direct deposition of particles and gases in the absence of precipitation to vegetation, soil and water surfaces (Lowett, 1994). Dry deposition is recognized as one of the three pathways of deposition while wet deposition (deposition of material involved in precipitation) and cloud deposition (deposition of non precipitating constituents of clouds and fogs) are the two other pathways. Whilst wet deposition fluxes are easy to quantify, large uncertainties are associated with the measurement of dry deposition fluxes of particles, which is particularly true for the finer ones (Quinn and Ondov, 1998).

There is a controversy in the literature on the relative importance of wet and dry deposition while latter is much more significant for the elements associated with the large particles, for instance, Fe, Ca and Ti (Wu et al., 1994; Quinn and Ondov, 1998) and where anthropogenic sources are present in close proximity of the water body. Moreover, Pike and Mogan (2001) showed that for a number of metals such as Ag, Al, Cr, Ni, Fe and V dry and wet deposition rates are comparable. However, wet deposition is responsible for 60 to 90 % of total atmospheric input of As, Cd, Pb, Sr, Zn, Co and Cu. In contrast to this, Grantz et al. (2003) claimed that dry deposition is continuous and dependable process for atmospheric cleansing though dry deposition rates are orders of magnitude smaller than rates corresponding to wet deposition.

Deposition of particulate bound metals is of interest since some of these metals such as As, Pb and Cd, pose significant toxicity to aquatic environment. Deposition of acidic species like  $\text{SO}_4^{2-}$  and  $\text{NO}_3^-$  is also especially crucial for lakes. These acidic species decrease the pH of lake water. Once pH drops in lake some of the nutrients necessary for life in the lake dissolves and leave it with the water outflow. Acid water has also impacts on the living biota and their reproduction. For example, increase in acidity in Scandinavian lakes accompanied by decrease in fish (Botkin and Keller, 1995). Not only acidic species but also dust, which is transported to Eastern Mediterranean from North Africa, influence the biogeochemical cycles in water environment. For example, Dulac et al.(1996) and Bergametti et al. (1992) showed that dust deposition stimulating the surface marine productivity by providing nutrients in Mediterranean Sea. Later, Guerzoni et al. (1997) put forward that deposition of dust to sea bottom affects clay mineral content of the marine sediments in Mediterranean. They found that Saharan dust flux ( $\approx 1$



mgcm<sup>-2</sup> year<sup>-1</sup>) is responsible for 10 to 20 % of the deep sea sedimentation, which is about 3-15 mgcm<sup>-2</sup>year<sup>-1</sup>, in the Western Mediterranean.

Weather at Antalya shows a typical Mediterranean climate having long dry months. Average monthly precipitation and temperature profile of city between 1993 and 2001 was illustrated in Figure 4.117. Average maximum precipitation was observed in May with a rate of 37 mm. Precipitation was recorded from January to June but the rates were often less than evaporation. Possessing long dry months, one could claim that dry deposition is the most crucial way of atmospheric cleansing in Antalya region. Kubilay et al. (2000) calculated total dust deposition at Erdemli station, which was also located at Turkish Mediterranean coast. Researchers have found out that only 7 percent of the total deposition was in the wet form while the remaining 93 % of the deposition in dry form in the dry summer season of 1992.

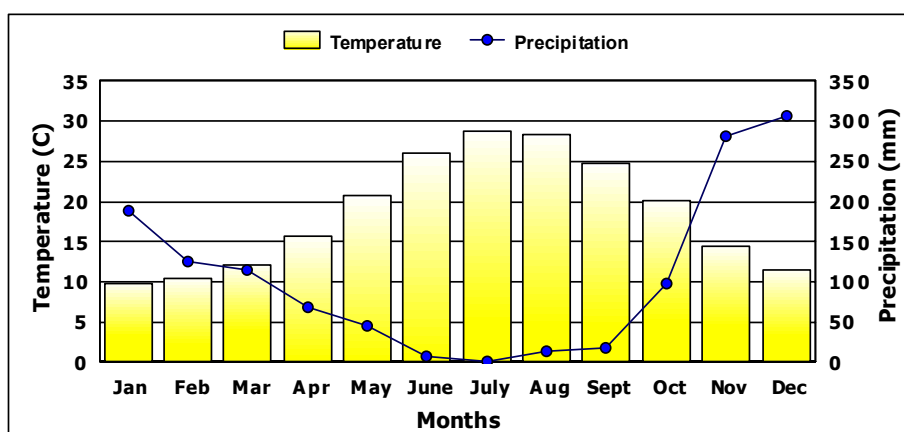


Figure 4.117 Average monthly precipitation and temperature profile of Antalya between 1993 and 2001

Dry deposition fluxes of particle associated elements and ions can be calculated by multiplying the corresponding concentration with a suitable velocity of the related parameter and can be formulized as:

$$F_d = V_d * C \quad (4.18)$$

Where;

$F_d$  stands for the deposition flux in terms of mass per square area per day,  $V_d$  is the corresponding dry deposition velocity in length per time and finally,  $C$  is the measured concentration of parameter of concern in mass per volume.

Dry deposition velocity,  $V_d$ , in this equation is inversely related with the resistance ( $R_t$ ), which is the sum of three types of bulk resistances. First resistance,  $R_a$ , representing the air movement in space, second one represents the resistance in the boundary layer adjacent to surface,  $R_b$ , and the last one stands for the chemical and biological absorption capacity of surfaces onto which air containing particles stick ( $R_c$ ).

$$V_d = -\frac{1}{R_t} \quad (4.19)$$

Where;

$$R_t = R_a + R_b + R_c \quad (4.20)$$

Negative sign in velocity resistance relation is due to the traditional use of fluxes toward the surface are considered as negative (Lowett, 1994). Accordingly, deposition velocity is variable depending on the type of surface and surrounding environmental conditions.

Dry deposition velocity is dependent on the particle size, climatological and physical conditions in the lower atmosphere, which is particularly true for sites located close to water bodies (Herut et al., 2001; Pereira et al., 2007). Quinn and Ondov (1998) investigated the influence of relative humidity on the particle growth and deposition fluxes. They have come up with the result that temporal variation in relative humidity is responsible for from 1.5 to larger than 4 fold increase in the deposition fluxes of particles bearing trace constituents. Particle growth due to humidity is the most important difficulty in estimating the dry deposition fluxes of trace constituents to water environment and is the main reason of large uncertainties associated with such sort of estimations. For instance, Sievering (1984) calculated the uncertainty associated with the dry deposition of particles with diameters less than 1  $\mu\text{m}$  to water surfaces as two orders of magnitude.

Pirrone et al. (1995) utilized a hybrid modelling to estimate the dry deposition of trace elements into southern Lake Michigan. The flux of trace elements associated with fine stage (particle size less than 2.5  $\mu\text{m}$ ) and coarse stage (particle size between 2.5 and 10  $\mu\text{m}$ ) was estimated. They suggested that fine stage deposition velocities were more variable as compared to large stage deposition velocities. Holsen and Noll (1992) suggested that the uncertainty related with estimations on dry deposition fluxes of particles could be reduced provided that size segregated samples were collected.

If one can find the dry deposition velocity of the measured species, then dry deposition fluxes can be calculated by simply multiplying concentration and corresponding velocity. Some of the dry deposition velocity values were obtained from the literature by taking account that studies were performed close to the aquatic environments, since our sampling station was located on Turkish Mediterranean coast. Most of the dry deposition velocity values were referred from a study that was conducted at the same sampling station. In this study, High Volume Cascade Impactor was used to collect samples in seven different size fractions, nominally, 10.2 microns and greater, 4.2 microns, 2.1 microns, 1.4 microns, 0.73 microns, 0.41 microns, and finally less than 0.41 microns. Particulate matter collected at different size fractions were analyzed by a combination of analytical techniques to determine Al, Ca, Cu, Fe, Mg, Zn, K, Na, Cd, Cr, Ni, Pb, V, Cl<sup>-</sup>, NO<sub>3</sub><sup>-</sup>, SO<sub>4</sub><sup>2-</sup> and NH<sub>4</sub><sup>+</sup> (Kuloğlu, 1997). Median dry deposition velocities of Al, Ca, Cd, Cl, Cr, Fe, K, Mg, Na, NH<sub>4</sub><sup>+</sup>, Ni, NO<sub>3</sub><sup>-</sup>, Pb, SO<sub>4</sub><sup>2-</sup> and V were obtained from Kuloğlu (1997) and used in the dry deposition flux calculations of related parameters.

In the dry deposition flux calculation, Biegalski and Landsberger (1999) dry deposition values for Au, In, La, Sm, Th and U were followed. Tin and Sr dry deposition velocities were obtained from Lim et al. (2006). Papastefanou and Ioannidou (1991) was referred for Be. Cobalt, Ce, Cs and Se dry deposition velocities were taken from Pierson and Cawse (1979). Finally, velocities corresponding to As and Sb were obtained from a study conducted by Pacyna et al. (1987) and Gatz (1975) was referred for the dry deposition velocity of Zn. The calculated dry deposition fluxes were tabulated in Table 4.31. It should be noted, however, that deposition fluxes should vary an order of magnitude due to uncertainties in followed  $V_d$  values. Calculated dry deposition fluxes might be investigated in four different groups in terms of their values. In the first group, Na, Cl, SO<sub>4</sub><sup>2-</sup>, Ca, NO<sub>3</sub><sup>-</sup>, Mg, Al, K, NH<sub>4</sub><sup>+</sup> and Fe can be considered. Highest dry deposition flux was calculated for Na ( $7704 \pm 9638 \mu\text{g m}^{-2} \text{d}^{-1}$ ) due to its highest dry deposition velocity ( $4.11 \text{ cm s}^{-1}$ ) and lowest dry deposition velocity was calculated for Fe with a value of

506± 876  $\mu\text{g m}^{-2}\text{d}^{-1}$  in this group. Second highest dry deposition flux was calculated for Cl owing to its highest deposition velocity (4.11  $\text{cm s}^{-1}$ ).

Table 4.31 Deposition velocities and corresponding calculated deposition fluxes of elements and ions

	Deposition Velocity	Deposition	Flux
	cm/s	avg $\mu\text{g/m}^2\cdot\text{d}$	sd $\mu\text{g/m}^2\cdot\text{d}$
<b>Al</b>	2.07	1136	2007
<b>As</b>	0.40	0.25	0.22
<b>Au</b>	0.03	0.0020	0.0072
<b>Be</b>	0.40	0.0083	0.0154
<b>Ca</b>	2.45	2321	4228
<b>Cd</b>	0.85	0.16	0.14
<b>Ce</b>	0.76	0.51	0.78
<b>Cl</b>	4.11	6592	8941
<b>Co</b>	0.80	0.15	0.21
<b>Cr</b>	1.91	5.59	7.58
<b>Cs</b>	0.36	0.036	0.038
<b>Fe</b>	1.90	506	876
<b>In</b>	0.31	0.0020	0.0082
<b>K</b>	2.68	761	811
<b>La</b>	0.91	0.32	0.59
<b>Mg</b>	3.23	1439	2121
<b>Mn</b>	1.10	7.77	9.69
<b>Na</b>	4.11	7704	9638
<b>NH<sub>4</sub><sup>+</sup></b>	0.61	597	602
<b>Ni</b>	1.74	3.51	3.85
<b>NO<sub>3</sub><sup>-</sup></b>	1.50	1624	1635
<b>Pb</b>	0.71	30	25
<b>Sb</b>	0.40	0.23	0.19
<b>Se</b>	0.16	0.057	0.085
<b>Sm</b>	0.84	0.061	0.121
<b>Sn</b>	0.34	0.19	0.16
<b>SO<sub>4</sub><sup>2-</sup></b>	0.63	4280	2812
<b>Sr</b>	1.50	5.18	11.69
<b>Th</b>	0.38	0.06	0.12
<b>Ti</b>	1.00	26	50
<b>U</b>	0.05	0.0032	0.0049
<b>V</b>	1.06	2.68	2.62
<b>Zn</b>	0.62	6.99	6.86

Dry deposition velocities corresponding to  $\text{NH}_4^+$  and  $\text{SO}_4^{2-}$  are considerably lower than other values of other parameters in this group. Size distribution of  $\text{NH}_4^+$  and  $\text{SO}_4^{2-}$  is considerably different from that of  $\text{NO}_3^-$ . Kuloğlu and Tuncel (2005) have reported that 75 % of the  $\text{NO}_3^-$  mass is associated with the coarse particles, which explains why significantly higher dry deposition velocity was assigned to  $\text{NO}_3^-$  as compared to  $\text{SO}_4^{2-}$  and  $\text{NH}_4^+$ . The calculated dry deposition flux for  $\text{SO}_4^{2-}$  and  $\text{NH}_4^+$  are  $4280 \pm 2812 \mu\text{gm}^{-2}\text{d}^{-1}$  and  $597 \pm 602 \mu\text{gm}^{-2}\text{d}^{-1}$ , respectively. The reason behind observing third highest flux for  $\text{SO}_4^{2-}$  is due to its highest concentration in the generated data set. It should be noted that mean concentration for  $\text{SO}_4^{2-}$  for the study period was found as  $7.93 \pm 5.14 \mu\text{gm}^{-3}$ . Other elements in this group, that is, Al, Ca, Mg, Fe, and K, are associated with the coarse particles in the atmosphere. Accordingly, their dry deposition velocities range from  $1.9 \text{ cm s}^{-1}$  to  $3.23 \text{ cm s}^{-1}$  for Fe and Mg, respectively. Calculated high dry deposition flux for these elements can be attributed to both their highest deposition velocities and their considerably high concentrations.

Second group includes Pb ( $30 \pm 25 \mu\text{gm}^{-2}\text{d}^{-1}$ ), Ti ( $26 \pm 50 \mu\text{gm}^{-2}\text{d}^{-1}$ ), Mn ( $7.77 \pm 9.69 \mu\text{gm}^{-2}\text{d}^{-1}$ ), Zn ( $6.99 \pm 6.86 \mu\text{gm}^{-2}\text{d}^{-1}$ ), Cr ( $5.59 \pm 7.58 \mu\text{gm}^{-2}\text{d}^{-1}$ ), Sr ( $5.18 \pm 11.69 \mu\text{gm}^{-2}\text{d}^{-1}$ ), Ni ( $3.51 \pm 3.85 \mu\text{gm}^{-2}\text{d}^{-1}$ ) and V ( $2.68 \pm 2.62 \mu\text{gm}^{-2}\text{d}^{-1}$ ). Lead is the major tracer of motor vehicle emissions and it is associated with the fine particles in the atmosphere. Consequently, its dry deposition velocity ( $0.71 \text{ cm s}^{-1}$ ) is considerably lower than other parameters in this group with the exception of Zn, for which deposition velocity was assigned to  $0.62 \text{ cm s}^{-1}$ . Except for Pb, other parameters in this group have mixed sources. For example, Ti present bounded to crustal material in addition to material released from incinerator and coal fired boiler (Chow, 1995). Therefore, these parameters are associated with both coarse and fine particles. With the exception of Zn and Pb, elements in this group have comparably high dry deposition velocities with a minimum value of  $1 \text{ cm s}^{-1}$  for Ti and maximum value of  $1.91 \text{ cm s}^{-1}$  for Cr.

Arsenic, Sb, Sn, La, Ce, Co, and Cd forms third group of elements. The minimum dry deposition flux was estimated for Co ( $\approx 150 \text{ ngm}^{-2}\text{d}^{-1}$ ) and maximum dry deposition flux was calculated for Ce ( $\approx 780 \text{ ngm}^{-2}\text{d}^{-1}$ ). Cerium and La are rare earth elements and it was previously shown that these elements are associated with the Saharan dust pulses observed at our station. Calculated highest dry deposition flux for Ce can be attributed to its deposition velocity ( $0.76 \text{ cm s}^{-1}$ ). Arsenic, Sb and Sn are associated with the fine particles in the atmosphere since they are mainly generated by the anthropogenic

activities, that is why low deposition velocities ( $0.40 \text{ cm s}^{-1}$  for Sb and As,  $0.36 \text{ cm s}^{-1}$  for Sn) were assigned for these elements.

Cesium, In, Th, U, Au, Se, Be and Sm constitute the last group. Estimated dry deposition fluxes of these elements range from 2 to  $61 \text{ ngm}^{-2}\text{d}^{-1}$  for In and Sm, respectively. The lowest dry deposition fluxes of this group of elements as compared to previously mentioned three other groups can be explained by their recorded very minor concentrations and assigned low dry deposition velocities. With the exception of Sm, for which deposition velocity was assumed as  $0.84 \text{ cm s}^{-1}$ , the rest of the parameters have deposition velocities equal and less than  $0.38 \text{ cm s}^{-1}$ .

#### ***4.5.8.1. Comparison with Literature***

Dry deposition data is scarce in the literature for Mediterranean region. For this reason, data generated at other parts of the world is used to compare with the estimated dry deposition fluxes in this study. It should be noted that all sites with the exception of site located in India were selected in a way that they are close to the aquatic environment. Therefore, differences arising from the dry deposition velocities due to humidity might not be completely eliminated but reduced.

In the comparison, two studies that were performed in Izmir and Bursa were referred. These two cities are western part of Turkey and expected to be considerably polluted owing to heavy industrial activity.

A high volume air sampler coupled with filter holder was used to collect TSP samples in Bursa. Collected samples were analyzed with ICP AES. Bursa is one of Turkey's highly industrialized cities. It contains many industries from textile to automotive. Samples were collected at three industrial districts; they are inland districts but close to Marmara Sea. Detailed information can be found in Tasdemir et al (2006).

Odabasi et al. (2002) estimated particulate dry deposition flux using a deposition plate. Particulate matter was collected on glass fiber filters using a high volume sampler. GFAAS and FAAS were used to analyze the collected samples in terms of their trace element content.

Wu et al. (2004) collected TSP samples at a metropolitan area surrounding the Taichung Harbor. Trace metals in the samples were determined by Hitachi Z-5000. They have found out that dust, vehicle emissions and marine salt are the main sources influencing the chemical composition of samples.

Samples were collected at Agra, which is located in north-central India, using polypropylene surfaces and analyzed by ion chromatography in the study of Saxena et al. (1997). Ferrous metal casting, ferrous alloy and non-ferrous industries, rubber processing, tanneries, lime oxidation and pulverization are listed in the Agra's major industrial activities.

Pirrone et al. (1995) was used a hybrid-receptor modelling approach to assess the trace element deposition to Lake Michigan, USA. Both temporal and spatial variations in the deposition flux were encountered in the study. The modeled deposition fluxes were compared with the direct measurements. The highest deposition flux was found for Al with a value of  $143 \cdot 10^3$  kg and this attributed to anthropogenic influences.

Total Suspended Particles (TSP) was collected by using high volume sampler at a station located at a coastal site of Israeli Mediterranean. Collected samples were analyzed through GFAAS. Dry deposition velocities assigned to values used by Duce et al. (2001). The calculated Al and Fe fluxes were at least factor of 2 higher than fluxes to Atlantic and Pacific Oceans.

Average dry deposition fluxes of common parameters determined in these studies were summarized in Table 4.32. The results indicate that Izmir had the highest Mg dry deposition fluxes ( $3100 \mu\text{g m}^{-2} \text{d}^{-1}$ ) and Taiwan had the lowest Mg dry deposition fluxes ( $106 \mu\text{g m}^{-2} \text{d}^{-1}$ ). The highest Ca dry deposition flux was calculated for Izmir in Turkey ( $43.1 \text{ mg m}^{-2} \text{d}^{-1}$ ) whereas the lowest one was calculated in Lake Michigan, USA ( $136.9 \mu\text{g m}^{-2} \text{d}^{-1}$ ). Among the stations used in comparison, Izmir had the highest Cr ( $16 \mu\text{g m}^{-2} \text{d}^{-1}$ ), Fe ( $12.09 \text{ mg m}^{-2} \text{d}^{-1}$ ), Cd ( $24 \mu\text{g m}^{-2} \text{d}^{-1}$ ), Ni ( $39 \mu\text{g m}^{-2} \text{d}^{-1}$ ) and Zn ( $1.91 \text{ mg m}^{-2} \text{d}^{-1}$ ) dry deposition fluxes. Highest Pb dry deposition flux was recorded in Bursa ( $77.2 \mu\text{g m}^{-2} \text{d}^{-1}$ ) while lowest dry deposition flux was calculated for Lake Michigan as  $56 \mu\text{g m}^{-2} \text{d}^{-1}$ .

Except for Mg and Pb dry deposition fluxes, former one was  $1439 \mu\text{g m}^{-2} \text{d}^{-1}$  and latter one was  $30 \mu\text{g m}^{-2} \text{d}^{-1}$ , all the calculated fluxes were smaller in Antalya station once compared with the sampling sites located in Turkey. When comparison was made in

terms of marine originated elements, that is, Na and Cl, for which data was available only for our station and station located in India, higher dry deposition fluxes were estimated for our station. This was expected since station in India was located away from marine environment. Highest K dry deposition flux was calculated for Indian site (average,  $860 \mu\text{g m}^{-2} \text{d}^{-1}$ ), which may be attributed to presence of heavy industrial facilities in the region since K is both soil derived and man made generated pollutant.

#### ***4.5.8.2. Seasonal Variation of Dry Deposition Fluxes***

The seasonal variation of the parameters, for which dry deposition flux were calculated, was also investigated. For most of the parameters, there is a clear seasonal pattern within January 1993- April 2001 winter (November-April) and summer (May-October). Observed seasonality in calculated dry deposition flux contradicts with the finding of Sandroni and Migon (2002). Researchers claimed that fluxes of trace metals do not show any clear seasonal pattern due to the homogenous anthropogenic European background in the Mediterranean atmospheric aerosol, on which Saharan dust pulses are occasionally superimposed.

Seasonality of dry deposition fluxes were investigated in four groups, which was previously formed based on the values of dry deposition fluxes, and results were demonstrated in Figure 4.118-4.121.



Table 4.32 Average deposition fluxes of measured aerosol variables reported in the literature ( $\mu\text{g m}^{-2}\text{d}^{-1}$ )

	<b>This</b>	<b>Bursa<sup>a</sup></b>	<b>Izmir<sup>b</sup></b>	<b>Taiwan<sup>c</sup></b>	<b>India<sup>d</sup></b>	<b>Lake Michigan<sup>e</sup></b>	<b>Israel<sup>f</sup></b>
	<b>Study</b>	<b>Turkey</b>	<b>Turkey</b>			<b>USA</b>	
<b>Mg</b>	1439	1204	3100	106	1730		
<b>Ca</b>	2321	4896.3	43100		5180	136.8	
<b>Cr</b>	5.59	10.7	16	11		0.24	<1
<b>Mn</b>	7.77	51.1	135	194		1.2	30
<b>Fe</b>	506	2165.4	12090	218		112.8	1184
<b>Zn</b>	6.99	250.5	1910	109		1.8	5
<b>Cd</b>	0.16	0.7	24				<1
<b>Pb</b>	30	77.2	22	56		0.53	4
<b>Cl</b>	6592				2590		
<b>Na</b>	7704				860		
<b>K</b>	761				860	36	
<b>Al</b>	1136					79.2	
<b>Co</b>	0.15	1.1					
<b>Ni</b>	3.51	5.1	39				

<sup>a</sup>Tasdemir et al., 2006;

<sup>b</sup>Odabasi et al., 2002;

<sup>c</sup>Wu et al., 2005;

<sup>d</sup>Saxena et al., 1997;

<sup>e</sup>Pirrone et al., 1995;

<sup>f</sup>Herut et al., 2001;

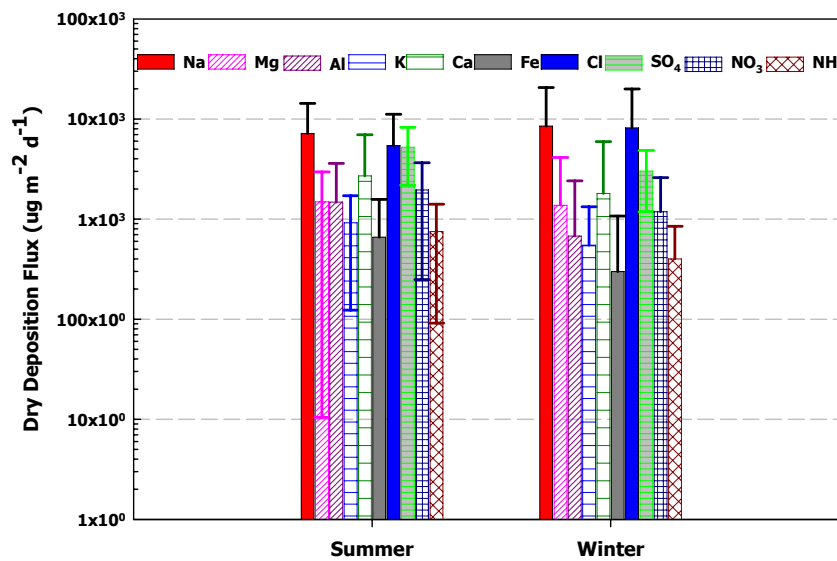


Figure 4.118 Seasonal variation of dry deposition flux of parameters evaluated in the first group

For the parameters evaluated in the first group (Na, Mg, Al, K, SO<sub>4</sub><sup>2-</sup>, NO<sub>3</sub><sup>-</sup>, NH<sub>4</sub><sup>+</sup>, Cl, Ca and Fe), seasonal variation is obvious as depicted in Figure 4.118. The summer to winter ratios for Na, Mg, Al, K, SO<sub>4</sub><sup>2-</sup>, NO<sub>3</sub><sup>-</sup>, NH<sub>4</sub><sup>+</sup>, Cl, Ca and Fe are 0.84, 1.08, 2.18, 1.67, 1.73, 1.65, 1.87, 0.66, 1.50, and 2.21, respectively. Parameters with summer to winter ratio is less than 1, that is, Na and Cl, are marine originated elements. Their high winter concentration may be attributed to increase bubble bursting process over the sea surface with increase strength of wind in winter time. High summer concentration of soil derived elements (Al, Ca, Fe, and K) is due to the increase resuspension of soil particles in summer months. Eventually, high summer to winter ratio of dry deposition fluxes of SO<sub>4</sub><sup>2-</sup>, NO<sub>3</sub><sup>-</sup> and NH<sub>4</sub><sup>+</sup> can be explained by the increase photochemical activity in the atmosphere facilitating the formation of secondary pollutants from their precursors in summer.

Seasonal variation of the parameters evaluated in the second group (Ti, Cr, Mn, Pb, Zn, Ni, V and Sr) was illustrated in Figure 4.119. The summer to winter ratio of the deposition fluxes are 2.08, 1.54, 2.05, 1.36, 1.65, 1.76, 1.40, and 2.11 for Ti, Cr, Mn, Pb, Zn, Ni, Sr, and V, respectively. With the exception of Ni and Sr, summer to winter ratio for all of the parameters was greater than 1.5. For all of the parameters, high summer to winter ratio implies that dry deposition is the most effective mechanism for the removal

of these pollutants from the atmosphere in summer season. In winter time, these parameters were cleansed from the atmosphere via precipitation that is why we observed lower winter dry deposition fluxes.

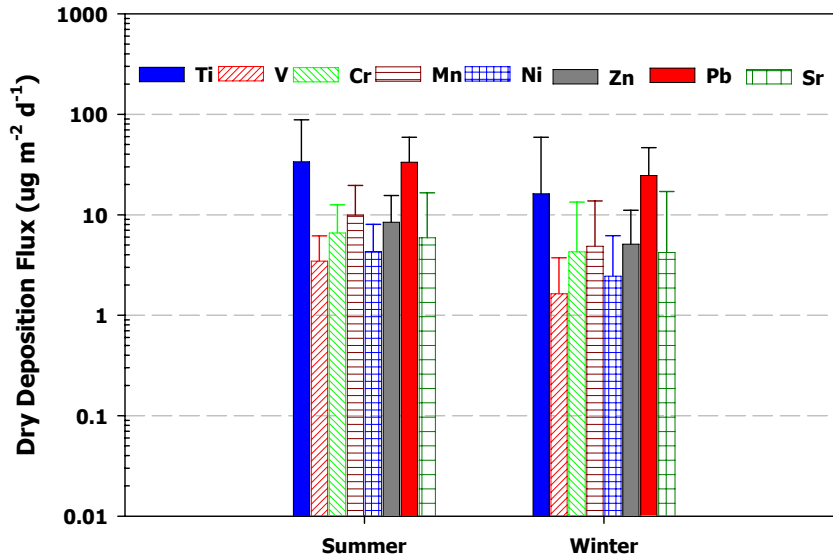


Figure 4.119 Seasonal variation of dry deposition flux of parameters evaluated in the second group

For the third group of elements (Co, As, Cd, Sn, Sb, La and Ce), all of the parameters have summer to winter ratio greater than one (Co: 1.77, Cd: 1.40, Sn: 1.62, Sb: 1.23, La: 2.17 and Ce: 2.10) except for As, for which ratio was calculated as 0.96, indicating that these pollutants are removed from the atmosphere mainly from dry deposition in summer whereas wet deposition is the main scavenging mechanism in winter. As it was shown previously in source apportionment section that As released to the atmosphere from local sources in Antalya region. Consequently, As concentration does not exhibit variation with time. Seasonal variation of dry deposition flux for this group of elements was depicted in Figure 4.120. Seasonal variation of dry deposition fluxes calculated for the last group of elements (Be, Se, In, Cs, Au, Sm, Th, and U) was shown in Figure 4.121. All of the parameters have summer to winter ratio greater than one (Be: 1.64, In: 1.02, Cs: 2.01, Au: 1.15, Sm: 2.18, Th: 2.45, Se: 1.13 and U: 1.76).

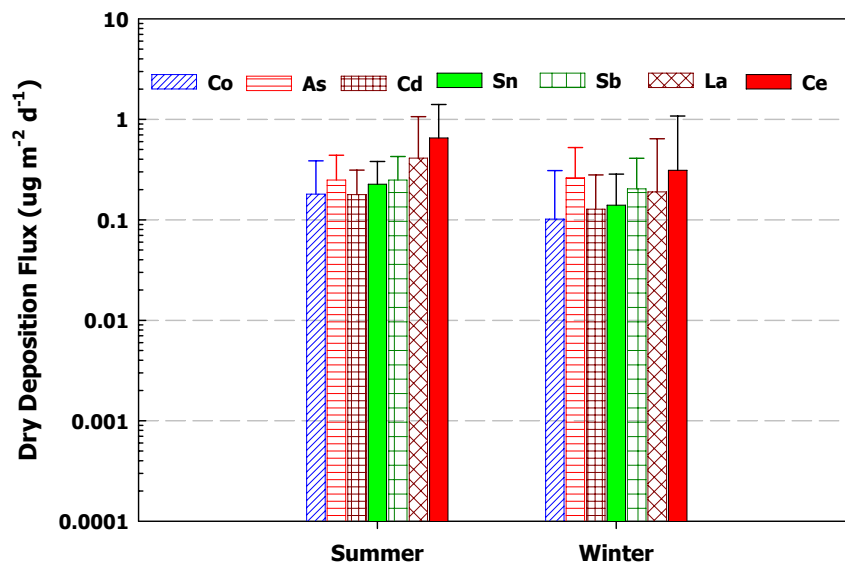


Figure 4.120 Seasonal variation of dry deposition flux of parameters evaluated in the third group

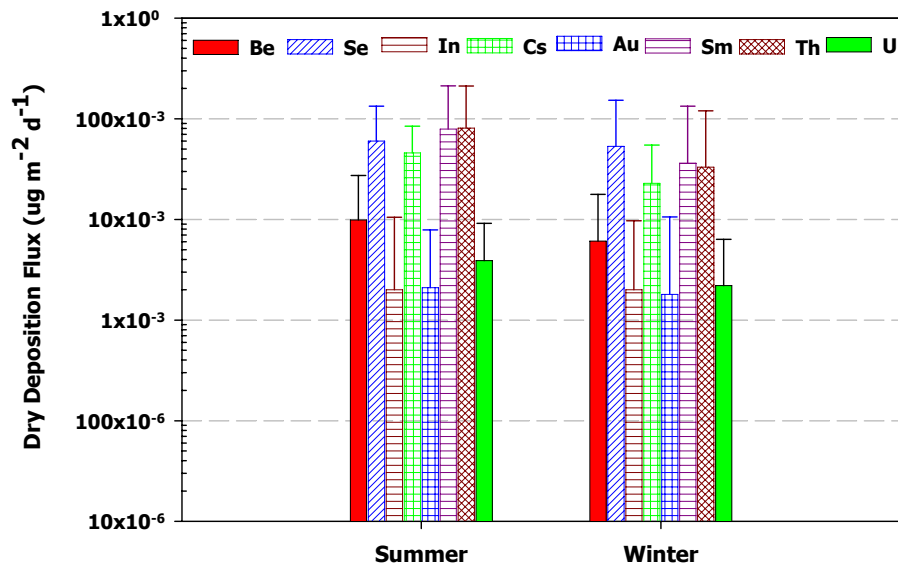


Figure 4.121 Seasonal variation of dry deposition flux of parameters evaluated in the fourth group

## CHAPTER 5

### CONCLUSION

Aerosol samples collected between 1993 and 2001 at Turkish Mediterranean coast were analyzed by a combination of three different analytical techniques in terms of trace element and major ions. Generated data set was interpreted to find the correlations between measured parameters, to evaluate their short and long term trends, to resolve major sources that determine their atmospheric concentrations and to identify possible regions that impact their chemical composition.

Measured concentrations range from 15.4  $\mu\text{g m}^{-3}$  for Ho to 7.93  $\mu\text{g m}^{-3}$  for  $\text{SO}_4^{2-}$ . With the exception of Al, B, Cd, Cl, K, Lu and Sr, applied K-S DN test for goodness of fit showed that all of the parameters were log-normally distributed.

In order to give insight about the pollution level determined in this study, parameters in generated data set was compared with the other stations located in both Eastern and Western Mediterranean region. Though all stations were close to Mediterranean Sea, differences in measured concentrations of marine elements (particularly for Na and Cl) were observed. Since these elements were associated with coarser particles in the atmosphere, their deposition increases as one goes from shore to inland. Consequently, observed difference was explained by different distances between the stations and shore. Concentrations of crustal elements such as Al, Ca, Ti, Co, Fe, K and Mg were higher than ones determined for Western Mediterranean sites and close to values measured at other stations located in Eastern Mediterranean. As these two stations in addition to Antalya station were close to arid regions of Mediterranean, greater concentrations of crustal elements were expected. Sulfate and Pb concentrations determined in this study were the highest for stations used in comparison. Use of leaded gasoline phase-out was begun in 2002 in Turkey though Europe began gradually phasing out leaded gasoline in 1980s and mandated elimination in 1990s. Since samples were collected before 2002 at our station, we observed considerably higher Pb concentrations in our station.

Background concentrations of the measured parameters were also calculated and compared with values determined for other stations in Turkey. Conducted comparison revealed that regional background concentrations of trace crustal elements such as Co, Cs, Dy, Sm, Th, and Sc were close for stations but the difference is obvious for other trace crustals including Ce, Hf, Nd, Rb and Tb. The difference observed in the concentrations of these elements was attributed to difference in soil profile of the regions.

With 9 years long back trajectory calculation, main air flow sectors affecting Eastern Mediterranean region were identified. This calculation revealed that air masses spent more time in West and North West direction before reaching to our station. Residence time of air masses in West and North West sector were determined as ~ 33 and 19 %, respectively. The contributions of N, NE, SW and E sectors to the climatology of region at 1500 m altitude were 15, 12, 9 and 7 %, respectively. Seasonality in the flow climatology was also investigated. Air mass flow frequencies from N and NE sectors increased about two folds in summer months.

Temporal variations in pollutants concentrations were discussed in three categories: (1) Short term (Episodic) variations; (2) Seasonal variations; (3) Year to year variations (Trend analysis). It was found that crustal and marine elements were more episodic as compared to anthropogenic pollutants. Total of 140 episodes were recorded for marine elements (Na and Cl). Seasonal distribution of marine episodes was almost equal though duration and magnitude of winter episodes were significantly different than ones observed in summer. Winter episodes associated with marine pollutants were longer in duration and higher in magnitude.

Two hundred fifty five crustal episodes were detected in the course of study period. Unlike marine episodes, crustal episodes are more frequent in summer season owing to increased resuspension of soil related material. Two sources of crustal episodes were detected as dust incursions from North Africa and Middle East and local soil. It was found that episodes from North Africa and Middle East were observed particularly in the months of transient seasons (April, May, September and October) while local dust episodes increased in August.

About 50 episodes were detected for anthropogenic elements between 1993 and 2001. Mean concentration for these elements increased by a factor of 6 to 10 in episode days. In contrast to long range transported pollutants such as  $\text{SO}_4^{2-}$  and Pb, episodes associated with anthropogenic pollutants having local sources (e.g., As) were more frequent in winter. Long range transported pollutants were removed from atmosphere mainly by precipitation; consequently, episodes for these pollutants were smoothed out on the way to sampling station.

Relation between pollutant concentrations and precipitation was also investigated herein. While concentrations of marine elements increased on rainy days, soil derived elements measured at lower concentrations on these days. Concentration of crustal elements increases more gradually after precipitation as compared to anthropogenic pollutants. Anthropogenic elements reached their pre-rain concentration in 1-3 days after precipitation recorded while this time much longer for crustal elements (7-10 days). Unlike crustal and anthropogenic elements, concentration of marine elements started to decrease after rain and their concentration increased after 3 days after precipitation again.

Most of the pollutants showed well defined seasonal cycle. Concentration of marine originated elements increased in the winter season due to increased sea salt production over sea surface through bubble bursting process, while concentrations decreased in summer season. For crustal elements, high summer concentrations were recorded and this pattern was attributed to dryness of both local soil and arid regions exporting dust to Eastern Mediterranean. Similar to crustal elements, we observed high concentrations of anthropogenic elements such as Cd, Pb,  $\text{NO}_3^-$ ,  $\text{SO}_4^{2-}$  and  $\text{NH}_4^+$  in summer season. Enhanced photochemical activity in atmosphere in summer season led to considerable higher concentrations of  $\text{NO}_3^-$ ,  $\text{SO}_4^{2-}$  and  $\text{NH}_4^+$ . Another factor determining the atmospheric concentrations of parameters is the scavenging. Pollutants were removed from the atmosphere by wet deposition in winter; consequently, lower concentrations were detected for crustal and anthropogenic pollutants in this season. Summer to winter ratio was calculated for measured species. For crustal elements, the calculated ratio changed from 2 to 4. Sodium and Cl had ratio of 1.20 and 1.00, respectively. Though both Na and Cl was marine originated, their summer to winter ratio was slightly different. This difference can be attributed to increased crustal contribution to Na and evaporation

of Cl as HCl from the aerosol surface in summer season. For Ge, As and Pt, summer to winter ratio was found around 1.00 indicating local sources for these pollutants.

Seasonal Kendall test was applied to generated data set to find the long term trends in the concentrations of measured parameters. Decreasing trend was detected for some of the anthropogenic elements such as Pt, As, Se, Ge and Pb. Decrease in Pb concentration were consistent with the decline observed in Europe for this element. The rate of decrease was calculated by Sen's slope estimator as 0.042, 0.022, 0.003, and 5.5 ng/m<sup>3</sup> per year for As, Se, Ge and Pb, respectively. Though about 70 % reduction was attained for SO<sub>4</sub><sup>2-</sup> starting from late 1980s in Europe, neither increasing nor decreasing trend was recorded for this ion in this study. For major crustal elements, for example, Al, Na, Mg, and K and rare earth elements (La, Ce, Pr, Nd, Sm, Eu, Gd, Tb, Dy, Ho, Er, Tm, Yb and Lu) decreasing trend was observed at 95 % confidence level. Highest rate of change was recorded for Na (-209 ng/m<sup>3</sup>/yr). For rare earth elements rate of change ranged from -0.001 ng/m<sup>3</sup> per year for Ho (Tb and Eu had also same rate of decrease in the course of study period) to -0.043 ng/m<sup>3</sup> per year for Ce.

Correlations between the parameters provide information about their sources and transport pattern in the atmosphere. Observed high correlation indicates either same source or similar transport in the atmosphere. Measured species were evaluated in five different categories in this study. In the first group, excellent correlation was observed for elements like Al, Fe, Ca, and Ti. Rare earth elements were also highly correlated with these parameters, which are soil derived elements. Consequently, first group contained crustal originated elements. Sodium, Cl and Mg showed good correlation ( $r > 0.7$ ) one to other, these elements are well known sea salt markers, hence, this group included marine originated elements. Lead showed moderate correlation ( $r > 0.55$ ) with Sn and Sb, and low correlation ( $r > 0.3$ ) with some of the crustal elements such as Cs, Ba, Li and K, implying that Pb transported to the atmosphere on soil particles. In the fourth group, SO<sub>4</sub><sup>2-</sup> showed moderate correlation ( $r > 0.5$ ) with V, Zn and Cd, and poor correlation with Pb ( $r > 0.3$ ). Sulfate, NO<sub>3</sub><sup>-</sup> and NH<sub>4</sub><sup>+</sup> were moderately correlated ( $r > 0.4$ ) with each other. This observed correlation was attributed to same generation mechanisms determining the concentration of these pollutants in the atmosphere.

Enrichment factor (EF) was also calculated for all of the pollutants. It was found that some of the anthropogenic elements for instance, S, Se, Cd and Pb were highly enriched



in aerosol samples ( $1000 > EF > 10000$ ). However, EF was calculated as less than 10 for V, Cr and Ni, which have both crustal and anthropogenic sources. Similar to these three elements, Na also had EF less than 10. Sodium released both from marine environment and earth's crust to the atmosphere. For crustal elements, EF ranged from 1 to 10.

In order to find the dominant sectors affecting chemical composition of Eastern Mediterranean aerosols two different methodologies applied, namely, residence time and cluster analysis. In the residence time analysis, study area was divided into six sectors (North, North East, East, South, West and North West) and samples were assigned to a specific sectors provided that trajectory for that particular day spent most of its time in that sector. Afterwards, average concentration of each element in each sector was calculated. With the exception of Pb, pollution derived elements for example,  $SO_4^{2-}$  and Zn, were identified in higher concentrations with the air masses originated from North, West and North East sector. South sector was determined as the predominant sector affecting Pb level at Antalya station. However, neither Mediterranean Sea nor North Africa could be the source of this observed Pb concentration. Local air circulation effective around the sampling station carries emissions from the highway, which is very close to sampling station. Concentrations of crustal elements were determined to be highest in the South sector, which was attributed to dust transport from North Africa.

Cluster analysis, grouping of trajectories according to their directions and speed, was also applied using 9 year long trajectory data. Cluster analysis identified 9 different sectors, which means that air masses originated 9 different directions. Some of the clusters (e.g., Cluster 4, 6 and 7) include short fetch of air masses, that is, slow moving trajectories while rest of them were fast moving trajectories. Average concentrations of soil derived elements were higher in Cluster 1, having south westerly flow, and Cluster 7, having south easterly flow. However, pollution derived elements were associated with trajectories allocated to Cluster 6, which includes short trajectories originated from Bulgaria and passing over Istanbul, and Cluster 4, which extends to Western part of Europe and covers Western part of Turkey.

Kruskal Wallis test, which is a non-parametric test, was applied to test whether the means of concentrations determined for each sector was statistically significant form one to another. With the exception of Pb,  $NO_3^-$ ,  $NH_4^+$ , Cl, W, Pt, Au, Ca and Cr, all of the parameters showed differences from one sector to another at 95 % confidence interval.

Measured aerosol species were apportioned to their sources by using Positive Matrix Factorization (PMF). PMF identified 8 different sources affecting chemical composition of collected aerosol samples: (1) Local dust factor (included high loadings of major crustal elements like Ca, Fe, Ti and Al); (2) Saharan dust factor (rare earth elements explained most of the variance); (3) Crustal-anthropogenic mixed factor (Cd, Ni, Zn, Se were enriched in addition to Cs, Ba, V and Cr); (4) Marine factor (Na and Cl explained most of the variance); (5) Motor vehicle emission factor (Pb, Sn and Sb were enriched in this factor); (6) Coal combustion factor (Ge and As explained most of the variance in this factor); (7) Oil combustion factor (V and Se were enriched in this factor); (8) Local Sb factor.

In order to find the source regions of pollutants identified in PMF, Potential Source Contribution Function (PSCF) was calculated and interpolated with a GIS software, namely, MapInfo. Western part of Turkey, Spain, France, Armenia, and Georgia were seemed to most probable areas determining the level of pollutants in oil combustion factor. For anthropogenic crustal mixed factor, northern part of Turkey, Romania, Ukraine, Spain and France were regions contributing to observed concentrations of pollutants including in this factor. Georgia, Russia, Romania, Belarus, Hungary and Germany were found as regions affecting levels of parameters apportioned to coal combustion factor. Check Republic, Ukraine, Romania, Germany, Spain were found as distant sources influencing parameters encountered in motor vehicle emission factor. In addition, countries located in North Africa having shore to Mediterranean Sea for instance, Libya, Tunisia, Egypt and Israel could be considered as major source regions of this factor.

High  $\text{SO}_4^{2-}$  concentration in Eastern Mediterranean atmosphere was put forward by many researchers and took attention. While about 70 % decrease was observed for Western Europe stating from end of 1980s, minor decrease was observed for Eastern Europe. Coupled with the cluster analysis, we saw that  $\text{SO}_4^{2-}$  concentrations is highest with the short trajectories from Balkans to Eastern Mediterranean. In this study, we were able to show that  $\text{SO}_4^{2-}$  concentration associated with southerly flow, from North Africa and Mediterranean Sea, had average  $\text{SO}_4^{2-}$  concentration of  $6 \mu\text{g m}^{-3}$ , which is about 6 times greater than one measured for Europe. Although the exact mechanism was not clearly herein, we believed that air masses from Balkans and Europe go to North Africa first and

then reached to our station, which is thought to be the reason of enrichment of air masses from Africa with  $\text{SO}_4^{2-}$ .

Dust transport is of special concern due to its role in the atmospheric chemistry. Dust particles impact biogeochemistry of the region that they transported to. Besides, they act as cloud condensation nuclei in the atmosphere and affect the earth's surface temperature. In addition, it accounts for the large portion of (70 % were recorded in the literature) daily  $\text{PM}_{10}$  exceedances in places close to North Africa. For this reason, people are trying to find the tracers of Saharan dust to estimate the exact quantity of dust transport to other regions of the world. In this study, we have found that Dy, Ho, Tm, Tb, Lu, Yb, Er, Sm and Eu can be used as potential tracers for Saharan dust. With the application of Seasonal Kendall test we have found decreasing trend for these trace crustal elements in addition to major crustals. Consequently, here we speculated that Saharan dust intensity decreased between 1992 and 2001. Seasonal variation of dust transport was also investigated. It has been shown that the Saharan dust intrusions mainly occurred in transient seasons such as April, May, September and October.

Weather at Antalya shows a typical Mediterranean climate having long dry months. Consequently, dry deposition is important mechanism for the removal of pollutants from the atmosphere. Dry deposition fluxes (DDF) of measured aerosol species were calculated by compiling dry deposition velocities reported in the literature. Calculated DDF ranged from  $7704 \mu\text{g m}^{-2}\text{d}^{-1}$  for Na to  $0.0020 \mu\text{g m}^{-2}\text{d}^{-1}$  for In and Au.

## CHAPTER 6

### FUTURE WORKS AND RECOMMENDATIONS

Aerosols account for the largest source of uncertainty in assessment of anthropogenic climate change. It is uncertain whether increase in aerosol intensity leads to a net increase or decrease in global average temperature. For these reasons, extensive research is going on for the determination of chemical composition, sources and temporal trends of aerosols.

PM<sub>10</sub> aerosol samples were evaluated in this study. It is well documented in the literature that anthropogenic particles are associated with the fine fraction of the particulate matter while natural pollutants such as soil derived and marine originated elements were transported to the atmosphere on coarse fraction. Consequently, multi element analysis of size segregated samples provides more information about the sources of pollutants. For this reason, dichotomous samplers or impactors should be employed during sampling periods. Nowadays, state of art instruments is taking attention in the scientific platform such as laser spectrometer, which enables one to count particle sizes down to 5 nm with significantly high time resolution.

First largest multi element data (56 element and 3 major ions were determined) was generated in this study. Unfortunately, organic tracers such as levoglucosan could not be measured. With the inclusion of organic tracers, emission from forest fires can also be identified by receptor modelling and contribution of forest fires to chemical composition of aerosols can be determined quantitatively. Alternatively, measurements of black carbon (BC) or elemental carbon (EC) in collected samples may also be useful in determination of forest fires and volcanic eruptions in the region.

In addition to particulate matter, gaseous pollutants such as SO<sub>2</sub>, NO<sub>x</sub> and O<sub>3</sub> should be monitored in the station, which altogether provide very detailed information on the pollution profile of the region.

Dust transport from North Africa and Middle East to Eastern Mediterranean was discussed in this study. While we determined high crustal element concentrations for specific days and requested back trajectories associated with these days, we hardly identified Saharan dust events since we did not have data related with vertical distribution of dust. Installation of instruments such as LIDAR would be useful to determine the vertical distribution of dust in the atmosphere. Therefore, the altitude of dust episodes in the atmosphere can be determined and correlation with the measured aerosol species can be found, accordingly.

## REFERENCES

- Ali, A.E., 2003. *J. Radioanal. Nucl. Chem.* 258, 391
- Abdalmogith, S.S., and Harrison, R.M., 2005. "The use of trajectory cluster analysis to examine the long-range transport of secondary inorganic aerosol in the UK". *Atmospheric Environment* 39, 6686-6695
- Abdalmogith, S.S., Harrison, R.M., Zlatev, Z., 2006. "Intercomparison of secondary inorganic aerosol concentrations in the UK with predictions of the unified Danish Eulerian model". *Journal of Atmospheric Chemistry* 54, 43–66.
- Air Quality Criteria for Particulate Matter, Volume I of III, EPA/600/P-95/001aF, 1996
- Al-Momani, I. F., Momani, K. A., & Jaradat, Q. M., 2000. "Chemical composition of wet precipitation in Irbid, Jordan". *Journal of Atmospheric Chemistry*, 35, 47–57
- Al-Momani, I.F., 2003. "Trace elements in atmospheric precipitation at Northern Jordan measured by ICP-MS: acidity and possible sources". *Atmospheric Environment* 37, 4507–4515
- Al-Momani, I.F., Aygun, S., Tuncel, G., 1998. "Wet deposition of major ions and trace elements in the eastern Mediterranean basin". *Journal of Geophysical Research* 103(D7), 8287-8299
- Al-Momani, I.F., Daradkeh, A.S., Haj-Hussein, A. T., Yousef, Y.A., Jaradat, Q.M., Momani, K.A., 2005. "Trace elements in daily collected aerosols in Al-Hashimya, central Jordan". *Atmospheric Research* 73, 87–100
- Al-Momani, I.F., Momani, K.A., Jaradat, Q.M., Masadeh, A.M., Yousef, Y.A., Alomary, A.A., 2008. "Atmospheric deposition of major and trace elements in Amman, Jordan". *Environmental Monitoring Assessment*, 136, 209-218
- Alpert, P., Kaufman, Y.J, Shay-El, Y., Tanre, D., da Silva, A., Schubert, S., Joseph, J.H., 1998. "Quantification of dust-forced heating of the lower troposphere". *Nature* 395, 367–370

Amouroux, D., and Donard, O.F.X., 1996. "Maritime emission of selenium to the atmosphere in eastern Mediterranean Seas". *Geophysical Research Letters* 23 (14), 1777–1780

Anderson, H.R., 2000. "Differential Epidemiology of Ambient Aerosols". *Phil. Trans. R. Soc. Lond. A* 358, 2771–2785

Anderson, J.M., Miller, S.L., Milford, J.B., 2001. "Source apportionment of exposure to toxic volatile organic compounds using positive matrix factorization". *Journal of Exposure Analysis and Environmental Epidemiology* 11, 295 – 307

Andrae, M.O., and Raemdonck, H., 1983. "Dimethyl sulfide in the surface ocean and the marine atmosphere-a global view", *Science*, 221, 744-747.

Andrae, T.W., Andrae, M.O., Ichoku, C., Maenhaut, W., Cafmeyer, J., Karnieli, A., Orlovsky, L., 2002. "Light scattering by dust and anthropogenic aerosol at the remote site in Negev desert, Israel". *Journal of Geophysical Research*, 107, D2

Anlauf, K., Li, S.M., Leaitch, R., Brook, J., Hayden, K., Sauntry, D.T., Wiebe, A., 2006. "Ionic composition and size characteristics of particles in the Lower Fraser Valley: Pacific 2001 field study". *Atmospheric Environment* 40, 2662–2675

Anttila, P., Paatero, P., Tapper, U., and Jarvinen, O., 1995. "Source Identification of Bulk Wet Deposition in Finland by Positive Matrix Factorization". *Atmospheric Environment* 29 (14), 1705–1718

Appel, B.R., Tokiwa, Y., Konthly E.L., Povard, V., 1988. "Evaluation of procedures for measuring atmospheric nitric acid and ammonia", *Atmospheric Environment*, 22, 1565-1573.

Arimoto, R., Duce, R.A., Savoie, D.L., et al., 1996. "Relationships among aerosol constituents from Asia and the North Pacific during PEM-West". *Journal of Geophysical Research* 101(D1), 2011-2023

Arruda, M.A.Z., 2007. "Sample Preparation of Atmospheric Aerosols for Elemental Analysis and Fractionation Studies, In: Trends in Sample Preparation". Nova Science Publishers, Inc., New York, pp.83-136, ISBN:1-60021-118-6

Artaxo, P., Oyola, P., Martinez, R., 1999. "Aerosol composition and source apportionment in Santiago de Chile". *Nuclear Instruments and Methods in Physics Research B* 150, 309–416

Ashbaugh, L.L., Malm, W.C., and Sadeh, W.D., 1985. "A residence time analysis of sulfur concentrations at grand canyon national park". *Atmospheric Environment* 19:1263-1270

Avila A, Roda F, 2002. "Assessing decadal changes in rainwater alkalinity at a rural Mediterranean site in the Montseny Mountains (NE Spain)". *Atmospheric Environment* 36(17), 2881–2890

Avila, A., & Alarcon, M., 1999. "Relationship between precipitation chemistry and meteorological situations at a rural site in NE Spain". *Atmospheric Environment* 33, 1663–1677

Avila, A., and Roda, F., 2002. "Assessing decadal changes in rainwater alkalinity at a rural Mediterranean site in the Montseny Mountains (NE Spain)". *Atmospheric Environment*, 36 (17), 2881–2890

Avila, A., Queralt, I., Alarcon, M., 1997. "Mineralogical composition of African dust delivered by red rains over North-Eastern Spain". *Journal of Geophysical Research* 102, 21977–21996.

Äyräs, M. , Niskavaara, H. , Bogatyrev, I. , Chekushin, V. , Pavlov, V. , Caritat, P. , Halleraker, J.H. , Finne, T.E. , Kashulina, G. , and Reimann, C., 1997. "Regional patterns of heavy metals (Co, Cr, Cu, Fe, Ni, Pb, V and Zn) and sulphur in terrestrial moss samples as indication of airborne pollution in a 188, 000 km<sup>2</sup> area in northern Finland, Norway and Russia". *Journal of Geochemical Exploration* 58(2-3), 269-281

Bandhu, H.K., Puri, S., Shahi, J.S., Mehta, D., Garg, M.L., Singh, N., Mangal, P.C., Suri, C.R., Swietlicki, E., Trehan, P.N., 1996. "An Evaluation of the sources of air pollution in the city of Chandigarh, India: A study using EDXRF technique". *NIMB Beam Interactions with Mterials and Atoms*, 114, 341–344

Bardouki, H., Liakakou, H., Ecobomou, C., Sciare, J., Smolik, J., Zdimal, V., Eleftheriadis, K., Lazaridis, M., Dye, C., Mihalopolos, N., 2003. "Chemical Composition of size resolved



aerosols in the eastern Mediterranean during summer and winter". *Atmospheric Environment* 37, 195–208

Baumann, K., Jayanty, R.K.M., and Flanagan, J.B., 2008. "Fine Particulate Matter Source Apportionment for the Chemical Speciation Trends Network Site at Birmingham, Alabama, Using Positive Matrix Factorization". *Journal of Air and Waste Management Association* 58, 27–44

Begum, B., Biswas, S.K., Kim, E., Hopke, P.K., Khaliquzzaman, M., 2005. "Investigation of Sources of Atmospheric Aerosol at a Hot Spot Area in Dhaka, Bangladesh". *Journal of Air and Waste Management Association* 55:227-240

Bencala, K.E., and Seinfeld, J.H., 1976. "On Frequency Distributions of Air Pollutant Concentrations". *Atmospheric Environment* 10, 941-950

Benkovitz CM, Easter RC, Nemesure S, Wagener R, Schwartz SE., 1994. „Sulfate over the North Atlantic and adjacent continental regions: evaluation for October and November 1986 using a three-dimensional model driven by observation-derived meteorology". *J Geophys Res* 9:20,725 –20,756

Bennet, C., Jonsson, P., Lindgren, E.S., 2005. "Concentrations and Sources of Trace Elements in Particulate Air Pollution, Dar es Salam, Tanzania, studied by EDXRF". *X-Ray Spectrometry* 34, 1–6

Bergametti, G., Dutot, A.L., Buart-Menard, Losno, R., Remoudaki, E., 1989. "Seasonal variability of elemental composition of atmospheric aerosol particles over the North-western Mediterranean". *Tellus* 41B, 353-361

Bergametti, G., Remoudaki, E., Losno, R., Steiner, E., Chatenet, B., 1992. "Source, transport and deposition of atmospheric phosphorus over the Northwestern Mediterranean". *Journal of Atmospheric Chemistry* 14, 501–513

Bevington, P.R., 1969. "Data Reduction and Error Analysis for the Physical Sciences". Mc Graw Hill Book Company, pp.99

Biegalski, S., and Landsberger, S., 1999. "An evaluation of Atmospheric Deposition of Trace Elements into the Great Lakes". *Biological Trace Element Research* 71–72, 247–256

Biegalski, S.R., Landsberger, S., and Hoff, R.M., 1998. "Source Receptor Modelling Using Trace Metals in Aerosols Collected at Three Rural Canadian Great Lakes Sampling Stations". *Journal of Air & Waste Management Association* 48: 227–237

Bonelli, P., Marcazzan, G.M., Cereda, E., 1996. "Elemental Composition and Air Trajectories of African Dust Transported in Northern Italy". Kluwer Academic Publishers. 275–283.

Borbely-Kiss, I., Kiss, A.Z., Koltay, E., Szabo Gy., Bozó , L., 2004. "Saharan dust episodes in Hungarian aerosol: elemental signatures and transport trajectories". *Journal of Aerosol Science* 35, 1205–1224.

Borja-Aburto, V.H., Loomis, D.P., Bangdiwala, S.I., Shy, C.M. and Pacheco, R.A. Rascon, 1997. "Ozone, Suspended Particulates, and Daily Mortality in Mexico City", *American Journal of Epidemiology* 145(3), 258-268

Botkin, D., and Keller, E., 1995. "Environmental Science: Earth as a living planet". John Wiley & Sons Inc., USA.

Brankov, E., Rao, S.T., Porter, P.S., 1998. "A Trajectory Clustering Correlation Methodology for Examining the Long Range Transport of Air Pollutants". *Atmospheric Environment* 32(9), 1525-1534

Braziewicz, J., Kownacka, L., Majewska, U., Korman, A., 2004. "Elemental Concentrations in the Tropospheric and Lower Stratospheric Air in Northeastern Region Of Poland". *Atmospheric Environment* 38, 1989–1996

Brody, L.R., Nestor, M.J.R., 1980. "Handbook for forecasters in the Mediterranean, Part 2. Regional forecasting aids for the Mediterranean basin". Naval Environmental Prediction Research Facility, Technical Report TR 80-10, Monterey, CA, pp.VII; VII-13

Brown, R.J.C., and Milton, M.J.T., 2005. "Analytical techniques for trace element analysis:an overview". *Trends in Analytical Chemistry* 24(3)

Brown, S.G., Frankel, A., and Hafner, H.R., 2007. "Source apportionment of VOCs in the Los Angeles area using positive matrix factorization". *Atmospheric Environment* 41, 227–237

Bundesminister des Inneren, 1971. „Gesetz zur Verminderung von Luftverunreinigungen durch Bleiverbindungen in Ottokraftstoffen für Kraftfahrzeugmotore (Benzin-Blei-Gesetz)“. vom 5.8.1971. RG Bl I, 1234–1236.

Buzcu, B., Fraser, M.P., Kulkarni, P., Chellam, S., 2003. "Source Identification and Apportionment of Fine Particulate Matter in Houston, TX, Using Positive Matrix Factorization". *Environmental Engineering Science* 20 (6):533-545

Buzcu-Guven, B., Brown, S.G., Frankel, A., Hafner, H.R., and Roberts, P.T., 2007. "Analysis and Apportionment of Organic Carbon and Fine Particulate Matter Sources at Multiple Sites in the Midwestern States". *Journal of Air and Waste Management Association* 57, 606-619

Charron, A., Harrison, R.M., Quincey, P. , 2007. "What are the sources and conditions responsible for exceedences of the 24 h PM<sub>10</sub> limit value (50 µgm<sup>-3</sup>) at a heavily trafficked London site?". *Atmospheric Environment* 41, 1960–1975

Cape, J.N., Metheven, J., and Hudson, L.E., 2000. "The use of trajectory cluster analysis to interpret trace gas measurements at Mace Head, Ireland. *Atmospheric Environment* 34, 3651-3663

Caquineau, S., Gaudichet, A., Gomes, L., Magonthier, M.C., Chatenet, B., 1998. "Saharan dust: clay ratio as a relevant tracer to assess the soil derived aerosols". *Geophysical Research Letters* 25, 983-986

Catinon, M., Ayrault, S., Clochiatti, R., Boudouma, o., Asta, J., Tissut, M., Ravel, P., 2008. "The anthropogenic atmospheric elements fraction: a new interpretation of elemental deposits on tree barks". *Atmospheric Environment* (2008), doi: 10.1016/j.atmosenv.2008.11.004

Cercasov, V., and Wulfmeyer, V., 2008. "Trends in airborne particulates in Stuttgart, Germany: 1972-2005". *Environmental Pollution* 152, 304-313

Chapman, R.S., Watkinson, W.P., Dreher, K.L., Costa, D.L., 1997. "Ambient Particulate Matter and Respiratory and Cardiovascular Illness In Adults: Particle-Borne Transition Metals And The Heart-Lung Axis", *Environmental Toxicology and Pharmacology*, 4, 331-338.

Charlson R. J., Lovelock J. E., Andreae, M. O. & Warren, S. G. 1987 Oceanic phytoplankton, atmospheric sulphur, cloud albedo and climate. *Nature*, Lond. 326, 655-661.

Charlson, R.J., Schwartz, S.E., Hales, J.M., Cess, R.D., Coakley, J.A., Hansen, J.E., Hofmann, D.J., 1992. "Climate Forcing by Anthropogenic Aerosols", *Science*, 255, 423-430.

Cheng, M.D., Hopke, P.K., Landsberger, S., and Barrie, L.A., 1991. "Distribution Characteristics of Trace Elements and Ionic Species of Aerosol Collected at Canadian High Arctic". *Atmospheric Environment*, 25A (12), 2903-2909

Cheng, M.D., Hopke, P.K., Zeng, Y., 1993. "A receptor methodology for determining source regions of particle sulfate composition observed at Dorset, Ontario". *Journal of Geophysical Research* 98, 16839-16849.

Chester, R., Nimmo, M., Alarcon, M., Saydam, C., Murphy, K.J.T., Sanders, G.S., and Corcoran, P., 1993. "Defining the Chemical Character of Aerosols from the Atmosphere of the Mediterranean Sea and Surrounding Regions". *Oceanologica Acta* 16 (3), 231-246.

Chiapello, I., Bergametti, G., Chatenet, B., Bousquet, P., Dulac, F., Soares, E.S., 1997. "Origins of African Dust Transported over the Northeastern Tropical Atlantic", *Journal of Geophysical Research*, 102 (D12), 13,701-13,709.

Chiapello, I., Prospero, J.M., Herman, J.R., Hsu, N.C., 1999. "Detection of mineral dust over the North Atlantic Ocean and Africa with the Nimbus 7 TOMS". *Journal of Geophysical Research* 104 (D8), 9277-9291

Chimidza, S., Viksna, A., Lindgren, E.S., 2001. "EDXRF and TXRF analysis of aerosol particles and the mobile fraction of soil in Botswana". *X Ray Spectrometry* 30:301-307

Chow, J.C., 1995. "Measurement Methods to Determine Compliance with Ambient Air Quality Standards for Suspended Particles". *Journal of Air & Waste Management Association* 45: 320–382

Christensen, J.M., 1995. "Human exposure to toxic metals: factors influencing interpretation of biomonitoring results". *The Science of the Total Environment* 166:89–135

Chueinta, W., Hopke, P.K., Paatero, P., 2000. "Investigation of sources of atmospheric aerosol at urban and suburban residential areas in Thailand by positive matrix factorization". *Atmospheric Environment* 34: 3319-3329

Chung, Y.S., Kim, S.H., Moon, J.H., Kim, Y.J., Lim, J.M., Lee, J.H., 2006. "(PM<sub>2.5</sub>/PM<sub>10</sub>) in an urban region of Korea Source identification and long-term monitoring of airborne particulate matter". *Journal of Radioanalytical and Nuclear Chemistry* 267(1): 35–48

CIA World Factbook, 2003 Edition

Coen, M.C., Weingartner, E., Nyeki, Cozic, J., Henning, S., Verheggen, B., Gehrig, R., and Baltensperger, U., 2007. "Long-term trend analysis of aerosol variables at the high-alpine site, Jungfraujoch". *Journal of Geophysical Research*, 112, D13213

Cokacar, T., Kubilay, N., and Oguz, T., 2001. "Structure of *Emiliania huxleyi* blooms in the Black Sea surface waters as detected by SeaWIFS imagery". *Geophysical Research Letters* 28(4), 4607-4610

Compendium Method IO-3.5. "Determination of Metals In Ambient Particulate Matter Using Inductively Coupled Plasma/ Mass Spectrometry (ICP/MS)". Center for Environmental Research Information Office of Research and Development U.S. Environmental Protection Agency Cincinnati, OH 45268

Convention on Long -range Transboundary Air Pollution, <http://www.unece.org/env/lrtap>, Last Access Date: 18/11/2008

Çetin, B., 2002. "Elemental Tracers of Saharan Dust". M.Sc. Thesis, Middle East Technical University, Ankara, Turkey

Danalatos, D. And Glavas, S., 1999. Gas phase nitric acid, ammonia and related particulate matter at a Mediterranean coastal site, Patras, Greece,. *Atmospheric Environment* 33, 3417–3425

David C. Dorman; DC., McManus;BE., Parkinson; CU., Manuel; CA., McElveen, AM., Everitt, JI., 2004. "Nasal Toxicity of Manganese Sulfate and Manganese Phosphate in Young Male Rats Following Subchronic (13-Week) Inhalation Exposure". *Inhalation Toxicology* 16:6-7, 481–488

Davis, B.L., and Jixiang, G., 2000. *Atmospheric Environment* 34, 2703

Dayan, U., 1986. "Climatology of back trajectories from Israel based on synoptic analysis". *Journal of Climate and Applied Meteorology* 25, 591-595.

Dean, John R., 1997. *Atomic Absorption and Plasma Spectroscopy, Analytical Chemistry by Open Learning, 2<sup>nd</sup> Edition, John Wiley & Sons Ltd., West Sussex, England*

deNevers, N., Lee, K.W., and Frank, N.H., 1979. "Patterns in TSP distribution". *Journal of Air Pollution and Control Association* 29, 32-35

Dentener, F., Carmichael, F., Zhang, Y., Lelieveld, J., and Crutzen, P., 1996. "Role of mineral aerosol as a reactive surface in the global troposphere". *Journal of Geophysical Research* 101, 22869–22889.

Determination of metals in ambient particulate matter using Inductively Coupled Plasma Mass Spectrometry (ICP/MS), Compendium Method IO-3.5, USEPA, Cincinnati, OH 45268, June 1999

Dockery, D.W., and Pope, C.A., 1994. "Acute Respiratory Effects of Particulate Air Pollution", *Annual Review of Public Health*, 15, 107-132.

Dolgoplova, A., Weiss, D. J. , Seltmann, R., Stanley, C. , Coles, B. and Cheburkin, A.K., 2004. "Closed-vessel microwave digestion technique for lichens and leaves prior to

determination of trace elements (Pb, Zn, Cu) and stable Pb isotope ratios". Intern. J. Environ. Anal. Chem. 84(12), 889–899

Donaldson, K., and MacNee, W., 1998. "The mechanism of lung injury caused by PM<sub>10</sub>". Environmental Science and Technology, 10, 21–32.

Dorling, S.R., Davies, T.D., and Pierce, C.E., 1992. "Cluster analysis: a technique for estimating the synoptic meteorological controls on air and precipitation chemistry-method and applications". Atmospheric Environment 26A (14), 2575-2581

Draxler, R.R. and Rolph, G.D., 2003. HYSPLIT (HYbrid Single-Particle Lagrangian Integrated Trajectory) Model access via NOAA ARL READY Website (<http://www.arl.noaa.gov/ready/hysplit4.html>). NOAA Air Resources Laboratory, Silver Spring, MD.

Duce, R.A., Liss, P.S., Merrill, J.T., Atlas, E.L., Buat-Menard, P., Hicks, B.B., Miller, J.M., Prospero, J.M., Arimoto, R., Church, T.M., Ellis, W., Galloway, J.N., Hansen, L., Jickells, T.D., Knap, A.H., Reinhardt, K.H., Schneider, B., Soudine, A., Tokos, J.J., Tsunogai, S., Wollast, R., Zhou, M., 1991. "The atmospheric input of trace species to the world ocean". Global Biogeochemical Cycles 5, 193–259.

Dulac, F., Buat-Menard, Arnold, M., Ezat, U., Martin, D., 1987. Atmospheric input of trace metals to the western Mediterranean Sea. 1. Factors controlling the variability of atmospheric concentrations, Journal of Geophysical Research, 92, 8437-8453

Dulac, F., Tanre, D., Bergametti, G., Buat-Menard, P., Desbois, M., Sutton, D., 1992. "Assessment of the African dust mass over the western Mediterranean sea using meteosts data". Journal of Geophysical Research 97, 2489–2506

Dye, J., Adler, K.B., Richards, J.H., Dreher, K.L., 2001. "Epithelial injury induced by exposure to residual fly ash particles: role of reactive oxygen species".

Dzubay, T.G. and R.K.Stevens (1984), Environmental Science and Technology, 9, 663

Howard, E.C., Henriksen, J.R., Buchan, A., Reisch, C.R., Bürgmann, H., Welsh, R., Ye, W., González, J.M., Mace, K., Joye, S.B., Kiene, R.P., Whitman, W.B., Moran, M.A., 2006. "Bacterial Taxa That Limit Sulfur Flux from the Ocean". *Science* 314, 649–652

Englert, N., 2004. "Fine particles and human health- a review of epidemiological studies", *Toxicology Letters* , 149, 235-242.

European Environment Agency, 2003b. "Europe's Environment: the third assessment", *Environmental Assessment Report 10/2003b*

European Environment Agency, 2005. "European Environment, State and Outlook 2005", *State and Environment Report No:1/2005*

European Monitoring and Evaluation Programme (EMEP), EMEP emissions, EMEP data, [www.emep.int](http://www.emep.int), Last access date: 18.11.2008

Favez, O., Cachier, H., Sciare, J., Alfaro, S.C., El-Araby, T.M., Harhash, M.A., Abdelwahab, M.M., 2008. "Seasonality of major aerosol species and their transformations in Cairo megacity". *Atmospheric Environment* 42, 1503-1516

Finlayson, P.B., and Pitts, J.N., 1986. "Atmospheric Chemistry: Fundamentals and Experimental Techniques". New York: Wiley- Interscience

Finlayson-Pitts, B.J., and Pitts, J.N., 1986. "Atmospheric Chemistry: Fundamentals and Experimental Techniques". John Wiley & Sons, Newyork, 816-818

Fiol LA, Fornos JJ, Gelabert B, et al., 2005. "Dust rains in Mallorca (Western Mediterranean): Their occurrence and role in some recent geological processes". *CATENA*, 63(1), 64–84

Foltz, G.R., McPhaden, M., 2008. "Trends in Saharan dust and tropical Atlantic climate during 1980-2006". *Geophysical Research Letters* 35(L20706), doi:10.1029/2008GL035042

Formenti, P., Andreae, M.O., Andreae, T.W., Ichoku, C., Schebeske, G., Kettle, J., Maenhaut, W., Cafmeyer, J., Ptasinsky, J., Karnieli, A., Lelieveld, J., 2001. "Physical and



Chemical Characteristics of Aerosols over the Negev Desert (Israel) during summer 1996". *Journal of Geophysical Research*, 106 (D5), 4871-4890

Formenti, P., Andreae, M.O., Andreae, T.W., Ichoku, C., Schebeske, G., Kettle, J., Maenhaut, W., Cafmeyer, J., Ptasinaky, J., Karnieli, A., Lelieveld, J., 2001. "Physical and Chemical Characteristics of Aerosols over the Negev Desert (Israel) during summer 1996". *Journal of Geophysical Research*, 106 (D5), 4871-4890

Foucault, A., Melieres, F., 2000. "Palaeoclimatic cyclicity in central Mediterranean Pliocene sediments: the mineralogical signal". *Palaeogeography, Palaeoclimatology, Palaeoecology* 158, 311-323

Fridell, M.D., Lindgren, E.S., Simpson, D., 1998. "Verification of air mass trajectories in Long-Distance Transport Using EDXRF Analysis of Intersite Element Ratios", *X-Ray Spectrometry*, 27, 121-138

Galasyn, J.M., Tschudy, K.L., Huebert, B.J., 1987. "Seasonal and Diurnal Variability of Nitric Acid Vapor and Ionic Species in Remote Free Troposphere at Mauna Lao, Hawaii". *Journal of Geophysical Research*, vol.92, No.D3, 3105-3113, 1987

Galindo, N., Nicolas, J.F., Yubero, E., Caballero, S., Pastor, C., Crespo, J., 2008. Factors affecting levels of aerosol sulfate and nitrate on the Western Mediterranean coast. *Atmospheric Research* 88, 305–313

Ganor, E., Foner, H. A., Bingemer, H. G., Udisti, R., and I. Setter, 2000. "Biogenic sulfate generation in the Mediterranean Sea and its contribution to the sulfate anomaly in the aerosol over Israel and the Eastern Mediterranean". *Atmospheric Environment*, 34, 3453–3462

Ganor, E., Levin, Z., and Grieken, R.V., 1998. "Composition of Individual Aerosol Particles above the Israelian Mediterranean Coast During the Summer Time". *Atmospheric Environment*, 32(9), 1631-1642

Ganor, E., Levin, Z., Grieken, R.V., 1998. "Composition of Individual Aerosol Particles above Israelian Mediterranean Coast During the Summer Time", *Atmospheric Environment* 32 (9), 1631-1642.

Gatz, D.F., 1975. "Pollutant Aerosol Deposition into Southern Lake Michigan". *Water, Air and Soil Pollution* 5, 239–251

Georgopoulos, P.G., and Seinfeld, J.H., 1982. "Statistical Distributions of Air Pollutant Concentrations". *Environmental Science and Technology*, 16 (7), 1982

Ghose, P.M., 1999. "Trace element analysis of airborne particulates by atomic absorption spectrometry, inductively coupled plasma-atomic emission spectroscopy, and inductively coupled plasma mass spectrometry". In *Elemental Analysis of Airborne Particles*. Amsterdam, The Netherlands: Gordon and Breach Science Publishers, 1–65

Gilbert, R.O., 1987. "Statistical Methods for Environmental Pollution Monitoring". John Wiley & Sons Inc., ISBN 0-471-28878-0

Ginoux, P., Prospero, J.M., Torres, O., Chin, M., 2004. "Longterm simulation of dust distribution with the GOCART model: Correlation with the North Atlantic Oscillation". *Environmental Modeling and Software* 19, 113–128

Glavas, D.S., Nikolakis, P., Ambatzoglou, D., Mihalopoulos, N., 2008. "Factors Affecting Seasonal Variation of Mass and Ionic Composition of PM<sub>2.5</sub> at a central Mediterranean coastal site". *Atmospheric Environment* 42, 5365–5373

Glavas, S., and Moschonas, N., 2002. "Origin of observed acidalkaline rains in a wet-only precipitation study in a Mediterranean coastal site, Patras, Greece". *Atmospheric Environment*, 36, 3089–3099.

Glavas, S., Kambezidis, H., and Danalatos, D., 1995. "Atmospheric Nitric Acid Concentrations in a Mediterranean Site, Patras, Greece", *Atmospheric Environment*, 29, 1849-1852.

Gobbi, G.P., Barnaba, F., Ammannato, L., 2007. "Estimating the impact of Saharan dust on the year 2001 PM<sub>10</sub> record of Rome, Italy". *Atmospheric Environment* 41, 261–275.

Goldberg, E.D., 1963. "The Oceans as a Chemical System, in the Sea". Edited By M.N. Hill, Vol.2, Ch.1, Interscience, NY

Gong, S.L., and Barrie, L.A., 2005. "Trend of Heavy metal components in the Arctic aerosols and their relationship to the emissions in the Northern Hemisphere". *Science of the Total Environment* 342, 175-183

Gordon, G.E., Zoller, W.H., Gladney, E.S., 1973. "Abnormally enriched trace elements in the atmosphere". In: *Trace Substances in Environmental Health*. University of Missouri Environmental Trace Substances Center, Columbia, MO, pp. 167–177

Goudie, A.S., and Middleton, N.J., 2001. "Saharan dust storms: nature and consequences". *Earth-Science Reviews* 56, 179–204

Grants, D.A, Garner, J.H.B., and Johnson, D.W., 2003. "Ecological effects of particulate matter". *Environment International* 29, 213–239

Groempling, A.H.J., Ostapezuk, P., and Emons, H., 1997. "Wet deposition in Germany: long-term trends and the contribution of heavy metals". *Chemosphere* 34, 2227–2236

Guerzoni, S., Chester, R., Dulac, F., Herut, B., Loye-Pilot, M., Measures, C., Migon, C., Molinaroli, E., Moulin, C., Rossini, P., Saydam, C., Soudine, A., Ziveri, P., 1999. "The Role of Atmospheric Deposition in the Biogeochemistry of the Mediterranean Sea". *Progress in Oceanography* 44, 147-190.

Guerzoni, S., Chester, R., Dulac, F., Herut, B., Pilot, M.D.L., Measures, C., Migon, C., Molinaroli, E., Moulin, C., Rossini, P., Saydam, C., Soudine, A., Ziveri, P., 1999. "The role of atmospheric deposition in the biochemistry of the Mediterranean Sea". *Progress in Oceanography* 44, 147-190

Guerzoni, S., Molinaroli, E., Chester, R., 1997. "Saharan dust inputs to the western Mediterranean Sea: depositional patterns, geochemistry and sedimentological implications". *Deep-Sea Research II* 44, 631–654.

Güllü, G., Ulutas, F., Belli, D., Erduran, S., Keskin, S., Tuncel, G., 1998. "Black Sea Aerosol and Long Range Transport", *Journal of Engineering and Environmental Sciences*, 22, 289-303.

Güllü, G., 1996. "Long Range Transport of Aerosols". Ph.D. Thesis, Middle East Technical University, Ankara, Turkey

Güllü, G., 1996. Long Range Transport of Aerosols. Ph.D. Thesis, Environmental Engineering Department, Middle East Technical University, Turkey, Ankara

Güllü, G., Doğan, G., Tuncel, G., 2005. "Atmospheric trace element and major ion concentrations over the eastern Mediterranean Sea: Identification of anthropogenic source regions". *Atmospheric Environment* 39, 6376- 6387

Güllü, G., Olmez, I., Tuncel, G., 2000. "Temporal variability of atmospheric trace element concentrations over the eastern Mediterranean Sea". *Spectrochimica Acta Part B*, 55, 1135-1150

Güllü, G., Ölmez, I., and Tuncel, G., 2004. "Source apportionment of trace elements in the Eastern Mediterranean atmosphere". *Journal of Radioanalytical and Nuclear Chemistry* 259 (1), 163-171

Güllü, G., Ulutaş, F., Belli, D., Erduran, S., Keskin, S., Tuncel, G., 1998. Karadeniz Aerosolü ve Uzak Mesafeli Atmosferik Taşınım. *Journal of Engineering and Environmental Science*, 22, 289–303

Güllü, H.G., Olmez, I., Aygun, S., Tuncel, G., 1998. "Atmospheric trace element concentrations over the eastern Mediterranean Sea: factors affecting temporal variability". *Journal of Geophysical Research*, 103, 21943-21954.

Günaydın, G.C., and Tuncel, G., 2003. "Source Regions Affecting Chemical Composition of Aerosols and Precipitation in the Eastern Mediterranean Atmosphere Determined Using Trajectory Statistics". *Air Pollution Processes in Regional Scale, NATO Science Series, VI. Earth and Environmental Sciences* 30, 121-133

Hacısalihoğlu, G.G., Balkas, T.I., Tuncel, S.G., Herman, D.H., Olmez, I., Tuncel, G., 1991. "Trace element composition of the Black Sea Aerosols". *Deep Sea Research, Part A, Oceanographic Research Papers*, 38, 1255-1266

Han, L., Zhuang, G. , Cheng, S. , Li, J., 2007. "The mineral aerosol and its impact on urban pollution aerosols over Beijing, China". *Atmospheric Environment* 41, 7533–7546

Harrison, R.N., and Yin, J., 2000. "Particulate matter in the atmosphere: which particle properties are important for its effects on health?", *The Science of the Total Environment*, 249, 85-101

Haupt, O., Linnow, K., Harmel, R., Schaefer, C., Dannecker, W., 1997. "Qualitative X-Ray Analysis of Emitted Aerosol Particles from Incineration Plants Sampled on Quartz Fibre Filters". *X-Ray Spectrometry*, 26, 79–84

He, Z., Kim, Y.J., Ogunjobi, K.O., Hong, C.S., 2003. "Characteristics of PM<sub>2.5</sub> species and long range transport of air masses at Tacan background station, South Korea". *Atmospheric Environment* 37, 219-230

Hedberg, E., Gidhagen, L., Johansson, C., 2005. "Source contributions to PM<sub>10</sub> and arsenic concentrations in Central Chile using positive matrix factorization". *Atmospheric Environment*, 39, 549–561

Henry, R. C., Chang, Y. S., & Spiegelman, C. H. (2002). Locating nearby sources of air pollution by nonparametric regression of atmospheric concentrations on wind direction. *Atmospheric Environment*, 36, 2237–2244.

Henry, R.C., 1991. "Multivariate receptor models, in *Receptor modelling for Air Quality Management*". P.K. Hopke (ed), Elsevier Science Publishers, Amsterdam, 117–147

Herut, B., Nimmo, M., Medway, A., Chester, R., Krom, M.D., 2001. "Dry atmospheric inputs of trace metals at the Mediterranean coast of Israel (SE Mediterranean):sources and fluxes", *Atmospheric Environment*, 35, 803-813.

Herut, B., Starinsky, A., Katz, A., & Rosenfeld, D., 2000. "Relationship between the acidity and chemical composition of rainwater and climatological conditions along a transition zone between large deserts and Mediterranean climate, Israel". *Atmospheric Environment*, 34, 1281–1292

Herut, B., Zohary, T., Krom, M.D., Fauzi, R. C. Mantoura, C., Pitta, P., Psarra, S., Rassoulzadegan, F., Tanaka, T., Thingstad, T.F., 2005. "Response of East Mediterranean surface water to Saharan dust: On-board microcosm experiment and field observations". *Deep-Sea Research II* 52, 3024–3040

Hinds, W.C., 1982. "Aerosol Technology". Wiley, New York

Hirsch, R.M., Slack, J.R., and Smith, R.A., 1982. "Techniques of trend analysis for monthly water quality data". *Water Resources Research*, 18, 107-121

Hitzenberger R, Jennings SG, Larson SM, Dillner A, Cachier H, Galambos Z, Rouc A, Spain TG., 1999. Intercomparison of measurement methods for black carbon aerosols. *Atmospheric Environment* 33: 2823 –2833.

Hoffmann, T., Odum, J.R., Bowman, F., Collins, D., Klockow, D., Flagan, R.C., and Seinfeld, J.H., 1997. "Formation of organic aerosols from the oxidation of biogenic hydrocarbons". *Journal of Atmospheric Chemistry* 26, 189–222

Holsen, T.M., and Noll, K.E., 1992. "Dry deposition of atmospheric particles: application of current models to ambient data". *Environmental Science and Technology* 26, 1807

Holynska, B., Ptasiński, J., Maenhaut, W., Anegarn, H.J., 1997. "Energy Dispersive X-Ray Fluorescence Spectrometer with Capillary Optics for the Chemical Analysis of Atmospheric Aerosols with High Time Resolution". *Journal of Aerosol Science*, 28 (4), 1455–1463

Hopke, P. K., Ito, K., Mar, T., Christensen, W. F., Eatough, D. J., Henry, R. C. et al., 2006. "PM source apportionment and health effects: 1. Intercomparison of source apportionment results". *Journal of Exposure Science and Environmental Epidemiology*, 16, 275–286.

Hopke, P.K, Ramadan, Z., Paatero, P., Norris, G.A., Landis, M.S., Williams, R.W., Lewis, C.W., 2003. "Receptor modelling of ambient and personal exposure samples: 1998 Baltimore Particulate Matter Epidemiology-Exposure Study". *Atmospheric Environment* 37, 3289–3302

Hopke, P.K., Li, L.C., Ciszek, W., Landsberger, S., 1995. "The use of bootstrapping to estimate the conditional probability fields for source locations of airborne pollutants. *Chemometrics and Intelligent Laboratory Systems*, 30, 69–79

Hopke, P.K., Paatero, P., Jia, H., Ross, R.T., Harshman, R.A., 1998. "Three-way\_PARAFAC/factor analysis: examination and comparison of alternative computational methods as applied to ill-conditioned data". *Chemometrics and Intelligent Laboratory Systems* 43:25–42

Hopke, P.K., Ramadan, Z., Paatero, P., Norris, G.A., Landis, M.S., Williams, R.W., Lewis, C.W., 2003. "Receptor modeling of ambient and personal exposure samples: 1998 Baltimore Particulate Matter Epidemiology-Exposure Study". *Atmospheric Environment* 37, 3289–3302

Hopke, P.K., 1991. "Receptor Modelling For Air Quality Management". Elsevier Science Publishers, Amsterdam

Hopke, P.K., 1985. "Receptor Modelling in Environmental Chemistry". John Wiley, New York

Hsu, S.C. , Liu, S.C. , Jeng, W.L., Lin, F.J. , Huang, Y.T. , Lung, S.C. C. , Liu, T. H. and Tu, J.Y., 2005. "Variations of Cd/Pb and Zn/Pb ratios in Taipei aerosols reflecting long-range transport or local pollution emissions". *Science of The Total Environment*, 347 (1-3), 111-121

<http://www.arl.noaa.gov/ready-bin/traj>, The Air Resources Laboratory, U.S. National Oceanic and Atmospheric Administration (ARL, NOAA), Last access date:1/4/2008

[http://www.webmet.com/met\\_monitoring/622.html](http://www.webmet.com/met_monitoring/622.html), The Meteorological Resource Center, Last access date:31/3/2008

Husain, L., Parekh, P.P., Dutkiewicz, V.A., Khan, A.R., Yang, K., Swami, K., 2004. "Long-term trends in atmospheric concentrations of sulfate, total sulfur, and trace elements in the northeastern United States". *Journal of Geophysical Research*, 109, D18305

Husain, L., Parekh, P.P., Halstead, J.A., Dutkiewicz, V.A., 1982. "Sources of aerosol sulfate and trace elements of Whiteface Mountain, New York". Presented at the 75<sup>th</sup> Annual Meeting of the Air Pollution Control Association, New Orleans, LA.

I. F. Al-Momani, K. A. Momani, Q.M. Jaradat, A.M. Massadeh, Y.A. Yousef, A.A. Alomary, 2008. "Atmospheric deposition of major and trace elements in Amman, Jordan", *Environ Monit Assess* 136:209–218

Ikavalko, E., Laitinen, T., Parkka, M., and Yliruokanen, I., 1995. "Intercomparison of Trace Element Determination in Samples from a Coal-Fired Power Plant". *International Journal of Environmental Analytical Chemistry*, 61, 207-224

Ikegawa, M., Kimura, M., Honda, K., Akabane, I., Makita, K., Motoyama, H., Fujii, Y. and Itokawa, Y., 1999. "Geographical variations of major and trace elements in East Antarctica". *Atmospheric Environment*, 33(9), 1457-1467

Injuk, J., Grieken, R.V., Klockenkamper, R., von Bohlen, A., Kump, P., 1997. "Performance and characteristics of two total reflection X-ray fluorescence and particle induced X-ray emission setup for aerosol analysis". *Spectrochimica Acta, Part B* 52, 977-984

Intergovernmental Panel on Climate Change (2001), *Climate Change 2001: The Scientific Basis*, edited by J. T. Houghton et al., Cambridge Univ. Press, New York

Işıkdemir, Ö., 2006. "Investigation of 8-year-long composition record in the Eastern Mediterranean precipitation". M.Sc.Thesis, Department of Environmental Engineering, Middle East Technical University, Ankara

Jacob, D.J., 2000. "Heterogenous chemistry and tropospheric ozone", *Atmospheric Environment*, 34, 2131-2159.

Jenkins, R., 2000. "X-Ray Techniques: Overview, In *Encyclopedia of Analytical Chemistry*". R.A.Meyers (Ed), pp. 13269–13288, John Wiley & Sons Ltd, Chichester

Jickells, T.S., An, Z.A., Baker, A.R., Bergametti, G., Brooks, N., Boyd, P.W., Duce, R.A., Hunter, K.A., Junji, C., Kawahata, H., Kubilay, N., Andersen, K.K., laRoche, J., Liss, P.S., Mahowald, N., Prospero, J.M., Ridgwell, A.J., Tegen, I., Torres, R., 2005. "Global iron



connections between desert dust, ocean biogeochemistry and climate". *Science* 308, 67–71

John Michael Trapp, Frank J. Millero, Joseph M. Prospero, 2008. "Temporal Variability of the Elemental Composition of African Dust Measured in TradeWind Aerosols at Barbados and Miami". *Marine Chemistry*, doi: 10.1016/j.marchem.2008.10.004

Johnson, B.J., Huang, S.C., Lecave, M., Porterfield, M., 1994. "Seasonal trends for nitric acid, particulate nitrate and particulate sulfate concentrations at a southwestern US mountain site", *Atmospheric Environment*, 31, 1657-1666.

Johnson, N.L., Kotz, S., 1985. *Encyclopedia of Statistical Sciences*, Volume 5, John Wiley, New York.

Jorba, O., Perez, J., Rocadenbosch, F., Baldasano, J.M., 2004. "Cluster analysis of 4 day back trajectories arriving in the Barcelona area, Spain, from 1997 to 2002". *Journal of Applied Meteorology* 43, 887-901 June 1999

Kallos, G., Astitha, M., Katsafados, P., and Spyrou, C., 2007. Long-Range Transport of Anthropogenically and Naturally Produced Particulate Matter in the Mediterranean and North Atlantic: Current State of Knowledge, *Journal of Applied Meteorology and Climatology* 46: 1230-1251

Kallos, G.; Kotroni, V.; Lagouvardos, K.; Papadopoulos, A., 1998. "On the long-range transport of air pollutants from Europe to Africa". *Geophysical Research Letters*, 25(5), 619–622

Kao, A.S., Friedlander, S.K., 1994. "Chemical signatures of the Los Angeles aerosol ( $dp < 3.5 \mu\text{m}$ )". *Aerosol Science and Technology*, 21, 283-293

Kao, A.S., Friedlander, S.K., 1995. "Frequency distributions of  $\text{PM}_{10}$  chemical components and their sources". *Environmental Science and Technology*, 29, 19-28

Karaca, F., Alagha, O., Erturk, F., 2005. "Statistical characterization of atmospheric  $\text{PM}_{10}$  and  $\text{PM}_{2.5}$  concentrations at a non-impacted suburban site of Istanbul, Turkey". *Chemosphere*, 59, 1183-1190

Karaca, M., Deniz, A., and Tayanç, M., 2000. "Cyclone Track Variability Over Turkey In Association With Regional Climate". *International Journal of Climatology* 20, 1225–1236

Karageorgos, E.T., Rapsomanikis, S., Wahlin, P., 2006. "Chemical characterization of the inorganic fraction of aerosols and mechanisms of the neutralization of atmospheric acidity in Athens, Greece". *Atmospheric Chemistry and Physics Discussions* 6, 12389–12431

Karakaş, D., 1999. "Determination of the european contribution on the aerosol composition in the black sea basin and investigation of transport mechanisms". Ph.D. Thesis, Department of Chemistry, Middle East Technical University, Ankara, Turkey

Kaskaoutis, G., Kambezidis, H.D., Nastos, P.T., Kosmopoulos, P.G., 2008. "Study on an intense dust storm over Greece". *Atmospheric Environment* 42, 6884–6896

Kato, N., 1996. "Analysis of structure of energy consumption and dynamics of emission of atmospheric species related to the global environmental change ( $\text{SO}_x$ ,  $\text{NO}_x$ , and  $\text{CO}_2$ ) in Asia". *Atmospheric Environment* 30, 2757–2785.

Katragkou, E., Kazadzis, S., Amiridis, V., Papaioannou, V., Karathanasis, S., Melas, D., 2009. "PM<sub>10</sub> regional transport pathways in Thessaloniki, Greece". *Atmospheric Environment* doi:10.1016/j.atmosenv.2008.11.021

Katsoulis, B.D., and Whelpdale, D.M., 1993. "A Climatological Analysis of Four-Day back Trajectories from Aliartos, Greece". *Theoretical Applied Climatology* 47, 93-103

Keene, W.C., Montag, J.A., Maben, J.R., Southwell, M., Leonard, J., Church, T.M., Moody, J.L., Galloway, J.N., 2002. "Organic nitrogen in precipitation over Eastern North America". *Atmospheric Environment*, 36 (28), 4529- 4540

Keler, G., Landis, M., Norris, G., Christianson, E., Dvonch, J.T., 2006. "Sources of Mercury Wet Deposition in Eastern Ohio, USA". *Environmental Science and Technology*, 40, 5874-5881

Kennish, M.J., 2001. "Practical Handbook of Marine Science". 3<sup>rd</sup> Edition, CRC Press, Boca Raton, FL., pp.60

Kim, E., and Hopke, P.K., 2007. "Source Identification of Airborne Fine Particles Using Positive Matrix Factorization and U.S. Environmental Protection Agency Positive Matrix Factorization". *Journal of Air and Waste Management Association* 57, 811-819

Kim, E., Hopke, P.K., Kenski, D.M., Koerber, M., 2005. "Sources of Fine Particles in a Rural Midwestern U.S. Area". *Environmental Science and Technology* 39, 4953-4960

Kim, E., Hopke, P.K., Qin, Y., 2005. "Estimation of Organic Carbon Blank Values and Error Structures of the Speciation Trends Network Data for Source Apportionment". *Journal of Air and Waste Management Association* 55, 1190-1199

Kim, J., Yoon, S.C., Jefferson, A., Zahorowski, W., Kang, C.H., 2005. "Air mass characterization and source region analysis for the Gosan super-site, Korea, during the ACE-Asia 2001 field campaign". *Atmospheric Environment* 29, 6513-6523

Kindap, T., Unal, A., Chen, S.-H., Hu, Y., Odman, M.T., Karaca, M., 2006. "Long-range aerosol transport from Europe to Istanbul, Turkey". *Atmospheric Environment* 40, 3536-3547

Kirkitsos, F.D., Sikiotis, D., 1991. "Nitric acid, ammonia and particulate nitrates, sulfates and ammonium in the atmosphere of Athens". *Ecistics* 348 349, 156-163.

Kocak, M., Nimmo, M., Kubilay, N., Herut, B., 2004. "Spatio-temporal aerosol trace metal concentrations and sources in the Levantine Basin of the Eastern Mediterranean". *Atmospheric Environment* 38: 2133-2144

Kocak, M., Kubilay, N., Herut, B., and Nimmo, M., 2005. "Dry atmospheric fluxes of trace metals (Al, Fe, Mn, Pb, Cd, Zn, Cu) over the Levantine Basin: A refined Assessment". *Atmospheric Environment* 39: 7330-7341

Koçak, M., Kubilay, N., and Mihalopolos, N., 2004a. "Ionic composition of lower tropospheric aerosols at a Northeastern Mediterranean site: implications regarding sources and long-range transport". *Atmospheric Environment* 38, 2067-2077

Koçak, M., Mihalopoulos, N., Kubilay, N., 2007. "Chemical composition of the fine and coarse fraction of aerosols in the northeastern Mediterranean". *Atmospheric Environment*, doi:10.1016/j.atmosenv.2007.05.011

Koçak, M., Mihalopoulos, N., Kubilay, N., 2007. "Contributions of natural sources to high PM<sub>10</sub> and PM<sub>2.5</sub> events in the eastern Mediterranean". *Atmospheric Environment* 41: 3806–3818

Kouvarakis, A., and Mihalopoulos, N., 2002. "Seasonal variation of dimethylsulfide in the gas phase and of methanesulfonate and non-sea salt sulfate in the aerosol phase in the Eastern Mediterranean Atmosphere". *Atmospheric Environment* 36, 929–938

Kouvarakis, G., Bardouki, H., and Mihalopoulos, N., 2002. "Sulfur Budget above the Eastern Mediterranean: Relative Contribution of Anthropogenic and Biogenic Sources", *Tellus*, 54B, 201-212

Kouyoumdjian, H. and Saliba, N.A. 2005. "Ion concentrations of PM<sub>10-2.5</sub> and PM<sub>2.5</sub> aerosols over the Eastern Mediterranean region: seasonal variation and source identification". *Atmospheric Chemistry and Physics Discussions* 5, 13053 – 13073

Kouyoumdjian, H., and Saliba, N. A., 2006. "Mass concentration and ion composition of coarse and fine particles in an urban area in Beirut: effect of calcium carbonate on the absorption of nitric and sulfuric acids and the depletion of chloride". *Atmospheric Chemistry and Physics* 6, 1865–1877

Kubilay, N., 1996. "The composition of atmospheric aerosol over the eastern Mediterranean: the coupling of geochemical and meteorological parameters". Ph.D. Dissertation, IMS, METU, Turkey, pp.219

Kubilay, N., and Saydam, A.C., 1995. "Trace Elements in Atmospheric Particulates Over the Eastern Mediterranean; Concentrations, Sources and Temporal Variability". *Atmospheric Environment* 29(17), 2289-2300

Kubilay, N., Kocak, M., Cokacar, T., and Oguz, T., 2002. "Influence of Black Sea and local biogenic activity on the seasonal variation of aerosol sulfur species in the Eastern Mediterranean Atmosphere". *Biogeochemical Cycles* 16(4), 27 1-15

Kubilay, N., Nickovic, S., Moulin, C., and Dulac, F., 2000. "An illustration of the transport and deposition of mineral dust onto the eastern Mediterranean". *Atmospheric Environment* 34, 1293-1303

Kubilay, N.N., Saydam, A.C., Yemenicioglu, S., Kelling, G., Kapur, S., Karaman, C., Akça, E., 1997. "Seasonal chemical and mineralogical variability of atmospheric particles in the coastal region of the Northeast Mediterranean". *Catena* 28, 313-328

Kulkarni, P., Chellam, S., Ghurye, G., Fraser, M.P., 2003. "In Situ Generation of Hydrofluoric Acid during Microwave Digestion of Atmospheric Particulate Matter Prior to Trace Element Analysis Using Inductively Coupled Plasma Mass Spectrometry". *Environmental Engineering Science* 20( 6): 517–531

Kulmala, M., 2003. "How Particles Nucleate and Grow", *Science*, 302, 1000–1001.

Kuloglu, E. and Tuncel, G., 2005. "Size Distribution of Trace Elements and Major Ions in the Eastern Mediterranean Atmosphere". *Water, Air and Soil Pollution* 167, 221–241

Kuloğlu, E., 1997. "Size Separation and Dry Deposition Fluxes of Particles in the Eastern Mediterranean Basin". MSc. Thesis. Middle East Technical University, Ankara, Turkey, 38 pp.

Kuschner, W.G., Wong, H., D'Alessandro, A., Quinlan, P., Blanc, P.D., 1997. "Human Pulmonary Responses to Experimental Inhalation of High Concentration Fine and Ultrafine Magnesium Oxide Particles". *Environmental Health Perspectives*, 105(11), 1234–1237.

Kvetoslav Rudolf Spurny, *Analytical Chemistry of Aerosols*, ISBN: 1-56670-040-X, 1999, Lewis Publishers, Washington D.C

Lai, SC., Zou SC., Cao JJ, Lee SC., Ho KF., 2007. "Characterizing ionic species in PM<sub>2.5</sub> and PM<sub>10</sub> in four Pearl River Delta cities, South China". *Journal of Environmental Sciences-China*, 19(8), 939–947

Lammel, G., Röhrig, A., Schreiber, H., 2002. "Atmospheric lead and bromine in Germany". *Environmental Science and Pollution Research* 9 (6), 397–404.

Landsberger, S. and Creatchman, M., 1999. "Elemental Analysis of Airborne Particles". *Advances in Environmental, Industrial and Process Control Technologies*, Volume 1, Gordon and Breach Science Publishers, ISBN 90-5699-627-4

Larssen, S., Sluyter, R., Helmis, C., 1999. "Criteria for EUROAIRNET, the EEA air quality monitoring and information network".

Lary, D.J., 1997. "Catalytic Destruction of Stratospheric Ozone". *Journal of Geophysical Research-Atmospheres*, 102 (D17), 21515-21526

Latha, K.M., and Badarinath, K.V.S., 2004. "Correlation between black carbon aerosols, carbon monoxide and tropospheric ozone over a tropical urban site", *Atmospheric Research* , 17, 265-274.

Laurent, B., Marticorena, B., Bergametti, G., Leon, J.F., and Mahowald, N.M., 2008. "Modeling mineral dust emissions from the Sahara desert using new surface properties and soil database". *Journal of Geophysical Research* 113(D14218), doi:10.1029/2007JD009484

Lawson, D.R., Winchester, J.W., 1979a. "A standard crustal aerosol as a reference for elemental enrichment factors". *Atmos. Environ.* 13, 925–930.

Lazaridis, M., Dzumbova, L., Kopanakis, I., Ondracek, J., Glytos, T., Aleksandropoulou, Voulgarakis, A., Katsiyela, E., Mihalopolus, N., Eleftheriadis, K., 2008. "PM<sub>10</sub> and PM<sub>2.5</sub> Levels in the Eastern Mediterranean (Aktotiri Research Station, Crete, Greece)". *Water, Air and Soil Pollution* 189, 85-101

Lee, J.T., Kim, H., Hong, Y.C., Kwon, H.J., Schwartz, J., and Chritiani, D.C., 2000. "Air Pollution and Daily Mortality in Seven Major Cities of Korea, 1991-1997", *Environmental Research*, Section A 84, 247-254.

Leifer, I., Caulliez, G., de Leeuw, G., 2006. "Bubbles generated from windsteepened breaking waves: 2. Bubble plumes, bubbles, and wave characteristics". *Journal of Geophysical Research-Oceans* 111 (C6) Art. No. C06021.

Lelieveld, J., Berresheim, H., Borrmann, S., Crutzen, P.J., Dentener, F.J., Fischer, H., Feichter, J., Flatau, P.J., Heland, J., Holzinger, R., Korrmann, R., Lawrence, M.G., Levin, Z., Markowicz, K.M., Mihalopoulos, N., Minikin, A., Ramanathan, V., Reus, M.D., Roelofs, G.J., Scheeren, H.A., Sciare, J., Schlager, H., Schultz, M., Siegmund, P., Steil, B., Stephanou, E.G., Stier, P., Traub, M., Warneke, C., Williams, J., and Ziereis, H., 2002. "Global Air Pollution Crossroads over the Mediterranean". *Science*, 298, 794–798.

Lelieveld, J., et al., 2002. "Global air pollution crossroads over the Mediterranean". *Science*, 298, 794– 799.

Lenschow, P., Abraham, H. J., Kutzner, K., Lutz, M., Preuß, J. D., & Reichenbacher, W., 2001. "Some ideas about the sources of PM<sub>10</sub>". *Atmospheric Environment*, 35(Suppl. 1), 123–133.

Lesson 6, Site Selection, Air Pollution Training Institute of U.S.EPA, 2000

Li, C., Kang, S., Zhang, Q., and Kaspari, S., 2007. "Major ionic composition of precipitation in the Nam Co region, Central Tibetan Plateau". *Atmospheric Research* 85, 351–360

Li, X., Maring, H., Savoie, D., Voss, K., Prospero, J.M., 1996. "Dominance of mineral dust in aerosol light-scattering in the North Atlantic trade winds". *Nature* 380, 416–419

Lim, J.H., Sabin, L.D., Schiff, K.C., Stolzenbach, K.D., 2006. "Concentration, size distribution, and dry deposition rate of particle-associated metals in the Los Angeles region". *Atmospheric Environment* 40, 7810–7823

Lindgren, E.S., Henriksson, D., Therning, P., Laursen, J., and Pind, N., 2006. "Possible Indicators for biomass burning in a small Swedish city studied by energy dispersive X-ray Fluorescence (EDXRF) spectrometry". *X-Ray Spectrometry*, 35, 19–26

Lingard, J.J.N., Tomlin, A.S., Clarke, A.G., Hay, A.W.M., Wild, C.P., Routledge, M.N., 2005. "A study of trace metal concentration of urban airborne particulate matter and its role in free radical activity as measured by plasmid strand break assay". *Atmospheric Environment* 39, 2377–2384

Lioy, P.J., Zelenka, M.P., Cheng, M.D., Reis, N., 1989. "The effect of sampling duration on the ability to resolve source types using factor analysis". *Atmospheric Environment*, 23 (1), 239–254

Lippmann, M., 1989. "Background on health effects of acid aerosols", *Environmental Health Perspectives*, 79, 2389-2399.

Lippmann, M., 1997. "The 1997 US EPA standards for particulate matter and ozone", *Environmental Science and Technology*, 10, 75-99.

Lobert, J., Keen, W., Logan, J., Yevich, R., 1999. "Global chlorine emissions from biomass burning: reactive chlorine emissions inventory". *Journal of Geophysical Research* 104, 8373–8389

Lodge, J.P., 1989, *Methods of Air Sampling and Analysis*, 3<sup>rd</sup> Edition, pp.763, Lewis Publishers, Chelsea, MI, USA

Lopes, F., Appoloni, C.R., Nascimento, V.F., Melquides, F.L., Almeida, L.C., 2006. "Chemical Characterization of particulate matter suspended in the atmosphere by energy dispersive X-ray Fluorescence (EDXRF)". *Journal of Radioanalytical and Nuclear Chemistry*, 270 (1), 43–46

Lovett, G.M., 1994. "Atmospheric Deposition of Nutrients in North America: An Ecological Perspective". *Ecological Applications* 4(4), 629–650



Lu, H.C., 2002. "The statistical characters of PM<sub>10</sub> concentration in Taiwan area". *Atmospheric Environment*, 36, 491–502

Lu, H.C., and Fang, G.C., 2002. "Estimation of the Frequency distributions of PM<sub>10</sub> and PM<sub>2.5</sub> by Statistics Wind Speed Data at Sha-Lu, Taiwan". *Science of Total Environment*, 298, 119-130

Mona, L., Amodeo, A., Pandolfi, M., and Pappalardo, G. "Saharan dust intrusions in the Mediterranean area: Three years of Raman lidar measurements". *Journal of Geophysical Research*, VOL. 111, D16203, doi:10.1029/2005JD006569, 2006

Lupu, A. , and Maenhaut, W., 2002. "Application and comparison of two statistical trajectory techniques for identification of source regions of atmospheric aerosol species". *Atmospheric Environment* 36, 5607–5618

Luria, M., Peleg, M., Sharf, G., Alper, D.S.T., Spitz, N., Ami, Y.B., Gawii, Z., Lifschitz, B., Yitzchaki, A., Seter, I., 1996. "Atmospheric sulfur over the east Mediterranean region". *Journal of Geophysical Research*, 101(D20), 25,917–25,930

Luria, M., Peleg, M., Sharf, G., Siman Tov-Alper, D., Spitz, N., Ben Ami, Y., Gawii, Z., Lifschitz, B., Yitzchaki, A., Seter, I., 1996. "Atmospheric sulfur over the Eastern Mediterranean region". *Journal of Geophysical Research* 101, 25917–25930.

Maenhaut, W., 1989. "Analytical techniques for atmospheric trace elements". In: Pacyna, J.M., Ottar, B. (Eds.), *Control and Fate of Atmospheric Trace Metals*, pp. 259–301.

Maenhaut, W., *Nucl.Instrum.Methods Phys.Res.Sect.B* 49, 518, 1990

Maden Tetk'ik Arama, [www.mta.gov.tr](http://www.mta.gov.tr), Last Access date:18.02.2009

Mahowald, N.M., Baker, A.R., Bergametti, G., Brooks, N., Duce, R.A., Jickells, T.D., Kubilay, N., Prospero, J.M., Tegen, I., 2005. "Atmospheric global dust cycle and ironinputs to the ocean". *Global Biogeochemistry Cycles*, 19, GB4025, doi:10.1029/2004GB002402.

Malm, W.C., Johnson, C.E., and Bresch, J.F., 1986. "Application of Principal Component Analysis for Purposes of Identifying Source-Receptor Relationships in Receptor Methods for Source Apportionment". Pace, T.G.,ed., Air Pollution Control Association, Pittsburgh, PA, 127-148

Marcazzan, G.M., Ceriani, M., Vali, G., and Vecchi, R., 2004. "Composition, components and sources of fine aerosol fractions using multielemental EDXRF analysis". *X-Ray Spectrometry*, 33, 267–272

Marcazzan, G.M.B., 1998. "Application of X-Ray Analysis to the Study of Air Particle Pollution in Northern Italy" *X-Ray Spectrometry*, 27, 247-256

Marenco, F., Bonasoni, P., Calzolari, F., Ceriani, M., Chiari, M., Cristofanelli, P., D' Alessandro, A., Fermo, P., Lucarelli, F., Mazzei, F., Nava, S., Piazzalunga, A., Prati, P., Valli, G., Vecchi, R., 2006. Characterization of atmospheric aerosols at Monte Cimone, Italy, during summer 2004: source apportionment and transport mechanisms. *Journal of Geophysical Research* 111, D24202. doi:10.1029/ 2006JD007145.

Marmer, E., and Langmann, B., 2005. "Impact of ship emissions on the Mediterranean summertime pollution and climate: A regional model study". *Atmospheric Environment* 39, 4659-4669

Mason, B., 1966. *Principles of Geochemistry*, 3<sup>rd</sup> Edition, John Wiley, New York, NY

Massey, F.J., Jr., 1951. The Kolmogorov-Smirnov Test for Goodness of Fit. *Journal of the American Statistical Association*, 46 (253),68–78.

Mateu, J., Forteza, R., Cerda, V., and Colomaltes, M., 1996. "Particle-Size Distribution and Long-Range Transport of Metals in Atmospheric Aerosols from the Alfabia Station (Majorca, Spain)", *Journal of Environmental Science and Health Part A-Environmental Science and Engineering & Toxic And Hazardous Substance Control*, 31 (1), 31-54

Mather, T.A. , Oppenheimer, C., Allen, A.G., McGonigle, A.J.S., 2004. "Aerosol chemistry of emissions from three contrasting volcanoes in Italy". *Atmospheric Environment* 38, 5637–5649

Matschullat, J., Maenhaut, W., Zimmermann, F., Fiebig, J., 2000. „Aerosol and bulk deposition trends in the 1990's, Eastern Erzgebirge, Central Europe". Atmospheric Environment 34, 3213–3221.

Matvev, V., Dayan, U., Tass, I., Peleg, M., 2002. "Atmospheric sulfur fluxes to and from Israel". Science of Total Environment, 291(1–3), 143–154

Meloni, D., Di Sara, A., Monteleone, F., Pace, G., Piacentino, S., Sferlazzo, D.M., 2008. "Seasonal patterns of intense Saharan dust events at the Mediterranean island of Lampedusa". Atmospheric Research 88, 134–148

Middleton, N.J., 1985. Effect of Drought on Dust Production in the Sahel". Nature 316, 431–434

Migon, C., and Caccia, J. L., 1990. "Seperation of Anthropogenic and Natural Emissions of Particulate Heavy Metals in the Western Mediterranean Atmosphere", Atmospheric Environment, 24, 399-405.

Mihalopoulos, N., Stephanou, E., Kanakidou, M., Pilitsidis, S., Bousquet, P., 1997. Tropospheric aerosol ionic composition in the Eastern Mediterranean Region, Tellus 49B, 314-326

Miller, J.M., Martin, D., Strauss, B., 1987. „A comparison of results from two trajectory models used to produce flow climatologies to the Western Mediterranean". NOAA Tech.Mem.ERL ARL-151, Air Resources Laboratory, Silver Spring, MD, 1987, pp.11

Milliman, J.D, Jeftic, L., Sestini, G., 1992., 1992. « The Mediterranean Sea and climate change-an overview". In: Jeftic, L., Miliman, J.D., Sestini, G. (Eds.), Climatic Change and Mediterranean, 1-14. UNEP, Great Britain

Mohan, S. V., Mouli, P. C., Balaram, V., Kumar, M. P., Reddy, S. J., 2006. "A study on trace elemental composition of atmospheric aerosols at a semi-arid urban site using ICP-MS technique", Atmospheric Environment 40, 136–146

Molinaroli, E., 1996. "Mineralogical characterization of Saharan dust with a view to its final destination in Mediterranean sediments". In: Guerzoni, S., Chester, R.(Eds), *The Impact of Desert Dust Across the Mediterranean*. Kluwer Academic Publishing, pp. 153-162

Mori , I., Nishikawa, M., Iwasaka, Y., 1998. "Chemical reaction during coagulation of ammonium sulfate and mineral particles in the atmosphere". *Science of the Total Environment* 224, 87-91

Mosher, B.W. and Duce, R.A., 1987. "A global atmospheric selenium budget". *Journal of Geophysical Research* 92, 13289–13298

Mouli, P. C. , Mohan, S. V. , Balaram, V. , Kumar, M. P., Reddy, S. J. , 2006. "A study on trace elemental composition of atmospheric aerosols at a semi-arid urban site using ICP-MS technique". *Atmospheric Environment* 40, 136–146

Moulin, C., Lambert, C.E., Dulac, F., Dayan, U., 1997. "Control of atmospheric export of dust by the North Atlantic Oscillation". *Nature* 387, 691–694

Muezzinoglu, A., and Cizmecioglu, S.C., 2006. "Deposition of heavy metals in a Mediterranean climate area". *Atmospheric Research* 81, 1–16

Muhs, D.R., Budahn, J.R., Prospero, J.M., and Carey, S.N., 2007. "Geochemical evidence for African dust inputs to soils of western Atlantic islands: Barbados, the Bahamas, and Florida". *Journal of Geophysical Research* 112 (F0209), doi:10.1029/2005JF000445

Murphy, D.M., Thomson, D.S., and Mahoney, M.J., 1998. "In Situ Measurement of Organics, Meteoritic Material, Mercury, and Other Elements in Aerosols at 5 to 19 Kilometers", *Science*, 282, 1664-1669.

N'Tchayi, M., Berrand, G., Nicholson, S.E., 1997. "The diurnal and seasonal cycles of wind-borne dust over Africa North of the Equator". *Journal of Applied Meteorology* 36, 868–882

Nastos PT, Alexakis D, Kanellopoulou HA, et al., 2007. "Chemical composition of wet deposition in a Mediterranean site Athens, Greece related to the origin of air masses". *Journal of Atmospheric Chemistry*, 58(2),167–179

Nicolás, J., Chiari, M., Crespo, J., Orellana, I.G., Franco, L., Nava, S., Pastor, C., Yubero, E., 2008. "Quantification OF Saharan and local dust in an arid Mediterranean area by the positive matrix factorization (PMF) technique". *Atmospheric Environment* (2008), doi:10.1016/j.atmosenv.2008.09.018

NOAA web page, <http://www.arl.noaa.gov/hysplitarc-bin/traj1arc.pl>, Last access date 05.01.2008

Nunes, L. S. S. , Tavares, T. M., Dippel, J. and Jaeschke, W., 2005. "Measurements of Atmospheric Concentrations of Reduced Sulphur Compounds in the All Saints Bay Area in Bahia, Brazil". *Journal of Atmospheric Chemistry* 50: 79–100

O'Dowd, C., Smith, M.H., Constardine, I.E., Lowe, J.A., 1997. "Marine Aerosol, Sea Salt, and the Marine Sulphur Cycle: A Short Review". *Atmospheric Environment*, 31, 1, 73-80

Oberdörster, G., Sharp, Z., Atudorei, V. , Elder, A. , Gelein, R. , Kreyling, W. , Cox , C.,2004. "Translocation of Inhaled Ultrafine Particles to the Brain". *Inhalation Toxicology* 16 (6&7):437–445

Odabasi, M., Muezzinoglu, A., and Bozlaker, A., 2002. "Ambient concentrations and dry deposition fluxes of trace elements in Izmir, Turkey". *Atmospheric Environment* 36, 5841-5851

O'Dowd, C.D., Hoffmann, T., 2005. Coastal new particle formation: a review of the current state-of-the-art. *Environmental Chemistry* 2 (4), 245–255

Ogulei, D., Hopke, P.K., Wallace, L.A., 2006. "Analysis of indoor particle size distributions in an occupied twonhouse using positive matrix factorization". *Indoor Air*, 16, 204–215

Ogulei, D., Hopke, P.k., Zhou, L., Paatero, P., Park, S.S., Ondov, J.M., 2005. "Receptor Modelling for multiple time resolved species: The Baltimore supersite". *Atmospheric Environment* 39, 3751- 3762

Ott, W.R., Mage, D.T., 1976. "A general purpose univariate probability model for environmental data analysis". *Computers and Operations Research* 3, 209-216

Ott, Wayne, 1990. "A physical explanation of the lognormality of pollutant concentrations". *Journal of the Air and Waste Management Association* 40, 1378-1383.

Owega, S., Khan, B.U.Z., Evans, G.J., Jervis, R.E., Fila, M., 2006. "Identification of long-range aerosol transport patterns to Toronto via classification of back trajectories by cluster analysis and neural network techniques". *Chemometrics and Intelligent Laboratory Systems* 83, 26-33

Ölmez, I., and Gordon, G.E., 1985. "Rare Earths: Atmospheric Signatures for Oil Fired Power Plants and Refineries". *Science* 229, 966-968

Özsoy, T., and Saydam, A.C., 2000. "Acidic and alkaline precipitation in the Cilician basin, north-eastern Mediterranean Sea". *Science of the Total Environment* 253, 93-109

Öztaş, N.B., 2001. "Solubility of Trace Metals in Atmospheric Aerosols". M.Sc. Thesis, Middle East Technical University, Ankara

P. Salvador, B. Artinano, X. Querol, A. Alastuey, M. Costoya, 2007. "Characterisation of local and external contributions of atmospheric particulate matter at a background coastal site". *Atmospheric Environment* 41 1–17

Paatero P., 1997. "Least squares formulation of robust non-negative factor analysis". *Chemometrics and Intelligent Laboratory Systems* 37 (1), 23-35

Paatero, P., 2000. "User's Guide for Positive Matrix Factorization Programs PMF2 and PMF3".

Paatero, P., and Hopke, P.K., 2003. "Discarding or downweighting High-Noise Variables in Factor Analytic Models". *Analytica Chimica Acta* 490, 277–289

Paatero, P., and Tapper, U., 1994. "Positive Matrix Factorization: A non-negative factor model with optimal utilization of error estimates of data values". *Environmetrics*, 5, 111–126

Paatero, P., Hopke, P.K., Begum, B.A, Biswas, S.K., 2005. "A graphical diagnostic method for assessing the rotation in factor models of atmospheric pollution". *Atmospheric Environment*, 39, 193–201

Pacyna, J.M., Bartonova, A., Cornille, P., and Maenhaut, W., 1987. "Modelling of Long Range Transport of Trace Elements. A case Study". *Atmospheric Environment* 23(1), 107–114

Pandis, S.N., Paulson, S.E., Seinfeld, J.H., and Flagan, R.C., 1991. "Aerosol formation in the photooxidation of isoprene and  $\beta$ -pinene". *Atmospheric Environment*, 21, 2275–2283

Papastefanou, C., and Ioannidou, A., 1991. "Depositional Fluxes and Other Physical Characteristics of Atmospheric Beryllium-7 in the Temperate Zones (40 °N) with a Dry (Precipitation Free) Climate". *Atmospheric Environment* 25A(10), 2335–2343

Partal, T., and Kahya, E., 2006. "Trend analysis in Turkish precipitation data". *Hydrological Processes*, 20, 2011–2026

Peirson, D.H., and Cawse, P.A., 1979. "Trace elements in the atmosphere". *Philosophical Transactions of the Royal Society of London, Series B, Biological Sciences* 288, 41–49

Pekney, N.J., Davidson, C.I., 2005. "Determination of trace elements in ambient aerosol samples". *Analytica Chimica Acta* 540, 269–277

Pekney, N.J., Davidson, C.I., Robinson, A., Zhou, L., Hopke, P., Eatough, D., Rogge, W.F., 2006. "Major Source Categories for PM<sub>2.5</sub> in Pittsburgh using PMF and UNMIX". *Aerosol Science and Technology*, 40:910–924

Pereira, P.A., Lopes, W.A., Carvalho, L.S., da Rocha, G.O., Bahai, N.C., Lotola, J., Quiterio, S.L., Escaleira, V., Arbilla, G., de Andrade, J.B., 2007. "Atmospheric concentrations and dry deposition fluxes of particulate trace metals in Salvador, Bahai, Brazil". *Atmospheric Environment*, doi:10.1016/j.atmosenv.2007.06.013

Perkin Elmer, ICP Mass Spectrometry Operator Manual, 2004

Peter K.K. Louie, P.K.K., Chow, J.C. , Chen, L.W. A., Watson, J.G. Leung, G. , Sin, D.W.M., 2005. PM<sub>2.5</sub> chemical composition in Hong Kong:urban and regional variations, *Science of the Total Environment* 338, 267– 281

Pierce, J.R., Adams, P.J., 2006. "Global evaluation of CCN formation by direct emission of sea salt and growth of ultrafine sea salt". *Journal of Geophysical Research-Atmospheres* 111 (D6) Art. No. D06203.

Pike, S.M., and Moran, S.B., 2001. "Trace elements in aerosol and precipitation at New Castle, NH, USA". *Atmospheric Environment* 35, 3361–3366

Pino, D.R., and Tian, R.C., 1995. "Simulation and prediction of anthropogenic lead perturbation in the Mediterranean Sea". *The Science of the Total Environment* 164, 135–150

Pirrone, N., Costa, P., and Pacyna, J.M., 1999. "Past, Current and Projected Atmospheric Emissions of Trace Elements in the Mediterranean Region". *Water Science and Technology* 39 (12), 1–7

Pirrone, N., Keller, G.J., and Holsen, T.M., 1995. "Dry deposition of trace elements to Lake Michigan:A Hybrid-Receptor Deposition Modelling Approach". *Environmental Science and Technology* 29, 2112–2122

Pitts, B.J.F., and Jr. Pitts, J.N., 1986. "Atmospheric Chemistry: Fundamentals and Experimental Techniques". John & Sons Publication Inc., 736

Pitts, B.J.F., and Jr. Pitts, J.N., 1997. "Tropospheric Air Pollution: Ozone, Airborne Toxics, Polycyclic Aromatic Hydrocarbons, and Particles". *Science* 276, 1045–1051



Plaisance, H., Galloo, J.C., and Guillermo, R., 1997. "Source Identification and variation in the chemical composition at two rural sites in France". *The Science of Total Environment*, 206, 79–93

Poirot, R.L., Wishinski, R.P., Hopke, P.K., Polissar, A.V., 2001. "Comparative Application of Multiple Receptor Methods to Identify Aerosol Sources in Northern Vermont". *Environmental Science and Technology*, 35, 4622-4636

Polissar, A.V., Hopke, P.K., Paatero, P., Kaufmann, Hall, D.K., Bodhaine, B.A., Dutton, E.G., Harris, J.M., 1999. "The aerosol at Barrow, Alaska: long-term trends and source locations". *Atmospheric Environment* 33, 2441-2458

Polissar, A.V., Hopke, P.K., Poirot, R.L., 2001. "Atmospheric Aerosol over Vermont: Chemical Composition and Sources". *Environmental Science and Technology*, 35, 4604-4621

Pöschl, U., 2005. "Atmospheric Aerosols: Composition, Transformation, Climate and Health Effects". *Atmospheric Chemistry International Edition* 44: 7520-7540

Priest, C., Panner, J., and Prather, M., 1997. "NO<sub>x</sub> from lightning: 1. Global distribution based on lightning physics". *Journal of Geophysical Research* 102, 5929–5241

Prodi, F., Belosi, F., Contini, D., Santachiara, G., Matteo, L.D., Gambaro, A., Donato, A., Cesari, D., 2008. "Aerosol fine fraction in the Venice Lagoon: Particle composition and sources". *Atmospheric Research* doi:10.1016/j.atmosres.2008.09.020

Prospero, J.M., 1996. "The Atmospheric transport of particles to the Ocean". In: Ittekkot, V., Schäfer, P., Honjo, S., Depetris, P.J. (Eds.), *Particle Flux in the Ocean*, SCOPE Report 57, John Wiley & Sons, Chichester, 19–52.

Prospero, J.M., Lamb, P.J., 2003. "African droughts and dust transport to the Caribbean: Climate change implications". *Science* 302, 1024–1027.

Prospero, J.M., Nees, R.T., 1987. "Deposition rate of particulate and dissolved aluminum derived from Saharan dust in precipitation at Miami, FL". *Journal of Geophysical Research* 92, 14723–14731.

Putuad, J.P., Raes, F., Dingenen, R.V., Brüggemann, E., Facchini, M.C., Decesari, S., Fuzzi, S., Gehrid, R., Hüglin, C., Laj, P., Lorbeer, G., Maenhaut, W., Mihalopoulos, N., Müller, K., Querol, X., Rodríguez, S., Schneider, J., Spindler, G., Brink, H.T., Törseth, K., Widensohler, A., 2004. "A European aerosol phenomenology-2: chemical characteristics of particulate matter at kerbside, urban, rural and background sites in Europe". *Atmospheric Environment* 38, 2579-2595

Pyle, S.M., Nocerino, J.M., Deming, S.N., Palasota, J.A., Palasota, J.M., Miller, E.L., Hillman, D.C., Kuharic, C.A., Cole, W.H., Fitzpatrick, P.M., Watson, M.A., Nichols, K.D., 1996. "Comparison of AAS, ICP-AES, PSA, and XRF in Determining Lead and Cadmium in Soil". *Environmental Science and Technology*, 30, 204–213

Querol, X., Alastruey, A., Ruiz, C.R., Artinano, B., Hansson, H.C., Harrison, R.M., Buringh, E., ten Brink, H.M., Lutz, M., Brückmann, P., Straehl, P., Schneider, J., 2004. "Speciation and origin of PM<sub>10</sub> and PM<sub>2.5</sub> in selected European cities". *Atmospheric Environment* 38, 6,547–6,555

Querol, X., Alastuey, A.A., Moreno, T., Viana, M.M., Castillo, S., Pey, J., Rodríguez, S., Artinano, B., Salvador, P., Sánchez, M., Dos Santos, S.G., Garraleta, M.D.h., Patier, R.F., Grau, S.M., Negral, L., Minguillón, M.C., Monfort, E., Sanz, M.J., Marin, R.P., Gil, E.P., Cuevas, E., de la Rosa, J., de la Campa, A.S., 2008. "Spatial and temporal variations in airborne particulate matter (PM<sub>10</sub> and PM<sub>2.5</sub>) across Spain 1999-2005". *Atmospheric Environment*, 42, 3964-3979

Quinn, T.L., and Ondov, J.M., 1998. "Influence of Temporal Changes in Relative Humidity on Dry Deposition Velocities and Fluxes of Aerosol Particles Baring Trace Elements". *Atmospheric Environment* 32 (20), 3467–3479

R. A. Cox , 1997. "Atmospheric Sulphur and Climate-What Have We Learned?". *Philosophical Transactions: Biological Sciences* 352(1350), Atmospheric Chemistry of Sulphur in Relation to Aerosols, Clouds, and Climate, 251–254.

R.G. Derwent and A. L. Malcolm, 2000. "Photochemical generation of secondary particles in the United Kingdom", *Philosophical Transactions: Mathematical, Physical and Engineering Sciences* 358 (1775), Ultrafine Particles in the Atmosphere, 2643–2657.

Rahn, K.A., 1976. "Silicon and aluminum in atmospheric aerosols: Crust-air fractionation". *Atmos. Environ.* 10, 597–601.

Raman, R.S., Hopke, P.K., 2007. "Source apportionment of fine particles utilizing partially speciated carbonaceous aerosol data at two rural locations in New York State". *Atmospheric Environment* 41, 7923–7939

Ramanathan, V., Crutzen, P.J., Kiehl, J.T., Rosenfeld, D., 2001. "Aerosols, Climate, and Hydrological Cycle". *Science* 294, 2119–2124

Reff, A., Elberly, S., and Bhave, P.V., 2007. "Receptor Modelling of Ambient Particulate Matter Data Using Positive Matrix Factorization: Review of Existing Methods". *Journal of Air and Waste Management Association* 57, 146–154

Reiff, J., Forbes, G.S., Spieksma, F.T.M., Reynders, J.J., 1986. "African dust reaching North-western Europe: a case study to verify trajectory calculations". *Journal of Climate and Applied Meteorology* 25, 1543–1567

Reimann, C., de Caritat, P., 2000. "Intrinsic flaws of element enrichment factors (EFs) in environmental geochemistry". *Environ. Sci. Technol.* 34 (24), 5084–5091.

Ribeiro, A.S., Borges, D.L.G., Vieira, M.A., Curtius, A.J., 2007. "Coupling of ultrasonic nebulization to flame furnace atomic absorption spectrometry—new possibilities for trace element determination". *Microchemical Journal* 85, 341–346

Riccio, A., Giunta, G., Chianese, E., 2007. "The application of a trajectory classification procedure to interpret air pollution measurements in the urban area of Naples (Southern Italy)". *Science of the Total Environment* 376, 198-214

Rodrigo A, Avila A, Roda E, 2003. *Science of The Total Environment*, 305(1–3),195–205

Rodrigo, A., Avila, A, and Roda, F., 2003. "The chemistry of precipitation, throughfall and stemflow in two holm oak (*Quercus ilex* L.) forest under a contrasted pollution environment in NE Spain". *The Science of Total Environment*, 305 (1–3), 195–205

Rodriguez, S., Querol, X., Alastuey, A., Mantilla, E., 2002. "Origin of high summer PM<sub>10</sub> and TSP concentrations at rural sites in Eastern Spain". *Atmospheric Environment* 36, 3101–3112

Rolph, G.D., 2003. Real-time Environmental Applications and Display sYstem (READY) Website (<http://www.arl.noaa.gov/ready/hysplit4.html>). NOAA Air Resources Laboratory, Silver Spring, MD.

Rudich, Y., Kaufman, Y.J., Dayan, U., Yu, H., and Kleidman, R.G., 2008. "Estimation of transboundary transport of pollution aerosols by remote sensing in the eastern Mediterranean". *Journal of Geophysical Research* 113(D14S13), doi:10.1029/JD009601

Rumburg, B., Alldredge, R., Claiborn, C., 2001. "Statistical distributions of particulate matter and the error associated with sampling frequency". *Atmospheric Environment* 35, 2907-2920

Russell, L.M., Singh, E.G., 2006. "Submicron salt particle production in bubble bursting". *Aerosol Science and Technology* 40 (9), 664–671.

S. Rodriguez, X. Querol, A. Alastuey, J. de la Rosa, 2007. "Atmospheric particulate matter and air quality in the Mediterranean: a review". *Environ Chem Lett* (2007) 5: 1–7,

S.R, Biegalski, and P.K.Hopke, 2004. "Total Potential Source Contribution Function Analysis of Trace Elements Determined in Aerosol Samples Collected near Lake Huron". *Environ. Sci. Technol.*, 38, 4276-4284

Salcedo, R.L.R., Alvim Ferraz, M.C.M., Alves, C.A., Martins, F.G., 1999. "Time series analysis of air pollution data". *Atmospheric Environment* 33, 2361-2372.

Saliba, N.A., Kouyoumdjiana, H., Roumie, M., 2007. "Effect of local and long-range transport emissions on the elemental composition of PM<sub>10-2.5</sub> and PM<sub>2.5</sub> in Beirut". *Atmospheric Environment* 41, 6497–6509

Salvador, P., Artinano, B., Querol, X., Alastuey, A., 2008. "A Combined Analysis of Backward Trajectories and Aerosol Chemistry to Characterize long-range transport episodes of Particulate Matter: The Madrid Air Basin". *Science of The Total Environment* 390, 495-506

Sancho, P., De La Cruz, J., Diaz, A., Martin, F., Hernandez, E., Valero, F., Albarran, B., 1992. "A five year climatology of back trajectories from Izana baseline station, Tenerife, Canary Islands". *Atmospheric Environment* 26A, 1081-1096

Sandroni, V., and Migon, C., 2002. "Atmospheric deposition of metallic pollutants over the Ligurian Sea: labile and residua inputs". *Chemosphere* 47, 753–764

Saxena, A., Kulshrestha, U.C., Kumar, N., Kumari, K.M., Prakash S., and Srivastava, S.S. 1997. "Dry deposition of sulfate and nitrate to polypropylene surfaces in a semi-arid area of India". *Atmospheric Environment* 31, 2361–2366.

Schauer, J.j., Rogge, W.F., Hildemann, L.M., Mazurek, M.A., and Cass, G.R., 1996. "Source Apportionment of Airborne Particulate Matter Using Organic Compounds as Tracers"., *Atmospheric Environment* 30(22), 3837-3855

Schauer, J.J., Wolfgang, F.R., Hildemann, L.M., Mazurek, M.A., Cass, G.R., 1996. "Source Apportionment of Airborne Particulate Matter Using Organic Compounds as Tracers". *Atmospheric Environment*, 30 (22), 3837–3855

Scheff, P.A., Valiozis, C., 1990. "Characterization and source identification of respirable particulate matter in Athens, Greece". *Atmospheric Environment* 24A, 203–211.

Schwartz, J., Dockery, D. W. & Neas, L. M. 1996. "Is daily mortality associated specifically with fine particles?". *J. Azr Waste Manag. Ass.* 46, 927–939

Sciare, J., Bardouki, H., Moulin, C., Mihalopoulos, N., 2003. "Aerosol sources and their contribution to the chemical composition of aerosols in the Eastern Mediterranean Sea during summertime". *Atmospheric Chemistry and Physics* 3, 291–302.

Seigneur, C., Pai, P. Louis, J.F., Hopke, P.K., Grosjean, D., 1997. "Review of Air Quality Models for Particulate Matter". Prepared for the American Petroleum Institute, Document No.CP015-97-1b

Seinfeld, J.H., Pandis, S.N., 1998. Atmospheric Chemistry and Physics, Wiley, NY.

Sen, P.K., 1968b. "Estimates of the regression coefficient based on Kendall's tau". Journal of American Statistical Association, 63, 1379-1389

Sen-chao, Lai, Shi-chun, Zou, Jun-ji, Cao, Shun-cheng, EEE., Kin-fai, HO., 2007. "Characterizing ionic species in PM<sub>2.5</sub> and PM<sub>10</sub> in four Pearl River Delta cities, South China". Journal of Environmental Sciences 19, 939-947

Shaka, H., and Saliba, N.A.,2004. "Concentration measurements and chemical composition of PM<sub>10-2.5</sub> and PM<sub>2.5</sub> at a coastal site in Beirut, Lebanon". Atmospheric Environment 38, 523–531

Sharma, S., Barrie, L.A., Plummer, D., McConnel, J.C., Brickell, P.C., Levasseur, M., Gosselin, M., and Bates, T.S., 1999. "Flux Estimation of Oceanic Dimethyl Sulphide around North America". Journal of Geophysical Research 104 (17), 21,327–21,342

Shinn, E.A., Smith, G.W., Prospero, J.M., Betzer, P., Hayes, M.L., Garrison, V., Barber, R.T., 2000. "African dust and the demise of Caribbean coral reefs". Journal of Geophysical Research Letters 27, 3029

Shuvayeva, O.V., Koutzenogii, K.P., Baryshev, V.B., Rezhikov, V.I., Smirnova, A.I., Ivanova, L.D., Sukchorukov, F.V., 1998. "Multi-elemental characterization of the atmospheric aerosols in frames of interlaboratory experiment". Atmospheric Research 46, 349–359

Siefert, R.L., Johansen, A.M., and Hoffmann, M.R., 1999. "Chemical characterization of ambient aerosol collected during the southwest monsoon and intermonsoon seasons over the Arabian Sea:labile Fe(II) and other trace metals". Journal of Geophysical Research, 104(D3), 3511–3526

Sievering, H., 1984. "Small Particle dry deposition on Natural Waters: Modelling Uncertainty". *Journal of Geophysical Research* 89, 9679–9681

Skjoth, C.A., Sommer, J., Stach, A., Smith, M., and Brandt, J., 2007. "The long-range transport of birch (*Betula*) pollen from Poland and Germany causes significant pre-season concentrations in Denmark". *Clinical and Experimental Allergy*, 37, 1204–1212

Sloss, L.L., and Smith, I.M., 2000. "PM<sub>10</sub> and PM<sub>2.5</sub>: International perspective". *Fuel Processing Technology* 65–66, 127–141

Small, H., Stevens, T.S., Bauman, W.C., 1975. *Analytical Chemistry*, 47, pg.1801

Smolik, J., Zdimal, V., Schwarz, J., Lazaridis, M., Havranek, V., Eleftheriadis, K., Mihalopoulos, N., Bryant, C., Colbeck, I., 2003. "Size resolved mass concentration and elemental composition of atmospheric aerosols over the Eastern Mediterranean area". *Atmos. Chem. Phys.*, 3, 2207–2216

Song, X.H., Polissar, A.V., Hopke, P.K., 2001. "Sources of Fine Particle Composition in the Northeastern U.S.". *Atmospheric Environment* 35:5277-5286, 2001

Stockwell, W.R., and Calvert, J.G., 1983. "The mechanism of HO-SO<sub>2</sub> reaction". *Atmospheric Environment* 17, 2231-2235

Stohl, A., 1998. "Computation, Accuracy and Applications of Trajectories: A Review and Bibliography". *Atmospheric Environment* 32(6), 947–966

Stohl, A., and Seibert, P., 1998. "Accuracy of trajectories as determined from the conservation of meteorological tracers". *Quarterly Journal of Royal Meteorological Society*, 124, 1465-1484

Stranger, M., Vermaak, S.S.P., Grieken, R.V., 2008. "Particulate matter and gaseous pollutants in the residences in Antwerp, Belgium". *Science of the Total Environment*, doi:10.1016/j.scitotenv.2008.10.019

Strayer, H., Smith R., Mizak, Connie, Poor, N., 2007. "Influence of air mass origin on the wet deposition of nitrogen to Tampa Bay, Florida-An eight year study". *Atmospheric Environment*, 41, 4310-4322

Swami, K., Judd, C.D., John Orsini Karl, X., Yang Husain, L., 2001. "Microwave assisted digestion of atmospheric aerosol samples followed by inductively coupled plasma mass spectrometry determination of trace elements". *Fresenius Journal of Analytical Chemistry* 369, 63-70.

Swap, R., Garstang, M., Greco, S., Talbot, R., Kallberg, P., 1992. "Saharan dust in the Amazon basin". *Tellus* 44B, 133-149

Szilagyi, V., Hartyani, Z., 2004. "Development of an X-ray Fluorescence Spectrometric Method for the Analysis of Atmospheric Aerosol Samples". *Microchemical Journal*, Article in Press

Szilagyi, V., and Hartyani, Z., 2004. "Development of an X-ray fluorescence spectrometric method for the analysis of atmospheric aerosol samples". *Microchemical Journal*, 2004, Article in Press

Tabor, K., Gutzwiller, L., Rossi, M.J., 1994. "Heterogenous chemical kinetics of NO<sub>2</sub> on amorphous-carbon at ambient temperature". *Journal of Physical Chemistry* 98(24), 6172-6186

Tamamura, S., Sato, T. , Ota, Y. , Wang, X., Tang, N. , Hayakawa, K., 2007. "Long-range transport of polycyclic aromatic hydrocarbons (PAHs) from the eastern Asian continent to Kanazawa, Japan with Asian dust". *Atmospheric Environment* 41, 2580-2593

Tasdemir, Y., Kural, C., Cindoruk, S., Vardar, N., 2006. "Assessment of trace element concentrations and their estimated dry deposition fluxes in an urban atmosphere". *Atmospheric Research* 81, 17-35

Taubman, B.F., Hains, J.C., Thompson, A.M., Marufu, L.T., Doddridge, B.G., Stehr, J.W., Piety, C.A., and Dickerson, R.R., 2006. "Aircraft vertical profiles of trace gas and aerosol



pollution over the mid-Atlantic United States: Statistics and meteorological cluster analysis". *Journal of Geophysical Research* 111, D10S07, 1-1

Taylor, S.R., 1964. Abundance of chemical elements in the continental crust: A new table. *Geochim. Cosmochim. Acta* 28, 1273.

Thermo X Series ICP-MS Operator Manual, 2006

Thurston, G. D., Ito, K., Hayes, C. G., Bates, D. V. & Lippmann, M., 1994. "Respiratory hospital admissions and summertime haze air pollution in Toronto, Ontario: consideration of the role of acid aerosols". *Environ. Res.* 65, 271–290.

Tiwari, M.K., Singh, A.K., and Sawhney, K.J.S, 2005. *Analytical Sciences* 21, 143-147

Trap, J.M., Millero, F.J., Prospero, J.M., 2008. "Temporal Variability of the Elemental Composition of African Dust Measured in Trade Wind Aerosols at Barbados and Miami". doi: 10.1016/j.marchem.2008.10.004

Traub et al., 2003. "Chemical characteristics assigned to trajectory clusters during the MINOS campaign". *Atmospheric Chemistry and Physics* 3, 459-468.

Truex TJ, Anderson JE. 1979. "Mass monitoring of carbonaceous aerosols with a spectrophone". *Atmos Environment* 13: 507 –509.

Tsitouridou, R., Voutsas, D., Kouimtzis, T., 2003. Ionic composition of PM<sub>10</sub> in the area of Thessaloniki, Greece. *Chemosphere* 52, 883–891.

Tuncel, G., Aras, N.K., and Zoller, W.H., 1989. "Temporal Variations and Sources of Elements in the South Pole Atmosphere: 1. Nonenriched and Moderately Enriched Elements". *Journal of Geophysical Research* 94(D10), 13025–13038

Tuncel, S.G., and Erduran, M.S., 2001. "Gaseous and Particulate Air Pollutants in the Northeastern Mediterranean Coast". *The Science of the Total Environment* 281, 205–215

Tuncer, B., Bayar, B., Yesilyurt, C., Tuncel, G., 2001. "Ionic Composition of Precipitation at the Central Anatolia". *Atmospheric Environment* 35, 5,989–6,002

Turekian, K.K., Wedepohl, K.H., 1961. "Distribution of the elements in some major units of the Earths crust". *Geol. Soc. Am. Bull.* 72, 175–191.

Turkish Air Quality Regulation, 2004

Turkum, A., 2004. "Investigation of the Relationship between Aerosol and Rainwater Composition". M.Sc. Thesis, Middle East Technical University, Environmental Engineering Department

U.S. Environmental Protection Agency. Determination of Trace Elements in Waters and Wastes by Inductively Coupled Plasma-Mass Spectrometry, revision 4.4, EPA-600-R-94-111, April 1991.

Uzun, B., 2000. "Investigation of Biogenic Sulfur in East Mediterranean Basin". M.Sc. Thesis, Middle East Technical University, Environmental Engineering Department, Ankara, Turkey

Valkovic, V. , Dargie, M. , Jaksic, M. , Markowicz, A. , Tajani , A., Valkovic, O. , 1996. "X-ray emission spectroscopy applied for bulk and individual analysis of airborne particulates". *Nuclear Instruments and Methods in Physics Research B* 113, 363-367,

Vallius, M., Lanki, T., Tiittanen, P., Koistinen, K., Ruuskanen, J., Pekkanen, J., 2003. "Source apportionment of urban ambient PM<sub>2.5</sub> in two successive measurement campaigns in Helsinki, Finland". *Atmospheric Environment* 37, 615–623

Van Belle G, Hughes JP. 1984. "Non-parametric tests for trend in water quality". *Water Resources Research* 20: 127–136.

Vascancelos, L.A.D., Kahl, J.D.W, Liu, D., Macias, E.S., White, W.H., 1996b. "A tracer calibration of back trajectory analysis at the Grand Canyon". *Journal of Geophysical Research* 101, 19329-19335

Vassilakos, Ch., Veros, D., Michopoulos, J., Maggos, Th., O'Connor, C.M., 2007. "Estimation of selected heavy metals and arsenic in PM10 aerosols in the ambient air of the Greater Athens Area, Greece". *Journal of Hazardous Materials* 140, 389–398

Viana, M., Kuhlbusch, T.A.J., Querol, X., Alastuey, A., Harrison, R.M., Hopke, P.K., Winiwarter, W., Vallius, M., Szidat, S., Prevoti, A.S.H., Hueglin, C., Bloemen, H., Wahlini, P., Vecchi, R., Miranda, A.I., Kasper-Giebl, Maenhaut, W., Hitztenberger, R., 2008. "Source apportionment of particulate matter in Europe: A review of methods and results". *Aerosol Science* 39, 827-839

Vinogradov, A.P., 1959. "The Geochemistry of Rare and Dispersed Chemical Elements in Soils". 2<sup>nd</sup> Ed. Consultants Bureau, Inc., New York, NY.

Von Mises, R., 1964. "Mathematical Probability Theory of Probability and Statistics". Chapters IX(C) and IX (E). Academic Press, New York

Wallace, J.M., and Hobbs, P.V., 2006. "Atmospheric Science: An Introductory Survey". 2<sup>nd</sup> Edition, Elsevier Inc., California, USA

Wang, C.F., Chang, E.E., Chiang, P.C., and Aras, N.K., 1995a. "Analytical procedures on multi-element determinations of airborne particles for receptor model use". *Analyst*, 120, 2521–2527

Wang, Y., Zhuang, G., Zhang, X., et al., 2006. "The ion chemistry, seasonal cycle, and sources of PM<sub>2.5</sub> and TSP aerosol in Shanghai". *Atmospheric Environment* 40 (16), 2935-2952

Washington, R., Todd, M., Middleton, N.J., Andrew S. Goudie, A.S., 2003. "Dust-storm source areas determined by the total ozone mapping spectrometer and surface observations". *Annals of the Association of American Geographers* 93 (2), 297–313

Watson, J.G., Chen, L.W.A., Chow, J.C., Doraiswamy, P., Lowenthal, D.H., 2002. "Source Apportionment: Findings from the U.S. Supersites Program". *Journal of Air & Waste Management Association* 58, 265–288

Watson, J.G., and Chow, J.C., 2001. "Source Characterization of major emissions sources in Imperial and Mexicali Valleys along US/Mexico border". *The Science of the Total Environment* 276, 33–47

Watson, J.G., Zhu, T., Chow, J.C., Engelbrech, J., Fujita, E.M., Wilson, W.E., 2002. "Receptor modelling application framework for particle source apportionment". *Chemosphere* 49, 1093–1136

Wehrens, R., Putter, H., Buydens, L.M.C, 2000. The bootstrap: a tutorial. *Chemometrics and Intelligent Laboratory Systems*, 54, 35-52

Wojcik, G.S., and Chang, J.S., 1997. "Reevaluation of sulphur budgets, lifetimes and scavenging ratios for Eastern North America". *Journal of Atmospheric Chemistry* 26, 109-145

Wolff, GT, Groblicki PJ, Cadle, SH, Countness, RJ., 1982. "Particulate carbon at various locations in the United States". In: Wolff GT, Climisch RL, editors. *Particulate Carbon: Atmospheric Life Cycle*. London: Plenum Press

World Bank, Phasing out lead from gasoline: worldwide experience and policy implications. *Pollution Management Series, World Bank Technical Paper No. 397*, Washington DC (1998)

Wu, S., Zhao, Y.H., Feng, X., and Wittmeier, A., 1996. "Application of inductively coupled plasma mass spectrometry for total metal determination in silicon-containing solid samples using microwave assisted nitric acid-hydrofluoric acid-hydrogen peroxide-boric acid digestion system. *Journal of Analytical Atomic Spectrometry*, 11, 287–296

Wu, Y.-S., Fang, G.-C., Chen, J.-C., et al. 2006. "Ambient air particulate dry deposition, concentrations and metallic elements at Taichung Harbor near Taiwan Strait". *Atmospheric Environment* 79, 52–66.

Wu, Z. Y., Han, M., Lin, Z. C. and Ondov, J. M. (1994) Chesapeake Bay atmospheric deposition study, year 1: sources and dry deposition of selected elements in aerosol particles. *Atmospheric Environment* 28, 1471–1486.

Xie, Y., and Berkowitz, C.M., 2006. "The use of positive matrix factorization with conditional probability functions in air quality studies: An application to hydrocarbon emissions in Houston, Texas". *Atmospheric Environment* 40: 3070–3091

Xu, X., Dockery, D.W., 1994. "Air Pollution and Daily Mortality in Residential Areas of Beijing, China". *Archives of Environmental Health*, 216–222

Y. Erel, U. Dayan, R. Rabi, Y. Rudich, and M. Stein, 2006. "Trans Boundary Transport of Pollutants by Atmospheric Mineral Dust". *Environ. Sci. Technol.* 40, 2996–3005

Yaalon, D.H. and Ganor, E., 1979. "East Mediterranean trajectories of dust carrying storms from the Sahara and Sinai". In C. Morales (Editor), *Saharan Dust*. Wiley, Ch.9, pp.187-193

Yao, X., Chan, C.K., Fang, M. et al., 2002. "The water soluble ionic composition of PM<sub>2.5</sub> in Shanghai and Beijing, China:1-inorganic ions". *Atmospheric Environment* 36(26), 4223-4234

Yatin, M., Tuncel, S., Aras, N.K., Olmez, I., Aygun, S., Tuncel, G., 2000. "Atmospheric trace elements in Ankara, Turkey:1. factors affecting chemical composition of fine particles". *Atmospheric Environment* 34, 1305–1318

Yeh, H.S., Cuddihy, R.G., Phalen, R.F., Chang, I.Y., 1996. "Comparisons of Calculated Respiratory Tract Deposition of Particles Based on Proposed NCRP Model and the New ICRP66 Model". *Aerosol Science and Technology*, 25, 134–140

Yu, S., Saxena, V.K., and Zhao, Z., 2001. "A comparison of signals of regional aerosol-induced forcing in eastern China and the southeastern United States". *Geophysical Research Letters* 28, 713–716

Zabalza, J., Ogulei, D., Hopke, P.K., Lee, J.H., Hwang, I., Querol, X., Alastuey, A., , Santamaria, J.M., 2006. "Concentration and Sources of PM<sub>10</sub> Constituents in Alsasua, Spain, *Water, Air and Soil Pollution*, 174: 385-404

Zerefos, C., Ganev, K., Kourtidis, K., Tzortsiou, M., Vasaras, A., Syrakov, E., 2000. "On the origin of SO<sub>2</sub> above Northern Greece". *Geophysical Research Letters* 27, 365–368.

Zhang, S.H., Shaw, M., Seinfeld, J.H., and Flagan, R.C, 1992. "Photochemical aerosol formation from  $\alpha$ -pinene and  $\beta$ -pinene". *Journal of Geophysical Research*, 18, 20717–20729

Zhang, XY., Gong, SL., Zhao, TL., Arimoto, R., Wang, YQ., Zhou, ZJ., 2003. "Sources of Asian dust and role of climate change versus desertification in Asian dust emissions". *Geophysical Research Letters*, 30, 24, 2272

Zhang, Z.W., Shimbo, S., Watanabe, T., Srianujata, S., Banjong, O., Chitchumroonchokchai, C., Nakatsuka, H., Matsuda-Inoguchi, N., Higashikawa, K., Ikeda, M., 1999. "Non-occupational lead and cadmium exposure of adult women in Bangkok, Thailand". *The Science of the Total Environment* 226, 65-74

Zhao, W., and Hopke, P.K., 2006. "Source Investigation for PM<sub>2.5</sub> in Indianapolis". In. *Aerosol Science and Technology* 40, 898–909

Zhu, X.R., Prospero, J.M., Millero, F.J., 1997. "Daily variability of soluble Fe(II) and soluble total Fe in North African dust in the trade winds at Barbados". *Journal of Geophysical Research* 102 (D17), 21297–21305

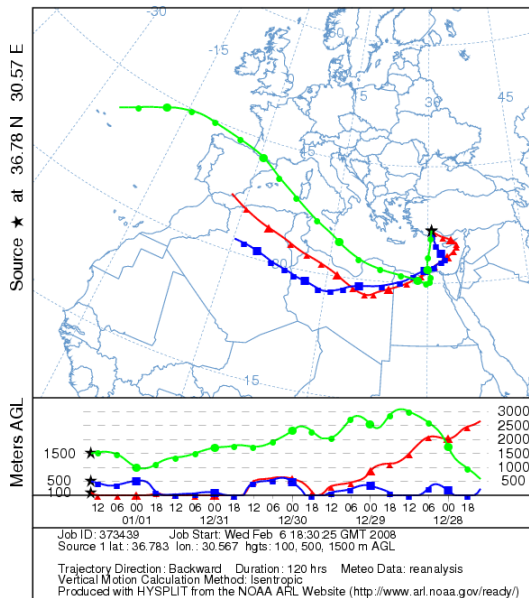
Zhuang, G., Yi, Z., Duce, R., and Brown, P.R., 1992. "Link between Iron and Sulphur Cycles Suggested by Detection of Fe (II) in Remote Marine Aerosols". *Nature* 355, 537–539

Zoller, W.H., Gladney, E.S., Duce, R.A., 1974. "Atmospheric concentrations and sources of trace metals at the South Pole". *Science* 183, 198–200.

## APPENDIX A. SAMPLE BACKTRAJECTORY FILE AND MAP

3	1	1	1	0	0													
CDC1	1	1	1	0	0													
CDC1	1	1	1	0	0													
CDC1	1	1	3	1	0													
3	BACKWARD	THETA																
1	2	1	14	36.783	30.567	100.0												
1	2	1	14	36.783	30.567	500.0												
1	2	1	14	36.783	30.567	1500.0												
3	PRESSURE	THETA	RAINFALL															
1	1	1	1	14	0	0	0.0	36.783	30.567	100.0	926.8	288.8	0.4					
1	1	1	1	14	0	0	0.0	36.783	30.567	500.0	882.5	289.8	0.4					
1	1	1	1	14	0	0	0.0	36.783	30.567	1500.0	779.3	292.4	0.4					
1	1	1	1	13	0	0	-1.0	36.681	30.447	0.0	941.3	288.9	0.4					
1	1	1	1	13	0	0	-1.0	36.680	30.346	431.5	893.9	289.7	0.4					
1	1	1	1	13	0	0	-1.0	36.653	30.259	1520.2	782.9	292.3	0.4					
1	1	1	1	12	0	0	-2.0	36.589	30.326	0.0	944.9	289.1	0.4					
1	1	1	1	12	0	0	-2.0	36.590	30.126	350.5	906.9	289.7	0.4					
1	1	1	1	12	0	0	-2.0	36.532	29.932	1543.7	786.1	292.3	0.4					
1	1	1	1	11	0	0	-3.0	36.498	30.196	0.0	948.6	288.6	0.2					
1	1	1	1	11	0	0	-3.0	36.503	29.917	271.8	921.5	289.0	0.2					
1	1	1	1	11	0	0	-3.0	36.412	29.596	1574.3	790.7	292.0	0.2					
1	1	1	1	10	0	0	-4.0	36.403	30.064	0.0	952.3	288.0	0.2					
1	1	1	1	10	0	0	-4.0	36.407	29.722	216.0	934.3	288.4	0.2					
1	1	1	1	10	0	0	-4.0	36.291	29.264	1611.9	793.7	291.6	0.2					
1	1	1	1	9	0	0	-5.0	36.303	29.927	0.0	956.7	287.5	0.2					
1	1	1	1	9	0	0	-5.0	36.301	29.532	186.8	943.0	288.0	0.2					
1	1	1	1	9	0	0	-5.0	36.169	28.937	1655.0	795.7	291.6	0.2					
1	1	1	1	8	0	0	-6.0	36.196	29.784	5.8	961.8	287.1	0.2					
1	1	1	1	8	0	0	-6.0	36.188	29.341	183.5	948.7	287.6	0.2					
1	1	1	1	8	0	0	-6.0	36.050	28.615	1701.8	796.7	291.4	0.2					
1	1	1	1	7	0	0	-7.0	36.086	29.631	42.6	963.8	286.9	0.2					
1	1	1	1	7	0	0	-7.0	36.066	29.146	202.1	952.1	287.4	0.2					
1	1	1	1	7	0	0	-7.0	35.934	28.300	1750.8	796.6	291.3	0.2					
1	1	1	1	6	0	0	-8.0	35.967	29.462	97.3	962.6	286.8	0.2					
1	1	1	1	6	0	0	-8.0	35.927	28.944	238.5	952.7	287.4	0.2					
1	1	1	1	6	0	0	-8.0	35.825	27.992	1801.3	795.8	291.2	0.3					
1	1	1	1	5	0	0	-9.0	35.843	29.275	145.9	959.6	287.3	0.2					
1	1	1	1	5	0	0	-9.0	35.804	28.729	274.6	951.7	287.7	0.2					
1	1	1	1	5	0	0	-9.0	35.713	27.677	1851.4	794.8	291.2	0.3					
1	1	1	1	4	0	0	-10.0	35.719	29.074	171.4	962.5	287.5	0.2					
1	1	1	1	4	0	0	-10.0	35.670	28.495	295.9	954.6	287.9	0.2					
1	1	1	1	4	0	0	-10.0	35.586	27.339	1899.2	793.3	291.3	0.3					
1	1	1	1	3	0	0	-11.0	35.593	28.858	179.2	966.9	287.7	0.2					
1	1	1	1	3	0	0	-11.0	35.533	28.240	307.1	958.4	288.0	0.2					
1	1	1	1	3	0	0	-11.0	35.443	26.974	1944.6	791.1	291.4	0.3					
1	1	1	1	3	0	0	-12.0	35.466	28.623	174.6	972.2	287.9	0.2					
1	1	1	1	3	0	0	-12.0	35.395	27.961	314.0	962.5	288.1	0.2					
1	1	1	1	2	0	0	-12.0	35.283	26.582	1989.6	789.1	291.4	0.3					
1	1	1	1	1	0	0	-13.0	35.337	28.374	163.2	978.1	288.0	0.2					
1	1	1	1	1	0	0	-13.0	35.255	27.653	323.3	966.1	288.2	0.2					
1	1	1	1	1	0	0	-13.0	35.106	26.159	2036.6	786.8	291.3	0.4					

NOAA HYSPLIT MODEL  
Backward trajectories ending at 14 UTC 01 Jan 01  
CDC1 Meteorological Data



## VITA

### PERSONAL INFORMATION

Surname, Name: Fatma Öztürk

Nationality: Turkish

Date and Place of Birth: Ankara, 10.04.1977

### EDUCATION

2001–2009	Middle East Technical University, Ankara, Turkey Ph. D. after BS in Environmental Engineering (3.61/4.00)
1996–2001	Middle East Technical University, Ankara, Turkey BS in Environmental Engineering (3.00/4.00)

### WORK EXPERIENCE

January 2002-Present	Middle East Technical University, Environmental Engineering Department Ankara, Turkey <b>Teaching Assistant</b>
Sept. 2006- Nov. 2007	University of Maryland, Chemistry and Biochemistry Department, Maryland, USA <b>Research Assistant, Fellow of The Scientific and Technological Research Council of Turkey</b>
June 2000-August 2000	Tugal Environmental Technologies Inc. Co., Ankara <b>Intern Engineering Student</b>
June 1999-August 1999	Ankara Metropolitan Municipality, Ankara <b>Intern Engineering Student</b>

### FIELD OF PROFESSION

Atmospheric Chemistry, Air Pollution and its Control, Environmental Chemistry